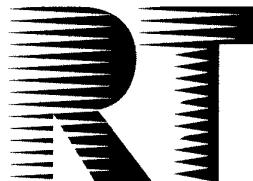NORTH ATLANTIC TREATY ORGANIZATION

R T

RESEARCH AND TECHNOLOGY ORGANIZATION

BP 25, 7 RUE ANCELLE, F-92201 NEUILLY-SUR-SEINE CEDEX, FRANCE

RTO MEETING PROCEEDINGS 35

Aerodynamic Design and Optimisation of Flight Vehicles in a Concurrent Multi-Disciplinary Environment

(la Conception et l'optimisation aérodynamiques des véhicules aériens dans un environnement pluridisciplinaire et simultané)

Papers presented at the Symposium of the RTO Applied Vehicle Technology Panel (AVT) held in Ottawa, Canada, 18-21 October 1999.

NORTH ATLANTIC TREATY ORGANIZATION

RT

RESEARCH AND TECHNOLOGY ORGANIZATION

BP 25, 7 RUE ANCELLE, F-92201 NEUILLY-SUR-SEINE CEDEX, FRANCE
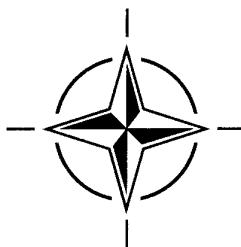
RTO MEETING PROCEEDINGS 35

Aerodynamic Design and Optimisation of Flight Vehicles in a Concurrent Multi-Disciplinary Environment

(la Conception et l'optimisation aérodynamiques des véhicules aériens dans un environnement pluridisciplinaire et simultané)
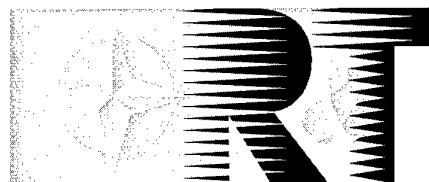
Papers presented at the Symposium of the RTO Applied Vehicle Technology Panel (AVT) held in Ottawa, Canada, 18-21 October 1999.

20010129 018

AQ - F01-04-0790

The Research and Technology Organization (RTO) of NATO

RTO is the single focus in NATO for Defence Research and Technology activities. Its mission is to conduct and promote cooperative research and information exchange. The objective is to support the development and effective use of national defence research and technology and to meet the military needs of the Alliance, to maintain a technological lead, and to provide advice to NATO and national decision makers. The RTO performs its mission with the support of an extensive network of national experts. It also ensures effective coordination with other NATO bodies involved in R&T activities.

RTO reports both to the Military Committee of NATO and to the Conference of National Armament Directors. It comprises a Research and Technology Board (RTB) as the highest level of national representation and the Research and Technology Agency (RTA), a dedicated staff with its headquarters in Neuilly, near Paris, France. In order to facilitate contacts with the military users and other NATO activities, a small part of the RTA staff is located in NATO Headquarters in Brussels. The Brussels staff also coordinates RTO's cooperation with nations in Middle and Eastern Europe, to which RTO attaches particular importance especially as working together in the field of research is one of the more promising areas of initial cooperation.

The total spectrum of R&T activities is covered by 7 Panels, dealing with:

- SAS   Studies, Analysis and Simulation
- SCI   Systems Concepts and Integration
- SET   Sensors and Electronics Technology
- IST   Information Systems Technology
- AVT   Applied Vehicle Technology
- HFM   Human Factors and Medicine
- MSG   Modelling and Simulation

These Panels are made up of national representatives as well as generally recognised 'world class' scientists. The Panels also provide a communication link to military users and other NATO bodies. RTO's scientific and technological work is carried out by Technical Teams, created for specific activities and with a specific duration. Such Technical Teams can organise workshops, symposia, field trials, lecture series and training courses. An important function of these Technical Teams is to ensure the continuity of the expert networks.

RTO builds upon earlier cooperation in defence research and technology as set-up under the Advisory Group for Aerospace Research and Development (AGARD) and the Defence Research Group (DRG). AGARD and the DRG share common roots in that they were both established at the initiative of Dr Theodore von Kármán, a leading aerospace scientist, who early on recognised the importance of scientific support for the Allied Armed Forces. RTO is capitalising on these common roots in order to provide the Alliance and the NATO nations with a strong scientific and technological basis that will guarantee a solid base for the future.

Aerodynamic Design and Optimisation of Flight Vehicles in a Concurrent Multi-Disciplinary Environment

(RTO MP-35)

Executive Summary

The theme of the Fluid Dynamics Sessions of the AVT Panel Fall 1999 Symposium was Aerodynamic Design and Optimisation of Flight Vehicles in a Concurrent Multi-Disciplinary Environment. The objective was to survey the current and future scene given the trend in industry towards a more concurrent and multi-disciplinary approach to aerospace vehicle engineering for air vehicle products procured by NATO Nations.

The conference included a Keynote Session where invited speakers, primarily from industry and military organisations, set the scene by discussing the lessons learnt from the past, the current and future capabilities in order to meet the military's operational requirements in Aerodynamics. The Sessions were well attended and there were lively discussions on the future needs of industries to develop competitive products. In particular there was a debate on the future role of the Aerodynamicist and the need for engineers who have both a broad appreciation whilst retaining depth in a particular specialist skill.

The impact of modern information technology and the move towards joint projects with a number of partners led to the question of how to appropriately support multi-national projects. During the other sessions consideration was given to the technologies being developed to support aerodynamic design optimisation particularly in the concept phase of a project. The importance of good quality data in the concept phase and its impact on early decision making was highlighted. This is an area in which the technical community could make a significant impact on the quality of the product and reduce the risk in future procurement programmes. The need for the scientific community to address this issue was emphasised.

The Technical Evaluator reflected that whilst optimisation with multi-disciplinary constraints was evident in the work presented, the impact of true multi-disciplinary optimisation was not clear. To ensure an optimum product for the military, the question was asked as to whether it was still relevant to train people to be purest aerodynamics engineers.

The meeting was considered to be successful in addressing and raising several issues of high priority which will need to be taken forward by the community for future events to ensure that military products are optimum and that the programmes to be developed are at minimum risk. A number of these issues are also discussed in the Technical Evaluator's Report.

la Conception et l'optimisation aérodynamiques des véhicules aériens dans un environnement pluridisciplinaire et simultané

(RTO MP-35)

Synthèse

Le symposium d'automne 1999 de la commission AVT a eu pour thème la conception et l'optimisation aérodynamiques des véhicules aériens dans un environnement fait de disciplines multiples et concomitantes. L'objectif a été de faire le point de la situation actuelle dans ce domaine et de prévoir les développements futurs, étant donné l'évolution générale vers une approche toujours plus concurrente et pluridisciplinaire du génie aérospatial en ce qui concerne les véhicules aériens achetés par les pays membres de l'OTAN.

La conférence comprenait une session d'ouverture au cours de laquelle des conférenciers, dont la plupart travaillent dans l'industrie ou pour des organisations militaires, ont introduit le symposium en débattant des enseignements à tirer du passé, ainsi que des possibilités actuelles et futures devant satisfaire aux besoins opérationnels des militaires en matière d'aérodynamique. Ses sessions ont accueilli de nombreux participants, avec des discussions animées sur la nécessité pour l'industrie de développer à l'avenir des produits compétitifs. En particulier, un débat a eu lieu sur le futur rôle de l'aérodynamicien et le besoin qui se fait sentir d'ingénieurs ayant à la fois une large culture technique et des connaissances approfondies dans un domaine particulier.

La prise en compte de l'impact des technologies modernes de l'information, associé à la tendance qui se dessine en faveur de projets conjoints réunissant un certain nombre de partenaires, a conduit à une réflexion sur le meilleur moyen de soutenir les projets internationaux. Les autres sessions ont pris en considération les technologies en développement devant concourir à l'optimisation de la conception aérodynamique, en particulier lors de la phase de conception initiale d'un projet. L'importance de disposer de données fiables lors de cette phase, ainsi que son impact sur la prise de décisions en amont, a aussi été soulignée. Il s'agit d'un domaine où les spécialistes techniques pourraient avoir une influence considérable sur la qualité du produit, tout en permettant de réduire les risques inhérents aux futurs programmes d'approvisionnement. La conférence a insisté sur la nécessité, pour la communauté scientifique, d'examiner ces questions.

L'évaluateur technique a noté que bien qu'il lui semblait évident, sur la base des travaux présentés, que l'optimisation soit accompagnée de contraintes pluridisciplinaires, l'impact d'une véritable optimisation pluridisciplinaire était loin d'être clair. La question a été posée de savoir s'il était encore utile, dans l'optique de la réalisation d'un produit militaire optimal, de former des ingénieurs en aérodynamique pure.

Il a été considéré que la réunion avait réussi à soulever et à examiner un certain nombre de questions prioritaires, qui devront être étudiées plus en avant afin de s'assurer que les futurs produits militaires soient optimisés, et que les programmes soient développés avec un risque minimum. Un certain nombre de ces questions sont aussi examinées dans le rapport d'évaluation technique.

Contents

Theme

Military air planes must fulfil a plethora of requirements which is continually growing. The impact of design objectives, compatibility and total life cycle cost requirements on design complexity is high. Reduction of design cycle time through concurrent engineering and reduction of risk through better multi-disciplinary interactions in the early stages of flight vehicle design are primary objectives of the military aerospace industry. Rapid turnaround aerodynamic, propulsion integration, structural and electromagnetic procedures are required for this purpose.

The symposium contributed to the understanding of the state of the art in the aerodynamic design and optimisation field, and that which can be expected from new developments in aerodynamics, information technologies, and optimisation theory. The objective is to survey the current and future scene given the trends towards a more concurrent and multi-disciplinary approach to aerospace vehicle engineering.

A particular theme of the symposium was the multi-objective, conceptual and preliminary design of flight vehicles in a concurrent, multi-disciplinary environment. Requirements for and capabilities of existing and new aerodynamic design and optimisation methods will be identified and discussed.

The format of the conference included an initial Plenary Session where invited speakers primarily from industry, set the scene by discussing: Requirements, lessons learnt from the past, current and future capabilities with regard to the role of aerodynamics in the future. This was followed by scientists and engineers contributing to better and faster design, and military technologists had the opportunity to express their views and needs.

Thème

Les aéronefs militaires doivent satisfaire à des spécifications multiples et en accroissement permanent. La réduction des délais de conception grâce aux techniques de conception simultanée et la diminution des risques par l'amélioration des interactions pluridisciplinaires lors des phases préliminaires de conception des véhicules aériens représentent les objectifs prioritaires de l'industrie aéronautique militaire.

Le symposium a contribué à définir l'état actuel des connaissances dans le domaine de la conception et de l'optimisation aérodynamiques, et les développements prévisibles dans le domaine de l'aérodynamique, des technologies de l'information, et de la théorie de l'optimisation. La réunion avait pour objectif de faire le point de la situation actuelle dans ce domaine et de prévoir les développements futurs, en tenant compte de la tendance générale vers une approche simultanée et pluridisciplinaire de l'ingénierie aérospatiale.

L'un des thèmes spécifiques du symposium était l'étude dès l'origine, de la conception des véhicules aériens dans un contexte pluridisciplinaire et avec des objectifs multiples. Les spécifications et les possibilités des méthodes de conception et d'optimisation aérodynamiques actuelles et futures furent identifiées et discutées.

La conférence débuta par une séance plénière au cours de laquelle les conférenciers, dont la plupart travaillent dans l'industrie, introduisirent le symposium en discutant des besoins, des enseignements à tirer du passé et des possibilités actuelles et futures de l'aérodynamique. Cette séance préliminaire fut suivie de contributions de scientifiques et d'ingénieurs visant à accélérer et à améliorer le processus de conception. Les technologues militaires eurent l'occasion d'exprimer leurs points de vue et leurs besoins.

Publications of the RTO
Applied Vehicle Technology Panel

MEETING PROCEEDINGS (MP)

Aerodynamic Design and Optimization of Flight Vehicles in a Concurrent Multi-Disciplinary Environment
MP-35, June 2000

Structural Aspects of Flexible Aircraft Control
MP-36, May 2000

Design for Low Cost Operation and Support
MP-37, Spring 2000

Gas Turbine Operation and Technology for Land, Sea and Air Propulsion and Power Systems (Unclassified)
MP-34, Spring 2000

New Metallic Materials for the Structure of Aging Aircraft
MP-25, April 2000

Small Rocket Motors and Gas Generators for Land, Sea and Air Launched Weapons Systems
MP-23, April 2000

Application of Damage Tolerance Principles for Improved Airworthiness of Rotorcraft
MP-24, January 2000

Gas Turbine Engine Combustion, Emissions and Alternative Fuels
MP-14, June 1999

Fatigue in the Presence of Corrosion
MP-18, March 1999

Qualification of Life Extension Schemes for Engine Components
MP-17, March 1999

Fluid Dynamics Problems of Vehicles Operation Near or in the Air-Sea Interface
MP-15, February 1999

Design Principles and Methods for Aircraft Gas Turbine Engines
MP-8, February 1999

Airframe Inspection Reliability under Field/Depot Conditions
MP-10, November 1998

Intelligent Processing of High Performance Materials
MP-9, November 1998

Exploitation of Structural Loads/Health Data for Reduced Cycle Costs
MP-7, November 1998

Missile Aerodynamics
MP-5, November 1998

EDUCATIONAL NOTES

Measurement Techniques for High Enthalpy and Plasma Flows
EN-8, April 2000

Development and Operation of UAVs for Military and Civil Applications
EN-9, April 2000

Planar Optical Measurements Methods for Gas Turbine Engine Life
EN-6, September 1999

High Order Methods for Computational Physics (published jointly with Springer-Verlag, Germany)
EN-5, March 1999

Fluid Dynamics Research on Supersonic Aircraft
EN-4, November 1998

Integrated Multidisciplinary Design of High Pressure Multistage Compressor Systems
EN-1, September 1998

TECHNICAL REPORTS

Recommended Practices for Monitoring Gas Turbine Engine Life Consumption
TR-28, April 2000

Verification and Validation Data for Computational Unsteady Aerodynamics
TR-26, Spring 2000

A Feasibility Study of Collaborative Multi-facility Windtunnel Testing for CFD Validation
TR-27, December 1999

Symposium Programme Committee

Programme Committee Chairman
Mr. C.D.S. Clarkson
Head of Aerodynamic Technology-MA&A
British Aerospace Defence Limited
Military Aircraft Division, Bldg W427D
Warton, Nr. Preston, Lancashire PR4 1AX

BELGIUM
Mr. J. Muylaert
ESTEC, Aerothermodynamic section
Postbus 299
2200 AG NOORDWIJK
The Netherlands

CANADA
Dr. L. Chan
High Speed Aerodynamic Lab.-U66
Institute for Aerospace Research
National Research Council Canada
Montreal Road
Ottawa, Ontario K1A 0R6

Mr. Joe. Templin
National Research Council
Montreal Road, Bldg. M-2
Ottawa, Ontario K1A 0R6

FRANCE
Mr. R. Lacau
Aerospatiale Missiles (E.SCG/N)
2-18, rue Béranger B.P. 84
92323 Chatillon

GERMANY
Dipl.Ing. P.W. Sacher
Daimler Benz Aerospace LMLE 3
Postfact 801160
D-81663 Munchen

ITALY
Mr. A. Galasso
CIRA SPCA
Via Maiorise
81043 CAPUA (CE)

NETHERLANDS
Dr. B. Oskam
National Aerospace Laboratory (NLR)
Anthony Fokkerweg, 2
1059 CM Amsterdam

Prof. Ir. J. Slooff
National Aerospace Laboratory (NLR)
Anthony Fokkerweg, 2
1059 CM Amsterdam

SPAIN
Mr. F. Monge
INTA – DeptoDinamica de Fluidos
Div. de Aerodinamica y Vuelo
Carretera Torrejon Ajalvir, km. 4.5
28850 Torrejon de Ardoz, Madrid

UNITED STATES
Mr. D. Selegan
AFRL/XPA
1864, 4th Street, Suite 1
Wright-Patterson AFB OH 54533-7131

Dr. N. Malmuth
Rockwell International Science Center
P.O. Box 1085, 1049 Camino Dos Rios
Thousand Oaks, CA 91358

TECHNICAL EVALUATION REPORT

Applied Vehicle Technology Panel Symposium on

AERODYNAMIC DESIGN AND OPTIMIZATION OF FLIGHT VEHICLES IN A CONCURRENT MULTI-DISCIPLINARY ENVIRONMENT

P.W. LIDDELL
BRITISH AEROSPACE
MILITARY AIRCRAFT AND AEROSTRUCTURES
FORT WORTH, TX

Introduction

The Fall 1999 Meeting of the Applied Vehicle Technology Panel comprised several discrete events. Following the opening session on the morning of October 18th, three separate Symposia were held. This report addresses one of these, the Symposium on Aerodynamic Design and Optimization of Flight Vehicles in a Concurrent Multi-Disciplinary Environment.

The following notes review this Symposium, assessing the degree to which the objectives apparent in its title and declared theme were actually met.

The Symposium

The published program for this Symposium comprised 35 papers, however, in the event, three of these were withdrawn.

The following was the declared "theme" for the Symposium;

> "Military airplanes must fulfil a plethora of requirements which is continually growing. The impact of design objectives, compatibility and total life cycle cost requirements on design complexity is high. Reduction of design cycle time through concurrent engineering and reduction of risk through better multi-disciplinary interactions in the early stages of flight vehicle design are primary objectives of the military aerospace industry. Rapid turnaround aerodynamic, propulsion integration, structural and electromagnetic procedures are required for this purpose.

> "The symposium will contribute to the understanding of the state of the art in the aerodynamic design and optimisation field, and that which can be expected from new developments in aerodynamics, information technologies, and optimisation theory. The objective is to survey the current and future scene given the trends towards a more concurrent and multi-disciplinary approach to aerospace vehicle engineering.

> "A particular theme of the symposium will be the multi-objective, conceptual and preliminary design of flight vehicles in a concurrent, multi-disciplinary environment. Requirements for and capabilities of existing and new aerodynamic design and optimisation methods will be identified and discussed.

> "The format of the conference will include an initial Plenary Session where invited speakers primarily from industry, will set the scene by discussing: Requirements, lessons learned from the past, current, and future capabilities with regard to the role of aerodynamics in the future. This will be followed by scientists and engineers contributing to better and faster design, and military technologists will have the opportunity to express their views and needs."

The Need for Concurrency and Multi-Disciplinary Operation

The keynote papers did make the case for developments in the areas of Concurrency and Multi-Disciplinary operation, highlighting the implications/consequences of real progress, including, for example, identifying the possible need for a different kind of aerodynamicist to ensure successful operation in the environments likely to emerge.

These and other references repeatedly make the compelling case for a fundamental rethink of the overall design process, within which specific aerodynamic problems are identified and addressed. These arguments typically cite the importance of rigorous work in the early phases of the process, often by identifying the particular importance of early decisions (the "cost committed versus cost incurred" argument which appeared, for example, in papers 2 and 3 in this Symposium). Of course, a key concern has to be the ability, or lack of it, to achieve significant improvements in "quality" in early program stages as, typically, tool and data/knowledge base development has been keyed to established, rather than novel,

processes. Given the role of this Symposium as a potential focus for future research efforts, it is disappointing that more emphasis was not given to the issues involved in achieving real improvement in this important (or even crucial?) domain.

Further, it seems ironic that following an opening plenary session, the screens were then drawn isolating the structures, aerodynamics and propulsion communities from each other, particularly as in at least two of the resulting enclaves the implications and the importance of multidisciplinary operation were then discussed in splendid isolation!!

This reviewer firmly believes that there is significant advantage to be captured if the issues surrounding the achievement of improved quality and depth of product understanding very early in the product realization process can be resolved. However, these are very real, even perhaps intractable, issues that warrant significant review and which will require much effort, even fundamental research, to resolve.

In my verbal report delivered at the end of the Symposium, I raised a series of deliberately provocative thoughts and questions. To prompt some contextual view of these, I showed the following diagram, taken from Norman Augustine's book "Augustine's Laws", essentially to focus thinking on just how improved "up-front quality" should impact beneficially on the overall process.
This particular chart shows the (predictable?) mismatch between "expectation" and "realization".
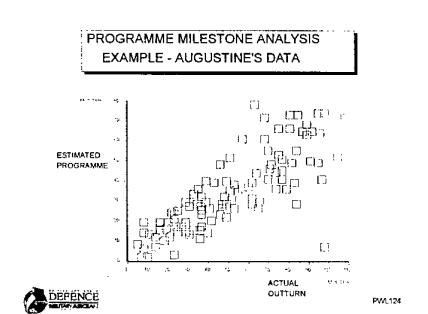
I suggested that this is probably a characteristic with which we are all too familiar. We all know that this happens. I surmised that we probably each have a good idea as to why this happens. I further suggested that we probably all would rather that this did not happen.

This trend is apparently endemic to many spheres of activity, not just aerospace. This mismatch between projection and outturn seems almost inevitable in any complex undertaking. Generally, organizations faced with the manifestation of such problems, i.e. the awareness that this relationship is actually developing, see the issue as one of "management", or perhaps the lack of it, and typically react by investing in "improvements" in their management processes. There can be little doubt that the "science" of program management has developed over the years and that organizations undertaking complex activities have introduced progressively more sophisticated management processes. What does seem remarkable, however, is that all these developments have had hardly any impact on the trend shown above. Indeed, where impact is discernible, often it is adverse!

This does rather suggest that all this investment of time and effort in fact is addressing the wrong problem. If overall performance is not sensitive to the quality of management against a prescribed plan, then the only conclusion possible is that the fault lies in the quality of the initial plan itself. If the plan is bad, no amount of management quality can change that.

This statement very closely paraphrases an observation that anyone working in the conceptual design domain will immediately recognize, that is that choice of the incorrect concept at the outset of the process can never be rectified, no matter how good the quality of the subsequent detailed design. Of course this similarity is hardly surprising as the proposed realization plan for a new product is an essential part of its conceptual description, i.e. the plan is part of the design.

It seems clear that success in complex product realization programs is critically dependent on conceptual "quality". Put another way, it seems obvious that we should (ideally) fully understand the problems inherent in any proposed endeavor before establishing plans and committing businesses to such programs, rather than discovering inherent problems after we have established the plans, resources, schedules, etc.

As I have already noted, several of the papers presented at the Symposium argued the importance of early decision making to ensuring overall success, generally by using the "cost committed v cost incurred" argument. A number of the papers presented built their theme on the need to complete the design process more quickly. However, the preceding paragraphs suggest that, however fast the initial parts of the design process might be completed, by far the overriding pressure must be to ensure that the design is "correct". This observation prompted the following question posed in my verbal report:

What is more important - to deliver our products quickly, or to deliver them when we say we are going to deliver them?

To determine the proper balance between haste and correctness is itself a subtle multi-disciplinary optimisation problem. This reviewer doubts that the tools exist properly to study such a trade-off. However, regardless of the precise balance that might ultimately be identified as "ideal", we cannot shift from today's position without the tools and capabilities necessary properly to improve quality in the early, conceptual, stages of the design process.

The Multi-Disciplinary Environment

I questioned whether "multi-disciplinary" was a unique descriptor. This was based on a belief that multi-disciplinary operation demands differ at different stages in the design

process. This was demonstrated by showing how the design process shifted from periods of "analysis" to "synthesis" in a cyclic manner. Conceptual design is dominated by the need for good "synthesis", but much of the tool development we have seen over the years has focused primarily on improved analysis.

This prompted me to ask a two-part question: 1) is there more than one distinct multi-disciplinary environment set?; 2) if so, do different conditions appropriate to such sets postulate distinctly different multi-disciplinary problems and issues? I was attempting to generate some thought as to whether multi-disciplinary synthesis might depend on different tool and competency sets than would be required for multi-disciplinary analysis.

I noted an observation by Douglas Adams, author of A Hitchhiker's Guide to the Galaxy, on an UK radio program some years ago. In answer to a particular question, he said:

"The real power of the computer is that it enables synthesis where previously we have been capable only of analysis"

This observation when coupled with an understanding of the overall process leads to the following line of reasoning:

1) Conceptual design is a process with heavy demands on "synthesis".
2) The product development processes we currently operate were established before the emergence of the computer and therefore primarily reflect "human" abilities, i.e. they are likely to be weak on "synthesis" and strong on "analysis".
3) Processes have evolved largely through development of analytical tools (log tables to slide rules to mechanical calculators, and so on). This begs questions regarding the extent to which computers are now used simply in lieu of these earlier analytical tools. How much of the IT in use now is simply dedicated to better analysis, i.e. failing to capture its "real power"?
4) What processes emerge if the real power of the computer were to be captured, i.e. if we really thought through the benefits to be derived from enhanced synthesis? If it is true that much of today's investment is aimed at solving problems caused by the lack of adequate early synthesis, rectifying that problem could render much of this development nugatory in future processes.
5) However finally, to what extent can the "real power" of the computer practically be captured?

This latter point expresses [my] concern over simulation based processes applied to the development new products, often entirely new concepts, when issues such as design validation have to be addressed.

This reasoning leads to a specific set of questions for a group such as the AVT Panel:

1) Does history actually support the contention that hitherto decision making within the preliminary design process has been inherently poor?
2) If so, do we understand why this has been the case?
3) What needs to be done to improve the quality of initial decision making?

This latter question is particularly germane if the group is to sponsor activities/research that are designed to "help".

The Conceptual Design Problem

Flight vehicles are complex.

Traditionally, complex problems have been addressed by subdividing them into sets of smaller, more manageable problems. Why has this been necessary? What are the limitations that cause this to be so?

The air vehicle design problem is highly multi-dimensional. At least one paper presented in the symposium attempted to quantify the levels of dimensionality (degrees of freedom) involved in air vehicle design. However the human has very limited ability to think in many dimensions. Thus, rather than "more manageable" problems, are we really simply reflecting our own limitations and generating "more understandable" problems?

If human capacity is indeed a limiting factor, how are we ever to achieve the ideal conceptual objective, assuming we support the view that the decision process should not be automated, i.e. we still wish the human to be fully involved and "in control" of the design process?

Many papers presented in this symposium confirmed not only that problems are still having to be subdivided, but even then are having to be further "simplified" to render them "manageable".

Subdividing a problem before it is addressed to some extent must predetermine the outcome of subsequent study. Further, the risks inherent in "sub-optimization", i.e. addressing only a small of part of the problem domain and seeking an "optimum" locally in that domain, should be clear. One wonders to what extent our development of truly integrated systems is being compromised by our need to subdivide these systems simply to allow them to be studied, particularly when this subdivision is almost always based on "traditional" architectures.

At least one paper noted that it is actually potentially dangerous to think in terms of "optimization", where design is complex and is inevitably about "compromise". A so called "optimum" solution in a highly multi-variate domain can easily be quite "unstable", i.e. very specifically dependent on the particular values of the many variables. This might be visualized as a solution "balanced" on a sharp peak in the design space. Alternative strategies involving the identification of solutions that are more highly robust, i.e. less sensitive, in the face of parameter variations might be more preferable and have been the subject of various research

programs to date. In other words, rather than seeking the ultimate "peak" in the multi-dimensional domain, a better solution may be in the middle of a "plateau", even if the "altitude" of this plateau is somewhat below the ultimate summit.

However, any "optimisation", or choice of alternative parameter sets, depends on assigning "value" to the alternatives. Do we properly understand value criteria that should be used to determine "best" compromise? Aircraft designers tend to think quantitatively (speed, range, technology level, etc.) but customers buy "capability" (effectiveness, reliability, availability, etc.). "Value" should only really be assessed in terms that matter to the customer, and selected value criteria need to reflect this.

The customer's preference, or otherwise, for any particular product is determined by his perception of that product's "benefit ratio", i.e. the ratio between what the product will do for him and what it will cost him. A product's benefit ratio is largely determined by its initial design. Remember the papers that presented the "cost committed" v "cost incurred" argument. As well as largely committing overall program costs, initial decisions have the tendency largely to determine the product's overall effectiveness as well. Thus the product's "benefit ratio", and hence customer acceptance, can be largely determined by decisions taken very early in the design process. Are we properly able even to consider, never mind to model robustly, all facets of this critical parameter in initial design?

The Presented Papers

This part of the report will review the extent to which the aims, both declared and implied, were actually met through the papers presented.

Each paper has been reviewed in the context of the Symposium's aims as expressed in the Symposium Title.

SYMPOSIUM ON *AERODYNAMIC DESIGN* AND *[AERODYNAMIC] OPTIMIZATION* OF FLIGHT VEHICLES IN A *CONCURRENT MULTI-DISCIPLINARY ENVIRONMENT*

Attachment 1 comprises a table that summarizes the extent to which, in the opinion of this reviewer at least, each paper actually addressed the four distinct elements captured in this title.

This table suggests that proportionately more attention was paid to "aerodynamic design and optimization" than to the "multi-disciplinary concurrent environment".

Many of the papers did allude to, make specific reference to, or claimed actually to address, "multi-disciplinary" optimisation, but more often than not this simply represented the addition of non-aerodynamic objective functions into the optimisation process. In other words, the papers had more to

do with "multiple-criteria" optimisation than with design in a true multi-disciplinary environment.

Those papers that did address the concurrency and multidisciplinary aspects of the problem admirably identified some of the key issues that need to be addressed. For example, development of required personal skills to work in a truly concurrent environment, development of tools appropriate to the fundamental objectives of improved concurrency in conceptual design, and so on.

Looking more specifically at the second and third paragraphs of the Symposium "aims" statement, i.e.;

> "The symposium will contribute to the understanding of the state of the art in the aerodynamic design and optimisation field, and that which can be expected from new developments in aerodynamics, information technologies, and optimisation theory. The objective is to survey the current and future scene given the trends towards a more concurrent and multi-disciplinary approach to aerospace vehicle engineering.

> "A particular theme of the symposium will be the multi-objective, conceptual and preliminary design of flight vehicles in a concurrent, multi-disciplinary environment. Requirements for and capabilities of existing and new aerodynamic design and optimisation methods will be identified and discussed."

it will be seen that generally the objective of the first of these paragraphs was met. However, the Symposium did not fully succeed in addressing the second of these paragraphs, specifically the final sentence.

Recommendations

Given the importance of these issues, and given that they were only partly addressed in this symposium, it is recommended that the Panel gives serious consideration to arranging a more complete session at some future date. At that time it would perhaps be better not to close the partitions between individual subsidiary seminars, but rather to address true concurrency in a necessarily more open forum.

This reviewer believes that there are numerous issues that will need to be addressed if real progress towards true concurrency is to be achieved. Some of these developments will necessarily require fundamental research, into, for example, process development, tool development, competency identification, and so on. A major objective must be to improve the level of human interaction with complex problem solution other than by merely simplifying the problem. It is highly desirable that such research, which probably will be happening anyway, be "channeled" to support a consistent objective vision.
It is Panels such as these that are in a position to establish such "vision".

Attachment 1 to the Technical Evaluator's Report for the Symposium on Aerodynamic Design and Optimization of Flight Vehicles in a Concurrent Multi-Disciplinary Environment.

Paper #	Aerodynamic Design?	Optimization?	Multi-Disciplinary?	Concurrency?
1	✓	✓	✓	
2			✓✓	✓✓
3			✓✓	✓✓
4	✓	✓	✓✓	✓✓
5	✓		✓✓	
6		✓✓		
7	✓✓	✓		
8	✓	✓	✓	
10		✓	✓✓	
11	✓✓	✓		
12		✓	✓✓	
13	✓	✓	✓	
14	✓	✓	✓	
16	✓✓			
17			✓✓	
18	✓	✓✓		
19	✓	✓✓		
20	✓	✓✓		
21	✓	✓✓		
23	✓	✓✓		
24	✓	✓✓		
25		✓	✓	✓
22	✓	✓✓		
27	✓			
28	✓	✓		
29	✓			
30	✓	✓✓		
31	✓	✓✓		
32	✓			
33	✓			
34	✓			
35	✓			

✓✓ = strong contribution
✓ = some contribution.

MULTI-DISCIPLINARY DESIGN
OF
COMBAT FLIGHT VEHICLES

G. A. HASEN
DIVISION CHIEF, AERONAUTICAL SYSTEMS SECTOR
AIR FORCE RESEARCH LABORATORY
1864 4TH STREET, SUITE 1
WPAFB OH 45433-7131, USA

INTRODUCTION

This paper discusses some of the multi-disciplinary technology development we are pursuing at the Air Force Research Laboratory. Although multi-disciplinary design is pervasive throughout the Laboratory, I will concentrate on the area of technology development for combat flight vehicles.

Our mission at the Laboratory in support of the United States Air Force is to "lead in the discovery, development, and integration of affordable warfighting technologies." A large portion of these development and integration activities, by their very nature, involve multi-disciplinary design. I might also add that the majority of this work is actually performed by the aerospace industry under research and development contracts; we in the Laboratory lead and coordinate these efforts, but they are executed by our industry partners.

INVESTMENT STRATEGY

Just over two years ago, the Air Force consolidated its seven science and technology organizations into one single Air Force Laboratory (Fig. 1). This consolidation has greatly aided in the integration of technologies across the broad spectrum shown in this chart. Today, it is much easier to tie these individual technology disciplines together as multi-disciplinary technology applications become ever more important. In our Air Vehicles Directorate, we have established a center of excellence for multi-disciplinary design in order to provide a focus for these high payoff efforts.

At AFRL, our investment strategy is to pursue a balance of technologies with high pay-off, some in the near-term, but many not until the long term of 20 years or more. In the present fiscally-constrained environment, we are pursuing technologies which give significant improvements in not just performance, but also in affordability and sustainment. In particular, we are highly interested in technologies which have the potential to reduce the cost of ownership for our systems by at least 50%.

In the aircraft arena, we have historically seen that as the capability of our weapons systems have increased dramatically, so has the cost (Fig. 2). Our current goal in the Laboratory is to break this trend, giving our warfighters high performance, yet affordable aircraft. One key to achieving this goal is through the application of multi-disciplinary design and technology integration

MULTI-DISCIPLINARY TECHNOLOGY EXAMPLES

Modern combat aircraft rely on a broad range of highly-integrated technology sets. Multi-disciplinary design is a key area required to bring these technology disciplines together in an integrated fashion. In this paper, I'll quickly cover five AFRL technology areas heavily dependent on multi-disciplinary design, followed by a quick look at an advanced combat flight vehicle demonstrator heavily dependent on multi-functional designs.

The five multi-disciplinary technology areas I'll cover are: Active Aero-elastic Wing; Advanced Inlet Integration; Advanced Fluidic Nozzles; Multifunctional Airframes; Turbine Engine High Cycle Fatigue. I selected these particular efforts to span the broad areas of aeromechanics, structures, avionics, and propulsion.

The first area, called the active aero-elastic wing, involves the integration of the areas of aerodynamics and structures known as aero-elasticity (Fig. 3). When coupled with the science of flight mechanics in a multi-disciplinary design approach, we can achieve great benefit in both aircraft performance and air vehicle weight. In this example, the wing design is no longer driven by static stiffness requirements, but uses multiple control surfaces to drive the wing shape at flight speeds. This approach can reduce the aircraft gross weight in the range of 5 to 20 percent. This approach is currently being demonstrated by the Laboratory in a cooperative program with NASA on one of their F-18 test aircraft with redesigned control surfaces and a much "floppier" wing.

This multi-disciplinary design approach will have a high potential payoff to a broad range of flight vehicles (Fig 4)In addition to potentially reducing the required structural weight and maneuver performance relative to traditional wing designs, this technology can also result in significantly reduced levels of drag, and thus greatly increased flight vehicle range.

Our second example is in the area of advanced inlet integration (Fig 5). In this case, to achieve our weight goals for the inlet system, we need a multi-disciplinary design approach in the areas of fluid dynamics and structures to overcome the limits imposed by traditional design approaches. Here, we want to exploit the advantages of advanced composite structures, while accurately predicting the maximum level of structural loading induced by flow distortion and phenomena known as hammershocks.

Specifically, we currently are pursuing this multi-disciplinary approach to develop and demonstrate an inlet system for an unmanned flight vehicle, which is 50 percent lighter than one that would be achieved using the present-day conservative approach (Fig 6).

Our third example deals with the area of advanced integrated nozzles (Fig 7). If you follow the arrow, you can see that historically, nozzle cost and weight have risen with increased nozzle performance. We are trying to achieve a major shift as shown by the down arrow that would reduce the weight and cost of the nozzle system simultaneously. In order to make such a revolutionary change, we need an innovative set of enabling technologies. We are currently investigating the technology of fluidics (Fig 8), using a secondary injection of compressed air from the engine, to allow these advances to be achieved. The promise of an advanced, thrust-vectorable nozzle with no moving parts may well be achieved if we are able to integrate fluidics with the traditional aspects of nozzle design in a multi-disciplinary manner.

The integration of these technologies will enable thrust vectored nozzles without all of the mechanical complexity present in the current generation of nozzles such as those on the F-22 fighter aircraft.

Our fourth example involves the integration of advanced structures technology with the area of avionics to achieve affordable, lightweight, multi-function structural components in future airframes (Fig 9).

A key enabling technology in this area is that of affordable composite structures. Under current aircraft structures methodology, assembly is the major cost driver, as shown by the huge number of components and fasteners used (Fig 10). Affordable composite technology promises to make a huge leap in the cost factor.

By applying multi-disciplinary design to the area of structurally integrated avionics, we can eliminate many of the compromises in both structural and avionics performance that currently result from traditional design methodology (Fig 11). Currently, the myriad of required apertures and antennas can degrade aircraft aerodynamics and LO performance, and compromise the structural integrity of an aircraft. The solution is to design and build high-performance, multifunction antennas and apertures that are integrally part of the load-bearing aircraft structure.

Our last example is in the area of turbine engine development. As we have developed increasing air breathing propulsion capability (Fig 12), we have frequently encountered multi-disciplinary phenomena that can drastically affect the durability of turbine engines in our combat aircraft systems. This is particularly critical for single engine fighters such as the F-16 and the future Joint Strike Fighter.

After solving numerous low cycle fatigue problems that emerged during the 1970's, high cycle fatigue has now become the principal area of concern regarding turbine engine durability. Although other problem areas such as acoustically coupled fatigue and thermo-mechanical fatigue are emerging, high cycle fatigue has the highest adverse impact to the combat aircraft fleet.

High cycle fatigue in turbine engines has serious implications in terms of both safety and maintenance cost.

By aggressively developing multi-disciplinary technology in this area, we hope to save both lives and Air Force resources for not only the present fleet, but also in future combat aircraft.

Current technology development efforts in our High Cycle Fatigue program are focused in the 7 areas shown in Figure 13. Many of these areas involve the application of multidisciplinary design in the areas of structural dynamics, fluid dynamics, and thermodynamics, and material properties.

This concludes our quick survey of some technology areas where multi-disciplinary design is of critical importance. To conclude my talk, I would like to give you a short overview of an exciting, near term technology demonstration program where the use of multi-disciplinary design is crucial. This program is our Unmanned Combat Air Vehicle advanced technology demonstrator program, which we are jointly developing with the Defense Advanced Research Projects Agency.

UNINHABITED AIR COMBAT VEHICLE

Shown in Figures 14 and 15 are six current Department of Defense Unmanned Air Vehicles, grouped by their primary mission areas for tactical support and for high altitude, endurance-type operations. All of these air platforms are used primarily in the roles of intelligence, surveillance, and reconnaissance.

The Unmanned Combat Air Vehicle, or UCAV, takes the concept of unmanned aircraft from the unarmed ISR role to a fully combat-capable role that involves carrying a lethal weapons load. Specifically, UCAVs are being examined for the roles of Suppression of Enemy Air Defenses, or SEAD, and Precision Strike against mobile targets (Fig 16). These missions have traditionally been very costly in terms of manned aircraft. These unmanned vehicles are meant to augment the future manned combat force structure, not replace it altogether. In addition to being an extremely lethal combat system, UCAV must also be significantly more affordable than the manned alternatives in order to be seriously considered. As this chart shows, we will be trying to achieve a 65 to 75 percent reduction in both acquisition and operating costs

The UCAV demonstrator is much more than just a flight vehicle demonstrator. The UCAV system consists of three tightly integrated segments: the air vehicle, a mission control station, and the external interfaces used for information transmission to and from the other two segments.

In the UCAV program, we are able to optimize the aircraft for the mission, not to accommodate the human pilot (Fig 17). This greatly expands our design trade space, and allows us to move away from traditional air platform configurations. Many of the advanced multidisciplinary technologies we just covered are naturals for UCAV applications. If we are able to aggressively apply new technologies in an integrated manner, our studies have shown that we can reduce air vehicle size by over 40 percent for the same mission performance.

Figure 18 shows the preliminary air vehicle design by Boeing, which will be building our UCAV Demonstrator system consisting of two flight vehicles, a mission control station, and associated support equipment for long term storage and world-wide transport. As you can

see, the UCAV is much smaller than either the F-16 or the F-117 aircraft. If this program proceeds as planned, we will have two of these flight test vehicles in the air within three years.

Just as we plan to optimize the air vehicle for the mission, we can do the same for the human interface. We are not envisioning taking the man out of the loop, just out of the cockpit. There is still a huge amount of work to be done to determine functional allocations between team members and the degree of autonomy of an unmanned flight vehicle carrying lethal weapons. A major goal in this area is to reduce the number of controllers handling UCAV missions in order to greatly impact operational costs.

Figure 19 lists the critical technologies and shows that UCAV is not just an air vehicle development program. Some of the most challenging aspects of this concept lie in

the areas of information links, command and control, and sensor integration. This is definitely an area where multi-disciplinary design can greatly help us in achieving both our cost and performance goals.

As we look beyond the near term for unmanned flight vehicles (Fig 20), we can see that in terms of system attributes and mission relevance, the level of technology challenges will continue to increase significantly. In my view, the requirement for multi-disciplinary design and technology integration will continue to grow at a quick pace

SUMMARY

We can see that over the span of 55 years, things haven't changed much. Research including multi-disciplinary design, will remain an essential for pre-eminent air power in the future.

Figure 1

GOAL FOR FUTURE AIRCRAFT
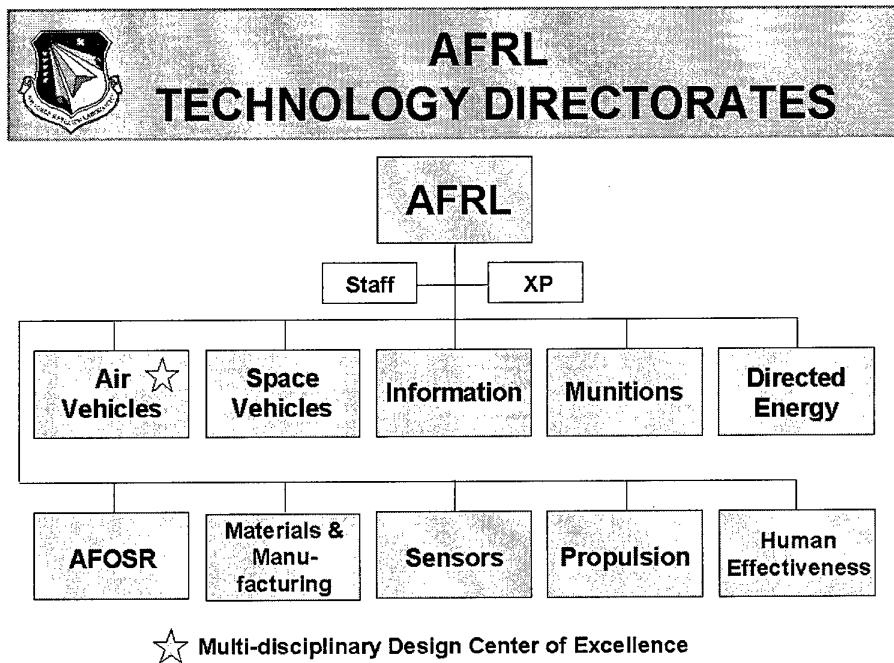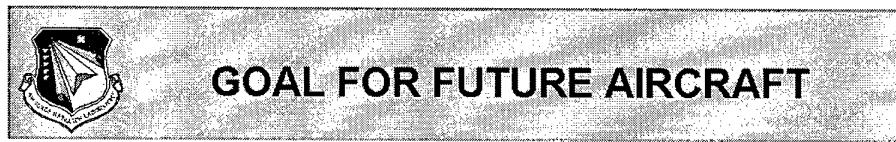
BREAK THE PARADIGM THAT HIGH PERFORMANCE
CAN ONLY BE ACHIEVED AT HIGH COST
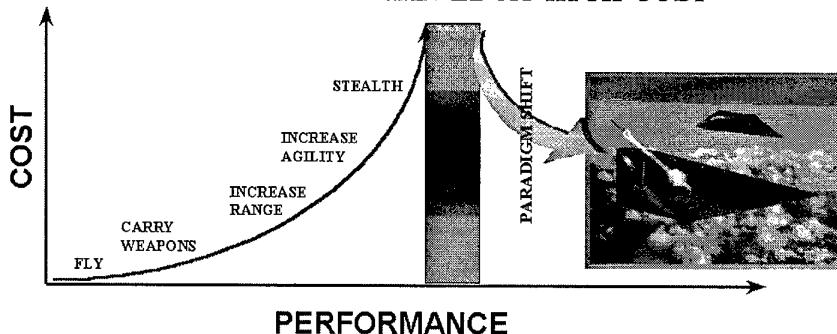
ENABLE DRAMATIC COST REDUCTIONS & PERFORMANCE GAINS
THROUGH THE DEVELOPMENT & INTEGRATION OF
MULTIDISCIPLINARY TECHNOLOGIES

Figure 2

ACTIVE AERO-ELASTIC WING (AAW) TECHNOLOGY

- **A Design Approach that Integrates Structures, Controls and Aerodynamics**

- **Uses Aero-elasticity For a Net Benefit**

  - **Multiple Control Surfaces Used as "Tabs" to Drive Wing Shape at High Dynamic Pressures**

  - **Wing Design no Longer Driven by Static Aero-elastic Stiffness Requirements**

GOAL:
Reduce Take-off
Gross Weight by
5-20%

Figure 3

AIRCRAFT TECHNOLOGY DEVELOPMENT

New Technologies In

HUMAN EFFECTIVENESS

AEROMECHANICS

STRUCTURES

FLIGHT CONTROL

SUBSYSTEMS

PROPULSION

WEAPONS

Integrate With Technologies In

SENSORS

DIRECTED ENERGY

INFORMATION

MATERIALS & MANUFACTURING

Yielding

Evolutionary / Revolutionary Technology Sets & Design Methods

To Enable New & Improved Aerospace Vehicles

Figure 4

ADVANCED INLET INTEGRATION

CHALLENGE: Minimize duct structural weight with acceptable level of damage probability and no catastrophic failure

- Overcome traditional, over-conservative design approach
  Validated probabilistic design criteria

- Reduce inlet hammershock prediction uncertainty
  Validated predictions of hammershock propagation

- Exploit damage tolerant composite structures
  Determine and define damage tolerant capabilities of composite structures

Hammershock Loads

Probabilistic

Traditional

Surge Pressure

Failure Criteria

First Crack — New Ultimate — Current Ultimate

Displacement

Figure 5

ADVANCED INLET INTEGRATION
STRUCTURALLY INTEGRATED COMPACT INLET DEMO

OBJECTIVE
- Demonstrate Reduced Weight and Life Cycle Cost for a Highly Survivable and Maintainable Inlet Aerostructure

APPROACH
- Scale component demos of UAV Inlet system
  - All weather capability
  - Inlet/engine compatibility
  - Structural integrity
- UAV Integrated Air Induction System/ Engine Demo
  - Static & Transient Loads
  - Thermal & Acoustic
  - Hammershock/Engine Coupled

PRODUCT
- All weather, damage tolerant, inlet system that weighs 50% less than F-22

Figure 6

ADVANCED NOZZLE APPROACH

Nozzle Weight & Cost

2-D CD Mechanical
- Pitch Vectoring
- Shaping

Axisym Mechanical
- Ejector Option
- Multi-Axis Vectoring

Axisym Mechanical
- Multi-Axis Vectoring

Fixed Aperture
- Mechanical A/B
- Fluidic Vectoring

Advanced Axisym
- Shaping
- Ejector Option

Fully Fixed
- Fluidic A/B
- Fluidic Vectoring

Axisymmetric Conventional Design

Increasing Nozzle Capability

Figure 7

FLUIDIC NOZZLE TECHNOLOGY

GOAL: Move from heavy, fully variable mechanically vectoring nozzles to fully integrated, light weight, fixed fluidic vectoring exhaust systems

F-22   Future UCAV

Figure 8

MULTIFUNCTIONAL AIRFRAMES

STRUCTURAL INTEGRATION IS AN

ENABLING TECHNOLOGY:

APPROACH: DEVELOP & VERIFY MULTIDISCIPLINARY DESIGN AND
STRUCTURAL DEMONSTRATION OF INTEGRATED AIRFRAME

DESIGN CRITERIA & LOADS

INTEGRAL THERMAL MANAGEMENT

FLEXIBLE AIRFRAME STRUCTURES

INTEGRAL SUBSYSTEMS & AVIONICS

INCREASE AIRFRAME UTILITY WITH MINIMAL COST IMPLICATIONS

Figure 9

Figure 10

Figure 11

Figure 12

Figure 13

AIR VEHICLE APPLICATION

Unmanned Combat Air Vehicle (UCAV)

Advanced Technology Demonstration

Figure 14

CURRENT UAV SYSTEMS

Predator   Global Hawk

Endurance   Endurance

Tactical   Tactical

Hunter   Outrider

Pioneer

Figure 15

UCAV VISION

- **Revolutionary New Tactical Airpower**
  - Force Enabler - Preemptive and Reactive SEAD
  - Provide Persistent All Weather Strike Capability
  - Augment Manned Force Structure
  - New CONOPS for High Risk or High Payoff Missions
- **New Paradigm in Aircraft Affordability**
  - Reduced Acquisition Costs (<1/3 JSF)
  - Dramatically Lower O&S Cost (>75% Reduction)
  - Maintain Mixed Force Structure

- Prosecution of Advanced IADS & Time Critical Targets
- High Survivable Design For First Day Penetration

Figure 16

REVOLUTIONARY AIR VEHICLE POTENTIAL

Optimize the aircraft for the mission, not to suit the pilot

Relocate the Pilot

Eliminate cockpit weight and volume

Eliminate cockpit side and frontal area

Remove physiological limitations

Design for minimized Life Cycle Cost
- Mission CONOPS
- Operator proficiency
- Low maintenance
- Extended storage
- Low cost manufacturing

Maintain proficiency via simulation

No Vertical Tail

Aperatures and Sensors

Inlet and Exhaust

Engine Position

Weapons Integration

Composite Processes

Vehicle Shape, Size & Wing Position

With Today's Technology:
- *Dramatically Reduced Acquistion Cost*
- *Reduced Size (-40%) for equal performance*
- *Inherently Reduced Observables*

Figure 17

UCAV AIR VEHICLE ATTRIBUTES

UCAV
F-16
F-117

- ~15,000 / 7,500 lb Gross/Empty Weight
- High subsonic med/high altitude
- 500-1000 nmi mission radius
- 1000-3000 lb weapons payload
- Wide range of current & advanced weapons
- ESM & On-Board SAR Targeting Solution
- All electric
- Affordable Stealth to the Next Level

66 ft.

Figure 18

UCAV KEY TECHNOLOGIES

- Information Superiority
- Agile C2 Architecture
- Minimal On-Board Sensors
- Small Accurate Munitions

- Affordable Vehicle Design
- Low System Maintenance
- Reduced Peacetime Operations

- Exploit Emerging Technologies
  - Miniature Air Launched Decoy
  - ISR Platforms & Architectures
  - Targeting Architectures

Figure 19

MULTIDISCIPLINARY DESIGN CRITICAL TO FUTURE UAVS

Near Term   Mid Term   Far Term

FY07   FY13   FY22

Attributes
- Affordable
- Light weight, compact
- Reliable
- Mixed manned and unmanned operations

Mission Relevance
- SEAD/Strike
- Recce

Attributes
- Affordable sets of vehicles
- Modular structure / subsys
- Enhanced strike
- Coordinated UAV package
- Extended range / endurance

Mission Relevance
- Battlefield Management
- ISR, Bomber, Tanker/Airlift

Attributes
- Affordable performance
- Customized adaptability
- Supersonic capability
- Intelligent swarms
- Seamless Ops

Mission Relevance
- AeroSpace Dominance
- DE UCAV

Figure 20

Eurofighter: Aerodynamics within a Multi-Disciplinary Design Environment

By

Keith McKay

British Aerospace
Military Aircraft & Aerostructures
Building W310C, Warton Aerodrome
Warton, Preston, Lancashire, PR4 1UN
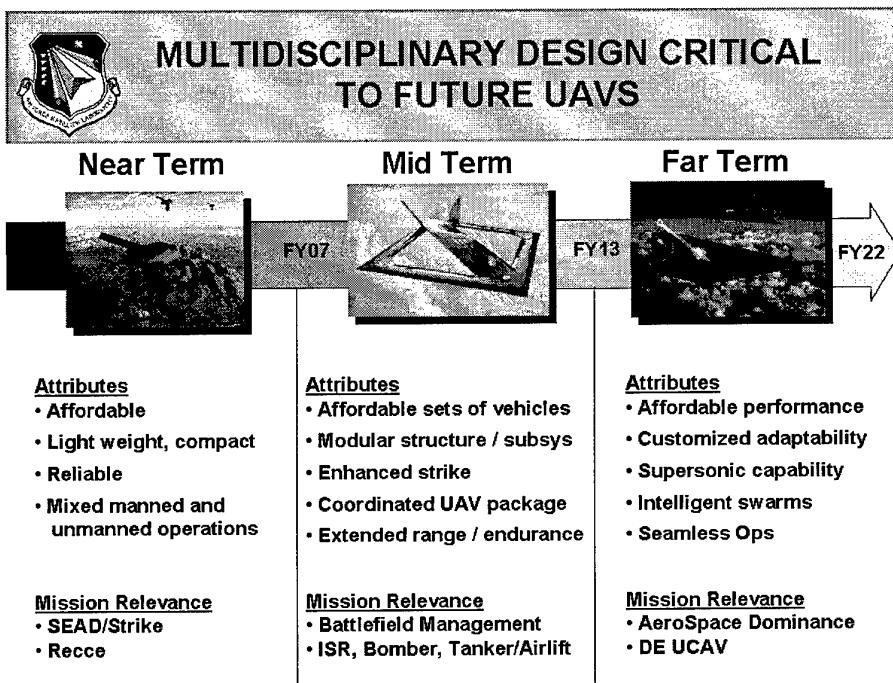United Kingdom

Abstract

The art and science of aerodynamics have been developing continually to meet the changing needs of aircraft of all types. in many cases, combat aircraft design drives this development farther and faster in the search for improved combat effectiveness. One result has been that an ever broadening of the individual but heavily integrated aspects of aerodynamics into a set of interdependent, diverse fields, covering fluid dynamics, structural dynamics, solid body mechanics, ballistics, acoustics and more recently electro-magnetics. Together, these individual disciplines are combined together into a term sometimes referred to as aerodynamic technology, as described in a recent Royal Aeronautical Society edition [1].

This paper will examine the requirements placed upon these disciplines in the light of the multi-disciplinary design optimisation process that took place on the Eurofighter project, specifically highlighting the roles of the aerodynamic technologies within that process and the lessons learned from their application in this environment. The paper will also provide some recommendations for improvements in the design capabilities based upon the experience gained and lessons learned from the design of the Eurofighter Weapon System.

Introduction - The Need for an Integrated Design Environment

The first air to air conflicts occurred in the Great War. Here, aircraft were, for the most part marginal with regard to performance, stability and controllability. Indeed, many combat losses could be attributed to these shortcomings rather than the action of the enemy. However, some of the aircraft were regarded, and still are, as models of the agile fighter, particularly in the hands of an expert pilot, or "ace". The basic skills required were the ability to remain in control and shoot accurately.

For subsequent conflicts, the same basic skills were required, although airframes were better stabilised and controlled and had increased power available, resulting in higher speeds. With radar and radio, it became possible to receive guidance towards the targets that the ground control perceived as the prime threat. Weapons remained visual range, however, but regardless of this, the increased speeds and the added information changed the difficulty of the pilot's task due to the implications on his situational awareness and choice of tactics. Increasingly, the combat results became more clouded by the interaction of the systems available to the pilot and his ability to assimilate the information provided.
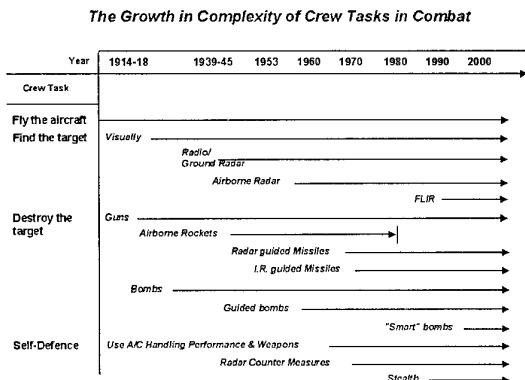
The advent of jets, airborne radar capability, missiles and counter offensive equipment have all tended to complicate the picture whilst attempting to improve the ability to perform the same basic tasks, i.e. finding the opposition and shooting him down. Korea demonstrated the benefits of high performance combined with good handling, to the detriment of the Communist forces. However, some lessons were forgotten, and had to be relearned in later conflicts.

Effectively, the processes described above have resulted in individual areas developing their capabilities for the goal of increased effectiveness, all with the aim of making the task of the pilot or crew easier to perform. However, what resulted was a management problem within the cockpit, i.e. each time a system improved to make it easier to use, another one or two were added.

In the case of Eurofighter, the decision was made to make the management of many of the systems automatic, such that they should look after themselves and allow the crew to concentrate on his tactics and operation, whilst the on-board systems do all the housekeeping. All of this was

required whilst achieving new levels of performance and handling of the aircraft, thereby ensuring that the crew always have the upper edge in any combat or other task.

The environment in which a fighter pilot operates is subject to continual change due to technology advances and the altering world situation. The only prediction that can be made with confidence is that profound change should continue to be expected.

The Growth in Complexity of Crew Tasks in Combat

Year	1914-18	1939-45	1953	1960	1970	1980	1990	2000
Crew Task								
Fly the aircraft								
Find the target	Visually							
		Radio/						
		Ground Radar						
		Airborne Radar						
				FLIR				
Destroy the target	Guns							
	Airborne Rockets							
		Radar guided Missiles						
		I.R. guided Missiles						
	Bombs							
		Guided bombs						
			"Smart" bombs					
Self-Defence	Use A/C Handling Performance & Weapons							
	Radar Counter Measures							
		Stealth						

The Eurofighter, now known as Typhoon for the export market, was designed into an age where this statement was never so true. The aircraft was conceived during the latter stages of the Cold War, where the primary threat was still considered to be the Soviet Bloc. Late in 1989, the Berlin Wall fell and the whole scenario changed politically across Europe. However, the various programme delays allowed for a re-assessment of the aircraft and its requirement, with experience of the Gulf War and early operation in the Balkans feeding into the military awareness. The result was that the need for the design was re-affirmed with relatively minor changes to the requirement being defined and accepted by the contract reorientation.

The primary reason for the success of the aircraft design concept lay in the inherent flexibility that could be achieved from the combination of the technologies employed in the aircraft and the integrated nature of the aircraft-weapon system design. From the outset, the aircraft was designed around air-air and air-ground roles, and this latter role has been strengthened in the recent past without requiring major upgrades to then design.

The whole weapons system design is driven by the need for agility, flexibility and availability, and rather than adopt a traditional approach, the vehicle and the weapon system has been designed to be blended and integrated to make this achievable.

A concise definition of agility is provided by the report from AGARD on agility [2], which states

"Operational Agility is the ability to adapt and respond, rapidly and precisely, with safety and poise, to maximise mission effectiveness."

This addresses the whole weapon system, but Operational Agility can be considered as being made of three essential components, i.e. the Airframe, which we will take to include the Flight Control System, the Mission Systems and the Weapons. Our concern within this review is the Airframe and the place of the Aerodynamic technologies within this design process.

The role of aerodynamics in this design optimisation was one of enabling the levels of performance required with the stability and control characteristics required for the generation of agility combined with carefree handling, which has proved to be a major engineering activity to ensure that this is achieved satisfactorily.

Whilst the work on the control system development is ongoing, the level of manoeuvre capability and airframe agility that has been demonstrated already is breath taking.

The Weapon System Specification

Traditional combat aircraft specifications and requirements were not really appropriate for the complex, integrated vehicles that have to result from attempting to meet the requirements. The more traditional processes often arrived a set of aircraft systems that had to be managed individually, rather than having an integrated management. The very complexity of the vehicles often means that decisions relating to the design options may not take into account all the influences, leading to engineering difficulties and expense later in the processes of development and procurement.

There was a need to change the way in which Weapon Systems were formulated. The concepts involved in total mission system engineering and simulation have assisted in the process of determining what the Weapon System Specification should contain and in the design and subsequent evaluation of the vehicle that results. Eurofighter, as a project, has followed this integrated approach and has been deeply influenced by the transition from a more serial process to one of extensive parallelism.

Process for Determination of the Vehicle Roles and the Integration of the Technologies to be applied.
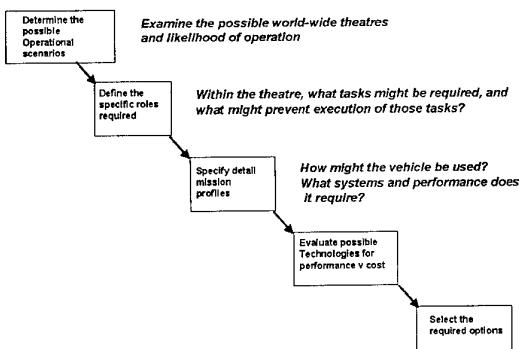
What was required was a method of defining the intended role of the vehicle, then breaking this down into a series of missions, then mission tasks, then mission task elements. From these, it should be possible to establish the interactions of the various technologies that can be applied to the aircraft. One of these technologies relates to the vehicle aerodynamics.

Eurofighter at Paris, 1999

In the case of Eurofighter, this process resulted in a Weapon System Specification being agreed and contracted in 1988. This Specification has been subject to continuous review, particularly during the period of reorientation of the contract, culminating in a re-signature of the contract in 1994 and the subsequent placements of the Production Investment and Production contracts during 1998 and 1999. The result is a total Weapon System, i.e. an aircraft, its sensors, processing and displays and weapons package, that is flexible, highly integrated and supportable, with low life cycle costs and high availability. Indeed, the specification places as much

emphasis on these latter aspects as it does on overall performance.

Aerodynamic Technology in the Initial Design

From the very outset of the project, aerodynamics played a very significant part in determining the nature of the vehicle that would fulfil the requirement to be met. Whilst a considerable data base had been constructed from the previous aircraft projects, such as TKF-90 in Germany, the tri-national ACA study and real projects such as X-31A and EAP (Experimental Aircraft Propgramme), the Eurofighter requirement also added something new. By changing the balance of the design requirements, changes to the configuration were allowed with a different optimum solution resulting.

A number of examples can be shown where this integrated design approach was required and in which the aerodynamics team played a significant role.

Aircraft Configuration and Wing Design

The requirement emphasis on a combination of agility, low and moderate speed manoeuvrability and supersonic sustained performance directly resulted in the choice of the delta-canard configuration. Extensive use was made of wind tunnels and CFD methods, as an integrated design activity, to ensure that the design met its particular requirements in terms of the aerodynamic performance.
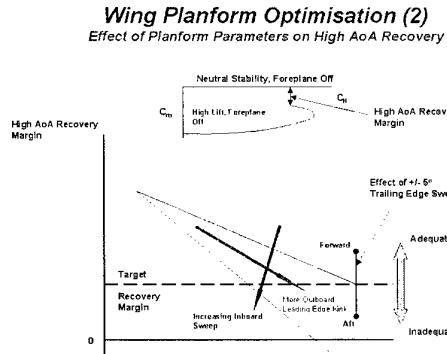
Wing Planform Optimisation (1)
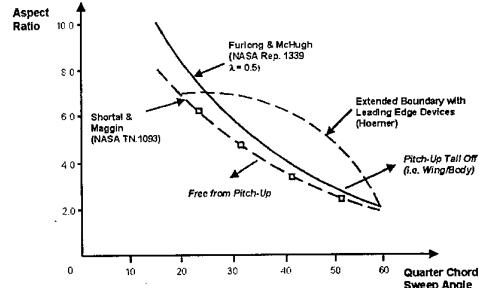
The design process required a closely integrated study with the aircraft structural designers, with information being regularly passed back and forth between the two areas. Key decisions for both disciplines resulted from the need to ensure that the aeroelastic stiffness of the wing was achieved, whilst being able to tailor the stiffness such

that the required aerodynamic shapes were maintained for both cruise and manoeuvre conditions.

relies upon the aircraft being controllable in a carefree manner throughout its envelope of normal operation.

Wing Planform Optimisation (2)
Effect of Planform Parameters on High AoA Recovery

Wing Planform Optimisation (3)
Optimisation of the wing torsion box determined by aeroelastic efficiency - wing bending v torsional stiffness for rolling

Wing trailing edge angle, flap position and sizing, including the size of the powered actuation system all result from the trade studies that were performed. This required the integration of the structural model, available via versions of Nastran, with aerodynamic models that existed in a number of different aerodynamic tools. The Nastran aerodynamic packages were not used as they were not sufficiently advanced to cope with some of the transonic and separated flow conditions that were of prime interest.

Significant effort was placed in correlating the results of the different aerodynamic design methods with experimental data from early wind tunnel tests to ensure that consistent results were being obtained, and that the overall aerodynamics of the wing matched the performance requirements and the needs of the flight control system. This latter demand placed significant burden on the aerodynamic designers to achieve as linear a design, in terms of pitch stability, as possible. Past experience from many previous projects with similar configurations indicated that some level of non-linearity was inevitable, however.

The demand for linear aerodynamics for the flight control system is always present with every aircraft design. However, there is also a view that, because the FCS is clever, it can cope with very non-linear aerodynamics. The phrase often heard was "never mind, the FCS will take care of it!" In the case of Eurofighter, the level of instability that was required for the overall aircraft was such that linear aerodynamics became a much firmer requirement, together with good aerodynamics from the flying controls. The whole success of the aircraft concept
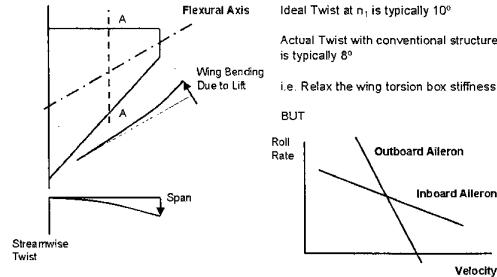
Further, having achieved a satisfactory theoretical design, the final step of the wing design activity is to take account of the wing structure to arrive at the shape that has to be manufactured in jig, in order that the shape in flight is correct. This reveals a "less traditional" interface with the manufacturing engineering organisations. Dialogue here reveals what can be built easily, and allows a further round of optimisation to ensure that the design is not so demanding that it cannot be built.
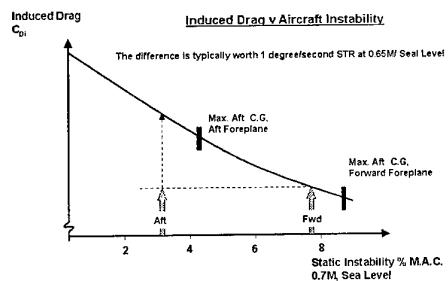
Foreplane
In regard to the foreplane, when factors such as aircraft layout, access, visibility from the cockpit and the aerodynamic interference with the wing are taken into account, then only two positions for the foreplane remain viable for further evaluation. These are forward and low or high and aft, using the wing plane and leading edge apex as a reference.

Extensive investigation over a period of years prior to defining Eurofighter had shown that intermediate positions were disastrous, regarding the aerodynamic interference with the wing, due to inadequate separation of the surfaces.

Consideration of aircraft performance dictates the maximum possible instability to avoid excessive induced drag penalties, which leads to the requirement for foreplane volume. The minimum induced drag occurs with a level of instability equivalent to about 16% of the mean aerodynamic chord, which is approximately twice that that the FCS can cope with. The high AoA recovery, i.e. the ability to pitch the aircraft down from high angle of attack, whilst at low speeds, dictates that the configuration should be neutrally stable with the
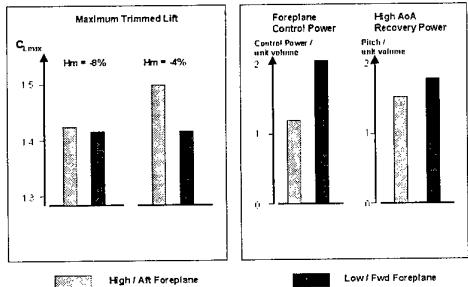
foreplane off, which is equivalent almost to an unloaded foreplane. This dictates that the foreplane volume has to be such as to generate around 8% m.a.c. instability at low speeds. A low forward foreplane position then results in the smallest foreplane area, with a consequent benefit on supersonic drag.

Choice of Foreplane Location (1)

Induced Drag v Aircraft Instability

C_{Di} Induced Drag

The difference is typically worth 1 degree/second STR at 0.65M/ Seal Level

Max. Aft. C.G. Aft Foreplane

Max. Aft. C.G. Forward Foreplane

Aft   Fwd

2   4   6   8

Static Instability % M.A.C. 0.7M, Sea Level

Further, at the level of instability chosen for the aircraft, there was little effect on maximum lift of either position, whilst for a less unstable aircraft, a high aft foreplane does provide some benefit on lift. Further, the low forward foreplane is more effective as a control surface, with consequent benefit for nosewheel lift, trim and manoeuvre capability. This increase in effectiveness is maintained, even at high angle of attack, where the effect is to provide more pitch recovery capability for high angle of attack recovery.

Choice of Foreplane Location (2)

Maximum Trimmed Lift

C_{Lmax} Hm = -8%   Hm = -4%

1.5

1.4

1.3

Foreplane Control Power

Control Power / unit volume

High AoA Recovery Power

Pitch / unit volume

High / Aft Foreplane   Low / Fwd Foreplane

Hence, with all these considerations, the foreplane position used on Eurofighter was chosen. It is to be noted that most of this particular design optimisation was performed from an experimental data base using empirical techniques, as adequate capability to fully model all of the aerodynamic interference did not exist within the CFD modelling capability in use at the time.

Fuselage Shaping

One of the key drivers for good sustained supersonic performance derives from the combination of stability level and flap or foreplane angles to trim. Clearly, the wing itself has a significant contribution, but a major effect comes from the fuselage itself. Recognising this as a result of experience flying EAP, significant effort went into developing a capability to predict the effect of the fuselage effective camber shape on the zero lift pitching moment.

EAP had shown a significant change in this term as the Mach number increased through M=1.0, with consequent larger flap angles required to trim than had been desired. To avoid this with Eurofighter, significant effort was placed on modelling the aerodynamics using CFD methods. Design changes were restricted to the wing root camber and overall fuselage camber, within the constraints provided by the need for good vision from the cockpit and the chosen chin intake configuration and the need to minimise the basic form drag of the aircraft. These changes were then evaluated via wind tunnel test at transonic speeds, before finalising the aircraft lines for build.

Optimisation of the Overall Aircraft Camber

Zero Lift Pitching Moment, All controls neutral
Change from EAP to Eurofighter due to body and wing root optimisation

C_{mo}

0.04

0.03

0.02

0.01

EAP, Wind Tunnel data

EF, Wind Tunnel Data

EF, Flight Test

1.0   2.0 Mach No
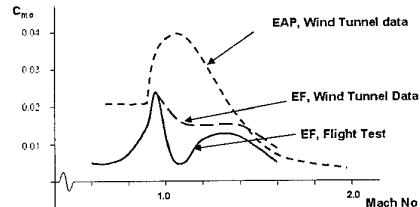
Interestingly, even with this effort, this has still proven to be an area where the aircraft in flight is slightly different to prediction, although the discrepancy is a fraction of that noted on EAP.

Fin design

From the early days of the configuration development, there has been a debate about the number of fins. The early configuration studies examined both single and twin

fins, but eventually the single fin was found to be the best optimum in terms of structural mass, drag, adverse flap-fin interaction for roll control transonically and effects on stability and lift.

However, this still left a decision as to whether the aircraft should adopt an all flying fin, or a more conventional fixed fin and rudder. The fin is sized by the directional stability requirement for flight at M=2.0. In the trade studies that followed, it became apparent that the fixed fin, because of its much greater structural efficiency, was smaller and lighter. Had control power been the more dominant requirement, then the all moving fin would have provided the better optimum.

In the end, the fixed fin and rudder was confirmed. The decision was again driven by the balance between reduced drag and greater control power, which would have been provided by a smaller all moving fin, against the aeroelastic stiffness problems it introduced in achieving the stability requirement, together with the size of the actuation system required.

However, the rudder is still the largest control actuator on the aircraft.

It should be said that there were some engineers, who had worked on the BAC TSR-2 project which was cancelled in 1966, who were extremely relieved at the outcome, despite the advances in technology that had taken place, due to concerns with that design over the structural coupling. Past experience suggested the likely outcome from the start, and even with the advances in materials for the aircraft structure, improved actuation systems and design techniques, the conventional fin is best, and that the all flying fin represented an unacceptable risk for the project, at least from this aspect.

Weapons Layouts

Whilst Eurofighter initially was thought of as an Air Superiority Fighter, it has always had a ground attack requirement, which is becoming stronger with time with all the partners Nations. One advantage of the configuration is that it provides a very large flying surface for the weapons engineers to hang a lot of external ordnance upon. This allows for a large number of weapon stations, and permits the aircraft to carry its Air-Air (A-A) and Air-Surface (A-S) weapons at the same time.

Improvements were being made in the ability to model weapons trajectories in the early phase of the release from

the aircraft. It was possible to consider packing the

Eurofighter
Illustration of the Weapon Packing Density
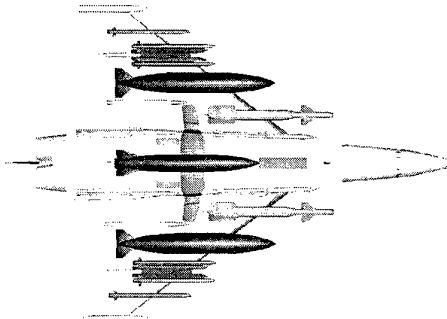
weapons together more densely and to reduce the amount of basic wind tunnel testing that was to be planned into the programme from the outset. Further, the aerodynamic modelling processes, as proven on current previous projects, had shown that the need for such test techniques as twin sting rigs, or for wind tunnel measurement of external flow fields, were no longer essential. As a direct consequence, all flow field data is generated via CFD calculation. The only test evidence that is now used are the installed loads data, or, in the case of missiles, loads measured at the end of stroke or end of rail positions.

Eurofighter
Configured with Air-Ground & Air Weapons

The Changing World

As the project moved through its Development Phase into the Flight Test Phase, and activity started to build up towards Production, a number of significant changes have come about to the world in which the aircraft was to operate. The Berlin Wall came down; there were numerous conflicts and a change in role for the Air Forces of the Nations within NATO. The role of the aircraft was reconfirmed, with an increased emphasis

being placed on the A-S capability, with the requirement moving to a very much more flexible aircraft, capable of operating autonomously for extended periods.

These changes do not affect the aerodynamics of the vehicle itself, but do have a very significant impact on the aerodynamicists involved in the project, and indeed upon every other engineer involved within the Eurofighter project and across all partner companies. The changes affect the way in which the engineers work, which in turn, impacts back onto what they have to do.

No longer could any area work in isolation from the other areas of the team. Affordability became a key driver for all the engineering and manufacturing areas, changing the working processes employed. This change is the move from the old cost plus environment, where everyone was paid for the work they did, to a fixed price contract structure, with both penalties and incentives. This has forced the adoption of parallel working in Integrated Product Teams, changing both the technical processes that are used and the management and leadership skills that are required to deliver the results.

Achievement of the recently placed Production Investment and Production contracts by the four Nations is totally dependent on the success of implementing the changed working practices, tool-sets and behaviours of the people involved in the project, wherever they work within the Customer – Supply chain.

This chain of events is set to continue throughout the life of the project, with every Customer and with every Supplier

The Changing Role of the Aerodynamic Technologies

As the project has developed with time, the role of the Aerodynamics specialists has changed, to meet the demands that have been placed upon the project by both the Customer and Industry. This situation is continually developing and is likely to increase the pace of change as the Customer base for the project increases.

The project is moving to a vision of being able to respond to changes in Customer needs on a regular basis, particularly as the need to integrate new weapons increases. This drives a range of Airframe related activities and the associated changes in Avionics or Flight Control System.

The aerodynamic technologies, which relate to optimising the design or installation, completing the design data and then generating the appropriate flight clearances have required significant modernisation and adaptation in order to be able to contribute to the overall integrated product.

Two main areas can be considered where the change can best be described, namely in the Processes involved in the technical work and in the management of the integrated product teams.

Process Changes

To maximise support for the project activity, dedicated project teams have been established. These teams are broken down into product based teams, populated with members drawn from those areas that have to work together to achieve a final, deliverable product. All the team members are focussed on delivery of their individual products to the project stream. This has resulted in significant changes to both the tool sets that are employed and to the development of concurrent engineering management practices, supported by excellent modelling environments.

Technical Processes

A key change that has occurred with the production activities is the change from a drawing based environment to an electronic product definition, with the concurrent activities requiring major attention to configuration control and release of data. This has enabled a change to the total process of design and manufacture, with the ability for the design teams to interact directly with the product being manufactured. To meet the challenges that this environment has posed, new working environments have been developed. This new environment is known as the Integrated Product Development (IPD) Process.

This process, supported by a software based configuration management tool, Product Manager, is becoming the established means of controlling the output of all engineering tasks on the project. Initial work with the process focussed upon the creation of the replacement for the traditional drawing sets, with all designers and the manufacturers having access to the data concurrently, but only able to use it for its defined purpose once formally released electronically. This is now being extended to cover the functional aspects of the design, such that the data pertaining to all the aircraft systems, which include all the aerodynamic "discipline" based systems, are all included. Hence all the design calculations, clearance calculations and performance verification data are to be

included within this tool, either directly or with a controlled reference, with consequent immediate access for all to properly configured data.

Currently, this is being extended to cover, not just the form and fit of the individual systems, but also the function of each of the systems. This tool will form the environment for management and control all of the data used for qualification, certification and verification of performance against the contracted levels. Any changes that occur in any of the data within the system has to be approved by the relevant stake holders before the data can go live, but it then goes live immediately to all potential users.

The use of desk-top processing, as opposed to the mainframe environment that existed on previous projects, has enabled the development of a new generation of engineering tools. The key drivers have been towards the development of interactive tools capable of producing their answers quickly, such that the engineers can develop the next step in the design quickly, as required by the parallel working practice now in use. In many cases, this has simply meant the porting of existing software tools into the new desk-top environment, but for some areas, completely new tool sets have been required.

As an example, further advances have been required in the analysis tools for extraction of the flight data. Experience with EAP had shown that the traditional Parameter Identification tools in use at BAe could no longer cope with an aircraft with a high level of basic instability combined with aerodynamic non-linearity, as experienced on Eurofighter and as predicted from wind tunnel testing. As identification of the aircraft remains a key to the final verification of many of the defined requirements, particularly relating to handling and performance, a capable tool was an essential requirement. This has lead to the development of regression techniques within Bae. These are now being applied successfully to a number of issues, with an example being described in a recent RTO Systems Integration Conference in Madrid[3].

Such techniques apply throughout the vehicle design and clearance cycle, and even into the flight test data analysis, where Eurofighter has brought its own specific challenges relating to the ability to derive data from flight measured parameters.

Management Processes

The changes that have been required of the processes and the team members have also required significant development of the management processes, in order to provide adequate support for the activities and their implications for individual team members.

Whilst team performance has been the required end result of the changes, to ensure that this is achieved requires a number of supporting actions to be put in place. This has resulted in significant re-thinking of exactly how such teams are led and managed, how they interact with their Customers and Suppliers, and the need to generate the involvement of the team in implementation of the changes that result.

The basis for the changes derives from the consideration of the five BAe Company values, as outlined in the BenchmarkBAe corporate cultural change programme and as recently described by the company chairman in his recent book[4], viz:

- ➤ Customers – our highest priority.
- ➤ People – our greatest strength.
- ➤ Performance – the key to winning.
- ➤ Partnerships – our future.
- ➤ Innovation – our competitive edge.

The BenchmarkBAe Values at Work
(The concept of Team Based Value Planning)

Customers   Partnerships

Performance

People   Innovation
& Technology
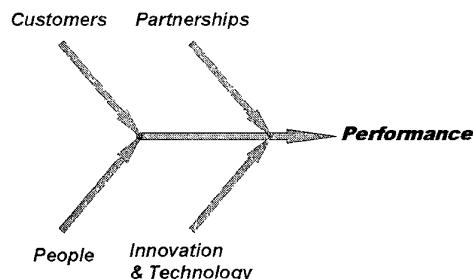
Benchmark drives thinking about behaviours related to each of the values, especially how any individual behaviour impacts upon those around that individual. Using an approach to planning tasks which addresses all of these values, the teams develop the overall plan of the work to be undertaken. Consideration of each of these values, for each major task, asks a series of questions that should be answered in the total plan being developed. Further, the process adds an ability to put the required events in the right order. Some of the issues that the approach would raise are obvious, but all too often in the past, it is the least obvious, softer, people management issues that are not considered and that cause a change-

process to fail. The process is referred to as Team Based Value Planning, and it is a major enabler to the achievement of a rigorous Earned Value Management System that is now being deployed across the project.

Role out of these techniques is taking place within all the teams operating on the Eurofighter project within BAe, and the key to success is the embedding of this approach without the team requiring conscious effort to achieve it. This will come with practice, but even thinking consciously through the questions that the values pose can lead to significant improvements in the overall team management and ability to meet the demands being placed upon them by Customers.

BenchmarkBAe - Achieving Customer Excellence

- *The ACE Tool - A simple self-assessment tool for use within all Project and Product Teams*

- *Identify the Customer - do we really know who this is and what he wants?*

  - *Where are we in terms of the service provided?*
  - *Where do we need to be?*

- *Develop a Customer Strategy and Customer Care Plan*

  - *Establish the contact maps*
  - *Establish metrics agreed with the Customer and measure the teams own performance against these*
  - *How do we handle complaints?*

Further Capability Development to support an Integrated Product Team Environment

A number of lessons have been learned from the design processes of the Eurofighter. In particular, the work stressed the need for a balanced and combined application of experimental methods, prediction techniques, whether based upon empirical data analysis or upon more sophisticated aerodynamic CFD modelling, as well as experience. The drive for faster turn around of change leads to the requirements for easy-to-use tools that enable the engineers to think about the job and not become experts in dealing with the quirks of an unfriendly piece of software.

Traditionally, many of the tools in use were developed for dedicated tasks. What is now occurring, is a move to more generic tools that cope with a multitude of different, but related tasks. The applications are then driven by the requirements of the user, with the possibility of customising the user interface for a specific application.

This leads to the development of user friendly front ends appropriate to the application. The days of taking months to set up geometry definitions for use in CFD calculations, as part of the normal working environment, are over in such a team.

There are areas where significant technique development is required.

One of the major concerns that remains is the ability to adequately predict the effects of unsteady aerodynamics, particularly due to aerodynamic separation and the large extent of the vortex flows that develop at high angles of attack. The areas of concern relate to being adequately model buffet loading, on the aircraft and the weapons it carries, to improving the modelling of the aero-servo-elastic characteristics to minimise the loss of phase that the current generations of filters can introduce into the flight control system.

The aerodynamic non-linearity that was seen in the wind tunnel has necessitated the development of very sophisticated flight analysis techniques, in order to enable a satisfactory resolution of the flight data, essential for verification of the aircraft models upon which flight clearance development and verification of performance are based.

One of the major, pleasant surprises has continued to be just how good a representation of the aircraft has been achieved in the wind tunnel modelling of the aircraft, especially regarding the non-linear behaviour.

It is also clear, that there is much more than the development of the required tools required for the success of a multi-disciplinary team. A major aspect remains the personal development of the teams and the personnel to take part in the teams. A key issue hinges around the encouragement of individuals to realise that they can do far more than their specialist knowledge might indicate, and that the best people to support them are the other team members, as well as their functional departments or home disciplines.

Concluding Remarks

Eurofighter required a significant involvement of the aerodynamic engineers from the very outset of the project design, across all of the partner companies involved in the project. Examples have been shown of the nature of some of the design decisions in which the role of the aerodynamicist has been a key.

As time has progressed, the Eurofighter Project has seen a significant change in the integration of the aerodynamics disciplines into a modern project and product focussed mode of operation.

This has impacted primarily in the areas of:

➢ Technical processes and tools
➢ Management processes
➢ Leadership styles and personal behaviour.

There is a definite move away from the tools which are not user friendly and which require detail knowledge and experience of the tool itself for successful application. There is a move towards tools that are easy to use and understand and quick to apply, wherever this is possible. Often this involves capturing of experience and building this into the user interface, such that the system leads the user through the right questions and decision points. There remains much to do in this respect.

Within British Aerospace, these changes are being focussed around the setting up of a product based work structure, in line with the requirements of modern Earned Value Management practices. However, to ensure that this is implemented successfully, the other major effort that is required is the recognition and acceptance of all the team members of their involvement in developing the plans by which the products are delivered. The key enabler being used for this is the Team Based Value Planning and the disciplines that this brings with it regarding the softer, non task focussed issues that are more readily overlooked in more traditional approaches.

References

1   RAeS Journal Volume 100, Number 1000, pp 411 - 424
     Aerodynamic Technology

2   AGARD FMP WG.19 AR-314
     "Operational Agility"

3   NATO RTO MP-11, Paper 12
     "System Identification for Integrated Aircraft Development and Flight Testing."
     R.Bava, G.T.Hoare, G.Garcia-Mesuro & H.-C.Olker.

4   Nicholas Brealey Publishing
     "Vertical Take-Off"
     Sir Richard Evans & Colin Price

The Future Role of 'Virtual' Design Teams

APPLIED VEHICLE TECHNOLOGY PANEL (AVT)
Keynote Session – Aerodynamic Design and Optimization of Flight Vehicles in a Concurrent Multi-Disciplinary Environment

18-21 November 1999

Charlie Guthrie
Director – Air Vehicle Advanced Design
Boeing Phantom Works
2401 E. Wardlow Road
Long Beach, California 90807-5309
U.S.A.

Summary: This keynote presentation will discuss the role that our aerospace engineers and their design teams and tools will play in the 'Virtual' design office of the future. Dramatically improving information technology is rapidly changing the design environment and the potential capability of the design toolsets. Along with these improvements in capability, there is a change in our expectations and requirements for both the design teams and the tools that enable the design teams to accomplish their tasks.

Today's Discussion: In this presentation we will describe the role of the 'Virtual' Design Team in a likely future design environment. We will take a quick look at the following influences and factors;

- **Design Environment Today**
- **Future Design Environment**
- **The 'Virtual' Design Team**
- **The Tool Requirements**
- **Snapshot of the Future**

This presentation will describe the quickly changing environment and consider how these changes may effect the future design office in which our design teams will be expected to perform. Lastly, what will the toolset needs and requirement be to support our design teams in the future design environment.

Today's Design Environment: Before discussing the future design environment, let's take a quick look at the design environment we are surrounded with today.

I will focus on a few key elements of today's environment centered around: How we pull our design teams together, how we handle our design information and knowledge, and some characteristics of our design toolsets.

For many years we have all seen the value of co-location of the project and design team. This is our preferred condition. We tend to rely predominately, if not entirely, on the co-located members of the design team and only reach outside this immediate group when absolutely necessary. As a result, we have the tendency to 'make do' with the group skills of the co-located team even when there are more experienced and better-qualified specialists within our companies.

We tend to rely on personal face-to-face contact both within our internal development team and externally with both our customer and supplier communities. We have all evolved a long list of interface, review, and follow-up meetings to ensure adequate communication during these design efforts. Sometimes we actually do provide good communication throughout a program's duration. But many times we fall short, and vow to incorporate yet an additional set of interface meetings in the next project we bring along.

Information is drawn into a design project from a wide range of sources. We draw from the company's history of similar and supporting projects through libraries of reports, data files, presentations, archives, and such. Each of the members of our design teams has personal experiences, files full of notes, collections of reference material and resources. We all have our phone lists of people who know a little more about some certain thing than we do. Or someone who knows someone who knows someone who does. Some of this database comes in the form of books and reports and pictures, some as computer files of text or modelling or algorithms, and much of it in hand-written notes and calculations or conversations or memories. Needless to say, much of the existing database is probably not in the appropriate form and format for the next analysis your design team performs or report they prepare.

Many of the toolsets used by our design teams originated, and are maintained, by the specialised functional disciplines that all contribute to the total system design process. There has been a strong push for many years to bring these various 'modules' together in a more integrated overall design toolset. We have all worked on this for a long time, and we still have a long way to go.

Impact of The Information Age: A lot can be said about the 'Information Age' and the profound impact that it is having on each of our lives. For a moment let's consider some of the rapidly improving capabilities that both cause and enable a significant change in the way our design teams will do their job is the near future.

New and rapidly improving capabilities include;

- **Immediate Access to Information**
- **'Paperless' Information**
- **Continuous Communication**
- **Telecommuting**
- **Electronic Assistance & Automation**
- **Increased Computing Speed & Capacity**
- **Electronic Media**

The 'Virtual Office' has become something we are all a part of in one way or another. There has been one shortfall up to now in the Virtual Office's ability to support high technology design teams. As the products we design have become more highly integrated, complicated, and sophisticated; the design tools and design databases have become electronically huge. The dramatically improving capability to rapidly, and in 'real-time', transfer huge amounts of electronic data to anywhere in the world, is now enabling design teams to be 'virtually' co-located while actually being geographically distributed. The 'Virtual Office' can now become the 'Virtual Design Office'.

The Future Design Environment: There is an almost endless number of things that will be a part of the future environment that will influence our design teams. Let's consider four key elements that will have a high level of impact to the design teams;

- **Geographically Distributed Teams**
- **Highly Diversified Teams**
- **Common Information & Database**
- **Common Processes & Toolsets**

At Boeing we are calling the distributed total 'enterprise' team capability - **"Design Anywhere, Build Anywhere"**. Organizational, Processes, Infrastructure, and Cultural changes are beginning to reflect this move into the future environment.

Future Design Teams must include a highly diverse technical skill group to address increasingly complex and highly integrated design challenges. The teams will have both company internal and company external participants that address all phases of the air vehicle's lifecycle from design and development, through manufacturing and operational support.

'Real time' communication of all forms of data and information will tie the design teammembers together as a cohesive unit. The large amounts of project related data and information will be quickly accessed from many legacy sources, will be traceable and controllable, and will be in directly usable forms and formats.

A design toolset built of common processes using a common database will provide effective and efficient utilization of all teammembers and design information. Analysis 'modules' using common geometry models and data formats will minimize wasteful reconstruction of unique databases. Having common databases also greatly simplifies all aspects of configuration control. Commonality will reduce the development, maintenance, and training costs associated with multiple unique processes and tools.

Broadening Customer Base & Marketplace: The industry has moved toward more consolidation over the past several years. Individual company's traditional customers and marketplaces, no matter what they were in the past, have expanded and now encompass a much wider industry perspective.

There are elements of both government and commercial, domestic and international in most companies' business base. This has created multiple customer interfaces, interactions, business relationships, and 'shared destiny' from what may have been a very focused 'company/customer' view in the past.

Future Design Process & Tools Requirements: Increasing focus on "affordable" aerospace vehicles demands wide ranging improvements in processes and integrated toolsets. Tool requirements will focusing on efficient utilization several key company resources: People, Time, and Knowledge base.

We must leverage the best people and their skills from across the entire company 'enterprise' regardless of where they live and work. This will drive us into the 'Virtual Design Office'.

We must effectively apply our 'enterprise' wide knowledge base of information, processes, and tools against the always more challenging design efforts.

To reduce the total investment of resources, we must shorten the time required to effectively study design options and make critical decisions. This also means we must provide improved design fidelity across a wider range of design options earlier in the design cycle.

The companies that achieve aggressive goals for improvement will have a strategic business advantage over their competitors.

Improved Decision Making in Early Phases: Lets step back and look at what is driving the design cycle time needs.

Program Cost Is Committed Early
**We Must Provide Data to Support Decisions**
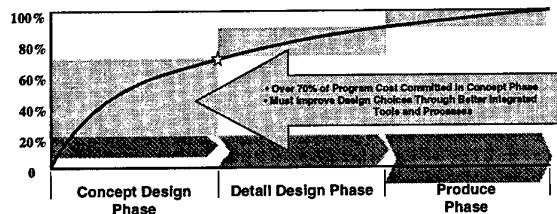
The majority of the cost of a program is determined in the very early phases of design. Because of this, it is important for us to make critical decisions early in the design process. And it becomes very important for us to improve the fidelity of design data as early as possible. Highly integrated design tools and improved processes are required to reduce cycle time while at the same time improving design choices, design fidelity and knowledge based decision making capability.

A Closer Look at the Concept Design Phase: The Conceptual Design phase moves through several different design cycle characteristics. These range from very rapid assessment of a very wide range of possibilities in the initial efforts, to a more focused and detailed analysis of the "best" design solutions later in the effort. The design solution needs and requirements evolve during this design phase. The needed design 'fidelity', to conduct early decisions of design solution screening and selection, initially requires less stringent design tolerance.


Design Cycle Time
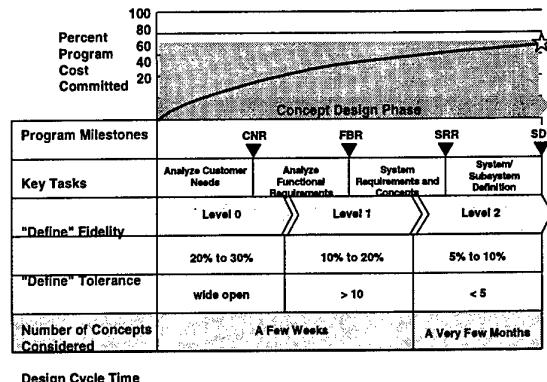
'Virtual' Design Office - Accommodating Distributed Teams: Computing infrastructures are evolving to support 'Virtual' co-location of high technology design teams.
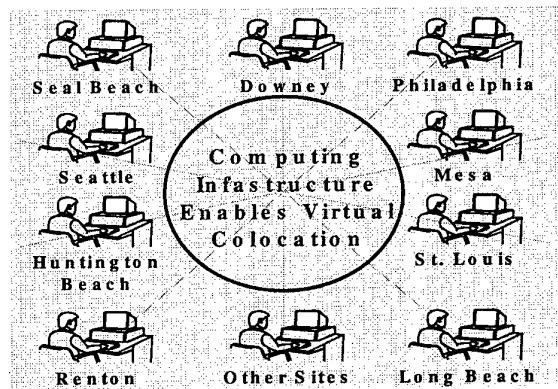
Web-based communication technology provides quick access to and transfer of the huge amounts of technical data design teams require.

Web-Based Computing Infrastructure: The new communication and computing infrastructure effectively ties the service providers (design toolsets , 'enterprise' technical experts, databases, and toolset developers & maintainers) directly together with the user groups (design teams) in 'real-time'.
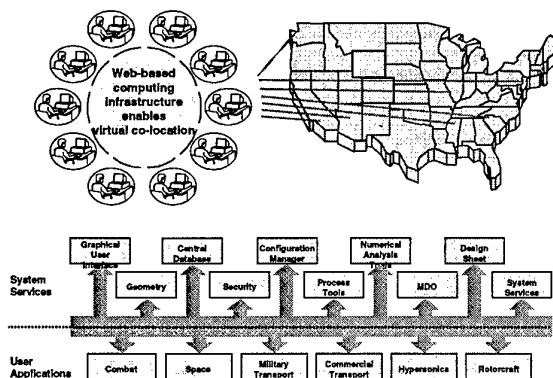
The ultimate success of 'Virtual' co-location and the 'Virtual' Design Team depends on this capability.

Design Practices, Processes and Tools Integrated Into One Common Design Environment: We will continue to address the evolving needs and requirements through new approaches and implementations of improvements to our tools and processes. The goal is to provide strategic competitive advantage for the company and to provide significant benefit to the customer through improved products and services.

- **Evolving Needs and Requirements**
- **New Approaches and Goals**
- **Benefit to the Customer**

A Day in the Life of "The 'Virtual' Design Team":

Lets imagine we are on that 'Virtual' Design Team in the near future. The day starts off with our daily 'stand-up' team meeting. Several teammembers are in each of three conference rooms hundreds of miles apart. Others are on their personal computers in even more locations. The 'virtual' meeting participants include teammembers from the company, several suppliers, and the customer. There is a design integration issue between the structures designers, the sub-systems installation designer, and two hardware supplier engineers. A decision is made to ask for help from an experienced consultant. Arrangements are made and that team-segments 'virtually' meets later in the day to work the details of the design problem. During that meeting, the current design is viewed in 3D and the lead designer describes the issues. Many questions are asked and different teammembers take control of the '3D visualization' to understand all the design implications and offer potential solutions. Someone remembers a similar design issue from a previous project, they quickly recall it from the 'enterprise' library archives and show it to the rest

of the group. The group identifies several potential options, the customer describes his concerns for support when in service, and the options are narrowed. The group discussed what analysis and supporting data must be generated to make the final decision, and the team agrees on a time to reconvene later in the week to review the results and make a decision.

Meanwhile, the manufacturing engineer, working with the Research group thinks that a new bonding process may eliminate several expensive assembly steps during production. He calls the vehicle design integration leader and they review the research results from their own work areas. A manufacturing assembly simulation using the common 3D design database is ready the next day to assess the affordability improvement of the new process. The integration leader convenes a 'virtual' meeting of the design area affected and ensures . . .

. . . And then we win that next contract, launch that next aircraft program, or design that next prototype. Sounds great doesn't it?

What Toolset Developers Need to Consider: As the 'Virtual' Design Office of the future drives and establishes needs for improving capabilities, both the design teams and tool developers will have to address many new implications:

- **Tools and Processes Must Support the 'Virtual Office' Environment**
- **Tools Must Provide Increased Fidelity Earlier in the Design Effort**
- **Consideration of Greater Number of Ideas**
- **Must Support 'Real Time' Data Links**
- **Common Data Formatting And/or Compatibility**
- **Tools Must be Transparent to All User 'Platforms'**

Above all, there is one important question we must always keep asking ourselves:

Are the Tools We Are Developing Going to Support the Future Environment ?

The Multidisciplinary Engineer in the Context of Concurrent Engineering

David J. Moorhouse
Air Force Research Laboratory/VAO
2130 Eighth Street, Suite 1
Wright-Patterson AFB, Ohio 45433-7542
United States

Throughout the evolution of the design of flight vehicles, the role of the individual engineer has also evolved. As aircraft have become more complex and performance envelopes have become ever larger, the role of the technical specialist has diminished in favor of the design team approach. Although the theme of the symposium deals with aerodynamic design and optimization, many comments apply to all technical disciplines. In this paper we review this design evolution very briefly. It is suggested that the evolutionary design process led to independent technical disciplines, technology development along the same lines and finally engineering education in the same engineering sciences. Concurrent engineering is discussed, together with the advantages and disadvantages from the viewpoint of the practicing engineers. It is suggested that the required approach leads to a requirement for engineers with a broader view than the traditional specialists. Next we consider the education process which, for design engineers, has evolved from apprenticeship to curricula that teach the engineering sciences. It is suggested that we may need to consider moving to the science of engineering. Finally, a possible view of future aerospace vehicle design is presented.

Introduction

The Air Force Research Laboratory does not design aerospace vehicles, per se, so the sense of our work is more from the aspect of analytical or conceptual design to analyze the impact of new technologies. The individual technologies mirror the ones considered in aircraft design, so that the same comments apply and are used interchangeably in this paper. In the Laboratory context, it is just as important to be able to demonstrate the potential benefit of a proposed technology if it were integrated into a system. In prioritizing technologies, whether in a design or a laboratory development, there is always the question of what is more important to the customer. Thus there is a need for a design and analysis capability, although not to the same level of detail as for a project to be built. There are similar pressures to use concurrent engineering practices and arrive at a valid interdisciplinary result. In fact, it is to be expected that many papers in this symposium will contain similar themes.

In the "old-fashioned" traditional design, many of the technical disciplines could be and were pursued in an independent or serial way. There are a variety of factors that have changed that simple view of aircraft design, and continue to change the design process at an ever-increasing rate. Aircraft are becoming more and more integrated, so this means that the traditional ways became less and less efficient. At the same time, the traditional pursuit of performance increases has given way to a strong emphasis on affordability, safety, environmental impact and information technology, etc. There have been a number of studies of the acquisition process within the US Department of Defense. The results have unanimously shown the need for drastic changes in the way major weapon systems are developed and acquired, but the relevant aspects for this paper are the design aspects. The need exists for new design concepts to be analyzed in great detail in the context of operational use in order to demonstrate benefits and uncover problems as early as possible. We should even take a fresh look at the mechanisms and strategies for optimizing aerospace vehicles, since the optimization constraints are also evolving. From the original requirements for basic stability and controllability, there was a period in time when increases in maximum speed were the primary focus. Then the focus became maneuverability for fighter aircraft. Now the primary focus is shifting away from performance aspects, and affordability is of equal or greater importance.

The foregoing discussion is only a very brief indication of the changes in the aircraft design process which have occurred and will continue. As the requirements change, such as the increasing importance of affordability rather than pure performance, the tools for designing, or even analyzing, systems with such constraints may not exist. The historical interactions may also change because of advancing technology, so that the historical data bases may need re-interpreting. As an example, aircraft cost models are predominantly based on weight and it is common to hear that we buy airplanes by the pound (or kilogram). Many factors are implicit in those correlations, however, that are part of the manufacturing process for the historical metal airframes. Thus the cost models are accurate for metal aircraft that are manufactured the same

way that the previous ones were. The actual models do not represent the "physics" of manufacturing an airframe, especially as we progress more and more towards use of composite materials with different detailed activities. With all of the changes, engineers need to be less specialized and more and more cognizant of related technical disciplines. It is important to understand the questions before working on the answers.

The theme of the symposium is "Aerodynamic Design and Optimization of Flight Vehicles ..." but many comments apply to the other disciplines with equal validity. The focus of the paper is that we can no longer afford to optimize any one particular discipline because that guarantees a suboptimum system. A more appropriate theme might be "The Role of Aerodynamic Design in System Optimization". The concurrent engineering process is discussed with some contrast to historical methods, followed by discussion of the implementation through Integrated Product Teams. Specific activities at the Air Vehicles Directorate of the AFRL are presented, including the creation this year of a Center for Multidisciplinary Technology which is tasked with addressing these issues. Some comments are presented relative to educating the new breed of engineers suggesting that we move forward from just teaching the engineering sciences towards the science of engineering. Lastly, there is a discussion of a possible future of vehicle design, although not as a forecast, but as a "vision of things that might come". Throughout this paper, examples are drawn from many sources, including the author's personal experiences in order to illustrate or prove various points.

Concurrent Design Processes

First, it is convenient to discuss the concurrent design environment that is the theme for both the symposium and this paper. We can consider the process for a new airplane system today, and contrast it with past practice. The concurrent design process relies on some form of systems analysis, or systems engineering. This has been expressed as:
1. Break the system under consideration down into component parts.
2. Gain an understanding of each individual part.
3. Determine how these parts interact.
4. Define the contribution of each component to the system performance
5. Put the system back together again.
6. Build it when the analysis shows that the design meets requirements.
At the risk of over simplifying the discussion, the old fashioned methods developed a reasonably good process for steps 1 and 2. It was not uncommon, however, to minimize the effort on steps 3 and 4 and then move on to step 5 and build a prototype and fly it to see if it met requirements. In

the "good old days" it was possible to build competing prototypes and choose the one that met requirements the best, rather than the analysis of step 6. The definition of the individual parts came early in the development of aircraft design. In this context, for instance, the aerodynamicist was responsible for predicting lift and drag and calculating mission performance (cruise speed and range, plus field length). History is replete with examples of the pitfalls of component optimization which yielded overall system sub-optimization. The original Spitfire wing was a perfect elliptical planform which minimized induced drag, i.e. optimized the wing performance. In combat it was soon learned that roll performance needed improvement, and the outer wing planform was cropped in later versions. The optimum wing for induced drag generated too much roll damping so that the total aircraft was not optimized for its primary mission.

In that example we see the negative aspect of the success achieved in breaking the system under consideration down into component parts. It led to the disciplines of aerodynamics, structures, controls and subsystems being defined, understood and analyzed as the essential components of an airframe. Each discipline could be studied, developed and analyzed separately. In the university setting these were taught as individual engineering sciences. In a project setting separate design groups were responsible for the same disciplines. Lastly, in the Laboratory setting, this approach led to those disciplines becoming individual technology empires.

Obviously, the disciplines were never completely independent of each other. In any real aircraft design project, connections and interactions between the individual disciplines that had to be considered were defined as in step 3. For example, 'the aerodynamics group' calculated loads for 'the structures group' to use in their design; 'the aerodynamics group' calculated control effectiveness and hinge moments for the 'the controls group' to use; etc. It is suggested, however, that it is not a gross exaggeration to claim that these interactions were often not really integrated. It is often referred to, facetiously, as passing your results over the partition to the other group. A significant area of research today is devoted to modelling such interactions, including the vision of complete physics-based models that can be used for the purposes of aerospace vehicle analysis and design.

Step 4 is one area that is still showing continual improvement in capability. Today it is common to simulate the predicted performance during the design development so that the above Spitfire problem and similar problems are avoided. In order to counteract such problems, we "apply knowledge earlier" to the extent that the future use can be predicted. As aircraft systems become more and more complex, we are faced with more and more integration with

non-traditional technical disciplines. An aerodynamicist today may be tasked with designing control surfaces that are integrated with thrust vectoring to produce the required total aircraft performance and response. Until recently, the powerplant for conventional aircraft was largely developed independently. "Integration" was mostly a definition of the interfaces. Even for V/STOL aircraft, thrust vectoring and reaction controls were only used as the aerodynamic controls lost effectiveness due to the reduced airspeeds. The design issue could be considered more of a blending than a true integration of effects.

A really critical part of the process is step 6. It seems deceptively simple and straightforward – analyze the system to show that the design meets the requirements. What analysis ? Because the wrong analysis, no matter how rigorous, will give the wrong answer (at least the vast majority of the time). Alternatively, how often is the answer "known" before the analysis is done to prove it ? How much analysis is enough, i.e. can we quantify a confidence level ? I will claim that we cannot perform analyses today to show with 100% confidence that a design meets all requirements. A design trade space may also exhibit local minima or optima that can guide an incomplete analysis to suggest something less than the global optimum. In addition, it may be more productive to show sensitivities or trade-offs between design options and some of the requirements. In order to accomplish that, however, we need to consider at which point in the 6-step process that should be done. This question leads to discussion of step 5.

Step 5, "put the system back together again", can be done on various levels. For a point design, a process of linear superposition may be adequate to define the primary contributions of the components. In order to perform trade-offs, however, the interactions between the components needs to be modelled. The higher the order and fidelity of that modelling, then the more credible the results will be. The extreme solution, for the very distant future, is to use physics-based calculations and generate a completely faithful design matrix of every design parameter vs the complete range of outputs. But these outputs will range from maximum speed to maintenance manhours. Then we can trade off an aerodynamic feature against life cycle cost. This will be discussed later.

Integrated Product Development

An aspect of system or concurrent engineering that has found its way into many projects today is known by different forms of the phrase: Integrated Product Team (IPT). In practice, it varies from a true interdisciplinary team to address a specific problem to the extreme of just the formation of an IPT is the management solution to any problem. The real intent is to assemble the appropriate team to work on specific interdisciplinary problems, such as the

design of an integrated flight/propulsion control system. The appropriate team consists of the personnel responsible for designing any portion of the system together with those affected by performance of the system. In this example from the author's experience (see Kisslinger and Moorhouse), the team represented the different contractor functional areas, all the major subcontractors and different Government agencies. The Interface Control Sheets had been defined in one-on-one meetings between the Contractor and the various Suppliers. In any complex system, however, there are likely to be indirect effects of one component on some other, apparently unrelated, component or function. For this to happen, it means that there was incomplete knowledge relative to step 3 above. The rationale was to anticipate and address integration questions as early as possible, and also to involve all the Subcontractors and Subsystem Managers in the discussions, so as to uncover any possible indirect effects as early in the development process as possible.
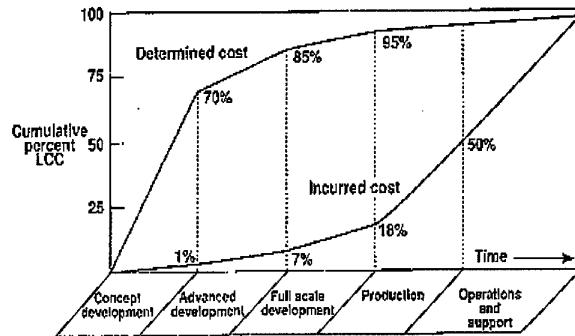

Figure 1. The Life Cycle Cost Problem

Another aspect that is receiving much attention is the timing of program decisions. It has been shown that the majority of an acquisition program's costs are essentially decided very early in the project design, see Figure 1. It is believed that this happens because many decisions are made before the knowledge to support such a decision has been obtained. It is also true, in many cases, that many costs were driven by inflated requirements. It has been tempting to ask for more than necessary "just in case", but this is also evidence of the lack of the right knowledge. The answer to the problem is to bring that downstream knowledge forward in the design process, as depicted in Figure 2. Although this seems like a contradiction, it is being implemented in many initiatives such as the US Department of Defense's Simulation Based Acquisition, NASA's Intelligent Synthesis Environment, and others. The basis of all these efforts is computational simulation and modelling, which relies on high-fidelity models of the total system. Once again, the basis is interdisciplinary or multidisciplinary

analyses rather than a concentration on any one discipline, or even a limited sub-set of disciplines. Again the ideal is for a group of engineers to address the problem where the team knowledge has to exceed the sum of the individuals, i.e. concurrent engineering.
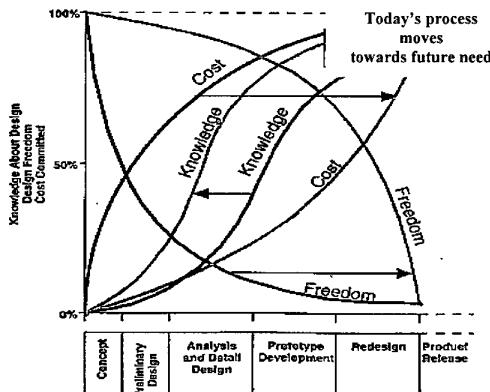

Figure 2. The Design Process Paradigm Shift

The Air Vehicles Approach

In the AFRL Air Vehicles Directorate, aerodynamic design and optimization is evidenced in a Center of Excellence for Computational Simulation. From its start in Computational Fluid Dynamics, i.e. the pure science of aerodynamics, the Center is now addressing various technical couplings such as the effects of structural modes on the aerodynamics. There is another drive to develop solutions for Maxwell's equation in addition to Navier-Stokes equations in Computational Electro-Magnetics. This computational center is also linked to a Center for Multidisciplinary Technologies. We are developing the physics-based models for an ever broadening range of technical disciplines. The ultimate goal has to be the creation of the capability to analyze, synthesize, design and optimize the complete aerospace vehicle.

Earlier this year (1999), the Directorate created a new Center for Multidisciplinary Technology. The Center was chartered to "invent and develop new and improved theories, processes and tools, using them to enable revolutionary vehicle concepts". It covers the range from basic research into the development of new and innovative optimization algorithms through to applied research into higher-order integration and development of technologies. The charter includes:

* Energy-based constraints
* Non-linear theories

* Cost-based optimization
* Synergistic interactions
* Futuristic integration
* Configuration inventions

A key component of the center is a technology application group, whose operation and activities are subject to all the constraints discussed above. This group is responsible for developing or acquiring the capability to perform the vehicle concept assessments, and support technology development from a total system aspect. It is also responsible for providing the links to two other Centers of Excellence. In this way, the basic technical disciplines of aeronautical sciences, control systems and structures can be assessed in an integrated fashion. Obviously, we are also faced with incorporating models of other disciplines, such as propulsion, in order to have a credible assessment. In DoD nomenclature Air Vehicles technologies plus Propulsion technologies add up to Air Platform technologies and all programs are subject to high-level review from that perspective.

As the Center looks into the future, the requirements to adhere to the concurrent processes will become mandatory. A vision of basing aerospace vehicle design on natural principles, see figure 3, will probably seem unnatural at first sight. It is based on an assertion that natural selection is a process of discovery through experimentation. In nature, if something is inefficient then it dies out. In the aerospace vehicle context, therefore, there is a need for better tools and processes for discovery through desining for maximum efficiency and minimum energy waste. This approach will require:

* High-order computational modelling
* High-level design tools
* Energy-based natural selection

The ultimate promise is to be able to realize a fully-integrated and fully-optimized vehicle design.

PAST: Discovery Through Experimentation
Also Nature's Process of Selection

NEED: Common Metric for Every Aspect ~ Energy ??
Maximum Efficiency/Minimum Energy Waste

FUTURE: **Numerical Experimentation** Using
* High-Level Design Tools
* High-Order Computational Modeling
* Energy-Based Natural Selection
* Fully-Integrated & Optimized Vehicle Design

Figure 3. Design Based on Natural Selection

In order to include all relevant technical interactions, we should probably start off by assuming that **all** interactions are relevant. The greatest barrier to achieving a successful result is accepting something as a given without question. In fact, if we refer back to Figure 2, the real problem may be that the practitioners start off the process with a set of assumptions and do not realize that they are starting off with zero knowledge. It may also be instructive to consider a variety of lines on Figure 2, e.g. assumed knowledge vs actual knowledge, program management knowledge vs engineering knowledge, etc.

Engineering Education

Based on the preceding discussion, we can consider what aspects of engineering education may require changes in order to be aligned with the needs of a multidisciplinary engineer in a concurrent design environment. The embodiment of today's reality can be seen in the stated goal of NASA's new Intelligent Synthesis Environment initiative: "To develop the capability for scientists and engineers to work together in a virtual environment, using simulation to model the complete life cycle of a product/mission before commitments are made to produce physical products". Notice also that this very ambitious statement also promulgates the tradition that engineers and scientists are distinct. Universities were founded to "teach learning, i.e. science". Engineers who built things learned their trade as apprentices. As time passed, universities taught the engineering sciences but not the science of engineering, in this author's opinion. The old-fashioned traditions were continued, however, in that when the young engineer began employment in "the real world" he was typically assigned to a senior engineer and trained on the job. The expectation was that a new graduate (at whatever level) did need training in the "real aspects of the job or project".

Universities today are becoming more involved in teaching what the aerospace industry really needs, i.e. graduates with some experience in working in a team environment on a multi-dimensional problem. In the USA, in this author's opinion, the Georgia Institute of Technology in Atlanta, Georgia, is the most advanced in offering graduate degrees in aerospace vehicle design. The philosophy has been expressed as producing a "T-shaped engineer" i.e. the student is taught a broad range of engineering subjects to a certain level of detail, plus at least one specialty subject in depth. As a purely personal opinion, I consider that I got a very good undergraduate training in the broad range of subjects required to receive a degree in mechanical engineering. I suggest that the real difference is that the engineering subjects need to be taught, not as separate engineering sciences, but linked together in the interdisciplinary nature of real world problems. The linking together of the engineering sciences to provide multidisciplinary understanding is what forms the top of the "T" in shaping an engineer, this is the science of engineering. This concept is depicted (humorously) in Figure 4. In order to accomplish this, graduate students are assigned to work on team projects. At Georgia Tech, this is accomplished through an Aerospace Systems Design Laboratory. Students are assigned design projects and use state-of-the-art computer programs, many of which are advanced by the doctoral thesis work. In addition, there has been a relatively recent trend for professional technical societies and organizations to encourage such team projects. A visible sign of these activities is the various "build and fly" competitions that are held as university challenges.
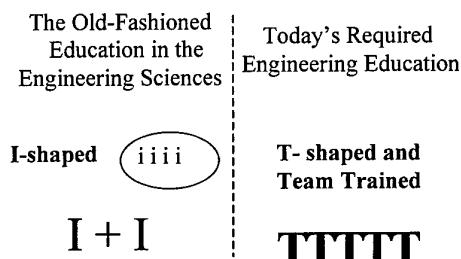

Figure 4. Education for Concurrent Engineering

The Future

Part of this discussion may also be considered as learning from history. It is known that the Wright Brothers studied birds as they were solving the basics of controlled flight, and the same is probably true of most of their contemporaries. Wing warping as a roll control device certainly came from the Wrights' observation of the aerodynamic shape of bird's wings in flight. This author has not seen any explanation for the design of the aileron that soon replaced wing warping for roll control. We know, however, that wings structures were made stiffer as speed and maneuvering increased. Very soon after those early flights aircraft design engineering became an evolutionary process of development from the preceding model. At AFRL today, however, wing warping is being researched again in the Advanced Aeroelastic Wing (AAW) program. So, is the aerospace vehicle design community at a point where we can learn again from nature in order to make the next major advance ?

The theoretical base is being developed that will allow the application of energy-based principles to aircraft design (Bejan 1997). It is a logical process to consider static systems such as power or refrigeration plants in terms of an energy balance, in order to analyze and minimize the losses. The same principle is being applied to aircraft

systems (Bejan 1999). That work is a discussion of "new opportunities for thermodynamic optimization" including the thermodynamic optimization of flight.

In a simple one-dimensional view, the aerodynamic optimization to reduce drag is already an example of minimizing the use of energy represented by fuel burned. We can write a balance of the fuel burned by the engine in order to do work overcoming the drag of the airframe. This is the implicit consideration of the traditional performance analysis, although it has been typically used to calculate the range or radius with specified mission constraints. This traditional analysis has been based on very simple models of an airplane that was designed through trial and error processes rather than a true integrated procedure. The engine also has to supply energy, in different forms, to drive the hydraulic pumps, to power the environmental control system, etc. The power that is required from the engine for these functions is not calculated on a real-time basis and is usually a simple average, so the analysis of a mission that includes combat maneuvering is only an approximation, at best. Further, that environmental control system has probably been designed as an independent subsystem and "integrated" via the definition of the interfaces.

Now, if we look into the future and consider the design of a total aircraft system in terms of an optimum balance of energy then all the classical engineering disciplines must be re-assessed. The first consideration is whether the engineering tasks can all be formulated in a common framework of energy or thermo-economic metrics. The answers to this question probably range from the trivial to the very complex. It is in vogue currently to claim optimization of life cycle cost, which is impossible to calculate with any degree of certainty using the available models. If we consider the potential of using energy-based optimization, then "everything" must be put in thermo-economic terms but to do this we must consider energy and cost to be equivalent units. The future of this methodology depends on being able to formulate the individual technical disciplines in this common framework for analysis and optimization, in parallel with the development of the necessary physics-based modelling.

Conclusions

A century of manned flight has been summarized in the briefest way possible to consider the role of the technical specialist, such as the aerodynamicist, in the modern design context. It is suggested that the time has already passed when the individual technical disciplines could be practiced independently. Optimization of individual disciplines leads to a sub-optimum system. This is probably obvious to many when considering design of a flight vehicle, but it is also just as true when considering applied research and technology development. Now, and

for the future, each technical discipline has to be considered in a multidisciplinary environment to satisfy the object of concurrent engineering. The theme of the symposium might be stated as "The Role of Aerodynamic Design in System Optimization".

The required education for "modern engineers" was discussed. No matter how good an engineering education was, it seldom prepared the graduate for the realities of a design team. I suggest that the next generation of engineers should be trained in the science of engineering rather than continue with separate treatments of the engineering sciences.

The original flight experimenters did study nature, and especially birds in flight. Aircraft design, however, soon became an evolutionary process. The question is posed: can we may new technology leaps by a return to nature? Further, nature is suggested as a minimum energy waste design constraint. For the future, maybe the emerging discipline of thermo-economics can be developed as a methodology for total vehicle system optimization. The AVT Panel might also consider that such an energy-based design methodology would be equally applicable to ships and land vehicles as well as aircraft.

Finally, within AVT are the technical disciplines of aerodynamics, structures and propulsion, i.e. three of the traditional technical disciplines. There needs to be integration with other RTO Panels in order to realize the full potential of a fully integrated concurrent engineering design process.

References

Bejan, A., "Advanced Engineering Thermodynamics", second edition, Wiley, New York, 1997.

Bejan, A., "A Role for Exergy Analysis and Optimization in Aircraft Energy-System Design", Proceedings of the ASME Advanced Energy Systems Division – 1999, S. Aceves, ed., ASME, New York, 1999.

Kisslinger, R. L., and D. J. Moorhouse, "Lessons Learned in Control System Integration & Management from the S/MTD Program", Society of Automotive Engineers Paper 901849, SAE Aerotech '90, October 1990.

DISCUSSION

Keynote Session, Paper #3

Dr Render (Loughborough University, UK) queried the applicability of "T-shaped engineers" to specialist tasks, particularly the production of the tools required by the multi-disciplinary engineers.

>**Dr Moorehouse's** ideal was that tools would be produced by "T-shaped engineers" with a specialty in computer science. He felt that engineers might write inefficient code, but code which would produce the correct answers. He expressed little confidence in tools written by computer specialists with no engineering knowledge. He suggested an IPT (Integrated Product Team) approach to capture the required engineering and computer skills.

Mr Woodford (DERA, UK) sought clarity on the distinction between "acquisition" and "production" costs. He also asked the author for his views on the establishment of cost as an independent technical discipline.

>**Dr Moorehouse** noted that his charts should have referred to three distinct components of life cycle cost, i.e. "development", "manufacturing" and "operations and support". He agreed that cost should be considered as a technical discipline subject to the same demands for fidelity and rules of optimization. He noted that cost is not an independent variable and should be taught and considered as a component of a multidisciplinary process.

ROLE OF THE AERODYNAMICIST IN A CONCURRENT
MULTI-DISCIPLINARY DESIGN PROCESS

By

Dr. Leland M. Nicolai
Chief Engineer, Advanced Development Projects

Atherton Carty
Aerodynamics/RCD Program Manager

Lockheed Martin Skunk Works
1011 Lockheed Way
Palmdale, Calif 93599
USA

ABSTRACT

As the affordability of new aircraft and missile systems becomes an essential element of new development programs, the time spent in the early design (conceptual and preliminary design) needs to be reduced. This paper will address the time and activities associated with the conceptual and preliminary design of an aircraft, the role of the aerodynamicist in this early design period and the tools that he uses. The question of how the design time can be shortened will be discussed and what the aerodynamicist can do about it.

INTRODUCTION

The Skunk Works has adhered to the motto "Quick, Quiet, Quality" in the development of many new and unique aircraft for over fifty years (Figure 1). The "Quality" was because the customer deserved (and demanded) it. The "Quiet" was because many of the Skunk Works programs were (and still are) "Black". The "Quick" was because "Time Is Money" and the faster a new product could be brought to the market, the less it cost. With the current world-wide emphasis on low cost and affordability, Quick is an essential new program parameter.

The design and development of a new aircraft (or missile) is naturally a serial set of tasks. Ideally, things should be done in order so that nothing has to be done over as new information becomes available. A notional serial schedule (to first flight) for developing an aircraft (excluding avionics and propulsion) is shown in Figure 2 (green depicts the conceptual design phase, yellow the preliminary design phase and the blue is the detail design). Unfortunately, this leads to a very long schedule and an expensive product. For Figure 2 it is 42-54 months from the start of conceptual design to first flight (with no problems that would stretch out the schedule). It is faster and cheaper if tasks can be done in parallel provided a serious design flaw doesn't precipitate scrapping a long and expensive task (ie; tooling and fabrication of parts). Typically, aircraft schedules are driven by the development of the VMS (vehicle management system, flight control), the engine (if it is a new engine) or delivery of the landing gear (simply because there are so few landing gear suppliers and they are very busy).

The Skunk Works has been relatively successful in shortening the time between contract award for a new design (usually the end of conceptual design) and first flight as shown on Figure 3. The two aircraft, A-12 and YF-22, that contradict this trend have reasonable explanations. The original schedule for the Mach 3+ A-12 was 20 months to first flight. The program turned out to be a tremendous technical challenge for the
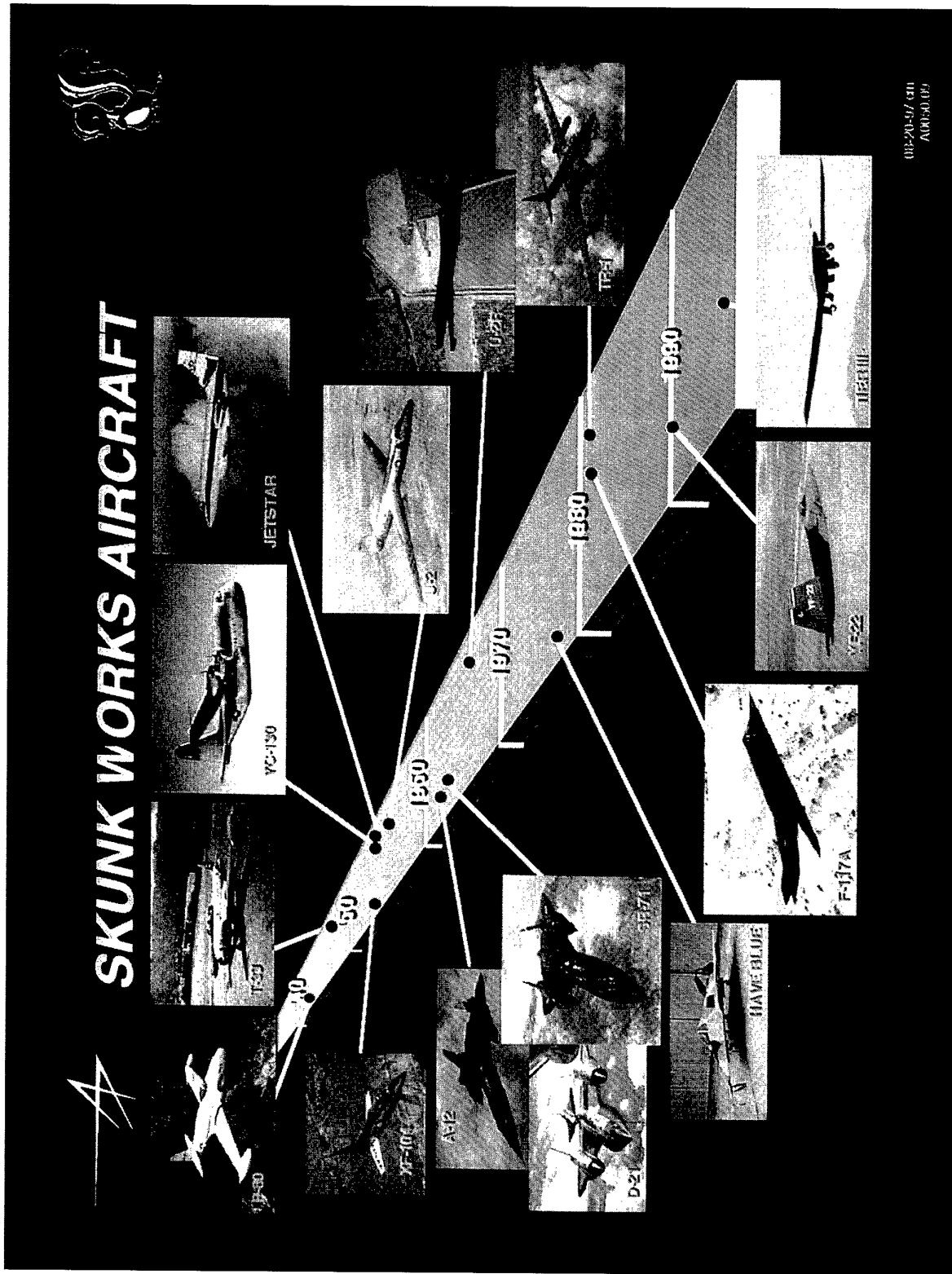
Figure 1. 50 Years of Skunk Works Aircraft

Skunk Works in the early 1960s (mixed compression inlet with translating spike, 85% titanium due to 600 °F surface temperature, fuels and lubricants operating at 350 °F, and the J 58 engine) and the program first flight slipped 10 months. Eight months after the dem/val contract award (October 1986) for the YF-22, the Lockheed team scrapped their prototype configuration and started over leading to the current configuration OML freeze in May 1988 and first flight in September 1990.

The Skunk Works success in reducing the time to first flight has been due partly to a close association and trust between LMSW and their customers leading to minimal specs, reviews and documentation. Also, being a quiet or black program helps shorten the schedule by keeping out the "lookie-loos". But most of the reduced time has come from parallel tasking (concurrent development) and encouragement to use off-the-shelf (OTS) equipment, either Mil-Spec or commercial. Having an experienced, enthusiastic and "workaholic staff of engineers, designers and manufacturing people always helps also.
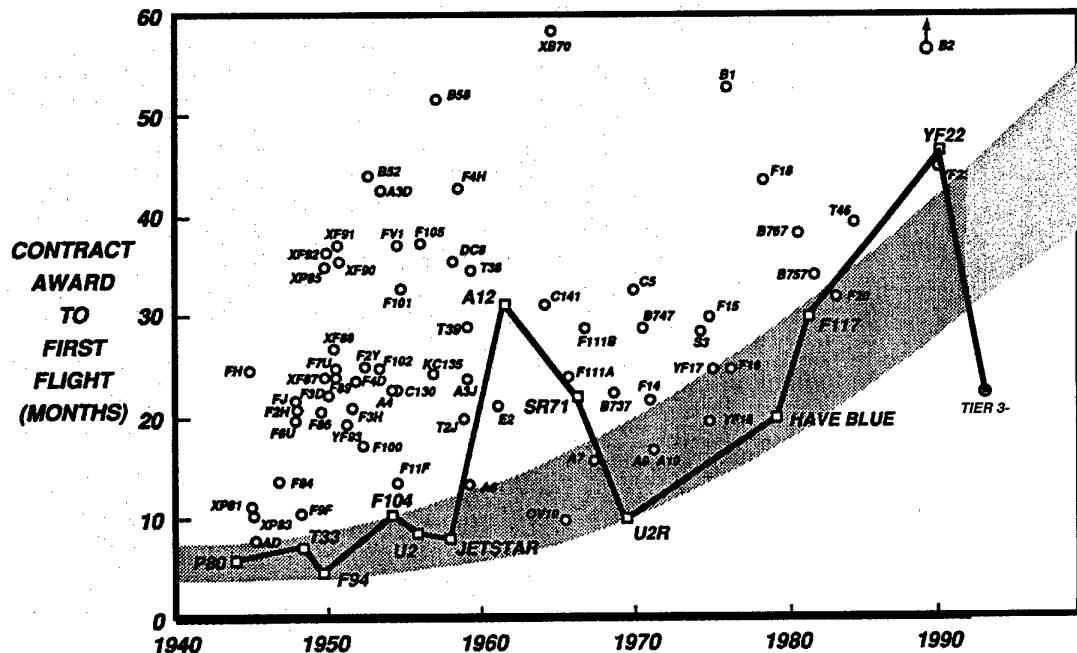
Figure 3 Aircraft Times To First Flight

FF

CDR

PDR

18-24 Mos

VMS Available

12-18 Mos

6-12 Mos

Baseline

Trade Studies
- Design
- Mission
- Tech

Predicted Loads

PSC

6 Mos

Functional Analysis

More Trades

9 Mos

Test / Risk Reduction
- Aero – S&C/Loads
- Propulsion
- RCS

OML Freeze

Structural Analysis

Loads

S&C

Predicted S&C

Design

Subsystem Design / Test

Simulation / Control Law Dev / Software Dev / Validation & Verification
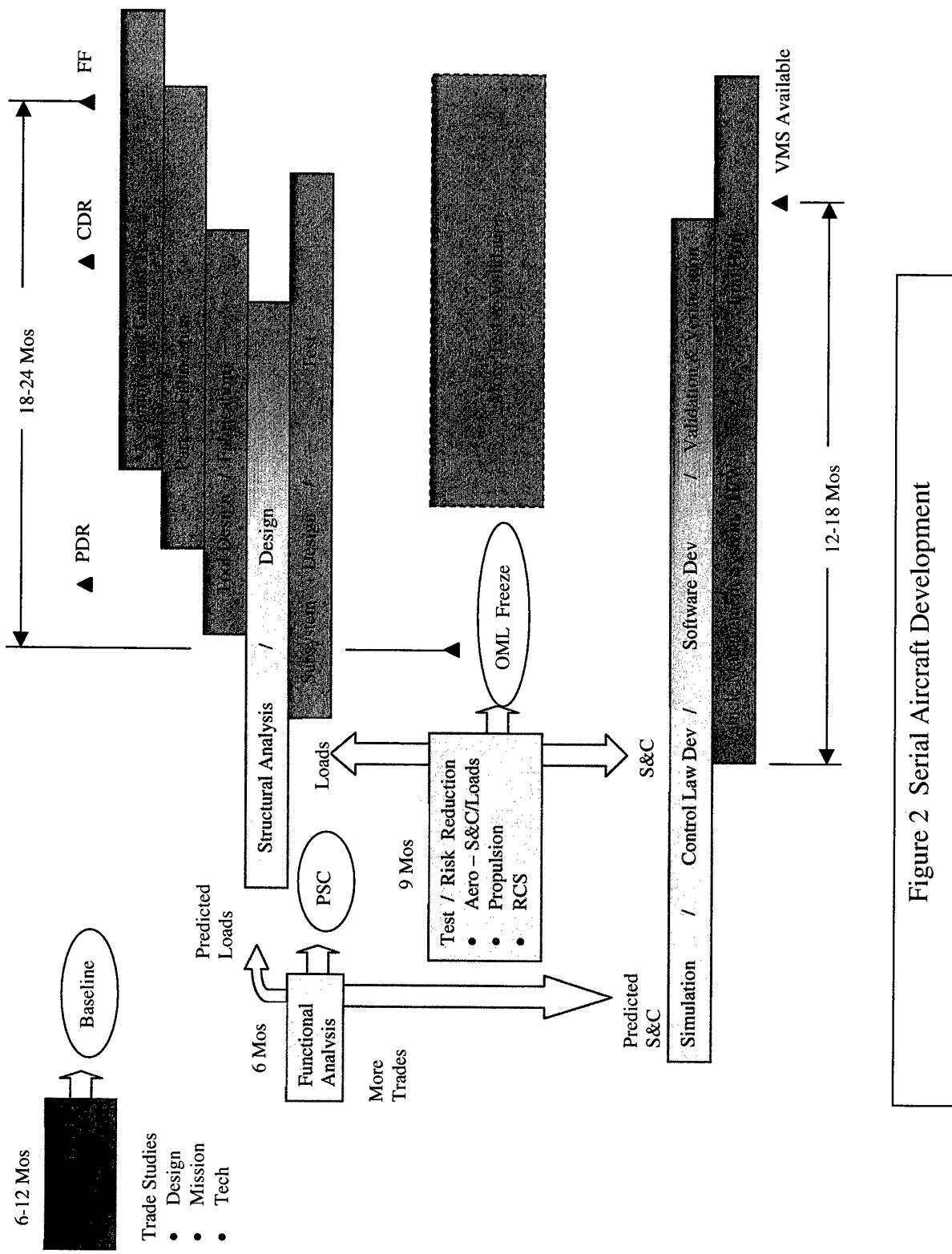
Figure 2 Serial Aircraft Development

It should be noted that the times shown on Figure 2 represents about half of the development time for a new aircraft. After first flight there is 3-4 years of developmental flight test (contractor clear- the-envelope testing, operational test and evaluation, etc.). In the past, the normal development program for a new aircraft was typically 8-10 years. With the emphasis on reducing cost, the industry is doing more concurrent development to reduce the total development time. The Skunk Works F-117 took 5 years to IOC (Initial Operational Capability) and the JASSM (Joint Air-to-Surface Standoff Missile) will take 76 months.

PARALLEL TASKING (CONCURRENT DEVELOPMENT)

Parallel tasking or concurrent development means overlapping the task blocks shown in Figure 2 as much as possible. This is always dangerous as decisions are made many times during the program before having a complete set of data or based upon predictions. For example:

1. The outer mold line (OML) is frozen before aerodynamics, propulsion and RCS testing is completed.
2. Structural loads are estimated before the wind tunnel testing is completed so that the structural design can proceed earlier.
3. Flight control laws are developed before the wind tunnel testing is completed so that the flight control software and hardware development can proceed earlier.

The risk associated with this parallel tasking depends upon the complexity of the design and the maturity of the functional analysis codes (ie; CFD and CEM). The U-2A flew in 8 months because the design was simple, subsonic and stable and the structural design was started very early based upon predicted loads. The loads were verified later and found to be very close to the predicted loads (lucky or good?).

The risks associated with parallel tasking are mitigated by the formation of a vehicle IPT (Integrated Product Team). The vehicle IPT meets weekly with all personnel involved in the development of the vehicle. The people represented on the IPT include the functional engineering plus manufacturing, RMS, avionics, flight test and cost. These meetings address and resolve downstream issues before they lead to a conflict and impact schedule. The old practice of one group completing its task and throwing the results over the wall to the next group inevitably lead to sub-optimization and conflicts.

The use of OTS equipment (either Mil-spec or commercial) will usually lead to a form/fit penalty for the design but will greatly reduce the risk of a schedule slip. It is a good policy to demand that any new equipment item "buy" its way onto the vehicle by showing that OTS equipment will not work. The F-117A used the flight control computer from the F-16A, cockpit displays from the F-18A, landing gear from the F-15 and brakes from the Gulfstream II.

ROLE OF THE AERODYNAMICIST IN THE DESIGN PROCESS

The aerodynamics group is at the center of activity during conceptual and early preliminary design because they "own" the OML (outer mold line) through their control of the configuration aerodynamic characteristics and performance. In conceptual design they define the initial configuration sketches and size the vehicles for the design group. Using their sizing tool they perform the design trades (wing loading, aspect ratio, sweep, thrust-to-weight, etc) and mission trades (range, payload, speed, etc). The design trades quickly reduce the design space and the mission trades answer the "what if" questions for the customer. The aero group is not working in a vacuum during this period because all disciplines are involved through the IPT process. The aero group, with help from propulsion, flight controls and RCS, develop the configuration OML for a baseline design.

During preliminary design the aero group leads the vehicle IPT towards the PSC (preferred system concept) by conducting configuration trade studies using a vehicle synthesis (sizing) tool. They then predict the configuration S&C characteristics for the flight controls group and verify the data base with

high fidelity wind tunnel tests. The aero group also works with the loads group to predict vehicle loads and verify the loads data base with high fidelity wind tunnel tests. Once these two important data sets are generated the center of activity shifts to designing and building the vehicle and integrating (stuffing) the subsystems (propulsion, flight control, ECS, etc) into the vehicle. The aero group continues to refine the PSC aerodynamics and performance.

Looking once again at Figure 2, it is quite clear that if aero doesn't do their assignment the whole schedule slides to the right. If aero misses on their wind tunnel test and has to modify the model and re-enter the wind tunnel, structural design and flight control law development slips. The responsibility of the aero group is to get it right the first time and shorten the design process. All engineering functions, but especially aero, must sharpen their analysis tools to consider multi-disciplinary issues. These tools must be user friendly and rapid turnaround.

RAPID CONCEPTUAL DESIGN (RCD)

LMSW uses a program called Rapid Conceptual Design or RCD to shorten the time spent in conceptual design, potentially reducing the cycle time in half. This software tool is used by the aerodynamics group to perform the multidisciplinary trades and optimization studies leading to the baseline design.

The implementation of RCD with its distributed modeling and analysis software package reduces the time to perform the multidisciplinary trades and optimization studies in three ways. First, the passage of data from one tool to another is automated (historically this has been done off-line and has been a major consumer of time). Secondly, the output from one analysis that is input for another analysis is scheduled automatically within the program and passed between modules as required. Finally, the RCD software automates system trades by enabling automated multivariable parametric studies and optimizations to be conducted (providing rapid resizing of the design when individual parameters in standalone disciplines are changed).

Conducting a multidisciplinary trade study by conventional methods is a time consuming process dominated by the reformatting, transforming, and translating of data between design disciplines and analysis modules. In order to conduct trade studies and evaluate a design, data must be passed from one of these analysis tools to another. Efficient design analysis and optimization requires data handling and initiation of appropriate analysis codes independent of interactive user input. The resulting design architecture can yield significant improvements in turnaround times as well as a substantial reduction of non-value added tasks performed.

The effective evaluation of a design at the conceptual level requires the integration of multiple disciplines. Currently there are many conceptual analysis tools from all the major disciplines utilized in the design process. Throughout the design process the output of one analysis is repeatedly used as input for a subsequent analysis. Multidisciplinary design software can facilitate this process by providing scheduling of the analysis codes and communication between the codes. Also, different classes of vehicles require the use of different analysis codes. Analysis tools do exist which combine portions of major disciplines into a single working environment in order to eliminate the need for translation of data. The primary drawback of these historically complex and aging codes is that they apply to a predetermined set of design problems and are difficult to expand, modify and maintain.

The objective of RCD was to develop a design tool to facilitate multidisciplinary design analysis and optimization at the conceptual level, and that would have the flexibility to address non-traditional design problems. Traditionally, vehicle design optimization is a chain of sub-optimizations of single disciplines (two-dimensional gradient or hill climbing). Trade studies are conducted on individual components or subsystems (i.e. wing, engine, fuel system, hydraulic system, etc) using an analysis code tailored for the particular item. The results of the trade are then passed to the other design disciplines, which in turn analyze the impact of the trade on their area of responsibility. If the affected disciplines approve of the trade, their components or subsystems are modified and the change distributed to the

remaining design disciplines for evaluation. This two-dimensional process of change and evaluation is repeated until the design is closed. Unfortunately, this path along local optimums can very often miss a global optimum solution.

Multidisciplinary design problems are by their very nature, extremely interconnected and nonlinear. Therefore, in searching for an optimum solution, one cannot simply assume that a given solution is optimal in the global sense simply because the solution may be optimal locally. The problem then becomes one of not simply 'climbing the hill' but rather, first finding the hill that is the tallest, and then climbing. The methods employed to solve this type of problem must therefore have the ability to either avoid local minimums all together or escape them once they are encountered in order to be effective. This fact alone puts traditional gradient based methods at a disadvantage, as the optimum solution which they locate is dependant largely upon the point in the function space at which they started. Non-gradient based methods such as genetic algorithms, for instance, are better suited to addressing the problem of locating a global optimum, but typically do not converge to a solution as effectively as gradient based methods. Ideally, a non- gradient based method would be used to determine which is the tallest hill, and a gradient based method to climb it. This 'hybrid' optimization strategy allows gradient and non –gradient methods to be employed in a complimentary fashion in order to most efficiently address the problem. The relative strengths of these methods are exploited while their respective weaknesses are neglected, thus yielding the analytical benefits of both. Future growth plans for RCD include the implementation of this capability.

The flexibility of RCD to address non-traditional design questions was incorporated by developing a framework that would allow the integration of existing analysis and optimization codes in a modular format in which the designer could choose appropriate analysis tools based on the level of fidelity required and type of problem the designer is facing. The user could then decide which data should be sent from one tool to the next in order to provide an efficient environment for performing the multidisciplinary optimization. Once this data is linked it is sent between analysis tools automatically thus allowing the designer to focus on the design problem. The Rapid Conceptual Design process as illustrated in Figure 4 is based upon the premise that all the systemic variables of the system should be available and monitored from a central location or framework. The analysis tools supplying these variables however, should be free to run on any platform independent of the controlling framework.
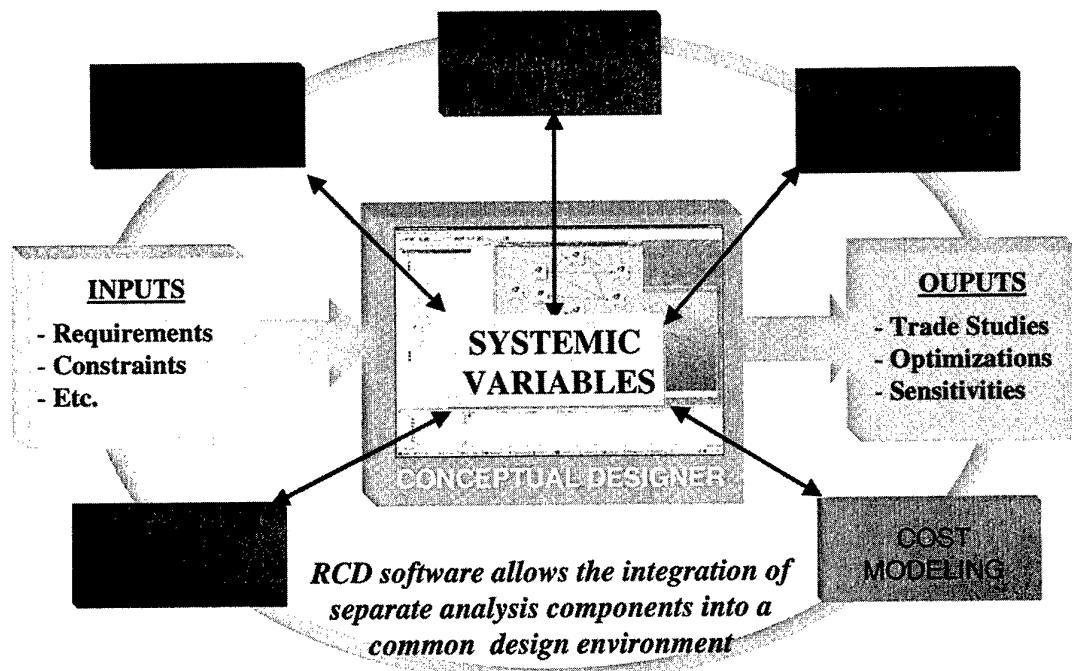

Figure 4 The RCD Process

RCD Case Study

The RCD program was recently used on a very unique problem where the solution vehicle bordered on the fringes of the classical design space. Due to the unique nature of the problem, the sensitivity of the design to operational methods / modes and systems design options was not initially well understood. The lack of known design drivers coupled with the limited duration of the study (only 48 days) meant that development of the vehicle by standard design methods could result in a sub optimal configuration. The customer had indicated that a solution to the problem existed and that the current effort would be competing with the existing solution on a cost basis. Therefore a design that met the technical requirements would not ensure a contract win. Optimization of the design would be required to increase the odds of a contract award. The only way to accomplish an integrated vehicle optimization effort in the time allotted was to employ Rapid Conceptual Design (RCD) techniques.

As previously mentioned, the proposed vehicle would be competing against an existing solution on a cost basis; as a result the primary design goal was to produce a minimum cost vehicle. For aerospace vehicles weight (i.e. size) is usually the primary cost driver. Thus the goal for the sizing code would be to minimize weight. If the proposed vehicle could be shown to outperform the existing solution on a cost basis, the next phase would most likely be a fixed price development program. Since cost is strongly related to size, the sensitivity of the solution vehicle's size to changes in subsystem performance and material weight and strength properties needed to be well understood. Without this data appropriate margins could not be added to cost model.

The uniqueness of this particular vehicle design made it difficult to determine many of the initial design values. Having linked sizing modules and a sizing routine, which allowed time-efficient closed vehicle parametric trades greatly de-emphasized the need for accurate initial design values. The final system model is a testament to the above statements. It consisted of 23 analysis modules, 87 inputs, passed 122 design values between the individual sizing modules, and had 107 output design values . Sixty three of the 87 model input parameters were varied during the course of the design study to determine the sensitivity of the design to individual input values. The final 20, two dimensional, 5 x 5 design point parametric runs were conducted in a 20 hour period whereas using conventional methods these trades would have taken weeks to run). The end result of the final 20 parametric trades was a vehicle whose size was reduced by 33%. One of the parametric trades revealed that the current design philosophy was 180 degrees out of phase with the actual physical phenomenon. The customer and the design team, at that time, believed that relaxing a particular constraint would have a positive effect on the vehicle. In actuality the vehicle size decreased as the constraint was tightened. Another parametric trade addressed the distribution of a design requirement between two different systems that were tasked to satisfy that requirement. The optimal distribution from a standalone system analysis (based on the incorrect belief described in the above parametric trade discussion) was to have one of the two systems satisfy 100% of the requirement. The final parametric trade of these systems revealed that the optimal solution was indeed a distributed share of the duty. These two parametric trades together were responsible for 28% of the 33% weight reduction. This illustrates the true power of multidisciplinary design optimization: The identification of counterintuitive solutions with optimums that can only be identified through multidisciplinary design.

Automated data transfers greatly reduced the time required to complete vehicle aerodynamic build-ups. Automated parametric trade studies significantly reduced the time to perform parametric analysis. RCD models linking standalone analysis tools also reduced the time required to evaluate the effects of a system parameter change at the vehicle level by an order of magnitude. Finally, complete integration of the multidisciplinary trades and optimization through the application of the RCD methodology has enabled the identification of optimal solutions that are counter intuitive and functions of multiple design disciplines.

The Rapid Conceptual Design Methodology

A required step in the RCD process is the creation of an 'integrated system model'. The system model should be capable of sizing the vehicle when given the design constraints. There are several steps to

creating the integrated system model. First the type of system which can best perform the mission must be determined from the design requirements. Next candidate configurations, systems architectures, subsystems, materials, etc. must be identified. For each candidate system the design input and output parameters must be identified.

Sizing modules, which determine the output design parameters given the input design parameters, must be selected or created. These sizing modules must then be integrated (i.e. the modules must be tied together such that the required information is passed between modules). Finally, a sizing closure module must be created to compile final design values and check for constraint compliance and design closure.

After the system model has been developed and verified, the optimization function (i.e. what constitutes the optimal vehicle) must be defined. The optimization function is usually a weighted function of the highest priority design parameters (range, speed, cost, etc.). Once the optimization function is defined, the optimum vehicle can be determined by varying the independent sub-system design inputs. The sensitivity of the optimal design to the design constraints can then be studied by performing parametric trades on each of the design constraints.

The next step in the RCD implementation process was to define a comprehensive list of disciplines and the information required from each discipline to design and develop an aircraft at the conceptual level. A sample minimum set of disciplines for an aircraft design trade study are: aerodynamics, propulsion, weights, thermodynamics, performance, stability and control and cost. Analysis tools capable of providing the minimum functionality in each discipline were assembled and integrated. With the basic library of analysis tools completed, verification cases and new design studies were conducted to evaluate the utility of implementing the RCD methodology in the conceptual design phases with the use of the distributed modeling and analysis tools.

Ideally, RCD software also provides an efficient user environment for the assembly and storage of individual analysis components into an integrated tool for the purpose of subsequent multidisciplinary design. These features will typically be tailored to the preferences of the user in order to extract maximum utility from the tool itself and subsequently ensure continued use of the code. The framework modularity allows the suite of available tools to be expanded to include future analysis tools. In addition, platform independent integration software allows analysis modules to be simultaneously coordinated on multiple computing hardware platforms.

STEREOLITHOGRAPHY (SLA) MODELS

In the past, wind tunnel testing of vehicle shapes was reserved for the preliminary design phase because of the time and expense involved. Typical high fidelity models for low speed wind tunnel testing cost several hundred thousands of dollars and took 3-4 months to fabricate. This cost and time was not appropriate for the conceptual design phase.

During this decade a model making process has been developed which has drastically reduced the cost and time of fabricating high fidelity, low speed wind tunnel models. This process, called stereolithography or SLA, consists of using a UV-curable epoxy resin and an ultraviolet laser to create plastic models from a 3-D file. In this process, the CAD (computer automated drawing) part file is converted to cross-sectional layers, or "slices " of the part .006 inches thick. Using the laser, the SLA machine draws a layer of the part onto the resin, curing a thin cross-section of the part being built. The part is then lowered .006 inches, and recoated with resin. The laser then draws the next layer, which attaches to the previous layer. In this way a part is "grown" layer by layer.

The SLA parts do not have the strength required for large high speed wind tunnel models but do very well for small (approximately 10 percent) and low speed (less than Mach 0.25) model testing. With the SLA process small, high fidelity, low speed models can be built for less than $10K and two weeks from

the time the NC tape of the loft is provided to the SLA operator. This cost and time fits within the conceptual design phase and competes with CFD for doing configuration trades.

The stereolithography process can be used for making parts for things other than wind tunnel models. At LMSW, SLA is used for making display models, RCS models, lay-up molds, patterns for molds, burnout patterns for investment casting, jig drill plates and welding jigs and example parts for proposals.

ADVANCED SYSTEM SYNTHESIS AND EVALUATION TECHNIQUE (ASSET)

The RCD methodology is extremely effective when employed during conceptual aircraft design as several concepts are simultaneously considered, analyzed and pertinent trade studies conducted in order to explore the design space. During conceptual and early preliminary design, the aero group at LMSW uses a higher fidelity analysis tool called ASSET (Advanced System Synthesis and Evaluation Technique) to provide the detail necessary for more focussed trade studies.

ASSET is an analytical design program and data integration tool which analyses the vehicle configuration, weight, and cost through mission and performance analysis. It is a comprehensive data integrating system and analysis tool consisting of contributions from all of the technical disciplines during the early phases of aircraft design. It combines data from configuration design, propulsion, mass properties (structures, materials and weights), aerodynamics, subsystems, cost, and program requirements. All of these disciplines contribute data based on the design concept, customer requirements, and a technology level.

The main function of ASSET is to size (dimensions and weight) the aircraft to meet design criteria. A measure of merit such as the lowest cost, or the lowest weight is the most often used design criteria. To accomplish aircraft sizing, ASSET evaluates the impact of requirements imposed on the design by mission profiles and performance constraints. Parametric studies, where vehicle design parameters are varied, are used to determine impact of constraints across a range of designs. Sample parameters are the thrust-to-weight ratio to represent power plant size, and wing loading to represent airframe size. ASSET can vary these parameters and others to create performance, weight, cost and mission data for comparison purposes. These parameters are often plotted on carpet plots, which show the valid, invalid, and critical regions of the design space. Using these parametric methods, ASSET can rapidly evaluate alternate configurations during the design process.

It should be noted at this point that ASSET is not simply a 'back of the envelope' calculation procedure to quickly generate airplane performance parameters and weights. ASSET requires input from technical disciplines and large amounts of propulsion, aerodynamics, and weight data are required. This often requires time and personnel to acquire data and includes cooperation by several departments (e.g. acquiring engine performance tables or wind tunnel data).

One of ASSETs main features is its geometry routine which will grow or shrink (subject to realistic constraints of crew station, engines, weapons, etc) the configuration to accommodate a change in wing area, engine size, payload or fuel required. Design rules are entered to accomplish the dimension changes. Too often sizing programs will determine the increase in fuel required but not adjust the configuration dimensions to accommodate the fuel. ASSET does not mislead the engineer with this fault.

Lockheed Martin began incorporating ASSET's analysis routine with the NASA Ames Aircraft Synthesis Tool (or ACSYNT) in 1993, forming the ASCENT program. The main menu of ASCENT provides a selection for most disciplines involved with aircraft design. Selecting most of these options will allow the user to edit the portion of the ASSET input file used by these disciplines. Another feature of ACSYNT is its parametric geometry modification capablility, accessed by the user in a 3-D parametric aircraft conceptual modeler. Employing this feature of the ASCENT program, the taper ratio and aspect ratio, for example, may be changed by altering values on the GEOMETRY template. When these parameters are changed, the entire B-spline surface definition of the vehicle is modified automatically.

Once the geometry is defined, aerodynamic analysis can be performed. A Lockheed-developed extension to ACSYNT allowed the parametric geometry to be analyzed by VORLAX, DATCOM, and WAVEDRAG II. The program then processes the output of these aerodynamic analyses and passes it on to ASSET for synthesis evaluation.

AERODYNAMIC PREDICTION CODES

LMSW uses a stable of CFD codes to predict the S&C characteristics, drag and loads during conceptual and preliminary design. These codes are:

Name	Code Type	Grid Type	Application	Full Config Setup Time
VORLAX	Potential Flow	Vortex Lattice	Conc Design, S&C, Prelim Loads	<1 hour
Quadpan	Potential Flow	3D Panel	Conc Design, S&C, Aero Flowfield	4-8 hours
Splitflow	Euler	Intern Gen Hybrid Cartesian Prismatic	Aero/Prop Flowfield	4-8 hours
COBALT (Wright Labs)	Euler/Navier Stokes	Unstructured Polyhedral	Prelim Design Prop Integration	1 week
USM3D (LaRC)	Euler/Navier Stokes	Unstructured Tetrahedral	Aero Flowfield Analysis, Loads	1-4 weeks
Penquin	Parabolized NS	Structured Hexahedral	High Mach Aero/Prop Flowfield Analysis	1-4 weeks
ENS3D	Euler/Navier Stokes	Structured Hexahedral	Prelim Design, Aero/ Prop Flowfield Analysis	1-4 weeks

The first three codes have full configuration setup times less than 8 hours and run times of minutes (VORLAX and Quadpan) to hours (Splitflow) and are used extensively during conceptual design to evaluate different configurations. The remaining CFD codes have setup and run times that limit their application to the fine tuning of baseline designs. In addition to the above CFD codes, LMSW has a complete stable of CEM (computational electromagnetic) codes for RCS predictions.

SUMMARY

The aerodynamicist is at the center of the early design of an aircraft or missile as he "owns" the configuration OML through his control of the aerodynamics data base and performance. The aerodynamicist must have tools to predict the aerodynamics, S&C, performance and loads that are accurate and rapid turn-around. With these tools the aerodynamicist can reduce the time spent in early design (conceptual design to OML freeze).

DISCUSSION

Keynote Session, Paper #4

Dr Khalid (NRC, Canada) offered thoughts on need for both structured and unstructured codes as each was suited to particular types of problem that were likely to be encountered in initial design.

> **Dr Nicolai** concurred.

Mr Woodford (DERA, UK) wondered whether aerodynamicits were in fact the people best qualified to drive the overall design of an air vehicle, for example given likely pressures to ensure an affordable design.

> **Dr Nicolai** sought to confirm that he had not intended his comments to apply to the overall vehicle design, but merely to its outer mold line (OML). He did not believe that OML was a first order cost driver.

Herr Sacher (DASA, Germany) wondered whether the design team's interactions described in the paper would still work if the teaming were "virtual".

> **Dr Nicolai** suggested that, whereas the interactions probably would work if the teaming were virtual, his preference was still for collocation, given the importance of direct personal contact.

Mr Templin (NRC, Canada) requested amplification of the author's assertion that "the aerodynamicists own the OML", citing as an example the F-117 where the shape was clearly constrained by other disciplines.

> **Dr Nicolai** accepted that aerodynamicists might very well have constraints, sometimes significant constraints, imposed on them but, nevertheless, they are the group that has to ensure that the vehicle will "fly". He was adamant that whatever these constraints might be, this responsibility determined that no-one was able to modify the OML without aerodynamics approval.

Prof Straznicky (Carleton University, Canada) wondered how much interaction there was between aerodynamics and the other disciplines in the early conceptual design phase.

> **Dr Nicolai** replied that the interaction described took place through normal operation of the IPT. He noted that this met at least weekly. He further noted that ideally all disciplines should be collocated "so that there is no excuse for not getting together daily".

LEARNING THROUGH EXPERIENCE: GROUP DESIGN PROJECTS ON THE MASTERS COURSE IN AIRCRAFT ENGINEERING

R I Jones
Aerospace Design
College of Aeronautics
Cranfield University
Cranfield
BEDS, MK43 0AL, UK

R G Scott
British Aerospace
Military Aircraft & Aerostructures
Warton Aerodrome
Warton, Preston
LANCS, PR4 1AX, UK

1. ABSTRACT

The successful completion of aerospace projects usually involves the bringing together of many different specialist skills. The need for aerospace engineers to be conversant with many disciplines and aware of the many facets of a project is today's reality. However, in today's working environment it is becoming increasingly difficult for individuals to achieve the necessary experience, with the timescales for major aerospace projects getting ever longer and their number decreasing.

The Group Design Projects within the Aircraft Engineering course have the specific purpose of addressing this issue. They provide the opportunity for aerospace engineers from a range of disciplines to be involved in a real project, with many of the difficulties and constraints of those they will meet in their working lives. These projects progress through the full design process and provide this experience within a limited time period and, relatively, limited risk environment.

In addition to meeting their basic objective, Group Design Projects commenced to-date have proved very demanding but provided further benefits to all concerned.

2. ABBREVIATIONS

ACSL	Advanced Continuous Simulation language
AE	Aircraft Engineering (course)
AVD	Aerospace Vehicle Design (course)
BAe	British Aerospace
BWB	Blended Wing/Body
CAA	Civil Aviation Authority
CAD	Computer Aided Design
CoA	College of Aeronautics
DERA	Defence Evaluation Research Agency
GDP	Group Design Project
GFRP	Glass Fibre Reinforced Plastic
LSWT	Low Speed Wind Tunnel
MA&A	Military Aircraft & Aerostructures
UAV	Unmanned Air Vehicle

3. INTRODUCTION

The Aircraft Engineering course is a three year part-time MSc course which comprises the same major elements as the very successful full-time MSc course in Aerospace Vehicle Design. That course has been running and attracting students from all over the world, with the same basic philosophy, since the College of Aeronautics(CoA) was founded in 1946.

The students on the Aircraft Engineering (AE) course attend lecture modules, perform a piece of individual research and work on a Group Design Project (GDP). It was this last element that particularly attracted the launch and predominant customer for the course, the then Military Aircraft Division of British Aerospace (BAe), with its basic philosophy of teaching the design process by placing someone in a project group with an individual responsibility but having to cater for the needs of the group as a whole. The basic objective of this is to provide a 'virtual industry environment' so as to better equip the students for the real situations in which they are likely to have to apply their aerospace engineering and science knowledge.

In this paper the basic organisation of the GDPs on the AE course is described, followed by details of all five GDPs commenced to-date. Due to both authors' direct involvement in the first GDP and one author's involvement in the third, these two will be described in rather more detail than the other three. Some general considerations, difficulties, plans for the future etc. are then discussed and finally some conclusions drawn.

4. GENERAL ORGANISATION OF GDPs

The GDP on the full-time course in Aerospace Vehicle Design concentrates on the initial design of parts of an aircraft, which has been previously defined in terms of basic geometry, mass, performance characteristics etc. by staff. However, BAe wished to address a greater extent of the design process in the AE MSc, with progression all the way from conceptual design, through preliminary and detailed design to manufacture, clearance and flight. In this way the students would, in the space of three years, be given first-hand experience of a much wider extent of an aerospace project than could ever be the case whilst working on major aircraft projects in a present military airframe manufacturer.

The detailed organisation of the GDPs on the AE course has varied slightly from one project to the next and in the sections covering each of the projects to-date these differences will be explained. However, there are some aspects which remain the same.

At present, there is no formal mechanism for choosing the subject of GDPs. It is hoped that this may change in the future but certainly there are a number of characteristics which are required for a subject to be suitable. To meet the basic objectives of the GDP, the subject must be such that it covers a wide extent of the whole design process from concept to flight and it is possible to do this within the constraints of a three year time frame, the effort available from the student group (with a little external assistance) and a restricted budget for the project. In addition, the subject should involve real clearance and safety issues (to concentrate the minds of all those working on the project) and should capture the interest of the students.

The projects commence soon after the beginning of each student intake's course and are formally progressed through GDP meetings held at regular intervals during the following three years. There is usually a meeting during each of the three lecture modules held at the CoA for that intake of students each year. In addition, there are usually two or three meetings in between these modules. These are usually rotate around the sites where the students are located and can give an opportunity to see and, in some case, make a tour around the sites, for the benefit of those who may not have visited them before.

The GDP meetings are jointly chaired by one member of staff from CoA and one senior engineer from BAe. The chairmen are directly involved in ensuring the overall progression of the project. However, they also act as a source of information and contacts, at BAe and CoA, useful to assist in the project.

In addition to the formal GDP meetings, the students are likely to hold further meetings, of the whole or part of the group, to address particular aspects. It has also been the case that the system of formal Design Reviews, used by BAe on there own projects, has been applied to the GDPs, though in a reduced fashion appropriate to the scale of these projects. This has both exposed the students to necessary preparation for such formal Reviews and performed the real function of subjecting the GDP work to the scrutiny of experienced engineers, independent of the project, to support the case for clearance to fly the results of the project.

As the GDP forms part, in fact the largest single part, of the assessment on the AE course, there is individual output required from each student on their personal contribution to the GDP. This takes the form of interim reports/presentations at around one and two years into each GDP that count towards a small part of the GDP assessment. The major part of the GDP assessment is through submission of a GDP final report or 'thesis'. This is submitted 3 months prior to the end of the student's three year course. Ideally, this would be following conclusion of the real work on the project. However, in practice, for the student intakes that have completed the course to-date, the GDP has not been completed at the point of submission of their GDP thesis. This is not a problem in terms of academic assessment of the work and, due to BAe's commitment to the GDPs, has not proved to be a problem in the students working on the GDP to see it to a real conclusion.

The tasks to be performed within the project, their size and whether they exist for the full length of the project obviously depend on the subject of the GDP. However, as a general principle, students are encouraged to have at least some say in selecting which tasks and responsibilities they will take on. This allows a student to either stay in an area with which they are familiar or broaden their own personal experience whilst possibly providing guidance to other students in there normal sphere. There is, of course, a need to cover all the necessary tasks and responsibilities for the project. Therefore, there sometimes needs to be an element of gently persuasion to ensure this is the case.

5. GDP FOR THE 1995 INTAKE

The Aircraft Engineering course was launched in February 1995 with 15 students, all from BAe Military Aircraft. The GDP that they were presented with was to work on modifications to Cranfield's own single seat A1 aerobatic

aircraft, which had resulted from previous MSc student work, to provide a two seat aerobatic trainer. This provided the realistic possibility for a project to progress through to manufacture and flight. However, it should be noted that at the outset there was no guarantee that it would do so.
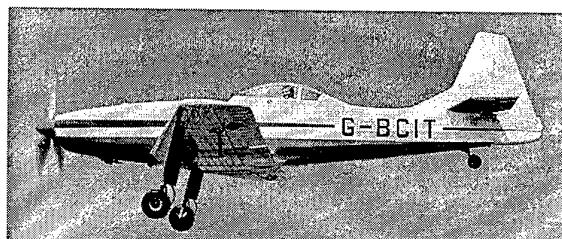

Figure 1 The original single-seat A1 MkII.

5.1 Initial Conceptual Phase

The students had been set an exacting specification for the two seat aircraft, with performance equal to or better than that of the existing single seat version, the A1 MkII, Fig. 1. This was an intentionally difficult requirement for an aircraft to be produced by modification , in order to get the students to consider some fairly radical modifications or even starting again with a blank sheet of paper.

	Existing A1 MkII	Two-Seat A1
Max. level Speed	76.1 ms^{-1}	80 ms^{-1}
Climb Rate	13.5 ms^{-1}	12.5 ms^{-1}
G limits	+7/-5	+6/-3
Roll Rate	150 deg/sec	150 deg/sec
Range	238 km	800 km
Stall Speed	25 ms^{-1}	25 ms^{-1}

Table 1 Comparison of the specification requirements set for the two-seat A1 with that of the existing A1 MkII.

During the initial phase, the students worked in three competitive groups, initially designated the Red, Blue and Green teams, to consider and present approaches to meet the specification. However, the students had soon renamed these the 'Well Red', 'Blue Sky Project' and 'Cranfield Aerobatic Project' teams.

Following consideration of a number of options by each team, they presented their chosen approach to the 'customer' consisting of senior staff of BAe and CoA. Not surprisingly, it was clear from the options presented, that the initial specification could only be met by major modifications to the existing airframe of the A1 and/or re-engining with a more powerful unit. Therefore, the 'customer' chose to specify a list of what became known as 'affordable' modifications to be progressed through the remainder of the project.

5.2 Definition of Individual Responsibilities

The affordable modifications were defined to provide the aircraft with a basic two seat capability and increased range with an attempt to approach the other specification requirements without the need to resort to replacement of major airframe elements or the engine. These modifications were split into the following task areas, each the responsibility of a student:

    Canopy
    Trailing Edge Flaps
    Fuel System Extension

Front Cockpit Seat, Controls and Instruments
Electrical System Extension

In addition, to these, however, some more radical changes were also to be progressed by other students. These would allow the possibility of meeting, or more closely approaching, the full list of requirements. These 'major' modifications, as they were termed, were as follows:

Composite Wing Design
Semi-Monocoque Metal Fuselage Design
Composite Fuselage Design 1
Composite Fuselage Design 2

The distinction between the two composite fuselage designs was to be that one would be suitable for one-off production, and thus treat production costs as paramount, whilst the other would treat the minimisation of mass as most important, and thus may only be suitable for series production.

As well as specific changes to the aircraft, a number of generic tasks, to be covered what ever changes were adopted, were also identified as necessary and defined as a responsibility of a student. These were:

Performance Evaluation
Wind Tunnel Testing
Mass & C.G. Control and Stability & Control Issues
Load and Fatigue Analysis
Structural Dynamics and Aeroelasticity
Flight Test, Instrumentation, and Certification

The student given the responsibility of Performance and Evaluation was also given that to design modified wing/fuselage fairings and wheel spats, which had been identified as a possible means of reducing drag. Whilst all the students needed to consider aerodynamic aspects, as they impacted on there particular area of responsibility, it was in these generic tasks that aerodynamics was particularly addressed.

5.3 Modification Design Phase

From the point that the students individual responsibilities were defined, they worked on as a single group, holding regular project review meetings. Professor Denis Howe had initially taken on the role as CoA GDP chairman and, due to his invaluable experience of the A1, was heavily involved in the project through-out. However, in February 1996 Robert Jones took on the role as CoA GDP chairman, joining Roy Scott, who was acting in this capacity for BAe.

Each of the students produced a statement of work for their responsibility area. These were then considered together to define the necessary timescales, due to dependency on outputs from other students.

Twelve months into the project a major Design Review meeting was held at Cranfield. At this the students presented their work to that date and plans for the remainder of the project to senior staff of BAe and CoA, again acting as both 'customer'. As a result of this, the commitment of both BAe and CoA to carry the project through to manufacture and flight was confirmed. Shortly after this, one of the students left BAe and his responsibilities for the cockpit controls etc. were redistributed amongst the other students.

Over the following few months facilities for manufacturing the necessary components within BAe and, where necessary, externally were investigated. Initial costs for manufacture,

bought out items and installation on the aircraft were gathered with one of the students taking on the role of co-ordination of these production related activities.

By approximately 18 months into the project it was clear that the students' other work commitments was slowing progress on the designs for affordable modifications to the extent that manufacture and installation could not be achieved within the timescale of the course. Therefore, BAe, took an important step in agreeing to students working on the affordable modifications taking part in an intensive two week placement at CoA to progress the designs with the advantage of co-location with the aircraft and the existing A1 drawings and information. In addition to the students who had responsibility for the affordable modifications, the other students and some senior engineering personnel from BAe joined the placement to assist in the design work for at least part of the two weeks. At this stage it was also decided that, due to the urgent need to progress the affordable modifications, teams for each modification would be formed with the student whose responsibility it initially had been acting as task leader. This required that work on the major modifications had to be suspended. Although it was the originally intention that the students working on the major modifications would return to these tasks once the affordable modification designs were completed, in practice little time remained to do this at the end of the project.

It was at this time that a second student, with the responsibility of the canopy design, left BAe. Thus, a further redistribution of responsibilities was necessary. One of the students, who had originally had one of the major modifications as his responsibility, took on this task.

The decision by BAe to allow the two week placement and the significant cost involved in the loss of students from their other commitments for that period was very important. During this period the state of the design for all the modifications was significantly advanced, providing an impetus without which the project would have been very difficult to complete.

5.4 Progression to Manufacture

Once drawings produced by the students were completed, these were checked, along with stressing calculations etc., by a further nominated student at each BAe site before despatch to Cranfield. The CoA retains full Design Authority on the A1, so whilst the drawings had been produced and checked within BAe and were usually issued back to BAe for manufacture, they were also checked by the Aircraft Design Group within Cranfield Aerospace Ltd. In particular, Chief Stressman Phill Stocking took on the responsibility of checking and issuing on behalf of the CoA.

The CoA had held discussions with the Civil Aviation Authority (CAA) at an early stage to inform them of intentions with regard to the modifications and discuss necessary procedures for certification in this case. The original A1 design had been performed to the British Civil Airworthiness Requirements, Section K. However, these have now been superseded by the Joint Aviation Requirements, Part 23. Thus, it was necessary to determine which areas should remain covered by the original requirements and which needed to satisfy the newer ones. The CAA were kept informed of progress and consulted on issues, as necessary, through out the project.

The majority of manufacture of items was performed by BAe at its Brough and Warton sites and for this purpose drawings and orders were issued to BAe for these. Therefore, BAe became a supplier to the CoA and, to satisfy the CoA's quality procedures, the CoA's Quality Co-ordinator and Chief Aircraft Inspector had to visit the BAe sites to assure himself that they were a fit supplier!

The CoA purchased all bought out items and, if necessary, issued these on to BAe for inclusion in the component assemblies to be supplied back to the CoA. At an early stage it was realised that there were a number of differences in methods and procedures between BAe and CoA. However, as the process of issuing drawings for manufacture commenced, other differences emerged and solutions to these were discussed and agreed, with up-dating of drawings etc. as necessary.

In order to progress the final stages of the design and address manufacturing issues as they arose, the full GDP review meetings, attended by all students, were supplemented by weekly progress meetings using teleconferencing between task leaders on the major modifications and others, as necessary.

5.5 Installation and Assembly of the A1-200

By the end of 1997 the initial components produced by BAe began to arrive at Cranfield for installation on the aircraft. In the meantime the aircraft had been substantially dis-assembled and stripped of its fabric covering . Necessary maintenance work on the airframe and in particular its undercarriage was performed. In addition, some preparatory work for modifications to the aircraft being worked on by the second (1996) intake on the Aircraft Engineering course was also performed.

Installation of the modification components on to the aircraft began with the items placed within the fuselage, prior to its re-fabricing. These included the control extensions, seat and instruments for the forward cockpit, the battery tray and mounting for a new GPS navigation/radio unit in the rear cockpit. The fuselage was then re-covered and painted, along with the wing, in a colour scheme to match the CoA's other aircraft. Next the canopy, which had been trial installed prior to re-covering, to ensure the new latching and hinging interface details were correct, was fitted.

5.6 Wind Tunnel Testing

Whilst manufacture of the canopy was progressing, one of the students, responsible for wind tunnel, testing was investigating the aerodynamic effects of it. The 1/7 scale wind tunnel model of the A1, produced during the original design work on the aircraft, was taken to BAe Warton and after some restoration work was used in the 4.0 m Low Speed Wind Tunnel (LSWT) facility there to investigate the effect of external modifications. The changes investigated included those from the addition of the trailing edge flaps but the canopy changes represented a major part of the tests carried out, Fig. 2.

The wind tunnel model had two new canopy shapes added to it for these tests, one representing a canopy composed of three single curvature shapes and a second modelling the canopy shape actually produced. Both these new canopy shapes were produced directly from Computer Aided Design (CAD) models using stereo-lithography techniques. The tests performed showed that canopy of the actual shape used had insignificant effect on the drag and acceptably small effect on stability derivatives.
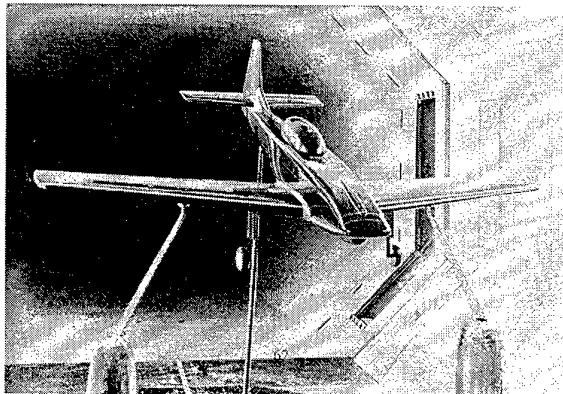
Figure 2 The A1 model in the LSWT at Warton

Whilst these wind tunnel tests did not identify any real problems for the two seat aircraft. They did provide a useful lesson in the measures necessary during the collaboration between organisations. The 4 m tunnel at Warton has a substantially automated system for recording measurements and converting them directly into the various non-dimensional derivatives. Initially, their appeared to be a significant alteration in the value of some of the lateral derivatives. However, it was then realised that the difference was almost a factor of two and the reason was the definition of non-dimensional derivatives produced by the Warton analysis system did not match with the standard notation used to define the same derivatives for the original two seat A1. This provided a useful reminder that even things which are expected to be and apparently are the same in different organisations may not be and should always be checked.

5.7 Predictions for the A1-200

It is worth noting at this stage that the other students with generic responsibilities showed through their work that structural dynamic problems would not result from the modifications (in particular the flaps), centre of gravity travel would remain basically within the limits of the A1 MkII and basic empty mass of the A1-200 would be just under 100 kg greater than the A1 MkII. The final generic task student, working on performance evaluation, predicted that whilst the A1-200 should meet or exceed the requirements set in the specification for range and roll rate and almost achieve those for maximum level and stall speed, it would fail to achieve the climb rate by a substantial margin, at only 10.6 ms^{-1}. However, without a substantial reduction in airframe mass and/or drag or a more powerful engine, it was accepted that this requirement could not be met.

5.8 Conclusion of the A1-200 Project

Following re-assembled in its two-seat configuration, the aircraft was readied for its official Roll-Out at Graduation Day on 12 July 1998. On that day all 13 of the students, who completed the course, graduated with a Masters in Aircraft Engineering. This must be judged a considerable achievement on their part. Whilst playing their part in the GDP work on the A1, they had attended and been assessed in lecture modules, performed research work on an individual topic, produced theses on there individual research and GDP responsibilities as well as holding down a full-time job at BAe and meeting their family commitments.

Following the roll-out the aircraft underwent further preparation and ground test prior to first flight. The official first flight took place on 30 September 1998, when the CoA's own Chief Test Pilot, Roger Bailey, provided a limited display of the aircraft in front of an audience of invited guests from industry and the media, following naming of the aircraft the Cranfield A1-200 'Eagle' by Dr Kenny-Wallace, Vice Chancellor of the BAe Virtual University, Fig. 3.

Figure 3 First demonstration flight of the A1-200 Eagle.

A great deal of documentation was created during the course of this project including meeting minutes, formal drawing, stressing calculations, orders etc. Much of this has now become part of the formal records of the A1 and is unpublished. However, for further detail on the project as a whole and the individual tasks performed by the students reference can be made to their GDP thesis (Refs. 1-13) which are lodged in the Cranfield University Library.

6. GDP FOR THE 1996 INTAKE

Ever since the A1 aerobatic aircraft first flew in 1976 there have been attempts to improve its capabilities and flying qualities. In particular, the following year the aircraft had a more powerful engine fitted than the original unit and a larger rudder. Even so, there are still aspects of the aircraft's handling qualities which could be further improved upon. One particular aspect is that the aircraft's flick roll capabilities leave something to be desired.

It has been generally accepted that the major factors affecting the A1's flick roll capabilities were a rudder effectiveness, which was too small in comparison to the aircraft's directional stability, and development of wing stall close to the root in the initial stages of the manoeuvre. Various measures had been introduced and attempted to address these problems including:

    Increase in rudder horn size
    Reduced size dorsal fin
    Removal of dorsal (subsequently replaced due to
    tendency to rudder overbalance)
    Addition of undercarriage leg fairings
    Measures to clean up flow over lower rudder

The problem with the lower rudder was the 'step' between the relatively wide fuselage and narrow fin was causing separation and thus loss of rudder effectiveness.

In 1989 a dedicated series of flight tests on the aircraft, using triangular stall breaker-strips on the wing leading edges at approximately mid-span of the ailerons and vortex generators on the rear fuselage in front of the lower rudder, provided a significant improvement in the aircraft's flick roll characteristics. The breaker strips were found to produce some problems at high incidence and during spin recovery but

the tests had proved the possibilities of improving flick roll performance. Therefore, the students on the 1996 intake of the AE course were set the task of improving the A1's lateral stability and control characteristics, in the knowledge that the aircraft that they would modify should, by then, be a two seat aerobatic trainer.

The GDP chairmen for the project were initially defined as Steve Jones from BAe Salmesbury and Steve Molnar from the CoA. However, Phill Stocking took over the role for the CoA when Steve Molnar left to return to BAe Airbus after approximately 12 months of this GDP.

Unlike the 1995 intake GDP, the 12 students who began the course were allocated individual responsibilities on the project from the beginning. These were initially as follows:
    Aerodynamic and CFD Analysis
    Novel Concepts
    Fin Design
    Structural Test
    Flight Controls
    Rudder Design
    Tailplane and Elevator
    Manufacture
    Fuselage Investigation
    Fatigue and Fracture
    Performance and Stability
    Project Management and Flight Test

However, during the first year of the course four students withdrew and a significant reallocation of tasks became necessary.

As might be expected, the modifications to the aircraft concentrated on methods of improving the flow over the lower section of the rudder but other methods of improvement were also considered. A lack of torsional stiffness of the rear fuselage was considered to be possibly adding to the loss of rudder effectiveness and thus one student investigated methods of increasing the stiffness of the tubular steel structure in this area. Another student considered novel methods of reducing the aircraft's lateral stability by addition of a 'canard fin' either above or below the forward fuselage or increase of size of the undercarriage leg fairings. Whilst none of these possibilities was in fact carried through to be embodied as actual modifications on the aircraft, they did form a useful part of the survey of possible approaches.

In practice, the major modification selected for progression to manufacture was the design of an increased thickness rudder and matching fin removing the step at the end of the rear fuselage. This required modifications to the control circuits for rudder and elevator in the rear fuselage area, of the dorsal fin and fin to tailplane fairings.

Fortunately, the modifications to the control circuits had been defined when the fuselage fabric was removed during the work prior to the installation of the modifications for the A1-200 and, therefore, could be achieved with little disruption. Some of the preparation for other changes, for what was termed the A1-400, were also made at this stage.

Whilst there was no specific requirement to do so, considerations of weight linked to the experience it would provide led to the choice of composites for the new fin and rudder to be manufactured for the A1-400. However, in considering the likely cost of production of two fins and

rudders, one for flight and one for structural test, it was found sensible to consider production of these items outside BAe. Following survey of and discussion with a number of potential manufacturers, Slingsby Aviation Ltd were chosen to manufacture the composite components incorporating metal hinges and brackets etc. produced within BAe.

The type of structure chosen uses substantially monolithic Glass Fibre Reinforced Plastic (GFRP) spar and rib construction with GFRP skins, Fig 4. This structure is being produced by manual wet lay-up of cloth laminates, with inclusion of metallic, foam and wood components as necessary, using minimum tooling.
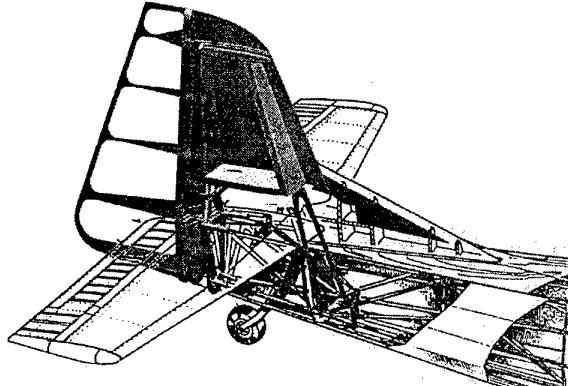
Figure 4 CAD representations of the GFRP fin and rudder for the A1-400.

The process of production of drawings and calculations by students followed by approval and issue by Cranfield Aerospace, as for the A1-200 modifications, was again followed in this case.

At the time of writing, seven of the eight students, who remained on the course at the end of the three years, successfully graduated in June 1999. The eighth student has been granted an extension to perform work towards his individual thesis. However, the GDP is not in practice complete. An order has now been placed with Slingsby Aviation for the two fin/rudder sets, with delivery to Cranfield planned for October 1999. One set will then be statically tested, prior to fitting of the second set to the aircraft for flight. It is possible that a first flight of the A1-400 may occur during 1999 but this is likely to be dependant on the weather.

Further detail on the A1-400 GDP and the student's individual work can again be found in the GDP thesis that they have produced (Refs 14-20).

7. GDP FOR THE 1997 INTAKE

Whilst the GDP subjects for the 1995 and 1996 intakes picked-up on Cranfield's unique position as a University having its own aircraft and holding design authority and approvals to modify it, the subject chosen for the 1997 picked-up on another unique area of the CoA's experience.

The CoA has for many years worked for and along with the UK Defence Evaluation and Research Agency (DERA) on development of all the aspects surrounding small Unmanned Air Vehicles (UAVs) particularly for surveillance purposes, Ref 21. For the 1997 intake GDP it was decided to utilise this experience to assist in the production of a UAV, to be designed from scratch, which would provide a tool for the investigation of the characteristics and suitability of various flight control laws and strategies when applied to unconventional aircraft configurations. This also recognised a rapidly growing general interest in the use of UAVs for various roles.

7.1 Specification

The initial specification for the UAV provided to the group of 16 students who started the course was, intentionally, rather vague but contained the following key design drivers:

1) The aircraft should be powered by jet propulsion with the capability of operation for around 15 minutes.

2) It should be able to take-off from its own landing gear, which should either be initially retractable or with the intention to retract it at a later stage, and approach speed should be limited to around 40 kt.

3) It should be capable of operating within the confines of a suitable airfield without the need for bank angles in excess of 45 degrees.

4) Adequate safety provision, in the event of a failure, should be provided to minimise the risk to third parties or property.

5) The vehicle span should be less than 2.5 m and its mass low enough to allow two people to safely lift it.

6) The vehicle should be of novel configuration to investigation of the characteristics of such a configuration, preferably with a construction which would allow alterations to the configuration without major alterations to the central core systems/engine element of the vehicle.

To minimise the work, and risk, involved in development of all the electronics and associated sensors and systems necessary to fly and control the UAV, permission was sought from and granted by DERA to use the electronics package developed by CoA in its work with DERA to fly conventional UAVs of a design which had become known as XRAE vehicles. This 'XRAE crate' contains all the electronics and sensors, or connections to sensors, necessary to control and fly an air vehicle with neutral or slightly negative stability, the electronics for a command and control link and electronics for a telemetry link.
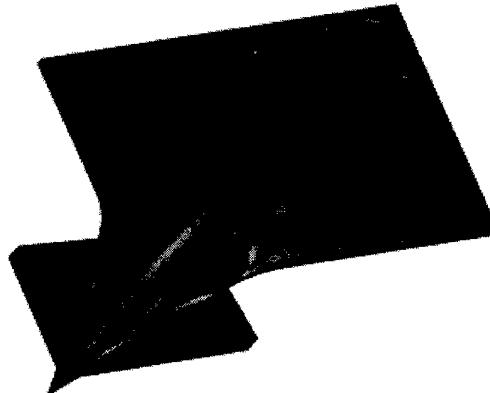
Figure 5 Initial 'Double Diamond' configuration.

7.2 Configuration Studies

The initial task of the group was to select a configuration for the vehicle. Configurations were suggested by most members of the group, ranging from the relatively conventional to the outlandish. Following parametric studies a 'Double Diamond' configuration (Fig. 5) was chosen.

However, following initial aerodynamic assessments, it was decided that the inclusion of the close-coupled canard represented too great a risk and the design evolved into a single diamond wing with dorsal engine intake, Fig. 6. Based on the students, ever optimistic, forecast of an expected first flight of the UAV in August 1999, they named it Eclipse due to the total eclipse of the sun over parts of the UK and Europe on 11 August 1999.
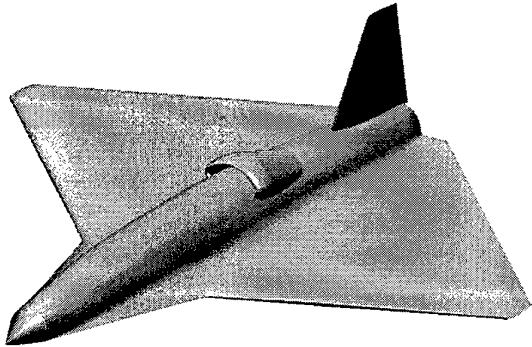

Figure 6 Final configuration of the Eclipse UAV.

7.3 Group Organisation

Although all members of the group took part in the initial configuration selection, they all selected individual roles for the project at the start. Due to the limited numbers involved, even at the start and to reduce to only 11 during this last year of the project, students generally took on more than a single role. However, in addition to the overall tasks of programme management, certification, cost etc., the group arranged itself into four major areas:
1) Aircraft systems (engine, fuel, flight controls, electrical power and physical interfaces with the XRAE crate).
2) Structural Design (including integration of all equipment).
3) Flight Controls and Simulation (concerning interpretation of aerodynamic data and development of the flight control laws to be programmed into the XRAE crate).
4) Aerodynamics (focusing on configuration issues, aerodynamic predictions, wind tunnel testing and intake design).

Roger Myers from BAe Brough Design took on the role of GDP chairman for BAe and Pete Thomasson, initially, took on this role for CoA. During 1999 Robert Jones took on the role of CoA chairman, to release Pete Thomasson to provide increased assistance to the project in his area of personal expertise, flight control law development and simulation.

7.4 Structural Design

The design of the Eclipse structure is based on construction techniques used in the production of previous vehicles of similar size for the CoA and DERA. These use hand lay-up of composites to provide foam core/composite skin, honeycomb sandwich and monolithic composite structures. Due to the restricted budget available, only a single vehicle was to be produced and so tooling costs had to be minimised. TASUMA UK Ltd, the supplier of previous similar size vehicles to CoA and DERA, was engaged to manufacture the air vehicle with the above considerations in mind.
The basic structure consists of a single piece foam core wing, skinned with carbon. A central bath tub in this wing houses the engine (with tail pipe and inlet duct) and the fuel tank. The XRAE crate is mounted on a carbon channel beam

extending forward of the wing. The fuselage is effectively a fairing simply reacting local aerodynamic loads.

It will be noted that the construction used does not allow a great deal of scope for modification of the configuration. However, there are some possibilities through alteration of the forward fuselage 'fairing' and through items which might be attached to this and the 'customer' (CoA and BAe) accepted the limitation in order to reduce design risks and limit cost. It should also be pointed out that the cost of airframe manufacture itself, whilst significant, is not the major cost when compared to aerodynamic and control law development that would be necessary, were the configuration to be changed in the future.

7.5 Systems

As previously indicated, the XRAE crate was to be used to provide many of the necessary functions for the UAV. However, it requires connection to a number of external items of equipment to do this. These include power supplies, antennas, actuators and air data sensors. Whilst many of the items are apparently off-the-shelf bought-out equipment, in practice some items have proved difficult to obtain at all and the restricted budget has caused difficulties for obtaining others. Credit must be given to the student responsible for identifying suppliers of the necessary equipment for obtaining it at not only significantly reduced cost but even, in one case, on 'free loan'.

The actuators necessary for operation of flight controls and undercarriage are high quality model aircraft items. They are in fact being used in the new small, delta configuration, surveillance UAV developed by CoA for DERA, the A3 Observer but it should be emphasised that they were selected only following testing by CoA to ensure they provided the desired characteristics, as manufacturer's data does not provide the necessary information.

The single main item of equipment open to selection by the group was that of the engine. After survey of a number of potential units the AMT Olympus engine was selected. This produces a maximum thrust of 190 N at a fuel consumption of 400 gm/minute. However, again the manufacturer was unable to provide all the information on the engine necessary to producing the control algorithms for integrating it into the flight control system. Therefore, the engine was obtained and a test rig produced to allow the necessary information to be gained.

The fuel system normally used for the AMT engine was not considered feasible for the durations required in this case. Therefore, a welded aluminium tank was designed allowing operation of the engine in all positive 'g' manoeuvres. Whilst this will not allow the aircraft to perform inverted flight, the XRAE crate cannot function in this attitude either.

The undercarriage and retraction mechanisms were initially selected to be off-the-shelf model aircraft items but the potential supplier ceased operation. Therefore, a similar design, using pneumatic retraction and brakes controlled, along with the nose wheel steering, by the same type of actuators as the flight controls has been developed.

7.6 Flight Control and Simulation

Whilst the XRAE crate provided the necessary hardware to support a fight control system for the Eclipse, a new set of control algorithms was necessary to match its characteristics. A full 6 degree-of-freedom model of the air vehicle has been developed. This uses aerodynamic derivative estimation from wind tunnel test data and empirical estimation methods such as ESDU and DATCOM.

The model and simulation have been developed using Advanced Continuous Simulation Language (ACSL), which has previously been very successfully used in support of the CoA/DERA work on UAVs. Two complete models are being produced. The first has all discontinuities removed and is used to develop the basic laws and augmentation requirements. The second model includes discontinuities and quantisation errors and will form the basis of the flight simulation work to assess the vehicle's anticipated behaviour. It can also be used to explore the flight envelope during normal flight and failure cases or determine the sensitivity to errors in the data used to build the model and develop strategies to deal with these.

7.7 Aerodynamics

From the outset it was intended that Eclipse would be longitudinally neutrally stable and that, although a fin and rudder would be present for initial flights, the vehicle might be flown later without these. Therefore, accurate prediction of the air vehicle aerodynamic characteristics, both lateral and longitudinal was essential to successful development of flight control laws for the vehicle.

A major contribution to determination of aerodynamic characteristics was obtained through the opportunity to perform wind tunnel tests on the configuration. A tenth scale flat plate wing model with fuselage shaping was produced with the intention of testing in a small blower tunnel at BAe Warton. However, at the point of testing, the 4 m LSWT was free and used instead, Fig. 7. The type of model used provides a relatively cheap method of obtaining representative aerodynamic data and the small model was 'calibrated' by also testing a flat plate model of a similar configuration for which data at a Reynolds number close to that of Eclipse was available.

One key objective of the tests was to determine the optimum forward fuselage strake design necessary to maintain neutral stability at high incidence and three strake configurations were tested. Trailing edge control surface effectiveness was investigated through bending of the wing plate using cuts in the trailing edges and the effects of spoilers, to provide lateral control in the 'fin-removed' case, were investigated.

The wind tunnel tests showed that the configuration has essentially linear characteristics in all axes, up to around 10° incidence. With increase in incidence the configuration becomes progressively more stable (longitudinally). The forward fuselage strakes counter this tendency and with the fin the configuration maintains positive lateral/directional stability up to around 20° incidence. This is close to the maximum trimable incidence using inboard trailing edge devices alone for pitch control and give a C_{Lmax} of around 0.8.

Data from the wind tunnel tests with regard to the spoilers suggested that these alone would have difficulty providing lateral control without the fin and, since they were not required for other reasons, they were deleted from the vehicle, at least for the present.
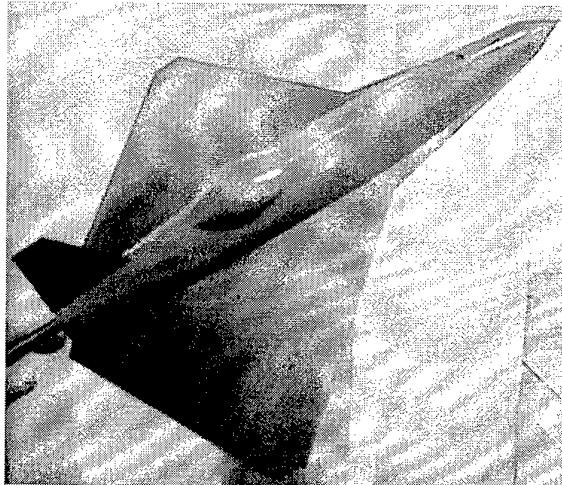
Figure 7 Eclipse model tested in the LSWT at Warton

One other area of aerodynamic risk not address by the wind tunnel tests was that of the engine intake. The choice of a dorsal intake and constraints on equipment positioning within the fuselage led to a short highly off-set 'S' duct, which, in addition, needed to accommodate a rapid expansion in area to cater for a cooling flow around the engine casing as well as one into the centre of its centrifugal compressor. CFD has been used to investigate this aspect. An Euler method was used to investigate the external flowfield in the vicinity of the intake. A Navier-Stokes method was used for examining internal flow characteristics in the duct. Whilst a 'dead' area close to the wall of the duct after the knee was identified using the latter analysis, the affected area would bypass the engine as cooling flow with the flow into the core predicted to behave well. This finding will, however, be born in mind particularly during ground testing of the engine when installed, with temperatures being monitored appropriately.

7.8 Overall Project status

At the time of writing, construction of the air vehicle is at an advanced stage, a number of the bought out items have been procured and arrangements for testing of the engine are being made. Development of the flight control system is well underway and, whilst this is recognised as one of the critical paths to first flight, additional resources from the student group and Pete Thomasson are being applied to this. Following completion of the airframe and some structural tests, it will be equipped with various equipment items at CoA and the XRAE crate, programmed with the relevant flight control laws etc. The aim at present is still to fly within the year of the eclipse of the sun, with a first flight programmed in November.

Three of the students involved in this project gained some useful additional experience earlier this year when they presented a paper on there work on Eclipse to the RPV/UAV Systems conference in Bristol, Ref 22. This paper provides further details on the work on the project up to that point in time.

8. GDP FOR THE 1998 INTAKE

There is considerable interest around the world at present in Blended Wing/Body (BWB) configurations. These have been suggested for a number of different roles, in particular, very large, 600+, passenger airliners and global range military transport aircraft. They represent an attempt to side-step the law of diminishing returns we see in trying to extract further gains in efficiency (both fuel and economic) from the conventional distinct wing, fuselage, trim surface configurations. However, they bring a number of difficulties, not least, the fact that many of our conventional design methods rely on essentially empirical data and are not easily applied to any novel configuration. In addition, the functions of the various elements and applicable analysis techniques for conventional aircraft allow us to break the design problem down in a way that the physically integrated BWB configuration does not.

In keeping with the world wide interest in BWB configurations, the CoA has put together a programme of research activities aimed at addressing some of the issues surrounding them. This involves individual research of MSc students on a number of courses and GDPs on both the Aerospace Vehicle Design (AVD) and AE courses. The estimated total commitment of staff and student time, at present defined for the full 3 year programme, is approximately 76,000 man-hours.

The GDP for the 1998 intake on AE is aimed at design, manufacture and operation of a sub-scale demonstrator of a BWB. Thus, the major initial task for the eleven students who began this project was to produce a preliminary design for the full-size BWB which would be demonstrated at full scale.

At the outset the students chose tasks for the preliminary design of the full-size vehicle covering the full range of disciplines that one would expect. In addition, they provisionally chose both technical and management tasks for the sub-scale demonstrator phase.

The CoA chairman for this GDP is Howard Smith, who is Course Director of the full-time AVD MSc and is also leading the BWB programme as a whole. He has performed a great deal of the preparatory work for this AE GDP and the AVD GDP, which worked on initial detail design of a full-size BWB and performed by students on that course during the period October 1998 to May 1999. The BAe chairman, Philip Wright of Design at Warton, is himself a former student on the AVD course.

At the time of writing, this GDP has completed the preliminary design of the full-size BWB (Fig. 8) and has now moved on to the design of the sub-scale demonstrator vehicle. Due to loss of one member of the group and some lessons learnt by the 1997 intake GDP, there has been some reallocation of the tasks relative to the provisional choices made at the beginning.

As with the 1997 intake, the XRAE crate will be used to provide the flight control etc. hardware. In addition, present intentions are to use the same propulsion unit, the AMT Olympus, with only a single unit occupying one of the nacelles of a demonstrator for a three-engined full-size vehicle. It is expected that vehicle construction techniques will be similar to those used for Eclipse and that TASUMA could well be the manufacturer. However, this vehicle is at

present planned to be around twice the size and mass of the 2.2 m span and 37 Kg mass predicted for the Eclipse UAV.
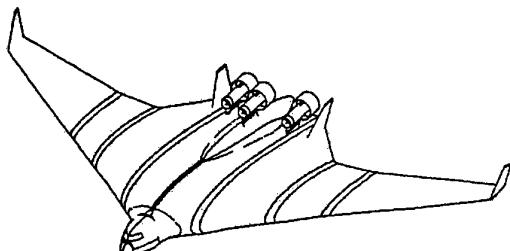
Figure 8 Full-size BWB configuration to form basis for 1998 GDP sub-scale demonstrator UAV.

9. GDP FOR THE 1999 INTAKE

The subject chosen for the GDP for the most recent intake on the AE course is again that of a UAV. However, the role is different to that of either of the previous two GDP UAVs.

The CoA has for some time had an interest in environmental monitoring of the atmosphere and in fact has operated a Jetstream aircraft to sample exhaust gas plumes for power stations etc.. In addition, the Astronautics and Space Engineering Group within the CoA has an interest in remote sensing, both the technologies involved and analysis of the data collected.

There have been a number of suggestions made that UAVs could be used as 'surrogate satellites' for remote sensing purposes, either proving payload or techniques prior to committing to a satellite launch or permanently replacing satellites in some roles. In fact, the CoA has already performed a small study funded by the European Community using very simple UAV systems at low altitude to prove some of the techniques.

For a number of the in-situ and remote sensing roles, for both environmental and other purposes, it is important that the vehicle stays on-station and often at reasonably high altitudes for long periods. This provides a challenge for all the disciplines of aeronautical engineering that has interested staff and students at the CoA for some time, Ref 23. Therefore, the GDP for the 1999 intake of the AE course has picked-up on these interests in attempting to design, build and fly a 'high' altitude 'long' endurance small UAV.

The 12 students in this group have been set the task of flying a proof-of-concept vehicle at 12 km altitude. Again, to reduce time and cost the XRAE crate will provide a basis for the vehicle systems. However, in this case the fact that this crate has been developed in stages, rather than as an integrated whole, and along with the various support equipment, batteries etc. weighs around 10 kg, becomes a real problem. Given time and money, a package performing the same functions as the present crate could easily be developed at half its present weight and probably much less.

Recognising the weight reduction in the crate which could be possible, the students have been asked to design an 'ideal' vehicle and a 'real' proof-of-concept vehicle. The former would have a re-engineered crate and be capable of carrying a 5 kg payload for 24 hours at 12 km with a 14 km ceiling, whilst the latter will use the present crate to carry a 1 kg

payload at 12 km for long enough to prove the fuel consumption figures etc.

At present the students are arranged in three competing teams, working on configuration designs to be presented to the 'customer' at their next lecture module in November 1999. Beyond that point they will move on to the design of the proof-of-concept vehicle, as a whole group. There are indications of possible interest from the Astronautics and Space Engineering group and companies they are involved with in production of a real demonstration payload for the vehicle to fly. This could, if all goes well, lead to the 'ideal' vehicle becoming a possibility.

The chairmen for this GDP are Robert Jones for CoA and Garry Shadbolt, one of the graduates from the 1995 intake of the AE course, for BAe.

10. DISCUSSION

10.1 The GDP as a Teaching Method
The general principle of a GDP as a teaching method, that the best way to learn the design process is to do it for real, has been well proven over the years on the full-time AVD course. However, that course only attempts to cover part of the design process and is particularly aimed at designers. The objective of the GDP on the AE course is more ambitious in that it attempts to bring in all the technical (and some non-technical) disciplines necessary to progress an aircraft project from specification to flight. As a result, the AE GDP has successfully allowed students from various backgrounds to play a full and useful part in the project.

In addition to providing first hand experience of technical aspects which must be considered in a real project, the GDP gives very real experience of the difficulties of managing and controlling a project with constrained manpower, budget and time and needing to prove safety. Experience with the GDPs on the AE course to-date have proved them to be all too 'real' with over-runs in terms of cost and time. At least these have been of manageable proportions and no-one's career or reputation has been destroyed be the problems (at least not yet!).

It has not only been the students that have learnt valuable lessons during the course of the GDPs. Staff at CoA and senior engineers at BAe have also learnt much about each other's capabilities. The advantages and disadvantages of each other's normal methods of working and how these might be applied to advantage on future projects outside the AE course have been highlighted.

There is no disguising the fact that the AE course as a whole is very demanding and, as a result, students have withdrawn from the course. It requires a student to study over three years a course equivalent to a full-time one year course, hold down their job and fulfil their family commitments, often at a point in their lives and careers when their circumstances are changing rapidly. The demands of the GDP adds to this. However, unlike the lecture modules and individual research elements of the course, it also brings with it a drive from being a member of a group, working towards a common end. In fact, it is clear from the intakes on the course to-date that, when a students time is limited, it is the other elements of the course rather than the GDP that suffer and particular emphasis

has continually to be placed on the individual research, particularly, to ensure this does not get left out.

One of the major non-technical benefits of the AE course and, in particular the GDP, to both the sponsor and students individually is the personal contacts that are made during the course. These provide links between BAe Military Aircraft & Aerostructures' (MA&A) sites and departments. Students have been drawn from BAe's sites at Brough, Dunsfold, Farnborough, Salmesbury and Warton. There disciplines have included:

> Aerodynamics
> Airworthiness
> Avionic Systems
> Design
> Flight Test
> Materials
> Manufacturing Dev. and Test
> Reliability
> Structural Test
> Structures
> Systems Engineering
> Wind Tunnels

The personal contacts formed between the students during the course and GDP, along with those made outside the groups to progress work on the GDP, are of lasting benefit to organisation. Whilst it may not actually be another student at another site or in another department that needs to be contacted in the future, they provide a useful and known starting point who is likely to be helpful in locating the person who is actually required.

As the second group of students on the course has only just graduated, it is a little early to judge the direct benefits to BAe and the students of the course and GDP. Certainly the course can not be seen as providing a guarantee of accelerated progression through the company for its graduates but indications are that some who have completed the course have already made good use of their experience.

10.2 Developments for the Future
As indicated above, the AE student intake covers a wide range of experience and discipline backgrounds within BAe. However, Cranfield University's regulations prevent a course being provided exclusively for a single employer. Therefore, it was always intended that its intake would be widened to encompass students from other employers from the aerospace sector. Therefore, although BAe MA&A remains the predominant customer for the AE course, there are students on the course from other parts of BAe , DERA and MoD.

In future. it is hoped to widen further the sponsors of students on the course. It should be emphasised that a particular attraction to BAe MA&A was that they could integrate lectures by some of their own staff with the material provided by Cranfield. Therefore, the effects of a wider audience on the allowed material for such lectures may need to be considered. However, the difficulties this might create are outweighed by the advantages gained by all sponsors of students in having their employees exposed to the knowledge and experience of students from other sponsors with a different perspective. In fact, it has long been recognised by the regular sponsors of students on the full-time AVD course, from around the world, that one of the major benefits of the course is the opportunity for the students to mix with those from other countries and parts of the aerospace industry.

To-date subjects of the GDPs have been limited to modifications of CoA's own A1 aircraft and UAVs. These have apparently provided topics which meet the basic objectives of this element of the course. Whilst further modifications to the A1 could be considered and further UAVs, or modifications of the present ones, are also possible, it would be good to find new subjects for GDPs, to ensure student interest.

The CoA does operate other aircraft which could be modified and often works on one-off modifications of BAe's own aircraft. Therefore, these could provide some possibilities. A more ambitious subject would be a manned aircraft designed from scratch but this would not sensibly be possible within a single GDP, so would need to be broken down into sections. At the other end of the scale would be a 'virtual project' which would not actually produce flight hardware but possibly wind tunnel models etc. This would certainly limit costs involved in the GDP but whether it would capture student interest and provide the same concentration of mind on safety issues is not clear.

11. CONCLUSIONS

Although the GDPs, and AE course as a whole, is and will continue to be very demanding of both students and staff involved, it provides an effective approach to tackling the problems of an engineer gaining real practical experience in today's employment environment. It also offers additional opportunities for all parties concerned to benefit.

Within the relatively short time period for which it has been running, the GDP element of the AE course has proved to be a very effect tool in teaching the students about the many technical and non-technical facets of typical aerospace projects. It has allowed students from many disciplines within BAe MA&A and beyond to be exposed to the real practical problems and difficulties in applying their own and other's aerospace engineering knowledge, in a relatively limited risk environment.

Personal links between students from different sites and departments and between CoA staff and a range of individuals in BAe have been formed, to the future advantage of all concerned. In addition, useful lessons about the general working practices within BAe and CoA and where/how these can be applied to best advantage in future have been learnt.

In the future, it is hoped to widen further the course intake to encompass more organisations within the aerospace sector. New subjects for GDPs will also need to be identified. However, the basic requirements of a project covering a wide extent of the design process, within real constraints, will need to be retained.

12. REFERENCES

1. Ali-Khan, S. A., "College of Aeronautics A1-200 Fuel System Design", MSc Thesis, Cranfield University, 1997.
2. Crane, A. P., "Aeroelasticity of the A1-200", MSc Thesis, Cranfield University, 1997.
3. Embley, N. J., "Conversion of the Cranfield A1 from Single to Twin Seat Aerobatic Aircraft Including Design of an Advanced Concept Material/Technique Based Fuselage", MSc Thesis, Cranfield University, 1997.
4. Franks, L. A., "The Design and Manufacture of the Cranfield A1-200 Aerobatic Trainer", MSc Thesis, Cranfield University, 1997.
5. Kelly, T. L., "Mass Control, Stability and Control Analysis and Front Cockpit Flight Controls Design", MSc Thesis, Cranfield University, 1997.
6. Massam, S. J., "Installation of Second Seat into College of Aeronautics A1 Aerobatic Aircraft", MSc Thesis, Cranfield University, 1997.
7. Radcliffe, N. J., "Cranfield A1-200 Group Design Project Wind Tunnel Tests and Front Cockpit Flight Controls Design", MSc Thesis, Cranfield University, 1997.
8. Ross, D. A., "The Modification of the A1 Aerobatic Aircraft Wing Including Aspects of a Plain Flap", MSc Thesis, Cranfield University, 1997.
9. Shadbolt, G., "The Design of a Trailing Edge Flap for the Cranfield A1-200 Aerobatic Training Aircraft", MSc Thesis, Cranfield University, 1997.
10. Shaw, J. M. R., "The Conversion of the Cranfield A1 to a Twin Seat Aerobatic Trainer, with Specific Reference to the Electrical System Design", MSc Thesis, Cranfield University, 1997.
11. Smith, D., "Conversion of the A1 to Twin Seat Trainer and Preliminary Design Work for a Replacement Metallic Semi-Monocoque Fuselage", MSc Thesis, Cranfield University, 1997.
12. Thomson, P. H., "Performance Evaluation and Drag Reduction of the Cranfield A1-200 Aerobatic Trainer Aircraft", MSc Thesis, Cranfield University, 1997.
13. Walker, S. J., "Twin Seat Conversion of the Cranfield A1 Aircraft (G-BCIT)-Fuselage and Canopy Aspects", MSc Thesis, Cranfield University, 1997.
14. Adams, J. M., "Cranfield A1-400: 'Novel' Lateral/ Directional Concepts, Flight Test Programme and Dorsal Fin Design", MSc Thesis, Cranfield University, 1998.
15. Duck, G., "Cranfield A1-400 Aerobatic Aircraft Group Design Project, Structural Testing and Rear Fuselage", MSc Thesis, Cranfield University, 1998.
16. Flux, P. K., "The Design of a Modified Rudder Control System for the Cranfield A1-400 Aerobatic Aircraft", MSc Thesis, Cranfield University, 1998.
17. Marshall, J., "Cranfield A1-400 Aerobatic Aircraft Group Design Project Fin Design", MSc Thesis, Cranfield University, 1998.
18. Pedley, N., "Group Design Project- Manufacturing Tasks for the Modifications of the Cranfield A1 Aerobatic Aircraft to Improve its Lateral Stability and Flick Roll Capability", MSc Thesis, Cranfield University, 1998.
19. Prus, R. L., "Cranfield A1/A1-200/A1-400 Aircraft - Fatigue Life Assessment", MSc Thesis, Cranfield University, 1998.
20. White, A. C., "Cranfield A1-400 Aerobatic Aircraft Group Design Project: Rudder Design", MSc Thesis, Cranfield University, 1998.
21. Dyer, D. J., Jones, R. I., Stevenson, A., Thomasson, P.G. & Walster, R. A., "'Reducing the Operator Workload' Short Range Unmanned Air Vehicle Research at Cranfield", 14th International RPV/UAV Systems Conference, Bristol, 12-14 April 1999.
22. Preston, A. M., Harrison, R. & Littlewood, R., "Eclipse - A Turbojet Powered UAV", 14th International RPV/UAV Systems Conference, Bristol, 12-14 April 1999.
23. Jones, R. I., "The Design Challenge of High altitude Long Endurance (HALE) Unmanned Aircarft", The Aeronautical Journal, Vol. 103, No. 1024, June 1999.

AN OPTIMISATION PROCEDURE FOR THE CONCEPTUAL ANALYSIS OF DIFFERENT AERODYNAMIC CONFIGURATIONS

G. Lombardi, G. Mengali
Department of Aerospace Engineering, University of Pisa
Via Diotisalvi 2, 56126 PISA, Italy

F. Beux
Scuola Normale Superiore di Pisa
Piazza dei Cavalieri 7, 56126 PISA, Italy

ABSTRACT

This paper addresses the problem to define a methodology for the analysis of the performances of different aircraft configurations in the phase of conceptual design. The proposed approach is based on a numerical optimisation procedure where a scalar objective function, the take-off weight, is minimised. The optimisation algorithm has obviously important consequences both from the point of view of the computational times and of the obtained results. For this reason a preliminary discussion is made where various different methodologies are critically compared. Although the best compromise between different approaches is probably given by an integration between a genetic algorithm approach and a classical gradient method, in this phase only the latter procedure has been used to perform the simulations. The methodology takes into account the high number of geometrical parameters and the flight mechanics requirements involved in the problem.
A basic example is described, and the use of the proposed methodology to investigate the effects of different geometrical and technological parameters is discussed.

NOMENCLATURE

A Sectional area of panel structure, m^2
AR aspect ratio
b span, m
c chord length, m
c_D global drag coefficient
c_l sectional lift coefficient
c_L global lift coefficient
c_{ma} mean aerodynamic chord of the wing, m
E efficiency (lift-to-drag ratio)
g acceleration of gravity, m/s^2
H cruise altitude, m
$h-h_n$ distance (non-dimentionalised with c_{ma}) between aircraft c.g. and neutral point
i stabiliser angle, deg
L length, m
$\bar{l}_t$ distance between aerodynamic centres of wing and stabiliser, m

M Mach number
q dynamic pressure, N/m^2
R range at cruise velocity, km
S surface area, m^2
S_{fc} specific fuel consumption, (N/hr)/N
T vertical gap, m
t/c thickness ratio
V cruise velocity, m/s
W weight, N
WS wing loading, N/m^2
x_{cg} c.g. position of the residual weight, ($\% L_{fus}$)
x_s position of stabiliser root leading edge from fuselage nose, m
y spanwise coordinate, m
α angle of attack, deg
Γ dihedral angle, deg
δ elevator angle, deg
θ twist angle, positive increases the tip angle of attack, deg
λ taper ratio
Λ sweep angle, deg
ρ air density, kg/m^3
ρ_M density of structural material, kg/m^3
σ_a admissible normal stress level, N/m^2
Φ diameter, m

Subscripts
BL bending due to lift
c cruise
ea elastic axis
f fuel
fus fuselage
M pitching moment
o take-off
p payload
r root
ref reference
res residual
rib wing ribs
s stabiliser surface
SL shear due to lift
t tip
w wing

1. INTRODUCTION

During the phase of conceptual design, the problem of evaluating the performance of different aircraft configurations is of great interest; however, difficulties arise due to the high number of geometrical parameters involved, which are necessary for defining such a configuration. A systematic analysis taking into account the effects of all these parameters appears to be difficult, given the complexity related to both aerodynamic load evaluation and the assessment of flight mechanics requirements. Furthermore, a sufficiently precise estimation of the weights of the different aircraft components is necessary. However this estimation is strongly related to aircraft lift distribution, hence the use of a satisfactory aerodynamic code is mandatory.

In order to tackle this problem, a direct numerical optimisation technique may be employed, giving rise to an attractive approach, since the problem may be addressed systematically, and the designer has a great flexibility in the choice of the design variables.

In the analysis through direct numerical optimisation, an aerodynamic code is coupled in a loop with an optimisation routine, so as to automatically manage the values of the design variables – typically concerning geometry modifications – with the aim of minimising a given scalar quantity (objective function). This approach is extremely flexible, and capable of meeting multidisciplinary requirements. The choice of the design variables is of fundamental importance, as they define the set of solutions within which the optimal one is sought. Finally, the design problem formulation requires the definition of the constraint functions, which can be of aerodynamic, flight mechanics or geometrical nature, or more generally involve any quantity that may be computed with sufficient reliability.

In a previous paper[1] an aerodynamic optimisation procedure, based on a potential flow model, has been developed for the study of the effects of the geometric parameters on the induced drag. The obtained code proved to be quite reliable in terms of efficiency in determining the optimum configuration for the induced drag, but, in the version presented in Ref. 1, only this aerodynamic aspect was taken into account. Consequently, the analysed configurations did not meet the constraints resulting from aircraft flight mechanics, nor was the structural weight considered. In Ref. 2 the above obstacles were overcame by including the constraints of a realistic configuration in the code, with the assessment of trim conditions, static stability requirements and with the addition of the evaluation of airplane structural weight, based on a methodology originally developed by Torenbeek.[3] The weight was included with a low level routine, the aim being to develop a code suitable for a conceptual design approach. This simplification, however, should not be considered a real limitation in so far as different modules, which make up the code, can be substituted by other ones, with more sophisticated mathematical models, without the need to modify the problem approach.

This paper is concerned with some improvements with respect to Ref. 2. In particular, in the present version the aerodynamic code takes into account the wing thickness and the real fuselage shape. From the flight mechanics point of view, the pitching moment at zero lift has now been considered.

The whole methodology is strongly dependent of the optimisation algorithm both from the computational performance point of view and the accuracy of the obtained results. Therefore, a critical analysis of the available methods has been carried out: this is described in the next section.

2. A CRITICAL REVIEW OF OPTIMISATION METHODS

The main limitation to aerodynamic shape optimisation in a difficult context is certainly related to his prohibitive computational cost due to complex and/or three dimensional geometry, and to multi-objective problems (multipoints and/or multidisciplinary optimisation). Among the different methodologies that are being pursued for direct optimisation, gradient-based methods, in which a specified objective is minimised, are often employed. These procedures require computations of both objective functional and its derivatives respect to each control variable. The gradient calculations are usually performed using black box finite difference methods which are simply to implement but require, for each control variable, at least a cost evaluation. For practical problems, a large number of control variables are needed to take care of geometry and multidisciplinary constraints. Accordingly, when the functional is expensive to compute, this kind of method gives poor computational performances.

A first possible solution is to use relative simple aerodynamic models, as for example, potential flows (see e.g. Refs. 4-6). The adjoint approach, based on control theory or variational analysis, is an interesting alternative procedure for the calculation of the functional derivatives, which makes use of a continuous as well as a discretised differentiation (see Newman et al.[7] for a review). Actually, it allows one to greatly limit the number of cost evaluations, and thus, can significantly reduce the computational cost. For the above reasons, in the last years, several optimisation computations for complex configurations and complex flow models have been performed using the adjoint method. Usually, this technique is combined with multigrid-like algorithms in order to reduce the dependency between cost and number of control variables and/or with the powerful of parallel computing. In this way, optimisations of realistic, complete aircraft geometries, using the 3D Euler equations as flow model, have been performed[8-11] as well as 2D airfoil shape optimisations using the Reynolds averaged Navier-Stokes equations coupled with turbulence models as flow model[11-13].

The hand-code exact derivation is extremely difficult to perform due to the complexity of both equations and discretisation, thus automatic differentiation techniques[14] have been used for the evaluation of the derivatives in a discrete adjoint method[13,15]. It should be noted that methods of second-order, .i.e. methods in which not only a gradient, but also, a Hessian must be evaluated, can be found in literature (see e.g.

Ref. 16). In a context of multidisciplinary design problems, gradient methods minimise a functional constituted by a combination of different criteria with different weights. Alternative methods, which do not require the use of gradients, can be also considered, in particular stochastic ones as the genetic algorithms (GAs) (see Hajela[17] for a review). GAs, which have found significant interest for applications in the aeronautical field (see e.g. Mosetti and Poloni[18], Crosslet and Laananen[19]). They are particularly attractive in a complex context because of their robustness. Indeed, they can overcome the limitations of gradient-based methods, i.e. they can operate with very poor regularity, especially with irregular non-differentiable functions and disjointed feasible domains. They can deal with a mix of different objects as continuous, discrete, integer or boolean variables, and, they are available to approach a global optimum whereas the gradient-based methods can yield only local optima. However, the major drawback of GAs is that they require a high number of evaluations of the objective function, and thus, these methods are poorly efficient in a context of expensive cost function. In particular, once the nearness of the global optimum is reached, the non gradient methods converge very poorly whereas this condition is well-suited for gradient-based methods.

To partially overcome the lack of computational efficiency, parallel computer architectures can be used (see e.g. Refs. 20-22) drawing profit from the structure of GAs which is well adapted to a fully parallelisation of the algorithm. Gradient-based methods and GAs have complementary properties, thus, in order to combine their favourable features, an interesting approach for complex configurations as multidisciplinary aeronautics optimisation is to couple the two methods. Starting from a large area of configurations, a GA can be used to get close to a particular configuration which is, then, optimised by a gradient-based method to reach the global optimum. This kind of hybrid strategies begins to be studied as it was reported in very recent works.[23,24]

In our opinion this latter approach appears to be the most effective for the problem at hand, but in the first phase of our research only a gradient method has been applied. Actually, this method has been used to obtain the simulation results for the present paper.

3. THE MATHEMATICAL MODEL

3.1 Evaluation of aerodynamic characteristics

The pressure distribution acting on the airplane was evaluated by means of a non linear panel method, based on the formulation due to Morino; the features of this method are discussed in detail in Ref. 25.

The code allows for wake relaxation, thus yielding non-loaded stream surfaces as required by the correct boundary condition. Once the pressure distribution is known, the lift distribution over wing, fuselage and stabiliser surfaces, as well as the induced drag, can be calculated.

In consideration of the aerodynamic code chosen, the analysis is naturally confined to flows at low angles of attack and subsonic Mach numbers; nevertheless, it can provide useful information without the need for complex and expensive experimental and/or numerical investigations.

Aircraft drag, at each step of the optimisation procedure, was estimated by using the component building method. The induced drag of the configuration was predicted by means of the previously described code. The profile drag of the lifting surfaces was evaluated by means of standard preliminary methodologies, as described in Refs. 26 and 27, while the drag of the non lifting bodies (fuselage and vertical tail) was evaluated following similar methodologies.[26,28] The drag increment caused by the propulsive system installation is very sensitive to the choice of a specific configuration; since in this phase no consideration at all is made on propulsion system choice and position, it was preferred to avoid the estimation of its effects. Consequently, the total drag is slightly underestimated, even if this simplification does not significantly affect the optimisation procedure. Obviously, there are no obstacles in taking into account this quantity where more detailed studies are performed.

3.2 The numerical optimisation routine

In the analysis through direct numerical optimisation,[29] an aerodynamic code is coupled in a loop with an optimisation routine, so as to automatically manage the values of the design variables – typically concerning geometry modifications – with the aim of minimising a given scalar quantity (objective function). This approach is extremely flexible, and capable of meeting multidisciplinary requirements. The choice of the design variables is of fundamental importance, as they define the set of solutions within which the optimal one is sought. Finally, the design problem formulation requires the definition of the constraint functions, which can be of aerodynamic, flight mechanics or geometrical nature, or more generally involve any quantity that may be computed with sufficient reliability.

It should be emphasised that a numerical procedure of this kind can never be regarded as a completely automated tool; user's experience and external control on the process are always needed to obtain the best results. In fact, the topology of the feasible region is unknown a priori.

The numerical optimisation routine adopted for the present study is the CONMIN code,[30] used extensively in the fields of aerodynamic and structural optimisation. CONMIN uses a gradient method for the search algorithm and includes three alternative first order methods for the calculation of the vector search direction. When all the constraints are satisfied for the current values of the design variables, the steepest descent method is used for the first iteration, and the conjugate direction method for subsequent iterations. When some of the constraints are active or violated the feasible directions method is used.

3.3 The optimisation procedure

In this paper the main objective is to evaluate the capabilities of the proposed methodology to obtain configurations with improved performances with respect to a reference one. The analysis is carried out upon assuming that the following design parameters have been arranged for cruise: payload, velocity, range, cruise height, engine specific fuel consumption. We stress that the different configurations were designed only for achieving a high-speed, long range cruise mission by matching the airplane design to cruise performance design. No dynamic analysis nor high lift conditions were directly considered. However, the high lift condition is implicitly inserted in the design trough a constraint on the wing loading, as discussed in the following.

It has been supposed that payload establishes the length and diameter of the fuselage, which have been considered known. Thickness ratio, sweep and dihedral angles for both wing and stabiliser, and the ratio between the wing and tail surfaces have been assumed as design parameters and have been kept fixed. As to tail volume (imposed here by means of the ratio between wing and tail surfaces), this is obviously imposed by mission segments different from cruise (typically, take-off and landing). The sweep angles are imposed by the Mach number, while dihedral angles comes from lateral stability considerations. Finally, as to thickness ratio, this is a function of both cruise and high-lift conditions. Cruise imposes a maximum t/c owing to drag problems; as to high lift conditions, it can be easily shown that the function c_{Lmax} versus t/c has a maximum which depends on the wing section. This entails another constraint on the maximum value of t/c. The choice of some of the above design parameters may have significant effects on the results; accordingly, the influence of a variation in thickness ratio and tail volume coefficient could be investigated, as shown in Ref. 2.

For each lifting surface, the design variables used in the optimisation process are aspect ratio, taper ratio and twist. Moreover, wing loading and stabiliser position (horizontal stagger and vertical gap) are also design variables. However, wing loading is a variable which is typically dependent upon flight phases other than cruise and, therefore, it is not possible to optimise this variable without a constraint which forbids it to assume unrealistic values. Moreover, stabiliser position is constrained by fuselage geometry, since its length and diameter have been fixed.

It is well known that one of the crucial aspects of the optimisation procedure is constituted by the choice of the object function. In the present analysis various considerations lead us to the conclusion that the take-off weight is a reasonable choice, even if it should be clear that the essence of the proposed methodology would not be affected by a different objective function. The main reason is that the aircraft take-off weight appears to offer a quite reasonable compromise between the need to obtain solutions that are sufficiently accurate to give significant results and the need to prevent such solutions from being excessively complicated, as it would happen by using, for example, Direct Operating

Costs as an objective function.[31]

The objective function is considered to be the sum of four terms: wing weight, stabiliser weight, fuel weight and residual weight. The latter comprises fuselage, payload, vertical tail, engines, gears and various systems; their weights and centre of gravity positions are assumed to be known, and have been established by statistical data.

The optimisation process includes the following steps:

1. On the basis of the above design parameters and with a fixed set of design variables, a first estimation of W_o and W_f is given and, as a function of W_o and W_f, an estimation of W_w and W_s is obtained by using formulae derived from statistical data.[32] Accordingly, wing and stabiliser planform is fixed as a function of the distance between wing and stabiliser aerodynamic centres. Centre of gravity of wing, stabiliser and fuel (supposed to be concentrated in the wing) are also evaluated. In the following examples the positions of the centres of gravity of various elements are obtained by means of simplified formulae.[33]

2. The angle of attack and elevator angle are computed to trim the aircraft in straight, horizontal flight, by using the following equations

$$c_{L_{trim}} = \frac{2W_o}{\rho_c S_w V_c^2} = c_L\big|_{\alpha=0,\,\delta=0} + c_{L_\alpha}\alpha + c_{L\delta}\delta \qquad (1)$$

$$c_M = 0 = c_M\big|_{\alpha=0,\,\delta=0} + c_{M_\alpha}\alpha + c_{M\delta}\delta \qquad (2)$$

The aerodynamic coefficients in Eqs. (1) and (2) are computed with an iterative procedure, by using the previously described non-linear aerodynamic code. The value of c_{Dtrim} is then evaluated with the previously described aerodynamics procedure and vehicle efficiency is obtained by $E=c_{Ltrim}/c_{Dtrim}$.

3. By means of the computed values of $c_{L\alpha}$ and $c_{M\alpha}$ the static longitudinal stability of the configuration is checked. The code constrains the difference between centre of gravity and aerodynamic centre positions (non-dimentionalised by c_{ma}) to be included between two imposed bounds. In the examples the inequality $-0.05 \le (h-h_n) \le -0.2$ was used. When the above constraint is violated, the code repetitively comes into play to modifying the value of l_t, by moving the wing with respect to fuselage, until the bounds are met.

4. At this point, the load distribution on lifting surfaces is known, therefore it is possible to give a new estimation of wing weight by using the methodology of Torenbeek[3] which binds wing weight to lift distribution along the wing span and mechanics characteristics of the employed materials (see Appendix). By this means it is possible to accurately estimate wing weight.
   Fuel weight is obtained from Breguet's formula:

$$W_f = W_o \left[1 - \exp\left(-\frac{RS_{fc}}{V_cE} \right) \right] \quad (3)$$

and the quantity $\overline{W} = W_w + W_s + W_f + W_{res}$ is evaluated. If $\overline{W} \neq W_o$ (except for numerically insignificant differences), a new estimation of W_o is given by using, for example, the updating formula $W_o' = (\overline{W} + W_o)/2$.

5. The points 1-4 are repeated until the condition $\overline{W} = W_o$ is met. It should be noted, however, that W_w at point 1 is now evaluated by Torenbeek's approach.

6. The optimisation routine updates the design variables and the procedure described at points 1-5 is repeated until the minimum weight configuration is obtained.

We stress the fact that, since the wing weight is evaluated by means an approach based on the real spanwise lift distribution, (and not simply on statistical data) it is possible to analyse canard configuration as well. Nevertheless, in this case the estimations based upon a statistical approach are defective due to the small number of available data.

4. THE OPTIMISATION PROCEDURE: A CASE STUDY

In this section the outlined methodology has been applied, as an example, to a typical light transport aircraft. Table 1 shows the values of the fixed parameters used in the optimisation procedure.

W_p	x_{cg}	M	R	S_{fc}	H
33000	40	0.4	2100	0.48	6100

L_{fus}	Φ_{fus}	Λ_w	Λ_s	Γ_w	Γ_s
11.2	1.7	0°	4°	4°	9°

Table 1 - Fixed parameters used in the optimisation procedure

In addition to the data of Table 1, the following design parameters have been fixed: (t/c) from 0.18 (at the root) to 0.12 (at the tip), both for wing and tail. Moreover a ratio $S_s/S_w = 0.25$ has been fixed.

The design variables are aspect ratio, taper ratio and twist of wing and tail, wing loading and tail position. The constraints are as follows: 1) maximum value of wing loading $WS = 1903$ N/m²; 2) the tail vertical position could only vary between the maximum height of the fuselage and two meters above that position; 3) tail horizontal position constrained by fuselage length. Note that a fully rotating tail has been assumed. It is interesting to note that the objective function was highly sensitive to wing loading which reached the value

given by the constraint. On the other hand, the optimisation of tail variables turned out to have a negligible effect, and the tail position reached, in all the cases presented, the upper values of the constraints. The most important results of the optimisation process have been summarised in Table 2a, where aircraft geometry is defined, and Table 2b, where trim conditions are shown.

	Wing	Tail
S	23.46	5.87
b	15.14	5.97
c_r	1.80	1.31
AR	9.76	6.07
λ	0.72	0.5
θ	-2.64°	0°
l_t	5.46	
x_s	10.9	
T	2.00	
i	0°	
W_w	5461	
W_s	514	
W_f	5686	
W_o	44652	

Table 2a - Aircraft geometry and weights

α	1.52°
δ	1.37°
c_L	0.361
c_D	0.0218
E	16.6

Table 2b - Trim conditions

The geometry of the optimised configuration is shown in Fig. 1 along with the mesh used in the computational analysis (for the body representation, about 2700 panels have been used). Typical computational times required to obtain an optimised configuration are of the order of 5h on a Pentium III Xion, 500 MHz and 512 MB RAM.

As far as drag analysis is concerned, wing loading being practically fixed by the constraint, it can be seen that wetted area is practically a constant (it is clear that, for a correct optimisation process, the final take-off weight cannot be significantly different from the initial estimation), hence friction drag does not vary to any remarkable extent and the optimisation process tends almost exclusively to decrease the induced drag. Accordingly, the optimised configuration is the best compromise between two opposite standpoints: an increase in wing span to decrease induced drag (thereby decreasing W_f and W_o) or, conversely, a reduction in wing span to reduce structural stress and, as a result, to diminish W_w and W_o.
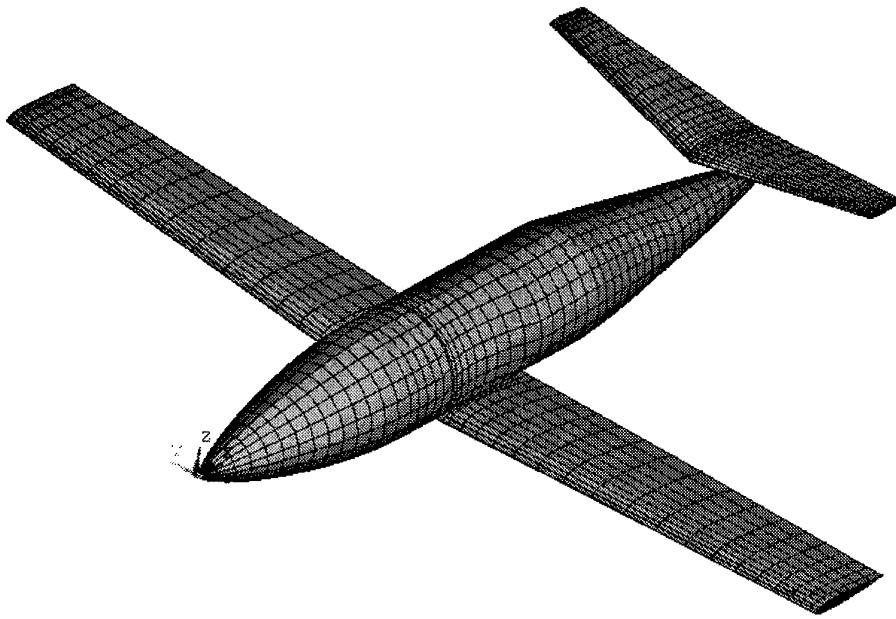
Fig. 1 – Reference optimised configuration

5. A COMPARISON OF DIFFERENT CHOICE OF THE GEOMETRICAL PARAMETERS

Although the above parameters are constrained, from a practical point of view, by mission segments different from cruise (especially take off and landing), it is interesting to obtain quick estimates of the order of magnitude of the improvements which would be related to a relaxation of these constraints. This in turn gives important information about the trade-off between an increase in costs related to more sophisticated solutions and an increase in the overall configuration performance.

The optimised configuration outlined in the previous section results from a number of different geometrical constraints. It is interesting to investigate the effect of the parameters which are not directly controlled by the optimiser. In particular, we analyse the differences in the configuration due to a different choice of the wing thickness ratio and to a different wing loading.

In Table 3 the optimised configuration obtained with a greater wing loading constraint is compared to the reference one.

A significant reduction in wing weight with an increase in wing loading is apparent, along with a less important effect on fuel consumption. Note that the increase in wing loading causes a decrease in wing span and an slight increase in aerodynamic efficiency, thus leading to both a reduction in wing weight and lower fuel consumption.

Value	$WS=1903$(Ref)	$WS=2093$
S_w	23.46	20.93
b_w	15.14	14.04
AR_w	9.76	9.41
λ_w	0.72	0.72
θ_w	-2.64	-4.64
b_s	5.97	5.64
λ_s	0.5	0.5
θ_s	0	0
l_t	5.46	5.14
c_L	0.361	0.396
c_D	0.0218	0.0237
E	16.6	16.7
W_w	5461	4752
W_s	514	461
W_f	5686	5549
W_o	44652	43813
$(W_o - W_{oref})/ W_{oref}$	-	-1.88%

Table 3 – Effect of a different wing loading

In Table 4 the optimised configuration obtained with a reduced value of thickness ratio at wing root is compared to the reference one. In particular, the reference value, corresponding to $t/c=0.18$ at wing root, is modified in $t/c=0.16$.

Value	t/c_{root}=0.18 (Ref.)	t/c_{root}=0.16
S_w	23.46	23.54
b_w	15.14	15.27
AR_w	9.76	9.90
λ_w	0.72	0.71
θ_w	-2.64	-2.68
b_s	5.97	5.98
λ_s	0.5	0.5
θ_s	0	0
l_t	5.46	5.34
c_L	0.361	0.360
c_D	0.0218	0.0220
E	16.6	16.4
W_w	5461	5505
W_s	514	524
W_f	5686	5763
W_o	44652	44806
$(W_o - W_{oref})/W_{oref}$	-	+0.34%

Table 4 – Effect of a different thickness ratio

It is clear that weight increases as t/c at the root decreases. Upon decreasing t/c at the root, performance decreases due to an increase in wing weight. It should be noted, however, that the higher structural efficiency is not "used" to increase wing span, which, indeed, shows a slight decrease. When t/c at the root is increased from 0.16 up to 0.18, the higher structural efficiency is "used" to increase wing span, thus reducing the induced drag, with a consequently lower fuel consumption, but without important differences in wing weight.

6. A COMPARISON OF DIFFERENT CHOICE OF THE TECHNOLOGICAL PARAMETERS

In this section, the outlined methodology has been applied to stress the importance of some of the most significant technological parameters over the final aircraft configuration.

6.1 Reduction in friction drag

It is known that the reduction of friction drag plays a relevant role in the current aerodynamic research. In what follows, we suppose that the friction drag may be reduced by 10% with respect to the nominal case. As a first example, this reduction has been applied to the optimised configuration of Table 2, which results in a fuel reduction of 370 N, which in turn corresponds to a reduction of 0.8% with respect to the take off weight.

It is interesting to investigate if the optimisation process would be different in this case: accordingly the whole optimisation procedure has been carried out with the new value of the friction coefficient and the results are shown in Table 5.

The optimised configuration obtained considering a smaller friction drag shows a reduction in the take off weight of 1.33%, significantly higher (+0.53%) than the

corresponding result obtained considering the reduction in friction drag applied to the reference configuration.

Value	Reference	c_f=0.9$c_{f_{ref}}$
S_w	23.46	23.15
b_w	15.14	14.64
AR_w	9.76	9.26
λ_w	0.72	0.74
θ_w	-2.64	-4.37
b_s	5.97	5.93
λ_s	0.5	0.5
θ_s	0	0
l_t	5.46	5.38
c_L	0.361	0.360
c_D	0.0218	0.0206
E	16.6	17.5
W_w	5461	5166
W_s	514	505
W_f	5686	5330
W_o	44652	44057
$(W_o - W_{oref})/W_{oref}$	-	-1.33%

Table 5 – Effect of a different friction drag

The new configuration shows an increased aerodynamic efficiency, even with a reduced wing span; therefore, both the wing and fuel weights are reduced. The lift coefficient remains practically constant, therefore the aerodynamic flow is practically the same, while the geometric configuration appears slightly different. Indeed, the new configuration has a reduced wing surface with a reduction both in wing span (-3.3%) and aspect ratio (-5.1%), a slightly higher taper ratio and an increased twist.

6.2 Reduction in specific fuel consumption

Another fundamental research area in the aeronautical field relates to the increase in engine efficiency. Accordingly, in what follows we suppose that the specific fuel consumption may be reduced by 10% with respect to the nominal case. As a first example this reduction has been applied to the optimised configuration of Table 2, which results in a fuel reduction of 569 N, which corresponds to a reduction of 1.3% with respect to the take off weight. Obviously, in this case the reduction in fuel weight is very close to the corresponding reduction in specific fuel consumption.

As in the previous example, the whole optimisation procedure has been carried out with the new value of the new value of the specific fuel consumption and the results are shown in Table 6.

The optimised configuration obtained considering a smaller specific fuel consumption shows a reduction in the take off weight of 1.98%, significantly higher (+0.68%) than the corresponding result obtained considering the reduction in specific fuel consumption applied to the reference configuration. The reduction in specific fuel consumption directly reduces the fuel weight, with a consequent reduction in the wing weight, mainly caused by the reduction in

required total lift.

Value	Reference	$S_{fc}=0.9S_{fcref}$
S_w	23.46	23.00
b_w	15.14	14.59
AR_w	9.76	9.26
λ_w	0.72	0.74
θ_w	-2.64	-4.55
b_s	5.97	5.91
λ_s	0.5	0.5
θ_s	0	0
l_t	5.46	5.38
c_L	0.361	0.360
c_D	0.0218	0.0220
E	16.6	16.4
W_w	5461	5135
W_s	514	501
W_f	5686	5119
W_o	44652	43767
$(W_o- W_{oref})/ W_{oref}$	-	-1.98%

Table 6 – Effect of a different S_{fc}

The new configuration shows an aerodynamic behaviour practically unchanged with respect to the reference configuration: the lift coefficient, the drag coefficient and the efficiency remain practically constant, therefore the aerodynamic flow is almost the same, while the geometric configuration appears to be slightly different. Indeed, the new configuration has a reduced wing surface with a reduction both in wing span (-3.3%) and aspect ratio (-5.1%), a slightly higher taper ratio and an increased twist.

6.3 Increase in structural efficiency

As a final example, we investigate the effect of an increase of 10% of the admissible normal stress level of the material over the optimised configuration. Upon applying this modified value to the optimised configuration of Table 2, a reduction of wing weight of 277 N is obtained along with a reduction of 35 N of fuel weight, which corresponds to a reduction of 0.6% with respect to the take off weight.

The whole optimisation procedure has been carried out with the new value of σ_a and the results are shown in Table 7.

The optimised configuration obtained considering a higher structural efficiency shows a reduction in the take off weight of 0.93%, higher (+0.33%) than the corresponding result obtained considering the increase in structural efficiency applied to the reference configuration, but not so important as in previous analysed cases.

The new configuration shows an aerodynamic behaviour practically unchanged with respect to the reference configuration: the lift coefficient, the drag coefficient and the efficiency remain practically constant, therefore the aerodynamic flow is almost the same. The geometric configuration appears substantially unchanged, with an increased twist as the only significant modification.

Value	Reference	$\sigma_a=1.1\,\sigma_{a\,ref}$
S_w	23.46	23.24
b_w	15.14	15.08
AR_w	9.76	9.79
λ_w	0.72	0.72
θ_w	-2.64	-4.49
b_s	5.97	5.94
λ_s	0.5	0.5
θ_s	0	0
l_t	5.46	5.29
c_L	0.361	0.360
c_D	0.0218	0.0218
E	16.6	16.5
W_w	5461	5024
W_s	514	508
W_f	5686	5656
W_o	44652	44235
$(W_o- W_{oref})/ W_{oref}$	-	-0.93%

Table 7 – Effect of a different σ_a

Therefore, the reduction in the take off weight is mainly produced by the direct effect of the increased structural efficiency on the wing weight and a consequent limited effect on the fuel weight.

7. CONCLUDING REMARKS

A methodology for the analysis and comparison of the performance of different configurations in the phase of aircraft conceptual design has been developed. In the analysis, a scalar objective function, the take-off weight, is minimised by means of a numerical optimisation technique, which takes into account the high number of geometrical parameters and the flight mechanics requirements involved in the problem. The approach proved to be extremely flexible, and capable of really meeting multidisciplinary requirements.

The obtained results highlight the order of magnitude of the improvements of the objective function due to an increase in technological characteristics. Moreover, it is clear that significantly higher improvements in the performances can be obtained if the configuration is developed by taking into account the above technological improvements from the initial phase of the project. This means that the optimised final configuration is different from the reference one (which in turn has been optimised with different values of these parameters).

We also note that the obtained results are "close" to the reference configuration. This is due to the fact that a gradient based optimiser may only give local minima. Actually, better results may be obtained by combining a global (GA based) optimiser, with a local gradient based approach. This matter is currently under development.

It is clear that the obtained results are not definitive, since a significant number of different configurations must be considered and several points need to be verified with a more accurate analysis. Among them the most important one is the

high lift condition which was not considered directly in the optimisation process, even if we assumed that it imposes a wing loading constraint. Obviously, this constraint must be accurately verified with an a posteriori analysis.

8. APPENDIX

According to Torenbeek's approach,[3] basic wing weight is considered as the sum of three contributions: 1) the weight of material required to resist bending, W_{BL} 2) the weight of material required to resist shear forces, W_{SL} and 3) the weight of wing ribs, W_{rib}. All three contributions are calculated as follows.

8.1 Weight due to bending moment

The bending moment due to lift at a generic (y) wing station is given by:

$$M_{BL}(y) = \int_{y}^{b/2} \frac{y'-y}{\cos \Lambda_{ea}} q c_l(y') c(y') dy'$$

and $c_l(y')$ is evaluated by the aerodynamic code.

The basic weight of two skin panels (upper and lower) can be estimated by the formula:

$$W_{BL} = 2\rho_M g \int_{0}^{b/2} A(y) dy$$

with $A(y)$ given by:

$$A(y) = \frac{M_{BL}(y)}{\eta_t t(y)\sigma_a}$$

where σ_a is the given admissible normal stress level, t(y) is the maximum thickness of the profile section and η_t is an efficiency factor which may be obtained from a drawing of the wing cross section or by simplified expressions.[3]

8.2 Weight due to shear forces

The weight due to shear forces can be expressed as

$$W_{SL} = \frac{2\rho_M g}{\bar{\tau}} M_{BL}(y=0)$$

where $\bar{\tau}$ is the mean value of shear stress which has been assumed constant. $\bar{\tau}$ can be estimated by means of the simple relationship:

$$\bar{\tau} = 0.5\sigma_a$$

8.3 Weight of wing ribs

Since a rational derivation for the weight of ribs is not feasible, the following (statistical) formulation is used:

$$W_{rib} = k_r \rho_M g S \cdot [t_{ref} + (t_r + t_t)/2]$$

where $k_r = 0.5 \times 10^{-3}$ and $t_{ref} = 1.0$ m.

Finally, basic wing weight estimation is the sum of the above three contributions, hence:

$$W_w = W_{BL} + W_{SL} + W_{rib}$$

REFERENCES

1. Lombardi, G. and Vicini, A., "Induced Drag Prediction for Wing-Tail and Canard Configurations through Numerical Optimization," The Aeronautical Journal, Vol. 98, No. 976 June-July 1994, pp 199-206.

2. Lombardi G., Mengali G. "A Methodology for the Preliminary Analysis and Comparison of Wing-Tail and Canard Configurations", The Aeronautical Journal, Vol. 101, No. 1004, April 1997, pp.169-177.

3. Torenbeek, "Development and Application of a Comprehensive, Design-Sensitive Weight Prediction Method for Wing Structures of Transport Category Aircraft", TU Delft, Report LR-693, September 1992.

4. Selmin V., "Optimization of Transonic Airfoils", Notes on Numerical Fluid Mechanics Vol. 61, Optimum Aerodynamic Design and Parallel Navier-Stokes Computations, ECARP - European Computational Aerodynamics Researsh Project, Périaux et al Editors, 1998, pp. 60-70.

5. Fornassier L., "Optimization of the Wing-Pylon-Nacelle Testcase TE5 by HISSS-D, a Panel Method-Based Design Tool", Notes on Numerical Fluid Mechanics Vol. 61, Optimum Aerodynamic Design and Parallel Navier-Stokes Computations, ECARP - European Computational Aerodynamics Researsh Project, Périaux et al Editors, 1998, pp. 99-108.

6. Labrujère Th.E., "Residual-correction type and related computational methods for aerodynamic design", AGARD Report R-803 Optimum Design Methods for Aerodynamics, 1994, pp. 4-1/5-31.

7. Newman III J.C., Taylor III A.C., Barnwell R.W., Newman P.A., Hou G.J.-W., "Overview of Sensitivity Analysis and Shape Optimization for Complex Aerodynamic Configurations", Journal of Aircraft, Vol. 36, No. 1, 1999, pp. 87-96.

8. Reuther J.J., Jameson A., Alonso J.J., Rimlinger M.J., Saunders D., "Constrained Multipoint Aerodynamic Shape Optimization Using an Adjoint Formulation and Parallel Computers", Journal of Aircraft, Vol. 36, No. 1, 1999, pp. 51-74.

9. Elliott J., Peraire J., "Practical Three-Dimensional Aerodynamic Design and Optimization Using

Unstructured Meshes", AIAA Journal, Vol. 35, No. 9, 1997, pp. 1479-1485.

10. Marco N., Dervieux A., "'Multilevel parametrization for aerodynamical optimization of 3D shapes", Finite Elements in Analysis and Design, Vol. 26, 1997, pp. 259-277.

11. Newman III J.C., Taylor III A.C., Barnwell R.W., "Aerodynamic Shape Sensitivity Analysis and Design Optimization of Complex Configurations Using Unstructured Grids", AIAA Paper 97-2275, 1997.

12. Anderson W.K., Bonhaus D.L., "Airfoil Design on Unstructured Grids for Turbulent Flows", AIAA Journal, Vol. 37, No. 2,1999, pp. 185-191.

13. Mohammadi B., "Optimal Shape Design, Reverse Mode of Automatic Differentiation and Turbulence", AIAA Paper 97-0099, 1997.

14. Bischof C.H., Carle A., Corliss G.F., Griewank A., Hovland P., "ADIFOR: Generating derivative code from FORTRAN programs", Scientific Programming, Vol. 1, 1992, pp. 11-29.

15. Malé J.-M., Rostaing-Schmidt N., Marco N., "Automatic Differentiation: an Application to Optimum Shape Design in Aeronautics", ECCOMAS'96 minisymposium on Automatic Differentiation of Programs and Large Scale Optimization, 1996, pp 87-91.

16. Jou W.H., Huffman W.P., Young D.P., Melvin R.G., Bieterman M.B., Hilmes C.L., Johnson F.T., "Practical considerations in aerodynamic design optimization" AIAA-95-1730-CP, 1995, pp. 950-960.

17. Hajela P., "Nongradient Methods in Multidisciplinary Design Optimization - Status and Potential", Journal of Aircraft, Vol. 36, No. 1, 1999, pp. 255-265.

18. Mosetti G., Poloni C., "Aerodymanic shape optimization by means of a genetic algorithm", Proc. of the 5th Symp. on Computational Fluid Dymanics, Sendai, Vol. II, 1993, pp. 279-284.

19. Crosslet W.A., Laananen D.H., "Conceptual Design of Helicopters via Genetic Algorithm", Journal of Aircraft, Vol. 33, No. 6, 1996, pp. 1062-1070.

20. Obayashi S., Yamaguchi Y., Nakamura T., "Multiobjective Genetic Algorithm for Multidisciplinary Design of Transonic Wing Planform", Journal of Aircraft, Vol. 34, No. 5, 1997, pp. 690-693.

21. Marco N., Lanteri S., Désidéri J.A., Périaux J., "A Parallel Genetic Algorithm for Multi-Objective Optimization in Computational Fluid Dynamics", Evolutionary Algorithms in Engineering and Computer Science, Miettinen et. al. Eds, J. Wiley & Sons, 1999, pp. 445-456.

22. Lee J., Hajela P., "Parallel Genetic Algorithm Implementation in Multidisciplinary Rotor Blade Design", Journal of Aircraft, Vol. 33, No. 5, 1996, pp. 962-969.

23. Dulikravich G.S., Martin T.J., Dennis B.H., Foster N.F., "Multidisciplinary Hybrid Constrained GA Optimization", Evolutionary Algorithms in Engineering and Computer Science, Miettinen et. al. Eds, J. Wiley & Sons, 1999, pp. 233-259.

24. Vicini A., Quagliarella D., "Airfoil and Wing Design Through Hybrid Optimization Strategies", AIAA Journal, Vol. 37, No. 5, 1999, pp. 634-641.

25. Morino, L., Kuo, C.C., "Subsonic Potential Aerodynamics for Complex Configurations: a General Theory", AIAA Journal, Vol. 12, No. 2, 1974, pp.191-197.

26. Anonymous "Usaf Stability and Control DATCOM", item 4.1.5.1., April 1978.

27. Anonymous "Usaf Stability and Control DATCOM", item 4.1.5.2., April 1978.

28. Anonymous "Usaf Stability and Control DATCOM", item 4.2.3.1-A., April 1978.

29. Vanderplaats, G.N., "Numerical Optimization Techniques for Engineering Design: with Applications", Mac Graw-Hill series in Mechanical Engineering, 1984.

30. Vanderplaats, G.N., "CONMIN, a Fortran program for constrained function minimization", NASA TM X-62-282, 1973.

31. Knowles and Martinez-Val "Conventional and Unconventional Configurations for Ultra-High Capacity Aircraft" ICAS paper 94-1.3.2, 1994, pp.656-664.

32. Raymer D.P., "Aircraft Design: a Conceptual Approach", AIAA Education Series, Washington DC, 1989.

33. Roskam, J. "Airplane Design", Roskam Aviation and Engineering Corporation, Ottawa, 1990, Part VI and VII.

Aero-Mechanical Design Methodology for Subsonic Civil Transport High-Lift Systems

C.P. van Dam, S.G. Shaw, J.C. Vander Kam, R.R. Brodeur
Department of Mechanical and Aeronautical Engineering
University of California
One Shields Ave
Davis, CA 95616-5294, USA

P.K.C. Rudolph
PKCR, Inc.
Seattle, WA 98166, USA

D. Kinney
NASA Ames Research Center
Moffett Field, CA 94035-1000, USA

Abstract:

In today's highly competitive and economically driven commercial aviation market, the trend is to make aircraft systems simpler and to shorten their design cycle which reduces recurring, non-recurring and operating costs. One such system is the high-lift system. A methodology has been developed which merges aerodynamic data with kinematic analysis of the trailing-edge flap mechanism with minimum mechanism definition required. This methodology provides quick and accurate aerodynamic performance prediction for a given flap deployment mechanism early on in the high-lift system preliminary design stage. Sample analysis results for four different deployment mechanisms are presented as well as descriptions of the aerodynamic and mechanism data required for evaluation. Extensions to interactive design capabilities are also discussed.

Introduction:

The aero-mechanical design of high-lift mechanisms is an important part of the total aircraft design process. In order to insure acceptable performance, a great deal of analysis must be done from both the aerodynamics and mechanism standpoints. Not only do high-lift systems account for 5-11% of the total aircraft cost for a typical subsonic transport, but high-lift configuration performance is important because it can have a large impact on the total mission performance of an aircraft. For example, an increase of 1% in take-off lift-to-drag ratio, L/D, for a typical long-range twin-engine subsonic transport can result in a payload increase of 2800 lb or a 150 nm increase in range (Meredith, 1993). Similarly, an increase of 1.5% in maximum lift coefficient, $C_{L_{max}}$, at a given approach speed can result in an additional 6600 lb of payload (Meredith,

1993). These analyses reveal the potential gain from detailed high-lift system design, but the actual details of how to obtain optimal aerodynamic performance with a given high-lift system can be tedious at best. A multidisciplinary approach has been developed in order to quickly and accurately predict the constrained performance characteristics of a trailing-edge flap system. This technique allows a general database of aerodynamic performance to be integrated directly into the mechanism design and analysis. This is accomplished through the use of a commercial software package along with a custom 'loads routine' which incorporates aerodynamic data from computational fluid dynamics (CFD) or experiment. Aerodynamic data is combined with kinematic data of the flap mechanism during deployment. The current method is limited to 2-D mechanisms, but can obviously be adapted to a 3-D wing. The aerodynamic database may be experimental or computational.

Aerodynamic Database:

The development of an aerodynamic database is the most time intensive portion of the process. The method of development of this database is up to the user, whether through CFD or experimental methods. The database should contain 2-D airfoil performance data as a function of flap gap and overlap. These flap geometry parameters are defined in Figure 1a. Note that flap gap is defined as the minimum distance between any point on the main element and the flap instead of the more common minimum distance from the trailing edge of the main element to the flap. The reason for adopting this slightly different definition is to allow better tracking of the distance between the two elements for flap settings with large overlaps.

Defining the aerodynamic database as a function of flap gap and overlap allows it to be used for any mechanism based on the location and orientation of the flap in relation to the main element of the airfoil. Clearly, this can be a large amount of data. For instance, in order to analyze five flap settings each ranging from 0 - 0.12c overlap and from 0 - 0.03c gap (where c is the chord of the cruise airfoil) at a resolution of 0.005c for each parameter, one arrives at 875 separate cases which must be analyzed. This number may be reduced through educated guesses at the probable gap and overlap ranges attainable at each flap setting. This data is all for a single angle of attack.

In this report, an angle of attack of 8° was selected in order to demonstrate the usefulness of the methodology. This angle is fairly representative for both take-off and approach/landing conditions. In the present study the aerodynamic data was compiled using INS2D which solves the incompressible Reynolds-averaged Navier-Stokes equations on structured, overset meshes (Rogers & Kwak, 1991). This flow solver has been extensively validated for multi-element flows and shown to provide sufficient accuracy in the prediction of these flows (Rogers, 1994). To resolve the complex flow phenomena related to high-lift aerodynamic components, a total of five meshes were used including a principal (background) mesh about the main element, a slat mesh, a flap mesh, and separate meshes for the main-element cove and the flap wake (Figure 1b). The high-lift configuration used is the Douglas LB-546 three element airfoil as shown in Figure 1. The airfoil in the cruise configuration has a maximum thickness-to-chord ratio of 11.55%. The slat chord is 14.48% and the flap chord is 30% of the cruise chord. This multi-element airfoil has been the subject of extensive experimental and computational studies by several researchers (Klausmeyer & Lin, 1997).

In order to further validate the ability of INS2D to predict the aerodynamic performance of this configuration as well as capture changes due to small flap rigging adjustments, a comparison with experimental results is performed. A study by Frank Lynch and his colleagues at the Boeing Company (Lynch, 1995) provides performance changes as a function of flap gap and overlap for this high-lift configuration. Comparisons in terms of ΔC_l and ΔC_d between the experimental results and the predictions based on INS2D are presented in Figure 2. The baseline configuration for this study is the airfoil with a flap gap of 1.27%c and overlap of 0.25%c (gap and overlap as defined by Lynch, 1995). From these comparisons, it is clear that though the values of ΔC_l and ΔC_d do not match up perfectly, the trends are generally very similar. Due to the

nature of the design methodology presented in this report, correct trends, specifically those in optimum flap gap and overlap, are sufficient for the technique to be useful. The disagreement between the experimental results and those predicted by INS2D in Figure 2 may be due to discrepancies in the transition location on the various elements of the high-lift system. No transition data is provided in the experimental results and the validation was done prior to integration of a transition prediction algorithm into INS2D. For the validation, transition was specified at the suction peaks of each element.

The geometries of the main-element cove and shroud as well as the flap of the LB-546 three element configuration were modified to allow retraction of the flap and to provide sufficient space for the flap actuation mechanism (Shaw, 1998). Comparison of the aerodynamic characteristics of the original and the modified configuration indicated only minor differences as a result of these geometry changes. Data is compiled in terms of the total 2-D airfoil lift coefficient, C_l, drag coefficient, C_d, and lift-to-drag ratio, $(L/D)_{2-D}$ as well as flap loading for flap settings of 5°, 10°, 20°, 30°, and 35° as functions of flap gap and overlap. The slat has three positions: stowed, take-off, and landing. The take-off position is used for the 5°-20° flap settings and the landing position used for flap settings of 20°-35°. Note that this results in two sets of data for the 20° flap setting. A Reynolds number based on the cruise airfoil chord and freestream conditions of 15.7 million was used based on typical approach speeds and wing chord lengths seen in current transport aircraft. In Figure 3 a very small portion of the database is shown for the configuration with 20° flaps and the slat in the landing position.

Figure 3a depicts the lift of the configuration at $\alpha=8°$ and Re=15.7 million as a function of flap gap and overlap. Optimum lift performance appears to occur for overlap and gap settings of approximately 0.010c and 0.015c, respectively. However, the performance is rather sensitive to small variations in the gap setting at these small overlap settings. Figure 3b depicts the $(L/D)_{2-D}$ of the high-lift configuration as a function of flap gap and overlap. Interesting to note are the need for the overlap to be small (0-0.02c) to maximize $(L/D)_{2-D}$, and the significant effect of flap gap on $(L/D)_{2-D}$ especially at small overlaps.

Due to the sensitivity of take-off lift-to-drag ratio to drag prediction, some attention must be paid to transition location on the airfoil elements. In the development of the database used in this study, transition is specified on each element at the suction peak of the pressure distribution. Since the development of this database, a transition prediction algorithm has been included within the INS2D

flow solver that makes it possible to determine transition location automatically as the flow solution converges. This methodology identifies several factors that influence laminar boundary layer stability, and hence, lead to boundary layer transition. In two dimensional airfoil flows, where surfaces are generally smooth and freestream turbulence levels are low, transition is governed by Tollmien-Schlichting (TS) instability, laminar separation or turbulence contamination (Kusunose & Cao, 1994). The latter phenomenon is often overlooked, but can be important when, for instance, the flap boundary layer is contaminated by the wake of the main element and/or the slat (van Dam et al, 1997).

TS instabilities, or TS waves, can be analyzed with the e^N transition criterion. This criterion is based on the growth of the TS instabilities in the laminar boundary layer. These instabilities, which are initially damped so that disturbances are suppressed, become neutrally stable at some critical point. After this point the disturbances begin to amplify. When they amplify beyond a certain level, boundary layer transition is imminent. The log of this amplification level is commonly referred to as the 'N-factor' and usually taken as N=9. However, depending on ambient conditions, the N-factor can be as high as N=13.5 (Horstmann et al, 1990).

In INS2D, the N-factor is analyzed with an empirical e^N method which relates the N-factor to the local boundary layer properties, shape factor and momentum thickness (Drela & Giles, 1987). Boundary layer properties are obtained through direct integration of the velocity profiles, which requires a highly resolved boundary layer mesh, or through an integral boundary layer method, which requires only the pressure distribution.

In addition, local skin friction is calculated so that laminar separation can be detected. Once laminar separation is detected through a negative skin friction value it is assumed a small bubble will form. To account for the bubble length, an empirical bubble model is used to delay the onset of transition beyond the point of separation (Schmidt & Mueller, 1989). This feature is especially useful for flows with low Reynolds numbers where laminar bubbles can be significant to the flow development.

Transition by turbulence contamination is predicted naturally by using the Spalart-Allmaras turbulence model (Kusunose & Cao, 1994). In the Spalart-Allmaras model, a source term is added at the transition onset point. This source term is only non-zero in the turbulent boundary layer or turbulent wake. If a turbulent wake intersects a trailing laminar boundary layer, this source term may already be non-zero. Hence, transition may automatically be triggered upstream of the specified location.

Overall, promising results have been obtained from this type of study (Kusunose & Cao, 1994, Duque et al, 1999). The present transition prediction formulation has been applied to the NLR 7301 flapped airfoil. The test was conducted for the airfoil with a flap angle of 20°, flap gap of 0.026c and flap overlap of 0.053c at a chord Reynolds number of 2.51 million and an angle of attack of 6°. This particular airfoil configuration was chosen due to the extensive experimental data available, which includes transition measurements (van den Berg, 1979). The predicted transition locations are compared to the experimentally observed locations in Figure 4. On the lower surface of the main element, transition is calculated within the range observed in the experiment, whereas transition on the upper surface is predicted slightly aft of the observed range. Transition on the flap element is predicted slightly ahead of that seen in the experimental observations. In general, the calculated transition points agree well with experimental observations.

The predicted lift and drag coefficients are in good agreement with the experimental results. Experimental results found C_l=2.42 while INS2D with transition free found C_l=2.44. The experimental drag results show C_d=0.0229 while INS2D with transition free found C_d=0.0217. Especially the drag results, although not in perfect agreement, correspond much better with the experimental data than previous Navier-Stokes results obtained for the same configuration (van Dam, 1999).

Mechanism Simulation:

Mechanism simulation is accomplished through the Pro/Mechanica™ software package. This is a kinematics package capable of simulating the motion of user-defined mechanisms using time-based equations of motion. It may be used in conjunction with the Pro-Engineer™ CAD package or as a stand-alone tool. Many different types of linkages, joints, drivers, and connections are available to the user as well as the capability to incorporate custom loading programs written in FORTRAN or C. The mechanisms used to deploy trailing-edge flaps lend themselves very well to the use of this package for analysis of their action. Assembly of the mechanisms in Mechanica is a point-and-click process similar to traditional CAD techniques. Four sample mechanisms are depicted in Figure 5.

Figure 5a depicts a four-bar linkage designed to increase the amount of Fowler motion at lower flap setting angles. This results in the Aggressive Four-Bar Linkage (Rudolph, 1998). The basis for this mechanism is derived from the initial Boeing design for the 777 outboard trailing-edge flaps. Figure 5c depicts a Link-Track mechanism based

on the Airbus 320 design (Rudolph, 1998). Additionally, a Conservative Four-Bar Linkage (Figure 5b) with less initial Fowler motion than the Aggressive Four-Bar Linkage and a Moveable Track Link-Track (Figure 5d) were modeled from the report by Rudolph. All of these mechanisms show rotary actuators driving the forward link. The rotary drive assembly is classically mounted to the rear spar of the wing, beneath the shroud assembly. Alternative means of driving flap mechanisms are available, but the rotary drive is very common in present designs due to its low maintenance requirements. There are many additional factors that enter into the design of these mechanisms. Side-load handling, conical motion in the 3-D configuration, and fairing size and movement are just a few of the issues that must be addressed. Since the aerodynamic performance of the flaps is the only concern in this study, the mechanism links are modeled as perfectly rigid and massless while the joints are frictionless. This modeling of the mechanisms used for the motion simulation are highly simplified, but sufficient for accurate flap position analysis. Capabilities for more detailed structural analysis are available, but are not part of the present study.

Pro/Mechanica™ is capable of tracking locations, velocities, and orientations of points and bodies in terms of global or local reference frames, but in order to keep track of the gap and overlap measures used in the aerodynamic database, a custom subroutine is required. This consists of an in-house code which interacts with the Mechanica simulation at each time step. The code takes in from Mechanica the flap angle and location of the trailing-edge of the flap and then calculates the gap and overlap based on the known airfoil coordinates. Based on this information, the subroutine then looks up aerodynamic performance based on the flap gap, overlap, and angle. An interpolation routine is included in this procedure. This information is then returned to Mechanica and is able to be presented by the on-board Mechanica plotting package. One may then analyze airfoil C_l, C_d, and $(L/D)_{2-D}$ as well as other parameters such as pitching moment coefficient, C_m, driver torque coefficient, C_T, and forces in the various mechanism linkages as a function of flap angle. Simulation time varies with the desired amount of time resolution and the speed of one's processor, but rarely exceeds a minute per mechanism for the full flap deflection range on older desk-top systems.

Analysis Results:

Results of the mechanism analysis are easily viewed directly from Mechanica. Figure 6 presents performance results for the four aforementioned mechanisms compared with the highest possible performance obtainable at each flap angle.

Figure 6a presents C_l performance for the four mechanisms. The discontinuity in the data at 20° is due to the fact that this flap setting was analyzed with the slat in both the landing and take-off positions. Note also that since the mechanism simulation is based on discrete time steps, data points do not necessarily fall exactly on deployment angles for which aerodynamic performance data exists. One must specify an envelope around the desired flap angle within which the simulation will output data for that angle. This accounts for the off-set seen in some of the mechanism performance data points. Further refinement of the time step and data point envelopes reduces this off-set, but significantly increases simulation time. The current time resolution provides data outputs within less than one degree of the desired flap deployment angles.

The differences in lift characteristics between the mechanisms are modest, with the largest variation in C_l being approximately 0.15. This is still an appreciable amount considering the previous examples on the impact small changes can have on typical airliners today. A more interesting result is presented in Figure 6b. This plot presents the $(L/D)_{2-D}$ performance of the four mechanisms compared to the maximum attainable performance. Lift-to-drag ratio is an important performance parameter for airplanes at take-off where the aerodynamic design is aimed at finding an acceptable compromise between lift capability at take-off and stall angles of attack and L/D efficiency (Flaig & Hilbig, 1993). For airplanes on approach for landing, L/D is less important. It may even be possible that the L/D of single-slotted flap high-lift devices may be too good at flap settings used during landing (Flaig & Hilbig, 1993). Obviously, the performance of a 2-D high-lift configuration differs from that in 3-D, but beginning with a good idea of which mechanisms perform well in 2-D will shorten the 3-D design and analysis process.

From Figure 6b, it is clear that no mechanism is able to achieve optimum $(L/D)_{2-D}$ for all flap settings, especially not at the lower flap angles of 5° to 20° where lift-to-drag ratio is important for good take-off performance. The best performers between 10° and 20° are the two link-track mechanisms with a $\Delta(L/D)_{2-D}$ of about 8 below optimum at each flap setting. At 5°, the Moveable Track Link-Track is the best performer with a $\Delta(L/D)_{2-D}$ of about 5 below optimum. It is important to note that the two mechanisms with the best Fowler motion progression show a $\Delta(L/D)_{2-D}$ of about 10 higher than the poorest of the four mechanisms considered at the lower flap settings. The take-off lift-to-drag ratio of a simple hinge would be considerably worse.

A third parameter of interest is the actuator torque required to deploy the flap mechanisms. Figure 7 presents actuator torque coefficient as a function of flap setting. Actuator torque is important for sizing the actuator and mechanism as well as determining the behavior of the flap mechanism. It is important to avoid load reversal throughout the deployment range of the flaps. Load reversal is said to occur when the loading on the actuator changes from a stowing load to a deploying load or vice versa. Load reversal can lead to flutter and fatigue problems. Additionally, in the case of structural or mechanical failure, trailing-edge flaps must stow themselves. The sign of actuator torque is indicative of whether or not this will happen. From Figure 7, one sees that the Aggressive Four-Bar Linkage mechanism comes close to actuator torque reversal at the 35° flap setting.

Analysis Benefits:

Final product price is often determined within the preliminary design phase through specification of configuration, mission, and size. The ability to accurately predict performance of a candidate configuration early on shortens development time and ensures a quality design.

Note that any known flap mechanism can move a flap from its stowed position to a desired landing position. Therefore, the flap mechanism has very little influence on landing performance. However the various flap mechanisms will cause significant differences in Fowler motion for typical take-off flap settings, thus greatly impacting take-off L/D. Mechanism choice also impacts complexity, actuation power requirements and weight which affect cost and overall airplane weight. Different flap mechanisms require different flap support fairing sizes which impact cruise and low speed drag as well as weight.

The results presented in the preceding figures may be obtained without knowledge of the flap deployment mechanism details. Early on, a designer may look at several candidate mechanism configurations and narrow the field of viable mechanisms through this type of analysis. For example, if airplane climb-out performance is of concern, from Figure 6b one may be able to eliminate several mechanisms right away based on their $(L/D)_{2-D}$ performance at low flap settings. This kind of information early on in the design process can aid the designer in selecting a mechanism type sooner rather than later. These simple mechanism models also give the designer an idea of the complexity and size of the final mechanism. An important issue to cruise performance is the flap mechanism fairing. The fairing size for each mechanism may be determined in a relative sense through these simple models by examining the configuration's vertical dimensions.

Design and Optimization:

In addition to providing analysis, this methodology is also capable of automated mechanism design. Using the on-board Mechanica design study features, mechanisms may be modified in order to improve performance. This requires some additional coding in the custom loads routine and the specification of design parameters within Mechanica. Successful optimizations have been conducted using airfoil C_l and for $(L/D)_{2-D}$ as the objective function and the mechanism linkage lengths as the design parameters. In this way, a designer is able to take a general mechanism type and tailor it to provide improved aerodynamic performance based on the mission goals. For example, one may define the objective function as $(L/D)_{2-D}$ at 5° and 10°, and C_l at the higher flap settings. These parameters can be combined into a single design factor by taking the root mean square (RMS) or some other average of the desired parameter over the range of flap settings. Then the mechanism linkages are changed in order to maximize that parameter.

An example of this type of optimization is seen in Figure 8. The aforementioned Aggressive Four-Bar Linkage is modified, or down-graded, to provide less C_l performance by altering the lengths of the driver arm and the aft-most link. The resulting performance is seen in Figure 8. This initial modification provides a less than optimal starting mechanism for the optimizer to adjust. The optimization routine was then set to maximize the RMS of C_l at each of the flap settings (5°, 10°, 20°, 30°, 35°) by varying the lengths of the two previously mentioned mechanism links. Design constraints are that the stowed position remains unchanged, that the final flap angle must be within 0.5° of 35° and that the gap must remain positive. The latter constraint ensures that no interference between the flap and the main element will occur. From Figure 8, it is clear that improvements have been obtained in the lift performance especially at higher flap settings. At the 35° flap setting, C_l has been raised from 3.25 to 3.35 and from 2.95 to 3.15 at the 30° setting. The focus on the higher flap settings is due in part to the relatively low sensitivity of C_l on gap and overlap at the lower settings as well as the fact that the displaced mechanism is still performing close to optimum at the lower settings. The nature of the objective function also allows for uneven improvements. Since the objective function is defined as the RMS of C_l at each flap deployment angle, optimization may not be focused evenly throughout the deployment range. In order to counter-act this phenomenon, weighting factors may be added to the individual C_l's, thus shifting the focus of the optimization

routine.

Though thorough validation of the optimization process remains to be completed, the technique shows great promise especially in the preliminary design of these types of flap deployment mechanisms. One may use this method to determine whether or not a certain mechanism layout has the potential to perform up to the desired standards before a final mechanism type is chosen.

Conclusions:

A multi-disciplinary design process such as the one presented here has great potential to decrease the amount of time and money spent in the preliminary design of trailing-edge flap mechanisms. The most time consuming segment of the study was the generation of an extensive aerodynamic database using CFD. The performance data contained in this database underscores the important effect of flap overlap/Fowler motion on $(L/D)_{2-D}$ efficiency especially for takeoff flap settings. Flap gap is also shown to have an important effect on $(L/D)_{2-D}$ especially at small overlaps. Once the aerodynamic database is developed, the designer may close in on a mechanism choice very quickly. Automated optimizations are possible and are being investigated further. This methodology is purely two-dimensional and the transition to 3-D mechanism design may alter performance evaluations and design constraints.

References:

Drela, M. and Giles, M.B., (1987) "Viscous-Inviscid Analysis of Transonic and Low Reynolds Number Airfoils," AIAA Journal, Vol. 25, No. 10, pp.1347-1355.

Duque, E.P.N., van Dam, C.P., Brodeur, R.R., and Chao, D.D., (1999) "Navier-Stokes Analysis of Time-Dependent Flows about Wind Turbines," FEDSM99-S295-2, 3rd ASME/JSME Joint Fluids Engineering Conference, San Francisco, CA.

Flaig, A. & Hilbig, R., (1993) "High-Lift Design for Large Civil Aircraft," AGARD CP 315, pp. 31-1 thru 31-12.

Horstmann, K.H., Quast, A., and Redeker, G., (1990) "Flight and Wind-Tunnel Investigations on Boundary-Layer Transition," Journal of Aircraft, Vol. 27, No. 2, pp. 146-150.

Klausmeyer, S.M. and Lin, J.C., (1997) "Comparative Results from a CFD Challenge over a 2D Three-Element High-Lift Airfoil," NASA TM 112858.

Kusunose, K. and Cao, H.V., (1994) "Prediction of Transition Location for a 2-D Navier-Stokes Solver for Multi-Element Airfoil Configurations," AIAA Paper 94-2376.

Lynch, F.T., (1995) "Subsonic Transport High-Lift Technology Review of Experimental Studies," AIAA Overview of High Lift Aerodynamics.

Meredith, P.T., (1993) "Viscous Phenomena Affecting High-Lift Systems and Suggestions for Future CFD Development," AGARD CP 315, pp. 19-1 thru 19-8.

Rogers, S.E., (1994) "Progress in High-Lift Aerodynamic Calculations," Journal of Aircraft, Vol. 31, No. 6, pp. 1244-1251.

Rudolph, P.K.C., (1998) "Mechanical Design of High Lift Systems for High Aspect Ratio Swept Wings," NASA CR 1998-196709.

Schmidt, G.S., and Mueller, T.J., (1989) "Analysis of Low Reynolds Number Separation Bubbles Using Semiempirical Methods," AIAA Journal, Vol. 27, No. 8, pp. 993-1001.

Rogers, S.E. and Kwak, D., (1991) "An Upwind Differencing Scheme for the Steady-State Incompressible Navier-Stokes Equations," Applied Numerical Mathematics, Vol. 8, No. 1, pp. 43-64.

Shaw, S.G., (1998) "An Improved Preliminary Design Methodology for High-Lift Systems for Subsonic Transport Aircraft," Master's Thesis, University of California, Davis.

Spalart, P.R., and Allmaras, S.R., (1994) "A One-Equation Turbulence Model for Aerodynamic Flows," La Recherche Aérospatiale, No. 1, pp. 5-21.

van Dam, C.P., Los, S.M., Miley, S., Roback, V.E., Yip, L.P., Bertelrud, A., and Vijgen, P.M.H.W., (1997) "In-Flight Boundary-Layer Measurements on a High-Lift System: Main Element and Flap," Journal of Aircraft, Vol 34, No. 6, pp. 757-763.

van Dam, C.P., (1999) "Recent Experience with Different Methods of Drag Prediction," Progress in Aerospace Sciences, in print.

van den Berg, (1979) "Boundary-layer Measurements on a Two-Dimensional Wing with Flap," NLR TR 79009U.
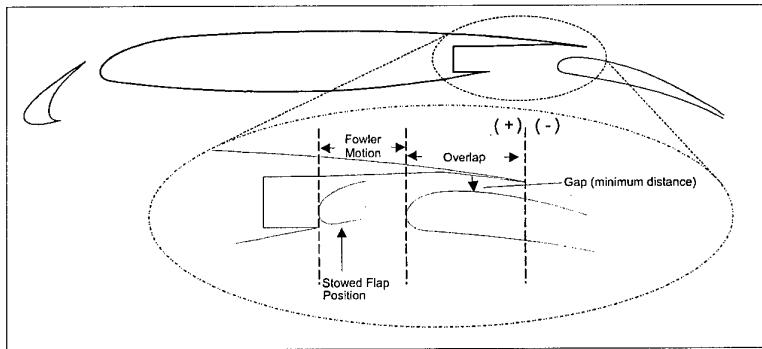
(a) Flap nomenclature
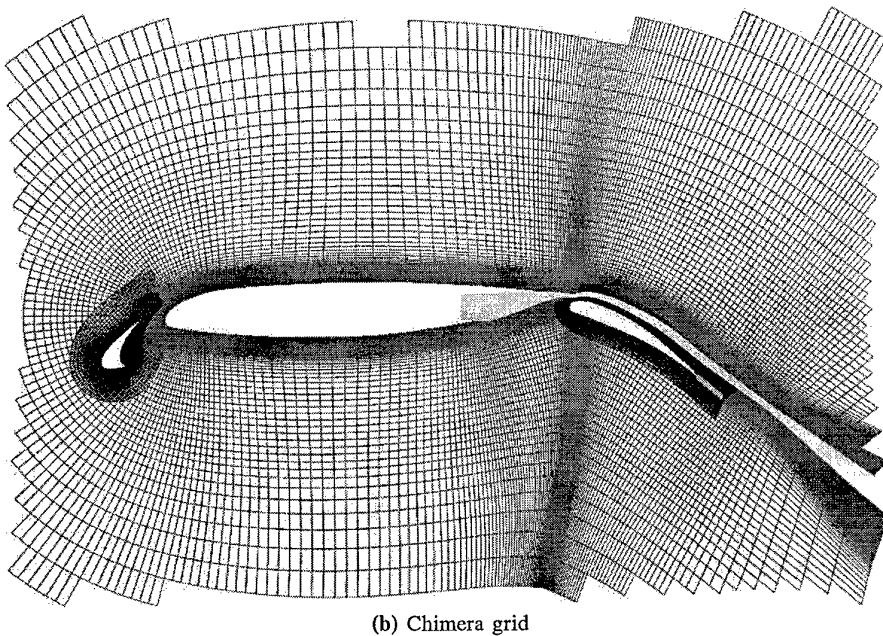
(b) Chimera grid

Figure 1: Douglas LB-546 three-element airfoil definition, flap nomenclature and computational grid definitions.

(a) Lift

(b) Drag
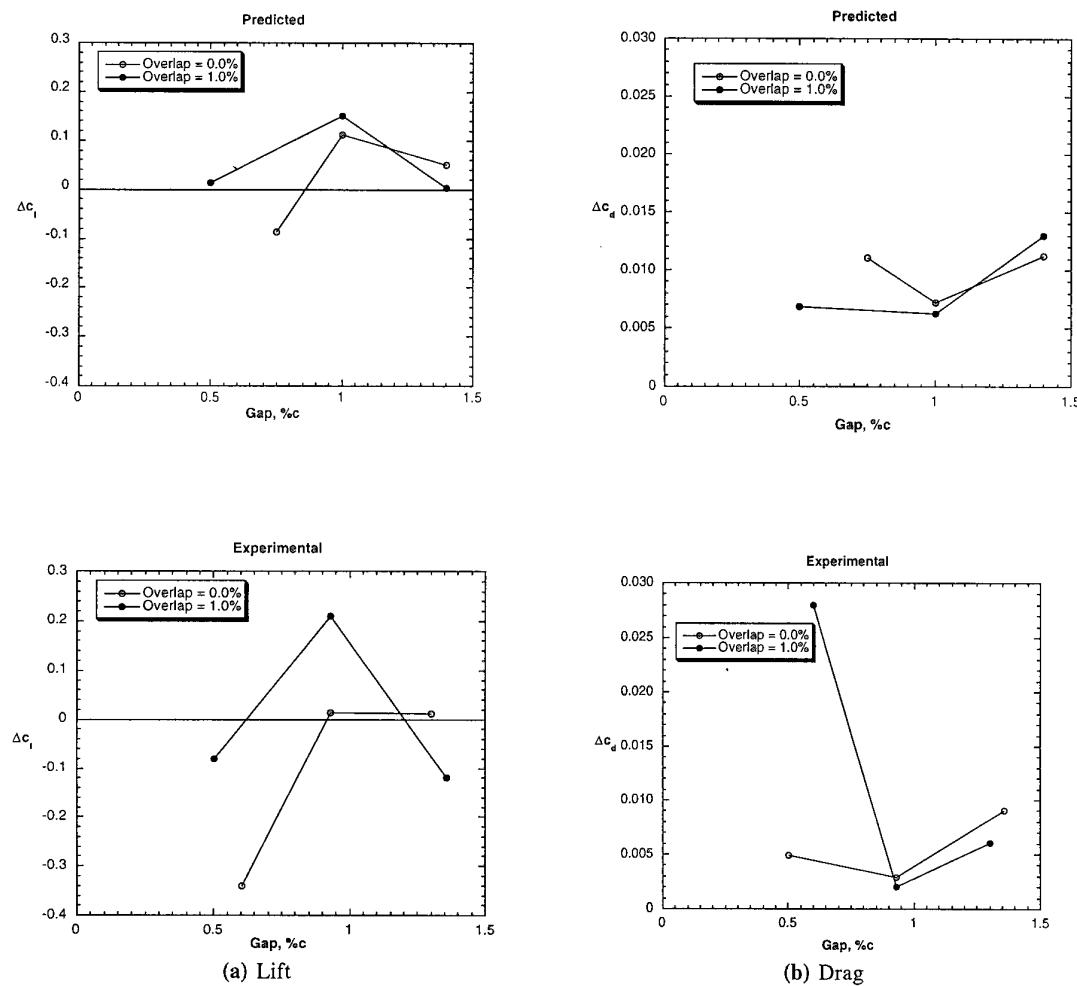
Figure 2: Comparison of predicted and measured effects of flap gap and overlap on lift and drag of LB-546 three-element airfoil at $\alpha=8°$, Re=9.0 million, $\delta_f=35°$. Baseline settings are flap gap of 1.27%c and overlap of 0.25%c.

(a) Lift
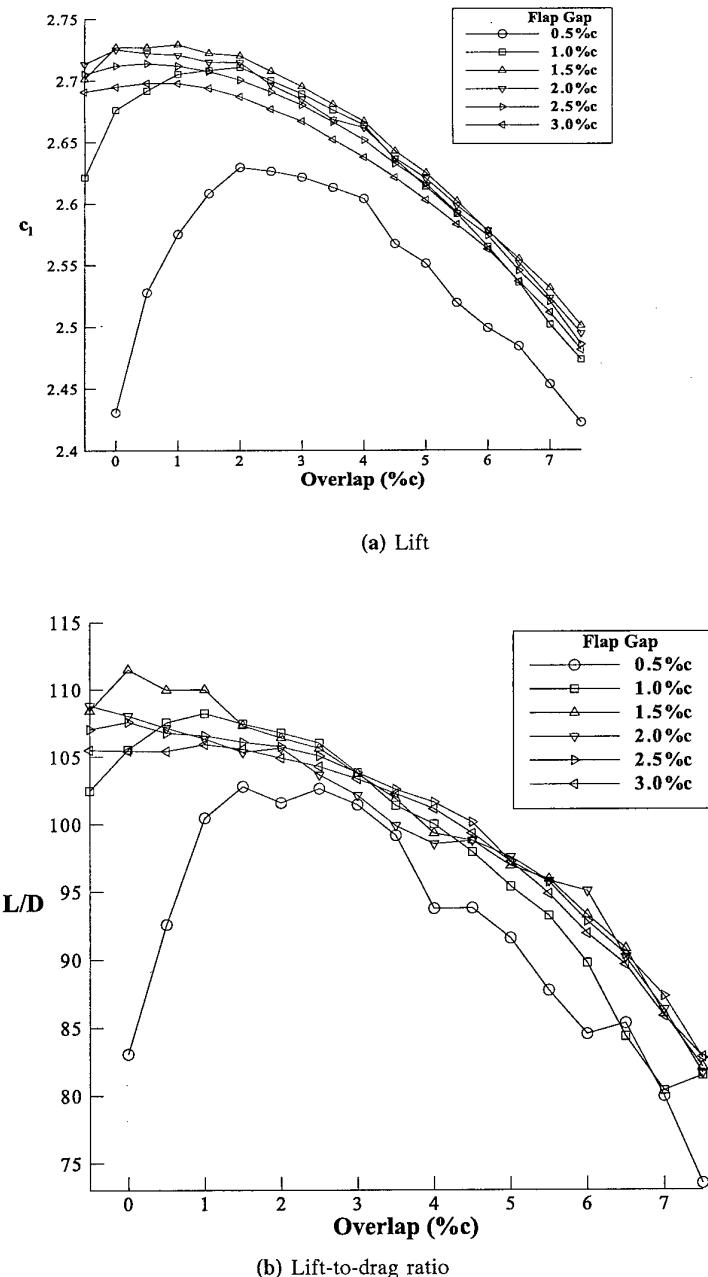
(b) Lift-to-drag ratio

Figure 3: Effect of flap gap and overlap for three-element airfoil at $\alpha=8°$, Re=15.7 million, $\delta_f=20°$, and slat in landing position.

Figure 4: Comparison of predicted and measured transition locations for NLR-7301 flapped airfoil (δ_f=20°, flap gap=0.026c, flap overlap=0.053c) at α=6° and Re=2.51 million.

(a) Aggressive Four-Bar Linkage

(b) Conservative Four-Bar Linkage

(c) Link-Track

(d) Moveable Track Link-Track
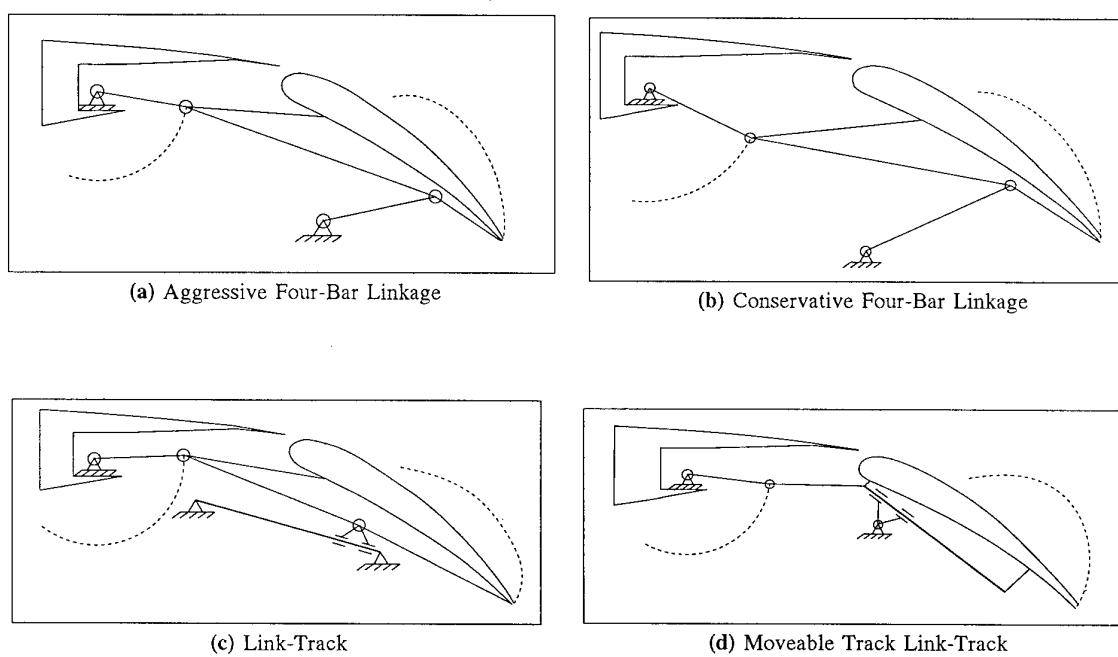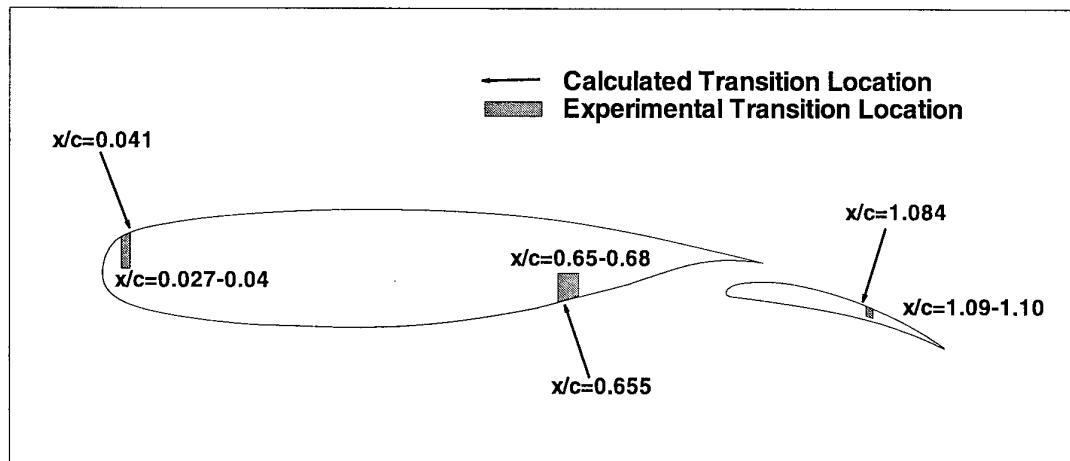
Figure 5: Flap mechanisms depicted at fully deployed setting (δ_f=35°).
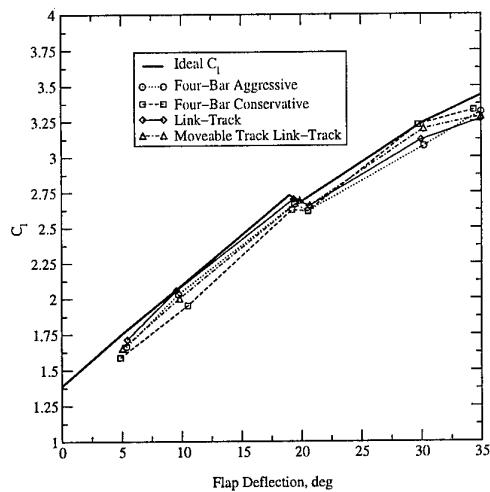
(a) Lift
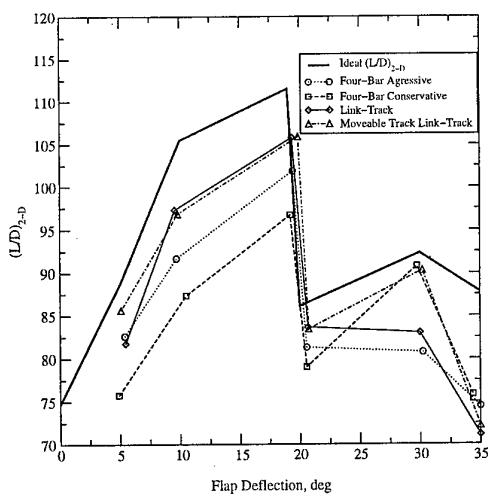
(b) Lift-to-drag ratio

Figure 6: Effect of mechanism on aerodynamic characteristics of three-element airfoil at $\alpha = 8°$, and Re=15.7 million.
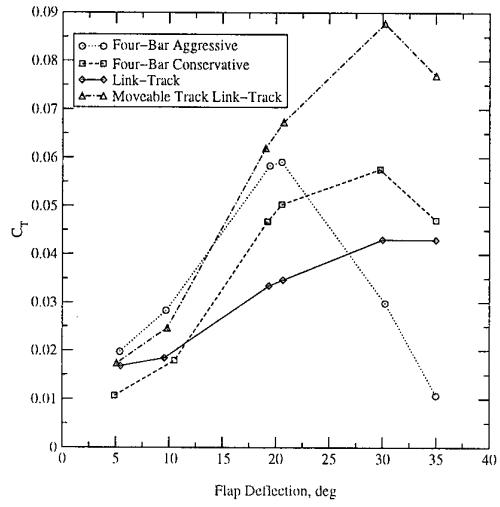
Figure 7: Effect of mechanism on actuator torque.
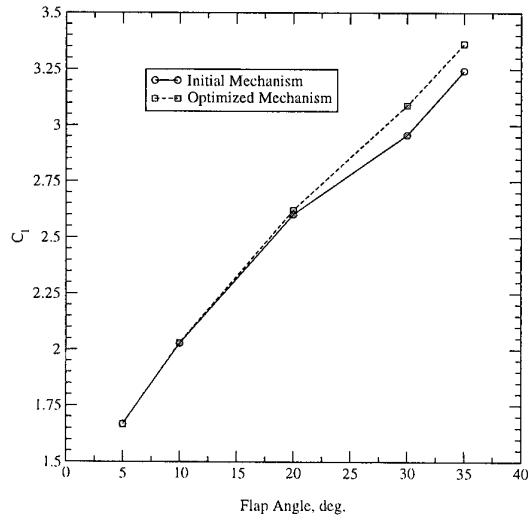
Figure 8: Lift optimization for the Aggressive Four-Bar
Linkage, $\alpha = 8°$, Re=15.7 million.

Conceptual Design and Optimisation of Modern Combat Aircraft

C A Crawford, S E Simm

Defence Evaluation and Research Agency
Pyestock, Room S9, Building 401
Farnborough, Hants, UK

1.0   ABSTRACT

The design of a combat aircraft is an extremely complex task, due to the large range of design variables available. A fundamental understanding of the effects of changes to these variables, and to changes in design/performance requirements, is necessary to achieve a balanced design. At the Defence Evaluation and Research Agency (DERA) this is achieved with the help of conceptual design and optimisation programs, developed and used extensively over the past 20 years or so. These Multi-Variate Optimisation (MVO) programs are rapid assessment tools, enabling the effects of variations in design variables and performance requirements, in terms of overall aircraft sizing and geometric shape, to be quickly demonstrated.

The programs are used routinely within the Air Vehicle Performance Group at DERA to conduct trade-off studies. These include assessments of the benefits of new technologies (e.g. in the fields of structures, aerodynamics or engines) and the impact of setting various levels of performance requirement. The results provide information and advice to the military customer, aiding balance of investment decisions and helping with initial concept definition.

2.0   INTRODUCTION

The design of a modern combat aircraft is a highly complex task, due to the large number of design variables available. The selection of key parameters such as the wing planform, number of engines and their thrust, the degree of stability and control required and the means of attaining it, requires a careful and systematic approach to ensure that a satisfactorily integrated design is achieved. In addition to meeting performance requirements, the design will also be required to meet some other 'measure of success', such as minimum aircraft mass. The optimum configuration will be one which not only meets the requirements, but which also achieves the best 'measure of success'. The process of optimising the configuration is complicated by the subtle inter-relation between the design variables, the performance obtained, and the measure of success employed.

A good appreciation of this process is essential in the assessment of proposed aircraft configurations, and in the planning and execution of forward-looking research. Over the last 20 years or so, the aircraft performance community within DERA (formerly RAE and then DRA) has developed a number of multi-variate optimisation (MVO) computer programs which can be used for preliminary synthesis and optimisation of air vehicle concepts according to user-specified criteria.

The MVO method for conceptual aircraft design consists of a specific aircraft design synthesis program, which is linked to a general program for constrained non-linear optimisation. MVO gives a rapid method for initial aircraft sizing and trade-off studies in advance of going to detailed design. The mass and aerodynamic estimation methods employed are relatively simple first-order methods, based mainly on empirical correlations, but with sufficient accuracy for work at this level. In avoiding the computational complexity of finite element (FE) structural methods and computational fluid dynamics (CFD), the MVO approach lends itself particularly well to broad-ranging parametric investigations. It thus represents a complementary technique and is often used within DERA as a precursor to deeper FE and CFD based design studies, providing the essential requirements-based starting parameters for the latter.

By the early 1990s several versions of MVO were in regular use in combat aircraft studies at DERA, namely ASTOVL for short take-off vertical landing aircraft, CANDEL for canard-delta configurations, and SWEPT for aft-tailed combat aircraft, as well as other versions for civil aircraft. The combat aircraft SWEPT program was used extensively in many studies, and continued to give good results in terms of the trends produced[1-3]. However it was restricted to the conventional swept wing / aft-tailed configurations of the 1970s and 1980s, with cylindrical and/or rectangular fuselage cross-sections.

With the advent of aircraft such as the F-22, JSF and other future combat aircraft concepts, it was clear that requirements for low observables (LO), were having a considerable effect on combat aircraft design. The MVO methodology needed to take account of LO constraints, particularly with respect to radar and infra-red signatures. Designing for low radar signature requires very careful attention to the entire airframe shape, (and may well influence the choice of airframe materials). Attempts to reduce the infra-red signature may include engine cycle choice, nozzle shielding by tailplanes/tailfins, two-dimensional nozzles, and choice of airframe materials and coatings. To meet the resultant modelling needs a new MVO code has been developed, known as STEALTH. This paper describes the program and gives examples from some recent design trade-off studies to illustrate its use and versatility.

3.0   A NEW CONCEPTUAL DESIGN PROGRAM

The new program, STEALTH, has been developed over the last five years. It aims to represent as accurately as possible the geometry of modern combat aircraft designs, including the main features required for low signature, while still remaining within the confines of a rapid optimising approach. It does not

however include the calculation of the signatures themselves. This complex task requires specialist software tools and definition of aircraft shapes and features to a much greater level of detail even than that used in STEALTH.

The following geometry features can be modelled by the program:

- internal weapons carriage

- canted fuselage sides and option for twin canted tailfins

- forebody chines

- aligned planform edges

- wing and tailplane in same horizontal plane

- option for no tails

- scarfed and raked air intakes

- option for two-dimensional engine exhaust nozzles

- option for tailplane and/or tailfin trailing-edge to extend beyond nozzle exit

Explanations of how the above features contribute to achieving a LO aircraft are well documented.[4-6]

Aircraft such as the F-22 and the latest JSF concepts are clearly low-observable designs. However in terms of their basic configuration they are all relatively conventional, in the sense that they retain a fairly distinct wing and body, aft tailplane, air intakes mounted on or near to the fuselage side, and a straight tapered trapezoidal wing.

Although flying wing configurations are attractive in terms of LO and subsonic aerodynamic efficiency, modelling them would require the development of an entirely new design synthesis program, including revised aerodynamic and mass estimation methods. Restricting STEALTH, at least initially, to wing+body layouts, meant that program development could start from the SWEPT program as a baseline, effort being concentrated on updating the geometry routines only, the mass and aerodynamic estimation methods remaining essentially unchanged.

Fig 1 shows a typical layout; the picture was generated by a commercial drawing package from geometry output by STEALTH.
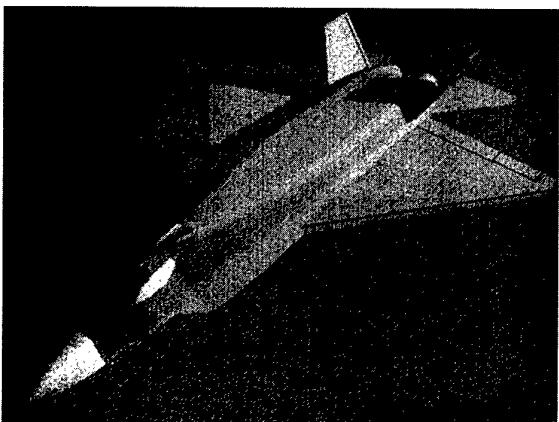
Fig 1: 3-D image of STEALTH-generated aircraft

3.1 Fuselage

3.1.1 External configuration

The longitudinal variation in fuselage cross-sectional area is governed by a 'fairing curve' to ensure a smooth distribution. This curve is defined by 5 independent variables in the optimisation process. STEALTH defines the external lines of the fuselage sections by Bezier splines and super-ellipses, and this detailed geometry definition enables both enhanced visualisation of the concept and improved accuracy of the mass and aerodynamic estimations.

3.1.2 Internal layout

In order to define the internal layout, the user must make a number of design choices at the outset

- Single or twin engine

- Number of internal weapons bays (0-3)

It must then be considered how these items, together with the main undercarriage bays and intake diffusers, are arranged within the fuselage, since all these items compete for space.

Illustrations of the 5 single-engine options and 6 twin-engine options catered for within the program are given in Fig 2. All are highly dependent on the weapons bay choice. A brief description of each layout follows.

Single engine options:

No weapons bays:

- main undercarriage bays canted with fuselage sides

- main undercarriage bays situated on fuselage bottom

One bay:

- single central weapons bay on bottom of fuselage beneath diffuser, main undercarriage bays canted with fuselage sides

Two bays:

- twin outer weapons bays canted with fuselage sides, main undercarriage bays horizontally housed in wing root

Three bays:

- main central weapons bay on bottom of fuselage beneath diffuser, twin outer weapons bays canted with fuselage sides, main undercarriage bays canted with fuselage sides aft of outer weapons bays

Twin engine options:

No weapons bays:

- main undercarriage bays canted with fuselage sides

- main undercarriage bays situated on fuselage bottom

One bay:

- Single central weapons bay on bottom of fuselage beneath intake diffusers, main undercarriage bays canted with fuselage sides

- Single central weapons bay on bottom of fuselage between intake diffusers, main undercarriage bays horizontal on bottom of fuselage beneath diffusers

Three bays:

- Main central weapons bay on bottom of fuselage beneath diffusers, twin outer weapons bays canted with fuselage sides, main undercarriage bays canted with fuselage sides aft of outer weapons bays

- Main central weapons bay on bottom of fuselage between diffusers, twin outer weapons bays in wing root, main undercarriage bays horizontal on fuselage bottom
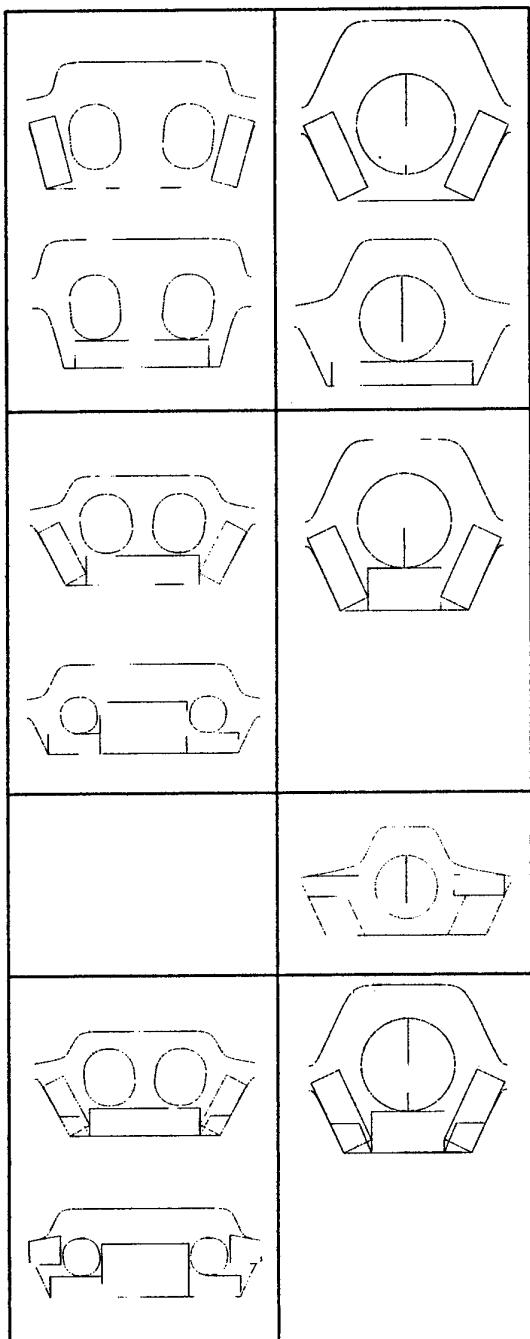
Fig2: Fuselage internal layout options

3.1.4   Geometry definition

The fuselage is modelled via the nine key reference stations shown in Fig 3. The location of these stations is chosen to coincide with major changes in fuselage cross section, and their shape is representative of the aircraft geometry at these points. The location of these stations is given below.

- Radome

- Station A: cockpit front bulkhead

- Station B: pilot's eyepoint

- Station C: intake face

- Station D: front of outer weapons bays

- Station E: front of main undercarriage bay

- Station F: engine front face

- Station G: rear of engine gas generator

- Station H: start of nozzles

Fig 4 presents the sections as they are situated longitudinally along the fuselage.

example1 - Fuselage sections
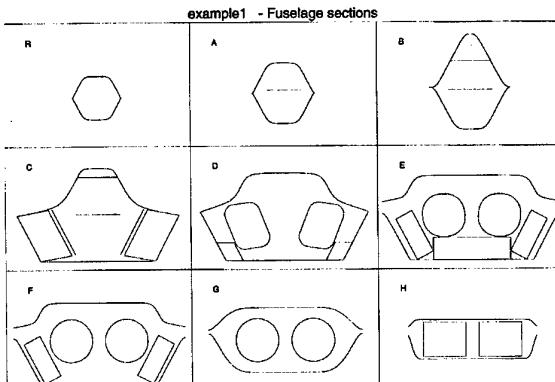
Fig 3: The 9 key fuselage stations (twin engine option)

example1 - Fuselage layout
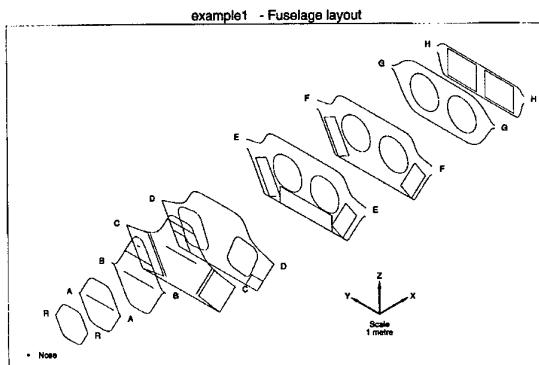
Fig 4: Key fuselage stations positioned along fuselage

3.1.4   Fuselage volume

Figure 5 gives a fuselage cross sectional area plot from a typical run of the STEALTH program.

When fuselage cross-sectional area is integrated along the length of the fuselage, an estimate of fuselage volume is obtained (V_F). This is a major parameter in the estimation of

supersonic drag, volume available for fuel, and mass of internal structure. The detailed geometry definition of the fuselage sections provided by the Bezier splines and super-ellipses enables accurate estimation of fuselage volume, and thus of the parameters dependent upon it.
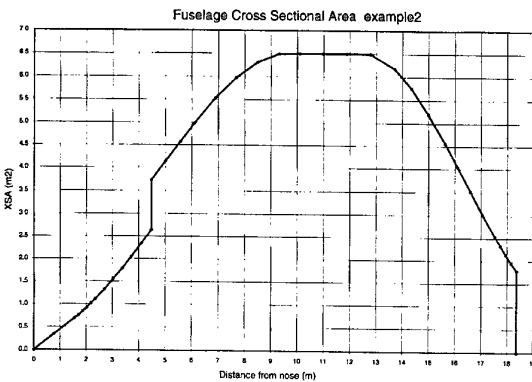
Fig 5: Fuselage cross sectional area distribution

The estimate of the fuselage volume available for fuel is a multi-stage process. The volume V_S, occupied by major items whose volumes are relatively easy to calculate (cockpit, undercarriage, intake diffusers, weapons bays, engines), is computed within the program and subtracted from the total volume obtained from the integration of cross sectional area described above. Then the volume occupied by the fuselage structure and the various systems (avionics, electrical, hydraulic, air etc) must be subtracted. This volume is very difficult to evaluate explicitly at the conceptual design stage, so here it is accounted for by defining a 'remainder fraction'. (A typical value for this parameter is 0.35, based on empirical analysis of a number of detailed aircraft designs. i.e. 35% of the *total* fuselage volume is assumed occupied by structure and systems). The remaining volume is available for fuel tanks, but some of this volume in turn will be occupied by tank structure, fuel pipes etc. A maximum fuselage fuel volume utilisation factor is therefore defined, usually 0.85. This leads to the following equation for useable fuselage fuel volume:

$$V_{fuselage\ fuel} = (V_F - V_S - 0.35 \times V_F) \times 0.85$$

3.1.5 Fuselage wetted area

Fig 6 gives a fuselage perimeter distribution plot from a typical run of the STEALTH program.
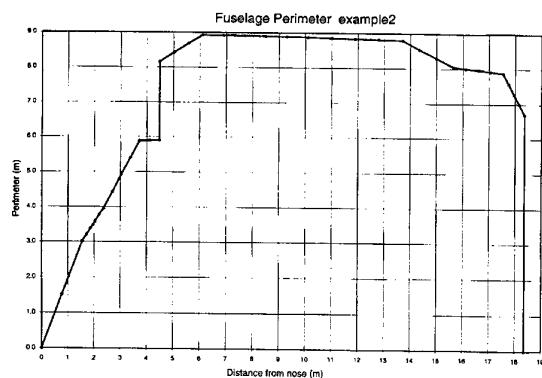
Fig 6: Fuselage perimeter distribution

When fuselage perimeter is integrated along the length of the fuselage, an estimate of fuselage wetted area is obtained. This is a major parameter in the estimation of subsonic drag, and the mass of the fuselage external shell. Again the detailed definition of the fuselage geometry enables an accurate estimate of wetted area to be made, improving the estimate of the parameters dependent upon it.

3.2 Wing

The wing is defined by the parameters

* area

* ¼ chord sweep

* aspect ratio

* thickness/ chord ratio

* taper ratio

all of which are independent variables in the optimisation process.

Currently the program does not cater for cranked wings, but this is an option which it is hoped will be incorporated in the near future.

The wing aerofoil section is a NACA 64 series.

3.2.1 Wing fuel volume

The volume potentially available for fuel tanks is calculated by integrating the wing section chordwise between the front and rear spars and spanwise between the fuselage side and a specified maximum spanwise position. Again a volume allowance must be made for the tanks themselves and associated pipework, so a maximum utilisation factor, usually around 0.7, is specified.

3.2.2 Controls

The program caters for the inclusion of leading and trailing edge devices, spoilers and ailerons. In previous MVO design syntheses, the chords of wing controls had been specified to be a constant percentage of wing chord. Now, as it is advantageous from the radar return point of view to have as few different angles as possible, the option for constant chord controls, giving hingelines parallel to wing leading and trailing edges, has been incorporated.

3.3 Empennage

The following empennage layouts are all catered for within the program

* No empennage

* Vertical (single or twin) tailfins, horizontal tails

* Canted twin tailfins, horizontal tails

* Butterfly tails

The sizes of the tailfins and tailplanes are governed by input values of fin / tail volume coefficients.

Tailplanes are assumed to be all-moving surfaces, so no elevators are modelled. The mass and geometry of the rudder(s) are calculated using input values of fractional chord and fractional span.

3.4 Mass estimation

First-order mass estimation methods from industry are used within the program to calculate masses of both structural components and systems. These are of sufficient detail to provide an aircraft mass breakdown to MIL-STD-1374A.

The methods for wing, fuselage, tailplanes and tailfins take conventional aluminium structure as the baseline, with 'technology factors' employed to account for alternative materials (e.g. composites) and/or other weight saving technologies such as advanced construction and manufacturing techniques. For example, for conceptual aircraft envisaged for the 2015 timeframe, typical factors used are 0.85, 0.90 and 0.85 for the wing, fuselage and tail surfaces respectively, these figures being chosen with industry guidance to represent aggressive targets. The additional mass due to the inclusion of internal weapons bays, associated with structural cut-outs, support structure, bay doors, actuation etc, is calculated within the program, using the same estimation methods as used in industry.

3.5 Aerodynamics

The aerodynamic estimations used within the program are simple first-order methods, based mainly on empirical correlations.

The aerodynamic drag coefficient of the aircraft is given by the expression:

$$C_D = C_{D0basic} + C_{D0base}(M<1.0) + C_{D0wave}(M \geq M_D) + C_{D0stores} + C_{DV}$$

where

M	= flight Mach number
M_D	= drag-rise Mach number
$C_{D0basic}$	= basic zero-lift drag
C_{D0base}	= zero-lift subsonic afterbody drag at reference condition
C_{D0wave}	= zero-lift wave drag (including supersonic afterbody drag)
$C_{D0stores}$	= zero-lift stores drag
C_{DV}	= lift-dependent drag

Zero-lift basic drag is calculated using empirical equations, and includes contributions from wing, tail, fin and fuselage including canopy, intake diverter and gun ports. In addition there are allowances to account for the drag due to interference effects between components and for excrescences and small surface irregularities.

Zero-lift wave drag is calculated, at M1.0 and M1.3, as the sum of contributions from wing, tail, fin, forebody (from aircraft nose to maximum fuselage cross sectional area), afterbody and canopy. The wave drag of the aircraft is assumed to be constant above M1.3. Variation of Mach number in the regions $M_D \leq M \leq 1.0$ and $1.0 < M \leq 1.3$ is determined according to expressions within the program containing empirical factors.

The drag-rise Mach number is the Mach number at which the drag of the aircraft rises sharply in the transonic region, due to supersonic flow over parts of the structure creating shock waves. This has some dependency on the overall aircraft shape, occurring earlier for aircraft of low fineness ratio. This

parameter is not estimated by the program but provided as input data.

Lift dependent drag is defined in two regions, for lift coefficients above and below the 'critical lift coefficient' C_{Lcrit}, joined by a cubic transition region.

In the low C_L region

$$C_{DV} = k_1 C_L^2 / \pi. AW \quad (AW = \text{wing aspect ratio})$$

In the high C_L region

$$C_{DV} = [k_1 C_{Lcrit}^2 + k_2(C_L^2 - C_{Lcrit}^2)] / \pi. AW$$

k_1 is calculated by the program from major wing geometric parameters. C_{Lcrit} and k_2 are extremely difficult to estimate at the conceptual design stage. Therefore these parameters are provided to the program via input tables of C_{Lcrit} and k_2-k_1 against Mach number. Values appropriate for the class of aircraft under consideration are chosen on the basis of data gathered from existing aircraft of similar configuration, wind-tunnel test results and from CFD predictions.

The maximum useable lift coefficient, C_{Lmax}, is a further parameter which is difficult to estimate empirically, and therefore representative values, chosen on a similar basis, are input as a table against Mach number.

Afterbody drag, at a reference (nozzle fully open) condition, is estimated by the program and accounted for in aerodynamic subsonic zero-lift drag.

For internally carried stores there is no additional drag. For externally carried stores a table of drag areas, D_0/q (m^2), against Mach number is input, the values incorporating airframe/weapon interference drag for a representative airframe. Variations as the airframe shape changes are not accounted for, as these effects are assumed to be small.

3.6 Engine

Engine data are provided to the program via a look-up table of gross thrust, fuel flow, air flow, jet exit area and spillage drag against Mach number, altitude and engine throttle setting. These data are given for the whole proposed aircraft flight envelope, and are for an engine at a reference scale. The mass and geometry of the engine at the reference scale are included in the input data.

The engine size is varied from the reference using a scale factor based on thrust. This scale factor is an independent variable in the optimisation process. Engine diameters are scaled with the square root of this scale factor; the lengths and masses of the gas generator, jetpipe and nozzle are adjusted according to slightly more complex scaling laws.

The gross thrust data take account of power off-take, air bleed, and the pressure recovery of an appropriate intake configuration. Different intake assumptions can be made when the engine deck is formulated, giving different pressure recovery and spill drag characteristics.

Variations in afterbody drag, from the reference condition accounted for in aerodynamic zero-lift drag, occur as the nozzle exit area varies from the fully open position. These throttle-dependent effects, strongly influenced by both engine characteristics and afterbody shaping, are very difficult to predict accurately. STEALTH incorporates a simple approximate expression for them, based on variation in jet exit area, but not considering the effects of nozzle pressure ratio. Lack of precision here is thought to be of secondary

importance as these plume effects are normally a small proportion of the whole airframe drag. However this is an area of potential improvement in the future.

4.0 THE OPTIMISER

The program is linked to a general-purpose gradient search code for constrained non-linear optimisation, RQPMIN. This optimiser has been used throughout the history of DERA MVO codes, and has itself undergone frequent and regular enhancement, including the addition of graphical features to aid visualisation of the process.

The problem posed to RQPMIN is of the form

minimise $f(x)$

Where $f(x)$ is termed the objective function, and x represents a list of n real-valued independent variables $x_1, x_2, \ldots x_n$.

At the solution to the optimisation problem, each of the variables x_i must satisfy a pair of inequalities

$$x_{iL} \le x_i \le x_{iU} \qquad (i = 1, \ldots, n)$$

where the values x_{iL} and x_{iU}, the lower and upper bounds, are constants and are specified in the input data file.

In addition, the x_i may be required to satisfy a set of $m \ge 0$ constraints of the form

$$c_j(x) = 0 \quad \text{or}$$

$$c_j(x) \le 0 \quad \text{or} \qquad (j = 1, \ldots, m)$$

$$a_j \le c_j(x) \le b_j$$

where a_j and b_j are constants specified in the input data file. It can be seen that these constraints can be one of three distinct types: an equality constraint, an inequality constraint, or a double inequality constraint.

4.1 Choice of objective function

Given the emphasis placed upon affordability in all modern combat aircraft procurement projects, the ideal quantity to optimise in a combat aircraft conceptual design program would be aircraft life-cycle costs. However cost data for such aircraft are notoriously difficult to establish, and thus creating a sufficiently reliable cost model is an extremely difficult task. Following work done at Cranfield University and continued at DERA[7], a study is underway to identify a first-order cost estimation method that would be suitable for incorporation into the STEALTH code in the future.

The parameter used to date as the objective function has in general been the Basic Mass Empty (BME) of the synthesised aircraft. This is in part because BME is a convenient and clear parameter to work with, but also because aircraft size has historically been seen as having a major influence on cost, and is therefore an indirect measure of the latter.

4.2 Independent variables

STEALTH uses 28 independent variables. 24 of these are geometric variables such as engine scale factor, wing area, fuselage fairing curve values, variables governing fuel distribution within the aircraft, longitudinal positions of the inner weapons bays etc. In addition there are 4 performance-related independent variables: Mach number and altitude in each of two specified sortie cruise legs, used when the option to allow these to be optimised is invoked.

4.3 Constraints

The program has 35 geometric constraints, to ensure that a sensible aircraft design is produced. For example there are constraints to ensure that there is sufficient cross-sectional area at the key fuselage stations to enclose the contents, that the centre of gravity is within the specified limits, and that geometric violations between parts of the structure and/or contents do not occur.

In addition there can be up to 18 performance related constraints. There is always a mission requirement to determine the payload-range performance of the aircraft, and this is formulated as a constraint to ensure that the aircraft carries the correct amount of fuel (including specified reserves) to complete this mission. Also there are always two field performance constraints, specified in terms of landing approach speed and take-off ground roll distance. In addition the user can specify up to 15 point performance constraints in terms of aircraft specific excess power, sustained turn rate, instantaneous turn rate, acceleration time, maximum Mach number etc.

5.0 PROGRAM OPERATION

The operation of the MVO process is outlined in Fig 7. As described previously, the program consists of aircraft design synthesis and performance estimation routines, linked to a general code for constrained non-linear optimisation. In the figure the parts of the operation undertaken by the synthesis program are represented by yellow boxes, while those involving the optimiser are shown as pale green boxes. Input consists of performance requirements (mission, point performance), design constants i.e. values for parameters which remain unchanged during the optimisation (e.g. cockpit length, weapons bay size, structural design factors), engine performance data at a reference scale (thrust, fuel flow etc throughout the flight envelope), and starting point values for those parameters which will change during the optimisation (e.g. engine size, wing area, fuselage length). The program then synthesises the aircraft geometry from the input data, estimates its mass and aerodynamic properties, and then, with the addition of the engine data, calculates its performance. Control now passes to the optimiser which considers whether the performance requirements are met, whether the design is sensible (e.g. centre of gravity within required range, fuselage volume sufficient to house the contents), and whether the synthesised aircraft is of minimum mass. If any of these considerations is not satisfied, the optimiser changes the value of one or more of the design variables, and a new aircraft geometry is synthesised. The process is iterated some several thousand times until all criteria are met and the details of the solution aircraft are then output. Time-history plots of the independent variables, constraint functions and the objective function are displayed to the workstation screen at run-time; a typical run takes in the order of 2-3 minutes.

Used in some complex optimisation problems, gradient search methods are known to be susceptible to finding local rather than global optima. Hence here, to ensure that the true optimum has been achieved, each case is generally run a number of times from a variety of start points. This can be performed automatically via a batch file which factors the values of key independent variables by specified amounts, runs the cases, and writes the results to a summary file to enable rapid selection of the best run.
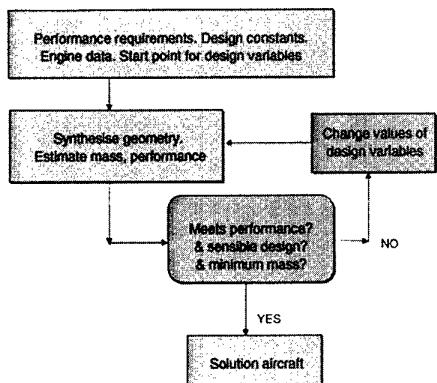
Fig 7: The MVO process

6.0 PROGRAM VALIDATION

MVO methods have been used within DERA for many years, resulting in the accumulation of considerable experience and confidence in the method. STEALTH uses the same optimiser as previous MVO programs, so the main effort of the validation concentrated on verifying the ability of the synthesis to model acceptable LO designs, rather than on the optimisation process.

The program was used to model a number of existing or projected combat aircraft with low observable features. Aircraft were selected for which sufficient design information, in particular performance requirements, were available, and which would exercise the different geometry layout options of the program.

The approach used was to fix the independent variables associated with the major geometrical features of the aircraft (e.g. fuselage length, wing and empennage geometries) at their known values. Thus the exterior airframe shape was, by definition, as representative as possible of the aircraft being modelled, but the program had freedom to manipulate all the interior packaging. The mission profile chosen was one for which the radius of action, with the given weapons load, was known; this profile and radius was then input as a requirement into the program. The 'measures of success' were then how well the synthesised aircraft BME and fuel load matched the real aircraft. A set of point performance parameters were also defined; these were not allowed to influence the optimisation process, but were calculated by STEALTH as a further comparison with the real aircraft.

Table 1 gives the comparison, in ratio terms (STEALTH prediction/real value), for two aircraft. BME, fuel load and a typical transonic sustained turn rate point performance parameter are presented.

	BME	Fuel load	Performance
Aircraft A	0.98	1.00	1.00
Aircraft B	1.02	0.99	0.94

Table 1: STEALTH validation

The results indicated not only that the geometry and packaging were being modelled correctly, but also that the relatively

simple mass and aerodynamic estimation methods incorporated were adequate at this conceptual sizing level.

7.0 EXAMPLE STUDY RESULTS

This section illustrates the uses and capabilities of the program, presenting results from a number of recent studies. These studies are quite different in nature, demonstrating the versatility of the program.

7.1 Engine technology study

This was a study into the impact of engine technology and performance requirements on the sizing of a future offensive aircraft. The work encompassed the effects of engine technology advances in the areas of aerothermodynamics, yielding engines of higher thrust / reduced fuel consumption, and materials and structures, giving engines of lower mass. A range of bypass ratios was considered, the study attempting to determine the optimum bypass ratio choice for a datum set of performance requirements.

Fig 8 presents aircraft BME. v engine bypass ratio for three levels of engine technology. Each point represents an individually optimised solution aircraft, incorporating the specified engine cycle, and meeting the datum set of requirements. It can be seen that each step in advancing engine technology gives strong benefits in terms of a lighter aircraft capable of achieving the same performance. The figure also shows that there is a strong increase in aircraft mass with increased bypass ratio, this trend being strongest at low technology.
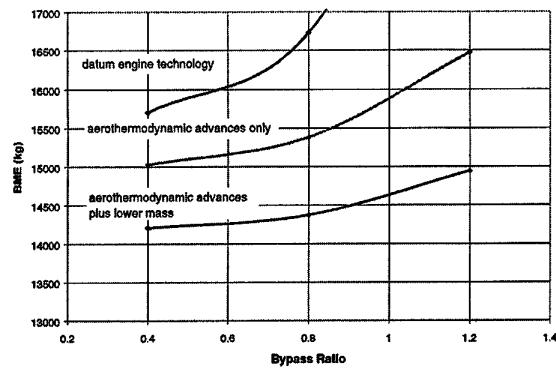
Fig 8: Engine technology effects
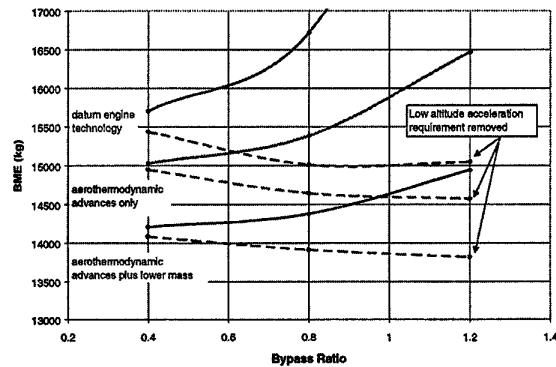
Fig 9: Effect of low-level acceleration constraint

It was discovered that the optimised solutions presented in Fig 8 were all strongly driven by a particularly demanding requirement for low-altitude ingress/egress acceleration. The dashed lines in Fig 9 show the results with this requirement deactivated; the solid lines, as shown in Fig 8, are included for comparison. With this new revised set of requirements the pay-off from increased engine technology is seen to be less than before, but still significant. The trend with bypass ratio is reversed.

Here the program has been used to show how engine technology can give substantial benefits in terms of a smaller, lighter aircraft able to achieve a specified level of performance, and how both BME and the optimum engine bypass ratio are very dependent on the performance requirements demanded at the outset.

7.2   Novel wings study

The aim of this study was to generate a family of conceptual aircraft designs, based around a selection of advanced wing planforms, to assist an informed selection of an aerodynamic configuration for a high speed wind tunnel model. Using the STEALTH program the aircraft were sized to a given level of mission, manoeuvre and field performance, enabling a comprehensive assessment to be made of the pros and cons of each planform when integrated into a complete configuration.

All aircraft had a single crew and twin engines. The air intakes were at the fuselage sides, with the intake ducts running up and over the main weapons bay to the engines, which were placed close together at the rear of the fuselage. The two smaller bays for the air-air missiles were situated immediately outboard of the main bay, with the main wheel housed parallel to the fuselage side. All aircraft had twin tailfins, canted parallel to the fuselage sides at 30°. Minimum leading and trailing edge sweep angles of 55° and 25° respectively were assumed.

A number of the wing planforms considered were of cropped trapezoidal shape, characterised by a trailing-edge crank, with the inboard trailing edge swept aft and the outboard trailing edge swept forward. Because STEALTH is currently unable to model cranked wings explicitly, these wings were emulated in the program by modelling an 'equivalent' uncranked wing. A cropped trapezoidal wing can be regarded as a trapezoidal wing with part of the inboard trailing edge 'cropped' or by an aft-swept wing with part of the outboard trailing edge 'cropped'.

The approach used was to model these wings as aft-swept wings, making some modification to the wing mass estimation. A mass saving of 5% was assumed since the redistribution of area - more inboard and less outboard – placed the spanwise centre of lift further inboard, reducing wing bending moment. The aerodynamic characteristics were assumed unchanged from those of the equivalent aft-swept wing.

The aft-swept wing of the solution aircraft was converted to an equivalent cropped trapezoidal wing of the same aspect ratio, area and leading & trailing edge sweep angles. By observing a minimum taper ratio of 0.10 for the cropped trapezoidal wing, the spanwise position of the crank could be calculated.

Figures 10-13 give some example solution aircraft from the study.
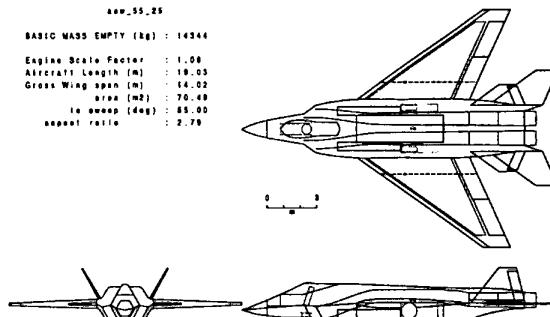
Fig 10: Aft-swept wing planform
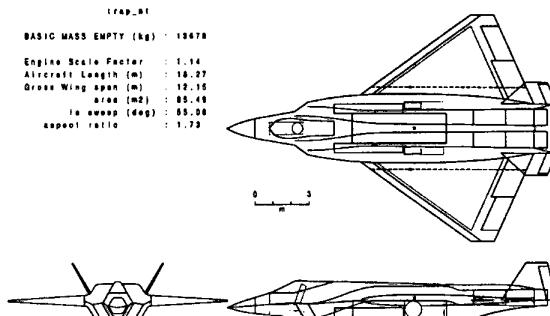
Fig 11: Trapezoidal wing planform
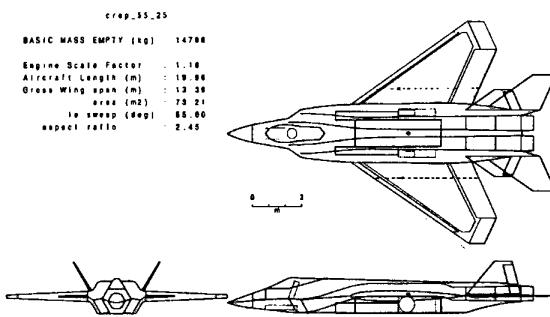
Fig 12: Cropped trapezoidal, 25° trailing edge sweep
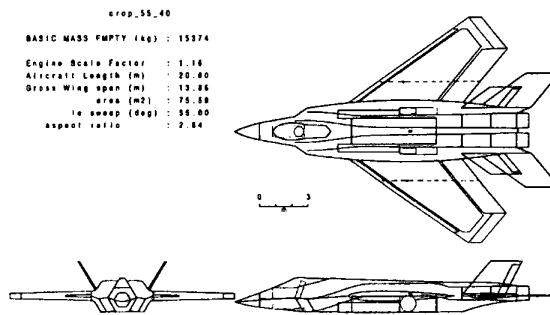
Fig 13: Cropped trapezoidal 40° trailing edge sweep

The trapezoidal wing planform of Fig 11 gives rise to the lightest aircraft. The wing is structurally efficient and has high internal fuel volume. The lightest of the tailed aircraft is that shown in Fig 10 with the relatively conventional aft-swept wing. The cropped trapezoidal wings lead to heavier aircraft, the comparison between Fig 12 and Fig 13 illustrating the mass penalty associated with moving to a higher trailing edge sweep.

This study example demonstrates how the program can provide an effective and rapid means of comparing different wing concepts on a consistent basis. Even where the program does not represent a selected planform explicitly (eg the cranked trailing edge), it is often possible to approximate the configuration in order to reach an MVO solution with sufficient fidelity for valid first order comparisons to be made. Once a suitable planform has been identified using STEALTH, design refinement can proceed using more detailed CFD-based and finite element methods.

7.3   LO trade-off study

The STEALTH program has been designed to model internal weapons carriage and other desirable features of low observable concepts. However, as indicated earlier, it is equally able to represent external carriage by specifying 'no weapons bays' and defining the locations of external stores hard points. This versatility is illustrated by our third example, which is taken from a study to investigate the penalties, in terms of aircraft mass and overall size, of designing for low observability. In this exercise, the STEALTH program was used to compare a 'conventional' aircraft (i.e. external carriage and no shaping concessions to LO requirements) with a low observable baseline aircraft.

The baseline was chosen to be similar to the trapezoidal wing design of Fig 11, although somewhat different mission requirements and technology assumptions between the two studies have led to differences in numerical results. Within the LO trade-off study, identical requirements and assumptions were of course used for both baseline and conventional designs. The essential differences in design constraints are set out in Table 2. Figs 14 and 15 show the resulting aircraft generated by STEALTH.

Fig 14: 'Conventional' aircraft

Fig 15: Low-observable aircraft

The resulting conventional design has considerably lower wing sweep and wing area, while aspect ratio is higher. Eliminating the need for internal weapons bays leads to a significantly smaller fuselage, with secondary benefits resulting from rather more freedom to distribute systems equipment and fuselage fuel efficiently within it. The conventional design is also not burdened with the weight penalty assigned to the incorporation of RAM. However it is not all gain for the conventional design. External carriage of weapons adds to aircraft drag and the effects of this are felt in the mission performance calculation part of the optimisation loop. Nevertheless the results of the exercise show a considerable net advantage in terms of BME for the non-LO design, because of its greater overall aerodynamic efficiency. Naturally, the extent of the difference will be mission-dependent and sensitive to the particular LO constraints chosen. Differences in any of these input specifiers will lead to different numerical results. Discussion of such issues lies beyond the scope of this paper.

'Conventional' aircraft	Low-observable aircraft
No wing sweep constraints	Wing leading edge sweep 55°
	Wing trailing edge sweep 25°
External weapons carriage	Internal weapons carriage
Vertical tailfins	Canted tailfins
Fuselage cant angle small (15°)	Fuselage cant angle 30°
	Additional mass to account for inclusion of Radar Absorbent Material (RAM)
Conventional propulsion installation effects	Propulsion installation effects due to LO design

Table 2: Modelling differences for conventional / LO aircraft.

8.0   FUTURE DEVELOPMENT

There is a program of work planned for the continued development and improvement of the STEALTH code.

As new airframe shapes develop there is a continuing need to ensure that the incorporated estimation methods correlate as closely as possible with a revised database of current combat aircraft. The mass estimation methods have undergone a recent overhaul, prior to a similar forthcoming review of the aerodynamic methods.

There are plans to add further geometric options to the program e.g. cranked wings and chin intakes. Also work is to take place to assess whether a suitable cost estimation method can be incorporated.

There is the potential to improve links with other more complex methods e.g. computational Fluid Dynamics (CFD), Finite Elements (FE) and programs for Radar Cross Section (RCS) estimation. STEALTH output geometry has on previous occasions been input to a CFD package, enabling a more accurate estimate of the aerodynamic parameters to be made for use in the next iteration of studies. However it is not intended to incorporate these methods within STEALTH, as the main value and versatility of the program is in its ability to carry out quick assessment studies. It is considered to be complementary to the Multi-Disciplinary Optimisation (MDO) programs currently in the early stages of development.[8]

It is envisaged that MVO methods like STEALTH will continue to be a major tool for initial conceptual and optimisation studies. Once the basic configuration and sizing has been established in this way, MDO methods will provide a means of refining the concept into an optimised structural/aerodynamic design at a more detailed level.

9.0   CONCLUSIONS

In summary, a new rapid design synthesis program has been developed which is capable of modelling low-signature combat aircraft. Incorporated with a code for constrained non-linear optimisation, the resulting MVO program has been demonstrated to be a powerful tool for initial aircraft sizing studies, and for illustrating the effects of advancing technologies and varying performance requirements.

10.0   REFERENCES

1   J A Kirk
         The use of multi-variate analysis to optimise design parameters for extended-range combat aircraft
         AIAA 92-4707 September 1992

2   S D Hodder, S E Simm
         The impact of advanced engine technology on combat aircraft performance
         AGARD-CP-572 June 1996

3   C A Crawford
         The impact of engine technology advancements on the range v performance trade-off for a future combat aircraft
         ICAS-98-1,10,1 September 1998

4   A C Brown
         Fundamentals of low radar cross-sectional aircraft design
         Journal of Aircraft, vol 30, no 3, 289-290 1993

5   A E Fuhs
         The no-see-um book: radar cross-section lectures
         AIAA New York 1982

6   D Howe
         Introduction to the basic technology of stealth aircraft (Parts 1&2)
         ASME/90-GT-116&117 in Transactions of ASME Journal of engineering for gas turbines and power, Vol 113, no 1, New York 1991

7   S Woodford
         Recent combat aircraft life-cycle costing developments within DERA
         RTO specialists' meeting: Design for low cost operation and support
         Ottawa 1999

8   D Lovell, P Bartholomew
         Progress towards a multi-disciplinary analysis and optimisation capability for air vehicle assessment and design – a UK view
         RTO conference: Aerodynamic design and optimisation of flight vehicles in a concurrent multi-disciplinary environment
         Ottawa 1999

DISCUSSION

Session I, Paper #8

Dr Nicolai (Lockheed Martin Skunk Works, USA) asked the authors to itemize the 22% empty weight increase shown for a stealth fighter when compared to a non-stealthy baseline. He asked how much of this difference was due to coatings and edges, to external v internal weapons carriage, and to propulsion installation.

> The authors noted that largest impact was due to internal weapons carriage and that the additional mass of radar absorbent material was the second strongest effect. In the example shown the propulsion effects were only modest because the concept had only a "limited LO propulsion installation. They noted that other studies had shown that this impact could be significantly greater with more stringent propulsion requirements.

Dr Render (Loughborough University, UK) asked how sensitive the optimization results were to the aerodynamic inputs.

> The authors concurred that the results can be very sensitive to aerodynamic input. They noted that the degree to which this is true, and just which inputs are particularly important, depends on the particular requirements driving the concept under study.

Multi-Disciplinary Constraints in Aerodynamic Design

by
P. Perrier
Dassault Aviation
78, Quai Marcel Dassault
Cedex 300
92552 St Cloud
France

Abstract

Paper nr. 11

A long tradition of aerodynamic design of combat vehicles shows that the expression of the targets and the constraints in the design are always difficult to select. Present long iteration processes hide such variable target/constraints continuous reassessment. Every processes of design unable to have flexibility in target/constraint handling is unusable.

Fortunately, the geometrical constraints are now better handled in new CAD software with features modeling.

The present development of new constrained features modeling will be described from its basic expression to the more complex and variable topology configuration.

Fitting the optimization process to the physics of multidisciplinary constraints may not be as easy as for geometry. It is proposed to select a family of constrained variations of geometry, each able to cope with a specific physical optimization and to generate a multiprojection of the multi-constrained operators. Some conceptual examples of such processes will be presented in the case of aeroelastic design, electromagnetic design and actively controlled configurations with variable geometry for improvement of flow control. The specific domains of use of deterministic and stochastic (genetic) algorithm and of self-adaptation by training (neural network) will be assessed.

New strategies will be proposed for sharing the work of optimization between different companies cooperating to the design of advanced aerospace vehicles.

0. INTRODUCTION

0.1. Past and future in basic design

Definition and data detailed qualification of advanced flight vehicles are becoming very difficult task for design in aerospace industry. Many experts are saying that the problems and their optimal solving procedures are now order of magnitude more complex with the new multidisciplinary requirements.

However the consideration of what was done before does not support the historical theory of past design only devoted to separated optimisation in each discipline ; multidisciplinary requirements were always present in the mind of the designers but only in a global intuition due to the lack of appropriate tools, but not of appropriate exchange between specialists. In fact it becomes a problem with the increase in size of the design office at the preliminary stage of design and much more in the development phasis. The number of experimental and numerical data has dramatically increased. Much more precise evaluations in each discipline and their sensitivity to interface with other discipline are available but true multidisciplinary work, at the peak of complexity and cost are less available at the time where human exchange become harder due to the number of specialists involved in the final choices. The synthesis of their studies becomes problematic whereas, in the past, global estimation of complex phenomena, multidisciplinary or not, was present for tractable although rough optimisation.

So the problems are first human and secondly of availability of convenient engineering tools.

0.2 Human problem - Organization methodology

The number of stages in decision making is well known as major parameter in the efficiency of a company. It is particularly true in multidisciplinary design whatever the help of convenient tools. The driving team in the design is a "trinom" : a trinom is a group of three men who have to work together in a close manner to succeed the integration of the three major general disciplines of importance in design : the system analysist, the architect and the shape designer. These three men are working under the supervision of the chief engineer. Denomination may be variable in each company but the functional attribute cannot change. It covers the three main drivers in design plus the interface and convergence leader :

1/ Future product seen as a system fulfilling given tasks for an operator, eventually in a more general system of defence, transportation ... Major interest for the system leader is to afford global performance and to share the contribution of each part of the system to the efficiency of the product by convenient allocation of targets in performances for platform and sensors and weapons.

2/ Future product seen as a technical achievement with the best cost - efficiency of each physical item as contributor to the elementary performances needed for support of global performances and cost of the system.

3/ Future product seen as a real hardware and software product, easy to manufacture, test and operate because detailed design is adjusted to the production and operation.

It is now easy to build a tree of technical relations derived from the "trinom" as the group supporting the final decisions of the engineering leader. The problem will be to have small number of people reporting to the trinom and large number of specialists helping them to succeed the multidisciplinary balance at the higher level. The 1 and 2 facets of the multidisciplinary work need specific tools for evaluation of complex multidisciplinary interactions and first adequate interaction between specialist involved. The facet 3 is more a user of output of optimisation of technical parameters but it appears as the main dealer of constraints : geometrical, industrial and economical constraints.

With convenient hierarchy that may be achieved with minimum number of levels for avoiding loss of confidence and of oral traditions (much more effective that any note or listings or figures).

0.3 General technical tools for multidisciplinary work

At this level, we consider the 3 items ; we can express them in another perspective as builders of three products :

- The system engineer <u>master objective</u> with allocation of performance targets. It needs specific system tools at two levels for building as products :
- First global estimation - second detailed prediction of performance - variations with characteristic parameters of interface between different disciplines that share the allocation of performances : for example, the size of the radar antenna and the electromagnetic detectability and the speed of the flying machine. Major output is specifications for the cost and/or performance index to be declined for each specialist. Its major tool is a mission simulator.

The "architect" engineer <u>master a set of constraints</u> that minimize the size weight and cost of the final vehicle taking in account all the allocation of volume and location for structural parts or fuel or engines ... . If the margins for tolerance, reparation and operations are included, it is easily seen that

reduction in size, weight and cost appears as bounded by geometrical constraints that are the major output of a good architecture. Major output is a virtual model or numerical mockup

The "physicist" and "shape" engineer master the physics of the final vehicle because the laws of the physics bound the achievements of the systems in performance and the margins taken versus limits of the physics are a measurement of the "state of the art" in each discipline. Its major output is now a virtual model of computation (simulation) of detailed performances figures and physical parameters necessary to the evaluation of the performance index and determination of each real hardware and software.

Due to the fact that the major interface between the second and third partner of the trinom is geometrical, and that the major stresses are at the outer limit of structure, the skin of any aerospace product is critical in the design loop, it is convenient to speak of the output of the third engineer as "shape" engineer and to summary the relationship in the trinom and their tools in the following table :
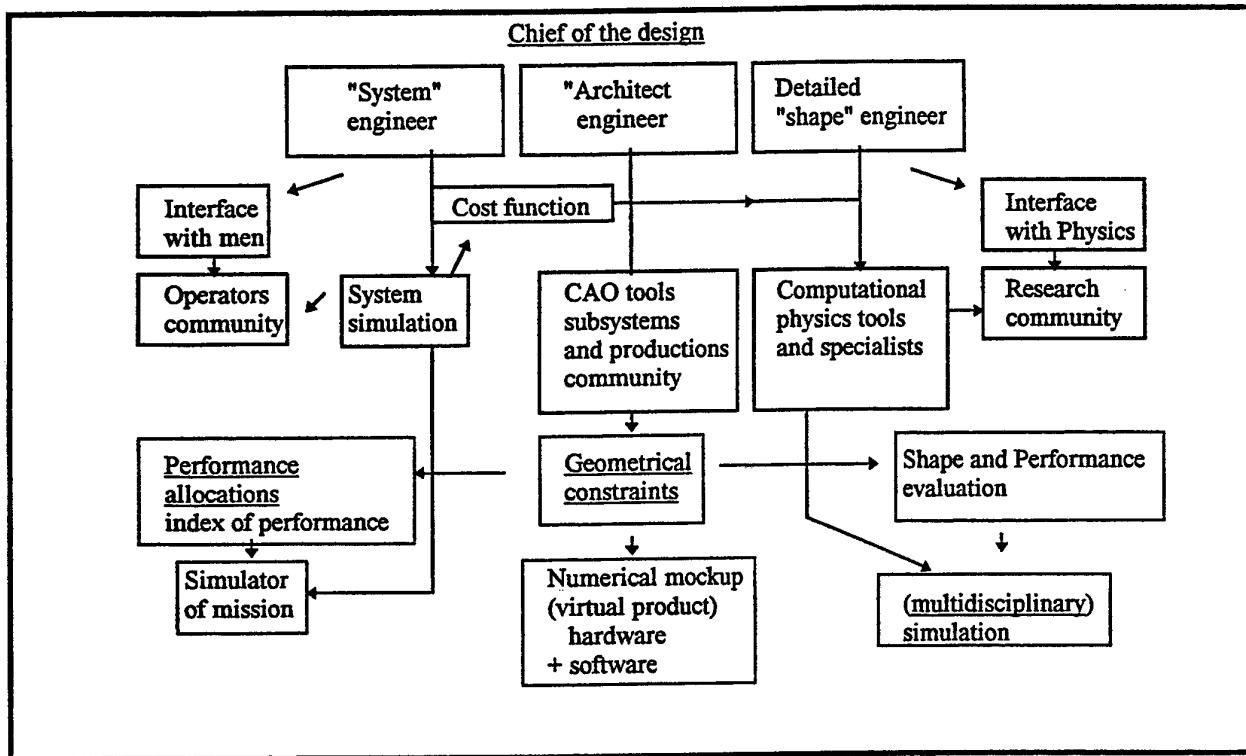
Generally the multidisciplinary work is considered only on the side of the "physics and shape engineer" and the teams of specialist that he federates. But this table shows that it is a true cooperative work where the function to optimize is coming from system engineer and the constraints from the "architect engineer" as a prerequesite to multidisciplinary optimisation (M.D.O.).

0.4 Gradual concepts to incorporate in M.D.O.

The major problem in optimization with many variables is to evaluate with reduced number of

"constrained" parameters cost function and its derivatives sensitivity analysis.

This paper is so organized as follows : first, geometrical constraints are taken as an example of reduction of number of parameters involved in multidisciplinary optimization. Next a thorough analysis of the rationale of physics related to variation in plysics emphasized the importance of numerical simulation and its validation in any multidisciplinary work. In conclusion some paths to cooperative multidisciplinary work between different companies will be proposed.

1.0. The problem of "constrained" geometry

First C.A.D. codes were derived from a mimic of the building of drawings in the design office with appropriate and traditional parameters and line and axis of reference. It excludes any direct volume generation and any variable parametrization of the quotations, so it excludes any distorsion, contraction or dilatation of separate parameters except the very scale of the part described. Such a definition is complete as is needed for a manufacturing plant, except some additive elements that appears by themself in the fabrication as for example the filets generated by path of a round cutting tool. Some elements defining completely the part may have to be added in the past to C.A.D. by manufacturing team, but now the effort tend to have complete geometry with details included in geometric data base. Thus it is possible to avoid hardware for mock-up and to rely on a completely virtual mock-up.

However the complexity of geometry is becoming so large that the preliminary design have to escape to so-detailed data base by simpler geometrical definition with the just-needed parametric description. It is the first effort to push in order to minimize the optimisation cost ; but it assumes the selection of relevant parameters, and the possibility of easy refinement or simplification of the geometric shapes, that can be done interactively if a trace-back of the work of definition on an interactive console is available. Parametric definition itself means that the tridimensional geometrical package of C.A.D. is able to reconstruct any complex shape for a given set of its basic parameters as retained in the definition. Such a parametric definition of the lines , surfaces and volumes is called : definition by "features" ; it has to give continuous threedimensional shapes varying with a continuous variations of the parameters. It is not generally possible outside of a limited range of variation of the parameters due to topological constraints : for example a torus has no interpenetration if the radius of centers is larger than radius of the basic circle and such interpenetration may be excluded if the volume of the torus is used as tank/link in geometry may also be excluded by stress or aerodynamic requirements.

So there appear two types of constraints :
- first topological
- second user or designer constraints as required by a specialist.

We may notice as example of architect or physics specialist requirements : the continuity in curvature for transonic design of airfoil and the generation by straight lines for easy fabrication of skins or fast milling.

1.1 The geometrical subset of constrainted shapes

We may include the previous requirement in the geometrical data base with features if the following rules are embedded in the variable geometrical package :

- for a given set of parameters only one shape is obtained

- for a given set of parameters continuity is enforced at the level of second order (aerodynamics) or first order (stress and electrodynamics) or zero order (part assembly)

- boundaries of change in topology with parameter variations may be easily computed : inequalities in the space of parameters may be then known, as a dual approach of acceptable topology (topology constraints).

- interaction between volumes or surfaces or lines may be precisely computed in order to take in account any architectural containment (e.g. volume of engine in a fuselage, undercarriage retraction without interference with a store ...)

1.2 Inclusion of relations between parameters in order to fulfill a geometrical requirement

The number of parameters involved in a complex geometrical requirement may be so high that a subset of acceptable deformation is often of great value. We have to define line of camber versus original reference line, surface of camber versus original plane of reference, volume of dilatation versus original volume. For the zero value of deformation parameter the shape is unchanged, for the 1 value the deformation is such that camber is completely applied. Many such deformations has been currently used in the past ; for example in a wing section change of the thickness or of camber, for a fuselage change in the mean line ...

On the figure 1 is given the family of deformation of a front fuselage when the line of sight of the pilot is changed ; it requires the position of the eye of the pilot, evaluation of the tangent to front fuselage and a camber line that allows such variations and may in addition keep for example the axisymetry of the nose radom and obviously the continuity in curvature at a given reference section of the fuselage.

This deflection of front fuselage for being tangent to a line of variable inclination is a very simple example. Much more complex constraints appear when complete internal architecture appear as a driver for geometrics. For example on figure 2 is given a typical interaction between localisation of radar, canopy, engine with its air intakes ; each

volume has to be specified with appropriate margins : clearance around engine, thickness of the skin of air intake ; one more step in definition has to take in account the structural requirements. For example in figure 2 the description of main frames, spares and ribs allows to express requirements in rigidity or minimal thickness of the structure. An appropriate specification of structural constraints is obtained by inclusion in the geometrical margins of the minimum thickness of structural parts.

The optimization may then cover parameters variations excluding two small carrying loads parts. Again the better description is to define minimal body plus maximal body and to allow variation of parameters constrained by the two extreme body geometry. One typical multidisciplinary optimization may search for maximization of mass of structural parts and minimization of wave and friction drag.

However, such a fixed geometry optimization is not at all convenient for optimality except if a set of points of optimization are selected (not the same for stress analysis and drag analysis). Real design has to take in account the variable geometry imbedded in true active control of aircraft. Such active control may involve three types of actuators : conventional slats and flaps, unconventional active control and jet deflections. In that case different targets may be fulfilled with different sizing requirements : all the devices may include geometry deformation for optimization of aerodynamic characteristics but may induce moments around center of mass. Similarly the conventional control surfaces are generating moments so that they generate angular accelerations taking in account the ellipsoïd of inertia and counteract the moments induced by external perturbations and optimal setting of slat, flap ... with margins for pilot actions. Figure 3 summarizes such constraints on surface, blowing, deflections that are essential parts in optimization of aircraft design. Such interaction of control requirements and basic aerodynamic requirements may be also express as constraints on size of flaps and necessary balance in moment not generally included in basic monodisciplinary design : different of margins for positive thickness of load carrying parts, it may appear as an allocated range of variation between two extreme values of moments covering the range of needed angular acceleration around the three axes.

Major problems of design are related to the boundaries of same topology of geometry : for example the maximum allowable pitching acceleration with an aircraft without tail is bounded by the relative size of main wingbox and elevon size when the aircraft without horizontal tail (i.e. separated flap with increased lever arm) ; but with horizontal tail, it may have more angular acceleration at the expanse of longer rear fuselage.

It is so possible to define a set of topology of aircraft that include each their own boundaries. The better geometrical description have to include a tree of branches, each with fixed topology with steps at bifurcation. The optimization may or may not be converge in the same branch ; if iterations of design converge at points with margins inside the iso-topology boundaries, the topology selected is acceptable ; if not the geometrical constraints along the boundaries will be the main driver in design, with risk of jump to another topology (for example with and without tail).

1.4 Flexibility in design by geometrical finite element method

From such considerations, it appears that the boundaries of constrained iso-topology geometry are first to be considered in design. Flexibility are given by sufficient margins added to that boundaries. Again the boundaries, with or without margins, appear as a reference for later optimization. In the same target of reduction of the number of free parameters in the design, all fixed point, curve, surface has to appear as constrained or fixed parameters : it is a "feature" modeling approach. We have to retain such approach for any multidisciplinary optimization.

A standard "feature modeler" for geometrical definition of aerodynamic shapes is operational from many years in the Dassault design office ; it relies on point, tangent and curvature vectors that define unambiguously the surface of the patches ; surfaces are fitted in curvature along the three dimensional parametric splines at the boundaries of each finite element patch.With such a vector definition any transformation of the space may give a new vector set by applying linear operator (matrix) coming from local distorsion of space : it allows a "feature" modeling to be easily generated. The transformation of the space may itself defined as a two "point" homothetic or affin projection along a camber line or surface, covering the boundary of topology as previously defined. Figure 4 summaries such modeler characteristics.

2. A RATIONAL APPROACH BY MATHEMATICS

2.1 General problem of optimum design

If it is possible to define explicitly the index of performance, the constraints, the state equations, it exists a rational procedure to derive the optimal set of geometric parameters giving the optimal shape for the body.

However one single optimum shape exist and that the "optimum optimorum" of the shapes may easily be

obtained if the cost function has a great number of local minima.

- The time of computation is tractable with present computer in as much that there is no exact solution to determination of flow with real Reynolds number accessible to computation for a long time, and that approximate solution with Reynolds average flow is also generally impossible to compute accurately with present computers.

- The constraints may be expressed with sufficient accuracy leading to realistic design.
- The optimal shape is stable for a small variation in cost fonction, constraints, external conditions or set of parameters fixed as representative of physics modelised.

Generally the designers avoid such cumulated uncertainties on the existence of an optimum design by taking as an initial point a design well known as robust and not so far from optimum, and trying to select a better design by iterative procedure. Of great help is however the research of local optimum with simplified analysis, giving more precise answer on a partial shape design. For example the selection of an optimum aerodynamic wing section may help greatly to design a wing for conditions too costly to be completely computed in 3D. The result of complex wing section design may then be transformed in a simplified cost function on pressure distribution, pressure gradient with penalty on lift and pitching moment.

If we turn to elasticity equation for materials and Maxwell equation for electromagnetics it is possible in the same way to simplify the geometry of load carrying parts, of antennas or bodies, to reduce the number of modes and of the frequencies, to assume ray tracing or simplified collapse criteria and so to have access on suboptimal parameter optimization. For example optimization of flutter speed or of radar cross section for fuselage section may be obtained at a realistic cost/time of supercomputer.

From a mathematical point of view, it can be seen as an optimization with a simplified set of state equations and with an alternate direction descent.
Such approach will be generally the only realistic optimization procedure for many years due to the complexity of state equations.
However computation of "not far from optimum" shape is possible if the number of parameters is not too large with a mix of such simplified optimum design and direct descent for small number of parameters.
If the cost function is sufficiently simple, its derivative may be evaluated and the cost of computation of the adjoint state of Euler, elasticity, Maxwell equation is not too large ; then an optimal

shape may be obtained iteratively for a cost equivalent at each step to some direct computations.
If the cost function is complex, and impossible to be derived, amongst a family of optimal shape with reduced number of parameters (typically less than 20) it is possible to select iteratively a better set of parameters defining a better shape.

2.2 Steepest descent to optimum multi-disciplinary shape

If we take the process of alternate descent, one with optimum design with derivable simplified cost function, the other with reduced number of parameters descent, the major time of computation will come from the later ; the sensitivities may then be compared, giving evaluation of uncertainties on critical parameters

There is three ways for solving such descent problem :

- The first one is to rebuild derivative from discrete variations. in that case, an estimate of the local constant cost curve will be obtained and a discrete conjugate gradient procedure may be initiated.

- The second one is to assume that the cost function is near optimum and so quadratic (or second order) versus the parameters. One fit a second order approximation of the cost function to the available cost values already computed for a set of parameters ; this optimum bowl will be more precise at each new computation and will give more effective determination of optimum set of parameters than conjugate gradient because all the points will contribute to the knowledge of the cost function.

- The third one is to mix heuristic and learning process in search of optimum. One way is the use of genetic algorithm : the new set of parameters will have an heavier weight as far as it will be better in cost evaluation. However that heuristic process is poor when deterministic cost function is to be addressed : the final convergence is slow (in square root of n) whereas it is steepest when a continuous convexity is present as usually. An approximation of cost function by neural network may also be used but it is not so effective as for dynamic system optimization.

2.3 Constrained optimization

If one make detailed analysis of the convergence towards optimum design, two cases appear :

- Optimum shape is between the constrained margins of variations of the parameters allowed by the different constraints in geometry or equivalent simplified cost boundaries. In that case, the process will be as much efficient as the parameters will be in small number, taken in a family of suboptimal shapes (for example smooth curvature family, including optimum shape previously obtained).

- Optimum shape is in constrained conditions. It is generally the case when the design is good, because the maximum of efficiency is to be compromised with other constraint. In that case, it will be better to follow the surface of constrained parameters because it has a lower number of degree of freedom.

For example, the optimal wing section will be in a family function mainly of maximum thickness, and such family will be bounded by the design Mach number and the weight of the wing box and its fuel capacity.
But the root of the wing will be deduced from that external wing section differently following the constraints in wing-fuselage shape intersection and respective degree of freedom (Figure 5).

2.4 Flexibility and robustness in design - least regret optimization

One important output of optimum design is the sensitivity to parameters. It will give the stiffness of the performance / geometry relation. Decrease of such stiffness relation will give more robustness to the design.

In the same direction, the adjoint equation will give information to the best location of sensor and actuator on the aircraft. The better actuation for an active aerodynamic control will be obtained by increase of the function of the adjoint equation at the location of the actuator, and it can be also a design driver to optimally select the actuators.

Anyway the optimal design will be more robust by multipoint design and by variable setting of slat and flap (variable geometry) around optimal shape as may be intuitively seen in Figure 6.

One way of expressing the robustness versus multidisciplinary optimization is the "least regret optimization". It corresponds to the concept of :

- maximisation of performance index in aerodynamics
- minimisation of sensitivity to other constraints or maximisation of the distance to the constraints.

Not far from optimum design for performance index is a "without-important-losses" improvement of the margins near critical constraints.

3. CONSTRAINTS OF PHYSICS

In the same manner that we have addressed specially the changes in topology in the geometrical expression of constraints, we need to delineate the boundaries of homogeneous physical subdomains (Figure 7).

Such subdomains are defined in the following manner :

- A boundary in a physical set of parameters is to be identified each time that a topology change occurs in the flow (in aerodynamics), in the deformations (type or mode of buckling or collapse in material analysis) or in wave propagation (diffraction vs reflection in electromagnetics)

- The boundaries are to be defined at the size larger than the phenomena observed in the modelling approach or at a smaller size if amplification takes place and appears in larger size.

- The boundaries are to be defined with the set of physical parameters relevant to the physics (Mach and Reynolds number, characteristic lengths or frequencies ...).

With the help of such domains, it is now possible to make a checking of the trajectory of the optimization process :

If it is bounded only by geometrical constraints validity of simulation may be established by validation of the codes on a : - same topology in geometry, same topology in physics - experiment.

If it is bounded by physics constraints, it is necessary to make evaluation of the jump of properties that comes from the change in topology. If there is a continuous behaviour of physical properties, it is just a matter of evaluation of the eventual effect of induced non-linearity on flight vehicle.

If there is a discontinuous behaviour of physical properties, perhaps it will be better to limit the acceptable physics by a constraint on physical parameter for avoiding optimization with such irregular output. For example a irregular instant jump in shock location or in separation line is against robustness in the optimization point.

Such a survey of the physics will be more and more a critical output, that need careful analysis by specialist in order to have assessment of the validity of optimal shapes output by computer.

4. TOOLS FOR MULTIDISCIPLINARY MULTI-COMPANY OPTIMIZATION

4.1. Multi-company design

The merging of different complementary companies not avoid in Europe the necessity to push high technology everywhere and the fact that aerospace insdustry is a traditional leader for such high technology emergence at the industrial level. So it is fruitfull for all european countries to be participants in some part of the high technology improvements induced by aerospace product engineering.

The answer by a centralised design office somewhere is not a good answer as far as the research on the physics is now correctly spread in all countries of EEC, and the research in systems is part of a general effort for mastering complex systems that will be present in all the advanced product of the future. For the architect (Table I) it is clear that the numerical model and the virtual product approach will help to exchange the mechanical interfaces for a large spreading of the work in the development phasis of any new project.

One major concept is emerging in management of complexity of advanced systems : the identification of the number and complexity of the interfaces will be the major critical output of preliminary design. Such complexity has to be mastered at the begining. It comes from the interaction of the components in greater number N than in the past and of interaction of larger number of specialists. It is to be reminded that N components gives birth to N ! interfaces that is a very large number as soon as N is not small number. Complexity comes from such combinatorial explosion and not of interaction of parts that constitue a chain :. a chain of N wagons has only N interfaces that can be normalized with just one interface standard, and it is the same for clock gears except that unique standard is not possible, each gear having a specific size and function. Complexity is not present, just complication, with N interface. Moreover the gear work as a discrete linear additioner ; such linear behaviour is not generally true for the parts of a complex system as an aircraft.

By consideration of linearized equations, it is possible to define a linear matrix interface that will be able to reduce the interaction to a linear operator and so to work with easy exchange of complete interface characteristics. For non-linear behaviour the complexity is "emerging" and only direct simulation of the complete system (with appropriate modelling of smaller sizes) may answer to the need of a global prediction of the system performances.

4.2 Common centers of computations and simulation

The only way of doing that global work will be to exchange modele of complete aircraft ; however if dynamic analysis is needed (separation of stores, transient loads, aerodistorsion and effect on lobes of antennas ...) the data and code exchanged is great and may engage the know-how of a company. So the best way is to keep the codes unaccessible to other partners but to open the total results exactly as it will happens in flight test many years after. Such integration of the best of modeling in a virtual physics simulator is mandatory for in advance evaluation of performances and above all for substantiation of the critical points of the design.

If, for example, margins are to be kept, with a least regrets approach in the optimisation, such a global fine grain simulation is needed. Convenient protection may be achieved by a common center of simulation where a super computer will receive proprietary codes from different partners and share only the global result of their work together : an agreed supervisor, plus access available only with multiple keys and separate proprietary code and data disk storage is a convenient solution to that problem.

The iteration optimization, with an agreed cost function is a good way of design in such multidisciplinary and multicompany situation. It affords to an international design team the same capability of managing as soon as possible the critical issues of the program as in a single company ; moreover various specialist teams may be involved in a sparse matrix of interaction for each company and in a complete set only for the managing team of the project. It requires an affordable C.S.C.W (Computing Support to Cooperative Work)

Due to the difficulty in validation of such complex numerical simulation tools, it seems useful to have alternate codes for critical computations ; so each partner is increasing the confidence in global answer, the global output alone being accessible to all partners.

REFERENCE

1. Korte S.S., Werton R.P., Zang T.A.
    "Multidisciplinary optimization methods for preliminary design"
    AGARD, Symposium on Futur Aerospace Technology, Paris 1997

2. Perrier P., Rostand P.
    "Hypersonic Airbreathing Aircraft"
    Integration through CFD : Global Simulation for Global Thinking
    AIAA paper 3090 in 30th AIAA/ASME/SAE Joint Propulsion , Conference 1994

3. Perrier P.,
    "Problèmes mathématiques posés par l'incertitude des simulations numériques" - Mélanges offerts à R. Dantray, Masson 1993

4. Werton R.P., Townsend J.C., Eidson T.M., Gates R.L.
    "A Distributed Computing Environment for Multidisciplinary Design
    AIAA paper 94, 4372

5. Hirschel E.H., Perrier P.
    "Vehicle Configurations and Aerothermodynamic Challenges"
    AGARD, Symposium on Future Aerospace Technology, Paris 1997
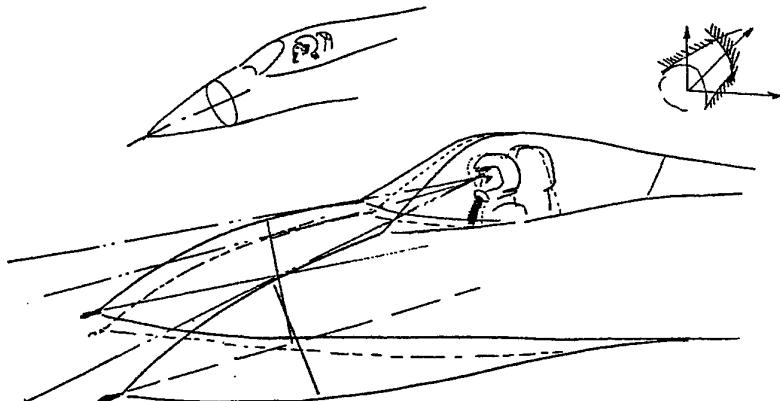
Change in a front fuselage with constraint on the line of sight
Figure 1

Variable aerodynamic shape
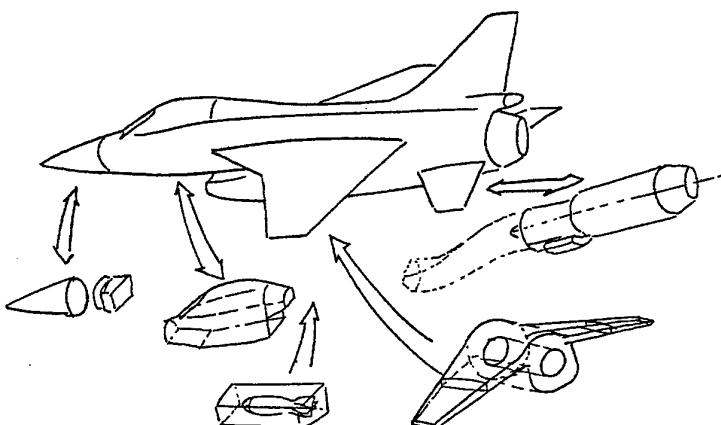
The architect specification of constraints (clean aircraft)
(critical lines) + critical volume and points

Figure 2

The architect specification of constraints (control of aircraft)
hinge lines + moments
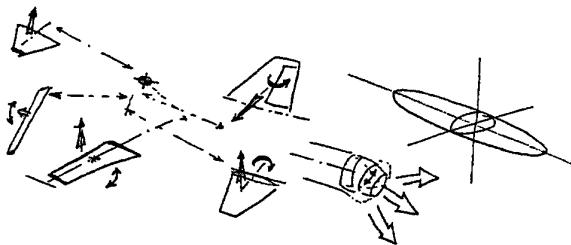
Variable setting of control surfaces

Variable setting of nozzle

Figure 3   Inertia ellipsoïd

Standard Dassault Modeler (David).

Ellipsoïd - bounded local
surface attached to a spline

Finite Element Surface
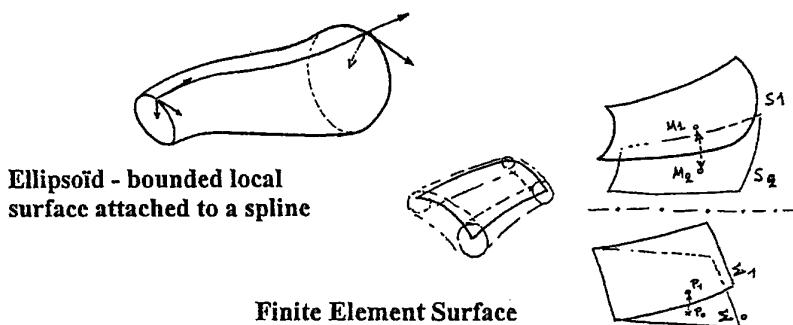
Transformation S1 → S2
Figure 4   as generated by a Σ0-Σ1 distorsion

Constrained optimization of wing fuselage

Figure 5

Multipoint and least regret optimization
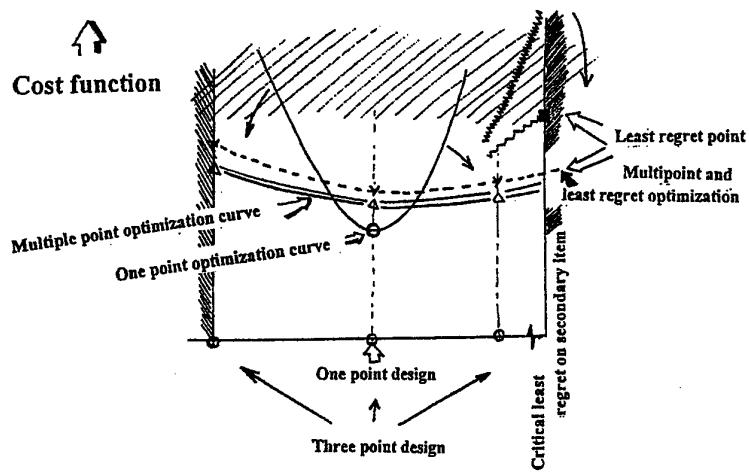
Figure 6

Constraints in physics parameters
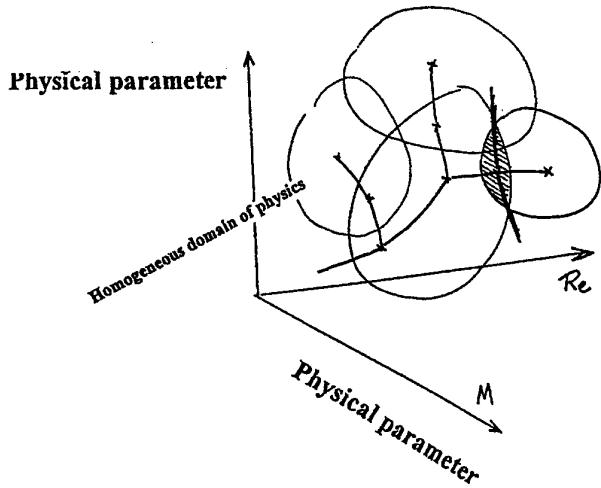
Figure 7

DISCUSSION

Session II, Paper #10

Prof Slooff (NLR, Netherlands) sought the author's opinion on the usefulness of "fuzzy logic" in the optimization process.

> **Mr Perrier** believed that fuzzy logic was a way to transform an unknown function joining definite extremal states into a derivable function. He was concerned over determinisation in an optimization process could be dangerous unless the smoothing function helps the convergence. However, how is this function reliably to be selected?

Aspects of Aerodynamic Optimisation for Military Aircraft Design

B. Probert
Aerodynamics Department, British Aerospace
Military Aircraft & Aerostructures
Building W427D, Warton Aerodrome
Preston, Lancashire PR4 1AX, United Kingdom

1   Summary

The paper considers the role of various optimisation strategies in the aerodynamic design of military combat aircraft.

The multi – design point targets of military aircraft implies that the final product must achieve a carefully judged balance between, often conflicting, requirements. The current established way of working to achieve this 'balance' is first reviewed including the use of rule based procedures, the application of linearised CFD codes in both direct and inverse/optimisation modes, and the role of initial experimental data leading on to more detailed CFD work and experimental verification. Practical examples are given relating to the design of various projects including the Experimental Aircraft Programme (EAP), which was the forerunner of Eurofighter.

The need for improvements is identified, being primarily brought about by considerations of affordability and reduced design cycle time and also by the challenge posed from novel configurations to met low observability requirements. The means of achieving these improvements is discussed, and these imply the development of Multi Disciplinary Optimisation (MDO) in a wide sense. Numerical optimisation experience is reviewed but it is strongly emphasised that there is a need for rapid experimental input to the configuration design choice programme. Means of achieving this are discussed and examples given.

The high incidence requirements have a strong impact on CFD developments and areas of improvement are identified. This leads to a proposed new way of working implying a much stronger interaction between the initial and detailed design phases of aircraft design.

2   Introduction

The increasing emphasis on achieving processes that are more efficient and adopting concurrent engineering practices through the Integrated Product Team approach is producing dramatic changes in the way the design of an aircraft project is progressed. However before considering the need and potential scope for such changes it is worth reviewing the previous, and indeed current, ways of working and the achievements made using 'conventional' methodologies, since such methods still have much to offer.

The paper illustrates this by describing the aerodynamic design aspects of a number of different types of configuration. These differ according to their design requirements and are divided into three classes - transonic design emphasis, supersonic emphasis but with good transonic performance, and a supersonic dominant design. All of these share a common need for a rigorous interaction between the disciplines: aerodynamics / structures / design / stability & control (S&C) / systems / etc. but the main subject of this paper is aerodynamic optimisation.   This covers shape optimisation for both performance and controllability, and the prospects for including this in a MDO environment.

In the context of wing design, it is recognised that the interaction between detailed shape optimisation for

performance and structural optimisation is weak. The former usually optimises a camber / twist distribution for a given wing overall thickness distribution, whilst the latter depends dominantly on the thickness. The twist requirement will influence the wing structural optimisation but on military aircraft this requirement may be dominated by other considerations of controllability, in particular achieving high levels of roll rate at high speed.

The wider optimisation issues for overall thickness, camber and twist design, particularly for supersonic performance has a strong link with structural optimisation and is an area which should benefit from MDO techniques.

Following the examples mentioned above the need for change is considered and means of achieving these is proposed. In this context, it is emphasised that not only increased automation and concurrency of existing methods are required but also there is a need to change the fundamental processes. It should be noted that the word 'change' is used, rather than 'improve', when considering an individual process. This reflects the increasing emphasis on affordability and reduction in design cycle time - not always compatible with quality improvements, though always adequate for the task in hand.

3   Requirements

The design of military aircraft is an extreme example of a multi-objective design problem. In the weapon system specification for performance requirements alone, there are usually a large number of point performances to be met along with many mission requirements. This is illustrated in fig. 1, which shows a typical set of requirements, viewed in the Mach Number - Lift Coefficient frame.

Fig 1 - Design Requirements
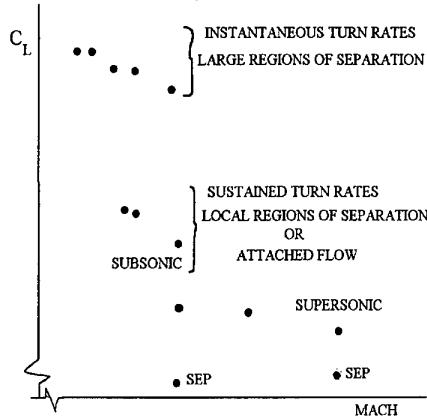
Thus, one cannot think of MDO as relating to the capture of all design requirements in one large design sequence. The development and application of MDO and optimisation systems will be sprinkled around different configuration issues and interfaces. In principle this will allow a better understanding of exchange rates and trade off studies and allow the consideration of a wider coverage of design parameters than achieved using conventional methods.

Even within the aerodynamic discipline itself there is a need to balance many related but conflicting requirements related to geometry / flight condition clashes. This is the case for an isolated wing - but in addition, there is a need to predict and allow for multi-component interference, e.g. wing - body interaction in the initial stages of design. Thus, it is usually not possible to think in terms of aerodynamic design for a wing in isolation. In addition, as the design progresses the full configuration will need to be evaluated using CFD and experimental facilities.

At the project feasibility stage there is a need, on a military project, to rapidly evaluate a large number of widely different layouts, in contrast to civil aircraft design where configuration changes tend to be perturbations of previous designs. This aspect has been compounded by the emphasis on achieving high standards of low observability leading to novel and non-ideal aerodynamic shapes, hence increasing the aerodynamic design challenge.

Referring to fig. 1 it can be seen that the major part of the flight envelope implies the presence of mild or severe regions of separated flow. Consequently, there is a need to predict both the onset of flow separation and the consequences on the configuration aerodynamics.

Finally, with all of the above in mind, there is a need to produce the best 'balance' in the configuration to meet the above objectives.

4   Current means of achieving requirements

Considering the aerodynamic aspects of design optimisation, the means of achieving requirements are illustrated via a number of examples. In the initial stages of design the skeleton layout, sizing, initial fuselage shaping, packing, wing planform, etc. will be done using a 'rule based' approach founded on previous experience and a host of empirical methods. For the wing planform and thickness selection, reference to guidelines as shown in figs 2 and 3 may be made.

Fig 2 - Pitch up Boundaries
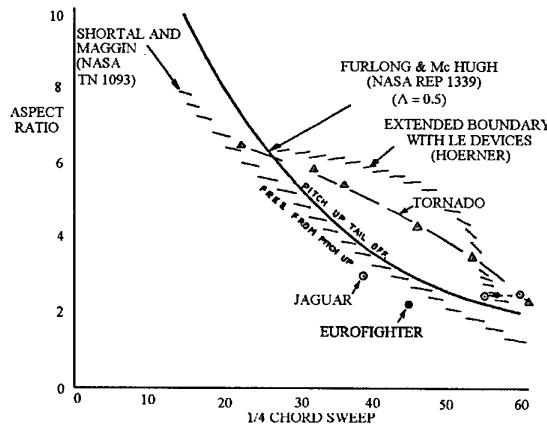
The first figure gives a relationship between wing aspect ratio and wing 'sweep that should ensure that the configuration avoids pitch up. However the empirical correlation is based on conventional trapezoidal planforms and its validity to more novel geometries is debatable. The latter figure shows a correlation between wing thickness and wing sweep which relates to the onset of severe buffet / shock stall, again based on trapezoidal planforms with the same doubts about general

applicability. The above two examples of simple rules in preliminary design will, if applied, lead to a configuration that needs thorough evaluation and that will usually need substantial enhancement to achieve an adequate design standard.

Fig 3 - Combination of Sweep and Thickness
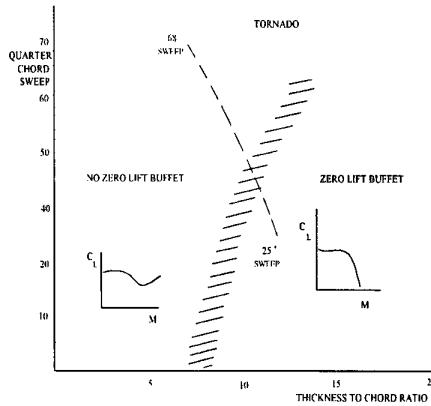
4.1   Transonic design case.

4.1.1   Thin Wing - supersonic performance as 'fallout'

The first example illustrates optimisation for a configuration with outstanding transonic flight performance using supercritical wing technology allied with variable camber at the leading and trailing edge (Refs 1, 2).

The configuration consisted of a high wing layout, with optional 'non interfering strake' to improve high incidence penetration with little detriment to low incidence drag. The wing LE sweep was 42° with a conventional trapezoidal planform. However, the initial wing design task was tackled by the design of aerodynamically equivalent 2D wing sections. The problem was to derive a section to meet at least two design points at high subsonic Mach number. The first was a high 'g' 'sustained turn rate' (STR) point and the second a low altitude high-speed dash point. If a fixed geometry is designed for the first condition then this will lead to separation on the lower surface for the second design condition. This leads to a pronounced reduction in drag rise Mach number at low lift as shown in fig. 4. (This figure also shows potential problems at high lift that can be improved, obviously, by additional LE flap deflection).

Fig 4 - Off Design Considerations
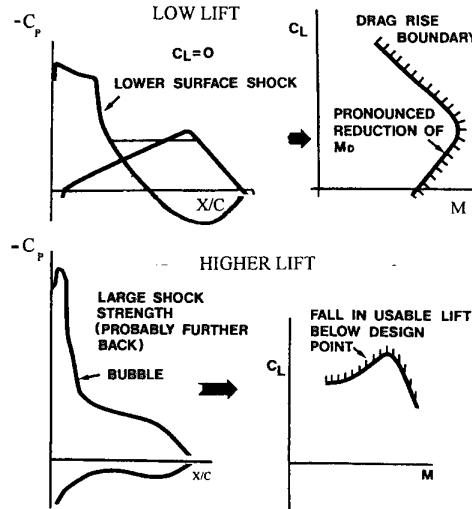
Use of variable camber solves the lower surface problem; the LE and TE flap are deflected upwards by 3.5° as indicated in fig. 5. This figure also indicates the large extent of supercritical flow achieved at the STR condition leading to a high value of lift to drag ratio.

Fig 5 - Benefits of Variable Camber
Theoretical Design Equivalent 2D Aerofoil Section

Fig 6 - Twist and Aeroelastic Effects
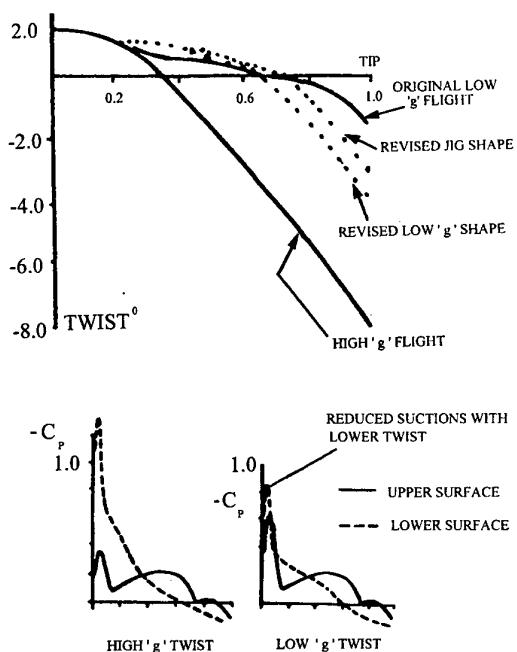
The final result, compared with a 1960's technology configuration, is illustrated in fig. 7 and shows excellent performance gains. It is not claimed that such a design represents the optimum solution for the problem but significant advances were made over previous design standards.

Fig 7 - Effect of Advanced Variable Camber Wing
Design on Lift/Drag Ratio

The resulting drag rise boundaries are shown in the lower part of fig. 5 where the extended penetration to higher speeds at low lift is evident.

This design was achieved through an iterative application of CFD codes designing the upper and lower surfaces separately at each design point and through the design and control of the surface curvature distributions. The 2D, and later the 3D design again adopting a repeated application of CFD codes, produced excellent standards of performance. The resulting 3D geometric shape for the STR point was deemed to represent the in-flight geometry and so included the effects of aeroelasticity. This was removed via an iterative procedure in order to derive the wing 'jig' shape for possible manufacture.

The flight and 'jig' twist values are compared in fig. 6. It was observed that 60% of the aeroelastic twist was obtained naturally through the wing bending contribution assuming a conventional aluminium alloy skinned multi-spar structure. The remaining 'jig' twist, when coupled with up LE flap gave satisfactory performance at the low lift design point.

4.1.2   Thick wing transonic design - subsonic aircraft

Here illustrated by the progress in design applications of CFD methods for the Harrier VTOL configuration wing design - as shown in fig. 8. The application of supercritical aerofoil technology and improvements in CFD methodology, including the incorporation of a vortical flow design, produced progressive increases in performance. These were achieved through repetitive CFD and geometry manipulation packages and led to 50% gains in maximum Lift to Drag ratio.

Fig 8 - Progress in Aircraft Wing Design CFD's Traditional Application
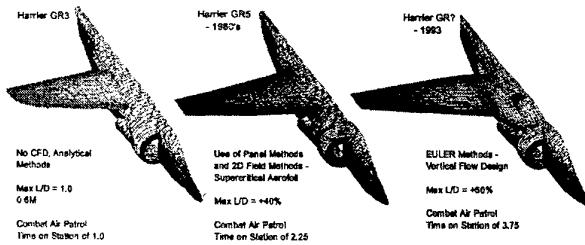
4.2   Supersonic bias design

The second example considers a conventional design approach as applied to the Experimental Aircraft Programme, a cranked delta with foreplane layout, which was the forerunner to Eurofighter. Here the supersonic requirement was severe, demanding a 'Beyond Visual Range' (BVR) capability at Mach 1.6 and requiring excellent transonic performance as well. Fig. 9 shows the configuration and the areas where CFD played a part in the overall optimisation. Here we concentrate only on the wing related optimisation.

Fig 9 - EAP: Areas of CFD Application - Canard Delta
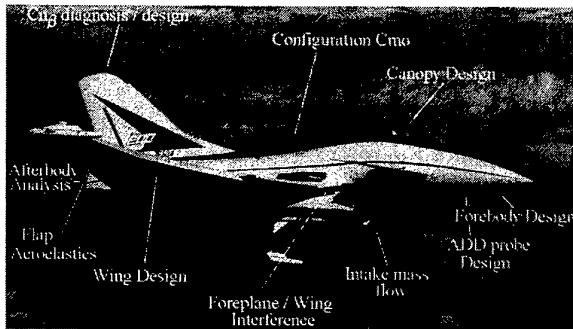
At the outset it was realised that the canard - delta configuration was a significant departure from previous experience and the first step was to carry out a large low speed experimental programme on a 1/10th scale model aimed at optimising the wing planform and wing to foreplane relationship. This study was outside the capability of CFD and configuration choice was strongly influenced by the S&C characteristics, dominantly at high incidence, including the ability to recover from high incidence. The experimental database allowed exchange rates to be quantified between S & C and performance (maximum lift) parameters. Example exchange rates are shown in figures 10 and 11 and these guided the final choice of planform.

Fig 10 - Use of Experimental Data in Configuration Design - Maximum Lift Trends
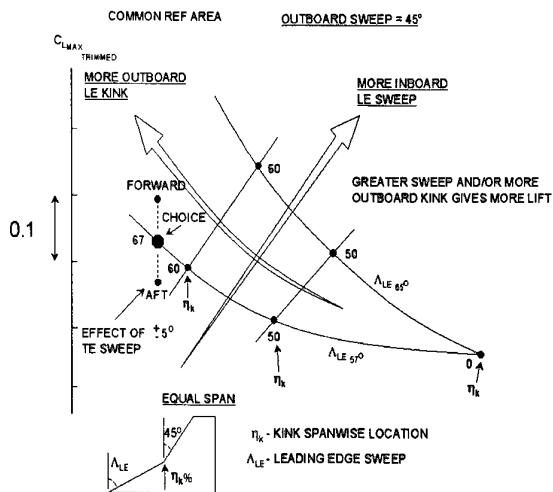
Fig 11 - Use of Experimental Data in Configuration Design - Recovery from High Incidence
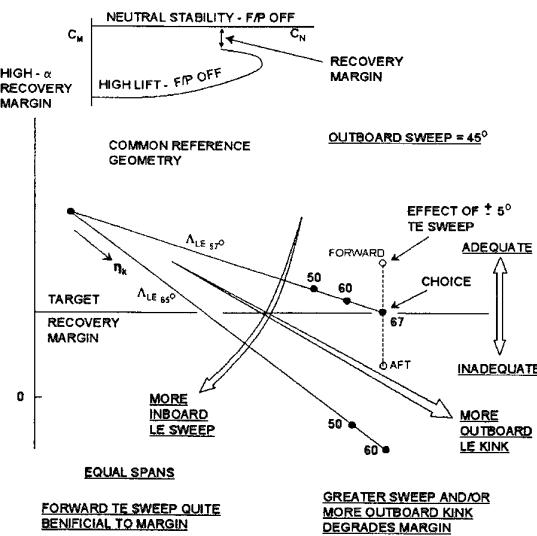
The best CFD code available at the time was an EULER code capable of treating a wing placed on a simple body composed of circular cross sections. This code gave good predictions of the wing pressure distributions and total lift at both sub and supersonic Mach numbers but poor prediction of the overall longitudinal pitching moment. To improve matters a hybrid procedure was derived which combined the strength of a potential flow panel method, to represent complex wing-fuselage geometry, with the non-linear wing flow capability of the EULER method. The resulting procedure gave accurate predictions of pitching moment for both stability and zero lift moment as shown in fig. 12.

The prediction of both these aerodynamic quantities are fundamental to achieve a balanced design as they affect controllability and efficiency. The new procedure also highlighted the complex nature of the wing to body interference for this configuration, which is shown in fig. 13 for the variation of zero lift moment with Mach number. The body on wing and wing on body effect increases dramatically

at transonic speeds though the wing alone trend is benign. The procedure also agrees well with the experimental data shown as the filled in symbols and was thus used to design and assess later developments.

Fig 12 - Comparison - Modified Euler v Experiment M = 0.9
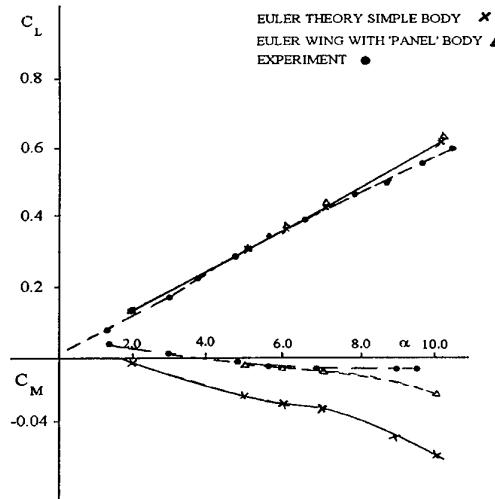
Fig 13 - Pitching Moment at Zero Incidence
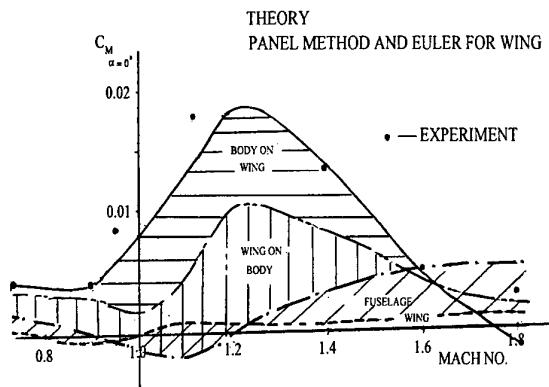
This is an example where the designer makes use of, at the time, an inadequate CFD capability but improvises to produce an effective design procedure. Had an automatic optimisation capability been available at the time it would not have been successful since use of the basic CFD alone would not have been adequate.

The search for a configuration with excellent supersonic performance coupled with very good transonic/subsonic performance is difficult. It was found that the best balance was achieved by designing for the supersonic manoeuvre point using a combination of linear theory and an EULER code and achieving the sub/transonic performance with LE and TE flap. The alternative of designing for the transonic case and decambering to achieve the supersonic case was not as successful. This is illustrated in fig. 14 for the early work done on the EAP at a Mach number of 1.4. The predicted drag values (via EULER) are plotted against pitching moment at two constant values of lift coefficient, effectively allowing comparison at trimmed conditions. The variation in drag with various LE/TE deflections is also shown and it is clear that

even a mild transonic design suffers a 4% penalty in zero lift drag compared with a supersonic design case. The final design selected was based on a refinement of a supersonic linearised theory optimisation.

Fig 14- Supersonic Drag - Lifting Surface Theory M = 1.4 Wing + Body
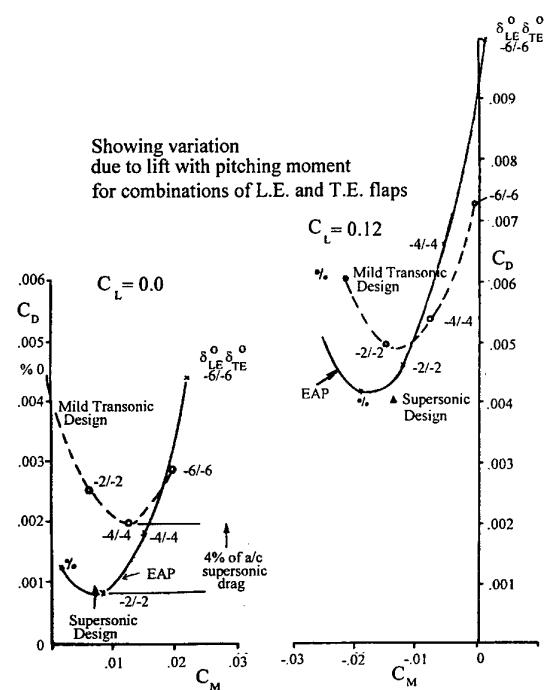
By a process of repetitive manual design using CFD an exchange rate was derived between wing maximum camber levels, subsonic STR performance and supersonic '1g' performance as shown in fig. 15. This served as a useful guide in checking permissible camber levels.

Fig 15 - Exchange Rate
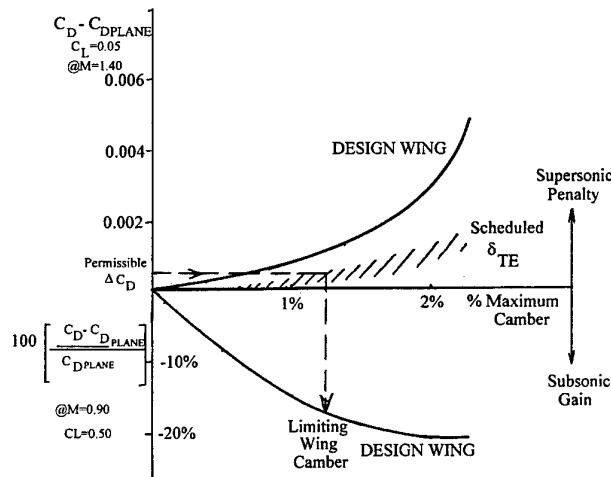
The final 'balanced' design gave large gains in sub/transonic performance with only a small penalty to supersonic cruise performance as shown in fig. 16.

In parallel with the shape optimisation work the conventional aerodynamic loading / structural / aeroelastic / flutter cycle was proceeding. In this instance the design and manufacture of the 'loads' fully pressure plotted large scale (1/10th) high speed tunnel model and subsequent testing covered a period of approximately two years from the start date. The information from the model was not available until after first flight and so it did not contribute to a better standard of loading estimate pre flight, though it did contribute to the check stress and flight clearance activities. The time expended and the cost of the model was significant.

Fig 16 - Benefits of Twist and Camber
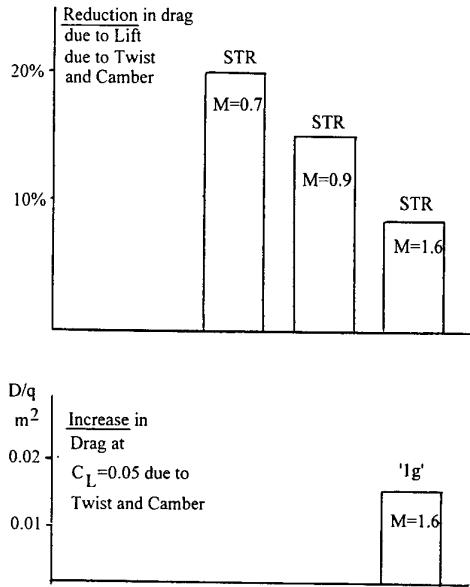
4.3   Supersonic design

The third example illustrates the design of a supersonic configuration. The second example above has already highlighted the importance of trim drag at supersonic speeds and to allow for this a procedure was developed to optimise the wing, using linearised theory, in the presence of the complex fuselage flow field derived from a panel method with the aim of minimising drag at trimmed conditions. The process is outlined in fig. 17. At each iteration the whole configuration is run on a panel method to check the 'out of trim' increment. Corrections are obtained and the process repeated until satisfactory convergence is achieved. Less than six iterations are required to obtain a satisfactory result. The final drag level is obtained using a 3D EULER code The above is an example of numerical optimisation using linear theory allowing for external interference. The process involves a 'man in the loop' due to only partial automation and the need to inspect intermediate results.

Fig 17 - Hybrid Supersonic Design Procedure
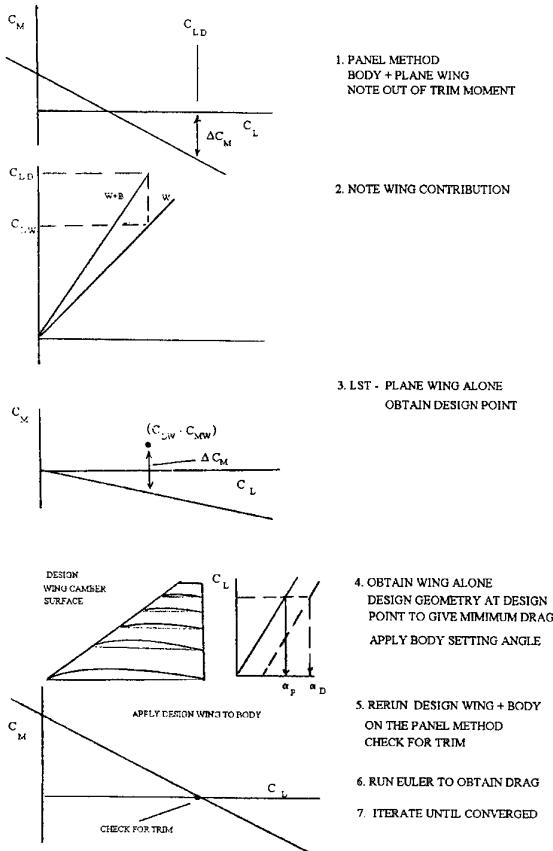
An example of optimisation using non-linear (EULER) theory (Refs 3, 4) is given in fig. 18(a/b) where a wing geometry is improved using the cross flow shock 'analogy' with 2D aerofoil design concepts. The need is essentially to increase L/D at supersonic manoeuvre conditions. The basic idea is to view the flow in a direction normal to the shock wave and to modify the wing geometry so as to weaken this shock wave. Such an exercise was undertaken (Ref. 5) and successfully reduced the drag but also showed the importance of allowing for trim drag at supersonic speeds - see fig. 19. Here trimming is done using the trailing edge flap.

Fig 18(a) - A Supersonic Design Approach
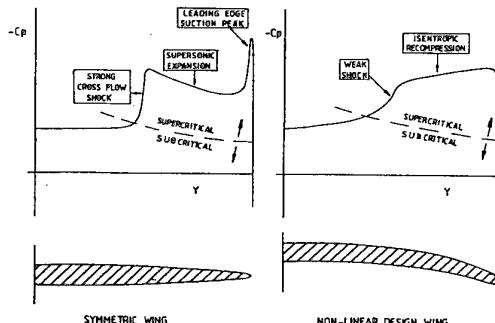
Fig 18(b) - A Supersonic Design Approach

UPPER SURFACE C_P

GRID = 160*32*32
C_L = 0.282

```
----    -0.320
------  -0.300
......  -0.280
-.-.-.  -0.260
-----   -0.240
-- --   -0.220
------  -0.200
......  -0.180
-..-..  -0.160
-----   -0.140
-- --   -0.120
------  -0.100
```

WING ISOBAR PATTERN AT THE SUPERSONIC
MANOEUVRE DESIGN POINT: M=1.6, n=4'g'
FINE GRID
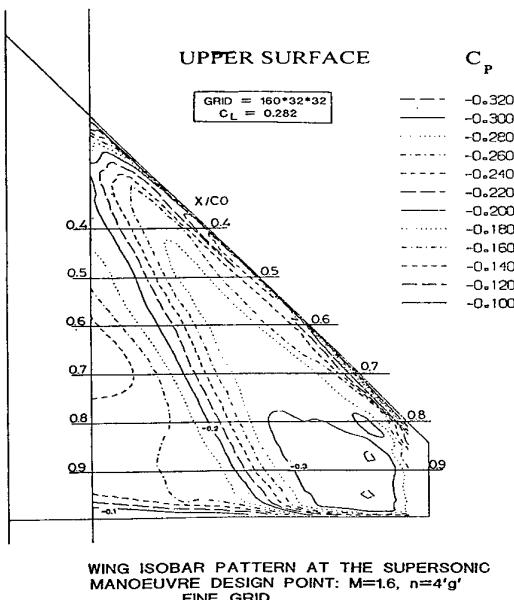
Fig 19 - Importance of Trim Drag
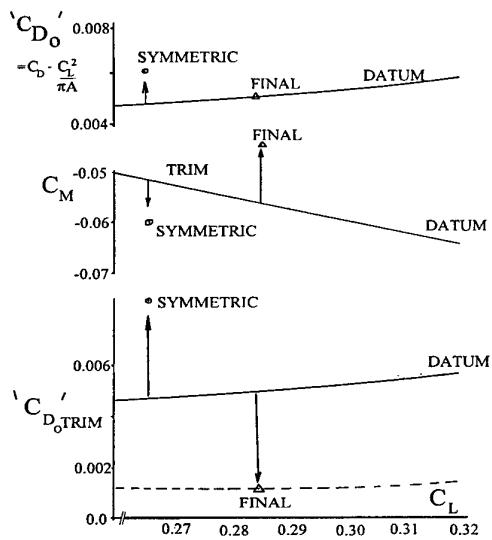
Three designs are shown - a datum wing, a symmetric wing and an improved wing at the same design lift coefficient. The latter and the datum have the same untrimmed drag, but its more positive pitching moment leads to a large reduction in overall drag when trimmed. This effect can be larger than the gain achieved by the 'cross flow' technique mentioned above and implies that a pitching moment constraint should always be used in supersonic optimisation. Again this optimisation was achieved using 'ad hoc' algebraic geometry modifications in both chordwise and spanwise directions, with manual intermediate inspection/decision making and repetitive use of CFD.

5   The need for improvements

The examples above have highlighted a number of tasks that are essential to the design process, but are time consuming to perform and could probably be done in a better way.

The first and the third design examples involved repetitive 'man in the loop' calculations and geometry manipulation to solve a multi-point performance problem. This is obviously a prime candidate for numerical optimisation but only since the design involved STR and low lift conditions where the design aim was to achieve attached flow (where the CFD method is valid). Extending this work to include 'instantaneous turn rate' (ITR) requirements at high incidence implies the ability to predict separated flow development. It is also evident that potential current low-observability requirements imply non-ideal aerodynamic options, where the onset of flow separations can begin at lower incidences than usual. The consequences can also be more severe. Hence, there is a need to include improved CFD capabilities in design optimisation both in terms of the flow physics modelling and to improve response times.

The second example showed that planform choice and wing to foreplane relationship was selected mainly on the results of wind tunnel data at high incidences and so was the first step in the detailed optimisation work which followed. The related loading / structural optimisation also covered a long elapsed time mainly due to the need for extensive pressure plot confirmation.

There are thus many areas for improvement.

6   Possible developments

6.1   CFD enhancements

Recent work on the application of a Navier-Stokes code to the flow over a generic novel geometry, where flow separation occurs early, has shown promise as shown in fig. 20 below.

Fig 20 - Navier-Stokes Comparison with Experiment
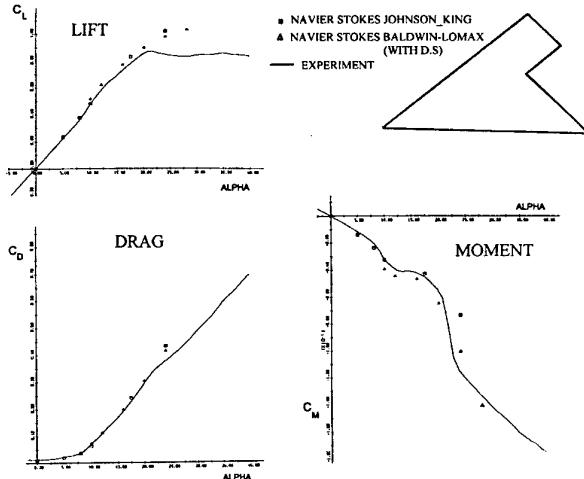
The method was run on the gross wing geometry alone and the results compared with low speed experimental data on a wing-body configuration. The body was narrow and of a simple nature with constant elliptic cross section and did not adversely interfere with the wing flow. The predictions agree well with the experimental force results up to high incidence. Maximum lift is not predicted but pitching moment and drag trends are well predicted. A more detailed look at the predicted skin friction lines on the wing upper surface is also compared with experiment in fig. 21. The experimental result lies in between the Navier Stokes predictions, shown for two turbulence models.

Fig 21 - Novel Wings
Theory (Navier-Stokes). v. Experiment
- Surface Friction Lines
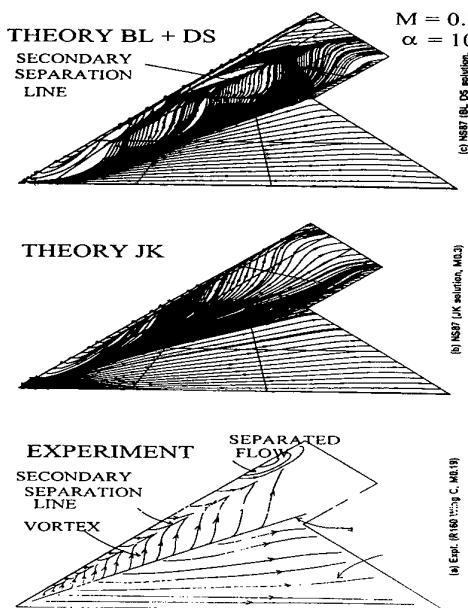
However current configurations exhibit more complex wing / body / chine / empennage geometries. The aerodynamics of these, on current evidence, are unlikely to be predicted adequately through the use of CFD at high incidences, though limited regions of separation can be qualitatively predicted. There is thus the limited possibility of introducing a Navier-Stokes capability into the optimisation problem but the computing requirements would almost certainly be prohibitive. Thus the use of such a method is likely to be intermittent, providing a 'physics reality' check when embedded in a design optimisation loop involving a lower order CFD code (e.g. EULER) - essentially a form of multi-level optimisation.

The inadequacy of CFD for treating complex configurations at high incidence places increased emphasis on experimental work, which formed an essential part of the second example in section 4.2 above.

6.2   Experimental developments

6.2.1   Simplified Experimental Models and Test

The approach adopted at BAe Military Aircraft & Aerostructures (MA&A) has been to increase productivity through the use of simplified and smaller wind tunnel models

(1/70th scale), which has also enabled the use of smaller and simpler low speed tunnels, e.g. a small open jet facility.

Models are constructed with a 'straight through' constant thickness 1mm flat plate metal wing to which the fuselage components are attached, with the empennage attached to the fuselage or wing as necessary.

There is no profile shaping and no LE shaping so the primary interest is simply to gain rapid information on a number of alternative body-chine-wing layouts. This technique has been successfully employed at MA&A after an evaluation of the procedure was made against conventionally gathered test data using a larger model (1/12th scale) and tunnel. A comparison of the two series of test data is shown in fig. 22 where it is seen that although an exact match is not produced, the trends and force changes occur at similar incidences so the data can be used to give relative comparisons between different configurations. It has also been demonstrated that the incremental effects of control surfaces are reliably predicted.

Fig 22 - Comparison of Small and Large Model Data
Lift and Moment
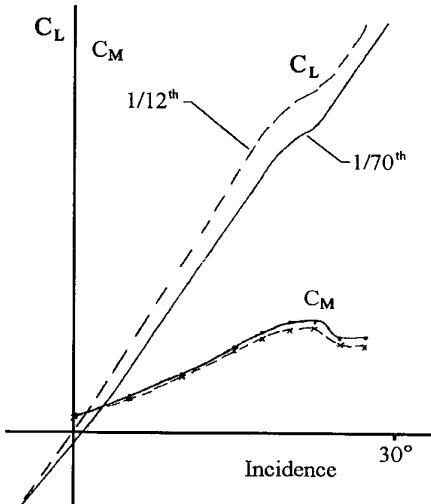
The savings in cost, design effort and in particular elapsed time are considerable. However the flow type on all the configurations tested in this development study was vortical in nature and thus not sensitive to scale effect or to wing geometry (for a model with a thin, but blunt, LE). It is an example where such an approach may be 'fit for purpose' but it can not be regarded as a generally applicable technique - especially for wings of lower sweep. However the rapid and extensive information gained with this approach allowed planform and configuration initial selection to be made on high incidence and control power characteristics.

6.2.2   Loading issues and Pressure Sensitive Paint

As noted earlier in section 4.2 the detailed surface pressure data was obtained at a very late stage in the design cycle, placing a heavy responsibility on the earlier estimates obtained based on past experience, related experimental data and CFD codes. This is especially true on novel configurations where past experience and databases may be inadequate and CFD is not well evaluated. The latter is also true for intended CFD shape optimisation work where early CFD evaluation is essential.

At BAe (MA&A) the current view is that pressure sensitive paint offers the best means of obtaining rapid and cost effective pressure data. Such a system (SUPREMO) (Ref. 6) is under development and several trials have taken place. The BAe system is based on a ' time decay' signal analysis rather than the usual luminous intensity based systems. In principle, the method is more accurate at and more tolerant of low intensity levels and high surface curvature regions. Typical results obtained on a 12 inch chord aerofoil model spanning the BAe (Warton) 1.2m HSWT are shown in fig. 23 and fig. 24 where comparison with experimental pressure tapping data is excellent. The detector was mounted so as to predict the development of the lower surface pressures, which accounts for the unusual pressure distributions.

Fig 23 - PSP Comparison with Pressure Tappings
2D Section   Mach 0.69 Incidence -4°
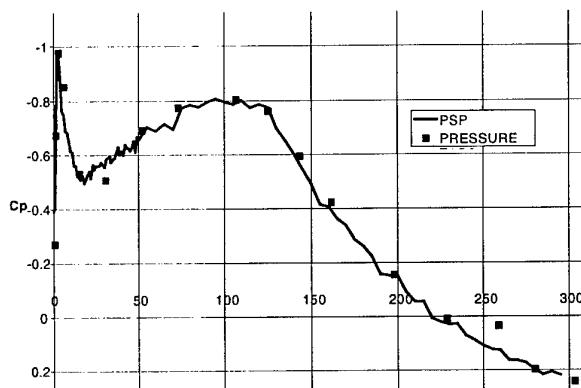
Both LE suction peak and the general chordwise development are well predicted though the position of the shock wave is slightly different in fig. 24. The possibility of a paint intrusion effect or a slightly non-2D development on the model is under investigation. In addition the method is being developed and assessed for 3D configurations.

Fig 24 - PSP Comparison with Pressure Tappings
- with shock   Mach 0.77 Incidence -2°
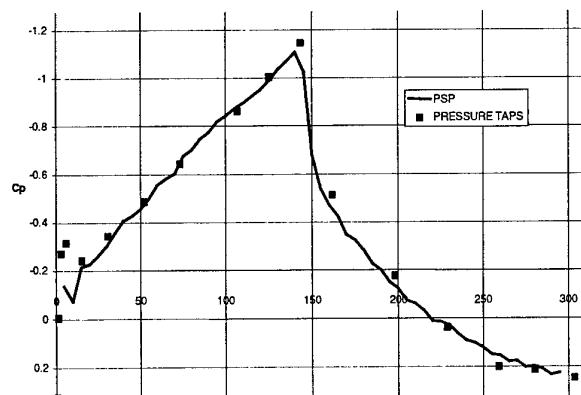
The technique offers reduced risks both in terms of loading and design optimisation work, reduced timescales, reduced model costs through the elimination of the 'loads' model, and continuous loading and design checks as the configuration evolves through the ability to 'piggy-back' conventional S & C testing.

6.3   Numerical Optimisation

A method which is receiving significant attention and evaluation at BAe is the shape optimisation system developed by DERA called CODAS (e.g. Ref. 7). This is a constrained non-linear gradient based optimisation code linked with a curvature based incremental geometry capability. It can be linked with a number of CFD codes, potential flow or Euler based codes in both 2D and 3D. Impressive evaluations and applications have been undertaken on both 2D and 3D wing designs though it must be stressed that such methods are to be considered as another 'tool' in the designers kit as great care is needed to drive the method to a proper solution.

Typical evaluations investigated the choice and number of design variables and their scaling, alternative formulations of objective and constraint setting, and considered both single and multi point designs. A resulting pressure distribution from the method is compared with a good datum standard of design in fig. 25 where a performance achievement is obtained through smoothing of an already weak upper surface shock and a modification of the rear surface loading.

Fig 25 - 2D Section Design
10-78-50 Aerofoil v 2D CODAS Optimisation
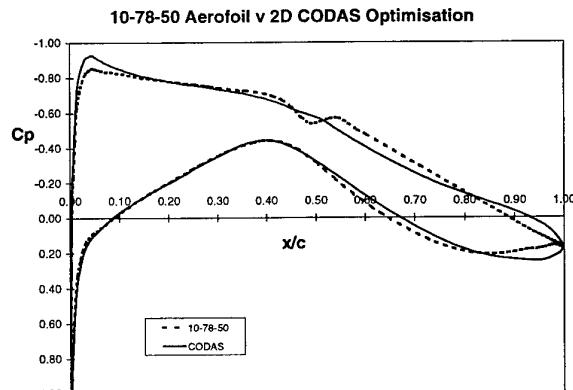
Further examples are too numerous to mention but the general conclusions reached were that the method worked best when adequately constrained, thus avoiding local minima, and that the effect of the design variable scaling should be investigated early on. For a 3D case this is difficult due to the computing requirements involved. However CODAS suggested options that may well have been dismissed using conventional approaches and it was noted that drag minimisation alone is not a sufficient objective, some form of control on the pressures is also required along with physical constraints to guide and control the optimisation process. Further evaluations and applications are planned.

The comments made above are reflected in a related but more extensive study undertaken by ESDU (Ref. 8). The same code was applied and evaluated for a range of 2D cases optimising section camber, upper and lower surface geometry independently and LE/TE flap schedules. The results illustrate the care that needs to be taken with gradient based optimisers. This is shown for an example where the objective is to minimise drag, at a design lift coefficient of 0.75, with no other constraint applied, by the deflection of optimum settings of LE and TE flap.

Fig. 26 shows the solution paths starting from five different starting points (i.e. values of LE/TE deflection) for a case where the incidence is started at a low value of 1°. The actual

minimum drag point is marked and it is clear that the process does not approach the correct solution from any of the starting points. Subsequent investigation of the results showed that the solution paths are strongly dependent on the scaling factors applied to the design and the fact that the initial starting point, in each case, is well outside the 'feasible' region (here, of lift coefficient). The method immediately attempts to reach the feasible region by changing the design variable that gives the largest increment towards that end. This increment is also a function of the input scaling factors.

In fig. 26 the scaling factors used are larger for the flap deflections than for incidence and so the method rapidly increases the former to reach the 'feasible region', but not an optimum.

Fig 26 - Effect of Different Starting Points on Design Variable Paths
Scaling Factors LE/TE/ALPHA (8/8/1)

Starting Point

	LE Flap	TE Flap
⬚	3.0	-2.0
X	0.4	0.5
◇	3.0	4.0
✚	-2.5	5.0
▽	-2.5	0.5
△	-2.5	-2.0
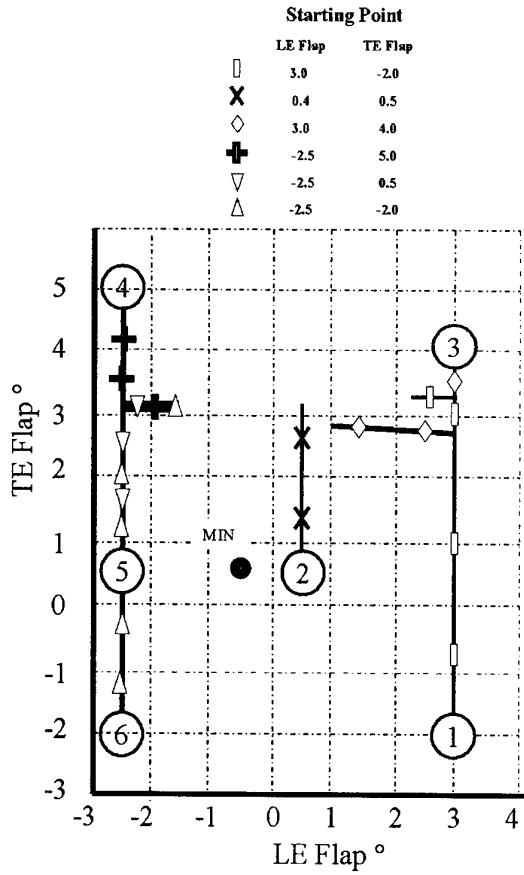
Inspection of the two-parameter design space for the problem at a lift coefficient of 0.75 in fig. 27 shows that a number of solutions are possible with the gradient based approach. If the scaling factors, in particular, are chosen appropriately one would expect this behaviour.

Revising the scaling factor on incidence does indicate the expected behaviour for four of the cases, as shown in fig. 28. Thus it is essential to try different starting points and to investigate such influences early on especially where a large number of design variables are employed where a simple

'visualisation' of the solution, as done above, may be impractical.

Fig 27 - Anticipated Effect of Different Starting Points on Solution Paths
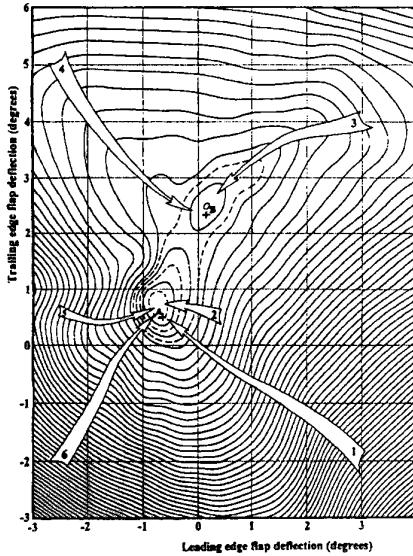
Fig 28 - Revised Scaling Factors LE/TE/ALPHA (8/8/5) Effect on calculation paths
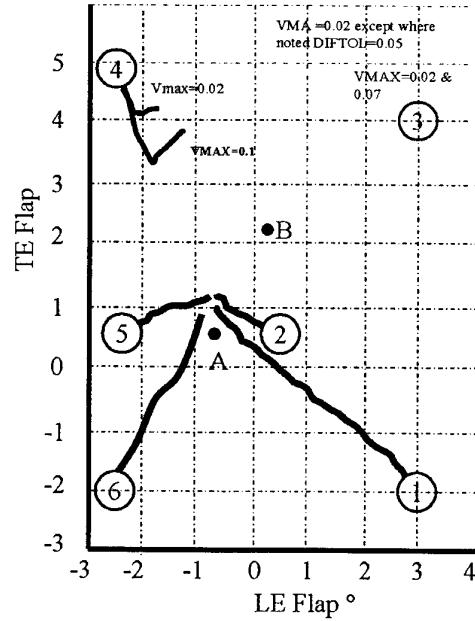
The option of treating this problem using a different (e.g. stochastic) optimisation procedure is yet to be addressed.

6.4   Multi-Disciplinary Optimisation

A system currently under evaluation at MA&A (Warton) is FRONTIER (Ref. 9), produced as a result of the FRONTIER European Framework IV project. This is essentially a framework that allows distributed processing using any user-required executables. Alternative optimisation packages are also available, including a genetic algorithm option. The system can be used to produce the Pareto boundary for key performance parameters and has already been applied by the

partner companies/developers to a number of design problems. Application by DERA and BAe to the optimisation of a thick delta wing has been reported in Ref. 10 while a more recent BAe application to a cavity / store release problem is given in this symposium as paper no. 14 (Ref. 11).

A further application is described below where the two disciplines involved are aerodynamics and radar signature. The case is simple in nature and attempts to assess the effect of aerofoil leading edge geometry on both the aerodynamics and Radar Cross Section, and whether a Pareto boundary exists for this type of interchange.

The aerodynamic problem posed is to assess the **off design** effect of leading edge changes by estimating the low Mach number (M = 0.50) upper surface flow separation boundary - thus the incidence at which separation starts is to be maximised. As a prerequisite, at low incidence (0°) a check is done to ensure that suction peaks on the lower surface also conform to a prescribed suction limit so that a 'high speed dash' can be achieved at low altitude.

The RCS problem posed is that of an aircraft, flying at low altitude, approaching a ground based radar operating at 3GHz. Thus incident elevation angles are small (0.5° to 1.5°). The RCS is averaged over this incidence range.

The problem is reduced to only three geometric design variables - the **leading edge radius** and the **two angles** which define the upper and lower surface blend point between the LE radius and the rest of the aerofoil. The latter is taken to be an elliptic profile back to the aerofoil maximum thickness on both surfaces. As these three variables are changed the leading edge droop or camber changes along with the curvature distribution. The flow process chart is shown in fig. 29. An Euler code has been used for the CFD calculations and a limiting pressure coefficient applied to derive the separation boundary. The RCS results were derived using a frequency domain code which solves Helmholtz' equation.

Fig 29 - Process Flow Chart
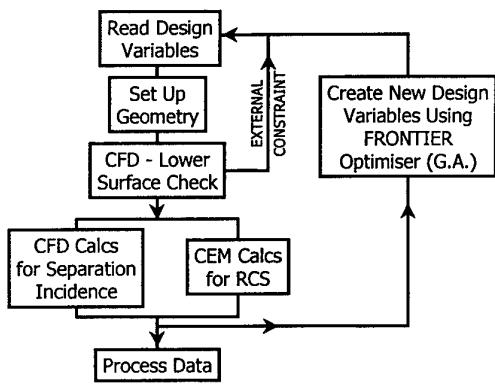
The first results obtained, where the allowable range of each design variable was restricted are shown in fig. 30. A clear demarcation boundary is seen, though the number of cases is not large. Analysis of this data and additional runs indicated definite trends; also shown in fig. 30. It is interesting to note that an increase in nose radius affects both separation incidence and the RCS return, assisting the first and penalising the latter, as expected. However increasing Θ_{upper} dominantly affects the separation incidence by increasing the LE 'droop'. Increasing Θ_{lower} dominantly affects the RCS. Both of these are more subtle effects and can be used to counter or balance a LE radius change.

Fig 30 – Narrow Range Variables and Trends

Trends for Each Design Variable
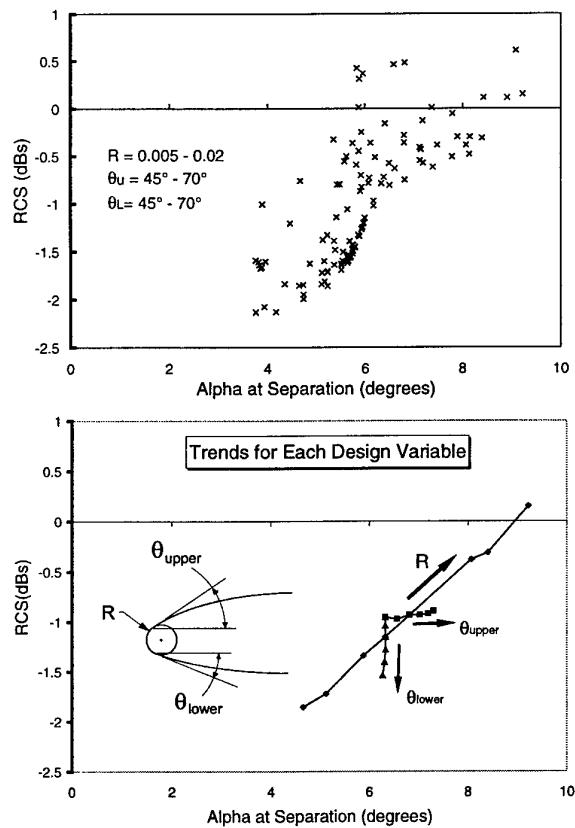
Fig 31 – Broad Range Variables

M=0.5, Freq = 3 GHz

Boundary Walk Plot
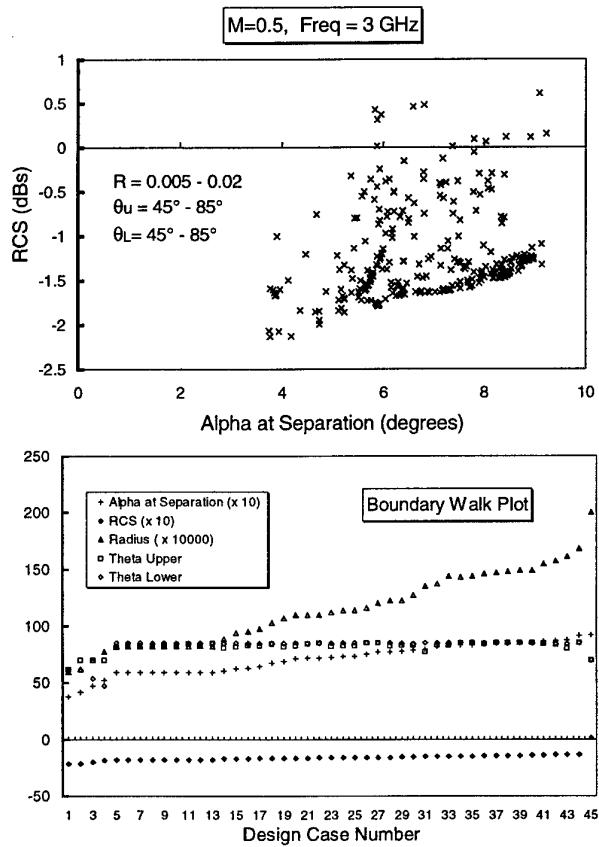
Extending the allowable range of the design variables results in the fuller boundary of fig. 31, but there is still a clear Pareto boundary. Also shown in fig. 31 are the variations of the design variables along this boundary, with trends reflecting the comments made earlier. In particular the LE radius is allowed to increase to improve the aerodynamic performance without major impact on the RCS. This is since the lower surface angle is at its maximum and since the radar threat is from below.

The above simple example has demonstrated the effectiveness of the FRONTIER system to easily obtain trends, exchange rates and Pareto frontiers. However many more evaluations and applications of increasing complexity are necessary to obtain a proper assessment.

7 Future ways of working

The airframe design cycle can be thought of as two design loops as indicated in fig. 32. The outer loop currently adopts empirical and rule based procedures, and dominates the configuration layout and component selection process. The inner, more refined design loop, has a secondary influence in this respect; thus, the controlling information is from the outer to inner loops.

It is anticipated that CFD enhancements, both in terms of physics modelling and faster response times, will enable an immediate feedback to a proposed configuration layout or change, especially on novel configurations where rule based procedures may be less sound. As acceptance of the new design procedures is gained, their use will spread to the outer design region. This will lead to a closer integration and gradual merging of the two design regions.

Fig 32 – Future Ways of Working
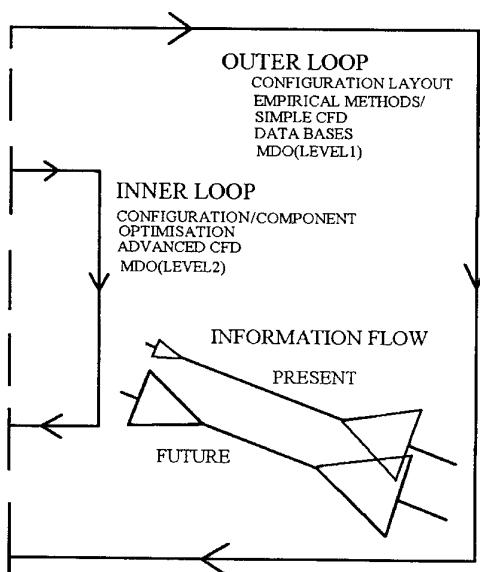
8 Conclusions

Optimisation of a combat aircraft is composed of many disciplines, but the aerodynamic database is probably the key component that needs to be in place before the detail optimisation can begin. The choice of the initial configuration is often made based on its high incidence characteristics, thus

any optimisation or MDO system needs to capture this component. As much of this is currently outside the scope of CFD there is a strong emphasis in developing a rapid means of obtaining experimental data, in order to bring this element into the MDO environment.

CFD plays a supporting role in the initial configuration study and this will increase as the methods are extensively evaluated and/or the algorithms improve, and a leading role in identifying multi-component interference and further downstream optimisation. The role of numerical optimisation and MDO is currently more sound when viewed in the detail design environment rather than the concept/feasibility stage, for military aircraft.

CFD enhancements, pressure sensitive paint and simplified model build and testing techniques have been highlighted as the means for progressing the design optimisation problem.

9 Acknowledgements

References

1. Holt, D. R. "Some particular configuration effects on a thin supercritical variable camber wing", AGARD CP - 285 Subsonic/transonic configuration aerodynamics (May 1980)
2. Probert, B. and Holt, D. R. "Advanced combat aircraft wing design", ICAS Congress (1980)
3. Mason, W. H. and Daforno, G. "Opportunities for supersonic performance through non-linear aerodynamics", AIAA Paper 79-1527, July 1979
4. Mason, W. H. "SC - A wing concept for supersonic manoeuvre", AIAA 83 - 1858, July 1983
5. Stanniland, D. R. "Supersonic manoeuvre design guidelines for a highly swept military aircraft wing", ARA Model Test Note Q85/3, June 1990
6. Davies, A. G., Bedwell, D., Dunleavy, M. and Brownjohn, N. "Recent developments in pressure sensitive paint measurements using the BAe system", Proceedings of the RAeS conference - Wind Tunnels and Wind Tunnel Test Techniques , April 1997
7. Lovell, D. A. and Doherty, J. J. "Aerodynamic design of aerofoils and wings using a constrained optimisation method", DERA, EAC 1994 paper 3.21, Oct 1994
8. Unpublished work - Engineering Sciences Data Unit International Plc
9. Spicer, D. FRONTIER: Open System for Collaborative Design using Pareto Frontiers. R.Ae.S. Conference on 'Multidisciplinary Design and Optimisation', London, Oct 1998.
10. Harris J ap C., Fenwick S.V. "The application of Pareto methods to multidisciplinary design optimisation" Proceedings of the Royal Aeronautical Society Conference on Multidisciplinary design and Optimisation, Oct 1998. Pages 7.1-7.9
11. Moretti, G., Spicer, D., Sharples, N. "An MDO application for a weapon released from an internal bay" RTO-AVT- Symposium on Aerodynamic Optimisation and MDO - Oct 1999, Ottawa

Progress towards a multi-disciplinary analysis and optimisation capability for air vehicle assessment and design - a UK research establishment view.

David Lovell[†] & Peter Bartholomew[‡]

Defence Evaluation and Research Agency,
Farnborough, Hampshire GU14 0LX
United Kingdom

ABSTRACT

This paper considers progress towards establishing a Multi-disciplinary Design Optimisation (MDO) capability for assessment and design. Some basic questions are posed and answered on the basis of experience gained by DERA as a result of participation in a series of recent National and International projects undertaken in partnership with UK and European industry and government research agencies. Issues addressed include the definition of MDO; its function within concurrent engineering; the role of product models; the definition and execution of the MDO process under user control; the use of trade-off studies for requirements capture; and the degree to which MDO can support detailed design work. The need for the adoption of standards in the definition of the product model is highlighted.

INTRODUCTION

Multi-disciplinary design optimisation enables the effectiveness of products to be optimised and supports trade-off studies between the design objectives from diverse disciplines. The MDO process is intended for use within the context of a modern engineering design environment, which is characterised by the commercial imperative to reduce time cycles and costs. These commercial pressures, together with the immense volume of design, manufacturing and maintenance data inherent to complex modern equipment, demand a heavily computerised environment.

Current practice, as exemplified by Concurrent Engineering (CE), is to move the design of complex equipment away from a process involving a sequence of specialist departments and to emphasise its multidisciplinary nature through the use of integrated product teams. Both the structural integrity of engineering products and the demonstration of the performance of proposed designs are increasingly reliant on the use of computer models created during the design process. Although the software tools existing within individual disciplines may be reasonably mature, the challenge is now to provide the tools necessary to support such an integrated approach.

The scope of MDO is limited to the design of products based on the simulation of physical objects in their environment. The use of multiple simulations is a key concept of MDO. This may involve diverse tools such as fluid flow solvers (to determine local and overall external forces), structural analysis and detail stressing (to determine structural deformations and internal stresses), electromagnetic analysis (to determine radar signatures from local and overall returns from incident beams), cost modelling, and tools for design for reliability. The physics modelling may be mathematical or experimental but the simulation of 'human interaction' effects, for example through the use of flight simulators, is excluded.

At a general level, when considering the overall mission performance of an aircraft, tools exist to aid the conceptual design of both military and civil aircraft, and are used during the early stages of the project. Figure 1 shows the 3 phases of project design and 3 corresponding levels of tools. Although a fully multidisciplinary approach is adopted at the conceptual design stage only the simplest, Level 1, empirical models are employed to approximate the physics which influence the overall design. Currently most MDO applications, for use in the preliminary design phases of a project, are based on major simplifications in mathematical modelling at level 2, such as beam structural models or panel methods for aerodynamics.

The objective today is to achieve the same degree of integration with Level 3, state-of-the-art analyses. The limiting factor in the use of proven models of this type is the capacity of current computation technology. Analyses using computational fluid dynamics, computational electro-mechanics, or detailed finite element models are separately capable of pressing computer resources to the limit, and this is compounded by the introduction of sensitivity calculations and optimisation. With the continuing advance of computation technology it can be expected that analysis methods will migrate up the pyramid shown in figure 1.

DERA has for many years been involved in multi-disciplinary optimisation in two areas; (1) using semi-empirical, Level 1, methods for concept assessment and to study the effect of changes in operational requirements, through the development and application of Multivariate optimisation (MVO)[1,2], and (2) using Finite Element methods in structural design, including linear methods for aerodynamic analysis, through the development and application of the

---

[†] Technical Manager, Aerodynamics & Hydrodynamics Centre
[‡] DERA Fellow, Structures Department
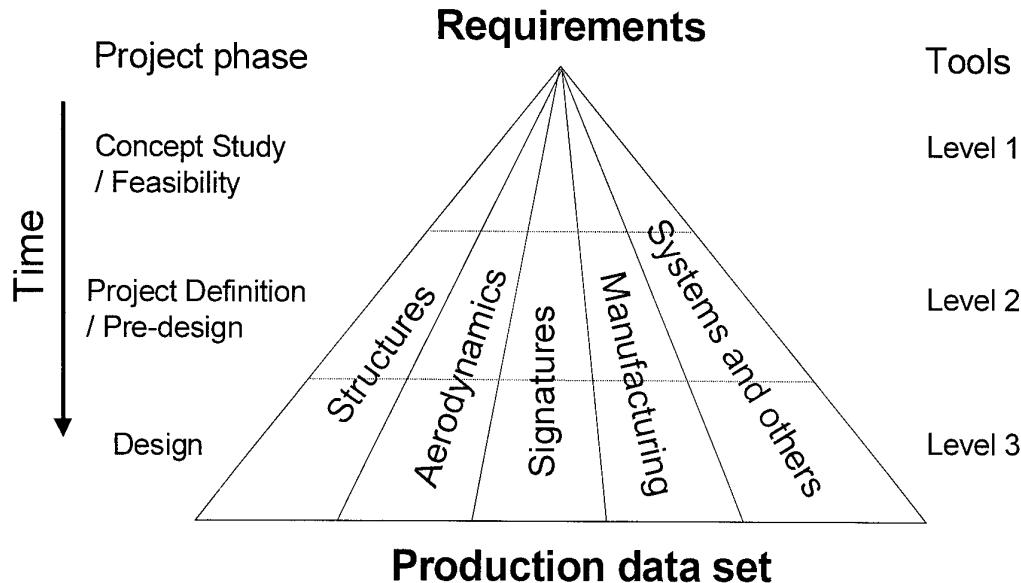
Fig 1 Project phases and tools for multi disciplinary design

STARS system[3]. From experience gained in these two areas the present authors embarked in 1995 on an examination of the potential and means for MDO. The fundamental difference of this MDO work from the earlier work has been that it has incorporated higher fidelity, Level 2 or 3, modelling in at least two disciplines. Because it was not clear what were the major issues and potential problems in achieving a viable MDO, a rapid-prototyping approach was followed initially. Previous work defining and building an MVO system had shown that it was not possible to predict in advance where the weakest link in the chain would occur, so development effort could have been misdirected if a rapid prototyping approach had not been followed. Subsequent work has comprised a series of relatively short-term projects, funded by UK government military and civil customers, and the Commission of the European Union. All the projects have had a strong industry participation.

In the next section of the paper the contribution of DERA to a series of projects is summarised. Several of these projects are the subject of separate papers at the RTO AVT Symposium on Aerodynamic Design and Optimisation of Flight Vehicles, and the reader is referred to papers 13, 14 and 15 for detail.

Drawing on the experience gained in these projects the following section attempts to identify the issues for implementation of an MDO process. This is approached via a series of questions and answers. The paper concludes by identifying the prime issues and some next steps required to progress towards providing an MDO tool that can be more generally used for air vehicle concept design and assessment.

CHRONOLOGY OF MDO PROJECTS

Wing Aeroelastic Optimisation

The GARTEUR Action Group SM(AG21) on multi-disciplinary wing design (1995-1999) covered the integration of strength and aeroelastic aspects of the design of high aspect ratio wings typical of modern regional transport aircraft, as illustrated in figure 2. The DERA contribution was based on the use of the in-house structural optimisation code, STARS[3] which, like several others, embodies aeroelastics as a tightly-coupled functionality. Both the aeroelastic predictions and design strategies to come out of the optimisation have been compared with those of the other partners within the group. While several European companies had long had the capability of combining aeroelastic design with basic strength requirements within the context of what are principally structural design codes, the GARTEUR Action Group provided a forum for the validation and comparison of the capabilities of the participants. Such comparison was felt to be important since experience has shown that significantly different 'solutions' can found by different groups. Unless analysis codes are thoroughly benchmarked valid conclusions on the relative merits of these codes in a design and optimisation environment cannot be made.
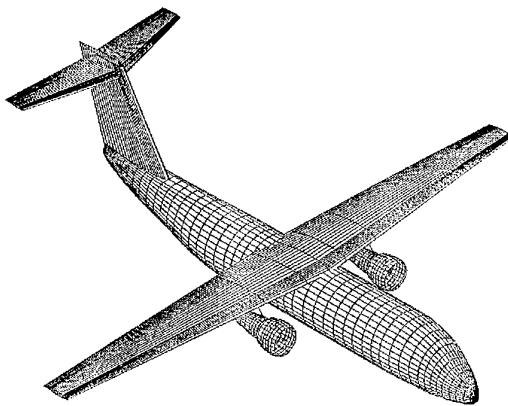
Figure 2 Regional transport aircraft used for wing aeroelastic optimisation

The MPEST project

In this 1 year project (1995-1996) an **MDO** Prototype for the Evaluation of **S**oftware **T**ools (MPEST) was constructed and demonstrated[4]. Funded by the UK MOD the prototype was assembled by British Aerospace Sowerby Research Centre, with additional contributions from DERA, BAe Airbus and Rutherford Appleton Laboratory. The prime aim was to assemble software for the key functional elements of an MDO framework and, by exercising these on a simple aerodynamic / structural optimisation problem, identify priority areas for

development. Figure 3a shows the framework used. A 2-dimensional Fowler flap design problem was used with the analysis methods being deliberately kept simple; a 2-d panel code for aerodynamic analysis and a simple beam model for the structural analysis of the trailing-edge flap track (figure 3b). This simple technical task had all the elements required to explore MDO issues. The framework consisted of elements for user-control, optimisation control, geometry generation, aerodynamic and structural analyses, and a data repository. The process by which an optimum solution to the flap problem was generated is shown in figure 3c.
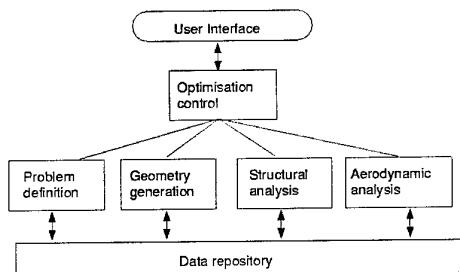
Figure 3a. MDO framework used in the MPEST project
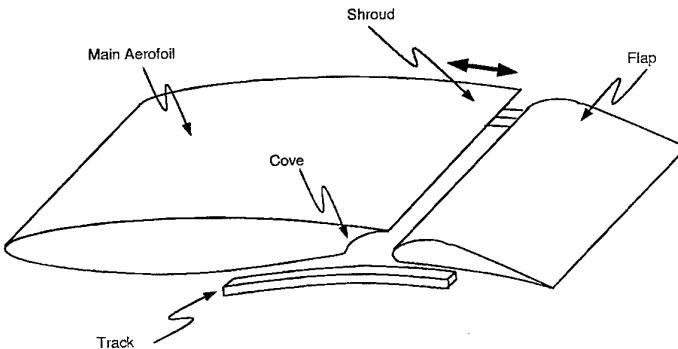
Figure 3b. Geometry of flap section used in the MPEST project

Initial Aerofoil

Parameterisation

Aerodynamic Analysis

Local
Constraint
Satisfaction

Structural Analysis

Local
Optimisation

Optimisation

**Storage of
Design sequences**

Visualisation
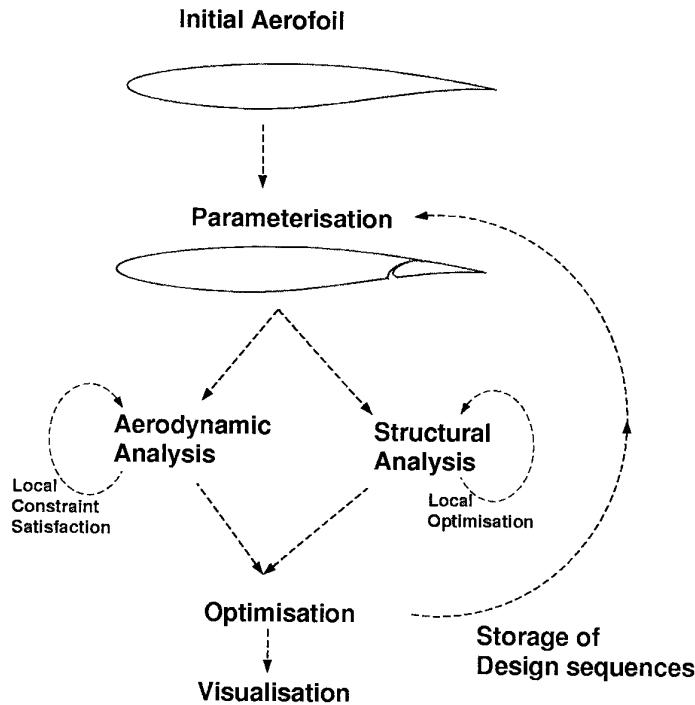
Figure 3c. MPEST optimisation process

This project showed the value of geometric parameterisation to accelerate re-design and the need for a plug-and-play capability for the software elements. The importance of process control, a user interface to track the solution of potentially complex problems and standards-based data structures were clear. The issue of whether MDO should be a distributed or integrated process was raised. While distributed processing can speed analysis and hence permit more comprehensive cross-discipline modelling, a single process would avoid complexity of control.

The EU MDO project

The next project, on the Multi-disciplinary Analysis and Optimisation of Aerospace Vehicles, was led by British Aerospace Airbus and funded by the European Commission. It comprised research on civil aircraft wing design by 14 partners. This two-year European project (1996-1998) represented a first step into multidisciplinary analysis and design optimisation of aerospace vehicles for many of the partners. The application selected to demonstrate new capabilities developed during the project was based on the A3xx concept currently under development by the Airbus partners. A whole aircraft model was provided for aeroelastic and controls studies, but the design activity was focused upon the wing. The project is described in detail by Allwright[5] from British Aerospace, who led the project.

All partners in the project participated in the definition of the research tasks and then separate groups were responsible for specialist investigations. The project was supported by the software infrastructure group with participants drawn from each of the research task groups. The final stage of the

activity was to draw together the lessons learnt from the project as recommendations. Further progress towards a full MDO capability was made, with the major advance being the introduction of aerodynamic design optimisation and the combination of aerodynamics and structural design to reduce the Direct Operating Cost (DOC). Some consideration was also given to issues of aircraft stability and control.

Groupings of partners within the project analysed a baseline configuration and examined alternative wing design aspects. This served both to ensure that corresponding product variants were modelled within each discipline and also to reduce the requirement for problem-specific data flow between disciplines. The issue of process control was also addressed with a variety of approaches being investigated. A range of approaches was also evident in the role of the optimiser, with some frameworks treating it as just another process within the chain and others allowing the optimiser to control the whole process. These areas are considered in more detail below.

Aerodynamic and Structural design. The objective of the work was to develop and demonstrate a capability for the aerodynamic and structural design of a wing which would minimise the direct operating cost (DOC) of the A3xx concept aircraft. The majority of the wing optimisation work used a few gross wing design parameters (area, aspect ratio, rear spar location, sweep, crank thickness and tip twist).

A strong need was perceived to use familiar legacy codes within a loose-coupled modular framework that enabled the output from every process to be evaluated before proceeding. The DERA-specific work introduced multiple flight conditions into the optimisation. This task illustrated the need

for flexibility within an MDO process, to allow the user to configure the optimisation process to accommodate multiple assessment tools, specific to each problem.

Product models and TDMB. The complexity of the data flow that links the disciplines of aerodynamics and structures, is illustrated in figure 4. This starts with a requirements system, which is assumed to be external to the MDO system, in which some freedom is assumed to exist to fine-tune the relative importance of various aspects of performance. An outline concept is then developed as a parameterised product model. This is followed by various assessments, here shown as aerodynamics and structures, with the possibility of making detailed shape and thickness changes for a given configuration.

Referring to figure 4 it is clear that large amounts of data, which may well be stored in separate databases, must be communicated between the component parts of the MDO system. The key issue for data transfer is the setting of common standards for the interpretation of information across disciplines. For MDO, the standards must cover all aspects of product geometry definition **and** design requirements, together with specific discipline-based data that reflects the constraints upon the design.

During the early meetings of the MDO project, a series of key activities were decided upon which defined the nature of the project. One was to adopt the BAe program TDMB[5] Technical Data Modeller and Browser) as the repository for the product model. TDMB provides a text editor user interface which supports a definition of data objects. It can then be expanded to store instance data capable of representing several variants of the product together with performance data derived from aerodynamic and structural analysis.

A fully parameterised representation of the aircraft configuration was developed, with tools to generate the aerodynamic data, finite element models and aeroelastic models used for performance assessment. This data-representation serves the project by providing partners with a common product model upon which design studies were based. The data models defined in TDMB will be exportable to the STEP/EXPRESS data definition language to enable future migration to other systems which conform to evolving standards for product models. The wider use of data which conforms to the STEP standards[6] is an important element of achieving the CALS objective of 'creating data once and using many times' through the product life cycle.

The use of a central data manager and browser in this project was shown to be of key importance to the success of the project in that it put in place a single product model from which specific contributing analysis models could be derived.

MDO process A major factor which will influence the overall success of any MDO implementation is the approach adopted to the co-ordination and scheduling of the diverse range of activities necessary to complete a full design cycle. This aspect of MDO must be adequately defined in the early

stages of the development process in order to draw together the different disciplines and allow concepts to be explored.

A framework specification document was written by a group of partners in the project and some software tools were provided for evaluation. These included tools for software version management, data definition, database technology, process definition, process execution on distributed networks, data visualisation and optimisation. Several alternative frameworks were employed and evaluated against the user and system requirements previously developed. The frameworks assessed included commercial MDO frameworks and toolsets, a process-driven Workflow Management tool and Network middleware. The frameworks tended to operate with a pre-defined sequence of operations and failed to provide the user with sufficient flexibility to reconfigure the process during the early exploratory phases of a design study. The interactive definition of a complex process is a prime requirement of any optimisation framework.

The strength of a work flow management tool is the traceability and control it offers, whereby only approved users may initiate processes and this may only be done if the input data has not been invalidated by changes by an upstream process. Network middleware systems enabled the computer resources of the network of machines to be utilised with the facility that one may expect of a single machine, but tended to require user-intervention and were weak at running chained processes.

As might have been expected the purpose-written MDO frameworks provided the most flexible integration support but did not necessarily distinguish the process support aspects (including the registration of tools, the definition of process chains and their execution) from data management (product models and requirements) or from embedded tools (for the visualisation of various categories of data or optimisation functionality). Further development is needed if the frameworks are to operate in a standards driven environment accessing data from corporate data bases.

The role of the optimiser The role of the optimiser was also the subject of slight variation within the various partner frameworks. At the simplest level, the optimiser calls for function evaluations, possibly including gradients, at a sequence of design points and, in effect, controls the process. As the function evaluations call for increasingly time-consuming analyses with complex data interactions and, possibly, requiring user-intervention, this becomes a less attractive option.

An alternative approach is still to start the design cycle with the optimiser initiating a design change, but to return control to the framework for the performance assessment phase. The optimiser must then be capable of being restarted once the performance assessment is complete. In software terms, the optimiser may then appear as just another MDO process, to be called as required, but its controlling role within the process of design should still be recognised.
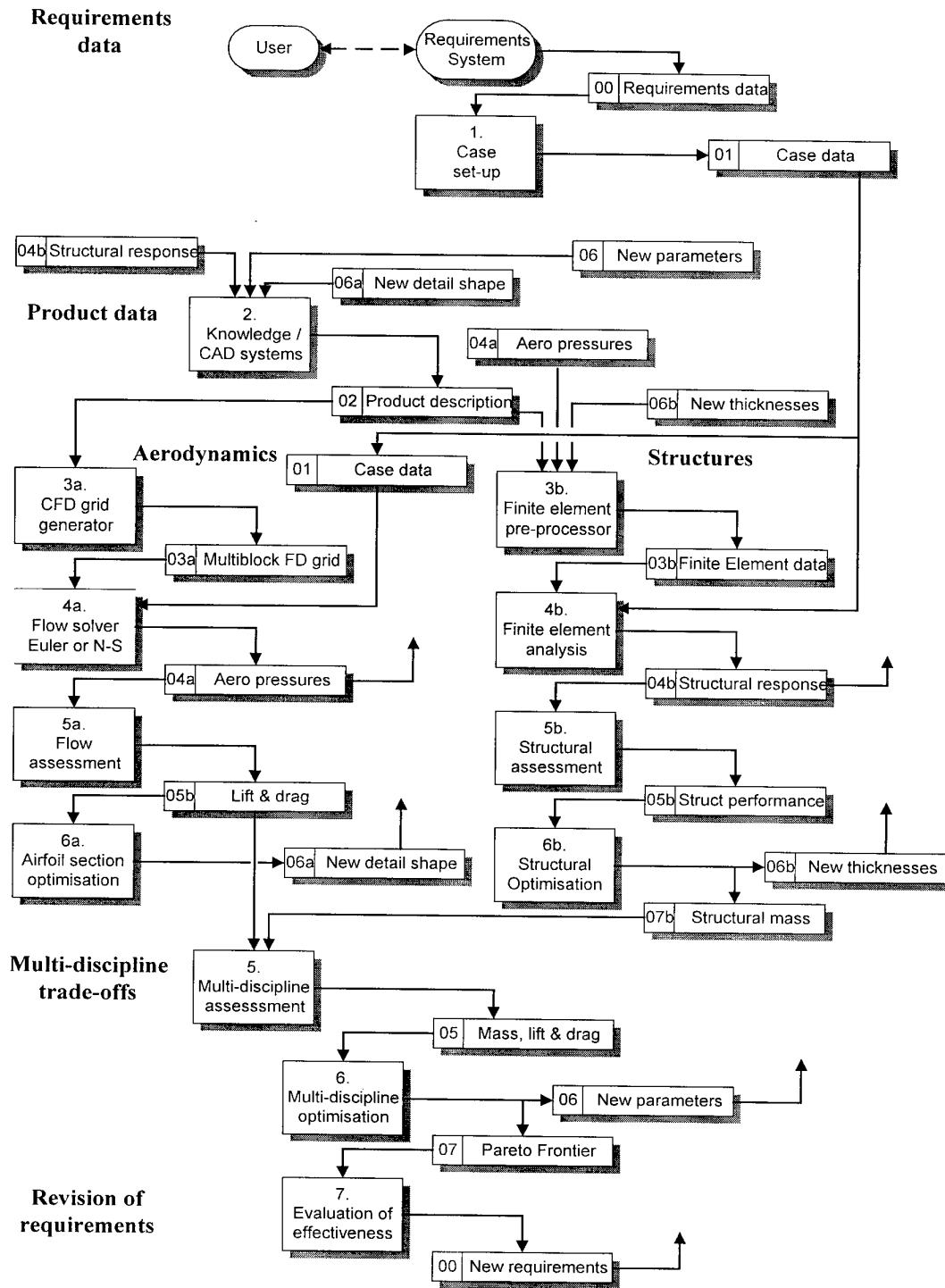
Figure 4. Data flow for multi-disciplinary design, showing software tools

The FRONTIER project

The FRONTIER project[7] (1996-1999) was led by British Aerospace Military Aircraft and funded by the European Commission. Although FRONTIER was a relatively small project, it had the widest scope in that it considered design against multiple objectives. The project partners consisted of universities who, in the main, acted as suppliers of new technology and industrial partners who provided user trials relevant to their industry sector. It comprised research to develop and evaluate a framework for multi-disciplinary optimisation, with multi-criterion decision making (MCDM) software to capture customer preferences, across a variety of mechanical engineering applications. The project also examined the capture of requirements. It is almost inevitable that the initial formulation of an MDO problem will not automatically lead to the required product, since the impact of constraints and the balance of conflicting requirements will not be fully understood at the outset. The Pareto frontier approach provides the user with visibility of potential design trade-offs and an ability to choose the relative importance placed upon multiple design objectives. Clearly, if cost were a criterion, this leads to a cost/performance assessment which is a key input to any requirement capture process.

In this project DERA evaluated the software tools developed for this purpose by other members of the FRONTIER Consortium, to explore combat aircraft wing design from a performance perspective. From multi-disciplinary aerodynamic and structural analyses, results for aircraft range (related to fuel volume, aircraft mass and drag) and supersonic sustained manoeuvre performance (related to aerodynamic drag) were derived. Figure 5, taken from the paper by Fenwick and Harris[8], shows that an envelope curve, the Pareto frontier, may drawn to encompass the performance results obtained for the family of wings of fixed planform which covered a range of wing thickness and spanwise thickness taper.

Requirement capture for military aircraft The user trial conducted by DERA in partnership with BAe was based on the design of a military wing and sought to achieve an acceptable compromise between aircraft range and turn performance. In this instance the aerodynamic model was taken as the master model, but in the longer term it would be expected that both the aerodynamics and structures models would be derived from a common product model. The approach taken is a multilevel Pareto-optimisation in which the wing thicknesses (wing-box depth) at various stations are used as top-level variables linking the structures and aerodynamic disciplines. The structural optimisation determines the sizes of the composite covers and sub-structure for each geometry, while the aerodynamic optimisation modifies the airfoil shape to maximise a weighted sum of lift to drag ratios corresponding to a supersonic turn condition and transonic cruise.

The supersonic turn rate and transonic range shown in figure 5 are then calculated from the drag, mass and fuel volumes. Each curve corresponds to a given spanwise thickness distribution but with the aerodynamic shape optimised to give differing levels of transonic to supersonic performance. In general the thicker wings give greater range due to their increased fuel capacity, but ultimately (case 9) higher drag will reduce the range.
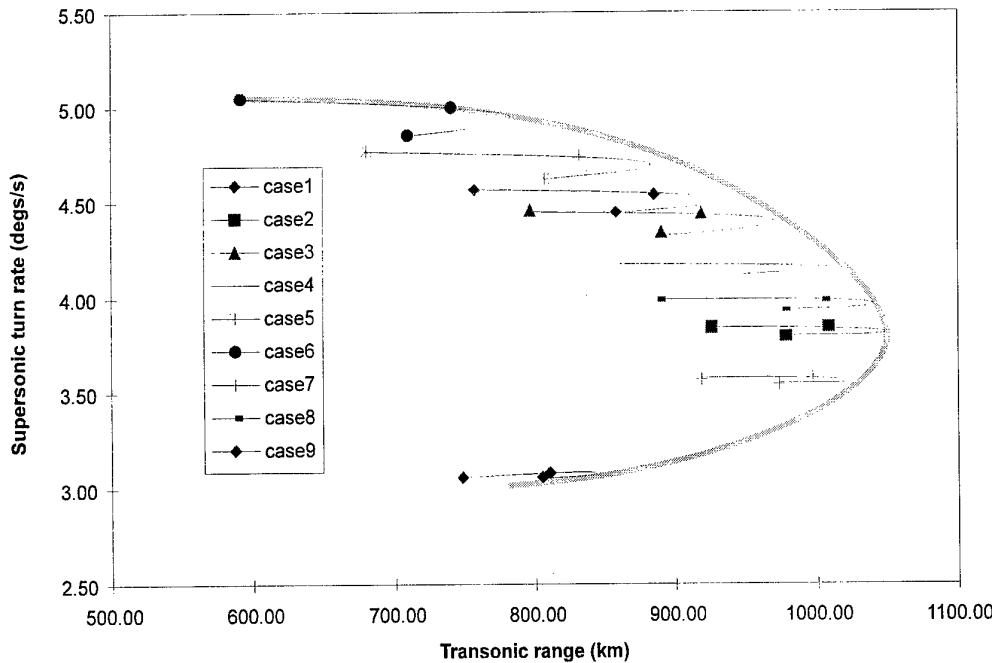
Figure 5. PARETO boundary

The Pareto frontier itself, indicated in grey in figure 5, bounds the region in which it is possible to design products to meet the conflicting requirements. The best products have performance characteristics which lie close to the 'top-right' part of the boundary. From here it is only possible to improve one characteristic at the expense of the other.

The use of genetic algorithms has been assessed as a method of achieving convergence to the boundary of the region. Typically such direct search methods require many function evaluations, each one of which calls a full structural optimisation for mass as well as an aerodynamic minimisation of drag for two flight conditions. The fact that these tasks are computationally intensive makes the activity appropriate for high-performance computing in the longer term, but to reduce the computing costs during the FRONTIER project, response surfaces were calculated for the wing mass and drag. The Pareto frontier could then be calculated on the basis of the cheaper response surface information rather than from further calls to the underlying design software. This enabled sufficient computing resources to be devoted to the assessment of genetic algorithms within the Pareto frontier approach, and to evaluating the MCDM software tool for deducing the weightings attached to the various design objectives from customer preferences. This aspect of the project was of particular interest as it extended the scope of MDO so that it assists with identification of the design requirements that the product should meet. The FRONTIER software provided a graphic demonstration of the ability to choose rapidly an appropriate mix of fighter and bomber requirements.

The ENHANCE project

The ongoing project ENHANCE (1999-2002), funded by the Commission of the EU, is addressing issues in Concurrent Engineering. This large European project (38 MEURO) has 53 partners drawn from the aeronautical industry and research community. The main objectives are to define new common ways of working, applicable from the initial design phase onwards, to propose a set of operational tools and to validate the new approach through a full range of industrial experiments. Central to the project is a set of 13 "COMMONs" each of which will define a common way of working within a given domain for engineering. It is planned to develop a set of Concurrent Engineering processes which will be adopted by all the parties. Implementation of these processes is expected to lead to large reductions in vehicle development timescales and costs, and to more effective and efficient utilisation of common exchange standards, leading to increased competitiveness.

DERA is contributing to the Common Scientific Calculation (COSCAL) element of the Product Engineering section of the project. Interfacing and integration of structural and aerodynamic analysis methods within a common data exchange environment are being defined and implemented.

DISCUSSION

Each of the projects summarised above has given a different perspective on MDO. In this section the discussions and conclusions from the individual projects are brought together and the major issues identified. To do this some basic questions need to be answered:

- Why do we need MDO?
- What are the necessary elements for MDO?
- How can these elements be put in place?
- What are the obstacles to be overcome?
- Who needs to take action?

Why do we need MDO?

Many answers have already been given to this question, but to summarise:

The military customer requires affordable and effective integrated air-vehicle systems, while industry aims to produce an air-vehicle system that meets customer requirements and produces a profit for its shareholders. To achieve these ends the military requirements and the potential solutions must be brought together with high fidelity of simulation, to reduce the cost and risk of a project. Industry needs a process to evolve concepts by bringing to bear quickly and effectively the full spectrum of their engineering design capabilities. The military customer needs a process to allow operational requirements to be evolved so that balanced concepts result for the warfighter. Thus responsiveness to evolving requirements is common to both parties. Reduced time for a design or assessment cycle allows more cycles to be completed in a given time, and a better product (cheaper for the same performance or higher performance for the same cost) to be defined. In the UK there is an increasing degree of overlap in the design and assessment processes because of the move to joint Industry / MOD project teams.

What are the necessary elements for MDO?

The following list captures all the elements required. They are listed in order of increasing difficulty of satisfaction across the potentially wide spectrum of users.

- Robust, compatible analysis codes
- Proven procedure for optimisation
- Data structure
- Requirements capture
- Framework architecture and hardware
- Control

Each of these is considered in detail in responding to the next question.

How can these elements be put in place?

Analysis codes The characteristics of any analysis code to be used for assessment, design or optimisation must be

thoroughly evaluated for the regime in which it is to be applied. The range of applicability needs to be defined. When used in an optimisation process any shortcomings in the modelling of physics within an analysis method can potentially lead to erroneous conclusions and hence invalidate the process. A standard interface to pre-processing (e.g. geometry input) and post-processing (e.g. flow field analysis and visualisation) is required. Although this can be achieved for legacy codes by writing a software 'wrapper', it is preferable to have a standard interface built into the analysis software.

Optimisation Flexibility is required in the means by which an 'optimum' can be defined. For optimisation within a local area of design space or for a well-understood problem gradient / line-search methods are most effective. When exploring a large region of design space the genetic-algorithm (GA) type of method has the advantage of being able to avoid local optima. Thus for mathematical optimisation in a new problem use of a variety of methods is likely to be preferable, if the potentially large computational requirement of a GA element can be accepted. Response surface methods provide a means of reducing the computational requirements while capturing many of the prime features of the design space.

In considering real engineering problems it is generally found that the definition of constraints is a critical element of the problem definition. While methods for unconstrained optimisation are mature and can produce well defined optima, this is not the case for constrained optimisation methods. In particular few gradient-based methods can produce well-converged solutions for problems with a large number of non-linear constraints. With the GA type of method constraints can be handled by including in the objective function a penalty term made up of the sum of the magnitudes of the constraint violations, but this approach can produce poor convergence. For engineering design in industry, visibility of the design space is an important requirement so that trade-off studies may be made to guide a decision on the 'optimum'. Thus a series of analyses and sub-discipline optimisations may be preferred to a total optimisation. For an MDO system to be of general use it is necessary to provide all of these options.

Data Structure To allow re-use of an MDO method data describing the product (i.e. aerospace vehicle) needs to be defined in a 'standard' form so that analysis programmes can retrieve and deposit the necessary parameters. The data describing the vehicle 'object' is not just geometric but will also cover the physical properties and performance of the product. To provide the widest possible commonality the product should be defined using an International standard with an associated data description language (e.g. STEP with the EXPRESS language). Because there are many ways in which an object can be described the choice of the model to characterise a product needs to be made by the prime customers for an MDO system, i.e. industry (for design, development and manufacture) and government procurement agencies (for requirements definition and project assessment).

With the current trend to integrated product teams the responsibility for model definition falls naturally to industry.

Parameterisation of geometry is a particularly important aspect of a product model. Historically different methods of parameterisation have been used for each engineering discipline (e.g. finite elements for structures, point data or bi-cubic patches for CFD, and CAD for manufacture). The requirement for a product model is thus to provide the reference detailed description of the object in such a form that the necessary information can be readily extracted for all disciplines. A potential difficulty arises from the fact that geometry parameterisation can be combined with geometric design rules if full advantage is taken of the capability available within modern CAD tools for implementing knowledge-based systems. As a result a product model can become proprietary, holding the accumulated knowledge of specialist designers. This type of product model could not therefore be released to the general R&D community so it is essential to separate the two functions.

Requirements capture Problems that are likely to be tackled with MDO are typically sufficiently complex that they have no unique definition. Requirements can be translated into alternative combinations of optimisation objectives, or constraints, or bounds on design variables, and can be applied at low or high-level in the MDO process. The capture of requirements for an MDO problem needs to be comprehensive as the omission of 'obvious' or 'trivial' requirements can result in unrealistic solutions. It is important to distinguish between requirements that are genuine constraints (e.g. to prevent overlap between components in a vehicle) and design 'rules' derived from established design practice that potentially limit the available design space. For design in industry the latter encapsulate best practice and thus they are often proprietary in nature, giving the company a competitive edge in the market place. It should be noted that the imposition of constraints of this nature removes some degree of design freedom and thus can potentially limit performance.

Framework architecture and hardware. Many alternative software architectures have been examined by workers in the MDO field. The most suitable approach will be determined by the particular problem being addressed and the computing resource available. While it is not possible to be more prescriptive than this, all frameworks should comprise elements with identifiably separate functions, and be implemented in an object-oriented form, so that the framework can be readily adapted as the design problem evolves (and typically grows in size). The framework needs to be suitable for implementation on networked computers, partly to link specialised analysis groups but also to allow parallelisation of any optimisation elements.

Control From an industry standpoint the weapon system designer wishes to make design judgements across a large number of issues, including commercial ones. Thus he will emphasise man-in-the-loop control of the MDO process, so that the process may be altered to provide the information on

the specific design trades he requires. At the other extreme an automatic large-scale optimisation could be defined that required no user interaction within the process. Experience indicates that results from a single optimisation of this type are of little use. Knowledge of the design space in the vicinity of the "optimum" is essential before any judgement on the worth of a design can be reached. Thus a series of optimisations is necessary, probably with systematic changes to constraints and / or objective functions. A user interface is therefore required which supports process definition and execution, and allows iteration without a man-in-the-loop (although, initially, user intervention is vital). Analysis methods must be automated and results displayed in a multi-disciplinary format. Experience from the MDO project recounted above indicates that the control element should also include the definition of the role of the optimiser: is it in control of the process or controlled by the process?

What are the obstacles to be overcome?

From the above discussion based on the experience of participation in MDO projects in the past 5 years, five issues need to be addressed to progress MDO from a research-based activity to one that will be of real value to industry and procurement agencies:

- Control of a distributed MDO process – who is in charge of the problem solution?

- Interactive definition of the MDO process to match problem requirements

- Definition of a product model for general use

- User confidence in results from analysis codes

- Audit of overall optimum by specialists from disciplines

Two other areas are important for improving the effectiveness of MDO, but progress is likely to be evolutionary and driven in part by advances in computation technology:

- Optimisation methods and strategy

- Geometric parameterisation

Who needs to take action?

Considering the first five issues listed above it is clear that the lead responsibility for their resolution rests largely with industry, as they are central to the concept definition process. In the UK this responsibility may devolve to a joint industry / military project team. Research agencies will continue to develop new technologies and demonstrate them. They can assist industry in the technology insertion process for the selected tools. The last two issues are likely to continue to be addressed by research projects developing new approaches and improved methods for the integration of disciplines. It will be essential for this work to be focused on realistic engineering problems generated in partnership with industry.

CONCLUSIONS

A number of developments relevant to the practical use of MDO have been identified by reference to a sequence of collaborative research activities in which DERA has participated. It is believed essential for the credibility of an MDO process that it should be able to accommodate the design processes used by engineers within industry to assess and validate their products.

Seven areas have been identified that need to be addressed to advance MDO. Of these the prime factor currently limiting further development of MDO is the lack of a product model to act as a standard for data accessed across disciplines. To achieve this it is essential that the data storage function be decoupled from rule storage (expert knowledge) function that co-exist in some CAD-based product models, because of the potentially proprietary nature of design rules. It is desirable to use STEP to standardise the form in which product data is shared and exchanged amongst processes.

A good framework for MDO that provides a flexible user interface for the definition, execution and monitoring of MDO processes is essential and further development of clear architectures for such software is still required. While conceptual design tools are often close-coupled, loosely coupled systems appear to be more appropriate to MDO in that they assist the verification of results by specialists. Some loss in process efficiency or even the generation of sub-optimal designs is acceptable provided the design process is understood and credible.

The future role of Research Agencies in advancing MDO is seen as developing and validating new technology for integrating analyses and optimisation, and assisting industry and procurement agencies in the insertion of the resulting tools into their design and assessment processes.

ACKNOWLEDGMENTS

REFERENCES

1 Lovell D A, "The application of multivariate optimisation to combat aircraft design." RAE TR88003, January 1988

2 Simm S, Crawford C, "Conceptual design and optimisation of modern combat aircraft." Paper 8, RTO AVT Symposium on Aerodynamic design and optimisation of Flight Vehicles. Ottawa October 1999

3 Bartholomew P, Vinson S, "STARS: Mathematical Foundations." In Software Systems for Structural Optimisation, Birkhauser Verlag, Basel 1993

4   Bodington R M, Sims P F, Allwright S E, *"MDO Prototype for the Evaluation of Software Tools (MPEST)"*. British Aerospace Sowerby Research Centre Report No JS13550. August 1996

5   Allwright S, *"Technical Data Management for collaborative Multidiscipline Optimisation."* AIAA-96-4160, 6th Symposium on Multidisciplinary Analysis and Optimisation." Seattle WA, Sept 1996

6   *ISO 10301, STEP*, http://www.ukcic.org/step/step.htm

7   *The FRONTIER Project*, ESPRIT Project 20082. http://frontier.ii.uib.no/

8   Fenwick S, Harris J ap C, *"The application of Pareto frontier methods in the multidisciplinary wing design of a generic modern military delta aircraft."* Paper 13, RTO AVT Symposium on Aerodynamic design and optimisation of Flight Vehicles, Ottawa October 1999

The application of Pareto frontier methods in the multidisciplinary wing design of a generic modern military delta aircraft[1]

Steven V Fenwick, John ap C Harris

Defence Evaluation and Research Agency, U.K.

Abstract

As a partner in the EC Framework IV "FRONTIER" project, DERA has investigated the application of a genetic algorithm (GA) and Pareto frontier methods to optimise the trade-off between multiple design objectives. A Pareto frontier is defined as the limit of design space beyond which one attribute of a design cannot be improved without detriment to another. DERA has applied the software produced within the project to the multidisciplinary design of the wing of a generic modern military delta aircraft, to trade-off the conflicting design requirements of range and agility. This paper recounts DERA's experience of the methods as an approach to the solution of a trial multidisciplinary design and optimisation (MDO) problem together with some of the results produced. Details of the software produced within the project are provided, along with conclusions and recommendations from its use.

Introduction

A characteristic of both military and civil aerospace engineering is the diverse range of disciplines contributing detailed information to the design task, such as aerodynamics, structures, signatures, manufacturing and support costs. The activities of these disciplines are commonly separate, and rely upon highly developed software tools for local analysis or optimisation of the discipline-based problem. In order to produce a viable design, the various disciplines must exchange subsets of their data, which will act as configuration definition or constraints data for the other disciplines. A MDO approach will simplify this process, whilst reducing design time and aiding the development of an equivalent or superior product. A detailed examination of the requirements and future potential for MDO, from a UK perspective is covered in reference 1.

The European Commission Framework IV project, "FRONTIER" [2] examined the increasingly important role of MDO in the design and assessment of new equipment. It explored the application of modern computing methods to link existing, complex engineering software tools in an easily accessible user environment, to enable engineers to optimise the trade-off of multiple objectives during the product design phase.

The project was a collaborative venture involving eight partners from industrial, academic and research establishments, and covered a wide range of engineering sectors, from household goods to aircraft. The partners were categorised according to their role within the project as either MDO users: DERA, British Aerospace (BAe), Daimler-Chrysler Aerospace (DASA), Calortecnica and Zanussi; or system suppliers: the University of Bergen, the University of Trieste and the University of Newcastle-upon-Tyne.

DERA investigated, in conjunction with BAe, the application of the multidisciplinary design tools produced by the

'supplier' partners to the wing design of a generic modern military delta aircraft. The user trial for the study comprised a tractable problem typical of aerospace concept development and design activities, which focused on examination of the effect of detailed aerodynamic and structural wing design on the overall aircraft performance. As such it was representative of the work of both BAe and DERA in their respective roles as equipment suppliers and advisors to the end users.

DERA user trial

The main aim of the DERA user trial was to guide the development and test the software produced by the supplier partners within the context of a typical aerospace design problem. The design problem selected for the software test phase involved the inter-disciplinary optimisation of the wing of a generic modern military aircraft (as pictured in figure 1a). To keep the problem at a suitable level of detail, only two disciplines were involved; aerodynamics and structures. It was intended that the user trial would prove the principle of inter-disciplinary optimisation, by using two already closely linked disciplines. The principle could then be extended in the future to include further disciplines, such as signatures and cost modelling.
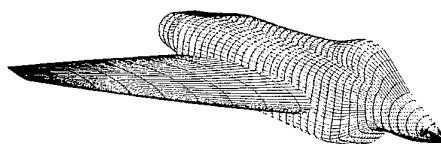
Figure 1a; CFD wing/body half model

Figure 1b; Finite element wing model (upper skin omitted)

The discipline specific models for the user trial were provided by BAe, and are shown in figures 1a and 1b. The objective of the study was to improve both the transonic penetration range and supersonic agility, as measured in terms of sustained turn rate (STR), of the aircraft. These conflicting performance requirements have historically been difficult to combine in a single design; a 'bomber' aircraft tends to have long range capability and poor manoeuvrability, whilst a 'fighter' aircraft generally exhibits good agility but short range.

Aerodynamic design optimisation is carried out at DERA using the Constrained Optimisation Design of Aerodynamic Shapes (CODAS) [3] software tool. This generally uses the Structured and Unstructured Numerical Analysis (SAUNA) computational fluid dynamics (CFD) suite [4] for the

---

aerodynamic analysis. CODAS uses a gradient-based optimisation algorithm, which attempts to minimise a user-defined objective function, subject to user-defined constraints, by varying the cross-sectional shape of the wing. The objective and constraint functions can be built from aerodynamic performance parameters (such as coefficient of lift, C_L and coefficient of drag, C_D), in addition to geometric parameters, such as thickness-to-chord ratio (t/c) and curvature.

DERA's structural design optimisation is conducted with the Structural Analysis and Redesign System (STARS) [5] which employs NASTRAN for the finite element analysis. The method uses a gradient-based optimiser to vary the thickness of the structural members, subject to constraints such as strength and stiffness, in order to minimise the overall structural mass.

Sequential operation of these two detailed discipline-based tools by their respective specialists is the traditional approach to an aerodynamic/structural wing design.

To reduce the complexity of the MDO task, the wing planform shape and location were fixed with respect to the fuselage. Initial studies into the performance of the aircraft at the required design points of transonic range and supersonic agility, indicated that the main aerodynamic drivers behind the differences in capability were wing thickness and wing camber due to their effect on lift, drag and internal fuel volume. The wing was therefore parameterised using the following 4 design variables:

i.   t/c at the wing root
ii.   t/c at the wing mid-semi-span
iii.   t/c at the wing tip
iv.   wing camber (3 discrete levels)

From the structures perspective, the objective was to minimise the mass of the wing structure, as this benefits both range and STR performance measures.

The output of the aerodynamic analysis of a single design instance included results such as transonic and supersonic C_L and C_D and internal fuel volume, whilst the structural analysis output the wing structural mass. These results are all low-level performance parameters specific to each discipline. In order to carry out a high-level optimisation of the wing as an element of the whole aircraft, incorporating both disciplines, high-level performance measures (such as range and STR) were required. Detailed models exist within DERA to analyse the performance of an aircraft as a whole based upon these performance parameters, but their use would have led to an over-complication of the user trial and have incorporated another detailed discipline into the high-level optimisation. Therefore for this user trial, simple equations derived from basic mechanics were used to convert the performance parameters detailed above into the high-level performance measures of range and STR.

Transonic penetration range was estimated for this approach using the Breguet range equation thus:

$$R = \left(\frac{Ma}{c'g}\right)\frac{L}{D}\ln\left[\frac{1}{1-(W_{fuel}/W_{take-off})}\right]$$

where: R   =   range (m)
       M   =   Mach number
       a   =   speed of sound (m.s^{-1})
       c'   =   specific fuel consumption (kg.N^{-1}.s^{-1})

g   =   gravitational constant (m.s^{-2})
L   =   lift (N)
D   =   drag (N)
W_{fuel} =   weight of fuel at take-off (N)
$W_{take-off}$=   total weight of aircraft at take-off (N),

and supersonic STR was estimated thus:

$$\omega = \frac{g}{Ma}\sqrt{\left(\frac{\frac{1}{2}\rho(Ma)^2 SC_L}{mg}\right)^2 - 1}$$

where the terms are as before, and:
    ω =   turn rate (radians.s^{-1})
    ρ =   air density (kg.m^{-3})
    S   =   gross wing area (m^2)
    C_L =   coefficient of lift
    m   =   mass of the aircraft (kg).

The FRONTIER framework

The software framework for MDO developed within the FRONTIER project comprises three separate functional entities; a graphical user interface (GUI), high-level optimisers, and a decision support tool as described below.

Graphical user interface (GUI) : The GUI was written by the University of Bergen, Norway [6, 7] and is intended to provide a user-friendly and easily accessible front-end to the rest of the FRONTIER system. The GUI provides a generic front-end for MDO which is applicable to most industrial design problems and consists of two main elements. The first element handles the interface with the user, and the second element is a framework to manage execution of the various analysis and optimisation processes involved in the task. The GUI interface is designed to be used across a network of heterogeneous platforms, and has been based on the JAVA language, in conjunction with HTML internet web page type screens. The portability of the GUI interface element between various hardware and software environments is therefore greatly enhanced, whilst also remaining highly configurable.

The GUI framework element involves the sequencing of the various stages of the MDO task based upon a user-defined logic script that indicates the required data files and software modules to be run. This relies upon an integral part of the GUI tool to automate the compilation of the run-time scripts needed to execute the discipline based legacy codes required for the analysis. The GUI framework deals with all the interactions between the various software modules as required, with only simple operations required of the user in order to set-up the optimisation problem. As part of the framework element, the Common Object Request Broker Architecture (CORBA) industry standard for message passing is used for communication between the various modules. This allows the modules to exist on separate, heterogeneous hardware platforms. The use of JAVA and CORBA will ensure the longevity of the software and enable future developments to the MDO framework to be readily incorporated.

Optimisers : The FRONTIER software includes two optimisers; a multi-objective genetic algorithm (MOGA) and a simple gradient-based method, both of which were programmed by the University of Trieste, Italy [8, 9]. The MOGA is the main optimiser for FRONTIER, and consists of a generational GA which can be appropriately configured by the users to suit their individual optimisation problem. Examples of the settings that can be altered by the user include the number of individuals and generations required, the

probabilities of crossover and mutation and the generational strategies (steady-state or standard) that are to be employed in the optimisation. Based upon either a random or user-defined initial set of individuals, the MOGA searches the design space for non-dominated solutions to the problem, subject to any user-defined constraints, which are represented as fuzzy penalty functions. Having thus explored the design space fully, the designs that form the non-dominated limit of the design space (ie. the Pareto frontier) can be filtered from the whole population, using the tools provided in the GUI.

To complement the MOGA, a gradient-based optimisation routine, based on the Broyden-Fletcher-Goldfarb-Shanno (BFGS) method is also supplied. This can be used to maximise a single objective function starting from a user-defined individual. With a choice of finite differencing schemes and the ability to use weighted combinations of the multiple objectives, the BFGS optimiser can be used to refine the current optimum as identified by the MOGA in a chosen region of design space.

Decision support tool : The multi-criteria decision maker (MCDM) has been written by the University of Newcastle-upon-Tyne, U.K. [10, 11] and is intended as an aid to the design engineer. The method employs the principles of utility functions to assess the relative merit of a series of designs, in order to assist the designer in selecting the alternative which most closely matches the user requirements. The facilities provided by the MCDM become particularly relevant at the later stages of the optimisation design process when a defined Pareto frontier set of designs can be compared against each other, and then ranked according to a declared set of user preferences. The subsequent output can then be used within the gradient-based optimiser to further refine the Pareto frontier in the area of interest to the designer.

The procedure used to rank the designs is based upon declared user preferences or indifferences for one design compared to another in the set of candidate designs. In addition, weightings can be applied between design variables to accommodate any specific needs. These judgements are used to calculate utility functions for each of the design variables. The software uses an exhaustive search method to refine the magnitude and curvature of each utility function, with the resolution of the search being refined as the best solution is identified. If no solution is possible, it is assumed that there is an inconsistency in the initial declared preferences, and the method suggests to the user which preferences should be reviewed. Once a solution is found, the composite utility function, formed from the amalgamation of the utility functions for each design variable, is used to rank the candidate designs. The magnitude and curvature of each of the design variable utility functions is also output, for use within the BFGS optimiser if required.

The general method for operation of the framework is firstly to link the existing analytical tools to the framework, using tools provided within the GUI. This provides the analytical functionality for the design optimisation process. The framework then needs to be configured for the specific design problem, such as number of design variables, number of constraints and the order in which the analytical tools will be used. Once these tasks have been carried out for a specific design problem, they do not need to be repeated. The optimisation is then usually begun with the MOGA for a specific number of individuals and generations, so that the design engineer can ascertain the nature of the design space, and if necessary adjust or incorporate further constraints. Following a successful MOGA optimisation and identification of the resulting Pareto frontier, the MCDM tool can then be used to rank a sub-set of the designs, in order to concentrate any subsequent optimisation effort into the area of design space of most interest to the design engineer. The best MOGA
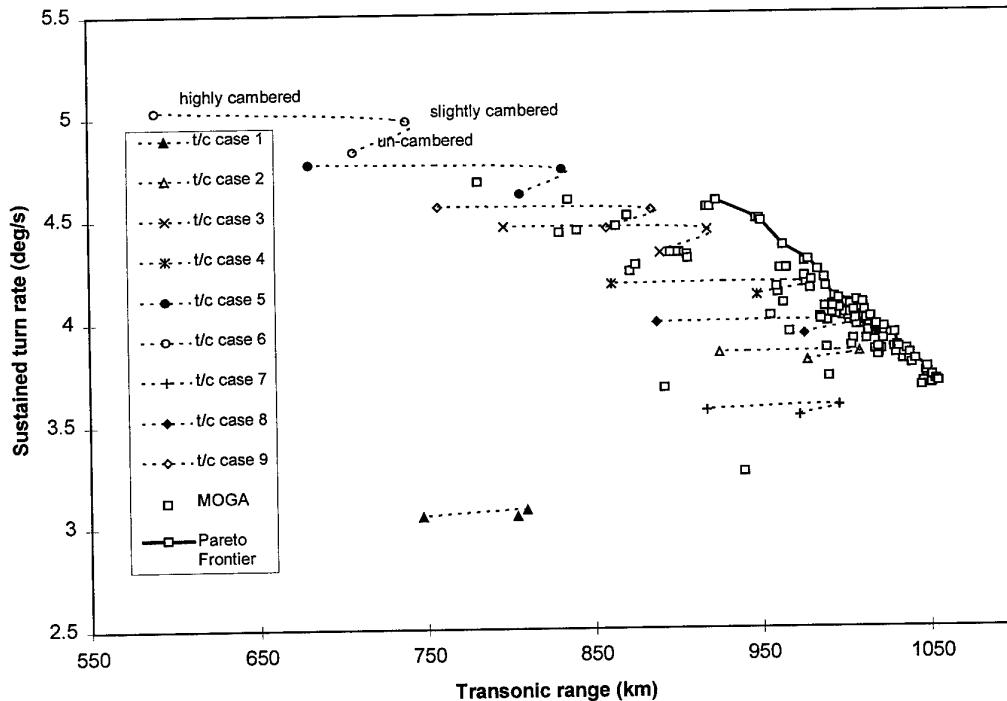
Figure 2; Initial response surface and Pareto frontier

generated design, calculated from the user requirements, can then be used as a starting point for the gradient-based optimisation to search for an improved design.

When using the FRONTIER software framework, the user has little direct interaction with the optimisers or decision support tool as all of the configuration and initiation of these modules is carried out using the GUI. It is therefore possible for a user inexperienced with the hardware and software of the host machine(s) to carry out an optimisation task.

Results

It was originally intended to encompass both CODAS and STARS within the DERA FRONTIER user trial, however cost implications associated with the coupling of a GA to such highly computationally intensive, low-level optimisation tools precluded this. Instead, an approach was adopted in which an initial set of designs were analysed with the detailed discipline tools, and the results used to populate a response surface. This could then be coupled directly to the FRONTIER system to identify the multidisciplinary optimum, with relatively little further computational cost beyond that required for the initial population of the response surface.

Accordingly, for the aircraft wing user trial an initial population of 27 designs were analysed with the detailed design tools to create a response surface which was a near quadratic for each of the design variables. These were produced from a set of 9 spanwise thickness profiles, each of which had 3 levels of camber applied to it; 'none', 'slight' and 'high'. The 'high' camber case was taken from initial studies carried out using CODAS, and the 'slight' camber was half of the 'high' camber case. For each design, estimates of its range and agility were made using the equations described earlier. It has been assumed that the wing structural mass is independent

of the wing camber. The high-level performance measures for the initial response surface population are shown in figure 2.

For the majority of cases, the highly cambered wing has the best supersonic STR, but the worst transonic range. This is because such wings are efficient at the high-lift design point, but must be flown at a reduced angle of attack to achieve 1g flight. This tends to produce shock waves on the underside of the wing, just aft of the leading-edge, which increases the drag, and hence reduces the aircraft's range. However, the un-cambered wings generally have the least turn rate, due to their reduced efficiency at high lift, but need to be flown at an increased angle of attack in order to generate the required lift for 1g flight. This tends to produce shock waves on the upper surface of the wing, again aft of the leading-edge, though these tend to be weaker than those on the highly cambered wing, and hence the aircraft show an improvement in range. For each spanwise thickness case, the slightly cambered wing has the best range. This is because it produces relatively weak or no shock waves for the range design point, yet is relatively efficient at the supersonic high lift design point, hence giving a good turn rate.

Interestingly, the results for each of the spanwise thickness cases shown in figure 2 are themselves low-level Pareto frontiers. These are approximated by the dotted lines, however it is not possible to determine the full extent of each curve from the available data.

The response surface was then coupled to the MOGA and an optimisation run of 10 generations, each of 32 individuals was performed. The results are shown in figure 2, together with the initial 27 designs for comparison. It can be seen that the MOGA has produced a wide ranging set of design instances, most of which show an improvement over the initial 27 designs. It is postulated that the Pareto frontier would not be
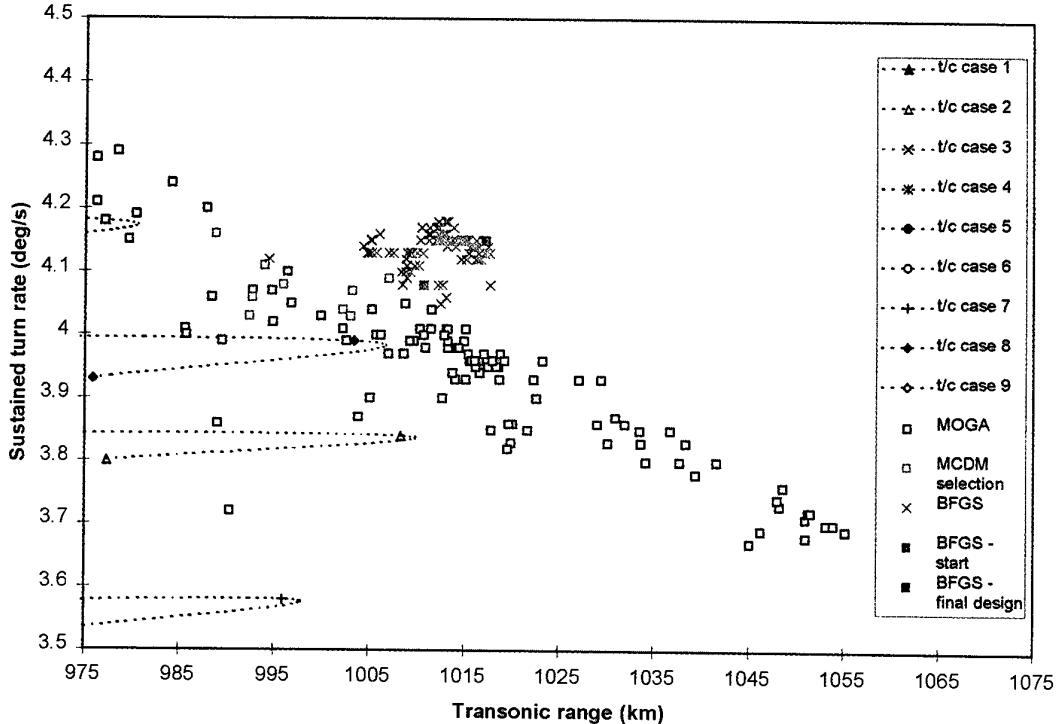
Figure 3; Refined high-level optimum design

advanced a great deal from the position shown in figure 2, without recourse to a very large number of generations and individuals within the MOGA. However, the Pareto frontier shown provides a useful aid to the design engineer, in that it demonstrates the nature of the design space involved.

To illustrate the use of the framework to optimise the wing to satisfy a defined set of user performance requirements, the designs identified by the MOGA on the Pareto frontier were then refined with the aid of the MCDM and gradient-based optimiser. Based on an assumed user requirement to maximise aircraft range and attain at least a 4°/s STR, a series of designs on and close to the Pareto frontier in the region of the required STR were passed to the MCDM decision support tool.

Several pairwise preferences were provided to the MCDM, together with the selection of designs from the MOGA Pareto frontier. The output of the MCDM software ranked the supplied designs, based on the indicated preferences and provided appropriate relative weightings for the objectives. The top ranked design, together with these weightings were then transferred to the BFGS gradient-based optimiser within the FRONTIER system, and a further optimisation carried out.

The results of the follow-on gradient based optimisation are shown in figure 3. It can be clearly seen that an improved design has been found in comparison to the MOGA Pareto frontier. This design is an improvement over the other designs, based on the preferences supplied to the decision support tool. It should be noted that this improved result is based upon the example user requirements of good range, and a minimum STR of 4°/s. If different user requirements had been specified, or different preferences used within the decision support tool, then it is likely that the final optimum design shown in figure 3 would be different. It is postulated that such refinement of the GA Pareto frontier could be carried out along the whole frontier, however this would require a large number of separate gradient optimiser runs, and this would have computational cost implications. Hence, the use of the decision support tool to concentrate optimisation effort only in the area of design space of interest to the designer.

Conclusions

The use of a GA allows the nature of the design space to be assessed, in addition to the well-publicised benefits for finding the global optimum of a problem. However, the shortcomings of such an approach are generally cited as being the relatively slow 'convergence' of such algorithms, in that they require a large number of design instances to be analysed to achieve the optimum design. It has been shown by these results that these difficulties can be partly addressed by the use of a GA in conjunction with a gradient-based optimiser. The GA can be used to populate the design space to sufficient detail for the design engineer to choose an area of interest, and then the designs can be refined just in that area, by the more efficient gradient-based method.

The critical step of the approach described above, is the transition from the more globally orientated GA, which may be using multiple objectives, to the more focused, single objective gradient-based approach. A great deal of time and effort can be spent in trying to devise weightings for the multiple objectives, in order to combine them into a single objective function. The use of a decision support tool at this stage, such as that in the FRONTIER system, can be very beneficial. Not only does it calculate which is the current best design, and therefore a suitable starting point for any subsequent gradient-based optimisations, but it also calculates the relative weightings of the multiple objectives. These

calculations are based on the initial information provided by the designer, and therefore reflect the user requirements in simple quantitative terms. However, for such decision support tools to be of use to the design engineer, the sensitivity of the output to the input should be examined closely, and the output only taken as guidance, rather than the definitive answer. Then, such tools can be highly valuable to the decision making process.

The use of a response surface approach, although utilised by this project primarily because of cost considerations has proved to be a success. It required the highly specialised low-level analysis tools to be used only by the respective specialists, and therefore the integrity of the data input to the response surface was assured. This avoids the possibility of the optimiser requesting analysis of designs which are incompatible with the underlying philosophy of the specialist analysis tool. In addition, when used with a GA a response surface requires relatively little computational effort to interrogate, in comparison to direct coupling of the analysis tools to the optimiser, and so a far wider reaching study can be performed. Similar findings are stated in reference 12.

The FRONTIER software tools at their current version of release, whilst clearly providing a valuable facility for MDO, have been developed over a relatively short period of time, and must be regarded as a pilot implementation of the techniques. As such, DERA has identified limitations in the current abilities of the framework. For instance, the FRONTIER system currently allows only for the use of the in-built optimisers, which are closely integrated with the rest of the framework. It is hoped that when the system matures the optimisers will be placed on the same level as the other software modules which perform tasks such as detailed design, design simulation, or performance assessment. This would allow the user to implement an in-house or "off-the-shelf" optimiser to suit the design task in hand, whilst also facilitating more advanced branching between tasks and disciplines as the design run progresses. In addition, the implementation of a common product model based upon industry standards such as the Standard for the Exchange of Product Data (STEP) would provide a database which could be used to store and access current and past optimised designs, without the need to re-run design tasks. It is hoped that the future exploitation of the FRONTIER software by a commercial vendor will address such shortcomings, and produce a FRONTIER framework that can be utilised as the basis for a generic MDO framework, applicable to a large number of engineering sectors in addition to aerospace.

- the UK Department of Trade and Industry, as part of the CARAD programme;

- the European Commission as part of the ESPRIT programme.

References

1   Lovell, D.A., Bartholomew, P.; *Progress towards a multi-disciplinary analysis and optimisation capability for air vehicle assessment and design – a UK view*; NATO RTA AVT symposium, October 1999

2   http://frontier.ii.uib.no/

3   Lovell, D.A., Doherty, J.J.; *Aerodynamic design of aerofoils and wings using a constrained optimisation method*; DERA, ICAS-94-2.1.2, September 1994

4   Peace, A.J., Chappell, J.A., Shaw, J.A.; *Turbulent flow calculations for complex aircraft geometries using prismatic grid regions in the SAUNA CFD code*; Aircraft Research Association Ltd., ICAS-96-1.4.2, September 1996

5   Bartholomew, P., Vinson, S.; *STARS: Mathematical Foundations.* In: K. Schittkowski, ed. Software Systems for Structural Optimisation. H.R.E.M. Horlein, Birkhauser Verlag, Basel, 1993

6   Cook, J., Moe, R., Mughal, K.; *Frontier Deliverable D2.3 – System Design*; Parallab, University of Bergen report, July 1997

7   Cook, J., Pickering, R.; *An Introduction to Frontier: An Environment for Design Optimisation*; Parallab, University of Bergen report, December 1998

8   Poloni, C.; *Design Optimisation Tools available in the Frontier System – User Manual*; University of Trieste report, 30 December 1998

9   Poloni, C., Pediroda, V.; *Optimisation Routine Prototype 4.3 – Final version of the selected optimisation routines to be interfaced to the system – Functionality Report and Interface Definition*; University of Trieste report, Frontier/UTS/ED4.3, 30 December 1998

10 Decision Support Group; *MCDM Software User Manual*; University of Newcastle Technical report, December 1998

11 Decision Support Group; *MCDM Software Technical Manual*; University of Newcastle Technical report, December 1998

12 Knill, D.L. et al; *Response surface models combining linear and Euler aerodynamics for supersonic transport design.* Journal of Aircraft, Vol. 36, No. 1 pp 75-86, January-February 1999.

DISCUSSION

Session II, Paper #13

Mr Perrier (Dassault Aviation, France) asked whether CORBA really worked for multiple users in a networking environment.

> **Mr Fenwick** replied that CORBA constructs are used to handle all the communication between the various software modules within the FRONTIER software. He believed that as an industry standard, CORBA allows easy and reliable communication between modules, whether they are hosted on one machine or many. Consequently, FRONTIER software is platform independent and allows easy use of network machines.

Mr Perrier asked how many GA iterations were used.

> **Mr Fenwick** noted that in the example presented there were 10 generations of 32 individuals in each generation, however not all are shown on the graphs as some of these were infeasible, i.e. they broke the imposed constraints.

An MDO application for a weapon released from an internal bay

Authors: G Moretti, D Spicer, N Sharples

British Aerospace Military Aircraft & Aerostructures
Warton Aerodrome
Preston – PR4 1AX
Lancashire
UK

1. INTRODUCTION

Multi Disciplinary Optimisation (MDO) process has always been identified as an essential tool for the development of an aircraft design. Recent engineering emphasis has been on improving the depth of optimisation within a reduced overall time frame, a goal which depends on the level of automation available and the capability and skill of each discipline.

The figure below shows an overview of the general design cycle in the military aircraft manufacturer's world. The large time spans involved in the full process should be appreciated: it may take between ten and twenty years to bring a new project to fruition.

DESIGN CYCLE

Figure 1.

The design process starts from a set of Operational Requirements, generated and substantiated by wargame scenarios. These requirements get translated into a set of design configurations which attempt to meet the requirements in various ways. Several iterations are needed to then select the final configuration(s).

Initial conceptual design takes place during the first two or three stages of this process and is conducted in a much reduced time scale. This allows many concept options to be examined and a knowledge database to be built up.

One of the key enabling factors for MDO over the past few years has been the introduction and widespread use of CAD within the initial design process. The use of a single model acting as a digital master allows the individual designer to take responsibility for all aspects of the initial layout and use the same controlling geometry for each task.

A fully integrated MDO process should cover all the factors which affect the major aircraft components from different engineering analysis viewpoints, and be embedded within a Synthetic Environment (SE) to meet the automation requirement. As a consequence, the optimisation of any particular concept design remains a complex problem because of the large number of variables to be considered. While the advent of large scale computing capabilities and the development of mathematical optimisation techniques has meant that artificial intelligence methods can now be applied to the configuration optimisation problem, the ultimate success or otherwise will depend on the skill, experience and judgement of the design team involved.

It should be noted that current MDO studies are limited to particular aspects of the overall configuration.

This paper shows the results of a study to demonstrate the advantages of a concurrent design process applied to an internal weapon installation and to report on the lessons learned.

2. STUDY BACKGROUND

For military aircraft, internal carriage is perceived as being one of the key ways of maintaining Low Observability (LO) during missions and offering enhanced survivability. Weapon bays have a significant impact on overall air vehicle configuration, and it is vital to ensure that the key constraints can be evaluated at relatively low cost early enough in the design cycle so as to minimise the overall air system development costs.

The weapon bay environment is one of the high risk features of LO platforms. The aerodynamics of deep weapons bays are characterised by highly unsteady flows, which generate high dynamic pressure levels throughout the bay [1 & 2], giving high aero-acoustic loads, which in turn lead to potential structural fatigue problems and equipment qualification challenges. Methods are required to predict these levels to a calibrated accuracy in order to assess interactively and quickly during the configuration development phase the effect of different options so as to reduce risk in the weapon bay design.

In order to assess the safe separation of stores from the weapons bay, current trajectory prediction methods and techniques also need to be assessed to account for the effects of the dynamic flow within and around the weapons bay.

Because these two major items tend to drive the bay shape in opposing ways, a compromise between them needs to be found in order to achieve a bay design capable of carrying and releasing weapons safely whilst maintaining equipment functionality and structural integrity. It should be noted that, once established, the bay cannot easily be altered.

The figure below describes pictorially the situation for stores release.
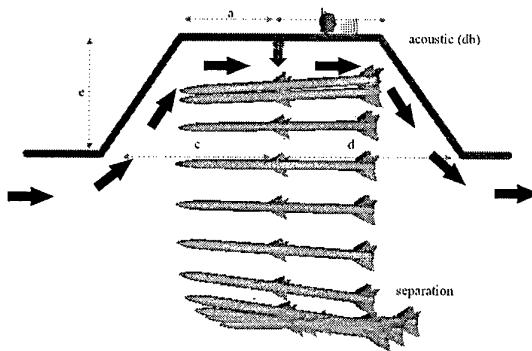
Figure 2.

3. WEAPON BAY TESTCASE

As part of the process of developing the overall MDO process for future design, an exercise has been carried out by the BAe MA&A Future Offensive Air System design group, to examine an internal weapon carriage and release case. The environmental aspects (i.e. acoustic noise levels) and the weapon safe release aspects were addressed simultaneously. This generic study has been performed with the major aim of proving that a more comprehensive and accelerated design process can be achieved by an automatic parallelisation of tasks. It was also a practical test case which identified some constraints and limitations of the optimisation method used.

The bay geometry has a strong influence on both the environment and the behaviour of the weapon during release. The acoustic characteristics of "deep" bays are notoriously very severe and release from "shallow" bays can be quite difficult, depending on the weapon and bay relative geometries. These are obviously simplifications and invariably other factors, such as flight conditions, ejector launchers, missile release controls, bay doors positioning, and noise suppression will also contribute to the overall solution. These additional terms have however been frozen for the purpose of this exercise.

The aim of this study is to demonstrate the design optimisation capability, based on the FRONTIER MDO tool, within the aerodynamics discipline on a simple 2D cavity test case. Although this is not a comprehensive 'multidisciplinary' demonstration, it does span a number of aerodynamic sub-disciplines, including dynamic loads and stores release.

The study aimed at demonstrating the feasibility of linking together a standard aerodynamic CFD tool with a mesh generator and a stores release code through the FRONTIER optimisation tool. Compromises had to be made at the expense of accuracy, in order to obtain quick solutions. The study was limited to a 2D case to ease the CFD processing time, since one current area of particular concern is the affordability (both in terms of supercomputing resource and elapsed time) of unsteady Navier-Stokes methods which are required to model cavity flows. Throughout the exercise, the accuracy of the CFD solutions was also assessed, but this was not a paramount consideration.

4. METHODOLOGY

In this section, we will state the design problem addressed, indicate the role of the general FRONTIER framework in integrating and supervising the design search, and define the analysis tools used to evaluate each design and how they are used.

4.1. THE EXAMPLE DESIGN PROBLEM

The weapons bay considered is represented by the following 2D geometry. The design variables, shown in figure 3, are; cavity base length L, cavity depth. D; and cavity rear face angle θ.

A conventional Heavy Duty ejector system with short stroke length (100 mm) is assumed. The ejector is mounted at the top of the bay and in the middle of the cavity base. On release, the weapon is fired down into the airstream, and is subject to forces from the ejector, the airflow, and gravity.
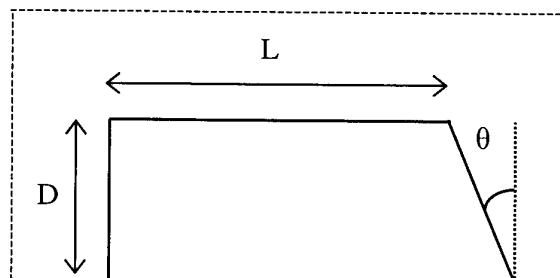
Figure 3.

The problem posed is:

minimise acoustic load A and maximise store separation S;

with respect to (L,D,θ) subject to the simple constraints:

$$1 < L/D < 10.$$

In this example, A is measured using the time history of the pressure at the upper rear corner of the bay. The fluid flow simulation is run for a 'settling period', then the pressure time history is recorded. At the end of the simulation, A is calculated as the total power in the spectrum of this pressure history. This metric keeps analysis simple and calculation time low. More sophisticated metrics may in future include automatically searching for tonal frequencies defining cavity

resonance.

S is the minimum vertical distance of any part of the weapon from any part of the structure, 0.5 seconds after release.

4.2. FRONTIER ENVIRONMENT ROLE

A typical optimisation exercise consists of a number of nonrecurring setup operations, followed by a recurring round of actions which create and evaluate a range of designs. Most of the tools needed are of course provided by the owner of the particular optimisation problem concerned. The role of the FRONTIER environment [3] is to provide systems integration, optimisation tools, and decision support tools.

The optimisation 'search engines' available include hill climber and probabilistic search algorithms. The search can also be controlled by the user. In the current study, we are addressing a multiobjective problem (minimising A and maximising S simultaneously), so a multiobjective algorithm is needed [4].

For each design proposed, the flow solver used for design evaluation expects a geometry input file, so the (L, D, θ) combination which defines each design considered needs to be turned into a full geometry using a geometry creation facility.

Then, the design needs to be evaluated, by activating the required analysis tools in the necessary sequence. Following this, the evaluation results are inspected, and also fed back to the search engine, to provide guidance for further searching.

This set of 'propose-create-evaluate-feed back' operations is continued until terminated by the designer.

4.3. GEOMETRY CREATION TOOLSET AND METHODS

The tools used in this case were the GAMBIT code incorporated within the Fluent CFD code together with a small in-house module to prepare GAMBIT input. In general, this geometry creation step would be carried out by the company's main CAD system, CATIA, using an interface appropriate to the data exchange format demanded by the evaluation tools.

4.4. DESIGN EVALUATION TOOLSET, PROCESS, AND METHODS

4.4.1. Toolset

The toolset included:
- the Fluent Inc. geometry and meshing tool GAMBIT 1 [5]
- the Fluent Inc. CFD analysis tool Fluent 5.1.1 [6]
- the CFD visualisation and post-processing code EnSight [7]
- the BAe NUFA semi-empirical weapon aerodynamics model, capable of operating with a non-uniform flowfield [8]
- and the BAe 6-DoF modeller STARS (Store Trajectory And Release Simulation) as the stores release trajectory prediction tool [9]

4.4.2. Design evaluation process

These tools were used to populate a design evaluation process. The process flow is shown in outline in figure 4.
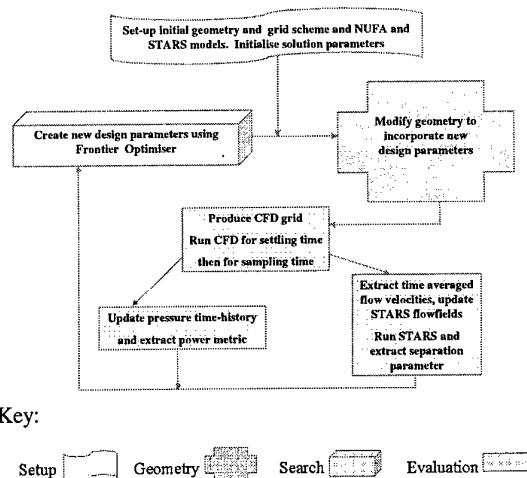
Figure 4.

4.4.3. Methods used for design evaluation

4.4.3.1. Flow modelling

The flow was modelled within Fluent by solving the unsteady Reynolds-Averaged Navier-Stokes equations with a 2 equation k-ε turbulence model using a 'dual time-stepping' scheme. All runs were carried out at Mach 0.90 onset flow at a Reynolds number of 20×10^6. Default Fluent tuning parameters were used. The time-marching inner solution was limited to 20 iterations per time step, while a physical time step of 0.002 seconds was used in order to pick up the primary modes of the unsteady oscillation. In a 'production' case, a smaller stepsize could well be used to capture higher frequencies of interest.

Run length is determined by the frequency resolution needed. In this study, this was not a consideration since total power was used as the metric of interest. However, in a 'real' case, a frequency resolution of around 3.5 Hz would be adequate to pick out frequency ranges of interest. Therefore, a run length of 150 steps, spanning 0.3 seconds, was adopted. Prior to this, an additional 'settling period' of 100 time steps was used, giving a total run length of 250 time steps.
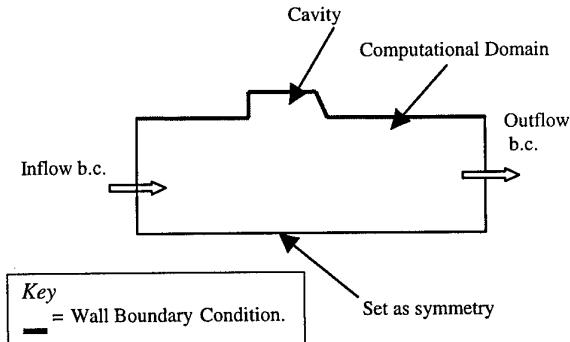
Figure 5.

It is necessary to set flow conditions for the boundaries of the computational domain. These were: prescribed mass flow into the region (based on Mach Number), prescribed pressure at outflow of the region, structural geometry wall boundary condition (upstream, all cavity walls, and downstream), and a symmetry plane condition (i.e. parallel streamwise flow) at the boundary opposite the cavity.

4.4.3.2.   Mesh Generation

The mesh generation was carried out using the Fluent mesh generator GAMBIT and was automated using a macro file. An example mesh is shown in figure 6.
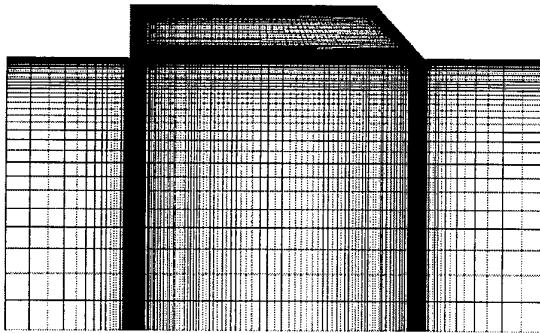
Figure 6.

The meshes used for all the runs in the study were topologically identical, and consisted of 47160 cells.

4.4.3.3.   Extraction of power levels from a time dependent solution space.

A monitor was set up to extract from the Fluent solution the pressure level at the upper rear corner of the bay at each time step. The total power in the spectrum of the pressure time history was derived using a simple in-house code. In future, the signal analysis can be made as complex as needed, commensurate with the aims of the study, e.g. specific frequencies can be extracted for assessment of structural response or spectra for equipment environmental qualification.

4.4.3.4.   Store release modelling

There are various options for utilising the time-dependent CFD data for a particular bay design, using the trajectory model STARS. One is to take several (or all) 'snapshot' flow fields from the flow solution and then simulate a trajectory for each case, selecting an average or 'worst case' from a safe separation viewpoint to give the optimisation measure. Another option is to reduce complexity by averaging all snapshot flow fields, and simulating a trajectory using this one field. One significant issue was the loss of higher frequency pressure content if this latter averaging process was used.

Separate STARS investigations showed that the effect of pressure variations on the store trajectory is only appreciable at relatively low frequencies (<30 Hz full scale). To ideally model the effective unsteady aerodynamic variation, a low-pass filter would be required and several trajectories would need to be generated from each filtered CFD solution.

However, in this exercise, the flow field values of x and y velocity, and mach number are produced at each time step and stored, and direct averaging of these is carried out subsequently to produce a single flow field covering the solution domain. This field then has to be interpolated onto a coarser regular grid of points covering the cavity and the immediately surrounding region using EnSight, to provide input suitable for the STARS simulator.

The flow field data extracted by this method was used with the NUFA package to calculate store loads. (N.B. within the cavity, there are regions of reversed flow i.e. angles >> 90 degrees relative to the weapon. The latest version of NUFA used in this exercise allows for these high local flow angles.) STARS was then used to calculate the missile trajectory. A utility program CRASH was used subsequently to assess safe separation and extract the separation parameter S.

4.5.   COMPUTING PLATFORMS USED

The basic modules of the system used are: user interface, process controller, search engine, geometry creation modules, 'A calculation' modules, and 'S calculation' modules.

The architecture supported by the FRONTIER software is such that any of these can reside on any IP-addressable platform reachable on the web. In this case, the primary concern in locating modules is firstly the need to run Fluent 5.1.1 and the geometry creation modules on a SG Origin 2000/120 remotely located; and secondly, the need to minimise data transferred between platforms. This led to deciding to locate the 'S calculation' modules (including STARS) on the Origin too. All other modules were sited on a local Unix workstation. The user interface was, on occasions, run on a convenient Windows NT PC.

The geometry and design evaluation parts of the process are identified in figure 4. These need to be run as a sequence. The FRONTIER environment implements runtime process definition and control, and provides wide area interprocess communications. This is done using CORBA internet protocol, with control and interface layers implemented in Java.

Fluent 5.1.1 can be run on a parallel computing architecture. The SGI Origin used in this study has 120 processors. Previous experience and computing resource availability suggested that each flow solution run should be done using 8 processors. Each time step took around 3 minutes to compute. Together with pre- and post-processing, the total time for one run varied, depending on computer load, between 5 and 10 hours.

5.   DESIGN SELECTION

The current study was limited in time and resource, and the design search process used reflects this. The aim was to exercise a simple strategy based on a probabilistic search employing a multiple objective genetic algorithm (GA). We thus implemented two generations of such an algorithm. The initial design set was determined using a quasiuniform Sobol sequence [3]. This distributes the chosen number of designs evenly in the space of the three design parameters. These cases were run and produced 8 measurement pairs (A, S). The search algorithm was then used to select a second generation

of cases. The probabilistic selection mechanism in the GA in this case chose to retain two previous cases and select six new ones. These were then run to produce another set of solutions, giving a total of 14 results for this exercise. A third generation of cases was generated for inspection, but was not run.

6. TESTCASE RESULTS

The geometries analysed are illustrated in figure 7.
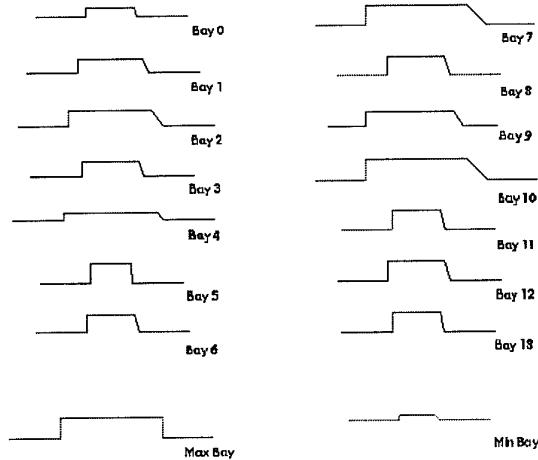
Figure 7.

The associated set of results is given in figure 8.

Design	Length	Depth	Theta	Acoustic	Separation
0	4.7569	0.8765	11.2941	5.5344E+11	3.4416
1	6.5137	1.2529	22.5882	5.1784E+11	11.726
2	8.2431	1.6235	33.7059	4.6454E+11	28.569
3	5.6353	1.4353	16.9412	1.2505E+12	12.726
4	9.1216	0.6882	39.3529	3.6439E+11	-1.177
5	3.8784	1.8118	5.6471	1.3923E+12	9.906
6	4.7569	1.6235	11.2941	1.1201E+12	9.034
7	10	1.9176	43.2353	5.9031E+11	1.151
8	5.6352	1.8118	16.9411	8.2732E+11	11.867
9	8.6824	1.4353	33.3529	5.1917E+11	5.9964
10	10	2	45	6.1934E+11	1.788
11	4.7568	1.9176	11.2941	1.3482E+12	10.102
12	5.6353	1.8118	16.9411	8.2732E+11	11.864
13	4.7569	1.8118	11.2941	1.3E+12	10.018

Figure 8.

N.B. Acoustic (A) is the total power in the pressure spectrum; separation (S) is the minimum separation distance (as defined earlier). A negative value of separation indicates that the missile has passed through the bay geometry.

Designs 0 through 7 were generated at the beginning of the exercise, designs 8 through 13 were the first generation of new designs created by the optimiser. The aim of the optimiser was to minimise A while maximising S. As can be see from figure 8, in general, the new designs generated have improved S without adversely affecting A. Clearly, the number of cases which has been run in this exercise is too small to achieve a meaningful optimisation. However, in the context of this

study, it was not affordable to run any more solutions and this should be an area for further work.

The following graph (figure 9) plots the case results showing the relationship between the acoustic metric 'A' and the separation metric 'S'. Clearly, there is no identifiable trend and as already stated, after so few design cases we would not expect to see one. Many more design cases would be required to define the boundaries of the solution space in terms of A and S and ideally to observe the points in figure 9 tending to an area close to the top left hand corner. (i.e. minimum A for maximum S).
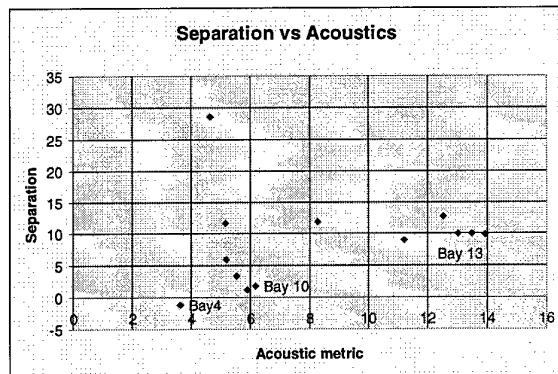
Figure 9.

Pictures of the *time averaged flow-field* (showing streamlines and contours of Mach Number) and store trajectory for four of the design cases is presented in Appendix I. The cases chosen are representative of the various flowfields and trajectories observed. As can be seen from these figures:

Bay 4 exhibits the aerodynamic characteristics of a 'shallow' cavity (L/D~13) with 'low' (comparatively) acoustic levels but with high flow angularity at the missile nose and tail (due to flow entering the cavity) which induces a nose up pitching moment on the missile. An unacceptable trajectory is achieved.

Bay 13 exhibits the aerodynamic characteristics of a 'deep' cavity (L/D~2) with 'high' acoustic levels predicted. However, the relatively low speed recirculating flow regions which occupy the entire bay and the approximately horizontal shear layer lead to a good release trajectory for the store. (Little pitching moment is generated on the store).

Bay 10 exhibits flow characteristics somewhere between those observed in bay 4 and bay 13. (L/D~5) When the missile is released, its nose passes through a recirculating flow region then through the shear layer which is approximately horizontal. However, the missile tail sees an angled shear layer which generates a tail up pitching moment on the store. The release trajectory appears to be unacceptable.

Bay 2 exhibits flow characteristics somewhat similar to Bay 13 though the vortex now occupies the whole cavity. The large resulting separation makes this case worth study and display. Although the general characteristics are those of a deep bay, the actual flow induces a pitch down moment on the store nose, due to the angled shear layer. The trajectory plot in figure A4.2 is somewhat curtailed. It illustrates the

complexities of metric definition, because this trajectory would be good for store jettison purposes, but not as attractive for the weapon's normal operational purposes.

The aerodynamic trends observed in the cavity are in good agreement with the trends identified in more accurate cavity simulations. It is acknowledged that neither of the metrics used in this assessment was ideal. In further studies we may require acoustic power (at some suitable location) against perhaps the store downward velocity.
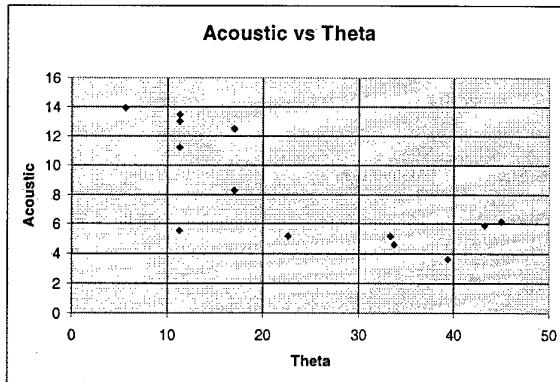
Figure 10.

As a further check on the qualitative accuracy of the solutions, the acoustic measurement was plotted against the cavity rear wall angle (figure 10). This replicates experimental trends observed in wind tunnel tests (outside this exercise) of reducing acoustic levels with increasing rear wall angle.

An initial exploration has been made of the use of a neural net model as a cheaper computational approach. The net was manufactured from the results of the 14 cases already shown. The neural net used had 3 inputs, 2 hidden layers of 8 nodes, and 2 outputs. The result of using this for around 400 design evaluations is shown in figure 11. The net model is clearly strongly influenced by the Bay 2 result.
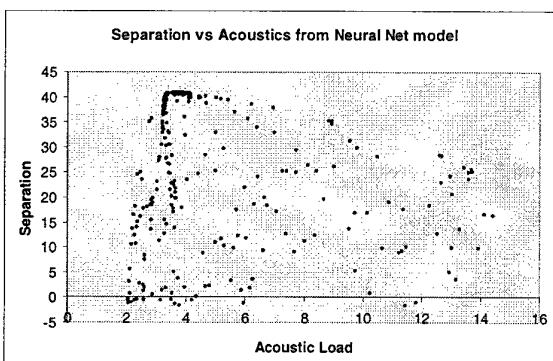
Figure 11

The function of this information would be to guide the selection of another set of full scale evaluations, and in turn use these to improve the net model.

7. LESSONS LEARNED

The exercise was intentionally quite short. It proved successful in highlighting that the process is potentially extremely useful during the early stages of a new design. The main aim of the exercise was to demonstrate the technique and establish confidence, particularly in the systems integration and automation aspects of the task. The validation of accuracy of the method is a subject for separate later assessment. The main lessons are in the following areas.

• CFD turnround times

In order to achieve a practically usable optimisation, considerably more sets of cases will need to be selected and run. The whole of the exercise has demonstrated quite clearly that a practical MDO process which matches the required design cycle timescales can only be implemented for bay installations if faster CFD turnround times are achieved. Defining acceptable levels of simplfication can assist here, together with rules for number of cases required for a given study.

• Search methods

Techniques for characterising the results from a limited set of CFD solutions and extracting maximum knowledge from them are needed. We need to develop a process in which a phase of using a limited number of expensive high fidelity simulations is alternated with a phase of using many more evaluations based on much cheaper models developed by extracting features and information from the accurate runs. The neural net approach illustrated above is one candidate. Ways to integrate CFD calculations with past evidence, theoretical, empirical or semi-empirical, also need to be found. A knowledge database needs to be developed.

• Initialisation

One of the problems with the CFD solution process has been the need to initialise and settle the solution for each case before the measurements can start to be taken. Ways of using the previous CFD solutions to initialise the next test case and hence shorten this process also need to be identified and assessed.

• Results storage

The need for an efficient storage of the CFD output is also required. Two extreme approaches need to be investigated: a) utilise a cheap memory storage system and increase the total storage space, and b) reduce the data size, by novel and extremely effective compression techniques.

• Flow / trajectory coupling

Ways to handle unsteady flow fields within quasi-steady trajectories also need to be addressed. Given the relatively short time required to calculate a trajectory compared to the current overall case run time, it is conceivable to consider a series of trajectory calculations for each CFD solution, but a means of reducing the number of trajectory calculations should be addressed.

• Signal analysis

Appropriate techniques need to be selected for any given exercise. Automation of some engineering tasks such as

cavity resonance frequency identification could increase process usefulness.

8. CONCLUSIONS

It can be appreciated from the foregoing that the design of a modern combat aircraft is quite a complex process. There are many conflicting issues to be resolved whilst trying to satisfy the dominant requirement. The execution of the process requires a wide range of skills and an overall appreciation of a large number of contributory topics. Work needs to continue into the application of artificial intelligence for the optimisation of future aircraft developments and weapon installations.

The use of MultiDisciplinary Optimisations or assessments needs to be encouraged, although it needs to be tailored to the resources available. This process cannot fully replace the engineering judgement and skill, but it can help in making decisions and choices. In some circumstances the MDO process needs to be limited to a parametric what-if rather than an intensive optimisation; nevertheless, the method can be extremely powerful and cost effective. Parallel developments in computing hardware and software need to complement this process.

What will eventually come about is a matter for speculation, but whatever the future, the need will remain for the military aircraft design to be responsive to time constraints.

9. REFERENCES

[1] Stallings R.L and Wilcox F, *Experimental Cavity Pressure Distributions at Supersonic Speeds*. NASA Langley, TP-2683, 1987.

[2] Plentovich E.B, Stallings R.L and Tracey M.B, *Experimental Cavity Pressure Measurements at Subsonic and Transonic Speeds*. NASA Langley, TM-3358, 1993.

[3] Dave Spicer, *FRONTIER: Open System for Collaborative Design using Pareto Frontiers*. R.Ae.S. Conference on 'Multidisciplinary Design & Optimisation'. London. Oct 1998.

[4] Carlo Poloni, Valentino Pediroda, *GA coupled with computationally expensive simulations: tools to improve efficiency*. Genetic Algorithms and Evolution Strategies in Engineering and Computer Science, Ed. by D.Quagliarella, J.Periaux, C.Poloni, G.Winter. John Wiley & Sons, 1998. Pages 267-288

[5] *GAMBIT 1 User's Guide*. Fluent Incorporated, 1998.

[6] *FLUENT 5 User's Guide*. Fluent Incorporated, 1998.

[7] *Getting Started With EnSight 6.2*. Computational Engineering International, EN-GS:6.2-2, 1998. http://www.ceintl.com .

[8] S McDougall, A.J. Press, and P.S. Barratt, *NUFA: A Semi-empirical Method for the Prediction of Isolated Weapon Aerodynamics*. AGARD-CP-493. Conference on 'Missile Aerodynamics'. April 1990.

[9] Graham Akroyd, *An Automated Method of Analysing Store Trajectory Simulations*. RTO. Conference on 'Aircraft Weapon System Compatibility and Integration'. Chester. Sept 1998.

10. ACKNOWLEDGMENTS

APPENDIX I – Flow Visualisation

Figure A1.1 – Bay 4 (L/D = 13.25, θ = 39.35 degrees) Flowfield coloured by Mach Number
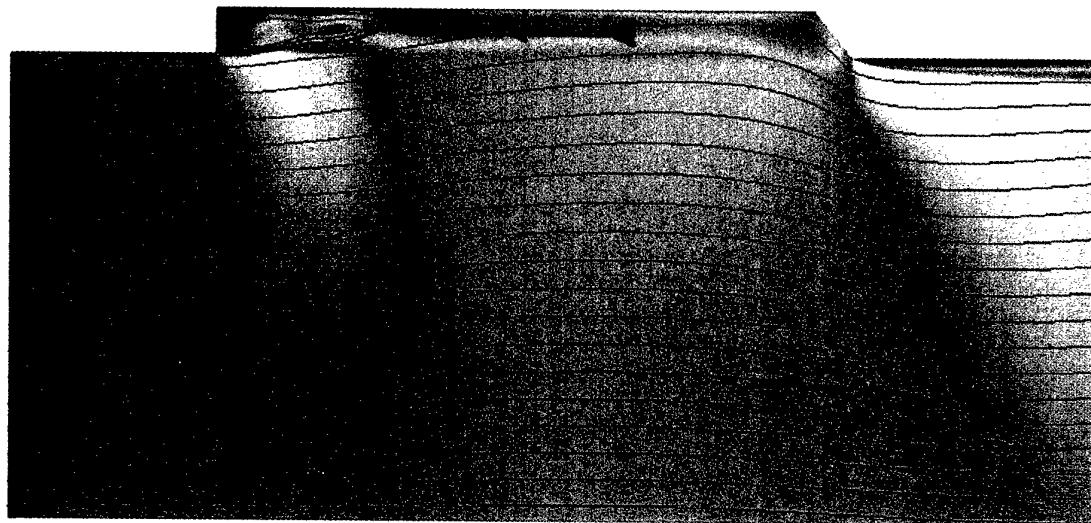
Figure A1.2 – Bay 4 (L/D = 13.25, θ = 39.35 degrees) Stillshot of Trajectory
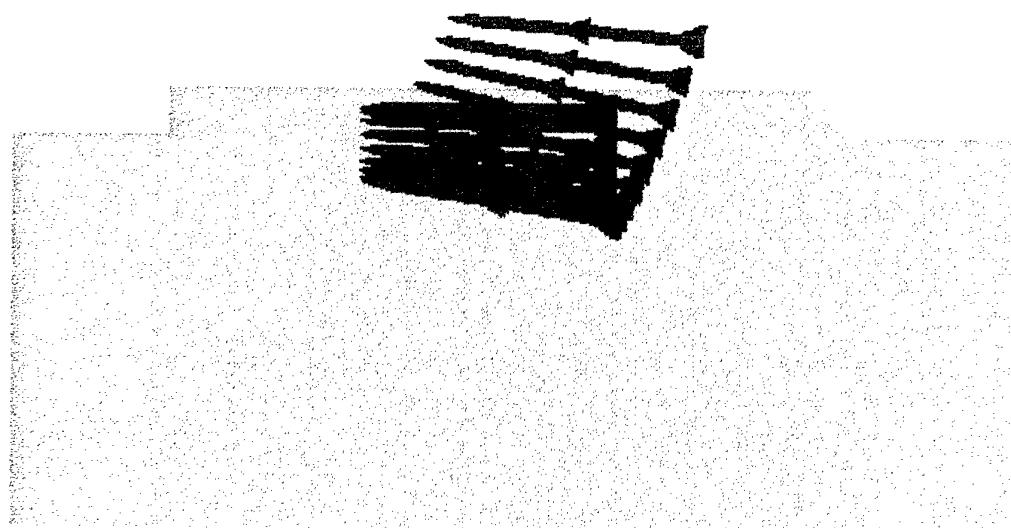
Figure A2.1 – Bay 13 (L/D = 2.63, θ = 11.29 degrees) Flowfield coloured by Mach Number
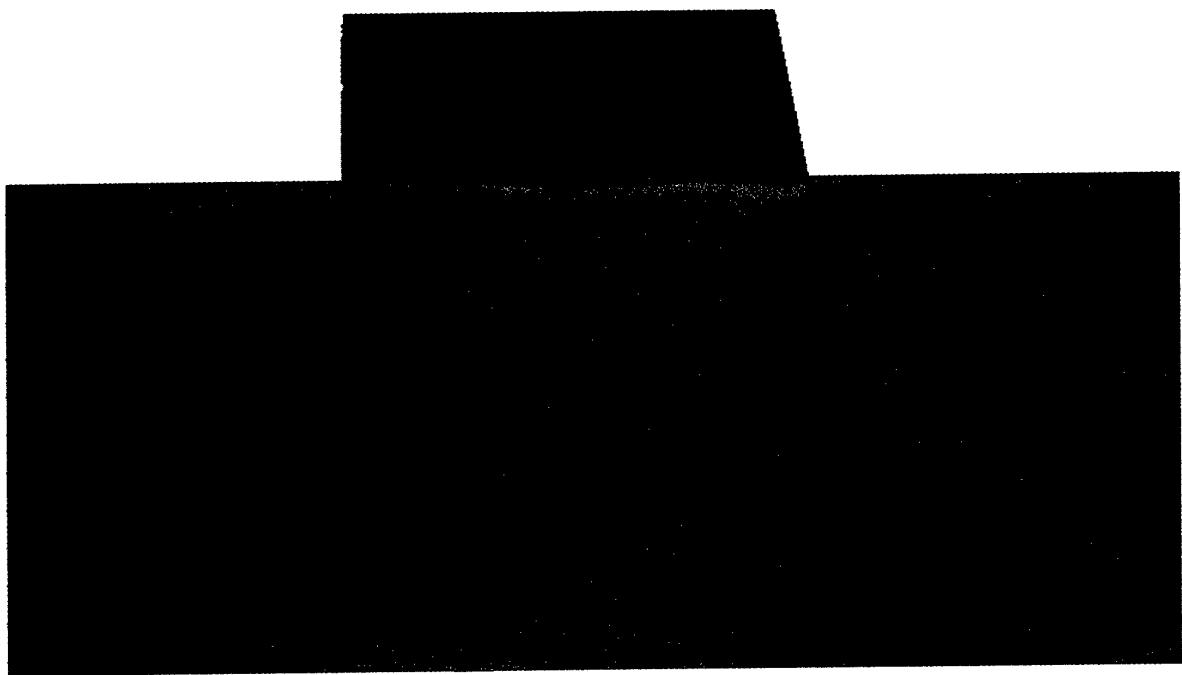
Figure A2.2 – Bay 13 (L/D = 2.63, θ = 11.29 degrees) Stillshot of Trajectory
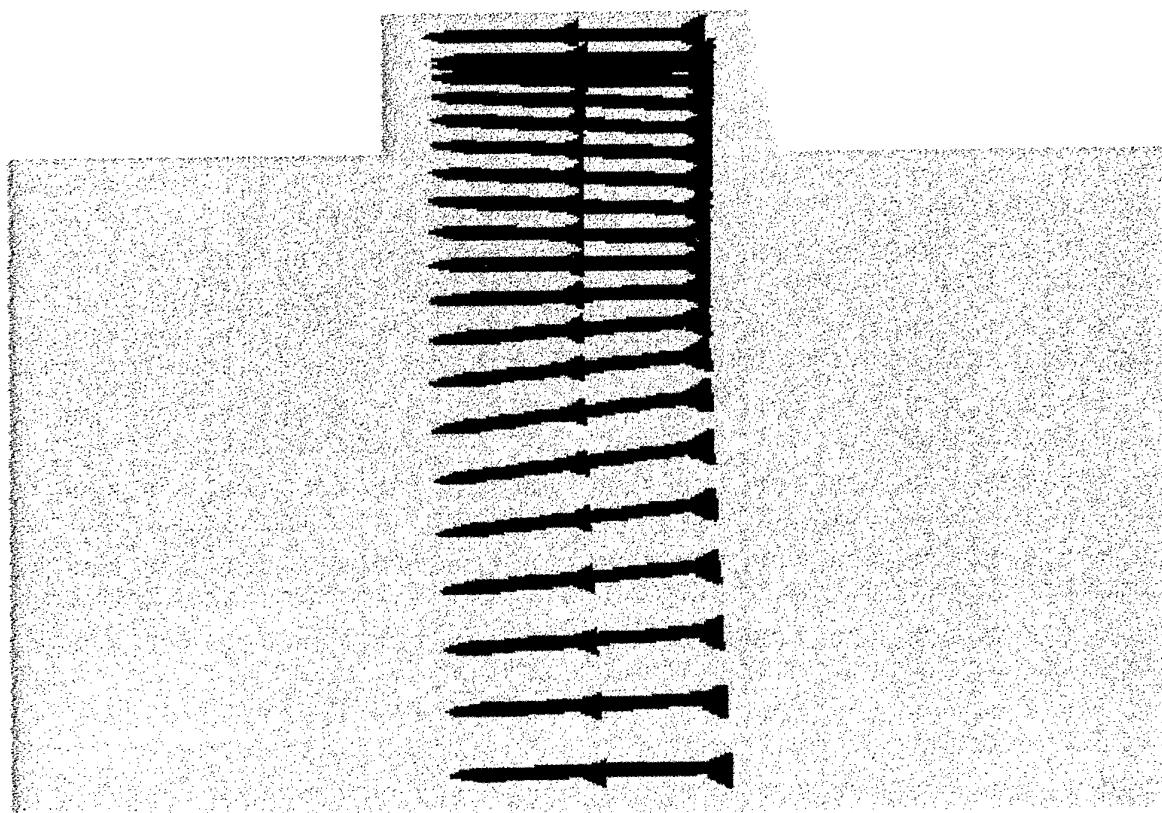
Figure A3.1 – Bay 10 (L/D = 5.0, θ = 45 degrees) Flowfield coloured by Mach Number
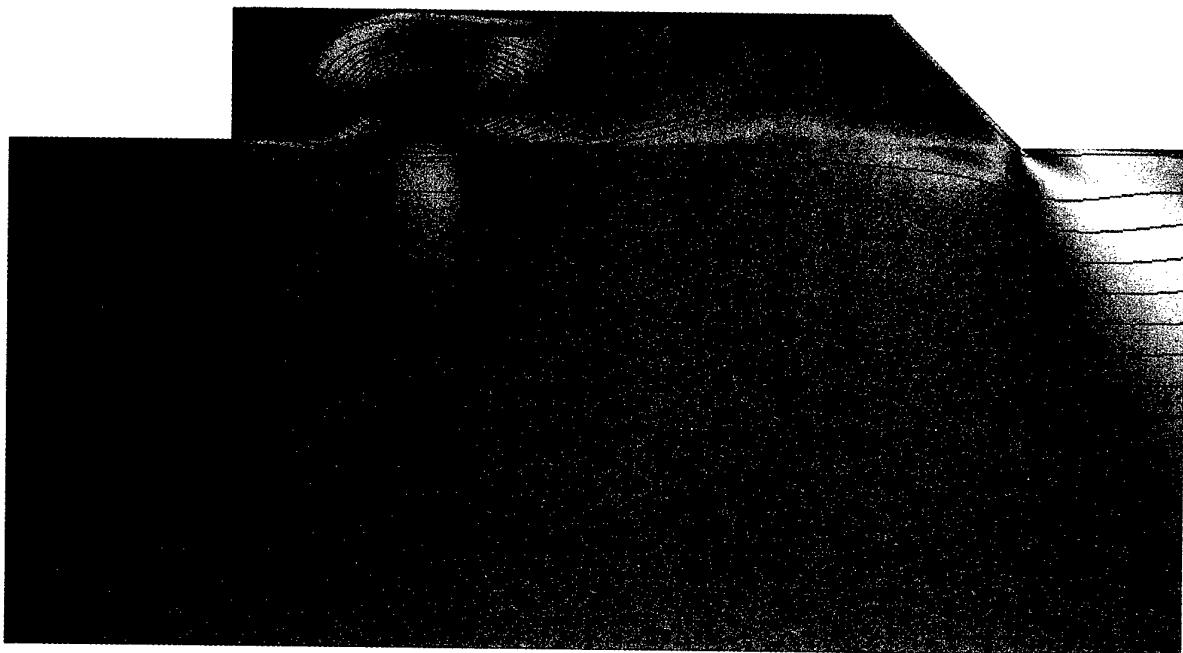
Figure A3.2 – Bay 10 (L/D = 5.0, θ = 45 degrees) Stillshot of Trajectory
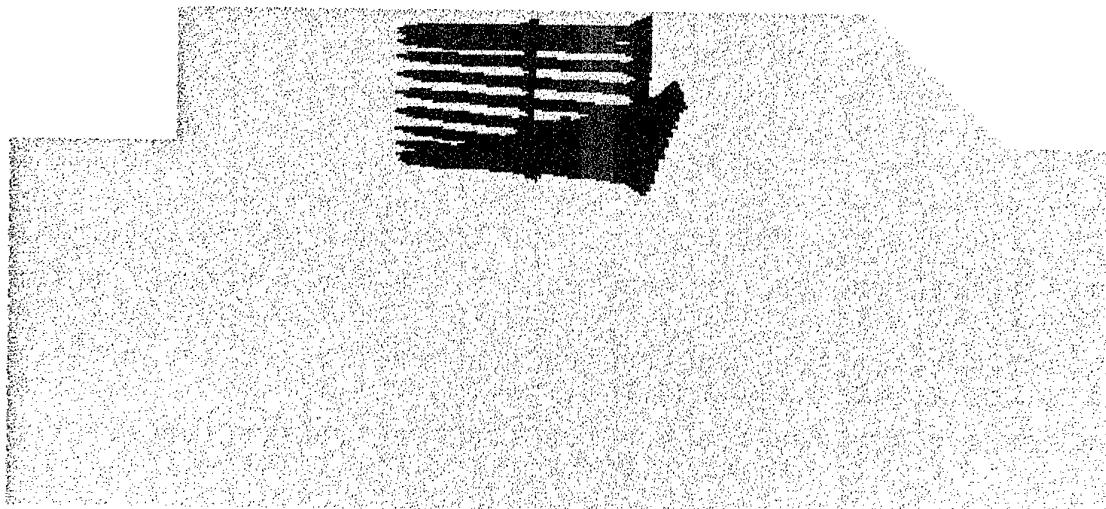
Figure A4.1 – Bay 2 (L/D = 5.08, θ = 33.71 degrees) Flowfield coloured by Mach Number

Figure A4.2 – Bay 2 (L/D = 5.08, θ = 33.71 degrees) Stillshot of Trajectory
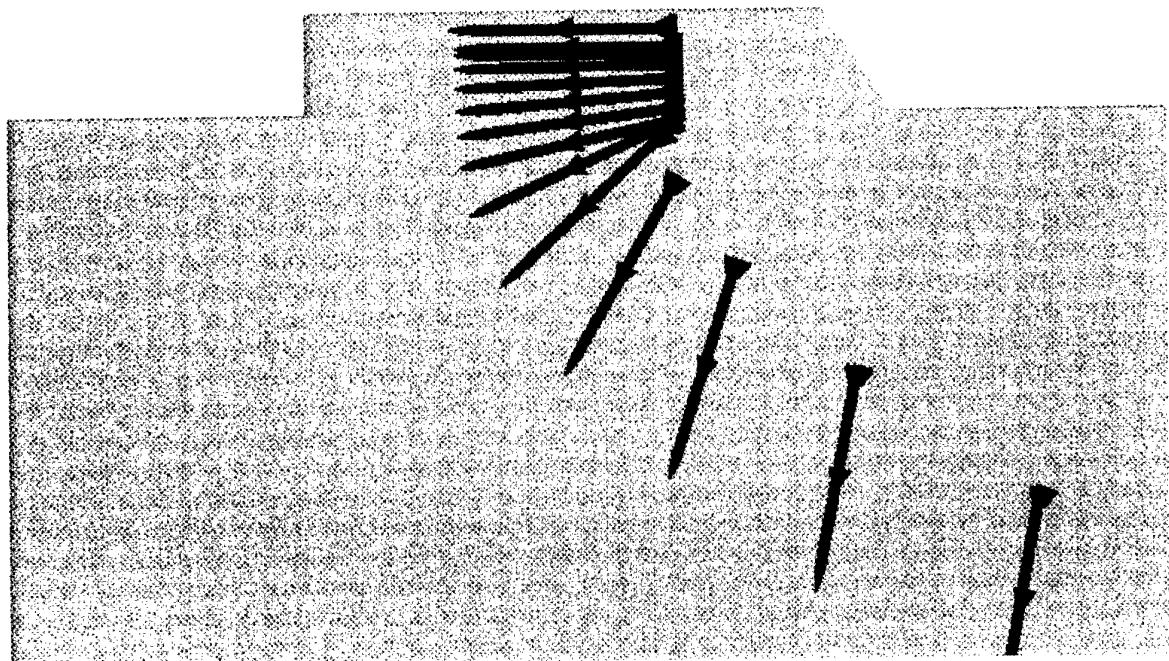
DISCUSSION

Session II, Paper #14

Mr Ohman (IAR/NRC, Canada) asked what effects angle of attack would have on the results presented.

> **Mr Moretti** noted that angle of attack has been considered but that its effects were not included in this presentation.

Aerodynamics for MDO of an innovative configuration

G. Bernardini, A. Frediani
Dipartimento di Ingegneria Aerospaziale
Università degli Studi di Pisa
Via Diotisalvi 2, 56126 Pisa, Italy

L. Morino
Dipartimento di Ingegneria Meccanica e Industriale
Università degli Studi *Roma Tre*
Via della Vasca Navale 79, 00146 Roma, Italy

Abstract

A numerical methodology for the evaluation of aerodynamic loads acting on a complex lifting configuration is presented. The work is limited to the case of attached high–Reynolds number flows. A viscous/potential interaction technique is utilized to take into account the effects of the viscosity. For the potential–flow analysis, a boundary element formulation is used; for simplicity, only incompressible flows are examined. The theoretical basis of the present methodology is briefly described. Comparisons with available, numerical and experimental results are included.

1. Introduction

The present work is an overview paper on recent results on viscous–flow analysis of innovative configurations (low–induced drag lifting configurations), obtained by the authors within the objective of developing an MDO methodology. The aerodynamic methodology is based on a boundary element formulation for the velocity potential introduced by Morino [16]; the effects of viscosity are taken into account by a classical viscous/inviscid coupling technique; a technique for extending this approach beyond the limits of the boundary–layer approach is also indicated.

In order to put this work in the paper context, note that, the increased request for low–cost air transportation has generated considerable interest for non–conventional configurations, such as biplanes with wing tips connected to each other directly (joined wing configuration) or through a vertical surface (box–wing configuration). These configurations are related to the early work of Prandtl [25] on multi-

planes, which shows that these configurations have certain aerodynamic advantages (outlined in the following sentences) with respect to isolated wings. First, the induced drag of a multiplane with elliptic distribution of circulation is lower than the induced drag of the equivalent monoplane (*i.e.*, of the monoplane having the same span and generating the same lift as the multiplane considered). In addition, the ratio, K, between the induced drag of a multiplane and that of the equivalent monoplane, decreases as the number of wings of the multiplane increases (with global height and lift kept constant). In the limit as the number of wings tends to infinity ("infinity–plane", according to the Prandtl [25] definition), K has the minimum value. Finally, there exists a box–wing type configuration that has the same distribution of circulation (and hence the same K) as the "infinity–plane"; such configuration is therefore designated, still by Prandtl [25], at the 'Best Wing System' (BWS).

After the work of Prandtl [25], valid only for the limited case of multiplanes with elliptic distribution of circulation, several numerical and experimental studies have been published. Of particular interest here is, the work of Nenadovitch [23] on the efficiency of bidimensional biplanes. Also, an experimental analysis of joined wing aircraft is presented by Wolkovitch [32], whereas experimental as well as numerical/empirical studies on biplanes and box–wing configurations are proposed by Gall and Smith [6].

In this paper, the attention is focused on an innovative configuration for a new large dimension aircraft (usually indicated as New Large Airplanes or NLA)

proposed by Frediani *et al.* [4], [5]. This configuration is a biplane, with counter–swept wings (positive sweep for the front lower wing and negative sweep for the back upper wing, which acts as a horizontal tail as well) connected to each other by aerodynamic surfaces (Figures 1 and 2). Following Frediani *et al.* [4], [5] we will refer to this configuration as the Prandtl–plane. Preliminary numerical and experimental studies (Frediani *et al.* [4], [5]) have shown that the induced drag of this configuration is lower than the induced drag of an equivalent monoplane. This fact allows one to reduce the wingspan of this configuration without drag penalties and introduces the possibility of respecting the maximum span–wise dimensions (critical for the NLA with classical wing configuration), which would allow compatibility with the existing airport regulations.

Still to in order to put the work in the paper context, note that through an unrelated activity, the authors have been involved in the developement of an MDO code. The weakest module in this code is the aerodynamic one. In fact, the aerodynamic module in such a code is limited to potential flows around simply–connected domains; on the contrary, the Prandtl–plane configuration is multiply–connected. In addition, a key for this configurations (and MDO in general) is the drag, induced and viscous.

These issues are addressed in this paper, as a first step towards generating a suitable viscous aerodynamic module around multiply–connected configurations, to be incorporated in the above mentioned MDO code. Specifically, because of the complexity and novelty of the configurations discussed above, it is desirable to develop an aerodynamic methodology for multiply–connected configurations capable of yielding accurate predictions with a relatively small computational effort (hence, not a CFD approach), which takes into account the effects of viscosity and of the wake roll–up (the geometry of the rolled–up wake is evaluated through the free–wake analysis of

Ref. [29]). The relatively recent state of our work in this context was presented in Bernardini *et al.* [1], which is based on the classical viscous–potential interaction, with the viscous flow (in boundary layer and wake) solved by using the strip–theory approach, with an integral two–dimensional boundary layer; the viscous/inviscid coupling technique is based upon the Lighthill [12] equivalent–sources approach. Matching of the boundary–layer solution with the corrected potential–flow solution is obtained by direct iteration. Here, the emphasis is on the most recent improvements with respect to that paper. First, we present an extension to higher order of the direct boundary element formulation used in the past by the authors for incompressible potential flows around lifting objects of arbitrary shape in uniform translation; this provides also an opportunity to clarify certain theoretical issues connected with the trailing edge conditions. Second, we discuss a three–dimensional integral boundary–layer formulation, which is based essentially on the algorithm of Nishida [24] and Milewski [15]. The solution is obtained through the simultaneous coupling technique introduced by Drela [3].

2. Formulation of Ref. [1]

The formulation of Bernardini *et al.* [1] is outlined here in order to emphasize the differences of the new formulation and also because, some new results presented here are based on this formulation. For a detailed discussion, see Ref. [18], where a review is also presented.

Potential–Flow Formulation: an inviscid, incompressible, initially–irrotational flow remains at all times quasi–potential (*i.e.*, potential everywhere except for the wake surface, which is the locus of the points emanating from the trailing–edge). In this case, the velocity field, $\mathbf{v}$, may be expressed as $\mathbf{v} = \nabla\varphi$ (where φ is the velocity potential). Combining with the continuity equation for incompressible flows, $\nabla \cdot \mathbf{v} = 0$,

yields

$$\nabla^2 \varphi = 0. \tag{1}$$

The boundary conditions for this equation are as follows. The surface of the body, $\mathcal{S}_B$, is assumed to be impermeable; this yields $(\mathbf{v} - \mathbf{v}_B) \cdot \mathbf{n} = 0$, *i.e.*,

$$\frac{\partial \varphi}{\partial n} = \mathbf{v}_B \cdot \mathbf{n} \qquad \text{for } \mathbf{x} \in \mathcal{S}_B, \tag{2}$$

where $\mathbf{v}_B$ is the velocity of a point $\mathbf{x} \in \mathcal{S}_B$, whereas $\mathbf{n}$ is the outward unit normal to $\mathcal{S}_B$. At infinity, in a frame of reference fixed with the unperturbed fluid, we have $\varphi = 0$. The boundary condition on the wake surface, $\mathcal{S}_W$, are: *(i)* the wake surface is impermeable, and *(ii)* the pressure, p, is continuous across it. These imply that $\Delta(\partial \varphi/\partial n) = 0$ (where Δ denotes discontinuity across $\mathcal{S}_W$), and that $\Delta \varphi$ remains constant in time following a wake point $\mathbf{x}_W$ (whose velocity is the average of the fluid velocity on the two sides of the wake), and equals the value it had when $\mathbf{x}_W$ left the trailing edge. This value is obtained by imposing the trailing-edge condition that, at the trailing edge, $\Delta \varphi$ on the wake equals $\varphi_u - \varphi_l$ on the body (subscripts u and l denote, respectively, upper and lower sides of the body surface).

In this paper, the above problem for the velocity potential is solved by a boundary element formulation. The boundary integral representation for the above problem is given by

$$\begin{aligned} \varphi(\mathbf{x}) &= \int_{\mathcal{S}_B} \left(G\chi - \varphi \frac{\partial G}{\partial n} \right) d\mathcal{S}(\mathbf{y}) \\ &\quad - \int_{\mathcal{S}_W} \Delta \varphi \frac{\partial G}{\partial n} d\mathcal{S}(\mathbf{y}), \end{aligned} \tag{3}$$

with $\chi := \mathbf{v}_B \cdot \mathbf{n}$, and $G = -1/4\pi \|\mathbf{y} - \mathbf{x}\|$. Note that, in the absence of the wake, Eq. 3, in the limit as $\mathbf{x}$ tends to $\mathcal{S}_B$, represents a boundary integral equation for φ on $\mathcal{S}_B$, with χ on $\mathcal{S}_B$ known from the boundary condition. Once φ on the body is known, φ (and hence $\mathbf{v}$ and, by using Bernoulli's theorem, p) may be evaluated everywhere in the field. The situation is similar in the presence of the wake, since, by applying the wake and trailing-edge conditions, $\Delta \varphi$ on the wake may be expressed in terms of φ over the body at preceding times.

In Bernardini *et al.* [1], the boundary integral equation for φ based on Eq. 3 is solved numerically by discretizing the body and wake surfaces in quadrilateral elements, assuming φ, χ and $\Delta \varphi$ to be piecewise constant, and imposing that the equation be satisfied at the center of each body element (zeroth-order boundary-element collocation method).

It should be noted that the geometry of the wake is not known *a priori*. For the case of isolated wings in uniform translation, a flat wake with vortical lines parallel to the unperturbed streamlines is typically used (prescribed-wake analysis). In the configuration of interest here, such *a priori* assumptions are not justified by past experience. Still in Bernardini *et al.* [1], the wake geometry is either prescribed (undisturbed) or obtained through a free-wake analysis, *i.e.*, the boundary integral equation is used to compute, at each time step t_n the flow velocity at nodes $\mathbf{x}_i$ of the discretized wake surface (free-wake analysis); the locations of $\mathbf{x}_i$ at t_{n+1} is then obtained by integrating the equation $\dot{\mathbf{x}}_i = \mathbf{v}_i(\mathbf{x}_p)$ by the explicit Euler method (in other words, in the case of free-wake analysis the shape of the wake and the flow-field solution are obtained step-by-step, as part of the solution). For the steady-state cases of interest here, the solution is obtained in the limit as the solution for $t \to \infty$ of a transient flow due to an impulsive start. Incidentally, this procedure resolves also the non-uniquess issue connected with steady-state flows around multiply-connected region; indeed, in the case of unsteady flow the solution is unique, because Kelvin's theorem allows one to obtain the circulation on the wing from the vorticity shed in the wake (see Ref. [20]).

Boundary Layer: the viscous flow analysis is limited to attached steady high-Reynolds number flows. Under these assumptions, a classical integral boundary-layer formulation may be used. Specifically, Bernar-

dini *et al.* [1] use a 2D integral boundary–layer formulation used as 'strip–theory'. The laminar portion is computed by using the Thwaites collocation method [30]. The transition from laminar to turbulent flow is detected by the Michel method [14]. The turbulent portion of the boundary layer and wake are studied by the 'lag-entrainment' method of Green *et al.* [9].

Viscous/Inviscid Coupling: once the boundary–layer equations are solved, the viscous correction to the potential flow is obtained as a transpiration velocity through S_B and S_W (equivalent source method by Lighthill [12]). The boundary condition for φ over the body surface is modified as follows

$$\partial\varphi/\partial n = \mathbf{v}_B \cdot \mathbf{n} + \chi_V,$$

where the transpiration velocity χ_V is given by

$$\chi_V = \frac{\partial}{\partial s}\left(u_e\delta^*\right) = \frac{\partial}{\partial s}\int_0^\delta \left(u_e - u\right)dz, \qquad (4)$$

where s denotes the arclength in the 2D boundary–layer and wake, and δ^* is the displacement thickness. In addition, u and u_e denote, respectively, the velocity within the vortical layer and at its outer edge (in a frame of reference fixed with the body). On the wake surface one has

$$\Delta\left(\partial\varphi/\partial n\right) = \left(\chi_V\right)_u + \left(\chi_V\right)_l,$$

where the subscripts u and l denote, respectively, the upper and lower sides of the wake surface.

3. Third–order extension

The specific formulation used here is based upon a high–order formulation introduced by Gennaretti *et al.* [8], and extended in Refs. [20] and [21], to which the reader is referred for details (here the emphasis is on the applications). This consists of using bicubic quadrilateral elements and the Hermite interpolation for φ in both directions. This yields a bicubic representation in terms of the nodal values of φ, $\partial\varphi/\partial\xi$, $\partial\varphi/\partial\eta$, and $\partial^2\varphi/\partial\xi\partial\eta$; the nodal derivatives are then expressed in terms of the unknowns of the problem,

φ_i, through suitable finite-difference approximations. Only steady flows are considered here; then, the wake geometry at the trailing–edge (typically tangents to one of the sides of the body surface at the trailing-edge) may be determined by the results of Mangler and Smith [13].

The above formulation generates new issues connected to the trailing–edge. The first one, is related to the existence of the trailing–edge potential discontinuity which implies that at any trailing–edge node there exist two unknowns, but only one collocation point. Gennaretti *et al.* [8] use two collocation points suitably located slightly ahead of the trailing edge (otherwise the collocation points coincide with the nodes).

In order to avoid ill–conditioned matrix here, as mentioned above, we use the approach introduced in Ref. [20], who, at the trailing–edge, use only one control point but two different integral equations: the first is the potential equation while the second is its derivative in the direction of the wake normal at trailing-edge.

An additional issue stemming from the third–order formulation is that of the evaluation of the derivatives of φ at the trailing edge. These may be obtained by imposing the two conditions of stagnation point and smooth flow (see Ref. [20] for details).

4. Three–dimensional boundary layer

In order to take into account the three–dimensional effects, the viscous flow in the boundary layer and wake, is modelled using the three-dimensional integral boundary–layer equations on non–ortogonal grids. Specifically, the integral method uses two equations for momentum (extention of von Kármán equation to 3D flows) coupled by two auxiliary equations. The first is the kinetic energy equation and the second is the transport equation for the maximum shear stess coefficient ('lag' equation). In order to complete the problem, we use, following Nishida [24] and Milewski [15], the streamwise closure relations pro-

posed by Drela [3] in his 2D integral boundary–layer method, along with the crosswise relations of Johnston [11]. The Mughal [22] finite–volume scheme is used for the solution.

Also in this case, the viscosity correction to the potential flow is evaluated as a transpiration velocity through $\mathcal{S}_B$ and $\mathcal{S}_W$ (equivalent source method by Lighthill [12]). However, as mentioned above, in contrast with the formulation of Bernardini *et al.* [1], the matching of the thin–layer solution with the potential–flow solution, is obtained by the fully simultaneous coupling method of Drela [3], which solves the viscous and inviscid equations simultaneously and is stable even for separated flows.

5. Numerical results and comments

The results presented here fall into three groups. In the first group are some new results obtained with the formulation outlined in Section 2 (some of the results of Ref. [1] are included here for the sake of clarity). The second and third group are based on the formulations of Sections 3 and 4.

For all the potential flow results, the airloads are determined by using the formulation of Ref. [7], which is an exact generalization of the Trefftz–plane theory [31] for the evaluation of aerodynamic loads around objects of arbitrary shapes. The viscous drag is evaluated by using the classical formula by Squire and Young [28].

First, a few results obtained by Bernardini *et al.* [1] are discussed as they help in putting the paper in the proper context. First of all, the potential flow formulation of Section 2 has been validated in Ref. [1] by a comparison with analytical results by Prandtl [25] either in the case of biplanes and box–wing configuration; this comparison has shown nearly perfect agreement between our numerical results and the analytical results of Prandtl. Also, in order to analyze the mechanism of induced–drag reduction, it is interesting to compare the efficiency K of: *(i)* a rectangular biplane; *(ii)* a rectangular biplane with facing tip winglets on the two wings and *(iii)* a box–wing. For, this show the graduality of the reduction (in the sense that the biplane corresponds to the zero winglet–length case and the wing–box to the full length case); this is apparent from Figure 3 (from Ref. [1]), which depicts a comparison of the curves $K = K(G/b)$ for a biplane without winglets, for the corresponding box–wing body, and for a biplane with winglets (winglet length $0.4c$, where c is the root chord).

It should be observed that the above results have been obtained using a prescribed–wake approach, in order to be consistent with the Prandtl model which is based on the lifting–line theory. However, the present methodology is able to capture the effects of the wake roll–up on the airloads by using a free–wake approach, as described above. Figure 4 (also from Ref. [1]) depicts the Prandtl factor K as a function of G/b, for free–wake and prescribed–wake analysis. The results obtained by a free–wake approach show that the wake roll–up effect is to reduce the value of K. For the range of G/b of practical interest in aeronautical applications (*i.e.*, $0.1 < G/b < 0.2$), we have that the reduction of K is about 6% for the case of a box–wing. This demonstrates the importance of including a rolled–up wake in the analysis.

Next, consider new potential–flow results obtained with the formulation of Ref. [1]. In particular, Fig. 5 present a parametric study of the effects of the sweep angle (of the front and rear wing) on the Prandtl factor K of the Prandtl–plane shown in Figures 1 and 2. Here, we have considered three different configurations characterized by: (a) Mid–chord front wing sweep angle $\Lambda_F = 35°$ and mid–chord rear wing sweep angle $\Lambda_R = -40°$, (b) mid–chord front wing sweep angle $\Lambda_F = 37°$ and mid–chord rear wing sweep angle $\Lambda_R = -37°$ and, (c) mid–chord front wing sweep angle $\Lambda_F = 40°$ and mid–chord rear wing sweep angle $\Lambda_R = -35°$. We can note that the Prandtl factor of all three configuration are hardly distinguishable,

and are very close to the value of the Prandtl factor of the Best Wing System (continuous line). This is very important because it shows that, even for the Prandtl–plane, we have a reduction of induced drag, with respect to a traditional wing configuration.

Next, consider some preliminary results for attached high–Reynolds viscous flows. The two–dimensional integral boundary–layer formulation, used a 'strip–theory' in three-dimensional application, has been validated in Ref. [1], by comparison with experimental results available in literature, in the case of: (i) isolated wing, (ii) biplane, and (iii) box–wing configuration. For the sake of completeness the results for the third case are presented here in Fig. 6 (also from Ref. [1]) which depicts the polar at $Re = 5.1 \cdot 10^5$ of a box–wing configuration with aspect ratio 5, gap $G = c$, stagger $S = c$ and section profiles NACA 0012. The numerical results are in good agreement, also in this case, with the experimental results by Gall and Smith [6]. Next consider new results. The formulation of Ref. [1] has been used for a parametric study of the effect of sweep angle on the polar of a Prandtl–plane. This is shown in Fig. 7 which depicts a polar for the same three configuration of Prandtl–plane used in Fig. 5. We can note that their difference is very small.

Next consider the validation of third–order formulation. Some results have been presented in Morino and Bernardini [21] for the case of simply (RAE wing) and multiply connected (nacelle) configurations. Here, we consider the particularly challanging case of a wing with strake (see Fig. 8), at angle of attack $\alpha = 5°$ and having symmetric NACA 0002 airfoil sections. Fig. 9 depicts the circulation $\Gamma = \Delta\varphi_{TE}$ as a function of $2y/b$, while Fig. 10 shows the chordwise distribution of the pressure coefficient (at $2y/b = .219$). The present results are obtained with a chordwise discretization $N_1 = 20$ and a spanwise discretization $N_2 = 12$, and are compared with those obtained with the method of Roberts and Rundle [26] with $N_1 = 39$

and $N_2 = 24$ and those obtained with the method of Rubbert and Saaris [27] with $N_1 = 28$ and $N_2 = 12$. The agreement among the three formulations is good, except at the trailing-edge, where the pressure predicted in our case is higher (see also Ref. [21] which shows why our results appear to be more reliable).

Finally, we present some preliminary results of the three-dimensional boundary layer formulation. In particular, Figs. 11 and 12 show respectively the chordwise distribution (at $\eta = 0.5$ and for the upper surface of the wing) of the streamwise displacement thickness, δ_1^*, and the shape factor, H, for a RAE wing with mid–chord sweep angle $\Lambda = 45°$, RAE 101 airfoil secton at $Re = 2.1 \cdot 10^6$ and angle of attack $\alpha = 6.3°$. Our numerical results, obtained using $N_1 = 60$ and $N_2 = 10$, have been compared with the numerical results of Milewski [15] (obtained using $N_1 = 64$ and $N_2 = 10$), and experimental results of Brebner and Wyatt [2]. The transition location, in this case, is fixed using experimental data. We have also included in the figure the two–dimensional boundary layer formulation (unfortunately with transition obtained by Michel method [14]). Our three-dimensional numerical results are in good agreement with both the Milewski [15] and with experimental data. On the contrary, the 2D formulation shows, at the trailing edge, a great difference. This could find a justification in the fact that, at the trailing edge, the 3D effects are higher.

To conclude the paper we wish to mention a technique that allows us to overcome the boundary layer limitations. This is based on a decomposition introduced by Morino [17] for the velocity field as $\mathbf{v} = \nabla\varphi + \mathbf{w}$, where $\mathbf{w}$ (obtained by direct integration of $\nabla \times \mathbf{w} = \boldsymbol{\zeta} := \nabla \times \mathbf{v}$) has the property that $\mathbf{w} = 0$ where $\boldsymbol{\zeta} = 0$. This decomposition has been successfully applied to 2D steady full potential flows with boundary-layer correction (see Morino *et al.* [19]) and to 2D steady Euler flows, obtained as an exact correction to the full-potential solver (see Iemma *et*

al. [10]). The coupling of Euler with the boundary layer is now under investigation.

References

[1] Bernardini, G., Frediani, A., and Morino, L., "MDO of an Innovative Configuration - Aerodynamic Issues," Proceedings of the International Forum on Aeroelasticity and Structural Dynamics, Williamsburg 1999.

[2] Brebner, G.G., Wyatt, L.A., "Boundary Layer Mesurements at Low Speed on Two Wings of 45° and 55° Sweep," CP 544, Aeronautical Research Council, 1961.

[3] Drela,M.,"XFOIL: An Analysis and Design System for Low Reynolds Number Airfoils," in T.J. Mueller, editor, *Low Reynolds Number Aerodynamics*, 1989.

[4] Frediani, A., Chiarelli, M., Longhi, A., D'Alessandro, C.M., Lombardi, G., "Structural Design and Optimization of the Lifting System of a Non–Conventional New Large Aircraft," Proceedings of the CEAS International Forum on Aeroelasticity and Structural Dynamics, Rome 1997.

[5] Frediani, A., Lombardi, G., Chiarelli, M., Longhi, A., D'Alessandro, C.M., Bernardini, G., "Proposal for a New Large Airliner with a Non-Conventional Configuration," Proceedings of the XIV AIDAA Congress, Naples, 1997.

[6] Gall, P.D. and Smith, H.C., "Aerodynamic Characteristics of Biplanes with Winglets," *J. Aircraft*, Vol. 24, No. 8, pp. 518-522, 1987.

[7] Gennaretti, M., Salvatore, F., Morino, L., "Forces and Moments in Incompressible Quasi-Potential Flows," *Journal of Fluids and Structures*, Vol. 10, pp. 281-303, 1996.

[8] Gennaretti, M., Calcagno G., Zamboni A. and Morino L., 'A high order boundary element formulation for potential incompressible aerodynamics,' *The Aeronautical Journal*, Vol. 102, No. 1014, p. 211-219, 1998.

[9] Green, J.E., Weeks, D.J., Brooman, J.W.F., "Prediction of Turbolent Boundary Layers and Wakes in Compressible Flow by a Lag-Entrainment Method," RAE RM 3791, 1973.

[10] Iemma, U., Marchese, V., Morino, L., "Euler Flows Via BEM: a Potential/Vorticity Integral Formulation," Proceedings of ICES Conference, Atlanta, USA, 1998.

[11] Johnston, J.P.,"On the Three-Dimensional Turbulent Boundary Layer Generated by Secondary Flow," *J. of Basic Engineering*, Series D, Vol. 82, pp. 233-248, 1960.

[12] Lighthill, M.J., "On Displacement Thickness," *J. Fluid Mech.*, Vol. 4, pp. 383-392, 1958.

[13] Mangler, K.W., Smith J.H.B., (1970) Behaviour of the vortex sheet at the trailing edge of a lifting wing, *The Aeronautical Journal*, Vol. 74, pp. 906-908.

[14] Michel, R., "Etude de la Transition sur les Profils d'Aile–Establissement d'un Point de Transition et Calcul de la Trainée de Profil en Incompressibile," ONERA Rep. No. 1/1578A, 1952.

[15] Milewski, W.M.,"Three-Dimensional Viscous Flow Computations Using the Integral Boundary Layer Equations Simultaneously Coupled with Low Order Panel method," PhD Thesis, Department of Ocean Engineering, Massachsetts Insitute of Technology, 1987.

[16] Morino, L., "A General Theory of Unsteady Compressible Potential Aerodynamics," NASA CR-2464, 1974.

[17] Morino, L., "Helmholtz and Poincaré Velocity-Potential Decomposition for the Analysis of Unsteady Compressible Viscous Flows," in: Banerjee, P.K., and Morino, L., (Eds.): *Boundary Element Methods in Nonlinear Fluid Dynamics*. Elsevier Applied Science Publishers, London, 1990.

[18] Morino, L., "Boundary Integral Equation in Aerodynamics," *Appl. Mech. Rev.*, Vol. 46, August 1993.

[19] Morino, L., Gennaretti, M., Iemma, U., Salvatore, F., "Aerodynamic and Aeroacoustics of Wings and Rotors via BEM - Unsteady, Transonici, and Viscous Effects," *Comp. Mech.*, N. 21, 1998.

[20] Morino, L., and Bernardini, G., "Singularities in Discretized BIE's for Laplace's Equation; Trailing-Edge Conditions in Aerodynamics," Wendland, W.L., (ed.): *Mathematical Aspects of Boundary Element Methods*, CRC Press, London, UK, (in print).

[21] Morino, L., Bernardini, G., "Recent Developments on a Boundary Element Method in Aerodynamics," IUTAM Symposium on Advanced Mathematical and Computational Mechanics Aspects of the Boundary Element Method, Cracow, 1999.

[22] Mughal, B.H.,'A Calculation Method for Three-Dimensional Boundary-Layer Equations in Integral Form,' Master's Thesis, Department of Aeronautics and Astronautics, Massachusetts Institute of Technology, 1992.

[23] Nenadovitch, M., "Recherches sur les Cellules Biplanes Rigides d'Envergue Infinie," Publications Scientifiques et Techniques du Ministere de L'Air, Institute Aerotechnique de Saint-Cry, Paris, 1936.

[24] Nishida, B.A.,'Fully Simultaneous Coupling of the Full Potential Equation and the Integral Bounday Layer Equations in Three Dimentions,' PhD Thesis, Department of Aeronautics and Astronautics, Massachsetts Insitute of Technology, 1986.

[25] Prandtl, L., "Induced Drag of Multiplanes," NACA TN 182, 1924.

[26] Roberts, A., and Rundle, K., "Computation of incompressible flow about bodies and thick wings using the spline–mode system," BAC(CAD) Report Aero Ma 19, 1972.

[27] Rubbert, P.E., and Saaris, G.R., "Review and Evaluation of a 3-D Lifting Potential Flow Analysis Method for Arbitrary Configurations," AIAA Paper 72 - 188, 1972.

[28] Squire, H.B. and Young, A.D., "The Calculation of the Profile Drag of Airfoils," ARC RM No. 1838, 1938.

[29] Suciu, E.O., and Morino, L., "Nonlinear Steady Incompressibile Lifting-Surface Analysis with Wake Roll-Up," AIAA Journal, Vol. 15, No. 1, pp. 54-58, 1976.

[30] Thwaites, B., "Approximate Calculation of the Laminar Boundary Layer," *Aeron. Quart.* Vol. 1, pp. 245-280, 1949.

[31] Trefftz, E., "Prandtlsche Tragflächen und Propeller Theorie," Zeitschrift für Angewandte Mathematik und Mechanik, 1, Berlin, 1921.

[32] Wolkovitch, J., "The Joined Wing: An Overview," *J. Aircraft*, Vol. 23, pp. 161-178, 1986.
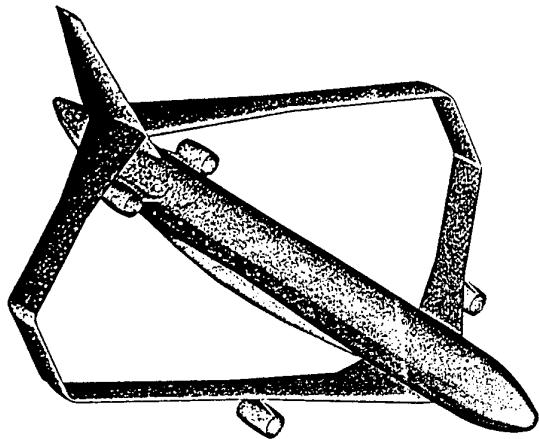
Fig. 1. Isometric view of Prandtl–plane.
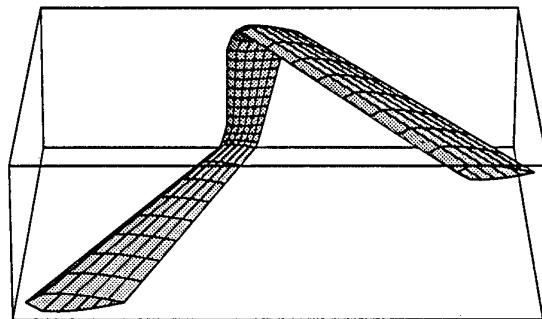
Fig. 2. Isometric view of wing of Prandtl–plane.
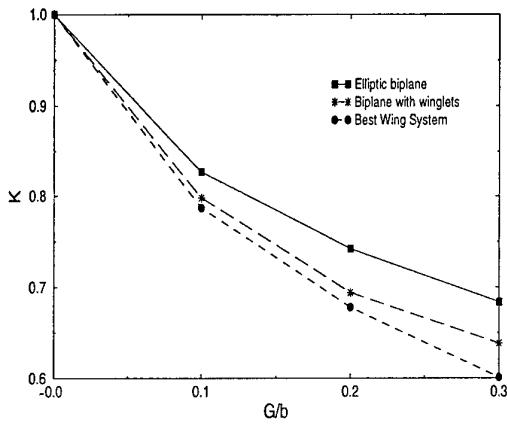
Fig. 3. Effect of winglets on Prandtl factor: rectangular biplane ($b/c = 10$, $\alpha = 5°$, unstaggered).
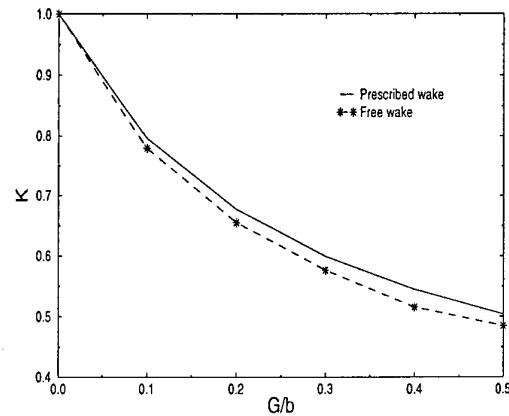
Fig. 4. Effect of wake roll–up on Prandtl factor: box–wing body ($b/c = 10$, $\alpha = 5°$, unstaggered).
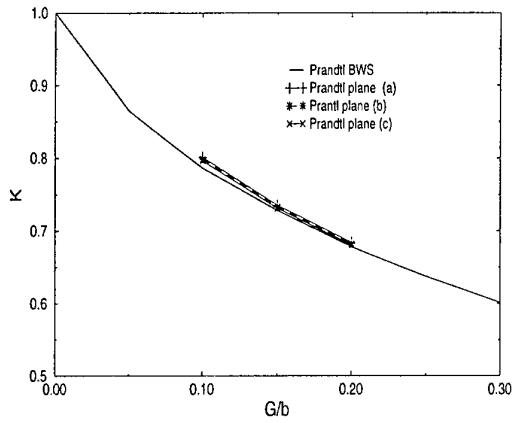
Fig. 5. Effect of sweep angle on Prandtl factor: Prandtl–plane.
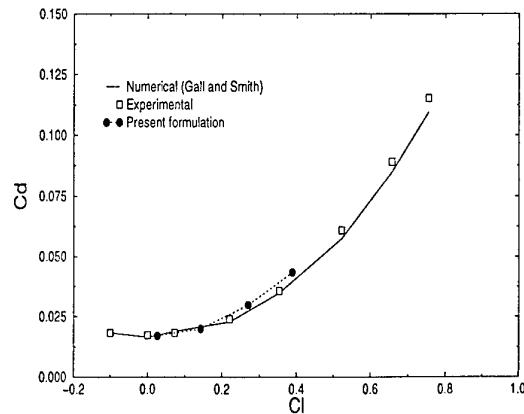
Fig. 6. Polar of box–wing body (aspect ratio 5, $G/c = 1$, stagger $= c$, section: NACA 0012) at $Re = 5.1 \cdot 10^5$.
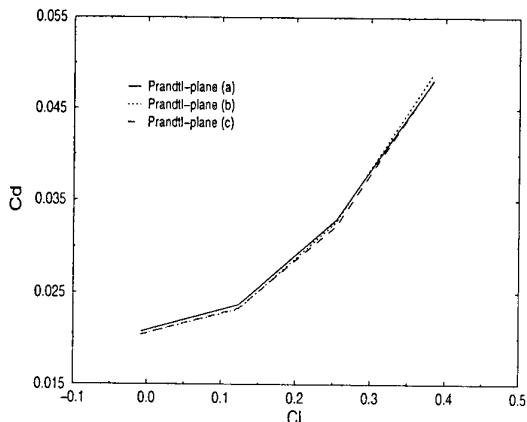
Fig. 7. Effect of sweep angle on polar of a Prandtl–plane at $Re = 2.7 \cdot 10^6$.
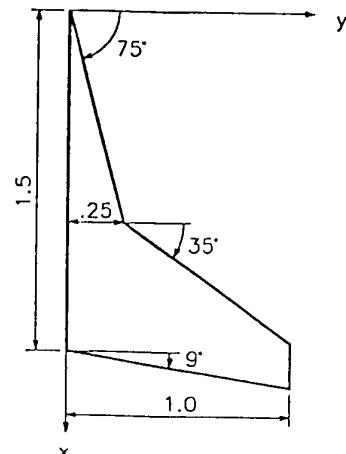
Fig. 8. Planform of wing with strake
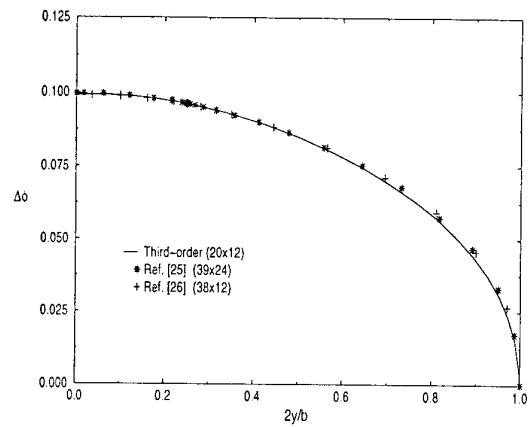
Fig. 9. Spanwise distribution of the circulation, $\alpha = 5°$.
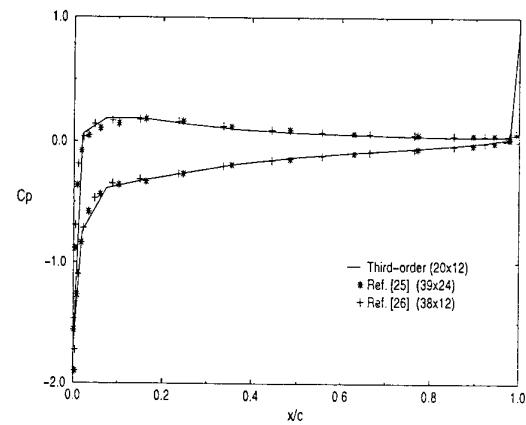
Fig. 10. Chordwise distribution of the C_p, $\alpha = 5°, \eta = 0.219$.
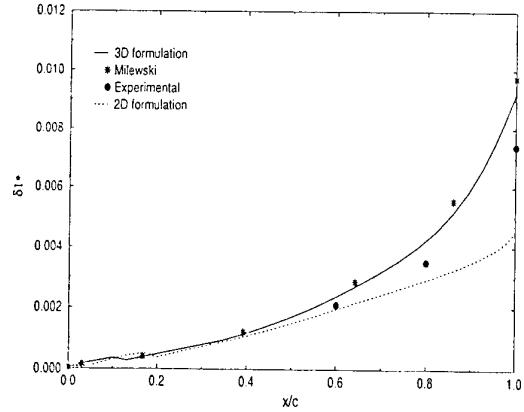
Fig. 11. Chordwise distribution of δ^*_1 at $Re = 2.1 \cdot 10^6$, $\alpha = 6.3°$, $2y/b = 0.5$.
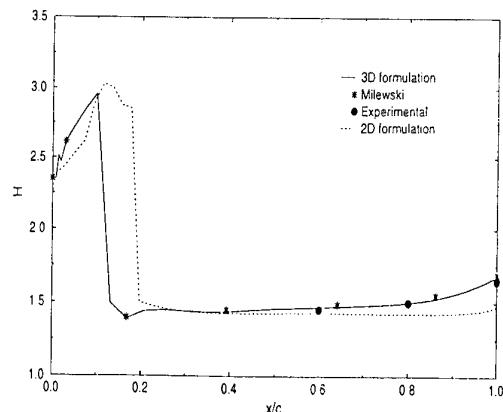
Fig. 12. Chordwise distribution of shape factor H at $Re = 2.1 \cdot 10^6$, $\alpha = 6.3°$, $2y/b = 0.5$.

DISCUSSION

Session II, Paper #16

Herr Sacher (DASA, Germany) asked how the engine would be represented in the potential approach.

> **Prof Morino** noted that in the past, the engine has been represented by a prescribed flow at the inlet with a rigid surface. As this rigid surface should be coincident with the actual stream surface, iteration is required to determine this shape. In this present work, the approach is to model the jet with a prescribed uniform flow plus a wake (doublet layer) to model the velocity discontinuity between the jet and the surrounding flow. It was noted that this would be an ideal application of the viscous flow extension discussed during the presentation.

Soft Computing in Multidisciplinary Aerospace Design - New Directions for Research

Prabhat Hajela
Mechanical Engineering, Aeronautical Engineering & Mechanics, Rensselaer Polytechnic Institute
5020 Jonsson Engineering Center, RPI Troy, New York, NJ 12180-3590, United States

Abstract

There has been increased activity in the study of methods for multidisciplinary analysis and design. This field of research has been a busy one over the past decade, driven by advances in computational methods and significant new developments in computer hardware. There is a concern, however, that while new computers will derive their computational speed through parallel processing, current algorithmic procedures that have roots in serial thinking are poor candidates for use on such machines - a paradigm shift is required! Among new advances in computational methods, soft computing techniques have enjoyed a remarkable period of development and growth. Of these, methods of neural computing, evolutionary search, and fuzzy logic have been the most extensively explored in problems of multidisciplinary analysis and design. The paper will summarize important accomplishments to-date, of neurocomputing, fuzzy-logic, and evolutionary search, including immune network modeling, in the field of multidisciplinary aerospace design.

Introduction

The optimal design of multidisciplinary systems has received considerable recent attention [1-3]. This initiative has been largely motivated by a recognition that the design and development of a complex engineering system can no longer be conducted by handling its different components in isolation. Both an increased level of complexity within the components, and the competition driven need to extract the advantages of a synergistic design process, dictate the need for a more comprehensive strategy. Inspite of an increased awareness of the potential of formal optimization methods in the design process, their application in real-life multidisciplinary systems continues to be a challenge. These challenges stem from the fact that practical scale multidisciplinary design optimization (MDO) problems are characterized by the presence of a large number of design variables and constraints, and analysis from various contributing disciplines which are not completely independent, involving one- or two-way couplings between the disciplines. In a number of situations, these analysis may be either very expensive, or in a worse case, simply unavailable to a design engineer in a form other than physical experimentation. MDO can be defined as a multifaceted entity with many conceptual components, and comprising of many established disciplines and technologies. Sobieski [1] defines the principal building blocks of the MDO problem in Figure 1. This taxonomy chart clearly shows the different areas in which research must be focussed if multidisciplinary optimization is to embraced as a standard procedure in industry design practice. These areas can be identified as follows.

- Approximations are needed to replace expensive exact analysis, where the latter can come from either sophisticated numerical codes or through physical experiments. Towards this end, the focus has resided in developing derivative-based extrapolations, or derivative-free approximations such as response surfaces, fuzzy-logic, and neural networks. In case of the latter, design of experiment approaches such as Taguchi methods have an important role in determining the data that must be used to develop such approximations.

- Mathematical modeling is critical to the success of the MDO approach. Such a model is required to predict the system behavior and its sensitivity to design variable changes. Models can be considered to belong to the broad categories of either physical or non-physical models. These models are necessary to answer 'what-if' questions.

- Design-oriented analysis basically deals with the issue of cost vs. accuracy in analysis for optimization. Inexpensive re-analysis is critical and is often based on a linear representation of the problem or on the basis of response-surface like approximations. In some cases, mathematical models can be constructed which only predict the gross system behavior, and provide crude models for preliminary design. Design oriented analysis must also consider how different components of the MDO problem must be executed so as to minimize the effort required in computing their interactions.

- Decomposition is a major concern in MDO, and entails the break-up of a large-scale problem into a sequence of smaller, more tractable subproblems. Depending upon the problem under consideration, the interactions between the decoupled subproblems may be either hierarchic or non-hierarchic.

- Design space search is a major component in MDO and is carried out by using traditional mathematical programming algorithms or newly emergent search techniques based on random sampling such as genetic algorithms and simulated annealing.

- Human intervention continues to be an important issue in MDO as the solution process is not a push-button operation. Operations such as algorithm termination, problem reformulation, interpretation of results, overriding the design process, require human intervention. Methods of artificial intelligence and expert systems have been explored in this context.

- Optimization strategies must continue to be studied in the context of the MDO problem. This includes optimization within a subproblem or a parallel optimization in all subproblems including ways to coordinate the solution towards a converged point.

A detailed discussion of all of these issue is clearly beyond the scope of this paper. This paper attempts to show how soft-computing methods have been adapted in the solution of some of the problems that are endemic to the multidisciplinary design problem. Discussions related to problem decomposition, coordination of solution in decomposed subsystems, design space search, and design oriented analysis, especially in the context of soft computing, are discussed in greater detail.

The MDO Problem

The design of a complex engineering system involves many interacting components or parts. Such interactions are clearly shown in Figure 2 for an aircraft wing structure. The design of this wing structure includes an interaction among the primary disciplines of structures, aerodynamics, controls and propulsion. Also central to this design is the input from the field of aeroacoustics. The figure schematically shows the multiple two-way couplings between the contributing

obtained in 8-10 revolutions of the blade. This process of obtaining trim condition prior to load calculation introduces additional computational costs.

The objective of the design problem was to design the blade geometry and internal structure to minimize a weighted sum of hub shear force and bending moments for a hingeless rotor blade in forward flight; aerodynamic, performance and structural design requirements are considered as constraints, and dynamic requirements constitute a multicriterion objective function. The premise behind the approach is that a minimization of the hub loads and moments translates into lower vibrations that are transmitted to the fuselage structure.

The planform geometry of the blade is shown in Fig. 5a. The blade is tapered in both the chord and the depth, and all loads are assumed to be carried by the structural box shown in Fig. 5b. The design variables for this problem are also shown on the figures and summarized in Table 1. The blade planform geometry is defined by the chord ratio λ_c and the point of inception of taper along the span denoted by τ_R. The blade twist varies from q_t at the root to zero at the tip; this variation maybe linear or nonlinear, and is controlled by the twist shape parameter δ. Both q_t and δ were design variables in the problem. Two nonstructural masses were positioned along the span of the blade, and the magnitude of these masses (m_1 and m_2) as well as their locations along the span (d_{m1} and d_{m2}) were considered as design variables. The rotational speed of the rotor Ω was also selected during the design process. The remaining variables, although descriptive of the internal structure of the blade, have a strong influence on both aerodynamic and dynamic performance. These were the horizontal flange thickness t_1, and the left and right vertical sections of the box beam denoted by t_2 and t_3, respectively. For the Graphite/Epoxy rotor blade, the horizontal flanges are symmetric +/-45 deg laminates; this layup is also present on the outer half of both vertical sections of the box beam. The inner half of the vertical walls are divided into two segments, with a layup of +/-θ_1 and +/-θ_2 deg, respectively. This accounts for a total of 14 design variables for the problem. Note that it is relatively easy to increase the problem dimensionality by simply varying the thickness and orientations of plies in discrete segments along the span.

The output quantities of interest are the maximum peak-to-peak values of the scaled shear force, flap bending moment, and lead-lag bending moment (F_z, M_y and M_z), the horsepower required during hover and forward flight (HP_h and HP_f), and the rotor thrust coefficient and solidity (C_T and σ). The last two must be bounded to limit the lift performance of the rotor disk so as to avoid blade stall. Bounds are also required on the blade autorotation (AI) capacity, and on the maximum allowed weight of the blade. A structural failure criterion based on the Tsai-Wu measure was used for the composite structure in this problem. Limiting values of σ_{buck}, the static stresses due to buckling were also imposed. For one given set of design variables, the analysis time required for the evaluation of the objective and constraint functions is substantial (about 18 CPU minutes on a SPARC station) and clearly not amenable to integration within an iterative optimization environment

Both the BP and CP neural networks were used to generate the mapping between the design variables and the response quantities of interest. Some of these mappings are quite nonlinear, and require careful consideration of the choice of network architecture and of the number of training patterns. A number of training patterns was generated, in the range of design variable variation, and this included both stable and unstable designs. A BP network with 14 input layer neurons, 10 hidden layer neurons, and 5 output layer neurons (a 14-10-5 network), corresponding to 5 output quantities, viz., vertical hub shear, flap moment, lag moment, rotor thrust, and the failure criterion index $\overline{R}$, was established and trained with 550 training patterns. This training presented problems in that it was difficult to reduce the training error to below 3%. The training data was then sorted to separate the designs that yielded stable and unstable responses; it was considered expedient at this stage to establish 5 networks, each mapping the design variables into one output only (14-10-1 networks for all but the lag moment, where a 14-10-8-1 network was used). The training of each of these networks could be done in parallel. The training using these separated patterns procceded well, converging to an error of less than 1%, with the exception of the lag moment (error was 2.6%). The observed pattern of time variation for the lag moment was quite nonlinear, and provides an explanation for the discrepancy in training. Table 2 shows the results of testing these networks for generalization performance using 7 sets of design variables that were not part of the original training set. Similar generalization performance was obtained from networks trained with the unstable data. The difficulty in training the networks for the combination of stable and unstable data can be attributed to either a) a completely different input-output relationship in one or more components or b) excessive data for the number of weights and bias constants in the network that could be varied to fit the data.

Similar experiments were also performed using the full CP network, that generates an identity mapping of the type [X,Y] -> [X',Y']. This network architecture requires a much larger number of input patterns, and the quality of generalization depends upon the number of Kohonen layer neurons that are permitted (indirectly a measure of maximum cluster radius). The results of numerical experiments designed to test this network are shown in Table 3.

Fuzzy Logic Based Function Approximations

In contrast to neural networks or other conventional function approximation techniques, fuzzy logic is based on natural languages. In a system, the problem description may be imprecise, not due to randomness, but because of inherent fuzziness. By taking advantage of the significance of natural language which has developed over many years, fuzzy logic can effectively model a complex real world without getting into the unnecessary detail.

The notion of fuzzy sets was first introduced by Zadeh in 1965 [12]. Since then, conceptual ideas were developed for nearly 10 years with very few applications. However, many recent successful uses of fuzzy set theory in various fields have established it as an effective tool to represent and manage vague information [13-15]. Fuzzy set theory has also gained much attention in the field of design optimization. Fuzzy optimal design of structures was introduced by Yuan and Quan [16,17]. Fuzzy optimization techniques were also applied in structural optimization problems with multiple

sitivity over the range of network training, and identifies the importance of any input component on an output quantity of interest. Such an analysis can be used to systematically partition the design space in a decomposition based design approach. This concept is discussed in a later section of this paper.

The counterpropagation (CP) neural network was first introduced by Hecht-Nielsen as a combination of two basic architectures - the Kohonen's self-organizing neural network and Grossberg's outstars neurons. However, the original version of the network did not receive widespread attention due to its unimpressive generalization performance, particularly in comparison to the multilayer perceptron model. As shown in Fig. 4, this network contains three layers - a fan-out layer as in the BP network, a layer of Kohonen or feature sensitive neurons, and an interpolating or Grossberg layer. The inputs to the network are directed to the Kohonen layer, which acts like a clustering device. In other words, neurons in this layer classify all input vectors based on some identifiable features in these vectors. Each neuron in the Kohonen layer represents one such cluster, and the interconnection weights between the input nodes and this neuron are representative of an average of all input patterns of that cluster. Similarly, the interconnection weights between each Kohonen neuron and the output or Grossberg layer neurons are representative of an averaged output of all patterns belonging to the cluster. Improvements to this basic format have been introduced wherein an input vector is classified as belonging to many different clusters, albeit to different degrees. A weighted average using the different clusters produces a much better generalization performance.

The primary differences between the CP and the BP model are in the time and data required for network training, and in the performance of their generalization capabilities. The former requires less computational effort to train, an issue of some importance when one considers modeling of extremely large multidisciplinary systems. However, its generalization performance is poorer when compared to the BP model. Improvements to the CP network have been implemented that partially circumvent this problem; however, large sets of training data continue to be required for their effective use. An advantage over the BP network is that CP networks provide a pattern completion capability, wherein, upon presentation of an input vector to the network, some components of which may be missing, the network approximates the missing components to produce a relevant output.

In using neural networks for approximate analysis, a set of input-output training patterns must be obtained from the real process that one is attempting to simulate. Determination of the number of such training pairs, and how they should span the intended domain of training, requires experimentation and experience. The same statement is applicable to the selection of the network architecture, i.e., the number of layers and the number of neurons in such layers. While mathematics can be used to assess bounds on such requirements, in a number of engineering problems, such approximations tend to be over conservative. This continues to be an active area for research.

Neural networks have been explored as function approximation tools in problems of multidisciplinary analysis and design, most commonly as a computationally inexpensive replacement for procedural analysis. In such cases, training data is generated from a procedural simulation of the multidisciplinary system, and a neural network is trained to mimic the input-output relations of this system (generalization). In such use, the neural network may be considered as a response surface approach where the order of the polynomial fitting function does not have to be specified. In fact, the neural network is a special form of response surface where the response function is a nested squashing function; the interconnection weights of the network that have to be learned correspond to the regression parameters in a typical regression model. Such a neural network is ideally well suited for an immersive design model, including one using a virtual reality environment.

ANN in Function Approximations - Example

At a preliminary design level, the multidisciplinary sizing of a rotor blade may require an integration of the disciplines of acoustics, aerodynamics, dynamics, and structural analysis within the optimization framework. This simplified example illustrates some of the inherent complexities in such design problems, and the use of neural networks in this context. The use of composites in rotorcraft blade design provide opportunities for enhanced aerodynamic, structural, and dynamic performance. With composites, it is practical to fabricate non-rectangular blades with variations in twist distribution and airfoil sections along the blade span, thereby contributing to increased flexibility in aerodynamic design. Satisfactory aerodynamic design requires that the required horsepower for all flight conditions not exceed the available horsepower, that the rotor disk must retain lift performance to avoid blade stall, and that the vehicle remain in trim. Important factors in structural design include material strength considerations for both static and dynamic load conditions. A combination of flapwise, inplane, torsion, and centrifugal forces typically comprise the static loading. Another important consideration that encompasses both structural and aerodynamic design, is the autorotation capability. The autorotation requirement pertains to maintaining the mass moment of inertia of the rotor in the rotational plane at an acceptable level. This is a function of the vehicle gross weight, rotor aerodynamic performance, and the rotor system mass moment of inertia. Finally, dynamic design considerations of the rotor blade pertain to the vibratory response of the blade under the applied loads; this design limits the dynamic excitation of the fuselage by reducing the forces and moments transmitted to the fuselage.

A finite element in time and space formulation was used to model the dynamics of the blade [11]. This formulation is based on a multibody representation of flexible structures undergoing large displacements and finite rotations, and requires that the equations of motion be explicitly integrated in time. An unsteady aerodynamic model is used to obtain the induced flow and to calculate the aerodynamic forces and moments in hover and forward flight. In addition to the geometric nonlinearities that are inherent in this problem, the loading on the blade varies as it moves around the azimuth - on the advancing side the flow velocity over the blade is additive to its tangential speed; on the retreating side, these velocities substract. Consequently, in order to maintain force and moment equilibrium, the pitch of the blade is continuously changed as it rotates around the azimuth, and the hub loads are a function of the blade rotational frequency. There is a transient period during which equilibrium of the vehicle is established (trim), and this is generally

subsystems. The interactions between the disciplines generally result from interactions between specific physical phenomena, two of which are illustrated in this figure. In such an environment where everything appears to effect everything else, design of subsystems in isolation is clearly not the strategy of choice. In an approach where the coupled multidisciplinary problem is treated as a single, large-scale optimization problem, the following difficulties have been identified:

- The dimensionality of the design space may increase to a degree that obtaining reliable solutions to the optimization problem is rendered questionable. Furthermore, there is a diminished capacity to evaluate the acceptability of solutions in higher-dimensionality design spaces.
- For an iterative analysis environment that is typical of optimization, the presence of coupling between disciplines would introduce an inner loop of iteration (analysis iteration) that adds to the computational costs.
- In a number of design problems, the design space may be nonconvex, and in some situations, even disjointed. Such characteristics call for the use of nontraditional search techniques that do not have a propensity to seek the nearest relative optimum from the nominal starting solution

Decomposition methods are introduced in multidisciplinary optimization to reduce large coupled optimization problems into a sequence of coordinated, smaller, more tractable subsystems. The subsystems not only allow for a reduction in problem dimensionality, but also allow for implementing specialized methods of analysis in each subsystem, and possibility of distributed, parallel processing. The interpretation of optimization results in each subsystem is also facilitated by the dimensionality reduction.

We start first with a generic mathematical statement for the optimization problem written as follows.

$$
\begin{aligned}
Minimize \quad & F(X) \\
Subject \ to \quad & g_j X \le 0 \qquad j = 1, m \\
& h_k(X)) = 0 \qquad k = 1, p \\
& X^L \le X \le X^U
\end{aligned}
\tag{1}
$$

Here X is the vector of design variables; superscripts 'L' and 'U' denote the lower and upper bounds, respectively; F(X) is the objective function and $g_j(X)$ and $h_k(X)$ are the inequality and equality constraints, respectively. If the dimensionality of the aforementioned design problem is manageable (of the order of a few hundred design variables), and if the gradient information is readily available, then traditional gradient based methods of nonlinear programming can be effectively used to obtain the optimal solution. However, in those problems where the design variables are a mix of continuous, discrete, and integer type, gradient information is not very useful, and alternative strategies must be investigated. A mixed-variable design space also limits the usefulness of traditional gradient-based optimization algorithms, and nongradient methods for optimal search have received attention in this context.

Another dominant concern in large-scale MDO problems is the high computational cost of analysis. Early implementations of multidisciplinary synthesis methods looked towards approximation methods for relief in this area (efficient structural reanalysis and Taylor approximations) [4,5]. While these ideas are still relevant and are broadly described as 'analysis for design', new requirements for developing nongradient based global approximations have emerged. This latter requirement is in part due to the increasing interest in applying optimization methods to real systems with mixed-variable design spaces. More importantly, it is driven by the need to generate 'mathematical models' for including disciplines such as manufacturability, cost, and maintainability, into the optimization problem. The use of response-surface like approximations based on neural networks and fuzzy logic have been explored in this context.

Approximate Models for Analysis

This section of the paper describes the use of artificial neural networks and fuzzy logic in developing approximate models for analysis, designed primarily to reduce the computational effort involved in MDO problems. The use of fuzzy logic in this application is motivated by the need to include in the optimization process, disciplines for which precise and well-defined analytical models are unavailable; these include, for example, issues pertaining to the cost, manufacture, and maintainence of designed artifacts. Both artificial neural networks and fuzzy logic based models are much like response surfaces, where a polynomial is fitted to given experimental or numeric data. Unlike the response surface approach where the order of the fitted polynomial must be specified, these methods provide greater flexibility to the user.

Among the most widely adapted neural network architectures in function approximation are the backpropagation (BP) network, counterpropagation (CP) network, and the radial basis network [6,7]. As shown in Figure 3, the BP network architecture consists of a layer of artificial neurons to which the external stimuli are presented, a series of hidden layers of artificial neurons, and a layer of neurons at which the output is available. The input neurons do not process the input stimulus; they simply serve as 'fan-out' points for connections to neurons in successive layers. Neurons in each layer are connected to all neurons in adjacent layers; there is an interconnection weight associated with this connection which defines the strength of the connection. Also associated with each artificial neuron is what is referred to as an activation function (sigmoid function or step function). The weighted sum of all inputs to a particular neuron are processed through this nonlinear activation function to produce a neuron output, which then feeds into all neurons of the next layer.

The presence of the hidden layer, and the nonlinear activation functions, enhance the ability of the networks to learn nonlinear relationships between the presented input and output quantities. This 'learning' or 'training' in these networks simply requires the determination of all interconnection weights of the network and characteristics of all activation functions, so that the network accurately produces the desired output for each of the input patterns used in the training. Once such a trained network is established, it responds to a new input within the domain of its training by producing an estimate of the output response. To this extent, it serves as a function approximation tool that provides inexpensive function information in stochastic sampling based search procedures [8]. The trained weights of this network can also be used to identify dependencies among design variables and design objectives/constraints [9,10]. This weight analysis may be considered as a smeared global sen-

objective functions [18,19].

Fuzzy sets are inherently different from classical sets; while the latter either wholly includes or excludes any given element, a fuzzy set can contain an element partially by using degrees of membership. An example which defines fuzzy sets is as follows. Consider the elements of a set defined as **heights** to include 5'0", 5'8", and 6'2". If another set is to include only the **tall heights** from the given elements, it would, most definitely, include the element 6'2" and exclude the element 5'0" since 6'2" is considered to be tall by most while 5'0" is not. For the element 5'8", it would be difficult to determine whether to include or exclude it from this set. Some will consider a height of 5'8" to be tall and others won't; this element sits on the fence. While classical sets have no way of accommodating this type of element, fuzzy sets can include them by assigning each of them a degree of membership. The degree of membership of each elements in a fuzzy set can be determined by its membership function. Since 5'0" is excluded from the set referred to as "tall", it is assigned a degree of membership of 0.0; in a similar vein, a degree of membership of 1.0 is assigned to the element 6'2", while some numerical value between 0 and 1 is given to the element 5'8". As an example, in fuzzy logic, 5'8" can be assigned a degree of membership of 0.7 which indicates that the person is somewhat tall.

If a classical set **tall heights** of a real number greater than 6 can be expressed as $tall = \{x | x > 6\}$, then a fuzzy set **tall heights** in X is defined as a set of ordered pairs $tall = \{(x, \mu_{tall}(x)) | x \in X\}$, where X is the universe of disclosure, x is an element of X, and $\mu_{tall}(x)$ is called the membership function of x in the fuzzy set **tall heights**. A membership function maps each element of x to a value between 0 and 1. Although the membership function can be any arbitrary curve whose shape is defined according to one's subjective perception, several most commonly used parameterized functions are available as a guideline. These include the triangular membership function, the trapezoidal membership function, the Gaussian membership function, the generalized bell membership function, and the sigmoidal membership function. Associated with each are a number of parameters that must be specified; they also offer a variety of smooth or nonsmooth functions to model variations of a quantity of interest.

Fuzzy logic is much like standard boolean logic except for the fact that in addition to 0 and 1, fuzzy logic can also operate with any numerical value between 0 and 1. There are a number of common operations such as intersection, union, and complement of fuzzy sets. The standard truth tables of Boolean logic are extended to fuzzy sets by replacing single-valued operations by multivalued logical operations [12]. Fuzzy rules are defined to map linguistic input and output values, and use conditional statements in the form of if-then-rules. In the case of boolean logic, if the antecedent part of if-then rule is true then the consequent part of if-then rule is also true. However, in fuzzy if-then rules, if the antecedent is partially true to some degree then the consequent is also partially true to that same degree. Given the freedom to choose from among different membership functions, fuzzy logic allows for the creation of an optimally tuned input-output function mapping. Evolutionary fuzzy modeling employs genetic algorithm based optimization to evolve fuzzy rules and membership function parameters. Genetic algorithms select from among discrete choices of membership functions and tune their parameters until the error between fuzzy outputs and target values are minimized.

Fuzzy logic approximation models are most appropriate for those situations when there is imprecise definition of parameters describing the desired model. One such model that has been constructed consists for creating a numerical model that relates the layup sequence of the individual plies in composite panels for rotorcraft fuselage, to the time required to fabricate such models on an automated fiber lay-up machine. In addition to limited numerical data that relates parameters such as panel geometry, location and frequency of cutouts, and fiber orientations in individual plies to the layup time, input from the machine operator was incorporated in construction of a fuzzy-logic based approximate model that was subsequently used in design optimization. Additional details on this model may be found in Reference [20].

Evolutionary Search and Genetic Algorithms

The strengths of evolutionary algorithms have been clearly established with reference to optimal search in generically difficult but very realistic multidisciplinary design problems such as those containing discontinuities or nonconvexities in function behavior, discrete variation in design variables, and where gradient information is generally unavailable. The genetic algorithm is based on an elitist reproduction strategy, where chromosomal representation of designs is evolved using random operations encompassed in operation like crossover and mutation, with bias assigned to those members of the population that are deemed most fit at any stage of the evolution process. In order to represent designs as chromosome-like strings, stringlike representations of the design variables are stacked head-to-tail. Different representation schemes have been adopted, including use of the decimal values of the design variable [21], use of integer numbers [21], or most popularly, a conversion of all design variables into their binary equivalent. In the latter case where the chromosomal string is a number of 0's and 1's, the numerical precision with which the design variable is represented is determined by the string length.

Increased adaptation into the multidisciplinary design environment has been accompanied by a number of modifications to the basic GA approach. Of these, direct schemes (non-penalty function methods) by which to account for design constraints [22,23], have received some attention. An approach applicable to a case where constraints are linear and the design space convex, has been described in [22]. Other methods, based on strategies that adapt useful features of the feasible designs into the infeasible population, have been proposed [23,24]. In [24], the process of adaptation is through the use of an expression operator, which like the crossover and mutation operations in genetic search, is probabilistic in nature. A similar process of adaptation ("gene-correction" therapy) is also at work in another strategy that is based on immune network simulation [23].

Binary coded GA's search for an optimal design from among a discrete set of design alternatives, the number of which depend upon the length of the chromosomal string. Large number of design variables, and/or considering a very fine precision in continuous design variable representation contributes to long chromosome string lengths which detracts

from the efficiency of the search process. These problems are particularly relevant in large-scale MDO problems, and several solution strategies have been proposed in this regard. Methods such as multistage search [25], wherein the granularity of the genetic algorithm based search is varied through a successive increase in the precision, and an approach which assigns significance to the previous generations of evolution in genetic search referred to as directed crossover [25], have been proposed. The latter simply attempts to determine through computations, significant bit positions on the string, and to constrain the crossover operation to these bit locations. A number of applications of both the basic GA and its enhanced forms, in problems of multidisciplinary structural design, structural layout determination, and composites design, are described in [26].

The implementation of genetic algorithms in a decomposition based approach has also been studied [27]. Consider the design problem to be formulated in terms of a design variable vector X. Also, let the design constraints $g_j(X)$ belong to the global constraint set G. The vector X and constraint set G are said to define a system level problem that is formulated as follows:

$$Min \ or \ Max \quad F(X)$$
$$subject \ to \quad G \equiv \{g_j(X), \ j = 1...NCON\} \ \leq 0 \quad (2)$$

Assume further that the best topology for decomposing the problem domain resulted in three subproblems A, B, and C, and the design variables and constraints for each of these subproblems are denoted by X_A, X_B, X_C, and g_A, g_B, and g_C, respectively. The objective function $F(X)$ for each of the subproblems is the same, and is the system level objective function. The system level problem of eqn. (2) is now represented by the following three subproblems.

$$Min \ or \ Max \quad F(X_A),$$
$$subject \ to \ g_A(X_A) \ \pounds \ 0, \ X_B, \ X_C = const$$
$$Min \ or \ Max \quad F(X_B),$$
$$subject \ to \ g_B(X_B) \ \pounds \ 0, \ X_A, \ X_C = const \quad (3)$$
$$Min \ or \ Max \quad F(X_C),$$
$$subject \ to \ g_C(X_C) \ \pounds \ 0, \ X_A, \ X_B = const$$

The principal challenge in this approach is to determine an appropriate topology for problem decomposition, and once such a topology has been established, to develop a procedure for coordinating the solution among the decomposed subproblems. The latter implies that the objective function obtained from each of the three subproblem optimizations be the same when the process converges to an optimal design.

A reasonable and logical approach for partitioning is one where balanced subsets of design variables would be assigned to different subproblems, and where each subproblem would be responsible for meeting the system level design objectives and for satisfying constraints most critically affected by the design variables of that subproblem. A trained BP network, can be used to extract the required causality. The weights of a BP network trained to relate the input design variables to the design constraints can be used to identify dependencies among design variables and design

objectives/constraints. This weight analysis may be considered as a smeared global sensitivity over the range of network training, and identifies the importance of any input component on an output quantity of interest. The approach results in the formation of a transition matrix [T], the components T_{ij} of which reflect the importance of the i-th input quantity on the j-th output component. First, the matrix product of the interconnection weight matrices is performed as indicated in Eqn. (4), and the elements of the transition matrix normalized as shown in Eqn. (5).

$$[T] = \prod_{k=1}^{N-1} W^k \quad (4)$$

$$\overline{T_{ij}} = \frac{T_{ij}}{max_j \ |T_{ij}|} \quad (5)$$

In the above, W^k is the k-th weight matrix, the coefficients w_{ij}^{kl} of which represents the interconnection weight between the i-th neuron of the k-th layer and the j-th neuron of the l-th layer; N denotes the total number of layers of neurons in the network architecture. This normalized matrix $\overline{T}_{ij}$ incorporates the effect of the sign of interconnection weights in the analysis. A systematic approach of using this transition matrix to decompose the problem is presented in Reference 27. For a larger version of the rotorcraft blade design problem defined earlier where the number of design variables has been increased to 42, the use of this transition matrix results in a decomposition of this problem as shown in Table 4. The form of partitioning allows for the most effective variables for a particular set of constraints to work in each subproblem optimization. It is also easy to recognize that such a split-up in variables could not be realized by a partitioning based on disciplinary concerns only, such as one that is largely used in current practice.

Once the design problem has been partitioned into a number of subproblems, the solution within each subproblem must proceed with adequate consideration of how a local design change influences the results of analysis in another subproblem. This is referred to as solution coordination and is required due to the fact that the subproblems are seldom completely decoupled. Two strategies that allow for consideration of these couplings are a) an approach based on the use of the counterpropagation (CP) neural network, and b) through the use of the simulation of a biological immune system modeling. As stated earlier, an important property of the CP network is a pattern completion capability - if an incomplete input pattern is presented to the network, the network estimates the most likely make-up of the missing components. This pattern completion capability can be of use in GA based decomposition design, by linking the GA optimizer in each subproblem with a trained CP network. In this mode of operation, the inputs to the CP network in each subproblem are the design variables for that subproblem, and approximations of the best combinations of variables in other subproblems. Details of how the progress of design variables of each subproblem are transmitted to other subproblems are described in [28]. The use of the biological immune system as an approach to communicate the coordination information is discussed in the following section.

Immune Network Modeling

In biological immune systems, foreign cells and molecules, denoted as antigens, are recognized and eliminated by type-specific antibodies. The task of recognizing antigens is formidable due to the very large number of possible antigens; it is estimated that the immune system has been able to recognize at least 10^{16} antigens. This pattern recognition capability is impressive, given that the genome contains only about 10^5 genes. This process can be simulated using the genetic algorithm approach, and has been the subject of considerable study [29,30].

A matching function that measures the similarities between antibodies and antigens, substitutes for the fitness function of the genetic algorithm. In a typical simulation of the immune system, the fitness of an individual antibody would be determined by its ability to recognize specific antigens, and a genetic algorithm using the matching function as a measure of fitness would evolve the gene structure of the antibody in an appropriate manner. In the context of a binary-coded genetic algorithm, the antibodies and antigens can also be coded as binary strings. The degree of match or complimentarity between an antibody and an antigen string indicates the goodness of that antibody. A simple numerical measure $Z = \sum t_i \; i=1,N_{string}$ can be defined, where N_{string} is the length of the binary string, and $t_i = 1$ if there is a match at the i-th location of the two strings, and is 0 otherwise. A larger value of Z indicates a higher degree of match between the two strings. Using a traditional GA simulation, a population of antibodies can be evolved to cover a specified pool of antigens, with Z used as the fitness measure for this simulation. The manner in which this pattern recognition scheme is invoked will determine whether the evolved antibodies are 'specialists', i.e. adapted to specific antigens, or generalists that provide the best match to a number of different antigens. From an applications standpoint, generation of both specialist and generalist antibodies is useful, and some of the applications have been discussed in [31].

In using this approach to account for interactions among temporarily decoupled subproblems, the motivation is to adapt changes in design variables from other subproblems into a particular subproblem with a prescribed frequency in the artificial evolution process. Note that updating the design variables of other subproblems must not simply involve introducing the best design from those subproblems but rather an average of the best few designs. In this regard, a generalist antibody would be developed that is the best representation of a number of good designs.

The proposed decomposition-based design procedure using immune network system may be summarized (see Figure 6) as follows. The stringlike chromosome structure representing the design contains a definition of all design variables. After partitioning of the design variable vector for each subsystem has been performed, genetic evolution is carried out in each subsystem in parallel, with the fitness function described in terms of the system level objective function. It should be noted that only that subsection of the chromosome string which corresponds to the design variables for that particular subsystem is changed. This process can be carried out for a fixed number of generations, and then a predetermined fraction of fit strings from each subsystem are introduced as

antigens to all other subsystems. A second stage of genetic search is then performed in each subsystem where the fitness function is defined in terms of each individual's ability to manufacture antibodies that match the newly introduced antigens. This stage of the genetic search is seen as a correction step that introduces compatibility between the different subpopulations, so that the process eventually converges on the desired design.

Computational Intelligence

Evolutionary search algorithms have a significant role in implementing ideas of computational intelligence in multidisciplinary design. Recent research has shown [32] how binary-coded rules in the IF-THEN form can be evolved using the genetic algorithm, based on information derived from a computational domain. In such classifier system type of machine learning approaches the rules may be completely arbitrary in the beginning but evolve into meaningful statements with information extracted from the computational domain. This approach has powerful implications in overcoming problems of a brittle rule-base that were endemic in traditional rule-based systems.

A classifier system is generally divided into two parts, a set of rules or classifiers, and a message list. The message list contains at least one input from the external environment and also provides the framework for the rules to interact (any rules generated internally are posted here as well). Hence, the message list is dynamic in nature, constantly evolving as the system changes. The classifier rules are made up of three distinct segments - conditions, actions and strength. To facilitate the use of genetic algorithms in this approach, all rules are coded as binary strings. The conditions allow the classifier to read the message list by searching for matches between the condition and the message list. If a match is found, the action is posted to the message list. The strength is a number associated with each rule designed to indicate its value to the systems, and forms the basis for learning. If a rule helps bring about useful responses, it gains strength. Similarly, an ineffective rule is weakened and perhaps ultimately purged from the system. The strength of the proposed approach would be to introduce new rules into the system based on principles of genetic search.

Consider for example, a heuristics based optimization procedure where the objective is to minimize the weight of a truss structure while ensuring that the bounds on maximum permissible stress in each element of the truss are not violated. A solution strategy would entail constructing a number of random classifiers in the IF-THEN (Condition-Action) format. The condition segment of the classifier can be chosen in a form that it allows for the classifier to be related to the current state of the design. One approach for doing this would be to construct a composite measure of all constraints of the problem. The action part of the classifier could be the changes required in each component of the design variable. A very simple-minded operation of the classifier would be to perform a match between the classifiers and the current state of the design; this match would be based on both the magnitude and sign of the constraint values. The winning classifier would be allowed to execute its action segment, and the resulting change in the state of the design as indicated by the weight and the constraint values, used to either increase or attenuate the strength of that classifier. Since both the condition and action segment of the classifiers are initially ran-

domized, the first set of design changes may be quite erratic, and the rules must evolve in a manner that subsequent steps will produce improvements in the results. This objective is attained by using a genetic algorithm to evolve the classifiers based on their fitness value as indicated by their current strengths.

The approach has also been used in enhancing the process through which neural networks are used to create function approximations. A rule learning procedure was implemented wherein computational feedback on the performance of a partly trained network was used to determine the amount and location of new training patterns required to improve the network generalization performance [33]. A similar approach to improve the quality of response surface based approximations is presented in [34]. The application of a classifier system approach in turbine design optimization is presented in Reference 35.

New Research Directions

This review would be incomplete without some reference to future directions for exploration. The role of soft computing tools in structural analysis and design is today on firmer ground than it has ever been before. Computing speeds today are in the MFLOPS-GFLOPS range and predictions indicate TFLOPS performance and better in the next decade. Analysis and design techniques must be revisited from a completely new perspective if such hardware is to be used in the most effective manner. Current algorithms, through all manners of software enhancement and efforts to parallelize, have their origins in serial thinking, and without the required intrinsic parallelism, are victims of the law of diminishing returns when placed on parallel machines. A completely new line of thinking born in the parallel processing environment is required for developing the next generation of structural analysis and design tools, and here is where soft computing tools are likely to have the most visible impact. What must result from new developments are real-time methods to analyze a design artifact - these tools should provide a design engineer with an immersive design capability in which not only search directions and step sizes are computed rapidly, but what-if questions pertinent to the design are available instantaneously. Research targeting these lofty goals has begun, albeit at very rudimentary levels. Specific goals of such research which spans the spectrum of soft computing tools includes the following

Use of neural networks and fuzzy-logic tools to develop response surface-like approximations for discrete and discontinuous functions which are significant in the context of topological design of structural systems, or in an immersive/ interactive analysis and design mode, where exploration of discrete concepts is most critical. The concept of using macro-neural networks (neuroelements) which can be adaptively interconnected during the evolution of design, has been considered. Efforts to expand the use of evolutionary algorithms to large-scale design problems through more efficient implementations in a parallel computing environment are worthy of consideration Similarly, extending these algorithms to better handle fuzzy design constraints and objective criteria through an effective integration with fuzzy-logic techniques must be explored. These are particularly relevant in an environment where manufacturing considerations must be included in the design cycle. Finally, an exploration of entirely different computational paradigms such as cellular

automata [36] to both analyze and design structural systems presents distinct possibilities. This approach represents a departure from the traditional procedural analysis. Instead of using fundamental equations of physics pertinent to a problem to analyze a domain, the idea here is to decompose the problem domain into a number of grids, where the property of each cell within this grid evolves or emerges through an interaction with the surrounding cells in the grid. This self-emergent or self-organizing behavior is thought to be significant in the development of the next generation of structural synthesis tools; it is an intrinsically decentralized computational paradigm ideal for multiple parallel processor machines. Preliminary results of work in this area are reported in [37,38].

Closing Remarks

The paper has described a subset of attempted applications of soft-computing tools in problems of multidisciplinary analysis and design. These tools represent significantly improved capabilities for solving generically difficult problems; more specifically, they overcome difficulties related to problem dimensionality, handling of a mix of discrete, integer, and continuous design variables, accounting for discontinuities or nonconvexities in the design space, and improved capabilities for modeling and design in the absence of gradient information. The last item is particularly relevant in a design for manufacturing environment, where manufacturing and production related constraints have received increased attention. Soft computing methods are expected to have a major role in the development of the next generation of tools for multidisciplinary analysis and design.

References

1. Sobieszczanski-Sobieski, J., "Multidisciplinary Design Optimization: An Emerging New Engineering Discipline", World Congress on Optimal Design of Structural Systems, Rio de Janeiro, Brazil, August 2-6, 1993.

2. Tolson, R.H. and Sobieszczanski-Sobieski, J., "Multidisciplinary Analysis and Synthesis: Needs and Opportunities", AIAA Paper No. 85-0584, 1985.

3. Abdi, F., Ide, H., Levine, M., and Austel, L., "The Art of Spacecraft Design: A Multidisciplinary Challenge", 2nd NASA/Air Force Symposium on Recent Advances in Multidisciplinary Analysis and Optimization, NASA CP-3031, Sep. 1988.

4. Noor, A.K., and Lowder, H.E., 1974. "Approximate Techniques of Structural Reanalysis", Computers and Structures, Vol. 4, pp. 801-812.

5. Schmit, L.A., and Farshi, B., 1974. "Some Approximation Concepts for Structural Synthesis", AIAA Journal, 12, 5, 692-699.

6. Hajela, P., Neural Networks - Applications in Modeling and Design of Structural Systems, CISM Lecture Notes, Udine, Italy, October 1998.

7. Haykin, S., 1994. Neural Networks - A Comprehensive Foundation, Macmillan Publishing Company, Englewood, New Jersey.

8. Hajela, P., and Lee, J., "Role of Emergent Computing Techniques in Multidisciplinary Design", proceedings of the NATO Advanced Research Workshop on Emergent Computing Methods in Engineering Design, Nafplio, Greece, August 1994, Springer Verlag, 1996, pp. 162-187, eds. D. Grierson and P. Hajela.

9. Goel, S. and Hajela, P., "Classifier Systems in Design Optimization", proceedings of the AIAA/ASME/ASCE/AHS SDM meeting, Kissimee, Florida, April 1997.

10. Hajela, P and Szewczyk, Z., "Neurocomputing Strategies in Structural Design - On Analyzing Weights of Feedforward Neural Networks", Structural Optimization, Vol. 8, No. 4, pp. 236-241, December 1994.

11. Bauchau, O. A. , and Kang, N.K..: "A Multibody Formulation for Helicopter Structural Dynamic Analysis", Journal of American Helicopter Society, Vol. 38, No. 2, pp. 3-14, April 1993.

12. Zadeh, L., "Fuzzy Sets," *Information and Control*, Vol. 8, pp. 338-353, 1965.

13. Uragami, M., Mizumoto, M., and Tanaka, K., "Fuzzy Robot Controls," Journal of Cybernetics, Vol. 6, pp. 39-64, 1976.

14. Dubois, D., "An Application of Fuzzy Set Theory to Bus Transportation Network Modification," Proceeding of the Joint Automatic Controls Conference, Philadelphia, 1978.

15. Kacprzyk, J., "Fuzzy Set-Theoretic Approach to the Optimal Assignment of Work Places," in G. Guardabassi and A. Locatelli (eds), Large Scale Systems Theory and Applications, Udine, pp. 123-131, 1976.

16. Yuan, W. G. and Quan, W. W., "Fuzzy Optimum Design of Structures," Engineering Optimization, Vol. 8, pp. 291-300, 1985.

17. Yuan, W. G. and Quan, W. W., "Fuzzy Optimum Design of Aseismic Structures," Earthquake Eng. Sturct. Dyn., Vol. 13, pp. 827-837, 1985.

18. Rao, S. S., "Multi-Objective Optimization of Fuzzy Structural Systems," International Journal for Numerical Methods in Engineering, Vol. 24, pp. 1157-1171, 1987.

19. Yoo, J. and Hajela, P., "Multicriterion Design of Fuzzy Structural Systems Using Immune Network Modeling", Proceedings of the AIAA/ASME/ASCE/AHS SDM meeting, AIAA 99-1425, St. Louis, MO, April 1999, pp. 1880-1890.

20. Yoo, J., Soft Computing Adaptations in Optimal Design of Structural Systems, Ph.D. Thesis, Department of Mechanical Engineering, Rensselaer Polytechnic Institute, Troy, New York, 1999.

21. Haftka, R.T., and Gurdal, Z., 1993. Elements of Structural Optimization, Kluwer Academic Publishers, Dordrecht.

22. Michalewicz, Z., and Janikow, C.Z., 1991. "Handling Constraints in Genetic Algorithms", Proceedings of the 4th

International Conference on Genetic Algorithms, pp. 151-157.

23. Hajela, P., and Lee, J., 1996. "Constrained Genetic Search Via Schema Adaptation: An Immune Network Solution", proceedings of the First World Congress of Structural and Multidisciplinary Optimization, Goslar, Germany, May-June, 1995, eds. N. Olhoff and GIN Rozvany, pp. 914-920, Pergamon Press.

24. Hajela, P. and Yoo, J., 1996. "Constraint Handling in Genetic Search Using Expression Strategies",AIAA Journal, Vol 34, No. 11, pp. 2414-2420.

25. Lin, C.-Y., and Hajela, P., 1993. "Genetic Search Strategies in Large Scale Optimization", proceedings of the 34th AIAA/ASME/ASCE/AHS/ASC SDM Conference, La Jolla, California, pp. 2437-2447.

26. Hajela, P., 1997. Stochastic Search in Discrete Structural Optimization - Simulated Annealing, Genetic Algorithms and Neural Networks, Discrete Structural Optimization, Springer, New York, pp. 55-134, (ed. W. Gutkowski).

27. Lee, J. and Hajela, P., "GA's in Decomposition Based Design - Subsystem Interactions Through Immune Network Simulation", Structural Optimization, vol. 14, No. 4, pp. 248-255, December 1997.

28. Hajela, P., "Biologically Inspired Computational Paradigms - Adaptive Solution Strategies for Multidisciplinary Structural Design", Invited Lecture at the 3nd International Conference on Computational Structures Technology, Budapest, Hungary, August-September, 1996, Advances in Computational Structures Technology, Civil-Comp Press, Edinburgh, Scotland, ed. BHV Topping, pp. 19-28.

29. Smith, R. E.; Forrest, S.; Perelson, A. S. 1992: Searching for Diverse Cooperative Populations with Genetic Algorithms. Technical Report CS92-3, University of New Mexico, Department of Computer Science, Albuquerque, NM.

30. Dasgupta, D., and Forrest, S., 1995. "Tool Breakage Detection in Milling Opeartions Using a Negative Selection Algorithm", TR No. CS95-5, Department of Computer Science, University of New Mexico.

31. Hajela, P., and Yoo, J., Immune Network Modeling in Design Optimization, New Methods in Optimisation, Editors: D. Corne, M. Dorigo and F. Glover, McGraw-Hill, 1999.

32. Richards, S.A., 1995. Zeroth-Order Shape Optimization Utilizing a Learning Classifier System, Ph.D. dissertation, Stanford University, California.

33. Hajela, P. and Kim, B., 1998. "Classifier Systems for Enhancing Neural Network Based Global Function Approximations", proceedings of the 7th AIAA/NASA/ISSMO/USAF Multidisciplinary Analysis and Optimization Meeting, St. Louis Missouei.

34. Hajela, P., and Lee, J., "A Machine Learning Based

Approach to Improve Global Function Approximations for Design Optimization", proceedings of the International Symposium on Optimization and Innovative Design, JSME Paper No 116, edited by H. Yamakawa, M. Yoshimura, S. Morishita and M. Arakawa, July 28-July 30, 1997, Tokyo, Japan.

35. Goel, S., 1998. Machine Learning Paradigms in Design Optimization: Applications in Turbine Aerodynamic Design, Ph.D. dissertation, Rensselaer Polytechnic Institute, New York, April.

36. Wolfram, S., 1994. Cellular Automata and Complexity, Addison Wesley, New York.

37. Hajela, P., and Kim, B., " GA Based Learning in Cellular Automata Models for Structural Analysis", 3rd World Congress on Structural and Multidisciplinary Optimization, Niagara Falls, New York, May 1999.

38. Hajela, P., and Kim, B.,"On the Use of Energy Minimization for CA Based Analysis in Elasticity", submitted to the 41st AIAA/ASME/ASCE/AHS SDM Meeting, April 1-3, Atlanta, Georgia, 2000.
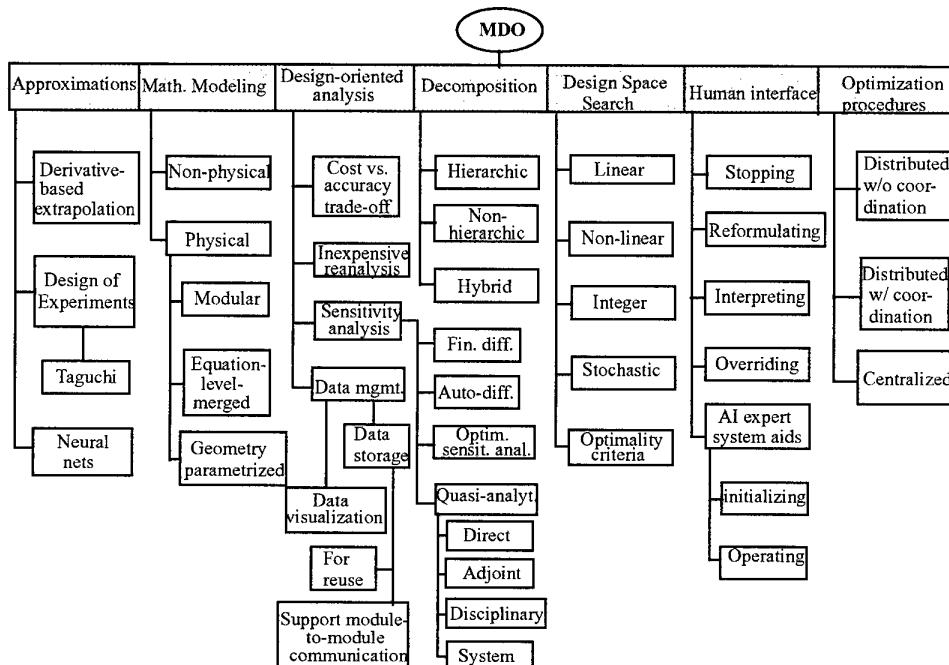
Figure 1. Taxonomy of the MDO Problem
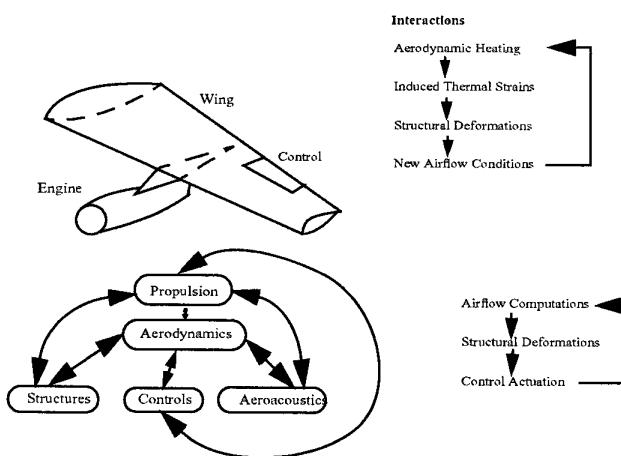
Figure 2. Schematic of a coupled MDO problem
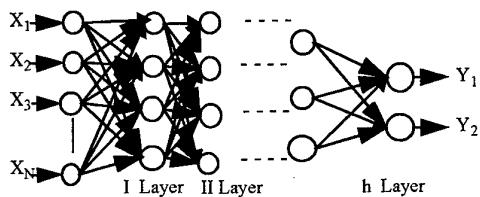
Figure 3. Schematic of a backpropagation neural network
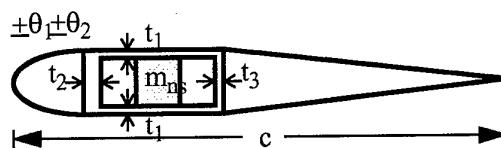
Figure 5b. Cross sectional profile of rotor blade
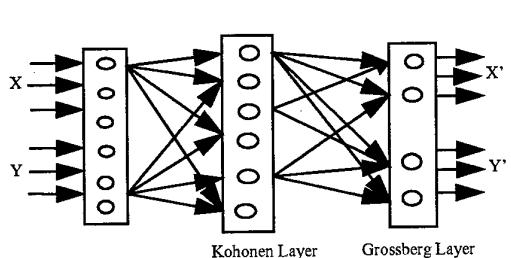
Figure 4. Schematic of a counterpropagation neural network
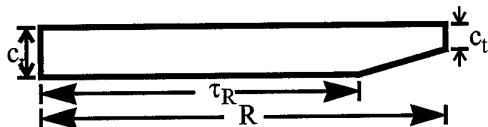
Figure 5a. Planform of rotor blade
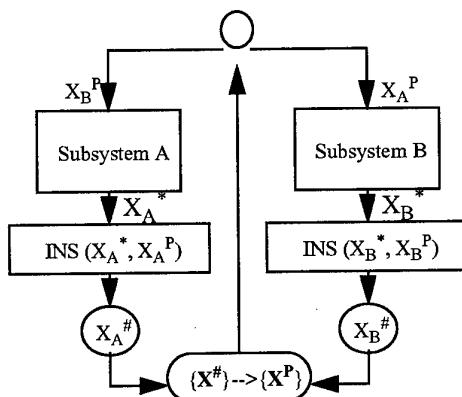
Figure 6. Subsystem interactions through IN simulation

	design variable	symbol
d_1	mass 1 location	m_1
d_2	mass 2 location	m_2
d_3	tuning mass 1 (kg)	d_{m1}
d_4	tuning mass 2 (kg)	d_{m2}
d_5	horizontal flange thickness ratio to box beam	t_1
d_6	left vertical flange thickness ratio to box beam	t_2
d_7	right vertical flange thickness ratio to box beam	t_3
d_8	blade twist (deg)	θ_t
d_9	twist shape parameter	δ
d_{10}	taper inception point	τ_R
d_{11}	chord ratio	λ_c
d_{12}	rotational speed (rad/sec)	Ω
d_{13}	layup angle of inner vertical flange (deg)	θ_1
d_{14}	layup angle of outer vertical flange (deg)	θ_2

Table 1. Descrition of the design variable set

shear force (N)			flap moment (N m)			lag moment (Nm)			thrust in cruise (N)			failure criterion		
NN	actual	%	NN	actual	%	NN	actual	%	NN	actual	%	NN	actual	%
13695	13546	1.10	11403	11711	2.08	5278	5266	0.24	778	784	0.76	0.261	0.261	0.01
8666	8649	0.19	6295	6891	0.50	4059	3994	1.65	517	506	2.17	0.243	0.241	0.83
6864	6790	1.09	6700	6745	0.67	4036	3880	4.72	369	374	1.33	0.247	0.249	0.84
9160	9373	2.27	8409	8406	0.04	3917	3772	3.84	498	502	0.79	0.313	0.308	1.62
14952	15028	0.51	12905	12984	0.61	4082	4086	0.10	857	873	1.83	0.250	0.250	0.02
17002	17001	0.03	12768	12736	0.25	5974	5899	1.27	926	921	0.54	0.319	0.316	0.94
7284	7339	0.75	6934	6957	0.33	11606	11559	0.40	435	427	1.87	0.238	0.244	2.45

Table 2. Testing of the trained BP network

shear force (N)			flap moment (N m)			lag moment (N m)			thrust in cruise (N)			failure criterion		
NN	actual	%	NN	actual	%	NN	actual	%	NN	actual	%	NN	actual	%
8942	8687	2.93	7316	7504	2.53	3663	3705	1.13	472	483	2.28	0.25	0.258	0.39
14963	14272	4.84	10056	10264	2.02	8273	7892	4.82	766	763	3.93	0.312	0.312	0.01
12384	12579	1.55	10568	10458	1.05	5894	5758	2.36	763	754	1.19	0.235	0.237	0.84
8926	8919	0.08	7045	7058	0.18	5685	5713	0.49	509	502	1.39	0.264	0.266	0.75
10253	10156	0.96	13093	13185	0.69	11796	11183	5.48	933	907	2.86	0.329	0.333	1.20
8113	8046	0.84	8936	8841	1.01	12529	11932	5.00	376	371	1.35	0.347	0.349	0.57
9735	9653	0.85	9618	9685	0.69	22940	23695	3.18	467	454	2.86	0.394	0.390	1.02

Table 3. Testing of the trained CP network

	subsystem [A]	subsystem [B]	subsystem [C]
objective	$F(X) = c_1 F_z + c_2 M_y + c_3 M_z$		
constraints	$HP_h \leq HP_a$ $\eta^L \leq \eta \leq \eta^U$ $AI \geq AI^L$	$HP_f \leq HP_a$ $C_T/\sigma^L \leq C_T/\sigma \leq C_T/\sigma^U$	$W_b \leq W_b^U$ $\overline{R} \leq 1$ $\sigma_{buck} \leq \sigma_{all}$
design variables	$m_1, m_2, m_3,$ $t_1^4, t_1^5,$ $t_1^6, t_2^3, t_2^6,$ $t_2^9,$ $t_3^6, t_3^8, t_3^9, \tau,$ $\pm\theta_1$	$t_1^3, t_1^{10}, t_2^4,$ $t_2^5, t_2^7,$ $t_2^8, t_3^2, t_3^3, t_3^5,$ $t_3^7, t_3^{10}, \theta_t, \delta,$ $\pm\theta_2$	$m_4, m_5, t_1^1,$ $t_1^2,$ $t_1^7, t_1^8, t_1^9,$ $t_2^1, t_2^2,$ $t_2^{10}, t_3^1, t_3^4,$ λ_c, Ω

Table 4 Topology of system decomposition

DISCUSSION

Session III, Paper #17

Mr Templin (NRC, Canada) observed that advanced search tools are potentially very complex and therefore perhaps require "specialist" users. He wondered whether the author saw the need for such people, or whether he anticipated another solution.

> **Prof Hajela** suggested that as the toolsets are changing, so is the education process. He believes that today's disciplinary-oriented graduates probably already have some training in advanced search methods. He further believes that it is these graduates who will lead industry in a "forced migration" towards at least some of these approaches.

An Optimal Control Theory Based Algorithm to solve 2D Aerodynamic Shape Optimisation Problems for Inviscid and Viscous Flows

S.Hiernaux[*] and J.-A. Essers[†]

Aerodynamics group, University of Liège
Rue Ernest Solvay 21 (Bât C3), B-4000 Liège, Belgium

March 2, 2000

1 Introduction

With the capacity of today's computers, one can envisage the resolution of shape optimization problems in aerodynamics. Nevertheless, optimization methods require many evaluations of different aerodynamic configurations, and so are much more expensive than a single analysis. It is therefore mandatory to find methods that evaluate aerodynamic functions and their gradient at the lowest possible computational cost, as well as fast and robust optimization methods.

Classical optimization techniques (descent methods) not only require the value of the function to optimize, but also of its gradient. The classical way to compute the gradient is to use a finite-difference formula; the main drawback of this method is due to the fact that $n + 1$ evaluations of aerodynamic functions are necessary at each iteration, n being the number of parameters defining the geometry to optimize. So, such methods are completely unsuited to aerodynamic shape optimization, because of the high computational cost of the single analysis. Alternative methods (stochastic optimization, genetic algorithms) that don't require gradient information are also highly costly in term of CPU time.

For a few years, techniques for sensitivity analysis based on the optimal control theory have been developed ([1],[13]). These techniques derive from the state equations another set of equations called "adjoint" or "costate" equations. The solution of these adjoint equations is used to compute the gradient

---
[*]F.N.R.S. Research Assistant
[†]Professor

at very low cost; since solving the adjoint equations is equivalent to solve the state equations, the cost of sensitivity analysis is greatly reduced. Some authors use adjoint equations derived from the discretized Euler equations ([5],[7]). In this paper, we focus on adjoint equations derived from analytical state equations.

2 Optimal control

A typical shape optimization problem can be stated as follows:

Let Ω be a subspace of $\mathbf{R}^2$. Find the shape of Γ_0, a boundary of Ω controlled by design variables $\mathbf{u}$, such that the functional:

$$\mathcal{J}(\mathbf{u}) = \int_{\Gamma_f} \Phi(\mathbf{s}, \mathbf{q}_x, \mathbf{q}_y, \mathbf{u}) d\Gamma_f \qquad (1)$$

computed on a boundary Γ_f (where Γ_f and Γ_0 can be different) is minimized

Over the domain Ω, the state variables $\mathbf{s}$ are governed by the advective-diffusive state equations:

$$\partial_x \left[\mathbf{f}(\mathbf{s}) - \mathbf{f}_v(\mathbf{q}, \mathbf{q}_x, \mathbf{q}_y) \right] + \partial_y \left[\mathbf{g}(\mathbf{s}) - \mathbf{g}_v(\mathbf{q}, \mathbf{q}_x, \mathbf{q}_y) \right] = 0 \quad \text{on } \Omega \,(2)$$

$$\mathbf{G}_i(\mathbf{q}, \mathbf{q}_x, \mathbf{q}_y, \mathbf{u}) = 0 \quad \text{on } \Gamma_i \,(3)$$

where $\mathbf{q} = \mathbf{q}(\mathbf{s})$ are the primitive variables and

$$\mathbf{q}_x = \partial_x \mathbf{q} = \mathbf{M} \partial_x \mathbf{s} \qquad (4)$$
$$\mathbf{q}_y = \partial_y \mathbf{q} = \mathbf{M} \partial_y \mathbf{s} \qquad (5)$$

with $\mathbf{M} = \frac{\partial \mathbf{q}}{\partial \mathbf{s}}$ the jacobian of the transformation between primitive and state variables.

In order to find an optimality condition, one have to form the *Lagrangian* of the problem:

$$
\begin{aligned}
\mathcal{L} \;=\; &\mathcal{J} \\
&+ \int_\Omega \psi^T \left[\partial_x \left(\mathbf{f} - \mathbf{f}_v \right) + \partial_y \left(\mathbf{g} - \mathbf{g}_v \right) \right] d\Omega \\
&+ \sum_i \int_{\Gamma_i} \mu_i^T \, \mathbf{G}_i \, d\Gamma_i \\
&+ \int_\Omega \lambda_x^T \left(\mathbf{q}_x - \mathbf{M} \partial_x \mathbf{s} \right) + \lambda_y^T \left(\mathbf{q}_x - \mathbf{M} \partial_x \mathbf{s} \right) \, d\Omega
\end{aligned}
\tag{6}
$$

where $\psi, \mu_i, \psi_x, \psi_y$ are the costate or adjoint variables associated with the state equations, state boundary conditions and primitive-conservative realtions respectively.

The optimal control theory states that the Lagrangian is stationary at the optimum solution, i.e. at the solution, the (independant) variations of the Lagrangian with respect to the state ($\mathbf{s}$), costate (ψ, μ) and design ($\mathbf{u}$) variables is zero.

The variation of the Lagrangian due to the design variables is the sum of two contributions:

- a *local variation* due to the variation of the design variables;
- a *convective variation* due to the displacement of the domain and boundaries.

The variations of the Lagrangian due to the state, and costate variables are local variations.

2.1 Local variations

The local variation of the lagrangian can be split in eight parts:

$$
\begin{aligned}
\delta \mathcal{L}_{\text{loc}} \;=\; &\delta \mathcal{L}_{\text{loc}}^{\mathbf{s}} + \delta \mathcal{L}_{\text{loc}}^{\mathbf{q}_x} + \delta \mathcal{L}_{\text{loc}}^{\mathbf{q}_y} + \delta \mathcal{L}_{\text{loc}}^{\mathbf{u}} + \delta \mathcal{L}_{\text{loc}}^{\psi} \\
&+ \sum_i \delta \mathcal{L}_{\text{loc}}^{\mu_i} + \delta \mathcal{L}_{\text{loc}}^{\lambda_x} + \delta \mathcal{L}_{\text{loc}}^{\lambda_y}
\end{aligned}
\tag{7}
$$

As the variations of the state, costate and design variables are independent, the variation of their contribution to the variation of the Lagrangian must be zeroed independently.

It is easy to demonstrate that setting $\delta \mathcal{L}_{\text{loc}}^{\psi}$ and $\delta \mathcal{L}_{\text{loc}}^{\mu_i}$ to zero leads to the state equations and boundary conditions, while setting $\delta \mathcal{L}_{\text{loc}}^{\lambda_x}$ and $\delta \mathcal{L}_{\text{loc}}^{\lambda_y}$ to zero leads to the primitive-conservative relations.

The local variation due to the design variables is:

$$
\delta \mathcal{L}_{\text{loc}}^{\mathbf{u}} = \sum_i \int_{\Gamma_i} \frac{\partial \mathcal{H}_i}{\partial \mathbf{u}} \delta \mathbf{u} \, d\Gamma_i
\tag{8}
$$

where the *Hamiltonians* $\mathcal{H}$ are defined as:

- $\mathcal{H}_f = \Phi + \mu_f^T \mathbf{G}_f$ on Γ_f;
- $\mathcal{H}_i = \mu_i^T \mathbf{G}_i$ on the other boundaries.

The local variation due to the state variable is, using Gauss' theorem:

$$
\begin{aligned}
\delta \mathcal{L}_{\text{loc}}^{\mathbf{s}} \;=\; &- \int_{\cup \Gamma} \left\{ \psi^T \left[\left(\mathbf{A} - \mathbf{A}_v \right) n_x + \left(\mathbf{B} - \mathbf{B}_v \right) n_y \right] \right\} \delta \mathbf{s} \, d\Gamma_i \\
&- \int_{\cup \Gamma} \left\{ \left[\lambda_x^T n_x + \lambda_y^T n_y \right] \mathbf{M} + \mu_i^T \partial_{\mathbf{s}} \mathbf{G}_i + \partial_{\mathbf{s}} \Phi \right\} \delta \mathbf{s} \, d\Gamma_i \\
&+ \int_\Omega \left\{ \left(\mathbf{A} - \mathbf{A}_v \right)^T \partial_x \psi + \left(\mathbf{B} - \mathbf{B}_v \right)^T \partial_y \psi \right\} \delta \mathbf{s} \, d\Omega \\
&- \int_\Omega \left\{ \partial_x \left(\mathbf{M}^T \lambda_x \right) - \partial_y \left(\mathbf{M}^T \lambda_y \right) + \lambda_x^T \frac{\partial \mathbf{M}}{\partial \mathbf{s}} \partial_x \mathbf{s} \right. \\
&\qquad \left. + \lambda_y^T \frac{\partial \mathbf{M}}{\partial \mathbf{s}} \partial_y \mathbf{s} \right\} \delta \mathbf{s} \, d\Omega
\end{aligned}
\tag{9}
$$

or

$$
\begin{aligned}
\delta \mathcal{L}_{\text{loc}}^{\mathbf{s}} \;=\; &- \int_{\cup \Gamma} \left\{ \psi^T \left[\left(\mathbf{A} - \mathbf{A}_v \right) n_x + \left(\mathbf{B} - \mathbf{B}_v \right) n_y \right] \right\} \delta \mathbf{s} \, d\Gamma_i \\
&- \int_{\cup \Gamma} \left\{ \left[\lambda_x^T n_x + \lambda_y^T n_y \right] \mathbf{M} + \mu_i^T \partial_{\mathbf{s}} \mathbf{G}_i + \partial_{\mathbf{s}} \Phi \right\} \delta \mathbf{s} \, d\Gamma_i \\
&+ \int_\Omega \left\{ \left(\mathbf{A} - \mathbf{A}_v \right)^T \partial_x \psi + \left(\mathbf{B} - \mathbf{B}_v \right)^T \partial_y \psi \right\} \delta \mathbf{s} \, d\Omega \\
&- \int_\Omega \left\{ \mathbf{M}^T \partial_x \lambda_x - \mathbf{M}^T \partial_y \lambda_y \right\} \delta \mathbf{s} \, d\Omega
\end{aligned}
\tag{10}
$$

where

$$
\begin{aligned}
\mathbf{A} &= \frac{\partial \mathbf{f}}{\partial \mathbf{s}} & \mathbf{B} &= \tfrac{\partial \mathbf{g}}{\partial \mathbf{s}} \\
\mathbf{A}_v &= \frac{\partial \mathbf{f}_v}{\partial \mathbf{q}} & \mathbf{B}_v &= \tfrac{\partial \mathbf{g}_v}{\partial \mathbf{q}}
\end{aligned}
\tag{11}
$$

The local variation due to $\mathbf{q}_x$ and $\mathbf{q}_y$ are, using Gauss' theorem:

$$
\begin{aligned}
\delta \mathcal{L}_{\text{loc}}^{\mathbf{q}_x} \;=\; &\int_{\cup \Gamma} \left\{ \partial_{\mathbf{q}_x} \Phi + \sum_i \mu_i^T \partial_{\mathbf{q}_x} \mathbf{G}_i - \psi^T \left(\mathbf{C} n_x + \mathbf{E} n_y \right) \right\} \delta \mathbf{q}_x \, d\Gamma \\
&+ \int_\Omega \left\{ \lambda_x + \left(\mathbf{C}^T \partial_x \psi + \mathbf{E}^T \partial_y \psi \right) \right\} \delta \mathbf{q}_x \, d\Omega
\end{aligned}
\tag{12}
$$

$$\delta \mathcal{L}_{loc}^{\mathbf{q}_y} = \int_{\cup \Gamma} \left\{ \partial_{\mathbf{q}_y} \Phi + \sum_i \mu_i^T \partial_{\mathbf{q}_y} \mathbf{G}_i \right.$$
$$\left. - \psi^T \left(\mathbf{D} n_x + \mathbf{F} n_y \right) \right\} \delta \mathbf{q}_y \, d\Gamma$$
$$+ \int_\Omega \left\{ \lambda_y + \left(\mathbf{D}^T \partial_x \psi + \mathbf{F}^T \partial_y \psi \right) \right\} \delta \mathbf{q}_y \, d\Omega$$

where

$$\mathbf{C} = \frac{\partial \mathbf{f}_v}{\partial \mathbf{q}_x} \quad \mathbf{E} = \frac{\partial \mathbf{g}_v}{\partial \mathbf{q}_x}$$

$$\mathbf{D} = \frac{\partial \mathbf{f}_v}{\partial \mathbf{q}_y} \quad \mathbf{F} = \frac{\partial \mathbf{g}_v}{\partial \mathbf{q}_y}$$

Equaling the integrals over Ω to zero in (12) and (13) gives the relations between ψ, λ_x and λ_y:

$$\lambda_x = - \left(\mathbf{C}^T \partial_x \psi + \mathbf{E}^T \partial_y \right) \quad (14)$$

$$\lambda_y = - \left(\mathbf{D}^T \partial_x \psi + \mathbf{F}^T \partial_y \right) \quad (15)$$

Equaling the integral over Ω to zero in (10) and using the two above relations gives the *adjoint equations*:

$$\left(\mathbf{A} - \mathbf{A}_v \right)^T \partial_x \psi + \left(\mathbf{B} - \mathbf{B}_v \right)^T \partial_y \psi$$
$$+ \mathbf{M}^T \left(\partial_x \tilde{\mathbf{f}}_v + \partial_y \tilde{\mathbf{g}}_v \right) = 0 \quad (16)$$

with:

$$\tilde{\mathbf{f}}_v = \left(\mathbf{C}^T \partial_x \psi + \mathbf{E}^T \partial_y \psi \right)$$

$$\tilde{\mathbf{g}}_v = \left(\mathbf{D}^T \partial_x \psi + \mathbf{F}^T \partial_y \psi \right)$$

the "adjoint viscous fluxes".

The adjoint boundary conditions are found by equaling integrals over Γ_i to zero in (10),(12) and (13):

$$\left(\mathbf{A}_n - \mathbf{A}_{vn} \right)^T \psi + \mathbf{C}_n^T \partial_x \psi + \mathbf{E}_n^T \partial_y \psi$$
$$+ \mu_i^T \partial_s \mathbf{G}_i + \partial_s \Phi = 0 \quad (17)$$

$$\partial_{\mathbf{q}_x} \Phi + \mu_i^T \partial_{\mathbf{q}_x} \mathbf{G}_i = \tilde{\mathbf{C}}_n^T \psi \quad (18)$$

$$\partial_{\mathbf{q}_y} \Phi + \mu_i^T \partial_{\mathbf{q}_y} \mathbf{G}_i = \tilde{\mathbf{D}}_n^T \psi \quad (19)$$

with:

$$\mathbf{A}_n = \mathbf{A} n_x + \mathbf{B} n_y \quad \mathbf{A}_{vn} = \mathbf{A}_v n_x + \mathbf{B}_v n_y$$
$$\mathbf{C}_n = \mathbf{C} n_x + \mathbf{D} n_y \quad \mathbf{E}_n = \mathbf{E} n_x + \mathbf{F} n_y$$
$$\tilde{\mathbf{C}}_n = \mathbf{C} n_x + \mathbf{E} n_y \quad \tilde{\mathbf{D}}_n = \mathbf{D} n_x + \mathbf{F} n_y$$

2.2 Convective variation

Let us first recall that the *convective* variation (i.e. the variation due to the movement of the domain)

of a functional of the form:

$$\mathcal{J} = \int_\Gamma f \, d\Gamma$$

is:

$$(13) \quad \delta \mathcal{J}^{conv} = \int_\Gamma \left(\vec{\nabla} f \cdot \vec{\omega} + \kappa f \right) \, d\Gamma$$

with:

$$\kappa = \frac{\partial_\sigma \vec{\omega} \cdot \vec{t}}{\|\vec{t}\|^2}$$

where:

- the boundary Γ is described by the parameter σ: $\Gamma : (x(\sigma), y(\sigma))$;

- $\vec{t}$ is the tangent vector: $\vec{t} = (d_\sigma x \; d_\sigma y)$;

- $\vec{\omega}$ is the boundary displacement due to the change of the design variables.

For a functional of the form $\mathcal{J} = \int_\Omega f \, d\Omega$, the convective variation is:

$$\delta \mathcal{J}^{conv} = \int_\Gamma f \omega_n \, d\Gamma$$

where ω_n is the projection of $\vec{\omega}$ to the normal to the surface Γ

Applying the formula above to the Lagrangian of the system (6) leads to the following convective variation (where Gauss' formula is applied):

$$\delta \mathcal{L}^{conv} = \int_{\Gamma_f} \vec{\nabla} (\mathcal{H} + \psi^T \mathbf{f}_n) \cdot \vec{\omega} + (\mathcal{H} + \psi^T \mathbf{f}_n) \kappa \, d\Gamma_f$$
$$+ \int_{\Gamma_f} \left[(\mathbf{f} - \mathbf{f}_v)^T \partial_x \psi + (\mathbf{g} - \mathbf{g}_v)^T \partial_y \psi \right] \omega_n \, d\Gamma \quad (20)$$

If the adjoint equations hold, the variation of the Lagrangian is formed by the convective variation (20) and the local variation due to the design equations (8). Considering that $\vec{\omega} = \vec{\xi} \delta \mathbf{u}$, the optimality condition is:

$$\delta \mathcal{L} = \mathcal{G} \delta \mathbf{u} \quad (21)$$

where:

$$\delta \mathcal{G} = \int_{\Gamma_f} \left[\frac{\partial \mathcal{H}_f}{\partial \mathbf{u}} + (\Phi + \psi^T \mathbf{f}_n) \kappa \right.$$
$$+ \vec{\nabla} (\Phi + \psi^T \mathbf{f}_n) \cdot \vec{\xi} + \mu_f^T \vec{\nabla} \mathbf{G} \cdot \vec{\xi}$$
$$+ \left. \left[(\mathbf{f} - \mathbf{f}_v)^T \partial_x \psi + (\mathbf{g} - \mathbf{g}_v)^T \partial_y \psi \right] \xi_n \, d\Gamma_f \right] \quad (22)$$

This equation is the *design* equation. The quantity $\mathcal{G}$ can be used as a gradient in an optimization procedure.

In summary, the optimality condition has the form of three sets of equations:

- the *state* equations (2) and boundary conditions (3);

- the *adjoint* equations (16) and boundary conditions (17,18,19);

- the *design* equations (22).

3 Application to two dimensional Navier-Stokes equations

3.1 The Navier-Stokes equations

The 2D Navier-Stokes Equations have the form:

$$\partial_x(\mathbf{f} - \mathbf{f}_v) + \partial_y(\mathbf{g} - \mathbf{g}_v) = 0 \tag{23}$$

where $\mathbf{f}, \mathbf{g}$ are the inviscid fluxes , and the viscous fluxes are given by:

- $\mathbf{f}_v = [0, \tau_{xx}, \tau_{xy}, u\tau_{xx} + v\tau_{xy} - h_x]^T$

- $\mathbf{g}_v = [0, \tau_{xy}, \tau_{yy}, u\tau_{xy} + v\tau_{yy} - h_y]^T$

The components of the stress tensor τ and the thermal flux $\vec{q}$ can be expressed in term of the first derivative of the primitive variables $\mathbf{q} \equiv [\rho, u, v, T]$:

- $\tau_{xx} = \frac{4}{3}\mu\partial_x u - \frac{2}{3}\mu\partial_y v$

- $\tau_{yy} = \frac{4}{3}\mu\partial_y v - \frac{2}{3}\mu\partial_x u$

- $\tau_{xy} = \mu\left(\partial_y u + \partial_x v\right)$

- $\vec{h} = -k\vec{\nabla}T$

with $\mu(T)$ the dynamic viscosity, and $k(T)$ the thermal conductivity.

The far-field boundary conditions are the same as for the Euler equations. The conditions for a wall are:

- the no-slip condition: $u = v = 0$

- the isothermal condition $T = T_0$ or adiabatic condition $\vec{\nabla}T \cdot \vec{n} = 0$

3.2 Optimization problem

The functional to minimize has the form:

$$\mathcal{J} = \int_{\Gamma_f} \Phi(p, \tau_w, \tau_n)d\Gamma_f \tag{24}$$

with p the pressure and τ_w the wall shear stress. The wall normal viscous stress τ_n, which is zero, has to be introduced for compatibility reasons in the adjoint boundary conditions [10][2].

3.3 Adjoint equations

The adjoint equations are given by (16). Expanding this equation leads to:

$$\mathbf{A}^T\partial_x\psi + \mathbf{B}^T\partial_y\psi - \mathbf{M}^T\left(\partial_x\tilde{\mathbf{f}}_v + \partial_y\tilde{\mathbf{g}}_v\right) = \mathbf{h}_v \tag{25}$$

with:

- $\tilde{\mathbf{f}}_v = [0, \Gamma_{xx}, \Gamma_{xy}, k\partial_x\psi_4]^T$

- $\tilde{\mathbf{g}}_v = [0, \Gamma_{xy}, \Gamma_{yy}, k\partial_y\psi_4]^T$

- $\mathbf{h}_v = \mathbf{A}_v^T\partial_x\psi + \mathbf{B}_v^T\partial_y\psi$, or in extenso:

$$
\begin{aligned}
\mathbf{h}_{v1} &= 0 \\
\mathbf{h}_{v2} &= \tau_{xx}\partial_x\psi_4 + \tau_{xy}\partial_y\psi_4 \\
\mathbf{h}_{v3} &= \tau_{xy}\partial_x\psi_4 + \tau_{yy}\partial_y\psi_4 \\
\mathbf{h}_{v4} &= k_T\left(\vec{\nabla}\psi_4 \cdot \vec{\nabla}T\right) \\
&\quad + \frac{\mu_T}{\mu}\left(\tau_{xx}\partial_x\psi_2 + \tau_{xy}\partial_x\psi_3 + \tau_{xy}\partial_y\psi_2 + \tau_{yy}\partial_y\psi_3\right)
\end{aligned}
$$

where μ_T, k_T are the derivatives of the viscosity and conductivity with respect to the temperature. The components of the adjoint tensor Γ are:

- $\Gamma_{xx} = \frac{4}{3}\mu\left(\partial_x\psi_2 + u\partial_x\psi_4\right) - \frac{2}{3}\left(\partial_y\psi_3 + v\partial_y\psi_4\right)$

- $\Gamma_{yy} = \frac{4}{3}\mu\left(\partial_y\psi_3 + v\partial_y\psi_4\right) - \frac{2}{3}\left(\partial_x\psi_2 + u\partial_x\psi_4\right)$

- $\Gamma_{xy} = \mu\left(\partial_x\psi_3 + \partial_y\psi_2 + u\partial_y\psi_4 + v\partial_x\psi_4\right)$

3.4 Adjoint boundary conditions on a wall

The adjoint boundary conditions for a non-slip wall ar computed by the equations (17,18,19). A lenghty calculation gives the following result:

- for ψ:

    - $\psi_s = \Phi_{\tau_w}$
    - $\psi_n = \Phi_{\tau_n} = -\Phi_p$
    - $\psi_4 = 0$ (isothermal BC), **or**
      $k\vec{n} \cdot \vec{\nabla}\psi_4 = \Phi_{\tau_w}\tau_w \left(1 - \frac{\mu_T}{\mu}\right)$ (adiabatic BC).

- for μ:

    - $\mu_n = -(\rho\psi_1 + \Gamma_n)$
    - $\mu_s = \tau_w\frac{\mu_T}{\mu} - \Gamma_s$
    - $\mu_3 = \Phi_{\tau_w}\tau_w \left(1 - \frac{\mu_T}{\mu}\right) - k\vec{n}\cdot\vec{\nabla}\psi_4$ (isothermal BC), **or**
      $\mu_3 = k\psi_4$ (adiabatic BC).

where (ψ_n, ψ_s) and (μ_n, μ_s) are the normal and tagential to boundary components of the vector (ψ_2, ψ_3) and (μ_1, μ_2); Γ_n and Γ_s are the normal and tangential components of the adjoint tensor Γ.

The adjoint boundary conditions also give a *compatibility condition* on the objective function Φ:

$$\Phi_{\tau_n} = -\Phi_p \qquad (26)$$

3.5 Design equation

The design equation is calculated using (22). Several terms in $\vec{\nabla}(\Phi + \psi^T \mathbf{f}_n)$ cancel each other due to adjoint boundary conditions, and the gradient is written:

$$\mathcal{G} = \int_{\Gamma_f} \frac{\partial}{\partial \mathbf{u}} \left(\Phi + p\psi_n - \tau_w\psi_s\right) d\Gamma_f$$
$$+ \int_{\Gamma_f} \left(\Phi + p\psi_n - \tau_w\psi_s\right) \kappa \, d\Gamma_f$$
$$+ \int_{\Gamma_f} p\vec{\nabla}\psi_n \cdot \vec{\xi} - \tau_w\vec{\nabla}\psi_s \cdot \vec{\xi} \, d\Gamma_f$$
$$+ \int_{\Gamma_f} \mu'_n\vec{\nabla}u_n \cdot \vec{\xi} + \mu'_s\vec{\nabla}u_s \cdot \vec{\xi} \, d\Gamma_f$$
$$+ \int_{\Gamma_f} \left(p\vec{\nabla} \cdot \vec{\psi} - \frac{\tau_w}{\mu}\Gamma_s - k\vec{\nabla}T \cdot \vec{\nabla}\psi_4\right) \xi_n \, d\Gamma_f \qquad (27)$$

with:

- $\mu'_s = \psi_4\tau_w \left(1 - \frac{\mu_T}{\mu}\right) - \Gamma_s$

- $\mu'_n = \rho H \psi_4 - \Gamma_n$

4 Discretization and numerical solution

The optimality condition is composed of three equations (state, adjoint and design). The most common method, which is the one used in this work, is to stand on the intersection of the state and adjoint surfaces, i.e. to have state and adjoint variables that satisfy state and adjoint equations, and to march to the design surface . This method is the well-known descent method, commonly used in mechanical optimization.

4.1 Navier-Stokes equations

The Navier-Stokes equations (23) are discretized by finite-volume method and solved by an implicit time marching method[9] .

Integrating the unsteady equations on a finite volume Ω_i and using the Gauss theorem yields:

$$\partial_t \int_{\Omega_i} \mathbf{s} \, d\Omega_i + \oint_\Gamma \left(\mathbf{F}(\mathbf{s}, \mathbf{n}) - \mathbf{F}_v(\mathbf{s}, \mathbf{n})\right) d\Gamma \qquad (28)$$

where $\mathbf{F} = \mathbf{f}n_x + \mathbf{g}n_y$ and $\mathbf{F}_v = \mathbf{f}_v n_x + \mathbf{g}_v n_y$ are respectively the advective and viscous fluxes through the boundary Γ of the cell.

Considering polygonal cells, and integrating the flux using an n_g-points Gauss formula, gives:

$$\partial_t \int_{\Omega_i} \mathbf{s} \, d\Omega_i + \sum_{j \in N_i} l_j \sum^{n_g} w_g \left(\tilde{\mathbf{F}}_j - \tilde{\mathbf{F}}_{vj}\right) = 0 \qquad (29)$$

where l_j is the length of the edge j, w_g the weight of the Gauss point, and N_i is the set of edges defining the control volume Ω_i. The numerical inviscid flux are computed using the Roe flux-difference splitting:

$$\tilde{\mathbf{F}} = \frac{1}{2}\left[\mathbf{F}(\mathbf{s}^L, \mathbf{n}) + \mathbf{F}(\mathbf{s}^R, \mathbf{n}) - |\tilde{\Omega}(\mathbf{s}^L, \mathbf{s}^R, \mathbf{n})| \left(\mathbf{s}^R - \mathbf{s}^L\right)\right] \qquad (30)$$

where $\tilde{\Omega}$ is the Jacobian matrix evaluated using Roe's average of s^R, s^L, the latter being the value at the right or the left of the edges extrapolated from the center of the adjacent cells. This reconstruction can be of order 0 (constant), 1 (linear) or 2 (quadratic), and may imply complex detector-limiter to deal with flow discontinuities (shocks or slip lines).

A centered discretization is used to discretize the viscous terms of the Navier-Stokes equations. The viscous flux is evaluated at one point located at the middle edge.

Once the spatial part is discretized, the equation is integrated in time with a fully implicit Newton-like method. The following non-linear equation is solved at each time step:

$$\mathcal{F}(s^{n+1}, s^n) = \frac{s^{n+1} - s^n}{\Delta t} + \mathcal{R}(s^{n+1}) = 0 \quad (31)$$

If this equation is linearized, the following linear system is obtained:

$$\left(\frac{\mathbf{I}}{\Delta t} + \mathcal{J} \right) s^{n+1} = -\mathcal{F}(s^n, s^n) \quad (32)$$

with $\mathcal{J} = \frac{\partial \mathcal{R}}{\partial s}$, the jacobian matrix. This system is solved by a 1-step Newton method using a ILU0 preconditioned GMRES Algorithm[14].

4.2   Adjoint equations

The continuous adjoint equations (16) are discretized with the same finite-volume method as the Euler equations: integrating (16) over a cell i gives (using Gauss theorem):

$$\partial_t \int_{\Omega_i} \psi \, d\Omega_i + \int_{\Omega_i} \mathbf{A}^T \partial_x \psi + \mathbf{B}^T \partial_y \psi \, d\Omega_i$$

$$+ \int_{\Omega_i} \partial_x \tilde{\mathbf{f}} + \partial_y \tilde{\mathbf{g}} \, d\Gamma = \int_{\Omega_i} \mathbf{h} \, d\Omega_i \quad (33)$$

or, using cell averaged values and applying Gauss theorem on integrals containing $\partial_x \psi, \partial_y \psi$,

$$\partial_t \psi_i + \sum_{j \in N_i} l_j \sum_{}^{n_g} w_g \left(\tilde{\mathbf{G}}_{ij} + \mathbf{M}_i^T \tilde{\mathbf{F}}_{vn} \left(\psi_{ij} \right) \right)$$

$$= \mathbf{A}_{vn}^T \sum_{j \in N_i} l_j \sum_{}^{n_g} w_g \psi_{ij} \quad (34)$$

where the numerical adjoint advective flux $\tilde{\mathbf{G}}_{ij}$ is computed with a Roe-like flux splitting formula:

$$\tilde{\mathbf{G}}_{ij} = \frac{1}{2} \left[\mathbf{A}_n^T(\mathbf{s}_i) \left(\psi^L + \psi^R \right) - \nu \left(\psi^R - \psi^L \right) \right] \quad (35)$$

with $\mathbf{A}_n = \mathbf{A} n_x + \mathbf{B} n_y$ and ν an artificial dissipation factor. This dissipation factor is mandatory for the convergence of adjoint equations used in transsonic flows problems. It will be shown that in such problems, the discontinuous state variables imply Dirac peaks in the adjoint solution. A lot of dissipation is then needed to avoid divergence problems.

As for the state variables, the adjoint variables on the edges are extrapolated from the nodal values using a constant, linear, or quadratic reconstruction. The adjoint viscous flux $\tilde{\mathbf{F}}_v$ is evaluated in a similar manner as the viscous flux of the Navier-Stokes equations.

Time derivatives are added to the adjoint equations to obtain a time dependent system of equations, which is then solved iteratively by using the same method as for the Navier-Stokes equations, i.e. fully-implicit Newton-like integration.

4.3   Optimization procedure

The optimization procedure presented here consists in transforming the highly non-linear shape optimization problem:

$$\begin{aligned} \min \quad & f(\mathbf{x}) \\ \text{with} \quad & c_i(\mathbf{x}) \le \bar{c}_i \quad \text{for } i = 1 \cdots n_c \end{aligned} \quad (36)$$

where the function and constraints are not explicitely known into a sequence of simpler (explicit) problems. At each iteration k, a subproblem P^k :

$$\begin{aligned} \min \quad & \tilde{f}^{(k)}(\mathbf{x}) \\ \text{with} \quad & \tilde{c}_i^{(k)}(\mathbf{x}) \le \bar{c}_i \quad \text{for } i = 1 \cdots n_c \end{aligned} \quad (37)$$

is constructed and solved by the CONLIN procedure developed at the University of Liège[6].

In this procedure, the key point consists in finding a good modelling of the objective function and constraints. Two different approaches were tested.

The first method is called "Method of Moving Asymptotes" (MMA)[11]. At iteration k, a function f is approximated by:

$$\tilde{f}^{(k)}(\mathbf{x}) = \sum_{i=1}^{n} \frac{p_i}{U_i^{(k)} - x_i} + \frac{q_i}{x_i - L_i^{(k)}} + r \quad (38)$$

The parameters r, p_i and q_i are adjusted such that :

$$\tilde{f}(\mathbf{x}^{(k)}) = f(\mathbf{x}^{(k)})$$

$$\left.\frac{\partial \tilde{f}}{\partial x_i}\right|_{x^{(k)}} = \left.\frac{\partial f}{\partial x_i}\right|_{x^{(k)}}$$

In addition p_i is set to zero when $\partial_{x_i} f < 0$ at $\mathbf{x}^{(k)}$ and q_i is set to zero when $\partial_{x_i} f > 0$, such that $\tilde{f}$ is a monotoneous increasing (resp. decreasing) function of x_i:

$$p_i^{(k)} = \max\left[0, \left(U_i^{(k)} - x_i^{(k)}\right)^2 \left.\frac{\partial f}{\partial x_i}\right|_{x^{(k)}}\right]$$

$$q_i^{(k)} = \min\left[0, \left(x_i^{(k)} - L_i^{(k)}\right)^2 \left.\frac{\partial f}{\partial x_i}\right|_{x^{(k)}}\right]$$

The parameters $U_i^{(k)}$ and $L_i^{(k)}$ are the asymptotes which are allowed to move from one iteration to another, in order to narrow or broaden the feasible space

The second method of approximation is the "Diagonal Quadratic" method [4]. At iteration k, a function f is modelled by:

$$\tilde{f}^{(k)}(\mathbf{x}) = f(\mathbf{x}^{(k)}) + \sum_{i=1}^{n} b_i(x_i - x_i^{(k)}) + \frac{1}{2} a_i \left(x_i - x_i^{(k)}\right)^2 \tag{39}$$

with:

$$b_i = \left.\frac{\partial f}{\partial x_i}\right|_{x^{(k)}}$$

$$a_i = \left.\frac{\partial^2 f}{\partial x_i^2}\right|_{x^{(k)}}$$

As the second derivatives of the function is usually not available, the term a_i has to be approximated. We have employed a rank-1 update procedure for the coefficients a_i:

$$a_i^{(k+1)} = a_i^{(k)} + \alpha \frac{v_i^2}{z} \tag{40}$$

with $\mathbf{v} = \vec{\nabla} f^{(k+1)} - \vec{\nabla} f^{(k)}$, $z = \mathbf{v}^T \left(\mathbf{x}^{(k+1)} - \mathbf{x}^{(k)}\right)$ and α a relaxation factor:

$$\alpha = \min\left(1, \frac{\sqrt{\sum_i a_i^2}}{z \|\mathbf{v}\|}\right)$$

5 Geometry considerations

5.1 Airfoil parametrization

The profile is defined by the formula:

$$y(x) = y_c(x) \pm y_t(x) \tag{41}$$

where y_t and y_c are the thickness and camber distributions defined as follow (see figures 1(a) and 1(b)):

- the thickness distribution is modelled by two Bezier curves (one curve of degree 3 on the front part and one of degree 2 on the aft part); the design variables are the position and value of maximum thickness, the leading edge radius and the trailing edge wedge angle.

- the camber distribution is modelled by two Bezier curves of order 2; the design variables are the position and value of maximum camber, and the first derivative at leading and trailing edges.

The airfoil section is then defined by eight parameters.

5.2 Mesh movement

During the optimization cycle, the geometry is modified and the computational mesh must be adapted. A straightforward method consists in generating a new mesh at each iteration, but this requires a fast and robust mesh generation technique. In the method used here, which is called "spring analogy", the vertices of the mesh are moved, without changing the connectivity nor the number of mesh points. The mesh is considered as a spring network that reacts to a perturbation of the boundary by adjusting the vertex position in such a way that the deformation energy is minimal. This leads to a system of non-linear equations that are solved by a Newton algorithm.

The spring analogy method is well suited for unstructured meshes for inviscid flows but needs some modifications to be used on hybrid meshes for viscous flows, because of the high aspect ratio of the cells in the boundary layer that can produce overlapping or highly distorted meshes. A vertex i near
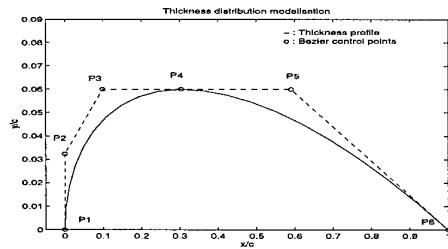
(a) Thickness distribution
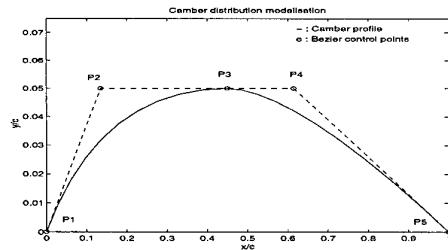
(b) Camber distribution

Figure 1: Airfoil modelisation

the moving boundary (in the boundary layer) is moved according to the formula:

$$\mathbf{x}_i^{\mathrm{new}} - \mathbf{x}_i^{\mathrm{old}} = \alpha(d)\left(\mathbf{x}_j^{\mathrm{new}} - \mathbf{x}_j^{\mathrm{old}}\right) \qquad (42)$$

where j is the nearest point on the boundary with respect to i, and $\alpha(d) \in [0\ 1]$ is a decreasing function of the distance to the boundary d, and vanishes for $d > d_{\mathrm{cut}}$. This procedure is applied to all the vertices for which $d < d_{\mathrm{cut}}$, and the remaining vertices are updated with the spring analogy.

6 Results

6.1 Inviscid transsonic Lift/Drag Ratio optimization

The test case consists in maximizing the lift to drag ratio at M=0.8 and an incidence of 2 degrees, with a lower bound to the maximumthickness of the airfoil (12% of chord). In such a configuration, there is a shock on the lee-side of the airfoil. This discontinuity in the state variable induces Dirac peaks in the

adjoint solution The first adjoint variable obtained at the first iteration step is shown on figure 2.
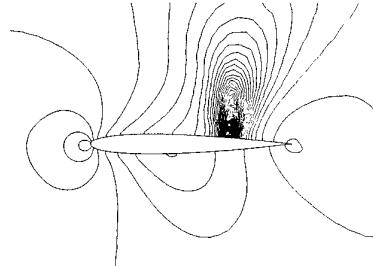
(a) ψ_1 field
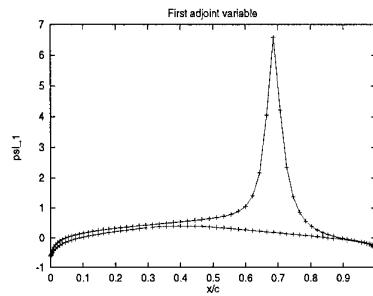
(b) ψ_1 on airfoil

Figure 2: First adjoint variable

This peak is smoothed by the numerical computation which involves a numerical dissipation scheme. Attempts to use a less diffusive flux (i.e. a Roe-type flux difference splitting) may lead to a failure of convergence.

This type of discontinuity is inherent to the problem, because the shock in the flow solution is not differentiable. Such Dirac discontinuities can be found also when using the flow sensitivity derivatives to compute the gradient[8].

The problem of minimizing the ratio $\frac{C_d}{C_l}$ is not obvious because the cost function cannot be written in the form (24), although C_l and C_d have this form.

The gradient of $f = \frac{C_d}{C_l}$ is

$$\nabla f = \frac{1}{C_l}\left(\nabla C_d - f\nabla C_l\right) \qquad (43)$$

One straightforward approach is to compute *two* adjoint problems, with functions C_l and C_d and to put their gradients in the formula above. The method used here consists in using the functional $\hat{f} = \frac{1}{C_{l0}}(C_d - f_0 C_l)$, defined at the current design point α_0, for the computation of the gradient. This function has the same gradient as the initial cost function at the current design point, and has the form (24), because it is linear in C_l and C_d. Its gradient only requires *one* adjoint computation.

After twenty iterations, the lift to drag ratio has increased from $2.03 \cdot 10^{-2}$ to 10.65. The final airfoil is slightly thinner than initial airfoil, with camber and a sharper trailing edge, see figure 3. The lee-side shock has slightly increased and moved backward (fig. 3).
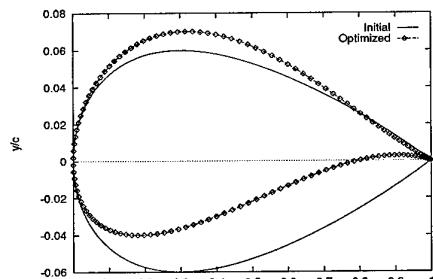
(a) Shape modification
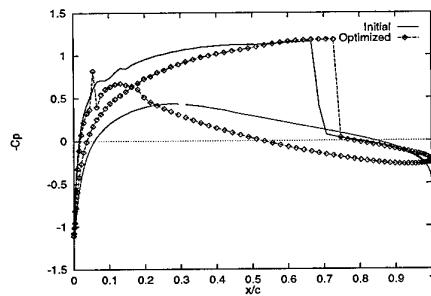
(b) Cp comparison

Figure 3: Shape and Cp comparison

6.2 Lift maximization

The first test case is a lift coefficient maximization of an airfoil in subsonic viscous flow (Mach=0.5, Re=100.000). The initial airfoil is a slightly cambered NACA0012, and an upper bound on the drag coefficient is imposed. This problem was solved with different approximations for the objective and the constraint (in the text below, MMA/QUA stands for "Method of Moving asymptots for the objective and diagonal quadratic method for the constraint", for example). Results are presented in table 1 and 2.

Method	C_L	C_D	$\frac{C_L}{C_D}$
Initial	$1.778 \cdot 10^{-1}$	$3.024 \cdot 10^{-2}$	5.88
MMA/MMA	$2.399 \cdot 10^{-1}$	$2.771 \cdot 10^{-2}$	8.66
MMA/QUA	$2.449 \cdot 10^{-1}$	$2.774 \cdot 10^{-2}$	8.83
QUA/QUA	$2.273 \cdot 10^{-1}$	$2.945 \cdot 10^{-2}$	7.72

Table 1: Aerodynamic coefficients

Method	ΔC_L	ΔC_D	$\Delta \frac{C_L}{C_D}$
MMA/MMA	+34.9%	−8.30%	+47.2%
MMA/QUA	+37.7%	−8.30%	+50.1%
QUA/QUA	+27.8%	−2.60%	+31.2%

Table 2: Performance of the different approximation techniques

It can be noticed that the all-MMA or MMA/QUA strategies work better than the all-QUA strategy. That can be due to two facts:

- the MMA approximation is well suited for monotonically decreasing or increasing functions (and that can be the case for C_L);

- the QUA method relies on the quasi-Newton approximation of the Hessian matrix, which can be quite inaccurate, especially during the first iterations.

Figure 4 shows the initial and optimized shapes for MMA/QUA and QUA/QUA computations (MMA/MMA gives almost the same airfoil as MMA/QUA).

Figure 5 shows the Mach field around the optimized airfoil (MMA/QUA).

The optimized airfoil is cambered (1.1%) to increase lift, with the position of maximum camber displaced
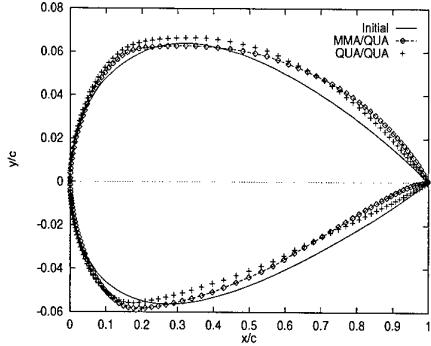
Figure 4: Initial and optimized shapes

Figure 6: Skin friction coefficient on initial and optimized airfoils

Figure 5: Mach field around optimized airfoil (Mach max.=0.89253)

toward aft (at 75% of chord), in such a way that the recirculation bubble is smaller (see figure 6), thus leading to a decrease in the viscous drag coefficient.

6.3 Inverse design

Inverse design problems can be treated as optimization problems, the function to optimize being the least square distance between a target pressure field and the actual pressure. Although optimization techniques are much more expensive in term of calculation time, they always succeed in finding an optimum value where inverse design techniques can fail. Inverse design problems are also useful when testing algorithms, because the optimal solution is known.

In the present test case, the pressure of an airfoil (Mach=0.5, Re=100.000) has to be matched to the pressure field of an RAE2822 airfoil in the same flow conditions. The initial airfoil is the same NACA0012 as in the previous test case. The optimization technique used is MMA.

As can be seen on figure 7, the final solution is very close to the target, in term of shape and pressure distribution.

The residual history gives valuables observations of the behaviour of the MMA algorithm: the initial oscillations of the objective functions, due to oscillations of the variable describing camber, are progressively damped by bringing the moving asymptots closer to each other. However this leads to a non-optimal solution; this difficulty was overcome by restarting the algorithm after iteration 13 (see figure 8).

In the previous calculation, the upper and lower bound on the design variables are chosen such that the optimal solution lies on the boundary of the design space. In such a case, the MMA approxiamtion is very efficient, because the objective function is generally a monotonous function. When the solution is inside the design space, MMA fails to find the real optimum because it cannot model functions with one (or more) extremum. Figure 9 shows the result of the same test case, with a larger design space: the computed solution lies on the design space boundary and is not the real optimum.
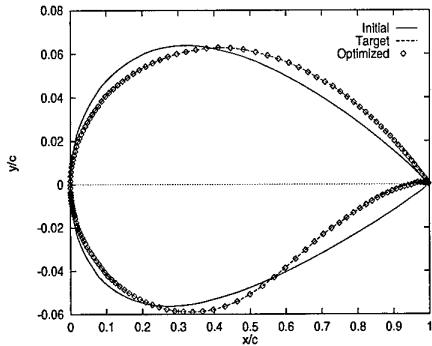
(a) Shape comparison
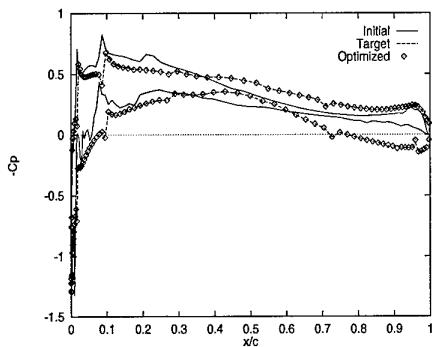
(b) Pressure coefficient comparison

Figure 7: Initial, target and optimized shape and Cp comparison

7 Conclusions and prospects

In this paper, we have showed that the adjoint method can give accurate gradient to aerodynamic coefficients. This method, together with fast flow analysis algorithms and a robust constrained optimization procedure, is mandatory for the resolution of aerodynamic shape optimization problems in 2D on small workstations (all the calculations were done on a single CPU HP-C160 workstation).

Further work is needed on the resolution of the adjoint equations, especially to derive the adjoint equations for turbulent flows. Another topic of interest is the study of approximations of the functions; a hybrid method involving both MMA and QUA could be very efficient[12] if a good approx-
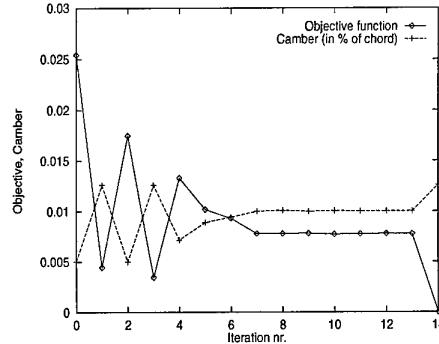
Figure 8: History of objective function and camber

imation of the Hessian matrices could be found. Further studies on Hessian matrices[3] could thus be valuable.

8 Acknowledgment

References

[1] J. Reuther A. Jameson. Control Theory Based Airfoil Design using the Euler Equations. AIAA Report 94-4272-CP, American Institute for Aeronautics and Astronautics, 1994.

[2] M.D. Salas E. Arian. Admitting the Inadmissible: Adjoint Formulation for Incomplete Cost Functionals in Aerodynamic Optimization. ICASE Report 97-69, NASA Langley Research Center, Hampton, Virginia, 1997.

[3] S. Ta'asan E. Arian. Analysis of the Hessian for Aerodynamic Optimization: Inviscid Flow. ICASE Report 96-28, NASA Langley Research Center, Hampton, Virginia, 1996.

[4] C. Fleury. Efficient approximation concepts using second order information. In *AIAA Structural Dynamics and Materials Conference, Williamsburg, USA*, April 18 – 20 1988.

[5] O. Baysal G.W. Burgreen. Three-Dimensional Aerodynamic Shape Optimization Using Dis-

(a) Shape comparison

(b) Pressure coefficient comparison
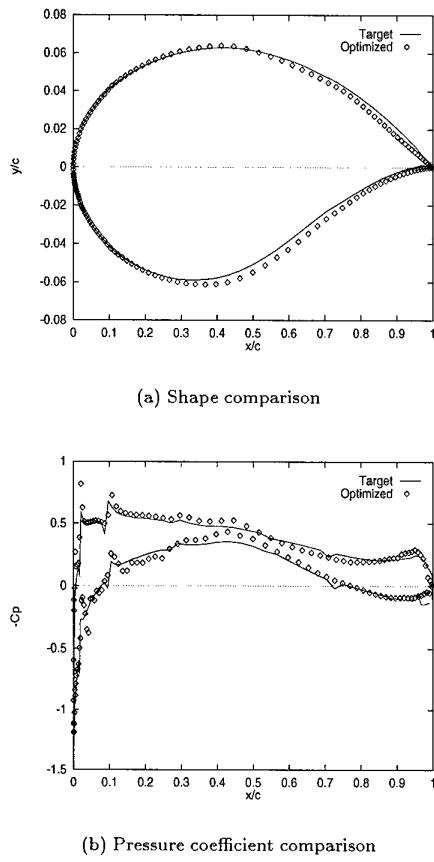
Figure 9: Target and final shape and Cp when widening the design space

crete Sensitivity Analysis. *AIAA Journal*, 34(9), September 1996.

[6] L.A. Schmit H. Smaoui, C. Fleury. Advances in Dual Algorithms and Convex Approximation Methods. In *AIAA/ASME/ASCE/AHS 29th Structures, Structural Dynamics and Materials Conference, Williamsburg, VI*, 1988.

[7] G.W. Burgreen J.C. Newmann III, A.C. Taylor. An Unstrucured Grid Approach to Sensitivity Analysis and Shape Optimization Using the Euler Equations. In *12th AIAA Computational Fluid Dynamics Conference, San Diego, California*, June 1995.

[8] M.D. Gunzburger J.R. Appel. Difficulties in Sensitivity Calculations for Flows with Discontinuities. *AIAA Journal*, 35(5), May 1997.

[9] J.A. Essers P. Rogiest M. Delanaye, P. Geuzaine. A Second Order Finite Vlume Scheme solving Euler and Navier-Stokes Equations on Unstructured Adaptive Grids with an Implicit Acceleration Procedure. In *77th AGARD FDP Symposium on Progress and Challenges in CFD methods and algorithms, Sevilla, Spain*, 1995.

[10] B. Soemarwoto. The Variational Method for Aerodynamic Optimization Using the Navier-Stokes Equations. ICASE Report 97-71, NASA Langley Research Center, Hampton, Virginia, 1997.

[11] K. Svanberg. The method of moving asymptotes – a new method for structural optimization. *International Journal for Numerical Methods in Engineering*, 24:359 – 373, 1987.

[12] K. Svanberg. Some second order methods for structural optimization. In *Optimization of Large Structural Systems, Vol. I*, pages 567 – 578. Kluwer Academic Publishers, 1993.

[13] V. Venkatakrishnan W. Kyle Anderson. Aerodynamic Shape Optimization on Unstructured Grids with a Continuous Adjoint Formulation. In *35th Aerospace Sciences Meeting and Exhibit, Reno, NV*, January 97.

[14] M. Shultz Y. Saad. G.M.R.E.S.: a generalized minimal residual algorithm for solving non-symmetric linear system. *SIAM J. Sci. Stat. Comp.*, 7, 1986.

A System for the Aerodynamic Optimization of Three-Dimensional Configurations

M. Orlowski, W. Tang

Institute of Design Aerodynamics, German Aerospace Center (DLR)
Lilienthalplatz 7, D-38108 Braunschweig, Germany

Summary

The paper presents a system for the aerodynamic optimization of three-dimensional configurations. This system is based on the repeated calculation of the flowfield around three-dimensional geometries by solving the Euler/Navier-Stokes equations. The basic structure of the system and the incoperated modules are described. Under the same conditions the system must provide the same solutions of classic aerodynamic optimization problems as given in literature. So the function of the system is checked with the Rhombus airfoil and the Sears-Haack body. The potential of the system is demonstrated with current aerodynamic optimization problems.

List of Symbols

A	area
C_D	drag coefficient
C_L	lift coefficient
c	chord length
D	drag
d	diameter
d_{CB}	diameter of capsule base
F_{CS}	area of capsule surface
G	objective function
L	lift
l	length
l_{REF}	reference length ($= 10$ m)
M	Mach number
r_{CN}	radius of capsule nose
S	parameter
$\overline{S}$	parameter set
$\Delta\overline{S}$	stepsize
U	volume utility ($= V/F^{3/2}$)
V	volume
α	angle of attack
δ	maximum thickness

Indices

B	body
C	capsule
SSB	SCT body
SSC	SCT cone
SSW	SCT wing
∞	freestream

1 Introduction

Future military and civilian aerospace vehicles must fulfil extensive and partially conflicting requirements. Technical aspects like flying characteristics or stealth capabilities have to be considered as well as economical aspects like life-cycle costs or fleet compatibilities and ecological aspects like noxious emissions or noise regulations. In order to fulfil these requirements the close interaction of all involved disciplines and the optimal use of all technical potentialities is necessary. Simultaneously, design cycle times have to be reduced.

Size and complexity of this task lead to growing importance of numerical design and optimization methods. In general, these methods can be divided based on their orientation into multidisciplinary methods and disciplinary methods. Multidisciplinary methods are used mainly in the predesign stage for a rough assessment of the vehicle characteristics and a preliminary interaction of the involved disciplines. An overview of multidisciplinary design and optimization methods is given in Ref. 1. Disciplinary methods are used mainly in the design stage for an exact calculation of the vehicle characteristics and their improvement. An overview of disciplinary design and optimization methods is given in Ref. 2.

Most aerodynamic design and optimization methods are still based on linear theory. They cannot or cannot exactly model non-linear phenomenons like separations or vortices. Hence, results represent only approximations of real optima. In order to improve these approximations the Institute of Design Aerodynamics of the German Aerospace Center (DLR) is working on new methods[3-5] based on non-linear theory, i.e. the solution of the Euler/Navier-Stokes equations.

Section 2 deals with the fundamentals of such an aerodynamic optimization method. The basic structure of the computational system and the incoperated modules are described. Tests of the system make up section 3. Its function is checked with solutions of classic aerodynamic optimization problems: the Rhombus airfoil and the Sears-Haack body. Section 4 presents applications of the system. Aerodynamic optimizations of a biconic re-entry capsule, an SCT wing as well as an SCT wing/body configuration and their results are presented.

2 Aerodynamic Optimization System

The Aerodynamic Optimization System is based on the repeated calculation of flowfields around three-dimensional geometries. A mathematical algorithm gives changes of the respective geometry according to an optimization strategy. These changes are carried out, the spatial mesh is created and the flowfield computed. The changes are characterized by the resulting aerodynamic coefficients and judged with an objective function. Finally, the mathematical algorithm determines the changes of the respective

geometry, which fulfil the demands formulated through the objective function best.

2.1 Basic Structure

The basic structure of the Aerodynamic Optimization System and the course of events is depicted in Fig. 1. Input parameters are start values for the geometric and aerodynamic parameters, which are included in the optimization process, constraints limiting their variations, start values for the stepsizes, which are used to determine gradients, and the objective function. These parameters have influence in the whole system. Further input parameters are values for the geometric and aerodynamic parameters, which are not included in the optimization process, and instructions for the generation of the surface mesh, the generation of the spatial mesh and the calculation of the flowfield. These parameters have influence only in certain modules.

At the beginning a geometry corresponding to the geometric parameters and a surface mesh are created. For that the instructions for the generation of the surface mesh prescribe the number of points in axial and spanwise direction, the location of points near edges and corners, the distribution of points near shocks and separations etc. Based on the surface mesh a spatial mesh is created. The instructions for the generation of the spatial mesh prescribe the number of points normal to the surface, the location of the farfield, the distribution of points etc.

Then the flowfield around the geometry is computed and the aerodynamic coefficients are determined. A numerical method is used to solve the Euler/Navier-Stokes equations at every point of the spatial mesh. The instructions for the calculation of the flowfield control this method. They give the number of iteration cycles, the damping of the method etc.

In the end the aerodynamic coefficients are put into the objective function and the function is analyzed. A decision on the continuation of the optimization process is made. In case the gradients of the objective function do indicate the possibility of improvements the process is continued. The parameters, which are included in the optimization process, are changed by a mathematical algorithm according to an optimization strategy. The constraints are checked and if necessary corrections are carried out. The described steps start again, i.e. a geometry corresponding to the changed geometric parameters is generated etc. In case the gradients of the objective function do not indicate the possibility of improvements, even after changes of the stepsizes, which are used to determine the gradients, the process is stopped. The geometric parameters and the aerodynamic coefficients are stored.

So the aerodynamic optimization system is a repeated cycle of four steps: geometry generation, mesh generation, flowfield calculation and optimization. These steps are carried out within the system by four independent modules. Their communication is completely based on data files. Here advantages regarding easy maintenance and development predominate disadvantages regarding higher computational effort. The four modules are described in the following sections.

2.2 Geometry Generator

The module for the geometry generation creates, as mentioned in section 2.1, a geometry corresponding to the geometric parameters and a surface mesh. The number of parameters, which are included in the optimization process, effects directly the number of optimization cycles and so the computational effort. Hence, the module for the geometry generation should be able to define a huge variety of configurations and extensive variations of these configurations with a minimum of geometric parameters. The available CAD systems as well as *MegaCads*, the module for the mesh generation, cannot guarantee this. Because of this a new code, *MegaGeo*, has been developed and integrated.

MegaGeo composes three-dimensional configurations out of two-dimensional curves describing elements of the configurations. Figure 2 illustrates two-dimensional curves describing an airfoil. Points at the leading and trailing edge divide the airfoil into upper and lower side. Further points divide upper and lower side into segments. The number and position of these points depend on the complexity of the airfoil and the expected flexibility of the parameterization. The order of the segments determines start and end points. A set of curve functions introduced by H. Sobieczky[6] is used to define the curve in the segments. In principle all functions are controlled by four parameters, which can be associated with the slope and curvature at the start and end points. But some functions have given parameters because of their mathematical background or constraints. The key number determing upper or lower side, the coordinates of the start point, the key number determing the curve function and the parameters of the function are the necessary information for a segment.

MegaGeo distinguishes two major elements of three-dimensional configurations: Wing and body. The elements forming a wing are shown in Fig. 3. A certain number of airfoils, the leading edge, the trailing edge and the twist axis, all defined by curve functions, together with information about the transition between the airfoils and their twist build up the basic structure. All airfoils are given in a normalized way and the leading and trailing edge are used to determine their magnitude. The elements forming a body are shown in Fig. 4. A certain number of body sections, the water line and the body axis, all defined by curve functions, together with information about the transition between the sections build up the basic structure. All body sections are given in a normalized way and the water line is used to determine their magnitude.

The surface of a wing, a body or a wing/body configuration develops with the surface mesh. For that a distribution of planes $x = const.$ is given. In these planes the intersection between wing and body results from a calculation. Also in these planes the number of mesh points as well as their distribution on wing and body, defined by curve functions too, is given. So the complete geometry and surface mesh generation is based on parameters controlling curve functions and can be carried out as an automatic generation. The instructions for the generation of the geometry and the surface mesh are more or less equivalent to these parameters.

2.3 Mesh Generator

The module for the mesh generation creates, as mentioned in section 2.1, a spatial mesh based on the surface mesh created by the module for the geometry generation. It has to guarantee an automatic generation of high quality within the optimization process. A huge variety of configurations and extensive variations of these configurations should not call this into question. Furthermore, it has to guarantee an automatic generation with minimum computational effort. The DLR code *MegaCads*[7] fulfils this and has been integrated.

MegaCads enables the definition of structured multi-block meshes around complex three-dimensional configurations using a parametric approach. Basic techniques for the generation of ge-

ometries and different algorithms for the determination of surface/surface intersections are integrated. Efficient algebraic methods for two and three-dimensional mesh generation are available. In order to smooth the algebraic meshes elliptic algorithms can be used allowing different controls for the point distribution at boundaries. Support features for multi-grid and chimera techniques are developed. The complete interactive mesh generation is stored in a protocol file using a simple script language and can be repeated for similar configurations or within an optimization process as an automatic generation. The instructions for the generation of the spatial mesh are more or less equivalent to this protocol file.

2.4 Flow Solver

The module for the flowfield calculation computes, as mentioned in section 2.1, the flowfield around the geometry and determines the aerodynamic coefficients. The flowfield calculation solving the Euler/Navier-Stokes equations has by far the greatest share of the computational effort. Hence, the module should be able to carry out one calculation with minimum computational effort as well as high robustness and accuracy. The DLR code *CEVCATS* and its successor *FLOWer*[8] fulfil this and have been integrated.

CEVCATS and *FLOWer* solve the Euler/Navier-Stokes equations using a second-order accurate finite-volume method. The spatial discretization is done by means of a cell-vertex scheme and central differences. In order to damp numerical oscillations first and second-order dissipative terms are added to the governing equations according to A. Jameson[9]. The integration in time of the resulting system of ordinary differential equations is carried out by means of an explicit five-stage Runge-Kutta scheme. To accelerate convergence local time stepping, residual smoothing and multi-grid algorithms are used. The instructions for the calculation of the flowfield are more or less equivalent to the input file of *CEVCTAS* or *FLOWer*.

2.5 Optimization Algorithm

The module for the optimization analyses, as mentioned in section 2.1, the objective function, makes a decision on the continuation of the optimization process, changes the parameters and checks the constraints. It has to guarantee a certain determination of global extreme. Complex structures of the parameter space or numerical fluctuations of the objective function should not call this into question. Furthermore, it has to guarantee a determination with minimum computational effort. The algorithm *EXTREM* developed by H.G. Jakob[10] fulfils this and has been integrated.

EXTREM determines the changes of the geometry, which fulfil the demands formulated through the objective function best, applying finite differences and parabolic interpolation. Figure 5 sketches the principle of the optimization strategy and the function of the mathematical algorithm. The start point of the optimization process, the parameter set $\overline{S}_0$, and the primary search direction $\Delta\overline{S}$ are given as input data. Search steps $\overline{S}_1 = \overline{S}_0 - \Delta\overline{S}$ and $\overline{S}_2 = \overline{S}_0 + \Delta\overline{S}$ lead to the parameter sets $\overline{S}_1$ and $\overline{S}_2$. Values of the objective function at the parameter sets $\overline{S}_0$, $\overline{S}_1$ and $\overline{S}_2$ are used for the assessment of the extreme in the primary search direction by means of parabolic extrapolation. The parameter set $\overline{S}_3$ results. At $\overline{S}_3$ a secondary search direction perpendicular to the primary direction is defined with an orthogonalization procedure. Further search steps lead to the parameter sets $\overline{S}_4$ and $\overline{S}_5$. The assessment of the extreme in secondary search direction by means of parabolic extrapolation leads to the parameter set $\overline{S}_6$. For a parameter space created by n parameters (n-1) secondary search directions are defined. Hence, for a parameter space created by 2 parameters a so called step is completed with the parameter set $\overline{S}_6$. After such a step a new primary search direction passing through the last parameter set and the last parameter set of the previous step (or the start point) is defined. The described procedure starts again, i.e. search steps lead to new parameter sets etc. It continues until the gradients of the objective function do not indicate the possibility of improvements, even after changes of the stepsizes.

EXTREM considers constraints of the parameters, which limit the variations, depending on the occurring violation. In case the violation of a constraint is caused by a search step, the step is neglected and the new parameter set results from a step with half of the previous size in the opposite direction. In case the violation of a constraint is caused by a parabolic extrapolation, the step is also neglected and the new parameter set results from a step with a quarter of the calculated size in the search direction. Of course EXTREM checks the constraints with the new parameter sets as well and carries out again necessary corrections in the same way.

3 Test of the Optimization System

Several solutions of classic aerodynamic optimization problems are documented in literature, solutions based on linear theory, extended linear theory or exact theory. Under the same conditions the aerodynamic optimization system must provide these solutions as well. Even under different conditions regarding the flowfield calculation the system must provide similar solutions. This has been checked with two classic aerodynamic optimization problems.

3.1 Rhombus Airfoil

The first problem is the symmetric airfoil of given length and thickness, which has minimum drag in supersonic flow. Linear theory[11] results in an airfoil with straight flanks before and behind the maximum thickness, a so-called rhombus airfoil. The maximum thickness of this airfoil lies at $x/c = 0.5$, i.e. exactly at half chord length. It depends not on the Mach number. The drag coefficient amounts to $C_D = 0.00208$ for Mach number $M_\infty = 2.0$ and $C_D = 0.00321$ for Mach number $M_\infty = 1.5$ assuming a relative thickness of $\delta/c = 0.03$. Extended linear and exact theory[12] result also in an airfoil with straight flanks before and behind the maximum thickness. But the maximum thickness lies not exactly at half chord length. It depends on the Mach number and lies at $x/c = 0.5191$ for Mach number $M_\infty = 2.0$ and at $x/c = 0.5192$ for Mach number $M_\infty = 1.5$, i.e. behind half chord length. The maximum thickness moves closer to the trailing edge with increasing Mach number. The drag coefficient amounts to $C_D = 0.00205$ for Mach number $M_\infty = 2.0$ and $C_D = 0.00317$ for Mach number $M_\infty = 1.5$ assuming a relative thickness of $\delta/c = 0.03$.

Several optimizations of a symmetric airfoil with respect to minimum drag in supersonic flow and based on solutions of the Euler equations have been carried out. They included five geometric parameters sketched in Fig. 6: the position of the maximum thickness in x-direction, the slope of the flank before the maximum thickness at the leading edge and at the maximum thickness as well as the slope of the flank behind the maximum thickness at the maximum thickness and at the trailing edge. Figures 7 and 8

depict initial and resulting airfoils for Mach number $M_\infty = 2.0$ using different start values for the parameters and stepsizes. All optimizations lead to the same airfoil. Hence, the resulting airfoil is not a coincidence. An effect of the start values could not be found. The optimizations lead to an airfoil agreeing very good with the solution based on extended linear and exact theory. The maximum thickness lies at $x/c = 0.5157$ compared to $x/c = 0.5192$ based on extended linear and exact theory. Difference between both values is about 1%. The drag coefficient amounts to $C_D = 0.00209$ compared to $C_D = 0.00205$ based on extended linear and exact theory. Difference is about 2%.

Figure 9 depicts initial and resulting airfoils for Mach number $M_\infty = 1.5$ Again, the optimization leads to an airfoil agreeing very good with the solution based on extended linear and exact theory. The maximum thickness lies at $x/c = 0.5162$ compared to $x/c = 0.5192$ based on extended linear and exact theory. Difference between both values is about 0.5%. The drag coefficient amounts to $C_D = 0.00322$ compared to $C_D = 0.00317$ based on extended linear and exact theory. Difference is about 2%.

Besides the effect of start values for the parameters and stepsizes the effect of accuracy as well as mesh density has been investigated. As mentioned in section 2.1, a numerical method is used to solve the Euler/Navier-Stokes equations at every point of the spatial mesh and to determine the aerodynamic coefficients. The accuracy, where this method stops, can be varied. Resulting airfoils for Mach number $M_\infty = 2.0$ determining the aerodynamic coefficients with different accuracies are shown in Fig. 10. Up to 10^{-4} an effect of the accuracy cannot be found. Figure 11 plots the computational effort on a NEC SX4 for the optimizations with different accuracies. Here an effect can be found. In accordance to expectations lower accuracies lead to lower computational effort. A spatial mesh is necessary solve the Euler equations and to determine the aerodynamic coefficients. The number of mesh points can be varied. Resulting airfoils for Mach number $M_\infty = 2.0$ using spatial meshes of different densities are shown in Fig. 12. Up to 1275 points only a small effect of the density can be found. Figure 13 plots the computational effort for the optimizations with different mesh densities. Again, in accordance to expectations lower densities lead to lower computational effort.

3.2 Sears-Haack Body

The second classic aerodynamic optimization problem is the body of revolution of given length and volume, which has minimum drag in supersonic flow. Linear theory[13] results in body with the maximum thickness at $x/l_B = 0.5$, i.e. exactly at half body length. The position depends not on the Mach number. The drag coefficient amounts to $C_D = 0.1104$ for Mach number $M_\infty = 2.0$ as well as for Mach number $M_\infty = 1.5$ assuming a volume of $V_B/l^3{}_{REF} = 0.0046$. The coefficient depends also not on the Mach number. Extended linear theory[14] results in a body with the maximum thickness not at half body length. The position depends on the Mach number and lies at $x/l_B = 0.5107$ for Mach number $M_\infty = 2.0$ and at $x/l_B = 0.5110$ for Mach number $M_\infty = 1.5$, i.e. behind half body length. It moves closer to the tail with increasing Mach number. A drag coefficient cannot be calculated.

Several optimizations of a body of revolution with respect to minimum drag in supersonic flow and based on solutions of the Euler equations have been carried out. They included six geometric parameters sketched in Fig. 14: the position of the maxi-

mum thickness in x- and z-direction, the slope of the contour at the nose, before the maximum thickness, behind the maximum thickness and at the tail. Some of these parameters are given because of constraints. The contour has to be continual at the maximum thickness. Hence, the slope of the contour before and behind the maximum thickness must be equal, i.e. zero. The volume has to be constant. Therefore, the slope at the tail must be chosen depending on the position of the maximum thickness and the slope at the nose. Figures 15 and 16 depict initial and resulting bodies for Mach number $M_\infty = 2.0$ using different start values for the parameters and stepsizes. All optimizations lead to the same body. Hence, the resulting body is not a coincidence. An effect of the start values cannot be found. The optimizations lead to a body agreeing very good with the solution based on extended linear theory. The maximum thickness lies at $x/l_B = 0.5028$ compared to $x/l_B = 0.5107$ based on extended linear theory. Difference between both values is about 1.5%. The drag coefficient amounts to $C_D = 0.0889$.

Figure 17 depicts initial and resulting bodies for Mach number $M_\infty = 1.5$. Again, the optimization leads to a body agreeing very good with the solution based on extended linear theory. The maximum thickness lies at $x/l_B = 0.4942$ compared to $x/l_B = 0.5110$ based on extended linear theory. Difference between both values is about 3%. The drag coefficient amounts to $C_D = 0.0949$.

Resulting bodies for Mach number $M_\infty = 2.0$ determining the aerodynamic coefficients with different accuracies are shown in Fig. 18. Up to 10^{-4} an effect of the accuracy cannot be found. Figure 19 plots the computational effort on a NEC SX4 for the optimizations with different accuracies. Here an effect can be found. In accordance to expectations lower accuracies lead to lower computational effort. Resulting bodies for Mach number $M_\infty = 2.0$ using spatial meshes of different densities are shown in Fig. 20. Up to 14985 points only a small effect of the density can be found. Figure 21 plots the computational effort for the optimizations with different mesh densities. Again, in accordance to expectations lower densities lead to lower computational effort.

So the aerodynamic optimization system provides the same solutions for classic aerodynamic optimization problems as given in literature. Input parameters, accuracy of the flowfield calculation and density of the spatial mesh have no effect on the solution. But they have a significant effect on the computational effort.

4 Application of the Optimization System

Different kinds of aerodynamic optimization problems are encountered during the design of aerospace vehicles. With several examples the potential of the Aerodynamic Optimization System has been proven. Three examples are documented in the following sections.

4.1 Re-entry Capsule

The aerodynamic characteristics of re-entry vehicles are very important for their mission. They decide the time frame of the re-entry, the place for the landing, the strain on the crew as well as the necessity for reactive or aerodynamic control systems. Hence, an improvement of the characteristics increases the possibilities for the mission and occasionally the financial requirements.

Several optimizations of a biconic re-entry capsule with respect to various objective functions and based on solutions of the Euler

equations have been carried out. The included seven geometric parameters are sketched in Fig. 22: the radius of the nose, the angles of the first and second cone, the length of the first and second cone, the inclination angle of the first cone and the diameter of the base. Some of these parameters are given because of constraints, which have been taken into account for a realistic background. The radius of the nose has to be larger than $r_{CN}/l_{REF} = 0.02$ in order to guarantee reasonable heat loads. The diameter of the base has to be $d_{CB}/l_{REF} = 0.35$ for good structural contact with launch systems. Finally, the volume of the capsule has to be $V_C/l^3_{REF} = 0.03$ in oder to accommodate crew, systems etc. Hence, the length of the second cone must be chosen depending on the angles of the first and second cone and the length of the first cone.

Figure 23 depicts resulting capsules for Mach number $M_\infty = 6.0$ with and without taking the stability into account. The objective function is identical. Taking the stability not into account leads to a long and slender capsule. A difference between the first and second cone angle cannot be found. Taking the stability into account by moving the center of gravity leads to a shorter capsule. A difference between the first an second cone angle can be found. Lift-to-drag ratios depending on the angle of attack are plotted in Fig. 24. Taking the stability not into account causes significantly higher lift-to-drag ratios.

Figure 25 depicts resulting capsules for Mach number $M_\infty = 6.0$ using different objective functions. The stability is taken into account. High weighting on the lift-to-drag ratio leads to a long and slender capsule again. High weighting on the volume efficiency leads to a shorter capsule. As expected high weighting on the lift-to-drag ratio causes higher lift-to-drag ratios, see Fig. 26. In this case bending of the capsule by an inclination angle of the first cone increases the ratios even more. In the other case, high weighting on the volume efficiency, bending provides no benefit.

Figure 27 depicts resulting capsules for Mach number $M_\infty = 6.0$ and Mach number $M_\infty = 1.5$. The objective function is identical, the stability is taken into account. For Mach number $M_\infty = 1.5$ the resulting capsule has a greater radius of the nose. Its lift-to-drag ratios are lower, see Fig. 28.

4.2 SCT Wing

The aerodynamic characteristics of the wing are crucial for an aircraft. The wing produces by far the greatest share of the drag. Hence, an improvement of the characteristics decreases the fuel consumption and by this way increases the economic efficiency of the aircraft.

Several optimizations of the wing for a Supersonic Commercial Transport with respect to minimum drag at cruise conditions and based on solutions of the Euler equations have been carried out. They included 31 geometric parameters. The parameters concerning the planform of the wing are sketched in Fig. 29: the position of the points at the wing tip in x-direction and in x- as well as y-direction, the position of the points at the leading-edge kink and the trailing-edge kink in x- as well as y-direction and the position of the point at the trailing edge root in x-direction. All points are connected with straight lines. The parameters concerning the airfoils at the root, at half of the half-span and at the tip are similar to those in Fig. 6: the position of the maximum thickness in x-direction, the slope of the flank before the maximum thickness at the leading edge and at the maximum thickness, the slope of the flank behind the maximum thickness at the maximum thickness and at the trailing edge, the shift of the air-

foils in z-direction, the chamber and the local angle of attack. Some of these parameters are given because of constraints, which have been taken into account for a realistic background. The area of the wing has to be $A_{SSW}/l^2_{REF} = 4.5$. Henc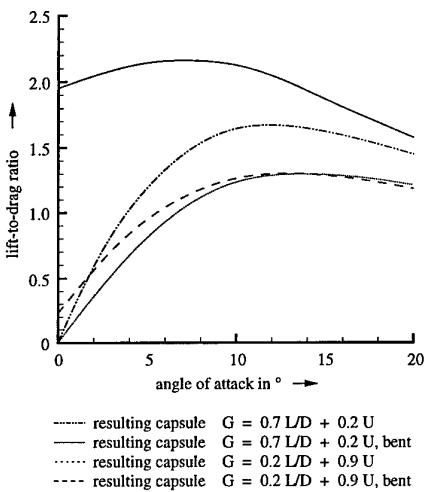e, the position of the trailing edge must be chosen depending on the span of the wing as well as the position of the leading-edge kink and the trailing-edge kink. The contour has to be continual at the maximum thickness of the airfoils. As a result the slop of the flanks before and behind the maximum thickness must be equal, i.e. zero. The volume of the wing has to be $V_{SSW}/l^3_{REF} = 0.0167$ and the maximum thickness of the airfoils has to be $\delta/c = 0.025$. Therefore, the slopes at the trailing edge must be chosen depending on the positions of the maximum thickness and the slopes at the leading edge. Furthermore, the lift coefficient of the wing has to be $C_L = 0.12$ at Mach number $M_\infty = 2.0$. This is ensured by the objective function.

Figure 30 depicts the initial and the resulting wing of one optimization. The resulting wing has a greater span than the initial wing. In order to keep the area its length is smaller. The resulting wing has a nearly straight leading edge. The kink has vanished. Figure 31 depicts the initial and the resulting airfoils in a normalized way. Chamber, local angle of attack etc. are very small and have been neglected here. The resulting airfoils are similar. They have a position of the maximum thickness slightly before half chord length. The lift-to-drag ratio of the resulting wing amounts at $M_\infty = 2.0$ to $L/D = 16$.

4.3 SCT Wing/Body Configuration

Several optimizations of an SCT wing/body configuration with respect to minimum drag at cruise conditions and based on solutions of the Euler equations have also been carried out. The included nine geometric parameters are sketched in Fig. 32: the length and diameter of the cylindrical body part, the length and diameter of the nose and tail cone, the position of the wing in x- and z-direction and the inclination angle of the body. Nose and tail cone have been shaped like Sears-Haack bodies, the wing has been taken from Ref. 15 and kept constant. Some of the parameters are given because of constraints, which have been taken into account for a realistic background. The body has to accommodate 250 passengers at 6 seats per row. Hence, according to guidelines the body must have a diameter of $d_{SSB}/l_{REF} = 0.35$ for 6 seats per row and based on this a length of $l_{SSB}/l_{REF} = 5.71$ for 250 passengers. The contour has to be continual at the transition from the nose cone to the cylindrical body part and from the cylindrical body part to the tail cone. Therefore, the nose and tail cone must have a diameter of $d_{SSC}/l_{REF} = 0.35$. Similar to the optimization of the SCT wing the lift coefficient of the configuration has to be $C_L = 0.1$ at Mach number $M_\infty = 2.0$ and angle of attack $\alpha = 3°$. This is ensured by the objective function. An assessment of viscous drag by the flat plate analogy is included in the objective function.

Fig. 33 depicts the initial and the resulting configuration of an optimization. The resulting configuration has a significantly greater length of the nose and tail cone than the initial configuration. It has a position of the wing closer to the nose and a greater inclination angle of the body. Lift-to-drag ratios depending on the angle of attack are plotted in Fig. 34. The resulting configuration has significantly higher lift-to-drag ratios than the initial configuration, not only in the design point, i.e. at angle of attack $\alpha = 3°$, but also at other angles of attack.

5 Conclusions

The described Aerodynamic Optimization System has proven to be a useful tool for the aerodynamic optimization of three-dimensional configurations. The system is based on the repeated calculation of the flowfield around three-dimensional geometries by solving the Euler/Navier-Stokes equations. Hence, non-linear phenomenons influence the optima. Under the same conditions the system has provided the same solutions of classic aerodynamic optimization problems as given in literature. Input parameters, accuracy of the flowfield calculation and density of the spatial mesh had in a reasonable range no effect on the solutions. But they had a significant effect on the computational effort. The Aerodynamic Optimization System has shown its potential for current aerodynamic optimization problems. Improvements of a re-entry capsule, an SCT wing and an SCT wing/body configuration before a realistic background have been achieved.

References

1   Sobieszczanski-Sobieski, J. and Haftka, R.T., *"Multidisciplinary Aerospace Design Optimization: Survey of Recent Developments"*, AIAA 96-0711.

2   Foster N.F. et al., *"Three-Dimensional Aerodynamic Shape Optimization Using Genetic Evolution and Gradient Search Algorithms"*, AIAA 96-0555.

3   Strohmeyer, D. and Seubert, R., *"Improvement of a Preliminary Design and Optimization Program for the Evaluation of Future Aircraft Projects"*, AIAA 98-4828.

4   Orlowski, M. and Herrmann, U., *"Aerodynamic Optimization of Supersonic Transport Configurations"*, ICAS 96-4.3.3.

5   Bartelheimer, W., *"An Improved Integral Equation Method for the Design of Transonic Airfoils and Wings"*, AIAA 95-1688.

6   Sobieczky, H., *"Geometry Generation for Transonic Design"*, In: Recent Advances in Numerical Methods in Fluids Vol. 4 (Ed. Habashi, W.G.), Pineridge Press, Swansea, 1985, pp. 163-182.

7   Brodersen, O. et al., *"The Parametric Grid Generation System MegaCads"*, In: Proc. 5th International Conference on Numerical Grid Generation in Computational Field Simulations (Eds. Soni, B.K., Thompson, J.F., Häuser, J., Eisemann, P.R.), Mississippi, 1996, pp. 353-362.

8   Kroll, N. et al., *"Accurate and Efficient Flow Solvers for 3D Applications on Structured Meshes"*, VKI Lecture Series 94-05 on Computational Fluid Dynamics, Brussels, 1994.

9   Jameson, A. et al., *"Numerical Solution of the Euler-Equations by Finite Volume Methods using Runge-Kutta Time-Stepping Schemes"*, AIAA 81-1259.

10 Jakob, H.G., *"Rechnergestützte Optimierung statischer und dynamischer Systeme - Beispiele mit FORTRAN Programmen"*, Fachberichte Messen, Steuern und Regeln Vol. 6, Springer Verlag, Berlin, 1982.

11 Miele, A. *"Theory of Optimum Aerodynamic Shapes"*, Academic Press, New York, 1965.

12 Ferri, A. *"Elements of Aerodynamics of Supersonic Flows"*, Macmillan Company, New York, 1949.

13 Sears, W.R., *"On Projectiles of Minimum Wave Drag"*, Quarterly Applied Mathematics Vol. 14 (1947), pp. 361-366.

14 Wellmann, J., *"Der Einfluß der Machzahl auf wellenwiderstandsoptimierte Rümpfe und Profile bei Überschallanströmung"*, DLR Report 151-73/5 (1973).

15 Doherty, J.J. and Parker, N.T., *"Dual-Point Design of a Supersonic Transport Wing Using a Constrained Optimization Method"*, In: Proc. 7th European Aerospace Conference, Toulouse, 1994, pp. 247-265.

Figures
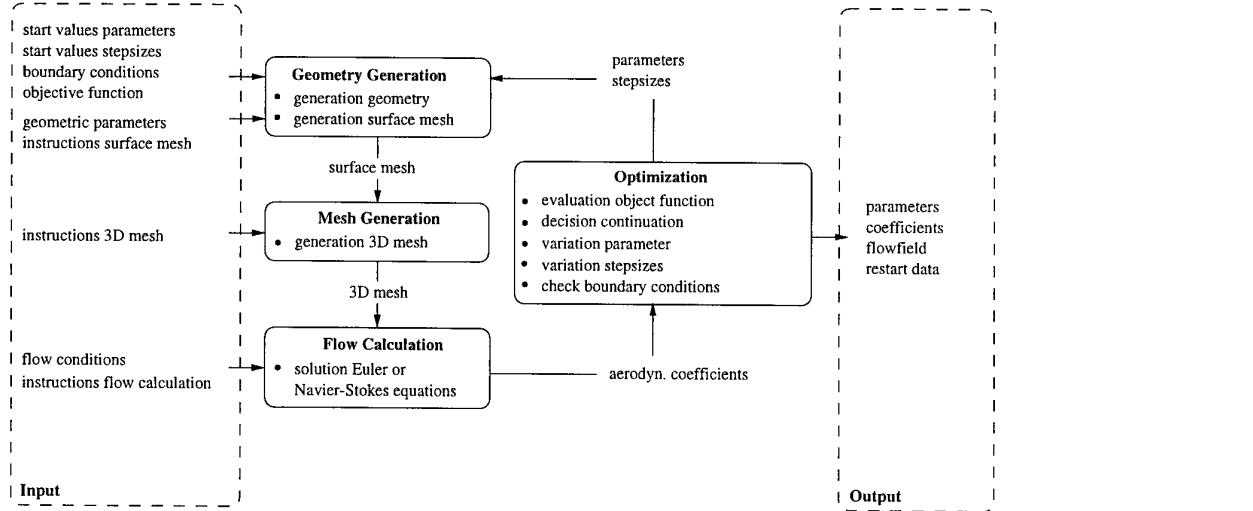
Figure 1: Basic structure of the Aerodynamic Optimization System.

Sketch:

Data:

key number upper/lower side	coordinate x/c start point	coordinate z/c start point	slope start point	key number curve function	slope end point	curvature start point	curvature end point
1	0.000	0.000		7	0.0	6.0	4.0
1	0.475	0.065	0.0	1	-0.2	4.0	2.0
1	1.000	0.000					
2	0.000	0.000		7	0.0	6.0	4.5
2	0.400	-0.050	0.0	1	0.0	4.5	8.0
2	0.920	0.005	0.0	1	-0.1	8.0	2.0
2	1.000	0.000					
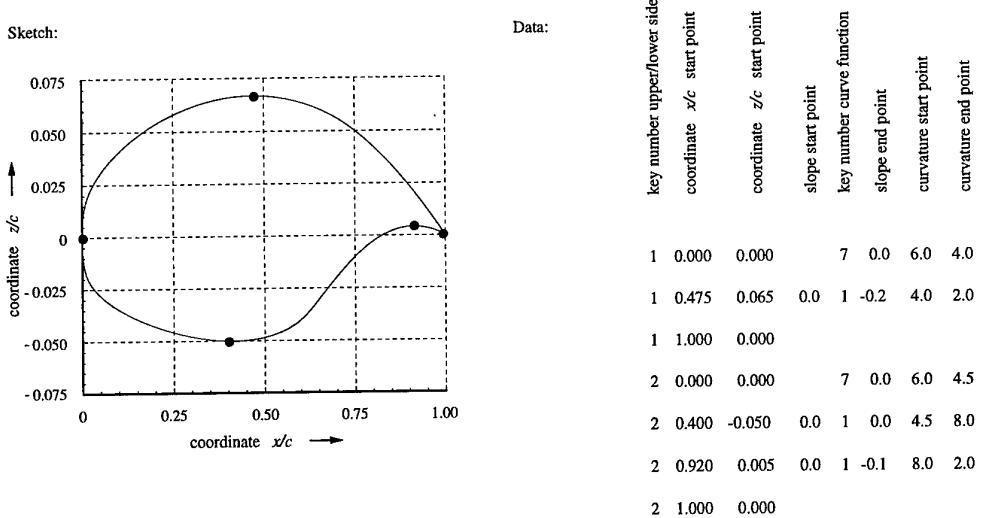
Figure 2: Example for curve functions describing an airfoil.
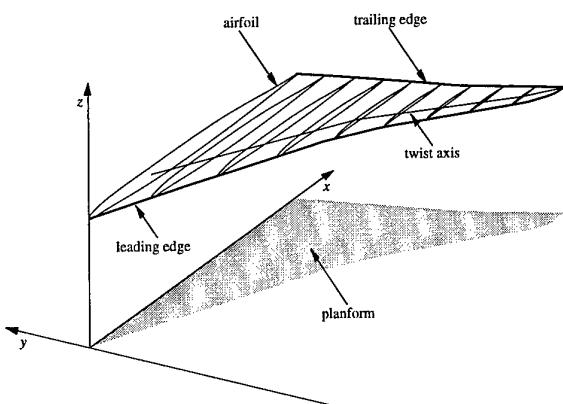
Figure 3: Elements forming a wing.
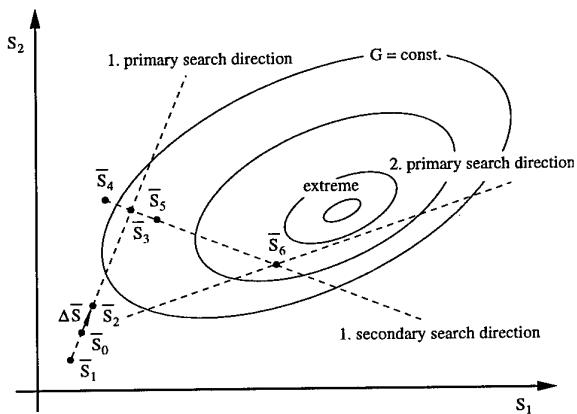
Figure 5: Principle function of the optimization algorithm.
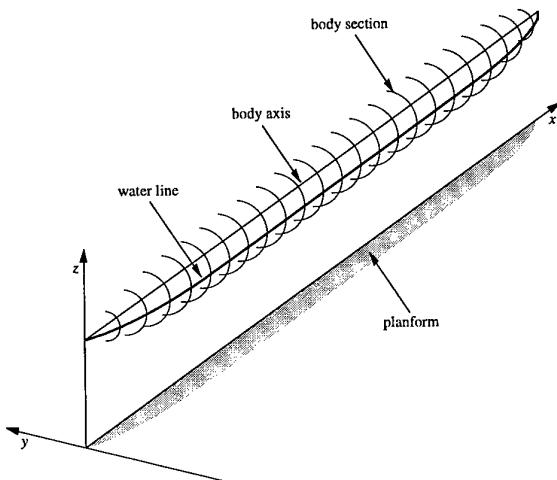
Figure 4: Elements forming a body.
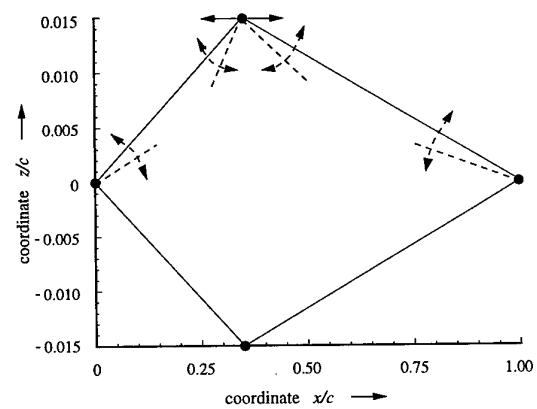
Figure 6: Symmetric airfoil with 5 geometric parameters, maximum thickness $\delta/c = 0.03$.
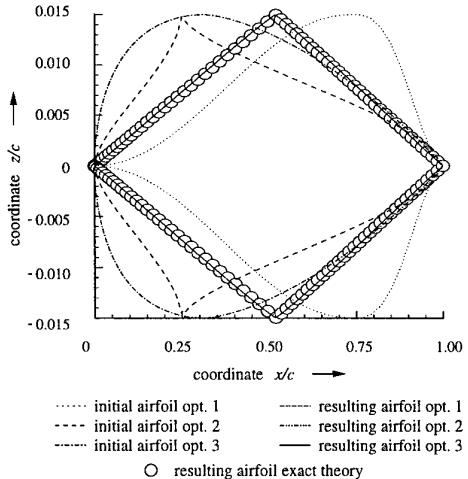
Figure 7: Initial and resulting airfoils of optimizations at Mach number $M_\infty = 2.0$ using different start values for the parameters.
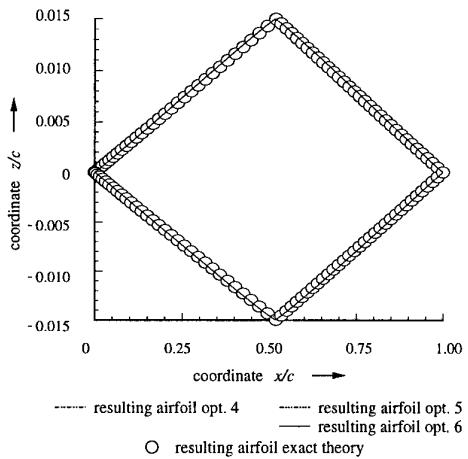
Figure 8: Resulting airfoils of optimizations at Mach number $M_\infty = 2.0$ using different start values for the stepsizes.
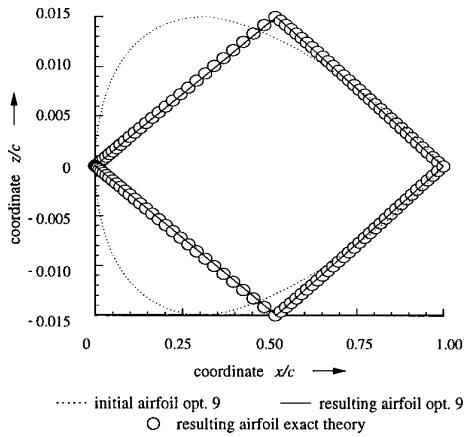
Figure 9: Initial and resulting airfoils of an optimizations at Mach number $M_\infty = 1.5$.
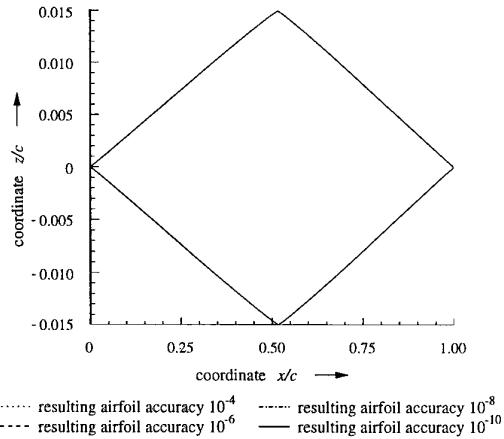
Figure 10: Resulting airfoils of optimizations at Mach number $M_\infty = 2.0$ determining the aerodynamic coefficients with different accuracies.
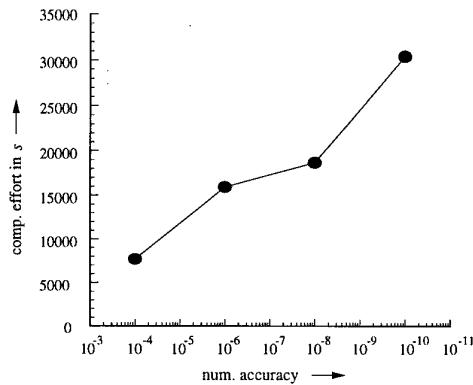
Figure 11: Computational effort for the optimizations at Mach number $M_\infty = 2.0$ determining the aerodynamic coefficients with different accuracies.
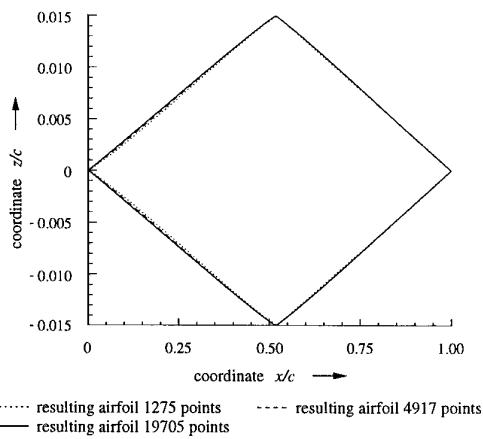
Figure 12: Resulting airfoils of optimizations at Mach number $M_\infty = 2.0$ using spatial meshes of different densities.
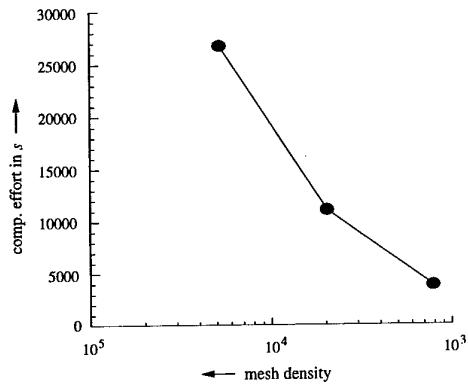
Figure 13: Computational effort for the optimizations at Mach number $M_\infty = 2.0$ using spatial meshes of different densities.
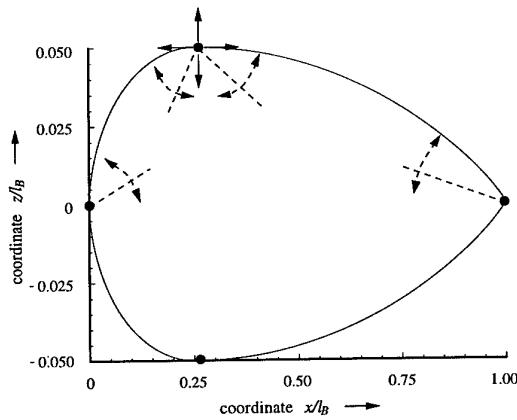
Figure 14: Body of revolution with 6 geometric parameters, volume $V_B/l^3_{REF} = 0.0046$.
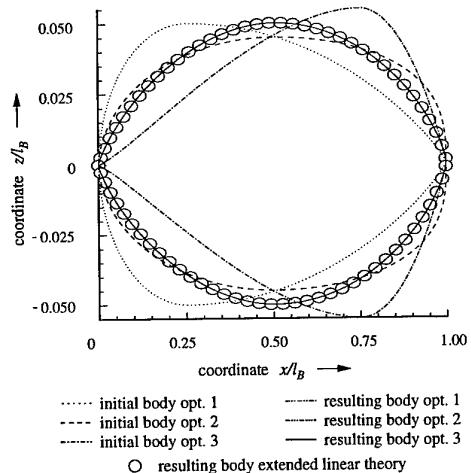
Figure 15: Initial and resulting bodies of optimizations at Mach number $M_\infty = 2.0$ using different start values for the parameters.
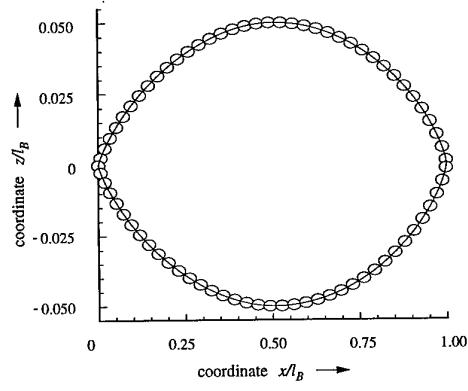
Figure 16: Resulting bodies of optimizations at Mach number $M_\infty = 2.0$ using different start values for the stepsizes.
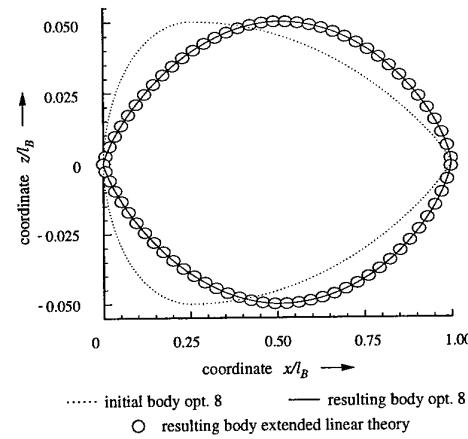
Figure 17: Initial and resulting body of an optimization at Mach number $M_\infty = 1.5$.
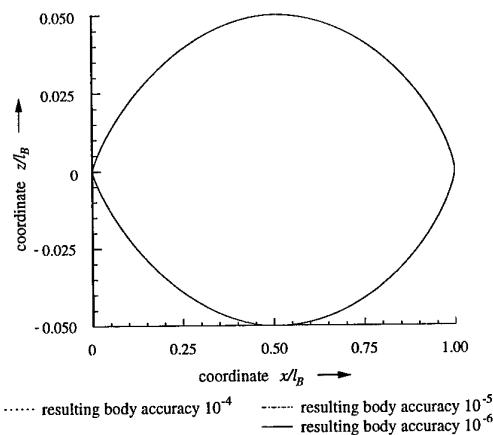
Figure 18: Resulting bodies of optimizations at Mach number $M_\infty = 2.0$ determing the aerodynamic coefficients with different accuracies.
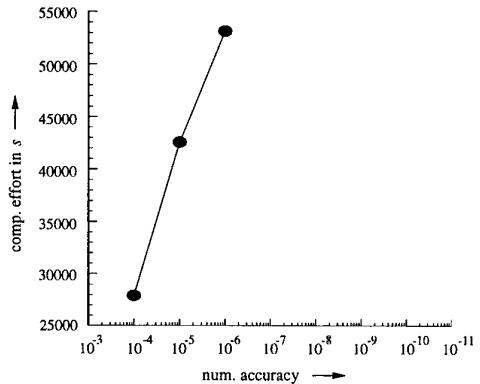
Figure 19: Computational effort for the optimizations at Mach number $M_\infty = 2.0$ determing the aerodynamic coefficients with different accuracies.

Figure 22: Biconic re-entry capsule with 7 geometric parameters, volume $V_C/l^3_{REF} = 0.03$, base diameter $d_{CB}/l_{REF} = 0.35$.

····· resulting body 14985 points   ----- resulting body 109707 points
——— resulting body 828755 points
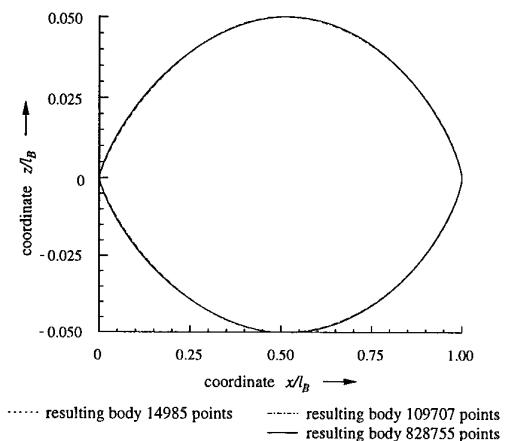
Figure 20: Resulting bodies of optimizations at Mach number $M_\infty = 2.0$ using spatial meshes of different densities.

——— resulting capsule   G = 0.5 L/D + 0.4 U, with stability
····· resulting capsule   G = 0.5 L/D + 0.4 U, without stability
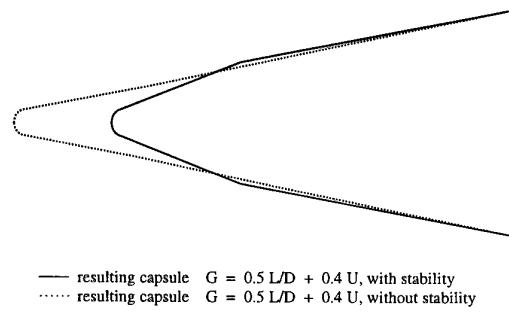
Figure 23: Resulting biconic re-entry capsules of optimizations at Mach number $M_\infty = 6.0$ with and without taking the stability into account.

Figure 21: Computational effort for the optimizations at Mach number $M_\infty = 2.0$ using spatial meshes of different densities.

——— resulting capsule   G = 0.5 L/D + 0.4 U, with stability
····· resulting capsule   G = 0.5 L/D + 0.4 U, without stability
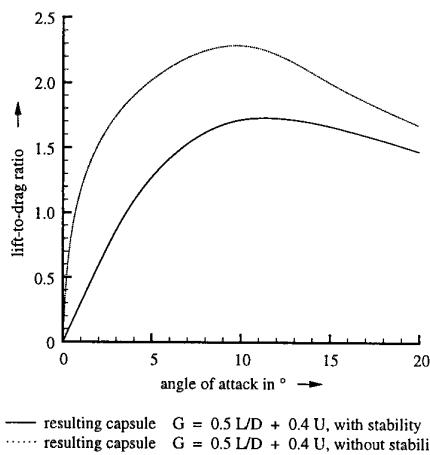
Figure 24: Lift-to-drag ratios of the biconic re-entry capsules resulting from optimizations at Mach number $M_\infty = 6.0$ with and without taking the stability into account.

Figure 25: Resulting biconic re-entry capsules of optimizations at Mach number $M_\infty = 6.0$ with different objective functions.

Figure 27: Resulting biconic re-entry capsules of optimizations at Mach number $M_\infty = 6.0$ and at Mach number $M_\infty = 1.5$.

Figure 26: Lift-to-drag ratios of the biconic re-entry capsules resulting from optimizations at Mach number $M_\infty = 6.0$ with different objective functions.

Figure 28: Lift-to-drag ratios of the biconic re-entry capsules resulting from optimizations at Mach number $M_\infty = 6.0$ and at Mach number $M_\infty = 1.5$.

Figure 29: Planform of the wing for a Supersonic Commercial Transport with 8 parameters, volume $V_{SSW}/l^3_{REF} = 0.0167$, area $A_{SSW}/l^2_{REF} = 4.5$ and lift coefficient $C_L = 0.12$.

Figure 30: Planform of the initial and resulting SCT wing of an optimization at Mach number $M_\infty = 2.0$.

...... initial airfoil
---- resulting airfoil at the root
-----·· resulting airfoil at half of the half-span
—— resulting airfoil at the wingtip
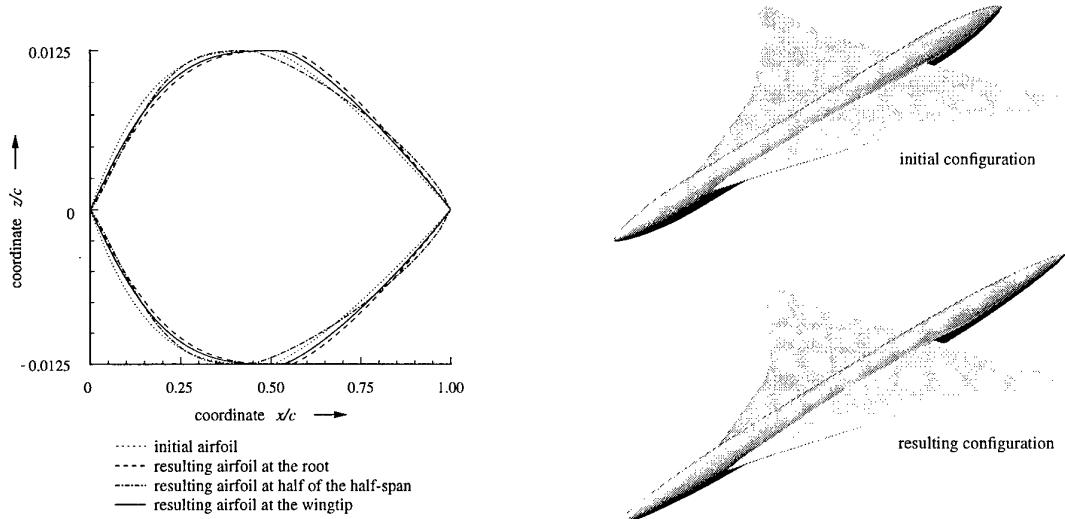
Figure 31: Normalized airfoils of the initial and resulting SCT wing of an optimization at Mach number $M_\infty = 2.0$.

Figure 33: Initial and resulting SCT wing/body configurations resulting from an optimization at Mach number $M_\infty = 2.0$ and angle of attack $\alpha = 3°$.
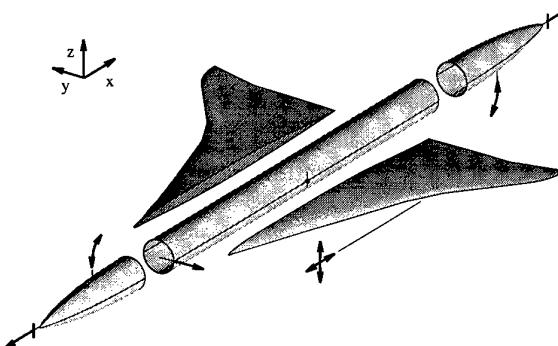
Figure 32: Wing/body configuration for a Supersonic Commercial Transport with 9 parameters, 250 passengers in 6 seats per row, wing fixed and lift coefficient $C_L = 0.1$.
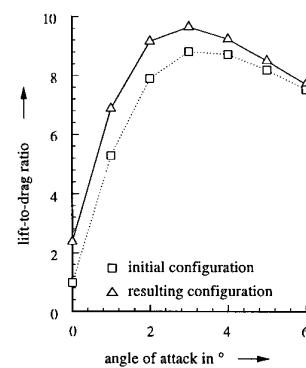
Figure 34: Lift-to-drag ratios of the initial and resulting SCT wing/body configuration resulting from an optimization at Mach number $M_\infty = 2.0$ and angle of attack $\alpha = 3°$.

DISCUSSION

Session III, Paper #19

Prof Knight (Rutgers University, USA) asked the largest number of design variables the author had considered. He wanted to know how the author's approach would "scale up" to problems involving large numbers of design variables.

> **Mr Orlowski** replied that the largest number of variables had been 35 optimizing an SCT wing. He noted that his approach using Euler equations was not cheap in terms of computational effort. He believed that with available high speed computing and experience with the system its use was acceptable, at least for the moment. He felt that further developments in computer systems available to industry should make the system acceptable to them also.

Mr Doherty (DERA, UK) asked whether it could be confirmed that the use of finite difference gradient generation rendered computation time independent of the number of constraints, unlike in an adjoint approach for gradient calculation.

> **Mr Orlowski** replied that the constraints affect the computational effort by reducing the number of parameters that are really included in the optimization process. However, the process itself was independent of this effect.

Alenia Multidisciplinary Design Optimisation - Topics and Approaches

V. Selmin*, P.L. Vitagliano, A. Pennavaria and L. Crosetta

*Alenia Aerospazio - Divisione Aeronautica
SPRT, Corso Marche 41
10146 Torino, Italy

Abstract

The purpose of this paper is to report on methods which have been developed or which are under development at Alenia Aeronautica for multidisciplinary optimum design, with particulary emphasis on aerodynamic shape design. Results of transonic 2D and 3D optimisation problems are presented.

1 INTRODUCTION

Multidisciplinary Design Optimisation (MDO) will provide designers a new array tools and approaches that will take them closer to that elusive goal, an "optimum airplane". MDO has been defined as "a formal design methodology based on integration of disciplinary analysis and sensitivity analysis, optimisation and artificial intelligence, applicable at all stages of the multidisciplinary design of aerospace systems". What this really means is that MDO is a way of getting engineers from various disciplines, such as aerodynamics, structures, weights, control systems, propulsion, etc., to work together. Mathematical tools, such as sensitivity analysis, modelling methods, and optimisation solvers, provide a mechanism by which this working together can be accomplished. The result is a process that can both reduce the design cost and flow-time, and improve the quality of aerospace systems.

Since the early nineties, Alenia Aeronautica has improved its optimisation design capability by participating to several ECC funded initiatives on optimisation (EUROPT, ECARP, MDO). The result is a highly automatised system that allows to solve near real life design problems. This paper describes in some details the optimisation system and its potentialities. In particular, the multidisciplinary (aerodynamics+structure) optimisation design of a wing-body configuration is presented. Although the system we have developed is general, emphasis will be done in the following to wing like geometries which are the subject of the section dedicated to applications.

2 OPTIMISATION SYSTEM

From a mathematical point of view, in order to solve an optimisation problem, the values assigned to the design variables $\mathbf{X}$ must be found so as to minimize the objective function $F(\mathbf{X})$ while maintaining that the possible constraint functions $G_j(\mathbf{X})$ are ≤ 0. The designer must derive these functions and choose the design variables that govern the transformation of the geometry.

The optimisation framework which was developed is formed by an optimisation module, an analysis module and an interface module that handles the geometry modifications (Fig. 1). The interface module is integrated within a Multi-Model Generator which provides the CFD system with a discretisation of the wing geometry and the CSM system with a finite element model of the wing torsion box and the forces acting on the model reference axis.
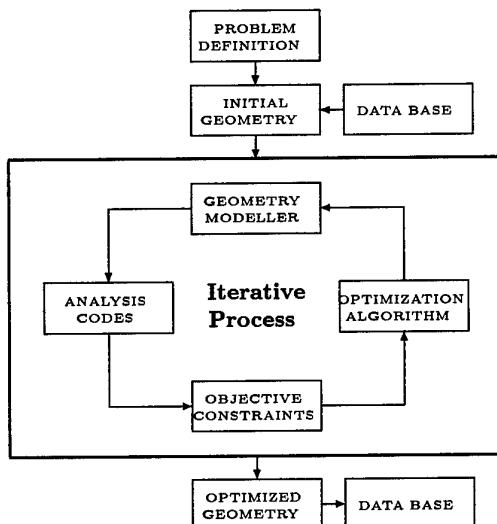
Figure 1: Optimisation system.

The optimisation module is based on optimisation routines coming from the commercial package ADS[1]. For unconstrained problems, a quasi-Newton method like the BGFS variable metric method is usually used; while for constrained problems, a method based on Zoutendijk's feasible direction algorithm[2] was selected. The optimisation routines are coupled with analysis codes which give the value of the derivatives of the objective function and of the constraints. Based on these derivatives, the optimisation routine chooses the most suitable modification direction. Aerodynamic coefficients are computed by using in-house CFD solvers, while wing mass is estimated through MSC NASTRAN structural optimisation module. The design variables can be any of the wing planform defining parameters or those that govern the modification of selected wing section shapes. The parametrisation technique is based on a shape perturbation method.

3 PARAMETRISATION

The wing is defined by:

1- The planform defining parameters such area(S), aspect ratio(AR) and sweep angle(Sweep).

2- The twist (Tw) and thickness (Tc) of key wing sections.

3- The shape of the key wing sections, which is generally given by the coordinates of a set of nodes.

Each section is defined with respect to a local frame, centred at the section leading edge and having the x-axis coincident with the section chord. Normalised coordinates are introduced by scaling each length with the chord length, which means that $x \in [0,1]$.

In the parametric model, the shape is modified using the following representation:

$$x(t) = x^*(t) \equiv t \qquad t \in [0,1]$$
$$z(t) = z^*(t) + \sum_{j=1}^{n} \Delta z_j \, B_{j,n}(t)$$

where (x^*, z^*) represents the position vector of the original shape and $B_{j,n}$ are general shape modification functions. The design variables are the parameters Δz_j. The original shape is recovered if they are all zero.
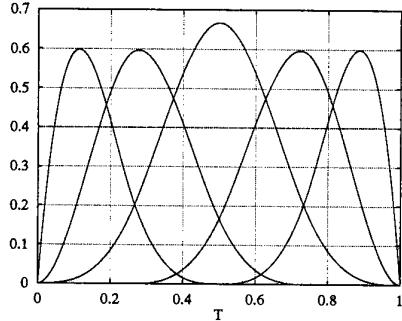
Figure 2: B-spline functions.

The present method greatly reduces the number of design variables with respect to a spline defining curve approach and may lead to a strong reduction on the computational cost of the optimisation. Various shape functions, including Hick-Henne functions[3], Bernstein polynomials and B-spline functions[4], have been studied. Among those, B-spline approach is preferred whereas the functions have a more compact support and allow to modify only locally the shape. Fig. 2 illustrates the 7th-order uniform cubic B-spline functions, which represents the default option implemented into the optimisation system. Only ten design variables are required to modify both upper and lower active wing section surfaces. Those sections without a design variables specified value are modified from the design variables associated to neighbouring sections using a linear relationship.

4 ANALYSIS TOOLS

4.1 Aerodynamic analysis

The aerodynamic analysis is performed using simulation systems based on in-house developed Euler and Navier-Stokes multiblock structured or unstructured solvers. Both take advantage of explicit time marching schemes employing finite-volume-based central difference spatial discretisations. Multiblock solvers are cell-centred based, while unstructured ones use a node-centred/cell-vertex approach. Nonlinear second-order and linear fourth-order damping terms are added for stability and shock-capturing properties. Time integration is performed using multistage algorithm. Convergence to steady state is accelerated with the aid of local time stepping, implicit residual smoothing and enthalpy damping (inviscid computations only). For turbulence modelling, Baldwin-Barth one-equation, together with $k - \omega$ and $k - R_t$ two-equation models are available. The unstructured solvers can accepted structured multiblock grids as input, which are converted into unstructured one-block meshes.

The flow solvers are implemented, together with a mesh generator and a procedure for domain modelling. Those allow automatic remeshing of the new geometry and of the associated field grid, during the optimisation, as the design parameters are modified. As an alternative, a Laplacian smoothing based node movement algorithm was developed. It has the capability to deform a grid while maintaining the characteristics of the initial one. This allows to introduce an automatic mesh deformation tool within the optimisation process, which we consider of paramount importance in order to deal with very complex geometries and with unstructured grids.

4.2 Mesh deformation algorithm

In the following, $\mathbf{x}_i$ will indicate the position vector of node i. We will indicate with $\mathcal{E}_i$ the set of elements belonging to the patch $\mathcal{P}_i$ of elements surrounding a given internal node i. $\mathcal{K}_i$ is instead the set formed by the nodes on the boundary of $\mathcal{P}_i$.

The method is based on an edge based data structure which has originally been developed for unstructured finite volume CFD codes. To move the mesh, it is first assumed that each node i of the grid is connected to each adjacent node j by a fictitious spring under the force $\mathbf{F}_{ij}$ defined by

$$\mathbf{F}_{ij} = K_{ij} \left(\mathbf{x}_j - \mathbf{x}_i \right) = K_{ij} \, \Delta \mathbf{x}_{ij} \tag{1}$$

where K_{ij} is the spring constant which, in general, will depend on some local grid features (grid metrics).

The resulting mesh is the solution of the equilibrium system for each vertex i:

$$\sum_{j \in \mathcal{K}_i} \mathbf{F}_{ij} = 0 \, , \tag{2}$$

which is also equivalent to minimize the energy of the overall spring system

$$\frac{1}{2} \sum_{j \in \mathcal{K}_i} K_{ij} \, \Delta \mathbf{x}_{ij}^2 . \tag{3}$$

In order to modify the grid while maintaining it close to the initial mesh characteristics, additional terms are introduced which modify the spring energy relation as follows

$$\frac{1}{2} \sum_{j \in \mathcal{K}_i} K_{ij} \left(\Delta \mathbf{x}_{ij} - \mathbf{Q}_{ij} \Delta \mathbf{x}_{ij}^0 \right)^2 \tag{4}$$

where $\mathbf{x}_i^0$ is the vector position of node i in the initial grid and $\mathbf{Q}$ is a mesh adaptation transformation matrix, which is related to the change between the original and deformed surface shapes. In the case of

$$\mathbf{Q} = \mathbf{I} \quad \text{and} \quad \Delta \mathbf{x}_{ij} = \Delta \mathbf{x}_{ij}^0 \quad ,$$

the spring energy is zero and the grid nodes do not move.

A conjugate gradient method is used to minimize the modified spring energy equation 4. The technique is valid for both regular and irregular grids.

Fig. 3 illustrates the application of the node movement method to the grid deformation which results from a 50% thickness increase of the NACA0012 airfoil.
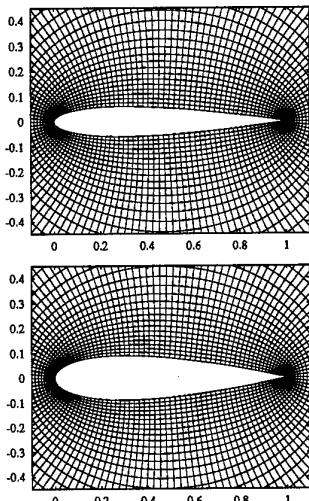
Figure 3: Mesh deformation: 50% increase in thickness.

4.3 Structural analysis

Starting from the finite element and loads models provided by the Multi-Model Generator, the wing mass is computed using the structural optimisation module of the MSC/NASTRAN code. The Sequential Quadratic Programming minimisation method is usually selected.

5 OPTIMISATION ALGORITHM

At each iteration q of the minimization process, the design vector $\mathbf{X}$ is updated according to the formula $\mathbf{X}^q = \mathbf{X}^{q-1} + \omega \mathbf{S}^q$, where $\mathbf{S}^q$ is a unit vector representing a search direction in a space having as many dimensions as the design variables, and where ω defines the displacement in the direction $\mathbf{S}^q$. In the Method of Feasible Direction, the search direction is built in such a way that it will reduce the objective function without violating the constraint for some finite move, and thus can be defined as a constrained steepest descent direction. The search direction $\mathbf{S}$ is determinated by considering the following problem:

Minimize:

$$\nabla F(\mathbf{X}) \cdot \mathbf{S}$$

Subject to:

$$\nabla G_j(\mathbf{X}) \cdot \mathbf{S} \leq 0$$
$$\mathbf{S} \cdot \mathbf{S} \leq 1$$

The last inequality is introduced to ensure that the search vector remains bounded. Solving this problem gives a search direction which is tangent to the critical constraint boundaries, unless the objective can be reduced more rapidly by moving away from one or more constraints.

In the optimization process, the gradients are calculated by a first order forward finite difference unless a variable is at its upper bound. In this case, a first order backward finite difference step is used.

6 APPLICATIONS

6.1 Single-point airfoil optimisation

The TE3 test case [5] adresses the problem of drag minimisation in transonic flows. Far field conditions are $M_\infty = 0.73$ and an angle of attack $\alpha = 2°$. The RAE2822 airfoil has been used as the starting profile. The objective was to search for a minimum drag based on a given lift coefficient. Although this test case was defined as an inviscid one, optimisation on the basis of a viscous flow has been additionally performed. Two different test cases were run:

1. An inviscid optimisation based on the above flow parameters and the constraint that the lift coefficient for $\alpha = 2°$ ($c_l = 0.865$) had to be kept unchanged.

2. A viscous optimisation with the same flow conditions as above, a lift coefficient of $c_l = 0.648$, a Reynolds number $Re = 6.5 \cdot 10^6$ and a transition fixed at $x/c = 0.03$.

Additional constraints have been applied to both test cases. These constraints read: $t/c = (t/c)_{\text{RAE2822}}$, α is kept fixed.
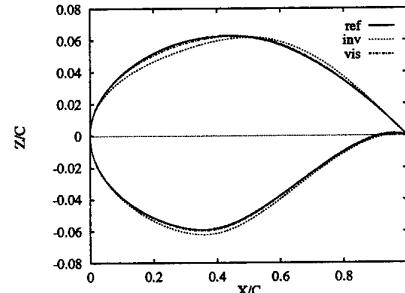
Figure 4: Problem TE3 - Comparison of Initial and Optimised Contours.

Inviscid Optimisation: The computation has been performed using an unstructured grid of 7809 triangles and 4009 nodes. Instead of rebuilding the grid each time the airfoil shape is modified, mesh deformation was provided by the Laplacian smoothing based node movement algorithm. The "best design" was reached after 69 functional evaluations resulting in a reduction of the initial drag coefficient which was driven down from its initial value of 0.00746 to 0.00096. The new shape shows a redesign of the camberline with very high negative value of the camber and a thinner thickness distribution in the first 40 % of the chord, while the thickness increases in the remaining 60 %. The maximum thickness location moves towards the

trailing edge to reach nearly 40 % of the chord (38 % for RAE2822 airfoil). The C_p distribution on the leeward side of the optimised airfoil is characterised by an increase of the suction peack and a reduction of the shock jump; the winward side remains almost unchanged.
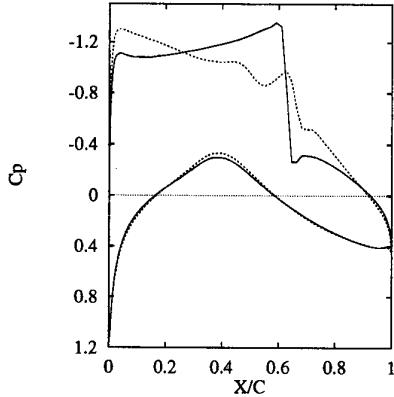
Figure 5: Problem TE3 - Transonic Inviscid Drag Minimisation - Comparison of Pressure Distributions.

Viscous Optimisation: The computation has been performed on an almost structured grid of 8200 elements and 8360 nodes. Here again, mesh deformations were obtained using the node movement algorithm. The "best design" was reached after 68 functional evaluations resulting in a reduction of 7 drag counts ($c_d = 0.0081$ instead of 0.0088). The shape is closer to the RAE2822 airfoil than those coming from inviscid optimisation. Here again, reduction of drag is mainly obtained by the redesign of the camberline but in a lower measure. The thickness distribution remains almost unchanged. The C_p distribution is characterised by a slightly higher suction peack and is shock free.
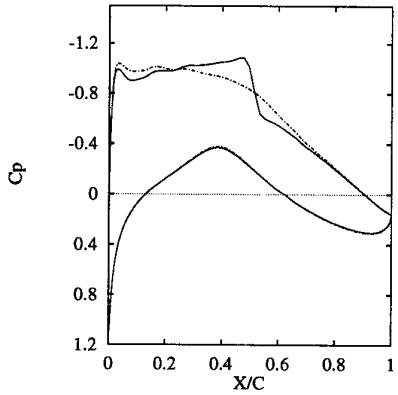
Figure 6: Problem TE3 - Transonic Viscous Drag Minimisation - Comparison of Pressure Distributions.

6.2 Multi-point airfoil optimisation

The problems consist in the improvement of an already existing airfoil in order to increase its maximum speed without deteriorating its characteristics at lower speeds. More precisely, the design problem was defined as to minimize drag at $M_\infty = 0.8$ and $C_l = C_l^t$, maintaining the C_l and C_d characteristics on the buffet onset curve of the original airfoil for $M_\infty = 0.55, 0.62, 0.71, 0.754$, which results in a five-point optimisation problem. The value of

the Mach number is $24 \cdot 10^6$ and the flow is assumed to be fully turbulent.

The new shape is obtained by a redesign of the camberline with higher values of the camber on both leading and rear parts of the airfoil, while the thickness is increased beyond 40% of the chord. The maximum thickness position moves from 35% to 42% of the airfoil chord.
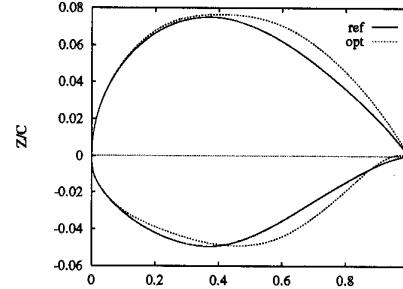
Figure 7: Multi-Point Optimisation - Comparison of Initial and Optimised Contours.
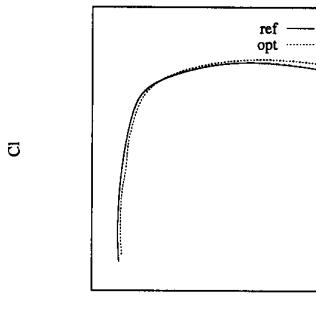
Polar at M=0.55.
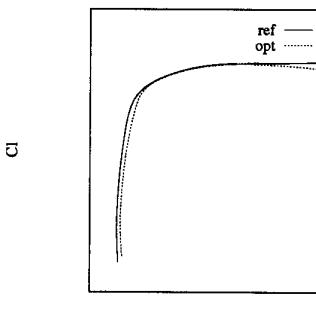
Polar at M=0.62.

Figure 8: Multi-Point Optimisation - Comparison of Aerodynamic Characteristics.

Figures 8 and 9 illustrate the aerodynamic characteristics ($C_l - C_d$ polars) of the two airfoils. At the main design point ($M = 0.80$), the drag is reduced along the overall lift range. For the secondary points, a small penalty on the drag (a few counts) is observed for low and intermediate values of the lift, while the drag is reduced at higer values. In general, an increase of the maximum lift of the airfoil is reached. This is particularily true at $M = 0.71$ and $M = 0.754$.

Polar at $M=0.71$.

Polar at $M=0.754$.

Polar at $M=0.80$.
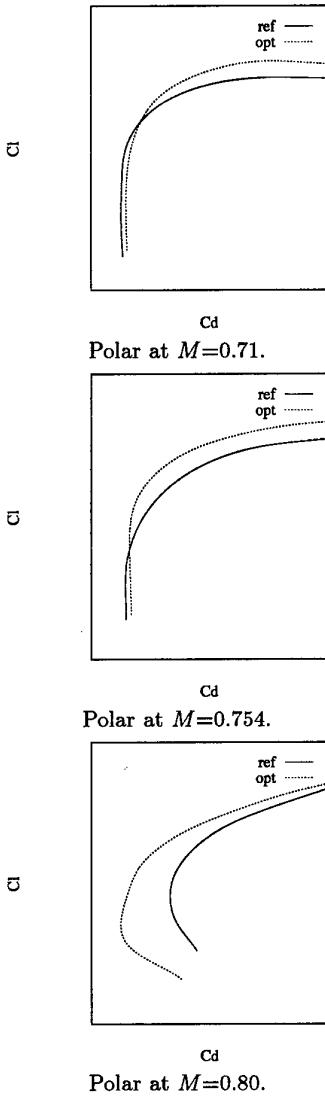
Figure 9: Multi-Point Optimisation - Comparison of Aerodynamic Characteristics.

6.3 Transonic wing optimisation

The reference aircraft geometry selected within the MDO project [6] is representative of a wide-body civil transport aircraft (650 passengers), with a wing span of nearly 80 meters and a maximum take-off weight of about 550 tons. The wing, whose exposed right component planform is illustrated in Fig. 10, has an area of 725 m^2, an aspect-ratio of 8.2, a span of 77.1 m and a sweep angle of 33°.

The optimisation problem, which has been solved, is summarized as follows:

Design Operation	Economic Cruise($M_\infty = 0.85$, $C_l^{tot} = 0.458$)
Objective Function	$\Delta DOC = \Delta D + \Delta W$
Constraints	$C_l = C_l^t$ $C_m = C_m^t$
Design Space	Crank and Tip section shapes; Crank thickness

where ΔD is the change of the wing-body drag expressed
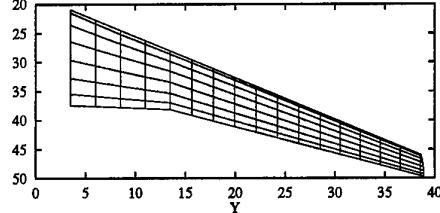
Figure 10: MDO wing - Planform View.

in counts and ΔW is the change in mass of one torsion box expressed in tons.

Starting from a reference trimmed configuration, the problem of reducing the DOC by only operating on the wing geometry without modifying other parts of the airplane is thus addressed. The trim condition is satisfied by maintaining the same angle of attack, the same lift and the same pitch moment than those of the original configuration. The root section is kept fixed. Crank and tip wing sections just as the crank thickness are allowed to change, which corresponds to 21 design variables. In addition, it is assumed that crank thickness modification induces the same percentage change in tip thickness.

The structural wing model consists in a centre wing box which is integrally built into the centre fuselage to which are attached the port and starboard lateral wing sections. The centre wing box is a conventional metallic structure with three spars. The structural optimisation model of the wing uses 156 design variables involving size parameters. The finite element model is formed by around 12000 elements. A fine grid of 54 blocks and about 204000 cells has been built around the wing body configuration. It is used to compute the trim condition of the reference geometry and to verify the aerodynamic characteristics of the optimised one. A coarse grid, which is the eighth of the fine, has been implemented into the optimisation system in order to maintain the overall optimisation cost at a reasonable level. For the same reason, the optimised wing mass was approximated by a curve fit as function of the crank thickness.

Table 1: Aerodynamic performance of the optimised configurations.

Case	Config.	Cl	Cm	Cd
Ref	w-b coarse grid	0.4946	-0.1963	0.02120
	w-b fine grid	0.5131	-0.2047	0.01700
	exposed wing	0.4550	-0.1835	0.01390
Opt	w-b coarse grid	0.4928	-0.1957	0.01790
	w-b fine grid	0.5154	-0.2049	0.01370
	exposed wing	0.4579	-0.1848	0.01060

The reduction of drag only results from a reduction of the wing wave drag, as it was expected from the problem definition. Aerodynamic performances of fuselage and tail are maintained unchanged. The use of a coarse grid seems to be adequate since the drag variation between the reference geometry and the optimised one is nearly the same for the two grids.

The improved configuration is obtained after a few global iterations of the optimisation process, which nevertheless corresponds to around 150 functional evaluations. The DOC is reduced while meeting the constraints at each iterations.

Table 2: Wing section thickness (%) and wing mass (Kg) of the optimised configurations.

Case	RootTc	CrankTc	TipTc	Wing Mass
Ref	14.00	10.00	8.800	28764
Opt	14.00	8.785	7.730	30562
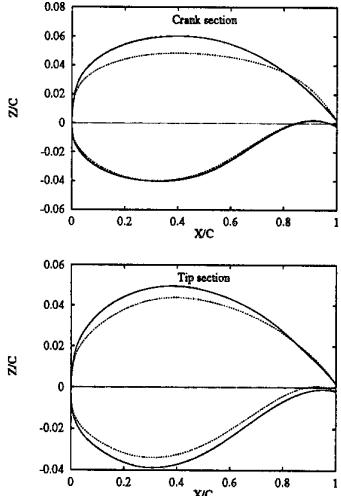
Figure 11: MDO wing - Comparison of Initial and Optimised Contours.

For the optimised geometry, the upper surface of the crank section is flattened. This effect has been mainly obtained by the redesign of the camber line. Except the decrease in the maximum thickness, the thickness distribution is only slightly altered in the rear part of the airfoil. In the case of the tip section, the major changes again apply on the camberline, with a tiny reduction of the leading edge curvature in the thickness distribution. The sectional pressure plots indicate a movement towards a two-shock structure on the upper surface.
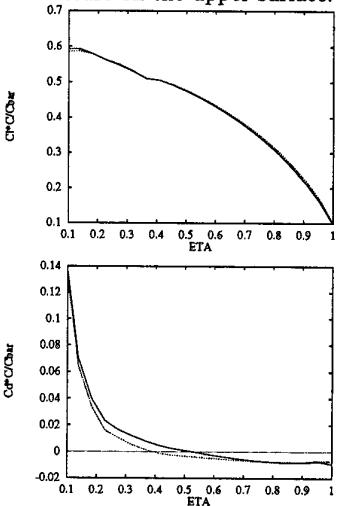
Figure 12: MDO wing - Comparison of Span Loads.

Spanwise loads distributions display a decrease of the drag in the central part of the wing, where lift and pitch moment are approximatively maintained at the same level than those of the reference wing. The loss of lift in the inboard part of the wing is recovered by the outboard sections. The opposite behaviour is found on the pitch moment. By comparison with the problem without
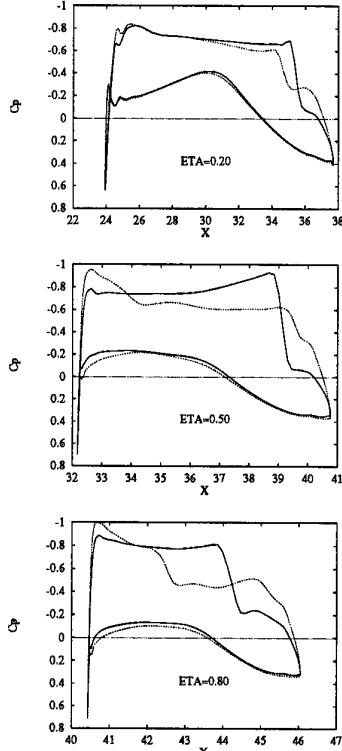
Figure 13: MDO wing - Comparison of Pressure Distributions.

crank thickness modification, the reduction of crank section thickness has the effect of further reducing drag not only in the central part of the wing, but also inboard. It leads nevertheless to an increase of the wing mass.

7 CONCLUSION

Mono- and Multi-disciplinary capability of the optimisation system has successfully been demonstrated for 2D and 3D applications. The capability of the design tool to be able to account for explicit constraints and multi-objectives within the optimisation process is of paramount importance for industrial applications. Nevertheless, the cost of sensitivities is a key factor when advanced modelling methods are used. Cheaper sensitivities and parallel implementations are requested. Future works will involve

1. more accurate gradients computation (adjoint equations, use of automatic differentiation),

2. introduction of other disciplines within the design loop (aeroelasticity, electromagnetism, ...).

8 ACKNOWLEDGEMENTS

References

[1] Vanderplaats, G.N., *ADS - A Fortran Program for Automated Design Synthesis*, User Manual, 1987.

[2] Vanderplaats, G.N., *Numerical Optimization Techniques for Engineering Design*, McGraw-Hill Series in Mechanical Engineering.

[3] Hicks, R. and Henne, P.A., *Wing Design by Numerical Optimization*, Journal of Aircraft, vol 35, n. 7, 1978.

[4] Farin, G., *Curves and Surfaces for Computer Aided Geometric Design*, Academic Press, 1989.

[5] Periaux J. et al eds., *Optimum Aerodynamic Design and Parallel Navier-Stokes Computations*, Vieweg, 1998.

[6] Allwright S., *MDO Process and Specification for the Primary Sensitivity Study*, MDO Technical Report MDO/SPEC/BAE/SA960430, 1996.

DISCUSSION

Session III, Paper #20

Prof Slooff (NLR, Netherlands) noted that in their work, optimising on the basis of Euler equations often led to non-unique solutions, that is several minima of about the same level. In such cases the additional constraints helped to reduce or eliminate this "non-uniqueness". Had the authors encountered this problem?

Dr Selmin indicated no specific experience of this issue, but agreed that adding constraints should help. He saw this as a requirement for a more precise definition of the original design problem.

Mr Perrier (Dassault, France) asked how better predictions of sensitivity could be ensured as he believed that decisions on constraints should come from good knowledge of constraint sensitivity.

Dr Selmin noted that his team intended to improve prediction of sensitivity by moving from the use of finite differences to automatic differentiation to evaluate the gradients.

Design and Optimization of Wings in Subsonic and Transonic Regime

Fernando Monge *, José Jiménez-Varona [†]

Instituto Nacional de Técnica Aeroespacial (INTA)

Carretera de Ajalvir km 4.5 28850 Torrejón de Ardoz (Madrid), Spain

* Director, Fluid Dynamics Department, e-mail: mongef@inta.es

[†] Research Engineer, Fluid Dynamics Department, e-mail: jimenezj@inta.es

For a realistic and practical aerodynamic optimization the most appropriate combination of the three sets of tools taking part in the process should be carefully studied. That is, the optimization should allow an easy implementation of constraints, and should be multipoint without the need to prescribe pressure distributions in the objective function; the design space should be broad enough; and the analysis tool should be fast and robust. Taking into account these criteria, a code for multipoint design and optimization of wings in subsonic and transonic regime has been developed and will be described in this paper. The objective can be any combination of the global aerodynamic coefficients, and geometrical and physical constraints can be applied. Results for subsonic and transonic cases will be presented. Flexibility in the use of the design variables allows many different tests to be performed before the best solution is achieved. Lastly, the computational cost is reduced by the use of a low level code for computing the aerodynamic coefficients.

1 Introduction

The quality of the results in the use of numerical optimization for the design of aerodynamic configurations depends on the appropriate choice of a lot of parameters. These are usually interdependent and do not always affect the solution in the same direction, especially when the gradient computation is required. For example, the use of more complex models for computing the flow does not necessarily improve the results because of the numerical noise; this also applies to the type and number of design variables; as well as the way in which the global aerodynamic coefficients are determined, whether by local or far field methods, among many other factors.

The first decision to be taken concerns the type and number of design variables, which is a subject that has not been sufficiently covered in our opinion. The design space should be broad enough to avoid the dependency of the starting geometry in the final solution as much as possible. As a first step we have found it is very important to replace the set of points usually defining the initial geometry by an analytical definition. For that purpose, an automatic adjustment by Bèzier polynomia has been used. After the validation with a data base of many different airfoils it was concluded that at least 25 control points are required to have an an error of definition less than 0.01%, which seems a reasonable criteria if the recommended initial changes in the design variables are 0.001. However, the shape functions originally included in the code (Wagner, Hicks-Vanderplaats, Legendre, etc ...) are still available for comparison purposes.

As regards the CFD codes to be used for computing the objective function robustness is their most essential characteristic for using them in an optimization loop, so that their sensitivity to the numerical data can be kept as low as possible. For this reason, and not only for the computing time, it is convenient to use low level codes as long as the nature of the flow allows us to do so, and particularly if the objective is a function of the global aerodynamic coefficients and, almost in any case, when we are in the first stages of the optimization, far from the final solution.

For the optimization itself a finite differences based commercial code [1] has been used with the options of following the steepest descent or conjugate gradients to where we have added the option of using a quasi-Newton method [2].

These three sets of numerical tools have been combined in a modular way to develop an optimization code for airfoils with high lift devices (OPTPER) and another one for wings (OPTWIN) that were employed for the application cases to be described in this report. They allow us to choose among different CFD codes ranging from velocity potential coupled with boundary layer until Navier-Stokes (2D) and until full potential coupled with boundary layer (3D). The objective function can be any combination of the global aerodynamic coefficients, and the equality or inequality restrictions to be imposed can be geometrical (leading edge radius, trailing edge angle, maximum thickness, camber, etc...) or physical (pitching moment coefficient, minimum pressure, etc...). Also we profited from the expertise collected in data bases such as ESDU for checking some other constraints like the maximum lift coefficient or the highest adverse pressure gradient along the optimization process.

2 Optimization procedure

The main code has been developed in a modular form in order to allow easy improvement or modification of any of its elements.

In general a geometry exists that requires aerodynamical improvement at certain flow conditions, but it is also possible to start the computation from any wing section selected from a given data base of airfoils, which always gives a kind of a guarantee that the final solution does not depend much on the initial wing. Its planform can also be optimized during the minimization process, but it is mainly designed using structural or handling qualities reasons.

Next the objective function has to be specified. It can be
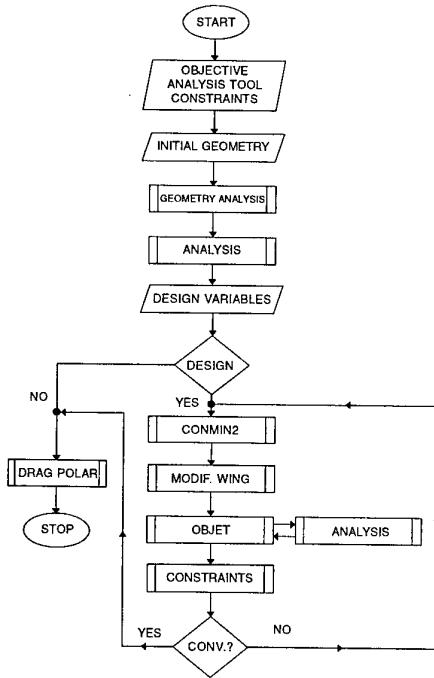
Figure 1: Flow chart for the aerodynamic optimization procedure

any combination of the global aerodynamic coefficients at one or several points of the drag polar. Apart from this, a pressure distribution can be prescribed as objective, but for this purpose the inverse methods are generally more efficient.

Carrying out an exclusively aerodynamic optimization other disciplines are not taken into account (structures, etc...). Generally it is also necessary to impose geometrical and/or physical constraints. At present it is possible to prescribe limits in the wing section area, leading edge radius, angles of thickness and camber line at the trailing edge, thickness at a given positions along the chord, minimum lift, maximum drag, absolute value of pitching moment and maximum velocity. This is also important in order to avoid unfeasible geometries, which is always a risk when the design space is sufficiently large.

For computing the objective function several analysis codes can be selected. In this report a 3D full potential method coupled with an integral boundary layer method has been used. It will be described in the following chapters along with the design variables.

As a minimization tool the original CONMIN code coupled with a BFGS routine to accelerate the convergence has been implemented (CONMIN2).

As regard as the data input, it was distributed in the following way: flow conditions and objective values, initial geometry, numerical parameters of the analysis, numerical parameters of the optimization, and number and type of design variables.

Before the minimization process starts the user may improve the initial geometry by distributing, smoothing and interpolating the original points if there are numerical oscillations in the curvature, which is internally evaluated.

Lastly, the following information can be obtained from the output: final geometry, evolution of design variables, aerodynamic coefficients and objective function. As the

new geometry is recorded at the end of every iteration, the user may stop the computation at any time without loosing the previous results, from which a new design strategy may start. In order to verify the quality of the final design a drag polar is computed at the end, and compared with that of the original geometry. The procedure described above is illustrated in figure 1.

3 Design variables

Concerning the design variables different possibilities have been included. First, a set of shape functions to be added to the original wing section was used: Wagner, Hicks-Vanderplaats, Legendre, cubic patches, etc ... After several trials the following functions were chosen [3]:

- Thickness

$$f_t(x) = 4 \cdot x^{p(x_{m_i})} \left(1 - x^{p(x_{m_i})}\right) \qquad (1)$$

being $p(x_{m_i})$

$$p(x_{m_i}) = \frac{\log\left(\frac{1}{2}\right)}{\log\left(x_{m_i}\right)} \qquad 0 \le x_{m_i} \le 1 \qquad (2)$$

and x_{m_i} is the percentage of chord where the maximum of $f_t(x)$ is located.

- Camber

$$f_c(x) = 4 \cdot (1 - x)^{p(x_{m_i})} \left(1 - (1 - x)^{p(x_{m_i})}\right) \qquad (3)$$

being $p(x_{m_i})$

$$p(x_{m_i}) = \frac{\log\left(\frac{1}{2}\right)}{\log\left(1 - x_{m_i}\right)} \qquad 0 \le x_{m_i} \le \frac{1}{2} \qquad (4)$$

whereas for $\frac{1}{2} \le x_{m_i} \le 1$ the expressions 1 and 2 are used.

They provide a more general design space than the other functions, and the number of design variables can be easily increased by an approppriate election of x_{m_i}. An infinite slope at the leading edge for the camber line has been avoided (fig. 2).

In this case we have considered nine design variables in order to control the radius of the leading edge, position and value of the maximum thickness and camber, angle of thickness and camber at the trailing edge, slope of the camber line at the leading edge and with at least one more degree of freedom.

However, when described as usual by a set of coordinates the numerical uncertainties in the definition of the original airfoil can have a negative effect in the optimization. It seems convenient to have the airfoil itself defined from the begining by analytical functions, and not only by the deformation shape functions. To this end a method for fitting the airfoil to a set of Bèzier polynomia has been developed and implemented into the code [4]. The control points are then used as design variables.
One function is used for each upper and lower side of the airfoil, where at the leading edge the continuity of first and second derivatives is imposed:

$$Y_{u,l}(s) = \sum_{i=0}^{NB} Y_{u,l}^B \left(\begin{array}{c} NB \\ i \end{array} \right) s^i (1 - s)^{NB-i} \qquad (5)$$
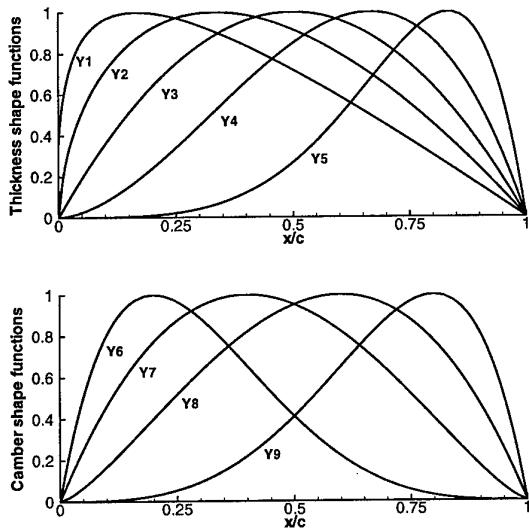
Figure 2: Thickness and camber shape functions

Figure 3: Bèzier fitting error for different airfoils

being Y the fitted coordinates, NB the number of Bèzier control points, s ranges between $0,\ldots,1$. The subscripts u and l denote upper and lower side respectively, whilst the superscript B means the Bèzier control point coordinates.

By solving two least square problems the control points $Y_{u,l}^{B}$ are computed. This can be done by numerical optimization or by directly solving the system of algebraic equations:

$$[A_{ij}]\{Y^{B}\} = \{B_{Y_i}\} \quad i,j = 1,\ldots,NB-1 \qquad (6)$$

where,

$$A_{ij} = \sum_{k=1}^{NP}\left[\left(\begin{array}{c}NB\\i\end{array}\right)\left(\begin{array}{c}NB\\j\end{array}\right)s_k^{i+j}(1-s_k)^{2NB-(i+j)}\right] \qquad (7)$$

and,

$$B_{Y_i} = \sum_{k=1}^{NP}\left[\left(\begin{array}{c}NB\\i\end{array}\right)s_k^i(1-s_k)^{NB-i}\cdot\left(y_0(s_k)-\right.\right.$$
$$\left.\left. y_0(s_1)(1-s_k)^{NB} - y_0(s_{NP})s_k^{NB}\right)\right] \qquad (8)$$

NP is the number of points defining the wing section and y_0 are the coordinates of the original wing sections.

We have used this last approach not only because of the much lower computing time required but also and mainly because not so many numerical parameters are required as in the first method.

Once the problem is posed and the solution method developed the main question is about the most appropriate number of control points for defining the airfoil and its deformations in order to have a large enough design space. A set of very different airfoils has been tested (conventional, laminar, supercritical, high-lift, etc...) and the outcome is that if the average error needs to be less than 10^{-4}, around 25 control points are required (fig 3). If an error of 10^{-3} is admissible then only 13 control points are needed. These errors are measured 1.0 being the chord of the airfoil. The results have been checked by using different solution methods:

Gauss-Jordan, Cholesky and QR.

We must also mention that, in any case, given to the nature of matrix $[A_{ij}]$, there are no additional benefits in using more than 30 control points due to numerical errors.

As a main conclusion, the use of 25 control points is recommended, which represents in general 21 design variables by taking into account the boundary conditions at the leading and trailing edges. This value is much higher than those mostly used up to now, but we consider it necessary for the solution to be independent of the design space.

4 Flow solver

The flow solver utilized in the present code for 3-D computations is the *FLO22vis* (INTA version). This code employs a viscous-inviscid interaction method in a direct iterative way to compute the flow past swept wings in transonic regime. It is based on the inviscid solver FLO22 by Jameson and Caughey [5] and the integral boundary layer code BL3D by Stock [6], recently modified by Yang and Wichmann at DLR [7]. The inviscid solver FLO22 has been modified at INTA to render the trailing edge as a grid line [8]. Additionally, the coupling procedure and the smoothing techniques for the displacement thickness have been improved. A more detailed explanation follows.

4.1 *Inviscid solver*

The inviscid solver is a finite differences code which solves the full potential equation in its non-conservative form in a non orthogonal co-ordinate system. The co-ordinate system is generated by a sequence of transformations. In its original formulation, the spanwise co-ordinate lines were aligned with the leading edge, but cut across the trailing edge in a tapered wing. In order to render the trailing edge as a grid line, an additional scaling by the local wing chord has been introduced in each of the wing sections. In the resulting co-ordinate system, both the leading and trailing edges are grid lines. New stretching transformations have been used outside the wing to increase the distance of the far field to the wing and to better implement the boundary conditions. The stretch-
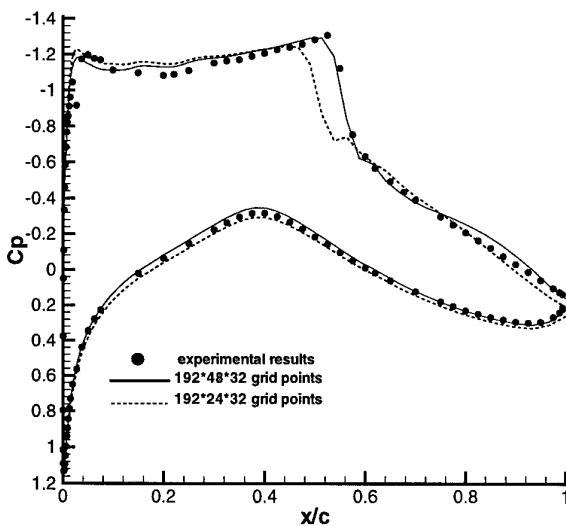
Figure 4: RAE 2822 airfoil. Cp distribution at $M = 0.73$, $Re = 6.5 \cdot 10^6$ and $CL = 0.8$

Figure 5: DLR F4 wing. Cp distributions on several spanwise sections at $M = 0.75$, $Re = 3 \cdot 10^6$ and $C_L = 0.5$

ing in normal direction at transonic flow is especially important. The resultant system of non linear algebraic equation is solved by an iterative relaxation procedure SLOR (Successive Line Over Relaxation).

4.2 Viscous solver

The viscous solver is an integral boundary layer code. It solves the laminar and turbulent boundary layers in a general non-orthogonal curvilinear coordinate system. In the laminar part, a family of similarity profiles of Falkner-Skan is used in the streamwise direction, whilst a combination of these profiles are used in crossflow direction. For the turbulent boundary layer, Coles velocity profiles of two parameters are used in the streamwise direction, and Mager or Johnston profiles are used in the crossflow direction. Transition is fixed or is computed by a set of empirical correlations. The 4th-order Runge-Kutta scheme is used for the numerical integration, in which the x-direction is the marching direction.

4.3 Coupling procedure

The concept of displacement thickness is used for the interaction of the external flow with the boundary layer. This method only provides a proper treatment of 'weak interaction' phenomena. An underrelaxation technique is introduced to avoid instabilities, and a special smoothing of the displacement surface by means of cubic Bèzier splines is employed to avoid strong irregularities in the shock region and in the trailing edge.

4.4 Validation

The flow solver has been widely validated after its improvement. Two sample cases in transonic flow will be shown below. It is important to compare not only global values but also pressure distributions. For potential flow, isentropic flow and irrotational flow are assumed. Discrepancy with the correct Rankine-Hugoniot result is small if the shock upstream Mach number is $M_1 \leq 1.3$. Moreover, the viscous-inviscid interaction takes into account only weak interaction phenomena. At $M_1 \geq 1.3$ incipient separation occurs, thus our viscous-inviscid coupling is less accurate.
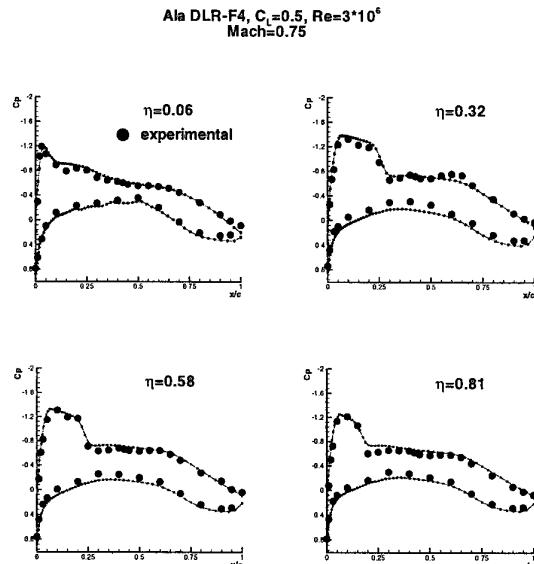
4.4.1 RAE 2822 airfoil

A limit case for comparison may be case 9 of reference [9]. At $M = 0.73$, $Re = 6.5 \cdot 10^6$ and $\alpha = 3.19$ deg. the boundary layer measurements show flow close to separation, and the shock upstream Mach number is $M_1 \approx 1.3$. Figure 4 shows the comparison of experimental and computed pressure distributions. The dashed line shows the result using a grid of $192 \cdot 24 \cdot 32$ points, and the solid line represents the results with a mesh of $192 \cdot 48 \cdot 32$ points. There is an important difference in the shock location. The reason is that, with the stretching transformation used in the normal direction, the far field is too close to the wing with the coarser mesh. A finer grid is needed to have the far field at a sufficient distance to avoid any influence of the far field into the supersonic zone. Although not shown here, the boundary layer parameters show good agreement with the experimental ones before the shock. After the shock, there are some differences, especially in the displacement thickness.

4.4.2 DLR-F4 wing

Another test case of a typical transonic wing will be shown. During 1997-98 INTA has participated in the *AEREA F4 Model Test Programme* to study the scale effects on the DLR-F4 wing-body model in the new criogenic european tunnel *ETW* (European Transonic Windtunnel). The range of Reynolds number was $3 - 33 \cdot 10^6$ and the range of Mach number was $0.6 - 0.81$. Thus, the amount of experimental information is very important and permits the validation and assessment of CFD codes [10, 11]. In this AEREA campaign, pressure measurements were not made, but there are experimental data obtained by the *Garteur Group AG-01* [12]. Figure 5 shows the C_p distribution in several spanwise sections of the DLR-F4 wing at $M = 0.75$, $C_L = 0.5$ and $Re = 3.0 \cdot 10^6$.

The computational mesh used had $192 \cdot 48 \cdot 64$ grid points and the computational time was about $1\frac{1}{2}$ hour in a SGI DN 10000 Power Challenge workstation (300 mflops). The mesh is finer than in the previous case to take into account the large variations of geometry in spanwise direction; otherwise the shock will not be
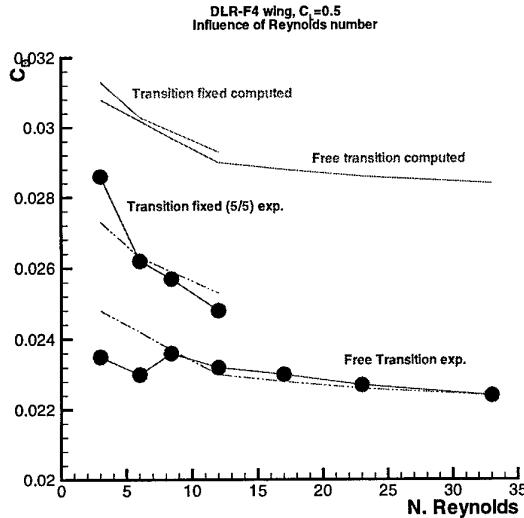
Figure 6: DLR-F4 wing. Reynolds effects on drag coefficient at $C_L = 0.5$
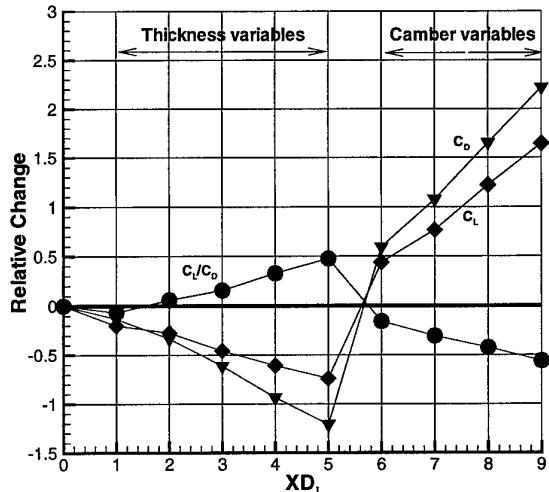
Figure 7: Sensitivity analysis for the subsonic case

properly captured. It can be seen that the comparison of the theoretical results with the experiments is good. There are some differences in the lower side due to the incapability of the flow solver to predict the influence of the body, and also to difficulties in the implementation of Kutta condition.

With regard to global values, figure 6 shows the drag coefficient at $M = 0.785$ and $C_L = 0.5$ at several Reynolds numbers. The comparison is done with fixed transition (5%/5%) and free transition. The fuselage drag has been computed using an analytical procedure. The figure shows that drag is overestimated using the code, but it is worth noting that the experimental results have not been corrected, and that Reynolds number effects include pseudo Reynolds number effects due to aeroelastic distorsion. Two curves representing a translation of the theoretical curves have additionally been plotted in the figure to compare the trends of both theoretical and experimental results. It can be observed that, despite the results at Reynolds number of $3 \cdot 10^6$ for fixed transition and $3 - 6 \cdot 10^6$ for free transition, the influence of Reynolds number in drag is well predicted. It must be underlined that at Reynolds number of $3 \cdot 10^6$ a small trailing edge separation is present in the kink region of the trailing edge [12], thus the drag increases.

A general conclusion is that the code can predict the flow past wings in transonic regime at attached flow conditions with sufficient accuracy. These are the cruising conditions. The advantage of using this kind of code is that an optimization code with this flow solver will not be highly time consuming.

5 Results

To show the capabilities of the method two cases (subsonic and transonic) have been tested. But before any optimization run can be started it is important to take into account several considerations. With the same engineering objective there are many different ways to proceed. For example, the aerodynamic efficiency could be optimized by using it directly as objective function, or by optimizing C_L with C_D as constraint or viceversa. But it is also possible that not all of those three strategies will provide a feasible design, if any.
On the other hand, when viscous effects are included in the analysis the changes in the objective function can be

highly non linear and it is very important to choose the most appropriate values for the initial design variables, not so small that the objective does not change, and not so large that the modified geometry can not be analyzed. That's why we have first computed the sensitivities of C_L and C_D to changes in the design variables. It also gives us an idea of the convergence criteria to use in the optimization run in order to avoid as many analyses as possible. Lastly, it provides useful information about the convenience or not for scaling the variables and for applying limiting values.

5.1 Subsonic case

The first exercise has been the optimization of the wing of an RPV called *SIVA (Sistema Integrado de Vigilancia Area)* designed at INTA. The flow conditions are $M = 0.2$ and $Re = 1.5 \cdot 10^6$. The wing has no twist, a surface of 4.5 sq.m., 5.81 m of span, 0.905 and 0.485 m of chord at the root and at the tip, respectively. Among a broad set of different airfoils, the *Eppler-580* was selected. At cruise conditions the angle of attack is 1.5 deg. and the lift coefficient $C_L = 0.56$.

By using the nine design variables described in § 3 (eqs. 1 to 4) the sensitivities computed for a change of 10^{-3} in each variable are plotted in fig. 7. There is an slight decrease in lift and drag when the thickness increases, but the efficiency $\left(\frac{C_L}{C_D}\right)$ in general increases, and more so when the deformation approaches the trailing edge. The opposite happens as regards the camber deformation.

From these values the following problem has been posed: improvement of $\left(\frac{C_L}{C_D}\right)$ at a weighted rate of 0.5 at 0.0 deg. and 0.5 at 2.0 deg. with the constraint of having a section area not smaller than that of the original one. By running a multipoint optimization, the use of an arbitrary constraint in the leading edge radius is avoided. It is also advisable not to use higher values of angle of attack when the accuracy of the results gets worse. The flow is supposed to be fully turbulent.

A design with the airfoil Eppler-580 as starting geometry was carried out. A sequence of three meshes, from coarse to fine, are utilized in order to accelerate the convergence and to save computing time. The geometry obtained is plotted in fig. 8 compared with the original one. As
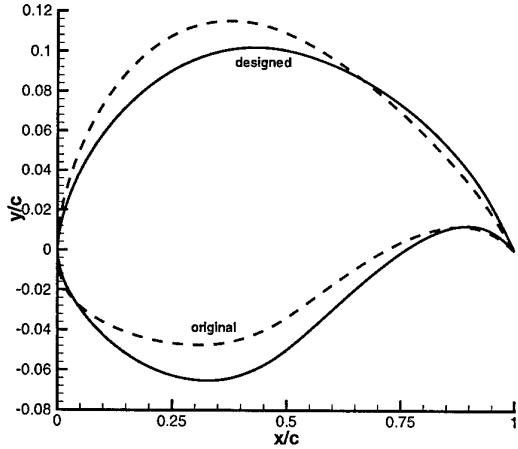
Figure 8: Geometries of both original and designed wing sections for the subsonic case
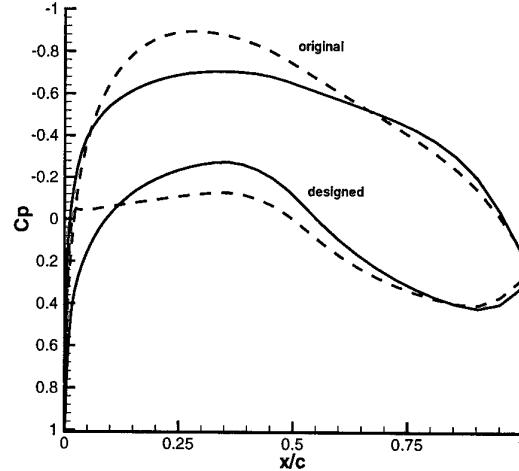
Figure 10: Pressure coefficient at central section of both original and designed wing (subsonic case)
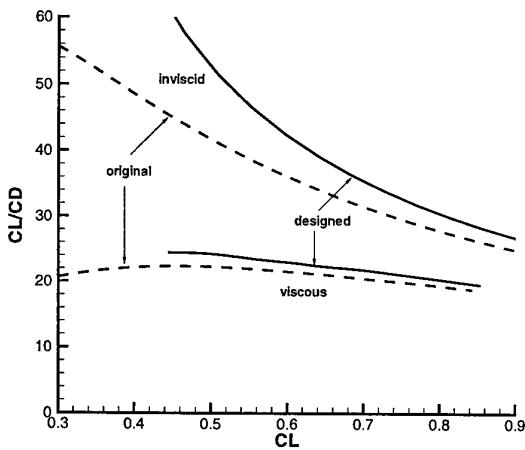
Figure 9: Efficiency vs lift coefficient for the original and designed wing in inviscid and viscous flow (subsonic case)


Figure 11: Geometries of NACA 0015, original and designed wing sections for the subsonic case

expected from the sensitivity results the camber has decreased for most of the chord. The efficiencies for a range of C_L's are plotted in fig. 9 where the results for an inviscid run are also included. For the viscous computation the efficiency is improved 9.4%.

The pressure distributions for the mid section of both wings are represented in fig. 10. It can be seen that the maximum velocity has decreased, which is usually positive in terms of drag. Besides, the pressure gradient around the leading edge on the lower side is much smoother. A further study should be made about the more adverse pressure gradient close to the trailing edge on the upper side, using different verification methods.

In order to check the dependency of the solution on the initial geometry an additional design has been carried out with the same objective and constraints as before, but starting from a conventional wing section (NACA-0015). The results are plotted in figures 11 and 12. It can be seen that even in this case the aerodynamic characteristics of the original section have also been improved,

showing in a broader sense the capabilities of the method.

Lastly, a test case using Bèzier polynomia has been carried out. It is enough using 13 control points (10 design variables) for an error of 10^{-3}, as it was pointed out in figure 3. A finer grid than in the previous cases has been used. The grid is a C-H mesh of $160 \cdot 24 \cdot 32$ points, fine enough in a subsonic case. The initial wing section is again the NACA 0015 airfoil. The total number of design cycles needed were 8, with 85 evaluations of the objective function. The search direction was that of the BFGS (quasi-Newton) method. Additionally, there is no asumption of fully turbulent flow. The transition is computed by means of empirical methods. The computing time was 24 *hours* 49 *min* in a SGI Power Challenge workstation (300 mflops). Figure 13 shows the initial section, the original section of the *SIVA* wing and the designed section using the Bèzier polynomia. The efficiencies of both the original and designed wing are plotted in figure 14. In order to increase confidence in the new design, two different codes have been used to analyze both the original and designed wings. One code is the solver employed by our

Figure 12: Efficiency vs lift coefficient for the original and designed wing with NACA 0015 as initial section (subsonic case)

Figure 14: Efficiency vs lift coefficient for the original and designed wing using Bèzier polynomia with NACA 0015 as initial section (subsonic case)

Figure 13: Geometries of NACA 0015, original and designed wing sections for the subsonic case using Bèzier polynomia

5.2 Transonic case

The design of transonic wings is more time consuming than in subsonic flow. In order to simplify the optimization procedure, the design shown in this paper was done fixing the planform and twist, and the wing sections are the same in every spanwise section of the wing. In these conditions, the improvement of wing features will depend on the airfoil features. The wing to improve is a trapezoidal wing of aspect ratio $AR = 8.0$, leading edge sweep angle $\Lambda = 27.5$ deg., taper ratio $\lambda = 0.4$ and linear twist. A typical grid for wing analysis has $192 \cdot 48 \cdot 48$ points. For the optimization, a coarser mesh will be used, because of the computational time. Figure 15 shows the transonic wing.

With the same design variables as used in the subsonic case, the sensitivities are plotted in figs.16,17. This time comparing the inviscid and viscous results.

As shown, the risk of obtaining very different designs when using viscous and inviscid analysis is high, as the sign of the gradients is different for some design variables and aerodynamic coefficients. For instance, by increasing the thickness in the rear part of the wing section the drag also increases when the analysis is inviscid but decreases for a viscous analysis.

The design conditions are $M = 0.82$, $Re = 6.0 \cdot 10^6$. The goal is to improve $\left(\frac{CL}{CD}\right)$ at a weighted rate of 0.5 at 1.5 deg. and 0.5 at 3.0 deg. with the constraint of having a section area not smaller than that of the original one.

The design is done using nine design variables described in § 3 (eqs. 1 to 4). The final wing section can be seen in fig.18 along with the original one. In the same figure the section designed by running the analysis as inviscid is plotted. It is not surprising that in this case the first impression is that the geometry does not look good due to the solution being much more dependent on the design variables used as there is a greater occurence of local minima. The need to take viscous effects into account is clear, especially in transonic flow where the interaction between the shock wave and the boundary layer can so greatly modify the designed geometry.

The efficiencies of the original wing and the viscous design are plotted in fig. 19. As expected in any transonic case, for the final evaluation of both two wings at

optimization method, i.e. *FLO22vis* code, and the other one is a commercial low order panel method coupled to an integral boundary layer method (*VSAERO* code). This code computes a lower drag than the former one, but it is worth noting that both codes show similar trends for both wings. There are some differences in the high C_L values range. In this case the results of the finite differences code are less accurate. In cruise condition both codes predict a similar improvement of the efficiency.

A final comment on this case is that, a design of the wing section of an RPV has been performed starting from an initial section far from the 'optimal' one. The result is an airfoil with similar behaviour of the selected airfoil (Eppler-580) at cruise conditions, and also at off-design conditions. A very few number of constraints have been imposed. This result shows the capabilities of the optimization method presented in this paper. The cost in terms of computational effort is not so high.

Figure 15: Planform view of the transonic wing. Typical surface mesh for analysis

Figure 17: Sensitivity analysis for the transonic case (con't)

Figure 16: Sensitivity analysis for the transonic case
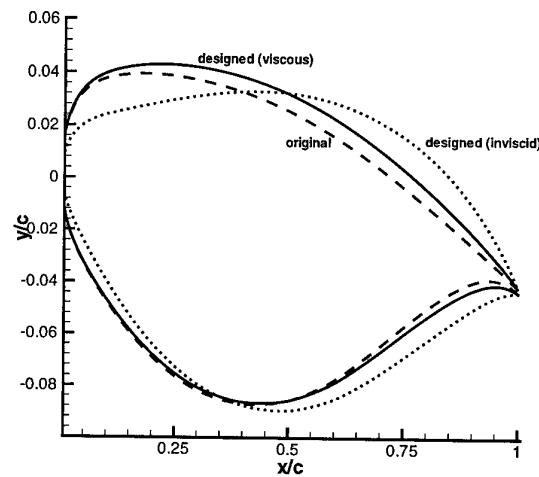
Figure 18: Geometries of both original and designed wing sections for the transonic case

off-design conditions this time it is not so important to include viscous effects compared with the subsonic case (fig. 9) as the relative contribution of friction drag is smaller. At the main design condition the efficiency is improved by 23.5%. As can be seen in fig.20, the main changes in the pressure distribution at the same flow condition are located, as expected, around the shock wave, which is now weaker, while it remains almost the same on the lower surface.

6 Conclusions

A modular optimization code for wings has been described. It allows any combination of the global aerodynamic coefficients to be used as objective function along with a broad set of geometrical and physical constraints. Even though it is possible to use a prescribed pressure distribution as an objective, it is not necessary to know anything about it. The examples shown here have been run on a SGI DN-10000 Power Challenge workstation (300 mflops). In any case, most designs can

be obtained from one day to another.

There are many more capabilities than those included in this paper, especially in the selection of the number and type of the design variables, including the planform modification, but the decision will be provided by the application to more different cases. At the moment, the following recommendations can be mentioned:

- From our experience in airfoil design (and we think it can also be extended to wings) it is not clear whether in any of the cases there are advantages in using high level codes instead of low level ones, taking into account that at design conditions the flow is expected to be attached and the shock waves, if any, are weak. Besides, the low level codes are generally more robust.

- On the contrary, care needs to be taken about the size of the design space. It has been shown that unless the changes in the geometry are expected to be small, around thirty design variables for a real wing
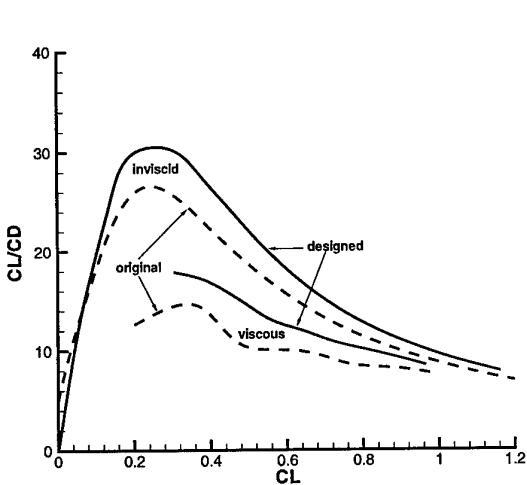
Figure 19: Efficiency vs lift coefficient for the original and designed wing in inviscid and viscous flow (transonic case)

Figure 20: Cp distributions on several spanwise sections at $M = 0.82$, $Re = 6 \cdot 10^6$ and $\alpha = 1.5$ deg. (transonic case)

design are needed, including planform modification.

- There is no engineering design without the possibility of running multipoint optimization.

- Lastly, even though the viscous contribution can be small, in any case the analysis should include viscous effects, especially in the transonic cases when no pressure distribution is prescribed, even if the friction drag is not included in the objective. Otherwise, the final geometry could be unfeasible or at least very dependent of the design variables used.

Finally, in the short term we plan to include the options already available in the 2D code OPTPER mentioned above for the design and optimization of airfoils; namely, to add the option of free transition as a new design variable [13] and to use control theory for computing the gradients [14].

Acknowledgements

References

[1] G.N. Vanderplaats. CONMIN -a Fortran Program for Constrained Function Minimization, User's Manual. Technical Report TM X-62,282, NASA, 1978.

[2] W. Press, W. Vetterling, S. Taukolsky, and B. Flannery. Numerical Recipes in FORTRAN, The Art of Scientific Computing. Cambridge University Press, 1992.

[3] V. Ibañez, F. Monge, and B. Tobío. Estrategias de Diseño Aerodinámico : Métodos Inversos y de Optimización. In 3er Congreso de Métodos Numéricos en Ingeniería, Zaragoza, Junio,3-6,1996.

[4] B. Tobío and F. Monge. Optimizacion numérica de perfiles aerodinámicos definidos mediante polinomios de Bézier. In V Encontro Nacional de Mecanica Computacional, Guimaraes, October,20-22,1997.

[5] A. Jameson and D.A. Caughey. Numerical Calculation of the Transonic Flow Past a Swept Wing. Contractor Report 153297, June 1977.

[6] H.W. Stock. Integral Method for the Calculation of Three-Dimensional, Laminar and Turbulent Boundary Layers. Technical Report 77/51 B, Dornier, 1978.

[7] Yang Q.-Z. and G. Wichmann. Calculation of Transonic Wing Flow by Interaction of a Potential and an Integral Three Dimensional Laminar-Turbulent Boundary Layer Method. Technical Report IB 129-98/11, DLR, August 1998.

[8] José Jiménez-Varona. Computations of DFVLR-F4 model using a Viscous Flow Solver for Transonic Wings. Technical Report AT/TNO/4510/001/INTA/98, INTA, February 1998.

[9] P.H. Cook, A. McDonald, and M.C.P. Firmin. Aerofoil RAE 2822 - Pressure Distributions, and Boundary Layers Measurements. In AGARD-AR-138, pages A6-1 to A6-77, 1979.

[10] D. Schimanski. The AEREA F4 Model Test Campaign. Technical Report E 9004 TR 0009, European Transonic Windtunnel, January 1998.

[11] D. Schimanski. ADDENDUM to TEST REPORT of the AEREA F4 Model Test Campaign. Technical Report E 9004 TR 0012, European Transonic Windtunnel, September 1998.

[12] G. Redeker et al. A Selection of Experimental Test Cases for the Validation of CFD Codes. In AGARD AR-303, volume 2, 1994.

[13] F. Monge and G. Vicente. Diseño aerodinámico de perfiles multicomponentes con transición libre. In V Encontro Nacional de Mecanica Computacional, Guimaraes, October,20-22,1997.

[14] F. Monge and B. Tobío. Aerodynamic design and optimisation by means of control theory. In IV World Congress on Computational Mechanics, Buenos Aires, Argentina, June, 29-July 2,1998.

DISCUSSION

Session III, Paper #21

Dr Nangia (Nangia Aero, UK) suggested that pitching moment should be included in the optimizations, as this would strongly affect Cl/Cd conclusions through the effect on trim drag, etc...

> **Mr Monge** agreed, pointing out that the option to take account of pitching moment as a constraint, or within the object function, is already included in his code. The sample cases presented in the paper were only intended to show some of the tool's capabilities.

A multiobjective approach to transonic wing design by means of genetic algorithms

A. Vicini, D. Quagliarella
CIRA – Centro Italiano Ricerche Aerospaziali
via Maiorise 81043 Capua (CE), Italy

1. Summary

In this work a transonic wing design problem is faced by means of a multiobjective genetic algorithm, and using a full potential flow model. The applications here presented regard both planform and wing section optimization. It is shown how both geometric and aerodynamic constraints can be taken into account, and how the multiobjective approach to optimization can be an effective way to handle conflicting design criteria. An interpolation technique allowing a better approximation of Pareto fronts is described. Two possible ways of improving the computational efficiency of the genetic algorithm, namely a parallel implementation of the code and a hybrid optimization approach, are presented.

2. Introduction

Transonic wing design is a very complex task, even if considered from a purely aerodynamic point of view. In fact, several criteria must be met in the design of any efficient transport wing, including good drag characteristics, buffet boundary high enough to permit cruising at design lift coefficients, no pitch-up tendencies near stall, no unsatisfactory off-design performances etc.[1]

Recent advances in computational techniques have made it possible to effectively address much more complex design problems than was previously possible, and concurrently reduce the design cycle flow time. The rapid improvements in the speed of computers have then originated a growing development of numerical optimization techniques for applications to aerodynamic design. Several techniques are today available[2], from mature gradient based methods to more recent approaches like automatic differentiation, control theory based methods and genetic algorithms (GAs). It is not possible, generally speaking, to state the overall superiority of one method over the others; in fact, there are several characteristics that must be considered, and that may assume different importance depending on the specific problem at hand. Among these characteristics we may mention: 1) the generality of the formulation, i.e. the possibility to rapidly set up different optimization problems, including also the use of different analysis tools; 2) robustness, intended as the capability to find global optima and reduce the need of human interaction and expertise; 3) the possibility to deal with multiple design objectives and constraints; 4) computational efficiency, for a practical use of the design approach.

On the other hand, because aerodynamic shape design represents only a part of the overall design of a flying vehicle, and because the need for an effective multidisciplinary approach to the design task is rising, it is important to identify the difficulties which are typical of multidisciplinary environments. Among these we may mention the necessity to operate at system level, and consequently managing and interrelating design objectives of different nature. Moreover, the dimensionality of the design space may increase to a point where traditional mathematical programming methods are likely to find severe difficulties. The design problem may be characterized by a mix of continuous, discrete and integer design variables, and the resulting design space can be non convex or even disjointed. For all these reasons, optimization methods which do not rely on the computation of gradients, in particular evolutionary programming and genetic algorithms, are receiving a considerable growth of interest[3]; in fact, these strategies are less susceptible to pitfalls of convergence to local optima, and generally offer a more robust approach to complex design problems. Indeed, the major weakness of such methods lies in their poor computational efficiency, which still prevents their practical use when the evaluation of the cost function is expensive, as happens with three-dimensional aerodynamic problems and complex flow models.

In this work a multiobjective genetic algorithm[4] is used for a transonic wing design problem, using a full potential flow solver as aerodynamic analysis tool. In the design examples here presented, the optimization of the wing planform is first addressed through a multiobjective approach, by taking into account both aerodynamic and structural weight considerations; afterwards, the wing sections are optimized to improve the aerodynamic performances by decreasing drag for a specified lift, while controlling some geometric characteristics of the airfoils and the pitching moment coefficient. Two different approaches for the enhancement of the computational efficiency of the procedure are illustrated; the first one is a parallel implementation of the code, which exploits the favourable structure of the genetic algorithm, while the second one is a hybrid approach obtained by including a gradient based optimization routine among the set of operators of the GA.

3. The Genetic Algorithm

Genetic algorithms belong to the class of evolutionary strategies, which common feature is the attempt to emulate the mechanisms of biological evolution. In their original formulation[5], a set of possible solutions to the problem at hand (population) are coded into bit strings (*chromosomes*); a number of operators are then used for the transformation and improvement of these solutions by evolving through subsequent generations[6]. The first component of a GA is therefore a scheme that allows for a coded representation of possible solutions; as stated above, a bit string codification is usually adopted, by representing each design variable through a fixed length binary number, and linking together all the coded variables in a single string. Then, there must be a criteria for the evaluation of the *fitness* of each individual of the population, which is a measure of how good the corresponding solutions are, allowing for a ranking of the individuals of the population; this criteria is of course problem dependent. The functions used for the simulation of the biological evolution when applied to the chromosome strings must then be devised. A criteria for the selection of the pairs of individuals that are going to reproduce must be chosen, such that selection probability is higher for individuals characterized by higher fitness. The parents chosen for reproduction are then mated through a *crossover* operator, which allows the recombination of their chromosomes; finally, the two strings obtained can undergo a mutation, consisting in a random variation of a little portion of the information coded in them. A number of different selection, crossover and mutation operators can be used; though the choice of these operators may have strong influence on the performances of the procedure, for a given optimization problem[7], it doesn't affect the basic scheme of the algorithm.

As already stated, a peculiar feature offered by GAs is their capability to face multiobjective optimization. When several design goals need to be achieved in an optimization problem, these are usually combined together so that a single scalar objective function is obtained. In this way, the problem becomes amenable to all classical optimization algorithms. The drawback of this approach is that the solution of the problem is strongly dependent on the (arbitrary) choice of the relative weights assigned to the objectives; moreover, if the objectives to be minimized are of different nature, as happens for example when multidisciplinary optimization problems are faced, it is difficult to understand how to interrelate them properly.

It can be convenient to follow a different approach, by classifying all potential solutions to the multiobjective optimization problem into *dominated* and *non dominated* (Pareto optimal) solutions. One solution is not dominated if there is no other solution which is better with respect to all design objectives. The Pareto front is the set of all the non dominated solutions; it follows from the definition that, if a solution belongs to the Pareto Front, it is not possible to improve one of the objectives without deteriorating some of the others.

By virtue of their structure, GAs are capable of facing multiobjective design problems in a more direct way; in fact, by selecting individuals according to the domination criteria instead of on the basis of a single fitness value, the set of Pareto optimal solutions can be closely approximated. In this way, a number of possible alternative so-

lutions are obtained, each one meeting the requirements of the problem at different levels of compromise. Hence, the characterizing feature of a multiobjective GA is the introduction of the domination criteria in the method used for individuals selection. In this work, this is accomplished through a *random-walk* operator: the current population is distributed over a toroidal landscape, a starting point is chosen at random, and the parents are selected as the locally non dominated individuals met in two subsequent *walks*, of a given number of steps, from that starting point; if more non dominated individuals are met, the first one encountered is selected.

In some of the applications here illustrated, an interpolation technique has been used to improve the quality Pareto front; this technique consists in what follows:

1) after each new generation G_i is completed, it is merged with the current Pareto front (P_{i-1}), and the new set of non dominated individuals (updated Pareto front, P_i') is extracted and stored;

2) afterwards, all the couples of adjacent individuals along the front are considered, and, if their distance (measured in the objectives plane) is higher than a specified percentage of the average distance between adjacent elements of the Pareto front, a new individual is generated by linear interpolation of their design variables;

3) after their evaluation, all the new individuals thus generated are merged with the current Pareto front set P_i', and the set of non dominated individuals P_i is extracted.

A flow chart of the resulting algorithm is illustrated in Fig. 1. This procedure has two positive effects: the first one is the enrichment of the Pareto front at the end of each generation, as many of the elements obtained through interpolation belong to the non dominated set; the second advantage is the exploitation of the first one, and it is obtained when an elitist strategy is adopted by selecting some of the individuals in the reproduction phase from the current Pareto front. The combination of these two effects allows to improve the approximation of the Pareto front with more and better distributed individuals.

4. Hybrid GA

Coupling a genetic algorithm with a different optimization technique can be an effective way to overcome its lack of efficiency while preserving its favourable features. Of course, many different strategies to hybridize the GA can be realized; the ideal approach is to combine the best features of both methods, so as to provide results better than those obtainable using either of the two techniques.

A simple GA may by itself be considered as the combination of two different search techniques, namely crossover and mutation, that are characterized by different behaviours. Crossover is a powerful tool to search the design space and single out the region where the global optima lie, but it lacks the capability of effectively refine the sub-optimal solutions found. On the other hand, mutation has a more local effect, since the modifications it produces are generally smaller in the coded parameter space. Hence, mutation has two important roles in simple GAs, i.e. to

provide the capability to effectively refine sub-optimal solutions, and to re-introduce in the population the alleles lost by the repeated application of crossover, maintaining population diversity. However, there is a broad class of problems, namely the ones where the fitness function is differentiable, for which gradient based techniques are much more efficient to locally improve a given solution. This suggests the introduction of a gradient based routine among the set of operators of the GA; mutation is then prevalently left with the role of keeping the diversity among population elements at an optimum level.

The genetic algorithm developed adopts a bit string codification of the design variables; anyway, this does not prevent the use of operators requiring real number list encoding, such as extended intermediate crossover and word level mutation.[4] In these cases the binary string is decoded into a real number list, the operator is applied and the set of modified variables is encoded back into a bit string. This scheme allows the use of a free mix of different type of operators.

A routine performing a gradient based optimization (with a conjugate gradients technique) has then been included as a GA operator, and called "hill climbing operator" (HCO). This operator is used as follows: through the application of the selection, crossover and mutation operators, an intermediate generation is created from the current one; afterwards, if the hybrid option is activated, some individuals may be selected and fed into the hill climbing operator to be improved, and then introduced into the new generation, as sketched in Fig. 1. Regarding the choice of the elements to be fed into the gradient operator, in the case of single objective optimization three different strategies are possible:

1. only the best fit individual of the current generation is chosen;

2. a number of elements determined by an assigned probability is picked using the selection operator;

3. a number of elements determined by an assigned probability is picked in a purely random fashion.

Of course, these strategies are characterized different levels of selection pressure, decreasing from strategy #1 to strategy #3; the relative performance will therefore depend on the optimization problem. The above described scheme can be naturally extended for multiobjective optimization: in this case, strategy #1 becomes the (random) selection of a number of elements determined by an assigned probability from the current set of Pareto optimal solutions, while strategies #2 and #3 remain the same. Of course, the hill climbing operator is by its nature capable of dealing only with scalar objective functions; thus, when multiobjective problems are faced, the objective function fed into the HCO is obtained through a weighted linear combination of the n problem objectives, i.e. as $obj = \alpha \ obj_1 + (1 - \alpha) \ obj_2$ in the case of $n = 2$. The weighting factor α can be chosen at random or assigned explicitly to favour one of the objectives.

An airfoil inverse design problem is used to illustrate the behaviour of the hybrid procedure. In this case, the objective function to be minimized, for a given Mach number and angle of attack, is computed by:

$$obj = 10 \int_S \left(c_p - c_p^{(t)} \right)^2 ds \qquad (1)$$

where c_p and $c_p^{(t)}$ are the current and target pressure distributions, respectively, and S is the current airfoil contour; the fitness is then obtained as $f = 1/obj^2$. A full potential transonic flow solver, with non-conservative formulation, has been used to calculate the flow field. The airfoil geometry is represented by means of two 5th order B-spline curves, for the upper and lower parts. The coordinates of the control points of the B-spline constitute the design variables;[7] 7 control points are used both for the upper and lower surfaces of the airfoil, including those fixed at the leading and trailing edges, for a total of 18 design variables (the first control points at the leading edge can move only in direction y). The problem here presented consists in the reconstruction of the CAST-10 airfoil[8] at $M = 0.765$, $\alpha = 0$. This problem has been solved using a NACA 0012 as initial guess, which can be considered an absolutely generic starting point.

The design variables have been encoded using 8 bit strings (giving a chromosome length of 144 bits), and a 50 individuals population evolved for 100 generations. A 3-step random walk was used for individuals selection, with one-point crossover ($p_c = 1$) and word level mutation ($p_m = 0.02$). The hybrid strategies have been activated so as to select on average only one individual every other generation, and carry out 2 gradient iterations $N_{it} = 2$, $\eta = 1$) Hence, to consider the same total number of objective function evaluations, the hybrid strategies must be judged approximately at generation 70. Fig. 3 illustrates the convergence histories, each one averaged over 10 successive trials characterized by different starting populations, obtained with the GA and with the corresponding hybrid strategies. The convergence history obtained by the application of the gradient based method by itself is also shown in the same figure; in this case, of course, there are no generations of individuals, but the convergence history is reported in such a way that the number of required objective function evaluations can be obtained from the same scale (1 generation = 50 evaluations). Besides, it must be noted that a restart procedure had to be used in this case to take the solution out of a local minimum where it got stuck after a few iterations.

As can be seen, for a given GA, hybridization is always beneficial, meaning that a better result can be found with the same amount of computations, or that the same result can be obtained with a substantial reduction of computation needed (ranging in this case from 50 to 75%). In particular, strategy #1, when the hill climbing operator is applied only to the best fit individuals, appear as the less effective, probably due to an excessive selection pressure. At the same time, the behaviour of the gradient based method is considerably improved from the point of view of the robustness.

Another important characteristic that needs to be considered is the statistical dispersion of the results obtained starting from different initial populations; in fact, if it is correct to judge the convergence characteristics of a given GA by averaging the results of a number of runs, from an application-oriented point of view it is more important for the algorithm to guarantee satisfactory convergence performances even on a single run basis. Fig. 4 shows all the values of the objective function obtained at the end of each of the 10 different runs, for each one of the algorithms used; it can be observed how the scatter of the results provided by the basic GA is much higher than that obtained using

the corresponding hybrid algorithms.

5. Parallel GA

The structure of GAs naturally adapts to the use of parallel computing, allowing to obtain remarkable efficiency improvements. When a population of individuals needs to be evaluated, it can be divided into a number of subpopulations which are sent to different processors; in this way, it is possible to evaluate the whole population in the same time required by a single analysis, if a sufficient number of processors is available. It is then also possible to take advantage by the splitting of the population, by using particular techniques. It has been shown for example[9] that, for some optimization problems, it can be convenient to let the different subpopulations evolve separately, with migrations between subpopulations allowed only to a controlled degree, and following particular strategies. Besides, it can be noted that, although this approach can be easily and naturally implemented on parallel computers, it is not exclusive domain of such kind of machines.

In this paper only a description of the parallel GA will be given. The individuals of each new generation are evaluated in a single loop, that follows the recombination phase and that can be carried out in parallel. The parallel programming model adopted relies on shared memory multiprocessing and the parallelism is implemented at the process level. The parallel machine adopted is a SGI POWER CHALLENGE system with 16 R-10000 processors. The parallel code has been implemented using the lightweight UNIX process primitives available on this machine[10].

The software is organized following the master-slave paradigm. In the initialization phase that precedes the first execution of the evaluation loop, the master process creates a pool containing a number of processes equal to the maximum number of processors available for the computation (NPROC). The child processes created are immediately put in a wait state, in which they remain until they receive a "go ahead" signal from the master to start the computation. This architecture has been chosen to avoid the inefficiency of creating a child process every time a computation is needed and killing it at the end.

When the master process enters the evaluation loop, it splits the population in subsets of maximum NPROC elements and then, for each subset, it copies the data relevant to a single computation in a shared memory area that is accessed by one of the child processes; afterwards, a signal is sent to the child, through a standard POSIX semaphore, so that the computation can begin. When the child terminates its computation, it copies the results in a memory region accessible to the master, but not over-writable by the other children. Thereafter, it sends a completion signal to the master (using another POSIX semaphore). The master waits for the completion of all child processes in a synchronization point. When this happens, the master collects the results and starts with the next subset of population elements. The child processes are terminated at the very end of the program, when all the evaluation loops related to each generation have been completed.

It can be observed that this architecture is efficient only when each sub-process has an even computational charge. If this does not apply, the computation process can loose efficiency because the master has to wait at the synchronization point for the completion of the slowest process.

Fortunately, this is not the case for the kind of application considered so that the efficiency decay can be neglected. However it is not difficult to modify the master so that it can assign a new task to a child as soon as this has completed the previous one.

6. Applications to wing design

6.1. Wing geometry parametrization

The parametrization of the wing geometry adopted for this work includes the possibilities to modify both the wing planform and the shape of the sections. For the sake of simplicity, in the application that will be illustrated the wing planform has been kept trapezoidal, so that all geometric characteristics vary linearly from the root section to the tip. In this case, a total of 6 design variables may be used: 4 of these act directly on the wing planform, namely the taper ratio λ, the sweep angle at 25% of the chord Λ, the aspect ratio AR and the twist angle θ; moreover, the (percent) thickness at the wing root and tip have also been included among the design parameters. The geometry modifications are made in such a way that the wing surface is kept constant, so that the average wing loading is not changed during optimization.

The wing geometry is assigned through a number of spanwise "control" sections, which shape can be modified in the optimization loop; intermediate sections are obtained by linear interpolation. The airfoil shape for each control section has been represented as a linear combination of the initial shape and a prescribed number of modification functions; the characteristic of these modification functions is that they are obtained as the difference between the initial airfoil shape and the shape of existing airfoils chosen from an available database, as follows:

$$y(x) = y_o(x) + \sum_{i=1}^{N} w_i \left[y_i(x) - y_o(x) \right] \qquad (2)$$

where y_o is the initial airfoil shape, y_i is the geometry of the $i - th$ airfoil of the database and w_i is the design variable associated with it. In this way, the design variable associated with each of these modification functions has an effect on the whole airfoil shape.

6.2. Wing planform design

As anticipated, the design of a transonic wing planform will first be illustrated; the design has been accomplished by minimizing inviscid aerodynamic drag, which combines induced and wave drag, and structural weight, at a given Mach number $M = 0.84$ and lift coefficient $c_L = 0.3$. The starting geometry chosen is the ONERA M6 wing[11]; this wing has an aspect ratio AR=3.8, a leading edge sweep $\Lambda = 30°$, a taper ratio $\lambda = 0.562$, and is untwisted. The shape of the airfoil is symmetrical, with a maximum thickness of about 9.8 % chord. A total of 5 design variables have been used; in Table 1 the initial values of the design parameters are reported together with the prescribed allowable ranges. The thickness at the wing tip has been fixed at the original value $t/c \mid_t = 9.8$ %. For all the cases that will be described, the constraint on the lift coefficient has been satisfied by

using the angle of attack as a free parameter, and letting the flow solver adjust it to meet the desired lift value.

The wing twist is distributed symmetrically between the root and the tip, so that a twist angle θ corresponds to an increase of local incidence of $\theta/2$ at the tip, and a decrease of $\theta/2$ at the root. The wing weight is computed using the algebraic equation of Ref. 12; this equation combines analytical and empirical (statistical) methods, and shows design sensitivity and prediction accuracy that make it possible to use it with success for preliminary design.

As can be seen from Table 2, individuals selection has been carried out through a 2 step random walk, with one-point crossover ($p_c = 1$) and bit mutation ($p_m = 0.1$), and a population of 16 individuals was let evolve for 10 generations.

The Pareto front obtained using the Pareto interpolation technique previously described is illustrated in Fig. 5 (where W_o and c_{Do} are the values of the original M6 wing), together with the planform of a few wings corresponding to the indicated positions along the front; the front is populated by 123 individuals. In the same picture also the Pareto front computed without the described interpolation technique is illustrated. In this case, 20 generations have been carried out, so that the two cases are compared approximately for the same total number of objective function evaluations; it can be seen how, in the latter case, a much coarser representation of the Pareto front is obtained (43 individuals).

In Fig. 6 the execution times of the parallel genetic algorithm are compared with those of the scalar version. The comparison is made running for 10 generations the same wing planform optimization problem described above. The speed-up obtained is generally very good, being very close to the number of available processors. It should be observed that the scalar version is faster than the parallel one when only one slave processor is activated; this behavior is due to synchronization and context switching overheads.

In Fig. 7 the values of the design parameters of the solutions belonging to the Pareto front are shown as a function of aerodynamic drag. It is interesting to observe how the variation of each design parameter along the front is far from being linear; in particular, "peaks" of some of the design variables can be found in correspondence of "valleys" of others. The distributions are nevertheless piecewise linear, which explains why also a linear interpolation between two elements on the Pareto front is likely to belong, in turn, to the Pareto front.

6.3. Wing section optimization

The design problem here presented consists in the minimization of (inviscid) drag for the ONERA M6 wing, at the design point $M = 0.84$, $c_L = 0.3$. The wing planform shape and the maximum thickness of the wing sections have been kept constant in the optimization process. This problem is first solved without additional constraints; only a geometrical constraint on the minimum allowable trailing edge angle (γ_{TE}) is used to avoid unfeasible geometries. The cases of a twisted and untwisted wing are considered separately. Afterwards, the same problem is faced introducing the requirement of controlling the value of the pitching moment coefficient during the optimization process, and an additional constraint on the leading edge radius to avoid undesirable off design performances. The

formulation of these design problems is summarized in Table 3.

6.3.1 Drag minimization

The results obtained for the optimization problems #1 and #2 of Table 2 are here illustrated. The objective function to minimize was c_D/c_L^2 (to account for small variations of the lift coefficient around the design value), with the fitness obtained as $f = 1/obj^2$. The constraint on the maximum thickness of the wing sections, so as to maintain it at the same value of the original geometry, is imposed by scaling the sections to the desired thickness after each geometry modification. Finally, the constraint on the trailing edge angle has been imposed as a filter, by assigning a very high value to the objective function of those geometries which violate it, and skipping the aerodynamic analysis.

The wing has been assigned using 4 spanwise sections, at the positions $\eta = 0$, 0.33, 0.66 and 1.0, and the optimization has been carried out beginning at the root and progressing to the tip in 4 subsequent cycles: in the first one, the modification to the airfoil shape was maintained constant in the spanwise direction; in the second cycle, the section at $\eta = 0$ was frozen, and the wing was modified from the section at $\eta = 0.33$ to the tip; in the third and fourth cycles, the same was done considering the remaining sections. A total of 12 design variables have been used for the wing sections modification.

The parameters used for the GA are reported in Table 2. As can be seen, selection was carried out using a 2 step random-walk, crossover was the extended intermediate recombination with probability 1, mutation was carried out at word level with probability 0.05, and the population size was 32.

As previously stated the described optimization run was first carried out considering an untwisted wing geometry; afterwards, a second optimization run with the same characteristics has been carried out, adding also the twist angle among the design variables. The twist was supposed to vary linearly from root to tip, so there was one extra design variable for it. Figure 8 illustrates the convergence histories obtained for the untwisted and twisted wings; as can be seen, 10 generations were used for the first modification cycle, and 5 for the subsequent ones. A total number of (approximately) 800 aerodynamic analyses were thus required. In Table 4 the aerodynamic coefficients of the original and modified wings at the design point are reported, including the values obtained at the end of the first optimization cycle; also the value of the twist angle θ is showed in the table. It can be seen that, in both the twisted and untwisted cases, most part of the gain in aerodynamic efficiency is obtained in the first optimization cycle, i.e. for a spanwise constant wing section. For the untwisted geometry the decrease obtained for inviscid drag is $\Delta c_D = 53.3$ d.c., which becomes $\Delta c_D = 58.0$ d.c. when twisting is allowed. This is essentially due to the reduction of wave drag, as induced drag is almost constant. Figure 9 illustrates the drag rise curves (at $c_L = 0.3$) of the ONERA M6 and the two optimized geometries. In Fig. 10 the shape of the airfoils of the control stations are illustrated, while Figures 11 and 12 show the Mach number distribution over the upper side of the original and optimized geometries. From these it can be observed how the suction peaks at the leading edge

are noticeably reduced, and the recompression from supersonic regime is moved close to the trailing edge, resulting in a marked decrease of the pitching moment coefficient. This situation is more apparent when twisting is allowed, especially in the outboard part of the wing; in fact, as can be seen from Fig. 10, the shape of the airfoils is supercritical from root to tip, whereas in the untwisted case the supercritical characteristic is lost when moving towards the tip. A difference between the two cases is also the leading edge radius of the wing sections, which is lower when the wing is twisted as can be expected.

6.3.2 Drag minimization with constrained pitching moment

In the second case considered an additional requirement regarding the pitching moment coefficient has been introduced as shown in Table 3. The pitching moment coefficient of the ONERA M6 wing at the design point is $c_M = -0.1315$ (evaluated using the full-potential flow model); thus, the considered constraint $c_M \geq -0.135$ corresponds to a maximum allowable decrease of about 2.5%. A multiobjective approach has been adopted in this case, with $obj_1 = c_D/c_L^2$, $obj_2 = (c_M - \tilde{c}_M)^2$. The value $\tilde{c}_M = -0.130$ has been used; in this way, the solutions on the final Pareto front will be characterized by pitching moment coefficients in the range from approximately $\tilde{c}_M$ to a lower value corresponding to the minimum drag solutions. Like in the optimization previously described, two separate runs have been carried out by allowing or not the wing twist to be modified; for the sake of simplicity, in this case the shape of the wing sections has been kept constant in the spanwise direction. The same parameters of Table 2 have been used for the GA, except for the population size which has been increased to 48 elements, and the length of the random walk which has been set to three steps. In Fig. 13 the solutions belonging to the final Pareto fronts are illustrated; it must be noted that the solutions are not reported in the objectives plane, but directly in the $c_d - c_M$ plane, which explains why their distribution doesn't look exactly as a Pareto front.

It is now possible to choose a solution with the desired characteristics among those obtained; the aerodynamic coefficients of the minimum drag solutions which satisfy the constraint on pitching moment are reported in Table 5. Fig. 14 shows the drag rise curves at $c_L = 0.3$ of these wings compared to the original wing. The twisted wing, though characterized by lower drag at the design Mach number, shows a higher drag at lower Mach numbers (drag creep) respect to the untwisted wing.

It can be seen that, in the case of the untwisted solution, the decrease in aerodynamic drag is approximately 45 drag counts, with the pitching moment coefficient within the acceptable value. On the other hand, with the twisted solution a decrease in aerodynamic drag of approximately 54 drag counts is obtained, and the pitching moment coefficient is even reduced with respect to the initial value. In Fig.s 15 and 16 the pressure distributions over the original and optimized wings are shown. When the wing is allowed to twist, it is possible to see how the intensity of the shock is reduced, while its position is to some extent anticipated in the outboard portion of the wing. Finally, In Fig. 17 the modified airfoil shapes are illustrated.

As can be seen, considering that the constraint on the pitching moment doesn't allow the optimizer to change the camber of the wing section very much, the final geometries in both cases are characterized by a significant reduction of the leading edge radius (see Table 5). This can be an unacceptable modification, as it may lead to unsatisfactory off design performances, in particular regarding high lift conditions (c_L^{MAX} of the clean wing). For this reason, the optimization procedure as described before has been repeated for the untwisted and twisted cases introducing an additional constraint on the leading edge radius, so that this could not be reduced to values lower than 1% of the local chord. In Fig. 18 the Pareto fronts thus obtained are shown, compared to those obtained without leading edge radius constraint. It may be observed how the solutions on these Pareto fronts are similar to those obtained without the leading edge radius constraint at the low drag end of the fronts, whereas they are characterized by higher drag values in the low pitching moment region of the fronts. Considering the same constraint $c_M > -0.135$, the characteristics of the solutions that can be extracted from these fronts are illustrated in Table 6.

As can be seen, the drag penalty of these solutions with respect to the corresponding ones without constraints on the leading edge radius is approximately 6.9 drag counts for the untwisted case, and 6.5 in the twisted one. In Fig. 19 the drag rise curves at the design lift coefficient of the optimized wings with and without the constraint on leading edge radius are illustrated.

Fig.s 20 and 21 illustrate the pressure distributions over the original and optimized wings, whereas the corresponding geometries are illustrated in Fig. 22. When the wing is twisted, the position of the shock wave is slightly anticipated, but its intensity is reduced.

7. Conclusions

A multiobjective genetic algorithm has been used for the optimization of a wing in transonic flow. In the design problems that have been described both geometrical and aerodynamic constraints have been taken into consideration. It has been shown in particular how multiobjective optimization can be an effective approach when conflicting design criteria must be met; in the application described this approach has been used to devise an optimum planform shape taking into account both aerodynamic drag and structural weight, and to control the value of the pitching moment while minimizing aerodynamic drag. A full-potential flow solver has been used as analysis tool; comparison of the results obtained with this flow solver with the corresponding ones obtained through Euler and Navier-Stokes solvers show that the full-potential model may be considered adequate for transonic cruise conditions, when viscous effects are not very important[14]. Simple semi-empirical criteria, like constraints on the maximum allowable Mach number ahead of shocks to avoid flow separation, may then be sufficient. On the other hand, if design problems of industrial relevance need to be faced, it is necessary to take into account complex geometries, and also viscous effects are to be included directly in the design loop to obtain more reliable solutions. Though genetic algorithms are effective and robust design tools, well suited for multidisciplinary environments, the critical issue still lies in

the computational effort they require. This makes their application unpractical when the fitness evaluation becomes computationally expensive. Two possible approaches to the problem have been investigated in this work, consisting in the hybridization of the algorithm to exploit the favourable features of gradient based search methods, and in the use of parallel computing.

References

[1] Lynch, F.T., "Commercial Transports - Aerodynamic Design for Cruise Performance Efficiency," Transonic Perspective Symposium, Progress in Aeronautics and Astronautics, Vol.81, D. Nixon ed., AIAA, New York, 1982, pp.81-147.

[2] *Optimum Design Methods for Aerodynamics*, AGARD-R-803, Nov. 1994.

[3] Hajela, P., "Nongradient Methods in Multidisciplinary Design Optimization - Status and Potential," J. of Aircraft, Vol.36, No.1, Jan.-Feb. 1999, pp. 255-265.

[4] Vicini, A., Quagliarella, D., "Multipoint Transonic Airfoil Design by Means of a Multiobjective Genetic Algorithm," AIAA Paper 97-0082, Jan. 1997.

[5] Holland, J. H., *Adaptation in Natural and Artificial Systems*, The University of Michigan Press, Ann Arbor, Michigan, 1975.

[6] Goldberg, D. E., *Genetic Algorithms in Search, Optimization and Machine Learning*, Addison-Wesley, Reading, Massachusetts, Jan. 1989.

[7] Vicini, A., Quagliarella, D., "Inverse and Direct Airfoil Design Using a Multiobjective Genetic Algorithm," *AIAA Journal*, Vol. 35, No. 9, Sep. 1997, pp. 1499–1505.

[8] *CAST-10-2/DOA 2, Airfoil Studies Workshop Results*, NASA CP 3052, 1989.

[9] Quagliarella, D., Vicini, A., "Subpopulation policies for a parallel multiobjective genetic algorithm with applications to wing design," IEEE SMC'98 Congress, San Diego, October 1998.

[10] D. Cortesi, A. Evans, W. Ferguson, J. Hartman, *Topics in IRIX^{TM} Programming — Chapter 8, Models of Parallel Computation*, Silicon Graphicsi Inc., 1996, Document Number 007-2478-004.

[11] Schmitt, V., Charpin, F., "Pressure distributions on the ONERA M6 wing at transonic Mach numbers," in *Experimental data base for computer program assessment*, AGARD-AR-138, Paper B1, May 1979.

[12] Torenbeek, E., "Development and Application of a Comprehensive, Design-Sensitive Weight Prediction Method for Wing Structures of Transport Category Aircraft," Technical Report LR-693, TU Delft, Sep. 1992.

[13] A. Vicini, D. Quagliarella, "Airfoil and Wing Design Through Hybrid Optimization Strategies," *AIAA Journal*, Vol. 37, No. 5, May 1997.

[14] A.Vicini "Transonic wing design using genetic algorithms", Report CIRA TR-98-212, December 1998.

design variable	initial value	allowable range
λ	0.562	[0.2 , 0.8]
Λ	30.0	[15 , 36]
θ	0.0	[-10 , 10]
AR	3.8	[3.5 , 4.2]
$t/c\,|_r$ %	9.8	[8 , 14]

Table 1 - Design parameters for the wing planform optimization.

	Planform optimization	Section optimization
Selection	Random-Walk, 2 steps	Random-Walk, 2 steps
Crossover	One-point	Extended Intermediate Recombination
P_c	1	1
Mutation	Bit	Word
P_m	0.1	0.05
Pop size	16	32

Table 2 - Parameters for the GA.

Design problem #	1	2	3	4	5	6
Mach	0.84					
c_L	0.3					
c_D	minimize					
c_M	free		$\geq$-0.135			
$t/c\%$	fixed = 9.8%					
twist	no	yes	no	yes	no	yes
γ_{TE}	$\geq 10°$					
L.E. radius	free			$\geq 1\%$ c		

Table 3 - Formulation of the design problems for the M6 section optimization.

Wing #	α	c_L	c_D	c_{Di}	c_{Dw}	c_M	θ
M6	3.3167	0.3000	0.01369	0.00700	0.00670	-0.13151	0.
1	1.6271	0.3002	0.00887	0.00705	0.00182	-0.22807	0.
2	1.4482	0.3004	0.00836	0.00711	0.00125	-0.23357	0.
3	1.1830	0.3007	0.00843	0.00706	0.00136	-0.22465	-1.4°
4	0.8530	0.3028	0.00789	0.00722	0.00067	-0.24006	-3.5°

Table 4 - Aerodynamic coefficients of the optimized wings (design problems 1,2).
Wing 1: untwisted, constant airfoil; wing 2: untwisted, variable airfoil;
wing 3: twisted, constant airfoil; wing 4: twisted, variable airfoil.

Wing #	α	c_L	c_D	c_{Di}	c_{Dw}	c_M	θ	r_{LE}
M6	3.3167	0.3000	0.01369	0.00700	0.00670	-0.13151	0.0	1.50%
1	3.4558	0.3000	0.00918	0.00700	0.00219	-0.13476	0.0	0.88%
2	2.8994	0.3002	0.00830	0.00731	0.00099	-0.12970	-4.09	0.37%

Table 5 - Aerodynamic coefficients of the optimized wings (design problems 3,4).
Wing 1: untwisted; wing 2: twisted.

Wing #	α	c_L	c_D	c_{Di}	c_{Dw}	c_M	θ	r_{LE}
M6	3.3167	0.3000	0.01369	0.00700	0.00670	-0.13151	0.00	1.50%
1	3.3823	0.3000	0.00987	0.00700	0.00288	-0.13475	0.00	1.14%
2	2.6742	0.3000	0.00895	0.00748	0.00147	-0.13237	-5.88	1.03%

Table 6 - Aerodynamic coefficients of the optimized wings (design problems 5,6).
Wing 1: untwisted; wing 2: twisted.
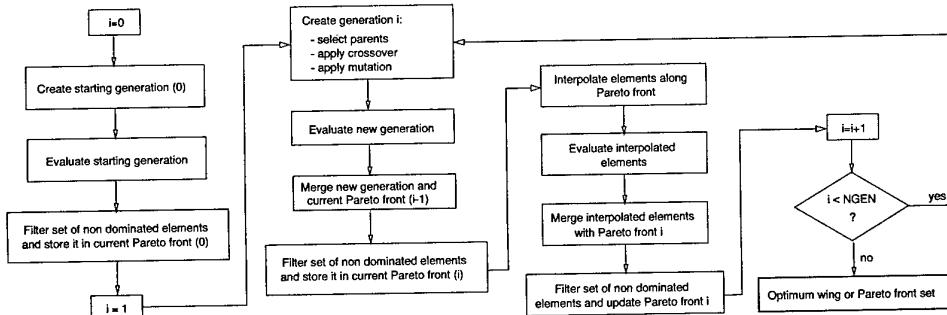
Fig. 1 - Flow chart of the multiobjective GA
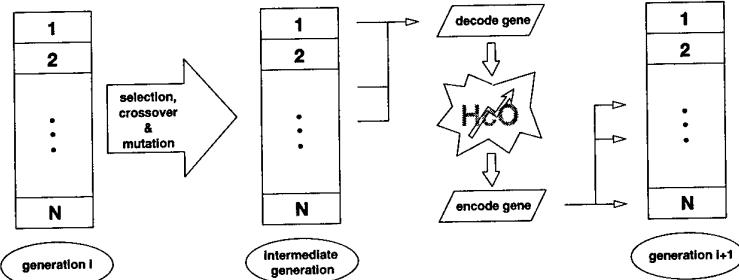
Fig. 2 - Sketch of the hybrid GA
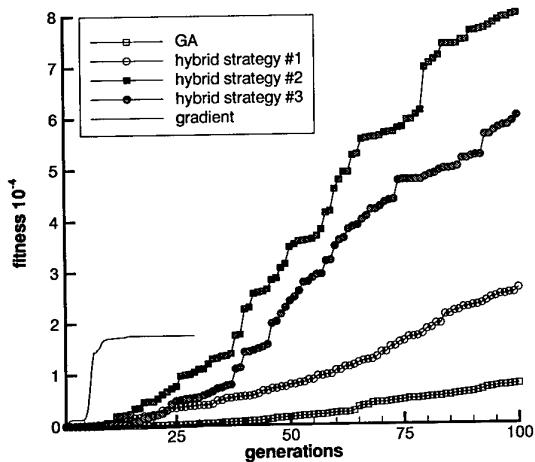
Fig. 3 - Convergence histories of the inverse airfoil design problem (averaged over 10 trials)
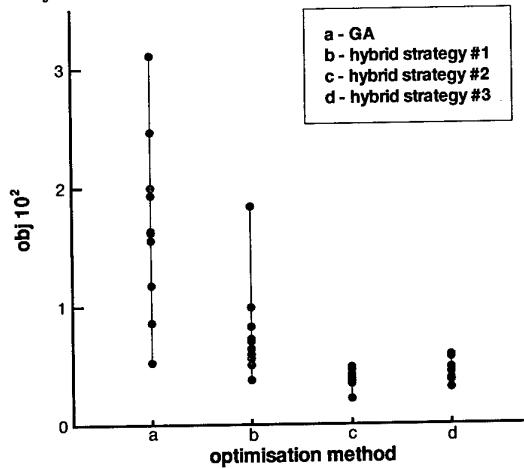
Fig. 4 - Scatter of results obtained in 10 different runs for the inverse airfoil design problem
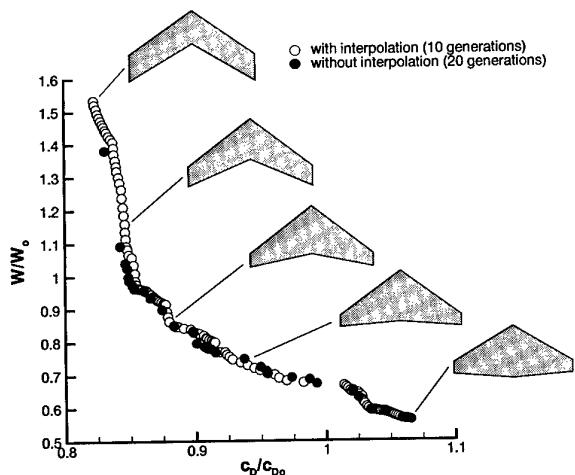
Fig. 5 - Pareto fronts for the planform optimization
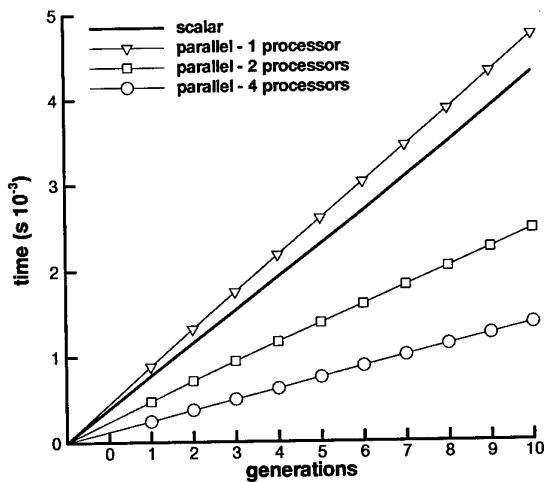
Fig. 6 - CPU times for the scalar and parallel GA
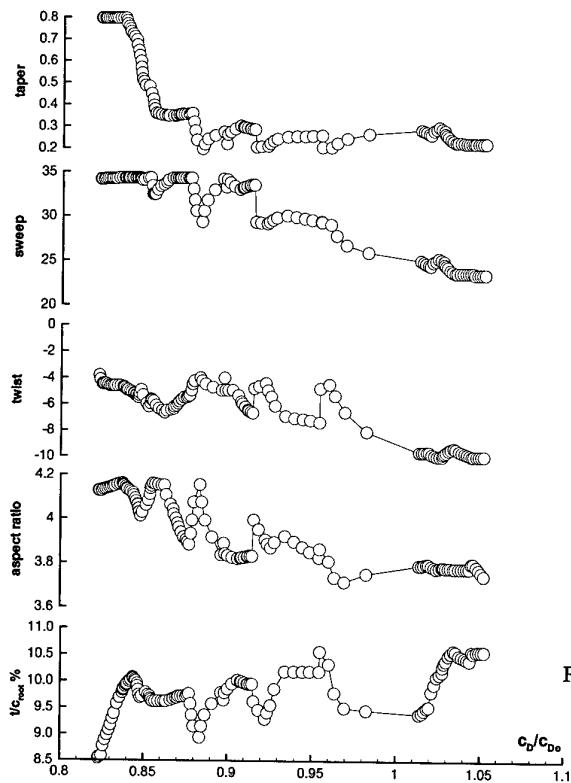
Fig. 7 - Parameters of the solutions on the Pareto front
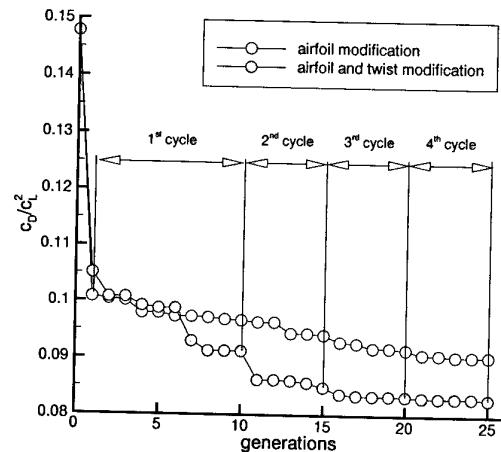
Fig. 8 - Convergence histories for the drag minimization problem
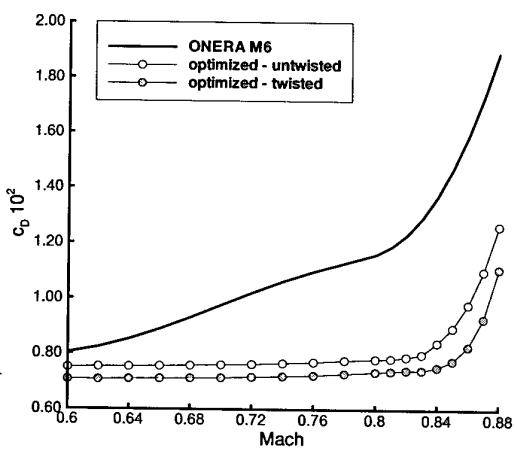
Fig. 9 - Drag rise curves for the original and optimized wings
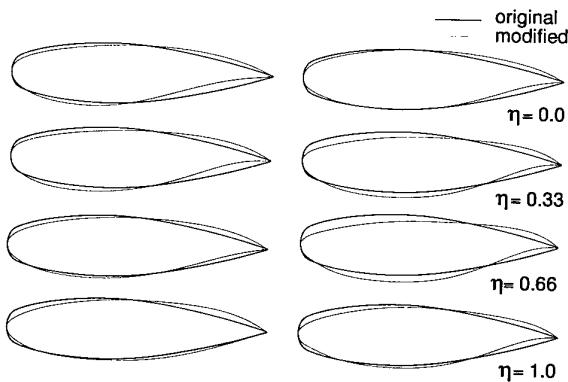
Fig. 10 - Shape of the modified airfoils;
untwisted (left) and twisted (right) wings
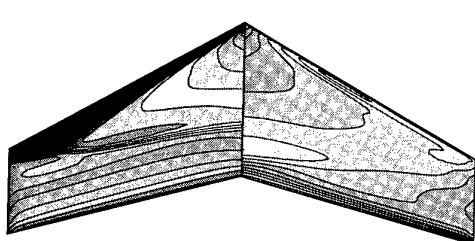
Fig. 11 - Mach number distribution on the original (left)
and optimized (untwisted) wing
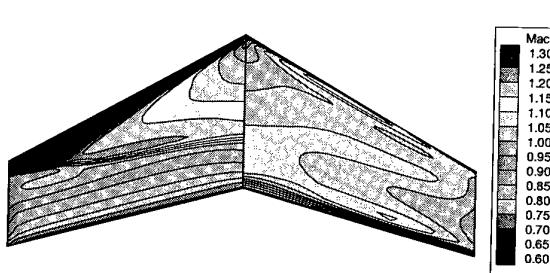
Fig. 12 - Mach number distribution on the original (left)
and optimized (twisted) wing
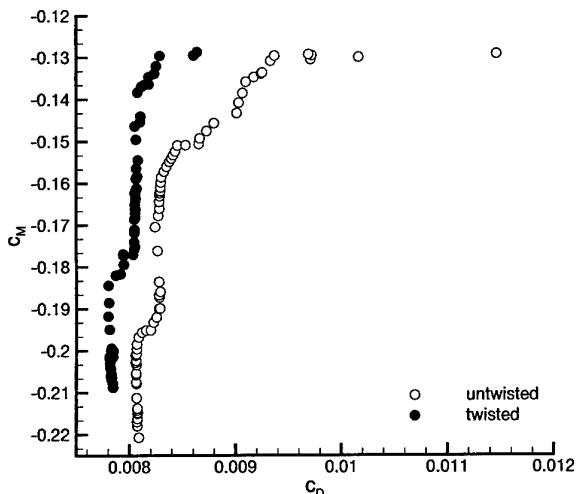
Fig. 13 - Pareto fronts obtained
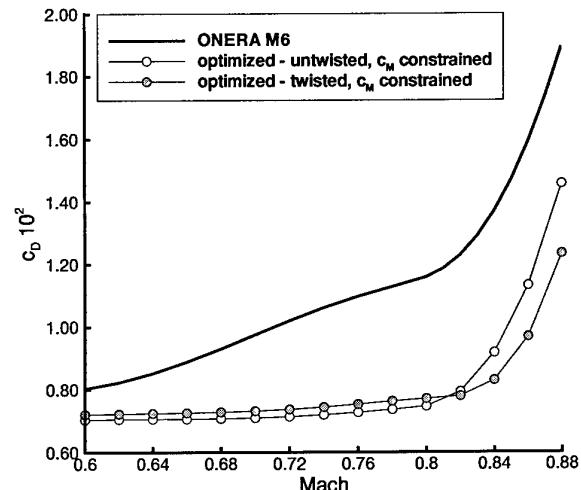
Fig. 14 - Drag rise curves for the original and optimized wings
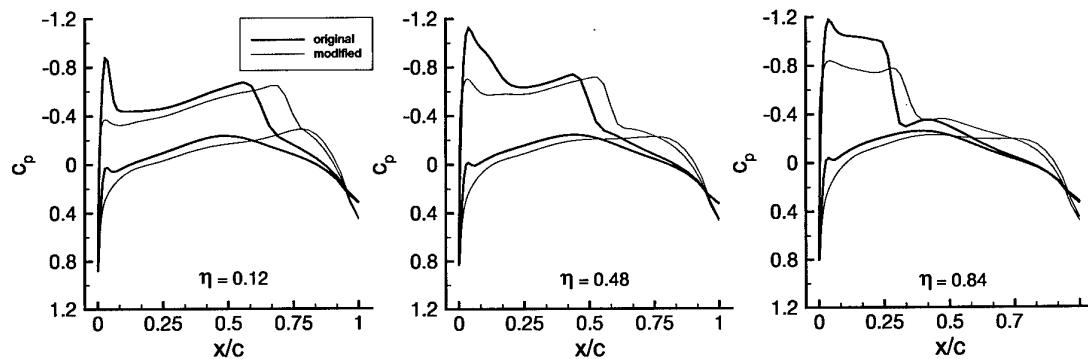
Fig. 15 - Pressure coefficient distributions on the original and optimized (untwisted) wings
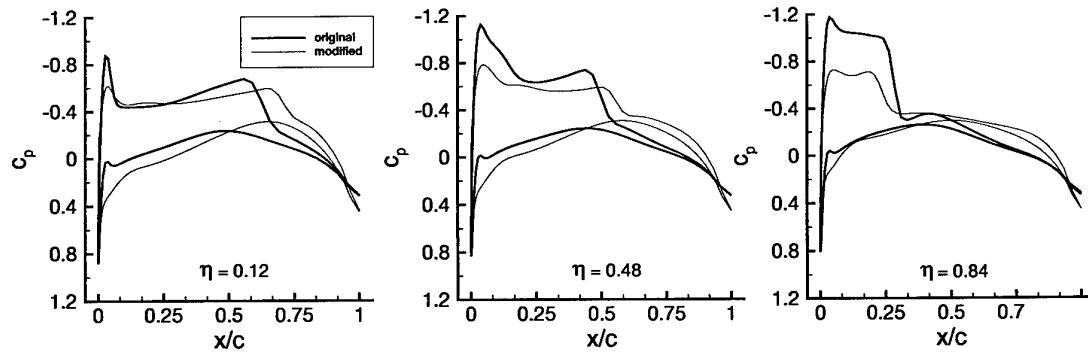
Fig. 16 - Pressure coefficient distributions on the original and optimized (twisted) wings

Fig. 17 - Shape of the modified airfoils for the untwisted (left) and twisted (right) wings
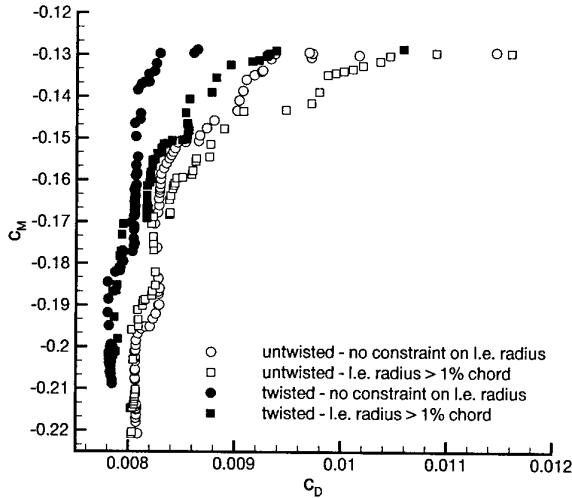
Fig. 18 - Pareto fronts obtained
with and without leading edge radius constraint
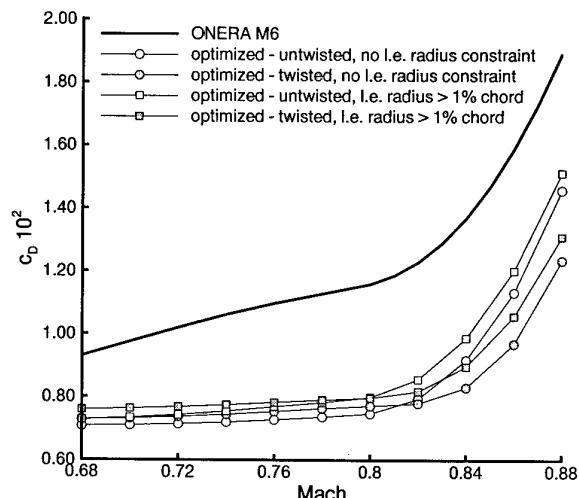
Fig. 19 - Drag rise curves for the original and optimized
wings with and without leading edge radius constraint
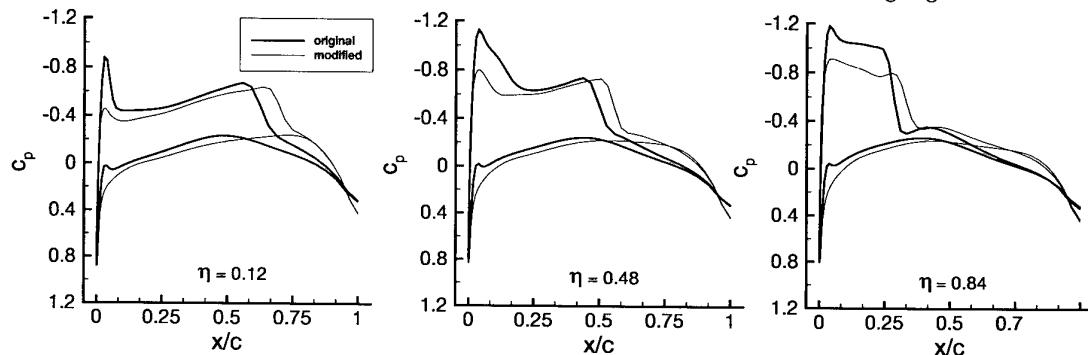
Fig. 20 - Pressure coefficient distributions on the original and optimized (untwisted) wings, with l.e. radius constraint
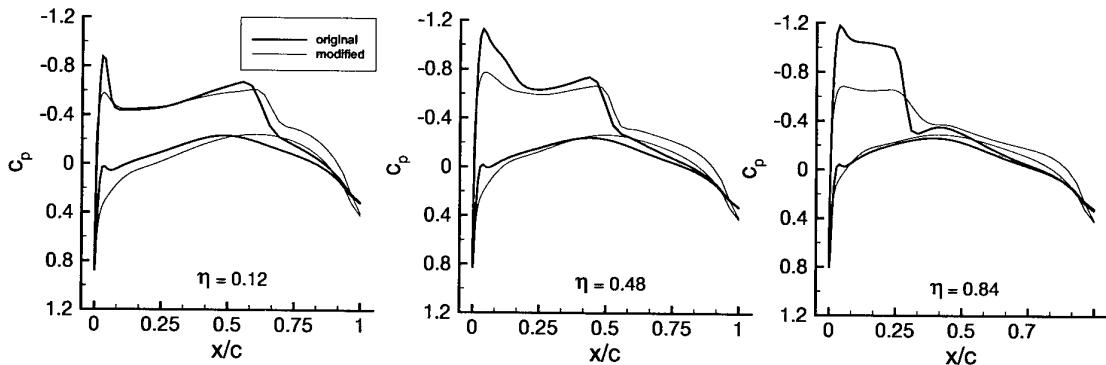
Fig. 21 - Pressure coefficient distributions on the original and optimized (twisted) wings, with l.e. radius constraint

Fig. 22 - Shape of the modified airfoils for the untwisted (left) and twisted (right) wing, with l.e. radius constraint

Application of Micro Genetic Algorithms and Neural Networks for Airfoil Design Optimization

Daniel C.M. Tse and Louis Y.Y. Chan

Institute for Aerospace Research
Aerodynamics Laboratory
National Research Council Canada
Ottawa, Ontario, Canada K1A 0R6

Abstract

Genetic algorithms are versatile optimization tools suitable for solving multi-disciplinary optimization problems in aerodynamics where the design parameters may exhibit multi-modal or non-smooth variations. However, the fitness evaluation phase of the algorithms casts a large overhead on the computational requirement and is particularly acute in aerodynamic problems where time-consuming CFD methods are needed for evaluating performance. Methods and strategies to improve the performance of basic genetic algorithms are important to enable the method to be useful for complicated three-dimensional or multi-disciplinary problems. Two such methods are studied in the present work: micro genetic algorithms and artificial neural networks. Both methods are applied to inverse and direct airfoil design problems and the resulting improvement in efficiency is noted and discussed.

1 Introduction

Aerodynamic design problems in the transonic regime are characterized by multi-modal topology in the design parameter space with possibilities of non-smooth variations. An example showing the multi-modal variations was constructed by Obayashi and Tsukahara (1997) who also pointed out that the presence of shock waves in transonic flow problems could introduce jump discontinuities in the design parameter space. The ability of genetic algorithms (GAs) to handle non-smooth topology and overcome local critical points in its search for a global optimum makes the method ideal for use in aerospace design optimization.

Although the ease of implementing GAs makes the method attractive, the use of the algorithm is hampered by the large number of fitness evaluations which is particularly costly for aerodynamic design problems. For such problems computational fluid dynamics (CFD) is often needed to provide aerodynamic data for evaluating performance. Thus, it is important to explore methods to improve the efficiency of GAs for on-going extension to three-dimensional applications and multi-disciplinary optimization (MDO).

Two-dimensional airfoil design problems provide a logical and economical means to explore strategies that have the potential to improve the performance of basic GAs. A special GA was designed by Zhu and Chan (1998) to deal specifically with the geometrical aspects of the problem; namely the positions and connectivity of the line segments that make up an airfoil profile. The method directly manipulates the coordinates of the airfoil surface to effect favorable changes, and has been demonstrated to show better efficiency than a standard binary coded GA for a number of two-dimensional examples that deal with geometrical shapes. However, the overall computational requirement is still high and the present work aims to explore methods to further improve the performance.

Two methods to improve the performance of genetic algorithms are studied in this paper, the first is the use of micro genetic algorithms (μGAs) and the second is the application of artificial neural networks (ANNs). The μGA strategy was derived by Goldberg (1989) and Krishnakumar (1989) to explore the use of small population sizes in genetic algorithm applications. Reeves (1993) also showed that for binary coding, a small population size is sufficient to reach the entire search space by cross-over alone. With a small population there will be rapid convergence to a possible sub-optimal solution, and the effective use of μGAs is to repeatedly generate new population members as soon as a measure of convergence has been achieved in a cycle of GA operation.

The implementation of the μGA concept is simple, and the method has been demonstrated to yield marked improvement over conventional large-population GAs. The use of μGAs can be found in Roy et al. (1997), Xiao and Yabe (1998), Abu-Lebdeh and Benekohal (1999), Chang et al. (1999), and the references contained therein. All the studies cited used binary-coded chromosomes, with applications ranging from process engineering to traffic scheduling. Although the range of application of μGAs is becoming extensive, their applicability has yet to be explored fully, and is certainly needed for aerospace design problems where computational requirement is enormous. Also there has not been much demonstration of μGAs for problems that use real number coding and our study provides information in this regard.

The second GA improvement strategy studied here is the use of artificial neural networks to supplement detailed computational analysis to provide fitness information for GAs to process. A properly trained ANN can provide fast and inexpensive data to assist engineering designs as demonstrated by Batill and Swift (1993) and Rai and Madavan (1998). The application of ANNs as approximate fitness evaluation tools for GAs, though suggested often, had seldom been put to practice. The combination of ANNs and GAs has been applied mainly for the construction of optimized neural networks through GA-based optimization techniques (Whitley (1995)).

Few applications of ANNs to GA processing have been reported. Podlena and Hendtlass (1998) used an ANN to classify regions in the search space to guide a GA to direct its search to high fitness regions. While details were presented on applications to the standard test cases given by De Jong (1975), only a little information was given for a more complex commercial application on aircraft trajectory planning.

Lingireddy (1998) presents a use of an ANN to provide quantitative data for GA search. In the study for a two-dimensional problem of aquifer parameter identification, GA coupled with finite element analysis (FEA) was found to be effective in estimating hydraulic conductivity but was computationally expensive. A feed-forward neural network was constructed for approximate function evaluation to save on computing cost. The simulation results show it was practical to use ANN and FEA within a genetic algorithm, but the study did not give any quantitative indication of reduction in computational effort.

To fulfill our second objective, an ANN is used as a quantitative alternative to provide aerodynamic coefficients for fitness evaluation so as to reduce the overall computational time of GA operation. The CFD results obtained during part of the GA operation are used to train the ANN in order to construct the response surface representing the design parameter space. With the topology of the design parameter space accurately represented, the fitness information can be obtained readily.

2 Optimization Examples

Two sets of numerical experiments are considered. The first is an inverse design problem where a target pressure distribution around an airfoil is specified and the airfoil shape is obtained by a GA operation to produce a profile that gives the desired pressure distribution. The second is a drag minimization problem with the constraint that the lift is fixed at a specified value.

The airfoil is assumed to operate in the transonic regime at Mach number 0.8 and angle of attack of 1.25°. For the first experiment the target pressure distribution is that of the NACA 0012 airfoil, and the NACA 64A410 is used to derive the starting airfoil samples. For the second experiment, both NACA 64A410 and NACA 0012 are modified to reduce the drag coefficient C_D at fixed values of the lift coefficient C_L

which are set to be 0.90 and 0.31 respectively for the two airfoils.

3 Coding Representation of Airfoils

Genetic algorithms work on a coding of design variables representative of the problem; therefore, efficient and effective parametric representation for airfoils is important for the success of the algorithm. For GA applications, airfoils should be represented by as small a parameter set as possible so the search space can be kept small. Also the smoothness of the profile forming an airfoil should be controllable to avoid inadmissible shapes.

Although less amenable to theoretical analysis, real number coding is a preferred choice for airfoil design problems. For such problems, multiple design parameters are involved and these parameters take values over different real number ranges. The use of real number coding eliminates the needs for coding and decoding of design parameters and can provide arbitrarily high resolution to the values of the parameters.

Zhu and Chan (1998) formulated a genetic algorithm for airfoil design problems that used the coordinate points on the airfoil as control variables. Although the underlying geometrical nature of the algorithm allows for the design of efficient GA operators for improved fitness evolution, the large number of design parameters causes difficulties for the mapping of the search space. The coding scheme uses over 100 control variables for a typical airfoil design study, and this number is significantly large to present difficulties in training an accurate ANN as observed by Tse and Chan (1999).

Open B-spline representation of airfoils is used in the present study as only a small number of control points are needed to represent satisfactorily a typical airfoil profile. Other useful advantages of B-spline are the smoothness of the profile can be specified explicitly and the information on concavity is readily available.

In open B-spline representations, the control nodes at the beginning and terminating ends coincide with the end-points of the resulting curve. Because the nose and tail points of an airfoil profile are fixed, the profile is split into a top half and a bottom half and a B-spline curve is used to represent each half.

To fit a B-spline curve to a prescribed profile, the order and number of nodes for the B-spline are specified first and then the resulting coordinates of the nodes are determined by a least square solution method. The B-spline fitting to the NACA 64A410 airfoil is shown in Figure 1. The order of the B-spline curve is six and a total of 10 control nodes are specified to fit each of the top and bottom profiles. A smaller number of B-spline nodes could also yield satisfactory results, but no effort was made to reduce the number of control nodes to an optimum. Details of the theory and numerical algorithms are presented in Rogers and Adams (1990).

4 Genetic Algorithm Operation

Each B-spline control node is considered a gene and the set of ordered control nodes describing a complete airfoil profile is considered a chromosome for GA operation. In subsequent discussion the fitness of a chromosome refers to the aerodynamic performance of an airfoil profile. Manipulation of the locations of the control nodes to obtain an optimal airfoil is the goal of GA operation and the various components of genetic operations are described in the following sections.

4.1 Fitness Evaluation

Fitness evaluation is the basis for the GA search and selection procedure and is usually the most costly part of the algorithm. An Euler flow solver is used as the primary means for obtaining aerodynamic information. This information is made available to train an ANN which then acts as a source for aerodynamic data for evaluating fitness. Detailed discussion of the CFD method and the implementation of ANN is discussed in following sections.

The numerical values of the fitness are also used to differentiate admissible profiles from inadmissible ones. To maintain physical realism, the airfoils should not have too many inflection points where concavity changes sign. If an airfoil exhibits too many inflection points, the fitness for that airfoil is assigned a very low value to ensure it has a low chance of surviving the genetic algorithm.

The fitness values for a generation of chromosomes are ranked and scaled linearly and uniformly. This scaling is necessary to prevent high fitness chromosomes from becoming overly dominant.

4.2 Selection and Population Replacement

Parents are chosen based on the Roulette wheel method where the probability of a chromosome being chosen is proportional to its fractional fitness value. Each pair of parents produces one offspring, and after a new population is produced, their fitness is compared to that of the parent generation and the best members are assigned to be the new generation. This elitist strategy has been observed to yield good performance.

4.3 Cross-over

A simple one-point cross-over scheme is applied. Given two parental chromosomes, an arbitrary cutting point is chosen where the genes positioned after the cutting point are interchanged. The smoothness of the resulting airfoil profiles is guaranteed by the B-spline formulation. The probability of cross-over is set at 80%, and smaller values tend to worsen the performance.

4.4 Mutation

Mutation is carried out by randomly selecting a gene and then changing its value by a random amount chosen within a prescribed range. Let $\{B_1, \ldots, B_{10}\}$ be part of a chromosome

that describes one side of an airfoil, with B_1 and B_{10} being the fixed nodes at the leading and trailing edges, respectively, as illustrated in Figure 2. For a gene chosen to undergo mutation (B_5 in Figure 2), its value will be altered by an amount (Δx, Δy) where

$$\Delta x = r_x \cdot \Delta x_{max}$$
$$\Delta y = r_y \cdot \Delta y_{max}$$

where r_x and $r_y \in$ (-0.5, 0.5) are random numbers distributed uniformly within the range. In this study Δx_{max} and Δy_{max} are both set to be 1% of chord.

As the above changes are applied to the selected control node, its neighboring control nodes are also adjusted so that the change in slope and curvature of the airfoil profile will not be too abrupt. The changes in the neighboring nodes ($B_2 \ldots B_4$, $B_6 \ldots B_9$) are done in proportion to the relative position from the node where the main change is effected as illustrated in Figure 2. The two end nodes B_1 and B_{10} are left unchanged.

As noted in Obayashi et al. (1998) the mutation probability for a GA using real number coding should be set at a higher value than when binary coding is used. The reason is that in binary coding a change in a single bit can effect significant change in the value of the design variable, but in real number coding a similar change has a lesser effect. Thus a higher mutation probability is justified as a means to enable the algorithm to search the design space thoroughly. The value of mutation probability is set to be 0.8 and lower values give degraded performance.

5 Micro GA Strategy

As discussed earlier, although µGAs have been demonstrated to provide faster convergence than regular GAs when applied to a range of engineering problems, their use has still been quite limited and apparently has not been tried on resource-intensive aerospace optimization problems. An objective of this study is to examine the applicability of µGAs to aerospace design problems where any reduction in computational effort would translate into significant saving in computer resources.

The efficiency of µGAs results from the use of small populations which leads to more rapid convergence and the frequent re-generation of random population members to ensure diversity during the search process. In this study, the µGA is implemented as follows. One cycle of µGA consists of evolving a small population of chromosomes of size *npsize* based on the GA operations described earlier for a fixed number of generations *ngen*. At the end of this cycle, the chromosome with the highest fitness is identified. Then (*npsize* − 1) chromosomes are generated based on mutating the fittest chromosome, and these newly generated chromosomes, together with the fittest individual from the previous µGA cycle, constitute a new population ready for the next stage of µGA operation. This cycling process continues until a desired level of performance criterion is achieved.

6 Methods for Evaluating Fitness

Fitness evaluation through CFD solution is accurate but costly. Hence, supplementary ANN prediction is exploited to provide the required fitness data. Details of the two methods are described below.

6.1 Direct CFD Solution

An efficient CFD solver is needed to yield aerodynamic data quickly for GA processing. A two-dimensional Euler flow solver is used as a compromise between physical realism and computational efficiency.

Central differencing scheme with second and fourth-order artificial dissipation terms is used. A 5-stage Runge-Kutta explicit scheme is used for time marching and the dissipation terms are evaluated at the 1st, 3rd and 5th stages. The optimal values for the coefficients used in the Runge-Kutta scheme are selected according to the suggestions by Jameson et al. (1981). To accelerate convergence a 3-level W-cycle multigrid combined with implicit residual smoothing is used.

For the calculation, an O-type mesh is constructed around the airfoil and far field boundaries are set at 50 chords away to minimize the boundary influence on the solution. There are 160 grid cells distributed around the airfoil and 32 cells along the direction normal to the airfoil surface. The multigrid solver used provides very fast convergence. Details on the solver performance can be found in Zhu and Chan (1998).

6.2 ANN-CFD Coupled Fitness Evaluation

An important consequence of the fact that a GA only needs function values during the optimization search is that the method can tolerate approximate function evaluation more readily than gradient-based methods. Therefore, as stated in Periaux et al. (1995), GAs are robust with respect to noise and accommodate well with less precise solutions. Additional robustness also results from the condition that convergence of the algorithm relies on the entire population and not on a single individual. This robustness quality could be exploited with the help of ANNs, which can construct an accurate response surface for the search space.

Applications of ANNs as response surfaces for aerodynamic data estimation and extraction have been reported by Chan and Zhu (1999) and Greenman and Roth (1999). The results indicate that a suitably trained ANN can provide accurate nonlinear interpolation for aerodynamic data.

The coupling between ANN and CFD for fitness evaluation proceeds as follows. First, specify those generations as *igen-cfd* where fitness information is obtained by the direct CFD method, and those other generations as *igen-ann* where approximate ANN evaluation is used. For each of the generations labeled *igen-cfd*, CFD is used for fitness evaluation and the results are stored for training the ANN. ANN training is commenced as soon as the CFD evaluation phase is over. Data for the whole generation of chromosomes

become training cases for the ANN, and the number of training cases is the number of chromosomes in a population.

Next, for each of the generations labeled *igen-ann*, the aerodynamic data for the chromosomes are obtained by the trained ANN. Because ANN results have lower fidelity compared to CFD predictions, the ANN results need scrutiny. Let *fmax* be the maximum fitness predicted by the CFD method; then if the ANN prediction for a chromosome has fitness greater than 90% of *fmax*, the fitness is re-calculated using CFD.

7 Neural Network Construction and Performance

The ANN used in this study is a single layer version of the Multilayer Perceptron network as shown in Figure 3. The neural network is designed to take the *(x,y)* coordinates of the B-spline control nodes as input and the pressure values around the airfoil surface are the output. Since there are 20 B-spline control nodes for an airfoil profile, the number of input nodes is 40 to account for the x and y values. Because 160 grid locations are defined in the CFD calculation for the surface pressure, the number of output nodes is the same at 160. Ten neurons are used in the hidden layer and numerical experimentation shows that the ANN results are not too sensitive to the number of hidden layer neurons used.

The training of the ANN is done by the well-known backpropagation algorithm. Techniques such as appropriate scaling of the input and output signals as suggested in Haykin (1994) are applied to accelerate the convergence.

When an ANN is used within a genetic algorithm, the training of the ANN is continued for the entire duration of the GA operation. The weights obtained from one set of training data are kept and are used as initial values to train the next set of data. This method reduces the training errors for a fixed amount of training epochs and enables a more comprehensive construction of the response surface for the search space.

Because the CFD flow solver is very efficient for the current applications, the training time required for the ANN becomes the bottleneck of the computational resource. Upon some experimentation, it was decided that 1000 epochs will be implemented for the neural network training. The choice represents a compromise between accuracy and computing time requirement. Typical prediction results are displayed in Figures 4 and 5, which show the surface pressure distribution for two airfoils obtained during the course of μGA operation.

In general, the ANN predictions are quantitatively reliable, with the shock jump magnitude and position predicted quite accurately for the case shown in Figure 4, but the position was a bit off for the case represented in Figure 5. For the results in Figure 4, the CFD method gives C_D to be 0.082 while the ANN method gives 0.077, an error of 6.1%. For C_L, CFD gives 0.93 while ANN gives 0.89, an error of 4.3%. For the results in Figure 5, the CFD method gives C_D to be 0.078 while the ANN method gives 0.069, an error of 12%. For C_L,

CFD gives 0.92 while ANN gives 0.84, an error of 8.7%. This range of accuracy represents what typically can be expected from the ANN predictions. Compared to the results presented in Tse and Chan (1999) where airfoil coordinates were used as design variables, the training time for the ANN is now shorter and the accuracy is higher.

8 Results of Numerical Experiments

For the numerical experiments, all the cases are executed for approximately 10000 fitness evaluations and the resulting performance of different strategies are compared based on the amount of CFD solver calls. For the cases where regular GA is used, a population size of 40 is chosen and 250 generations are computed to attain the desired number of fitness evaluations. The GA parameters are kept fixed in all cases.

8.1 Pressure Distribution Matching

A target pressure distribution is given as $\hat{p}_i$, $i = 1, 2, \dots, N_g$; where $N_g = 160$ is the number of surface grid cells around the airfoil. Let p_i be the pressure distribution around an airfoil design candidate, the goal is to minimize the following objective function obj:

$$obj = \frac{1}{N_g} \sum_{i=1}^{N_g} (p_i - \hat{p}_i)^2$$

The fitness function used in GA processing is defined as the reciprocal of obj.

8.1.1 Performance Comparison

Different Parameters for µGA

A parametric study is made to vary the values of *npsize* and *ngen* for µGA operation. The case *npsize* = 10 and *ngen* = 10 is chosen as the base case. The case *npsize* = 5 and *ngen* = 10 is done to examine the effect of reducing the population size. Following the work by Krishnakumar (1989), most applications with µGA use a population size of 5, usually without much investigation.

The work by Abu-Lebdeh and Benekohal (1999) shows that mid-sized populations (*npsize* between 9 and 15) consistently exhibited lower internal variability, defined as the variation in fitness value caused by changes in the initial population. Hence, a comparison of the effect of different *npsize* is desirable. In addition, the case *npsize* = 10 and *ngen* = 20 is tried to observe any changes in the fitness performance when a better convergence is established within each µGA cycle.

Results of the parametric study are shown in Figure 6. It is of interest to observe that for the case *npsize* = 5, the initial performance is far superior to the other two cases, but the performance levels off after the initial stage. This shows it is indeed favorable to use *npsize* = 5 in µGA operation, especially for dynamical modeling problems where real-time

solutions are needed. The case with *ngen* = 20 does not provide any performance improvement. For the rest of this study, the base case parameters are used because of the better performance when sufficient GA processing is allowed.

Comparison between µGA and GA

The significant improvement in fitness evaluation of µGA over GA is demonstrated in Figure 7. In the example, µGA is operated for 100 cycles and the GA for 250 generations, making the number of fitness evaluation or CFD solver calls to be about 10000 for both cases. Note that the actual CFD solver calls are slightly less than 10000 because some chromosomes generated do not satisfy the concavity constraints as stated earlier and are rejected. The superiority of µGA is evident: the µGA gives higher fitness prediction during the entire course of the optimization process.

Results with ANN Coupling

Figure 8 shows the fitness performance when ANN is used for part of the fitness evaluation. The implementation of ANN is as follow: during a cycle of µGA with *ngen* = 10, the aerodynamic data for the first five generations are calculated with CFD and the results are used to train the ANN. For the sixth generation CFD is also used but the data are for validating the ANN and not for training. For the remaining four generations the ANN is solely responsible for providing aerodynamic data.

The performance result is plotted with CFD solver calls alone, with the computational effort of ANN training not represented. The purpose is to highlight the computational saving achieved by reducing the overhead on the CFD solver. For the particular type of problems under study and the particular flow solver used, the CPU time for calculating one airfoil is about 3.9 seconds on an SGI Octane computer. In contrast, the CPU time for 1000 epochs of ANN training is about 7.4 seconds, almost twice that of the CFD calculation. However, for more complicated three-dimensional applications, the amount of CFD solver usage would dominate the CPU time consumption.

Figure 9 illustrates the benefit of using a larger training set by comparing the case with 4 generations of data available for training to that with 5 generations. Although the computational requirement is slightly higher for the latter case, a larger training set could give better definition for the underlying response surface and the advantage is reflected in the resulting improvement in the fitness evaluation.

8.1.2 Inverse Design Results

Figure 10 shows the pressure distribution for the target design (NACA 0012) and the initial design (NACA 64A410). The transformation of one profile to the other effects readily as indicated by the fitness results. The final profile obtained by the µGA is very close to the desired profile, as shown in Figure 11.

8.2 Drag Minimization Studies

For drag minimization at fixed lift, the objective function is defined as

$$obj = C_D + \beta \cdot (C_L - C_L^*)^2$$

where the constraint $C_L = C_L^*$ has been incorporated by a penalty function formulation with β being the penalty coefficient, chosen to be 10. The aim is to minimize obj and the GA fitness function is defined as obj^{-1}. The value for C_L^* is 0.90 for the NACA 64A410 case and 0.31 for the NACA 0012 case.

8.2.1 NACA 64A410

Figure 12 shows the performance of various strategies for the calculation starting with the NACA 64A410. Again μGA performs better than the regular large population GA, but the improvement is not as marked as in the previous example. When ANN is used, the performance is slightly better. Figure 13 illustrates again that it is beneficial to use a larger training set despite the slightly higher ANN training overhead.

The Mach contours of the original NACA 64A410 and the μGA optimized airfoil are shown in Figures 14 and 15 respectively. The airfoil designed by the μGA has $C_L = 0.91$ and $C_D = 0.0056$, a mere 7.4% of 0.076, the C_D value for NACA 64A410.

It is striking to see that without any thickness constraint, the airfoil would evolve into a very thin structure with a large leading edge curvature as shown in Figure 16. The large curvature encourages a rapid flow expansion, and the flattened upper surface then reduces the flow expansion to a near roof-top type distribution with a lower pressure level as shown in Figure 17. Consequently the shock strength is weakened as shown in both Figure 15 and Figure 17.

8.2.2 NACA 0012

Figure 18 shows the performance of μGA for this problem. Again, using ANN for part of the fitness prediction enhances the performance: for the same amount of CFD solver calls, calculation with ANN tends to give similar or better fitness results.

The Mach number distributions for the original NACA 0012 and the μGA optimized airfoil are shown in Figures 19 and 20 respectively. The μGA optimization process essentially eliminates the shock near the aft part of the airfoil. Figure 21 shows a detailed comparison of the profile shapes between the initial and optimized airfoils. Again, the optimization aims to increase the leading edge curvature and flatten both the upper and lower surfaces. The elimination of the shock is also seen in Figure 22, which shows the surface pressure distribution. For the μGA optimized airfoil, C_L is 0.31 while C_D is 0.0012, a mere 5.2% of 0.023, the C_D value for NACA 0012.

9 Conclusion

The examples shown suggest micro genetic algorithms can work well for problems that use real number coding. The performance of micro genetic algorithms is consistently better than regular genetic algorithms, although the improvement is more striking for some cases than others. With plenty of GA processing, the use of mid-sized populations yields higher fitness performance, but for solving real-time dynamical problems, a small population size appears to be more beneficial.

The artificial neural network constructed in this study performs well for the prediction of the surface pressure distribution. The use of B-spline control nodes as design variables instead of airfoil coordinates leads to a smaller network which enhances the performance, both for reducing the time required to train the network and for reducing the errors associated with the prediction. The good quantitative comparison indicates that ANN can realistically replace some of the solver calls in aerodynamic design applications.

Within a genetic algorithm, the use of ANNs can reduce the amount of CFD solver calls needed to achieve the same level of fitness performance. This saving of solver calls is essential for further applications of genetic algorithms to design problems under more complex conditions such as three-dimensionality, more complicated flow physics, and integration with other disciplines.

References

Abu-Lebdeh, G. and Benekohal, R.F. (1999), "Convergence Variability and Population Sizing in Micro-Genetic Algorithms", *Computer-Aided Civil and Infrastructure Engineering*, Vol.14, No.5, pp.321-334.

Batill, S.M. and Swift, R.A. (1993), "Structural Design Space Definition using Neural Networks and a Reduced Knowledge Base", AIAA-93-1034, AIAA/AHS/ASEE Aerospace Design Conference, Feb.16-19, Irvine, CA.

Chan, L. and Zhu, Z. (1999), "Neural Networks Modeling of Aerodynamics and Applications to Store Separation", AIAA-99-0685, 37th AIAA Aerospace Sciences Meeting and Exhibit, Jan. 11-14, Reno, NV.

Chang, C.S., Jiang, W.Q. and Elangovan, S. (1999), "Application of genetic algorithms to determine worst-case switching overvoltage of MRT systems", *IEE Proc.-Electr. Power Appl.*, Vol.146, No.1, pp.81-87.

De Jong, K.A. (1975), "Analysis of the Behavior of a Class of Genetic Adaptive Systems", Ph.D. Dissertation, Department of Computer and Communication Sciences, University of Michigan, Ann Arbor, MI.

Goldberg, D.E. (1989), "Sizing Populations for Serial and Parallel Genetic Algorithms", Proceedings of the Third International Conference on Genetic Algorithms, pp.70-79.

Greenman, R.M. and Roth, K.R. (1994), "Minimizing Computational Data Requirements for Multi-Element Airfoils using Neural Networks", AIAA-99-0258, 37th AIAA Aerospace Sciences Meeting and Exhibit, Jan. 11-14, Reno, NV.

Haykin, S. (1994), Neural Networks: A Comprehensive Foundation, Prentice Hall.

Jameson, A, Schmidt, W. and Turkel, E. (1981), "Numerical Solutions of the Euler Equations by Finite Volume Methods Using Runge-Kutta Time-Stepping Schemes", AIAA-81-1259, AIAA 14th Fluid and Plasma Dynamics Conference, June23-25, Palo Alto, CA.

Krishnakumar, K. (1989), "Micro-Genetic Algorithms for Stationary and Non-Stationary Function Optimization", SPIE Vol.1196, Intelligent Control and Adaptive Systems, pp.289-296.

Lingireddy, S. (1998), "Aquifer Parameter Estimation using Genetic Algorithms and Neural Networks", Civil Eng. and Env. Syst., Vol.15, pp.125-144.

Obayashi, S. and Tsukahara, T. (1997), "Comparison of Optimization Algorithms for Aerodynamic Shape Design", AIAA Journal, Vol.35, No.8, pp.1413-1415.

Obayashi, S., Takahashi, S. and Takeguchi, Y. (1998), "Niching and Elitist Models for MOGAs", Parallel Problem Solving from Nature – PPSN V, Lecture Notes in Computer Science, Springer, Berlin, Germany, pp.260-269.

Periaux, J., Sefrioui, M., Stoufflet, B., Mantel, B. and Laporte, E. (1995), "Robust Genetic Algorithms for Optimization Problems in Aerodynamic Design", Genetic Algorithms in Engineering and Computer Science, edited by G. Winter et al., Wiley Publishers, pp.371-396.

Podlena, J.R. and Hendtlass, T. (1998), "An Accelerated Genetic Algorithm", Applied Intelligence, Vol.8, pp.103-111.

Rai, M.M. and Madavan, N.K. (1998), "Aerodynamic Design Using Neural Networks", AIAA-98-4928, 7th AIAA/USAF/NASA/ISSMO Symposium on Multidisciplinary Analysis and Optimization, Sept.2-4, St. Louis, MO.

Reeves, C.R. (1993), "Using Genetic Algorithms with Small Populations", Proceedings of the Fifth International Conference on Genetic Algorithms, pp.92-99.

Rogers, D.F. and Adams, J.A. (1990), Mathematical Elements for Computer Graphics, second edition, McGraw-Hill Publishing Company.

Roy, S., Ghosh, S. and Shivpuri, R. (1997), "A New Approach to Optimal Design of Multi-Stage Metal Forming Processes with Micro Genetic Algorithms", Int. J. Mach. Tools Manufact., Vol.37, No.1, pp.29-44.

Tse, D. and Chan, L. (1999), "Optimization of Airfoil Designs using a Geometric Genetic Algorithm and a Neural Network", Proceedings of the 46th Annual Conference, Canadian Aeronautics and Space Institute, pp.1-8.

Whitley, D. (1995), "Genetic Algorithms and Neural Networks", Genetic Algorithms in Engineering and Computer Science, edited by G. Winter et al., Wiley Publishers, pp.203-216.

Xiao, F. and Yabe, H. (1998), "Microwave Imaging of Perfectly Conducting Cylinders from Real Data by Micro Genetic Algorithm Coupled with Deterministic Method", IEICE Trans. Electron., Vol.E81-C, No.12, pp.1784-1792.

Zhu, Z.W. and Chan, Y.Y. (1998), "A New Genetic Algorithm for Aerodynamic Design Based on Geometric Concept", AIAA-98-2900, 29th AIAA Fluid Dynamics Conference, June 15-18, Albuquerque, NM.
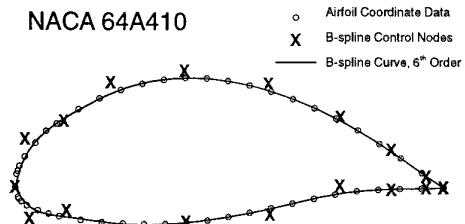
Figure 1: B-spline representation of the NACA 64A410 airfoil; 20 B-spline nodes, 6th order B-spline curve, vertical scale expanded.
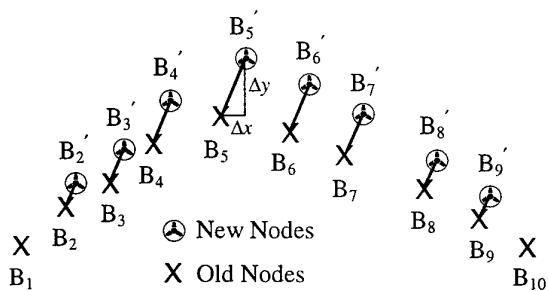
Figure 2: Schematic drawing showing the effect of mutation at the node B_5 and the subsequent smoothing.
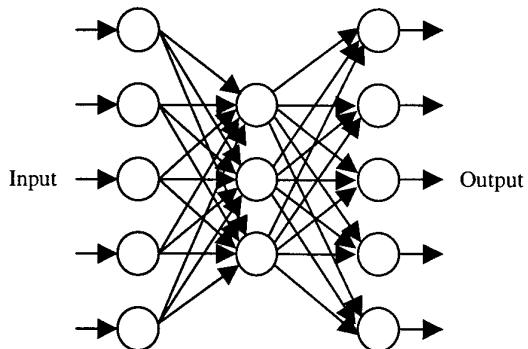
Figure 3: Schematic layout of a Multilayer Perceptron ANN.
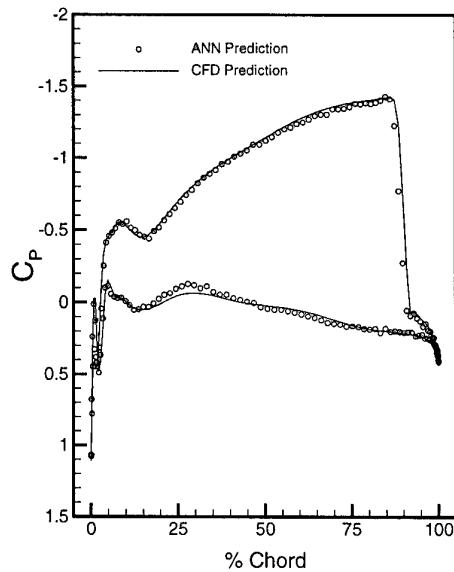
Figure 4: Pressure distribution prediction, CFD vs. ANN results; C_D error = 6.1%, C_L error = 4.3%.
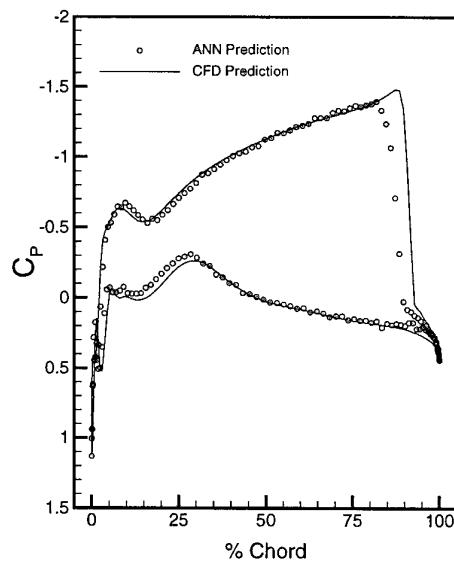
Figure 5: Pressure distribution prediction, CFD vs. ANN results; C_D error = 12%, C_L error = 8.7%.
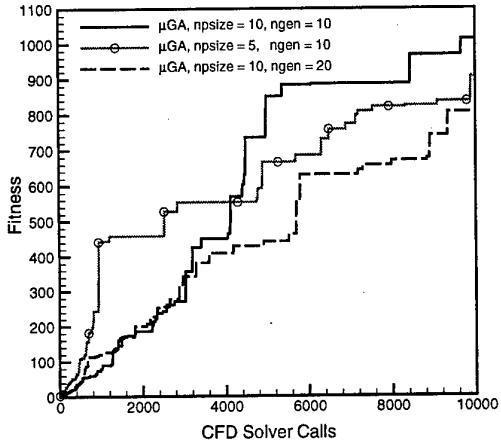
Figure 6: Performance comparison for μGA using various parameters.
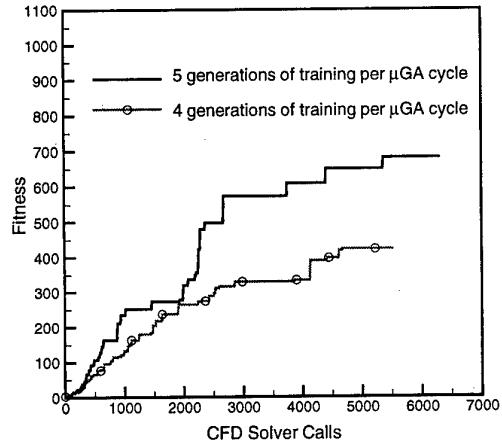
Figure 9: Comparison showing more ANN training sets can be beneficial.
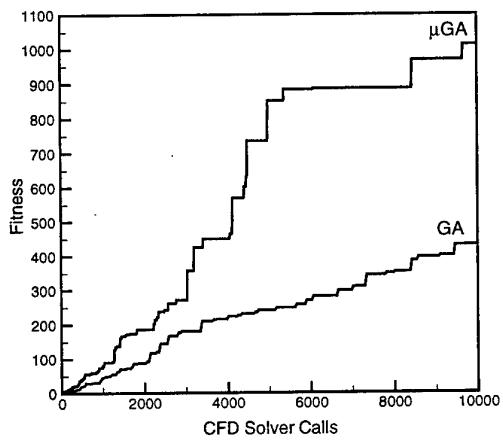
Figure 7: Performance comparison between μGA and GA.
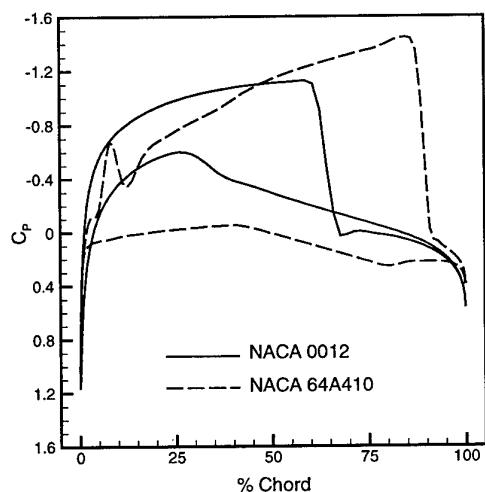
Figure 10: Surface pressure distribution; NACA 64A410 is used as the initial distribution, NACA 0012 is the target. Airfoils operate at Mach 0.8, angle of attack 1.25°.
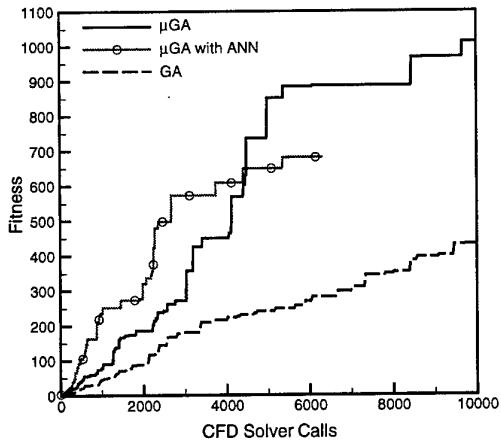
Figure 8: Performance comparison when ANN is used in fitness evaluation.
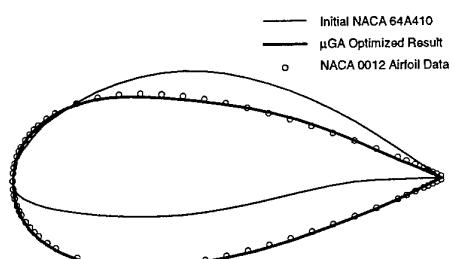
Figure 11: Results of the inverse design optimization showing the initial profile, the target profile and the μGA result, vertical scale expanded.
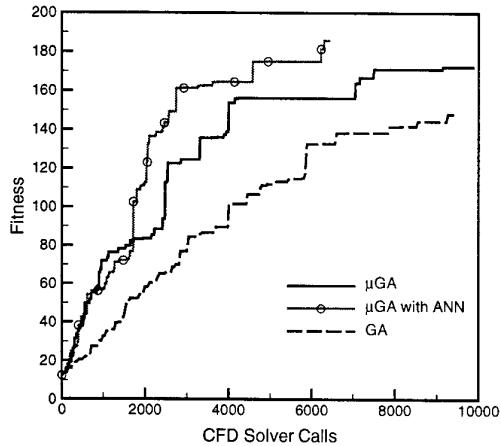
Figure 12: Performance comparison for the NACA 64A410 airfoil drag minimization study.

Figure 13: Performance comparison showing the benefit of more training per μGA cycle.

Figure 14: Mach number distribution for the NACA 64A410.
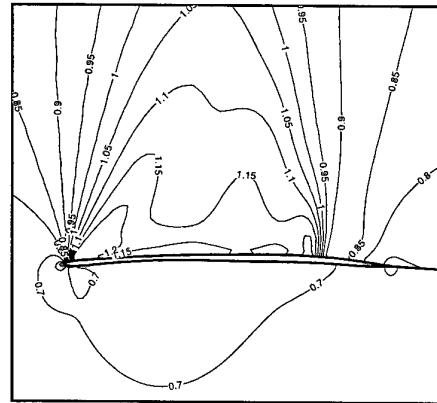
Figure 15: Mach number distribution for the μGA optimized profile.
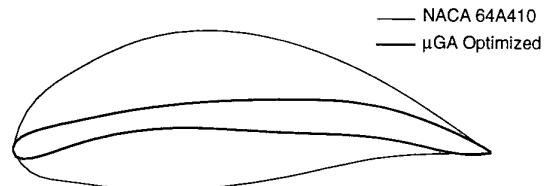
Figure 16: Results of drag minimization showing the initial NACA 64A410 and the optimized profile, vertical scale expanded.
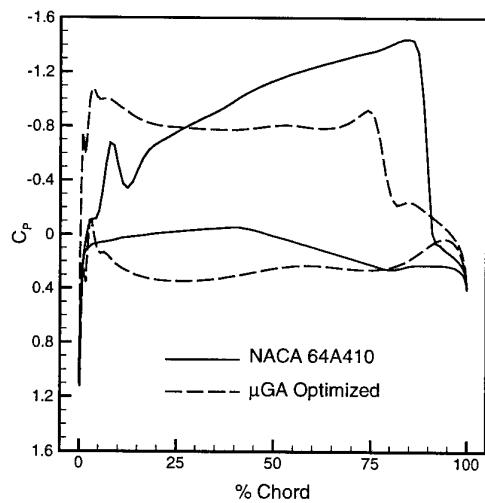
Figure 17: Surface pressure distribution for the initial NACA 64A410 and the μGA optimized profile.
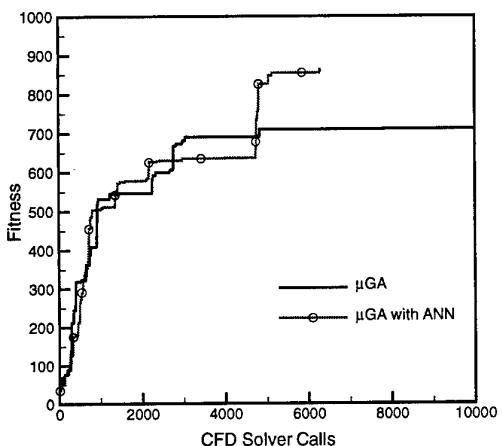
Figure 18: Performance comparison for the NACA 0012 airfoil drag minimization study.

Figure 21: Results of drag minimization showing the initial NACA 0012 and the optimized profile, vertical scale expanded.

Figure 19: Mach number distribution for the NACA 0012.
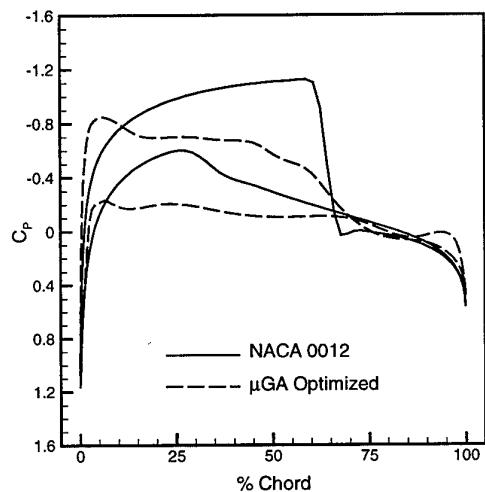
Figure 22: Surface pressure distribution for the initial NACA 0012 and the μGA optimized profile.
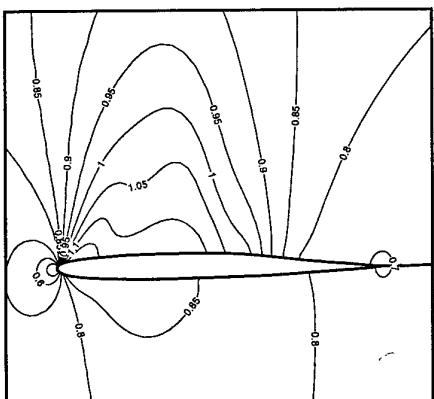
Figure 20: Mach number distribution for the μGA optimized profile.

Multi–Objective Aeroelastic Optimization

M. Stettner, W. Haase
DaimlerChrysler Aerospace AG
P.O.Box 80 11 60
D–81663 Munich
Germany

1. SUMMARY

The present work is aiming at an aeroelastic analysis of the X31 delta wing and particularly at the aeroelastic optimization problem of maximizing the aerodynamic roll rate and minimizing the structural weight at supersonic flow speeds. Results are achieved by means of a multi–objective genetic algorithm (GA) utilizing a GUI–supported software being developed in the European–Union funded ESPRIT project FRONTIER.

2. INTRODUCTION

In early aircraft design stages, the lifting and control surface sizes, shapes, and positions are determined in order to meet given manoeuver performance requirements. In these manoeuvers, aerodynamic and mass loads are imposed on the structure, creating stresses which the structure must withstand. The structure also yields to these loads, which usually degrades the manoeuvre performance predicted for a rigid aircraft. Therefore, a very stiff structure is desired. In order to meet both the strength and stiffness requirements, material needs to be added, which increases the structural weight. The increase may be prohibitively large, so that a change of the control surface planform is preferred, which, in turn, requires an additional loop of aeroelastic assessments. This trade–off between manoeuvre performance, for example the steady–state roll rate, and weight, both as a function of lifting and control surface configuration, is a common problem of aircraft design.

The work presented in this paper describes methods which visualize the dependency between achievable roll rate and the minimum structural weight required to achieve this performance <u>and</u> withstand the loads in this flight conditions, where parameters related to structural stiffness and control surface shape are used. The goal is to provide a means for selecting the "best" structural and control surface layout for given requirements on performance and weight. To achieve this goal, the minimization of weight and the maximization of performance are formulated as separate objectives in a multi–objective optimization. The following sections describe two levels of aeroelastic analysis used, the optimization framework FRONTIER [1] in which they were embedded, the problem as posed to the framework software, and results.

3. DESIGN EVALUATION SOFTWARE

LAGRANGE [2] is an in–house code of DaimlerChrysler Aerospace AG, Military Aircraft, used for structural analysis and optimization. The code bases on a finite element method and enables consideration of stress, strain, buckling, dynamic, static aeroelastic, and dynamic aeroelastic constraints. Objective function is commonly the structural weight. For static aeroelastic analysis, aerodynamic loads are calculated using linearized aerodynamic influence coefficient matrices for a simple panel method [3]. The constraints in this case are the ratios between aerodynamic loads values on the flexible structure and those on the rigid structure, the so–called "effectivenesses". For example, for ailerons the moment about the aircraft roll axis generated by a specified aileron deflection is decisive. Aileron effectiveness is defined as the moment generated by a wing that is free to deform elastically due to aerodynamic loads, divided by the moment generated by an undeformed wing in the same flow condition.

In the present application, LAGRANGE minimizes the structural weight while maintaining structural integrity in five critical static load cases. Simultaneously, the effectiveness of each aileron is required to exceed a given target value. With the actual aileron effectiveness and wing roll damping values of the minimum weight structure as calculated by LAGRANGE, the achievable roll rate as well as the required aileron deflections are calculated by an additional program. Upper bounds for aileron deflections and hinge moments are considered in this step. In summary, the aeroelastic analysis as described calculates a minimized structural weight and the achievable roll rate for a given aileron split ratio and aileron effectiveness target values. This analysis is referred to in the following as "method A".

Since this first approach is based on very simple, linear aerodynamics, a second aeroelastic analysis was developed which involved higher fidelity aerodynamics. The specific method is the HISSS–D code [4], a higher–order inviscid sub– and supersonic panel method for design which allows iterative and constraint aerodynamic optimization for general three–dimensional flows. HISSS–D may be coupled with LAGRANGE in the system HCSI to perform aeroelastic analysis and optimization. In the approach called "method B" in the following text, HCSI is inserted before the roll rate trim calculation of method A. The system thus uses the structural model as optimized by LAGRANGE with its simple aerodynamics, and re–calculates the actually achieved aileron effectiveness values. In effect, HCSI is used to correct the results of the simple aerodynamic analysis. The trim analysis is performed just as in method A. The following paragraphs describe the details of HCSI.

Aerodynamic and structural analysis are coupled by a procedure which determines the equilibrium of aerodynamic loads and the structural reaction forces. The "structural" relation between load and displacement is commonly assumed to be linear. The "aerodynamic" relation between deflection of the aerodynamic shape and aerodynamic load, however, is not linear. In contrast to widespread practice, this fact is considered in HCSI. As another novel element, analytic sensitivities of the equilibrium loads are determined and provided to the structural optimization.

A major challenge was the (automatic) coupling between the aerodynamic analysis code and the structural method. Flow analysis and structural codes usually use topologically very different meshes. Moreover, "more sophisticated" fluid dynamics analysis methods rely on much finer meshes compared to those used to model the structure. In order to feed the displaced geometry calculated by the structural method back into the flow solver, accurate interpolation in three dimensions must be obtainable. In HCSI, transformations between the meshes are performed using an approach based on statically correct distribution of discrete aerodynamic loads onto a limited set of structural nodes called "beaming". The reverse transformation is used for translating the structural displacements into aerodynamic surface mesh deformations. Conservation of virtual work in the process if these transformations is guaranteed.

The structure of HCSI is displayed in Fig. 1. The trans-

formation functions described above are generated by BEA5. The figure also shows the data flow from the mesh generation system PGRID to HISSS–D and, particularly, the intersection of HISSS–D with CPELA5, LAGRANGE and STRULA. STRULA uses the structural model of LA-GRANGE and loads due to unit deflections from CPELA5 to trim the aircraft for a certain target value of, say, steady–state roll rate. The actual trim displacements – and sensitivities with respect to the structural design variables – are then calculated by CPELA5 and returned to LAGRANGE. LA-GRANGE performs structural optimization with constraints on stresses resulting from these aeroelastic load cases. In the FRONTIER test case, however, the roll rate is an objective function, that is a *result* of the structural optimization. For this reason only CPELA5 is executed to calculate the aileron efficiencies.
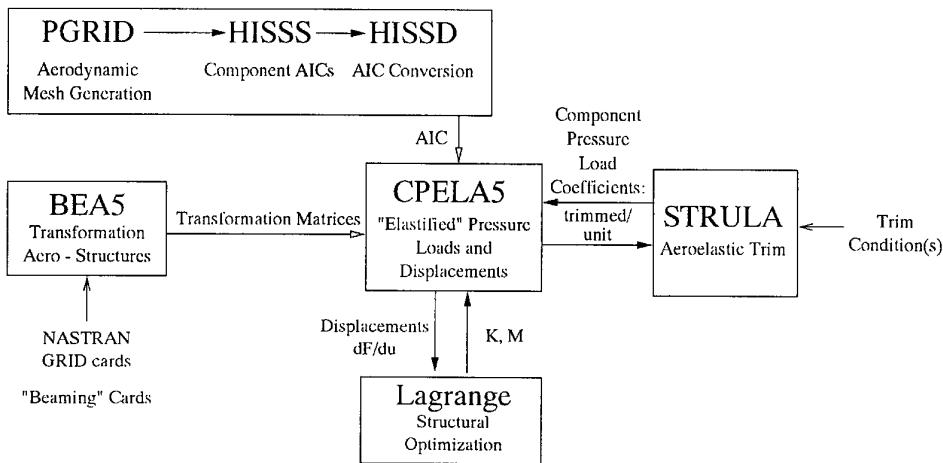
Figure 1 Flow chart of HCSI

4.   THE FRONTIER OPTIMIZATION ENVIRONMENT

One of the major results of the European project FRONTIER [1] is an optimization software which can be applied to multi–disciplinary, multi–objective optimization. It employs a genetic algorithm (GA), a "hill climber" (gradient–based optimization algorithm), and a Multi–Criteria–Decision–Making tool, MCDM. A graphical user environment/interface guides the (non–experienced) user. Parallelization of individual generation in the GA cycles is explicitly supported.

The FRONTIER technology is an open system for collaborative design optimization using Pareto Frontiers. The communication between applications on different platforms is enabled by CORBA service calls which provides a high degree of platform independence. The baseline implementation language of FRONTIER is Java [4]. This has proved very advantageous since only one source code is needed for Unix and Windows NT and, moreover, both single and parallel processor platforms are covered.

The multi–objective genetic algorithm (MOGA) for global exploration uses a generational and steady state GA with user–defined number of individuals and generations. A li-

brary of selection schemes is available with defaults defined on the basis of performance in mathematical test cases. The operations applied to parents to generate children are cross-over and mutation. These are applied to a chromosome encoding of the variables defining the design. Crossover, applied to solutions on or near the Pareto boundary, tends to generate other solutions near the boundary, while mutation tends to create variation in the design set. The user can specify crossover and mutation probabilities – or simply use default values.

Constraints can be handled by objective penalisation with hard and soft constraints or by a supplementary objective. A local hill climber (with constraints) can be used for improvement of GA results but also as a stand–alone tool. The gradient based optimization algorithm used is a BFGS (Broyden–Fletcher–Goldfarb–Shanno) algorithm adapted with modifications for constraint handling. The basic method is a Quasi–Newton method rather than a conjugate gradient method.

The MCDM tool generates a set of utility functions which are selected by the user in the form of pairwise comparisons (judgement) of designs. The total utility is treated as the (weighted) sum of utilities for several criteria (objectives).

The multi–objective–genetic–algorithm (MOGA) optimization provides a Pareto Frontier and, hence, a means to distinguish between results that either fulfill a single objective or results from composite objectives. Moreover, results on the Pareto Frontier can be easily taken as starting points for further engineering evaluations. The FRONTIER optimization technology also allows for hybrid optimization since the gradient based method may be used in order to improve GA results. Of course this latter step is limited to continuous variables, while the GA can manage mixed discrete/continuous design spaces.

5. TRIAL DESCRIPTION

5.1 Two–Level Optimization Procedure

The test case chosen a two–level, two–objective optimization of the composite X31 delta–wing at supersonic flow conditions. The wing model features two leading edge flaps, a wing box, and two trailing edge ailerons, see Figure 2 below. The leading edge flaps are fixed and treated as part of the wing planform. The ailerons may be deflected independently of each other in order to generate a rolling moment.
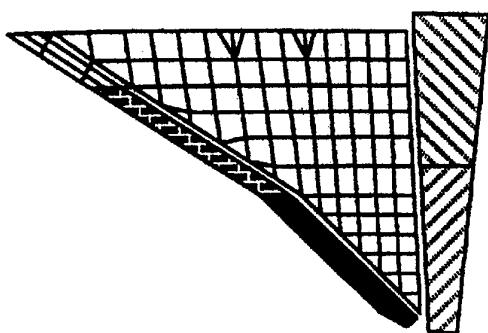
Figure 2 The X31 delta–wing structural model

The objective functions are minimum weight of the wing and maximum achievable roll rate. Three design parameters were used on the FRONTIER framework (upper) level: Roll efficiency goals for inboard and outboard ailerons, and the flap split. The former are continuous parameters, constrained to lie between reasonable bounds. The latter is a discontinous value since rib positioning in the wing box limits possible hinge positions – and thus flap splits – to three discrete values. Hence a coupled set of continuous and discontinuous design parameters had to be treated in a two–objective optimization space. Constraints are not used explicitly on this level.

Figure 3 provides a sketch of the general topology of the upper level design space, where the two efficiencies are combined into one value for the sake of simplicity and presentation. This aileron effectiveness, η, is an indicator of the stiffness of the wing. With increasing stiffness, the achievable roll rate, P, will converge to the value reached by a rigid structure. In order to create a rigid structure, however, it must be infinitely stiff, and therefore infinitely heavy. As a result, as η approaches 1.0, the weight, W, approaches infinity. It is therefore reasonable to provide an

upper limit to η. On the other hand, if the effectiveness requirement is very low, the stiffness of the structure necessary to sustain static loads may be suffient to generate efficiencies higher than the requested value. Therefore, one can provide a lower bound to the η–dimension of the design space without changing the outcome. Although qualitatively identical, the quantitative situation depends on the third design parameter, the aileron split ratio, t, which is equivalent to a specific spanwise split position, y_{fl}.
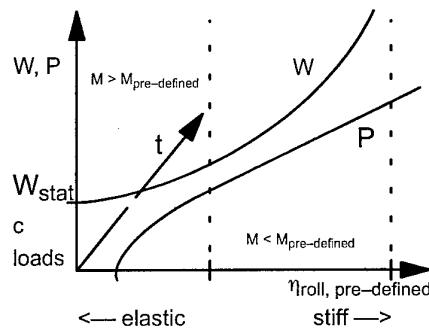
Figure 3 Top level design space topology

In order to receive the minimum weight of the X31 wing, LAGRANGE performs a second type of optimization. Design parameters at this (lower) level are thicknesses and composite fiber orientations of the structural members. These are varied to achieve minimum structural weight while satisfying constraints on allowable stresses and strains, buckling, and aileron roll effectiveness, $\eta \geq \eta_{predefined}$. The latter constraints are the design parameters of the upper level optimization. In the trim calculation, geometric limits are applied to the aileron deflections, $\alpha_{flap,in}$, $\alpha_{flap,out}$, and the hinge moments are limited to values which can be sustained by the actuators installed in the actual aircraft. Thus, while explicit constraints are not set to these parameters at either optimization level, they are implicitly constrained.

5.2 Geometry Parametrization

One of the most crucial items of optimization is reliable parametrization of the geometry. The success and performance of the entire optimization process is closely related to such application–dependent parametrization.

The geometry parametrization of the X31 delta wing is presented in Figure 4. Three design parameters used in the optimization process are highlighted. All other parameters for the complete wing parametrization are kept constant for the current flap efficiency study. It becomes evident from Fig. 4 that the original wing has been extended up to the symmetry plane of the fuselage.

According to the inner layout of the wing structure, Table 1, and based on the limitations that the actuators may not be moved and each aileron requires two hinges, the possible aileron–split domain is bound by the location of the outboard hinge of the inner aileron, and the actuator position of the outer aileron, including a tolerance, ε, for their spanwise dimension:

$$1777 \text{ mm} + \varepsilon < y_{fl} < 2330 \text{ mm} - \varepsilon$$

Three variants were finally selected: variant 1, at the baseline split location, variant 2 at the upper split limit, and variant 3 at the lower bound. These variants are represented by numerical values of the discrete design parameter "aileron split" of 1, 2, and 3, respectively.
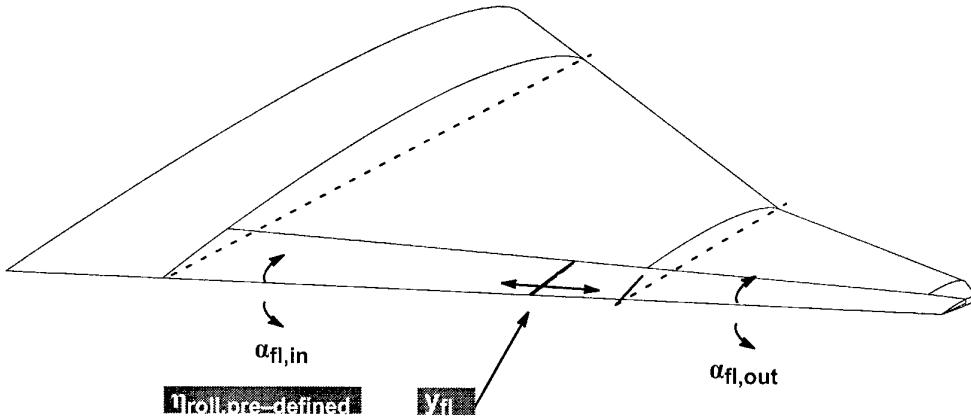

$\alpha_{fl,in}$

$\alpha_{fl,out}$

Figure 4 Geometry parametrization

Table 1 Geometry constraints

Geometry item	at position [mm]
Innermost edge of flap	616
Inner rib	783
Hinge with actuator	1046
Hinge	1777
Current yfl–value	2028
Hinge with actuator	2330
Hinge	2845
Hinge	3360
Hinge	3632

5.3 Design and Fixed Parameter Settings

Based on the previous considerations, the design parameters were specified in the FRONTIER environment in the form shown in Table 2. Additional parameters were supplied to the aeroelastic analysis, but not varied:

Mach–number   [–]   = 1.2
Angle–of–attack   [°]   = 5.73
Stagnation_pressure   [N/m**2]   = 102,100
Max. Inb_flap_setting   [deg]   = 15.0
Max. Outb_flap_setting [deg]   = 15.0
Max. Inb_hinge_moment   [Nm]   = 4500.
Max. Outb_hinge_moment [Nm]   = 4500.

Table 2 Design parameter settings

Design parameter	Min Value	Max Value	Steps
Aileron Split	1	3	3
Inboard Efficiency	0.2	0.5	151
Outboard Efficiency	0.2	0.5	252

6. RESULTS

6.1 Method A

Based on the values provided in Table 2, optimization was carried out on an SGI ORIGIN–2000 with 16 processors and 8GB shared memory, both as sequential runs and in parallel. The total computation time by using 8 processors 16 generations with 16 individuals each was roughly two hours.

The speedup of the parallel application can be taken from Fig. 5 below. It exhibits a reasonable speedup of about 6 when using 8 processors.

no. of processors
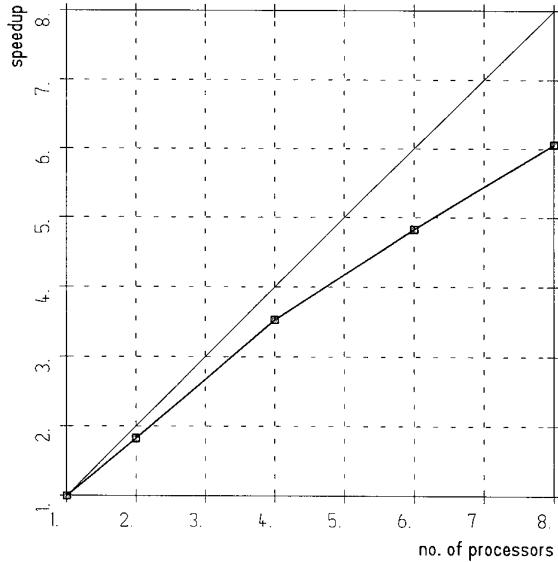
Figure 5 Speedup for parallel treatment of the X31 wing performance trial

It should be noted at this point that – on the basis of 16 individuals per generation – only 2, 4, and 8 concurrent designs might have been the correct choice for the "standard MOGA". However, as

for all trials the "steady MOGA" was adopted, the parallel run with 6 concurrent designs denotes an additional – possible – trial.

In Fig. 6, the computed pressure(–coefficient) distribution on the X31 wing surface is shown for the untwisted wing at Ma=1.2, 5.73° incidence, an inboard aileron setting of 20° and an outboard aileron setting of 10°. It very well exhibits the high pressure loads on the aileron which correspondingly lead to the deformations of the aileron, actuator, actuator support, and finally of the wing box.

Optimization results using 16 individuals and 8 generations – utilizing the steady MOGA approach for a total of 128 individuals – are presented in Fig. 7. The simple aeroelastic method A was used to evaluate the individuals.

The corresponding Pareto frontier is presented in Fig. 8. Taking into account an initial weight of about 173N, it becomes evident that there is some room for improving the weight limit, however under the drawback of reduced turning rates.

| cp |
| 0.913379 |
| 0.828144 |
| 0.74291 |
| 0.657675 |
| 0.572441 |
| 0.487206 |
| 0.401972 |
| 0.316737 |
| 0.231503 |
| 0.146268 |
| 0.0610336 |
| -0.024201 |
| -0.109435 |
| -0.19467 |
| -0.279905 |
| -0.365139 |
| -0.450374 |
| -0.535608 |
| -0.620843 |
| -0.706077 |
| -0.791312 |
| -0.876546 |
| -0.961781 |
| -1.04702 |
| -1.13225 |
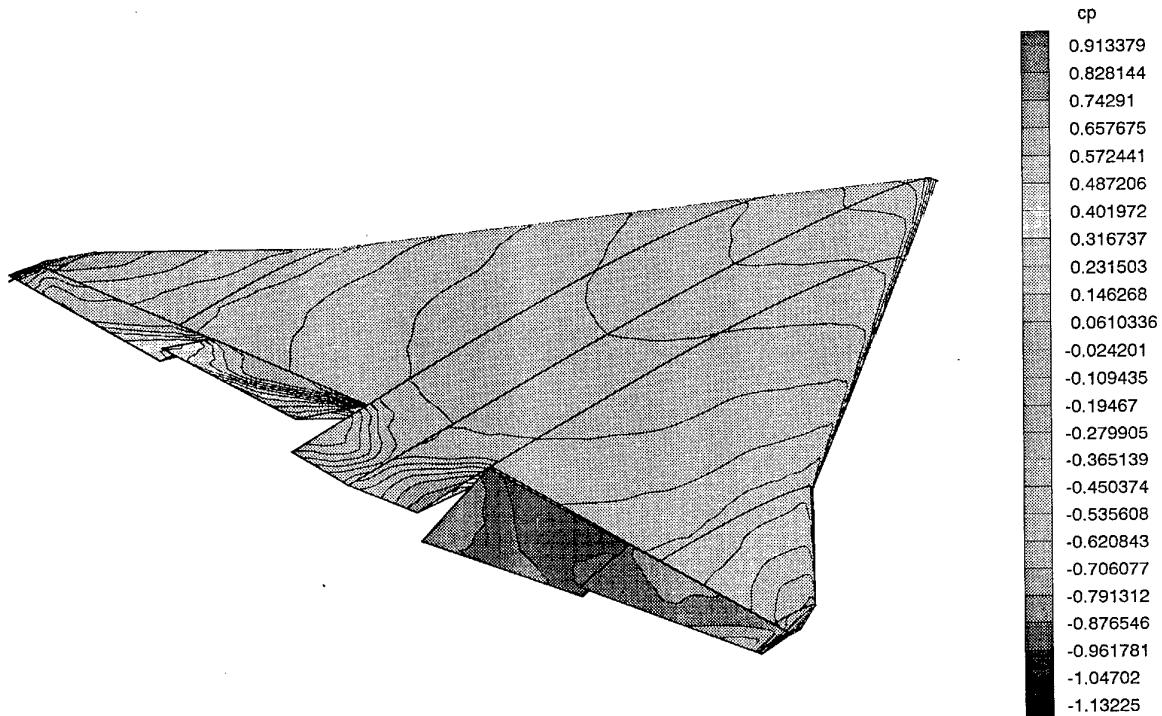
Figure 6 Computational pressure–coefficient results for specific individual
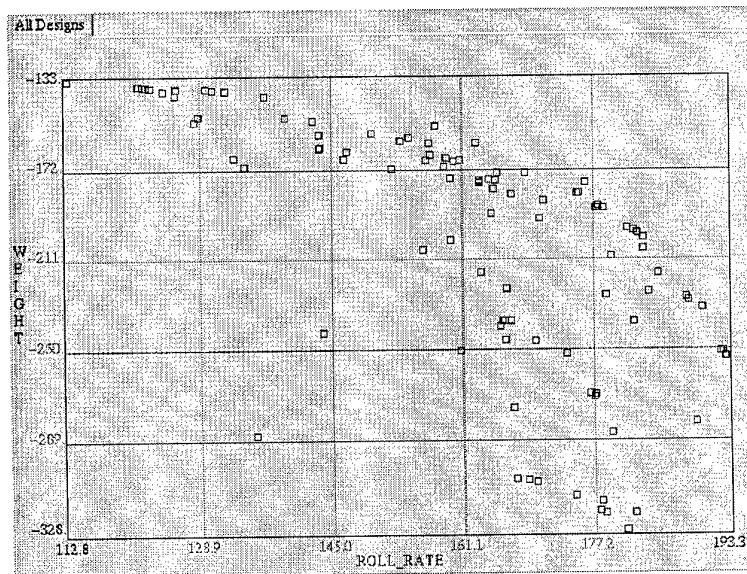
Figure 7 Objective space: Design parameters for 16x8 MOGA run with aeroelastic method A
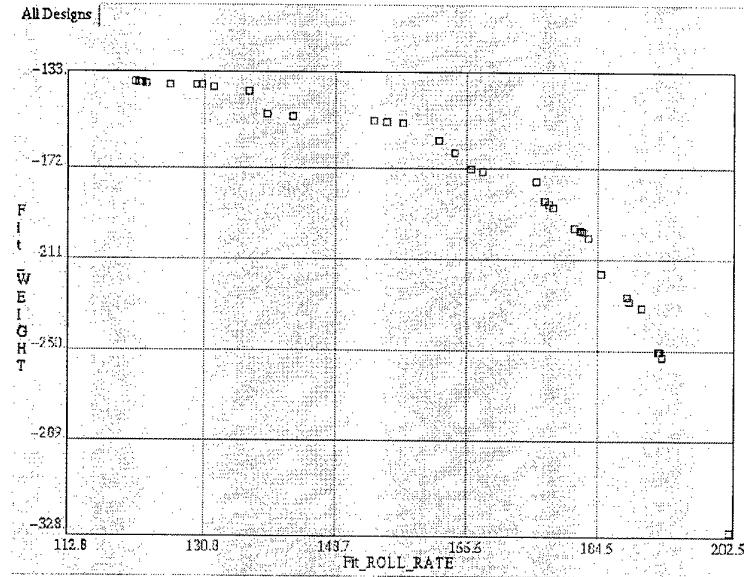
Figure 8 Pareto frontier: Design parameters for 16x8 MOGA run with aeroelastic method A
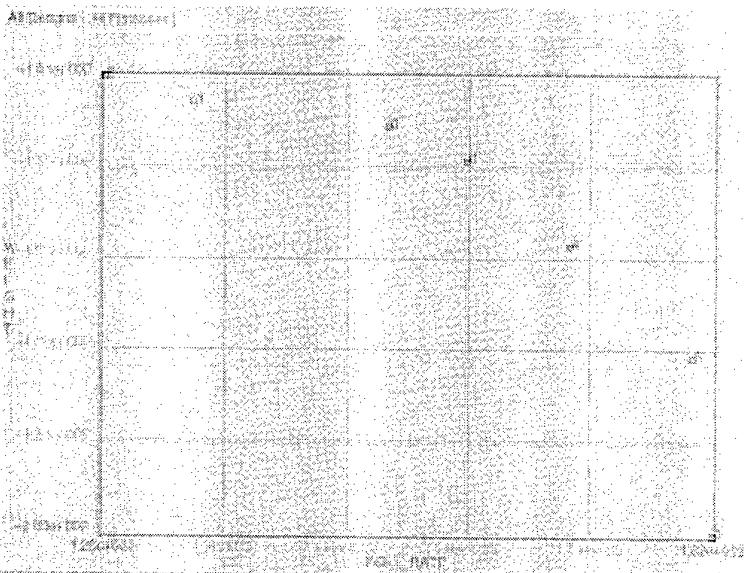
Figure 9 Buffered design for MCDM usage with results selected from to Figure 7 (8)

It should be noted at this point that – although the prescribed numbers of individuals and generations have been fixed in the input file for the FRONTIER run, the "real" number of usable designs differs slightly for the different parallel runs. This is due to the problem that some individuals are non–physical ones and are not taken into account for the design space evaluation. Therefore, the data in Fig. 7 provide the results obtained for the sequential/non–parallel run.

It was mentioned before that a further improvement of the Pareto results by using a hillclimber is possible but has not been used in the present investigation due to the discontinuous aileron–split design parameter. However, the possibility to fix the aileron's in-

board–outboard split by selecting a preferred "best" result from the Pareto frontier and then applying a gradient based method merely with the remaining two design parameters (the flap efficiencies) might be investigated in future trials.

When comparing the different results on the Pareto frontier, it becomes quite evident that the use of a evolutionary strategy – the GA in the current trial – can be efficiently applied to complex test cases. Moreover, for the selected set of design parameters, a gradient based method could have provided results *only* for one flap split, i.e. the present investigation would have been impossible to treat *without* an evolutionary strategy.

The complete set of results further indicate that the roll rate governs the optimization process, i.e. in the low structural–weight area larger improvements of the corresponding roll rate can be obtained – a fact that will be underlined by using the MCDM tool. For the MCDM investigation of the results obtained by method A, Table 3 presents the set of individuals that have been buffered from the Pareto frontier. In addition, Fig. 9 presents the design chosen and their location on the Pareto curve together with the numbering (according to the sequence in the data buffer) used by the MCDM.

It is initially suggested that an experienced engineer would select the same individual from the frontier as a novice user would receive by applying the MCDM method.

Table 3   MCDM trial: Buffered designs

Design no. on Pareto	44	35	49	92	77	90	27
Buffered individual for MCDM	2	1	3	6	4	5	0

In order to rate the different designs given in Table 3, the following set of preferences has been selected for the MCDM run:

5	preferred to	4
2	preferred to	3
7	preferred to	6
6	preferred to	1

The best (priority) result was computed to be individual no. 92, achieving reasonable roll rates together with relatively low structural weight. The two–objective case in that trial is, of course, not a real challenge for the MCDM tool, however it has proven to be in line with the "engineer's nose", i.e. it it suggested that an expe-

rienced engineer, properly checking the Pareto frontier, might have chosen a similar result.

Based on prescribed hinge moments of 4500 NM, the design and objective values for individual no. 92 read:

flap split   1
inboard flap efficiency   0.332   (resulting in $\alpha_{Flap,in}$=3.52°)
outboard flap efficiency   0.3308 (resulting in $\alpha_{Flap,out}$=6.85°)

resulting in

roll rate   159.022 deg/sec
strucural weight of X31 wing   151.668 N
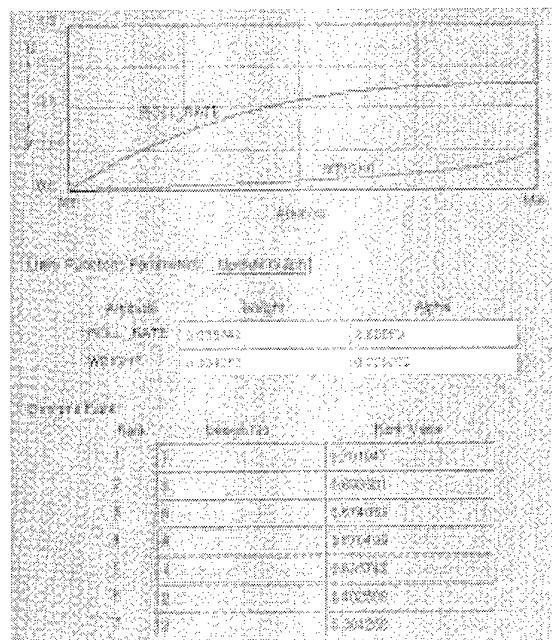
Figure 10 MCDM output
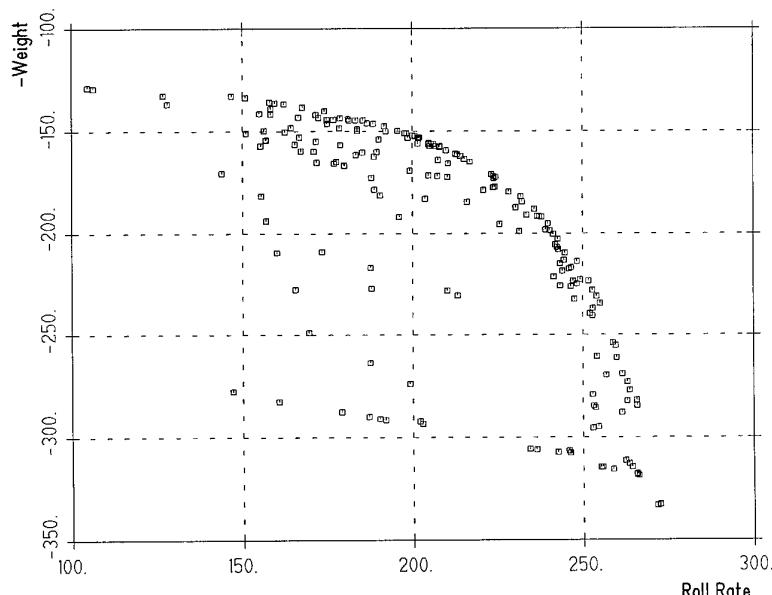
Figure 11 Objective space: Design parameters for 16x16 MOGA run with aeroelastic analysis method B

Fig. 10 presents the MCDM results, indicating the dependencies of roll–rate and structural weight and confirming that the roll rate is dominating the weight. On the other hand, it can be seen for higher weight factors that the roll rate cannot be improved with "although" the structural weight is drastically increasing. In addition, Fig. 10 also provides the obtained rating sequence.

6.2 Method B

Optimization results using 16 individuals and 16 generations – utilizing the steady MOGA approach for a total of 256 individuals – with aeroelastic anaylsis method B are presented in Fig. 11. A rather smooth Pareto frontier – often showing up in "physical", i.e. "non–mathematical", applications – has been obtained.

In comparison to the use of method A, the roll rate obtained by method B has increased by roughly 30%, compare Fig. 7. Checking again against the initial weight of 173 N which corresponds to a roll rate of about 240 deg/sec, the optimization result obtained is very close to flight test results and underlines the maturity of the improved method B in the chosen flight regime.

7. ACKNOWLEDGEMENT

8. REFERENCES

[1] *Spicer, D., Cook, J., C. Poloni. C., Sen, P.*: EP 20082 Frontier: Industrial multiobjective design optimisation. In: D. Papailiou et al (Eds.), Computational Fluid Dynamics '98, John Wiley & Sons Ltd., 1998.

[2] *Schweiger, J., Krammer, J., Hörnlein, H.R.E.M.*: Development and Application of the Integrated Structural Design Tool LAGRANGE. 6th AIAA/NASA/ISSMO Symposium on Multidisciplinary Analysis and Optimization, Bellevue, Washington, September 1996. AIAA–96–4169.

[3] Aeroelastic Tailoring of Advanced Composite Structures for Military Aircraft, Volume III–Modifications and User's Guide for Procedure TSO. General Dynamics Corporation/ Air Force Flight Dynamics Laboratory, Analysis and Optimization Branch (FBR), Wright Patterson Air Force Base. Technical Report AFFDL–TR–76–100, Vol. III, Feb. 1978.

[4] *Fornasier, L.*: Optimization of the wing–pylon–nacelle test case TE5 by HISSS–D, a panel method–based design tool. In: Notes on Numerical Fluid Mechanics, J.Periaux et al, Vol. 61, Vieweg, 1997.

[5] *JAVA language*: www.javasoft.com/doc/language_environment

Emergent Aerospace Designs Using Negotiating Autonomous Agents

Abhijit Deshmukh, Timothy Middelkoop
University of Massachusetts, Amherst
MIE Department
Elab Building, Box 32210
Amherst, MA 01003-2210, United States
Anjaneyulu Krothapalli
Dept. of Aerospace Engineering
Florida State University
2525 Pottsdamme Street, Room 229
Tallahassee, FL 32310-6046, United States
Charles Smith
NASA Marshall Space Flight Center
Bldg 4203 – Room 6145
Mail Code TD03
Alabama 35812, United States

Abstract

This paper presents a distributed design methodology where designs emerge as a result of the negotiations between different stake holders in the process, such as cost, performance, reliability, etc. The proposed methodology uses autonomous agents to represent design decision makers. Each agent influences specific design parameters in order to maximize their utility. Since the design parameters depend on the aggregate demand of all the agents in the system, design agents need to negotiate with others in the market economy in order to reach an acceptable utility value. This paper addresses several interesting research issues related to distributed design architectures. First, we present a flexible framework which facilitates decomposition of the design problem. Second, we present overview of a market mechanism for generating acceptable design configurations. Finally, we integrate learning mechanisms in the design process to reduce the computational overhead.

1 Introduction

Design of highly engineered aerospace components involves a variety of tradeoffs, such as cost versus quality, strength versus speed and weight versus stiffness. The need for efficient design methodologies, which capture these tradeoffs, is driven by the requirement to introduce cost effective and reliable products into the market quickly. This is especially true in the aerospace industry, where shrinking defense budgets and international competition are forcing manufacturers to significantly reduce the concept–to–delivery time for new products. In the space vehicle industry the challenges are even greater due to the need to produce extremely reliable designs with limited full scale testing capabilities. In order to achieve these objectives integrated synthesis environments, which incorporate high fidelity analysis, experimental testing, manufacturing and cost information at the design stage, are needed. Such systems enhance the probability of creating high quality products, without cycling through the product redesign iterations [1]. Most of these systems use multi–disciplinary design optimization methods to capture performance tradeoffs and prescribe a configuration with optimal design parameters. However, the complexity of several competing design objectives and diverse nature of the analysis tools makes the design optimization process computationally expensive. As a result, the design cycle is either extremely long or the designers have to rely on approximations.

The use of multi–disciplinary knowledge at the product development stage presents opportunities for improving the product cost to performance ratios. However, this desired capability, along with the changing customer requirements, places a heavy burden on the design decision makers who must constantly re-engineer products to comply with the customer needs. In this environment it is critical to have a set of integrated tools that can efficiently handle the re-current design cycles and at the same time manage the complex relations between the different design criteria.

This paper presents a Multi–Agent Design Architecture (MADA) which incorporates both the needs by providing a computational environment suitable for evaluating numerous design scenarios and a distributed solution search method that can handle multiple design criteria. The distributed search methodology uses negotiations between different stake holders, or design decision makers, to guide the search in the design parameter space. An important aspect of this method is the absence of a centralized design optimization module.

This paper is organized as follows. Section 2 gives an overview of the agent based design architecture. We use a high speed civil transport (HSCT) nozzle as an example throughout the discussion. Section 3 details the distributed design search methodology used in MADA. Section 4 discusses learning techniques that can be used to enhance the system performance. Finally, we present a summary of the developments and plans for future research.

2 Multi–Agent Design

Agents provide an efficient architecture for distributed design systems by encapsulating both data and process intelligence into autonomous decision making packages. MADA, shown in Figure 1, is a community of agents which represents a collection of tools, knowledge and procedures required for collaborative design and analysis tasks. We define the portion of the MADA system which transforms input parameters into a complete design as the *design ecology*. While the design ecology can produce a single design instance, the market based decision framework, which we term the *design economy*, searches the design space for a configuration that is acceptable to along all the decision criteria.

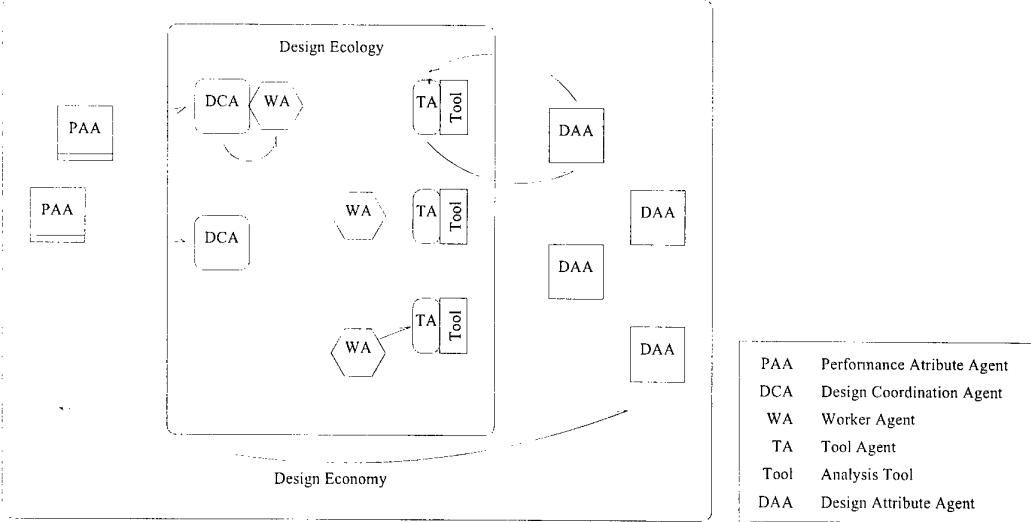| PAA | Performance Atribute Agent |
DCA	Design Coordination Agent
WA	Worker Agent
TA	Tool Agent
Tool	Analysis Tool
DAA	Design Attribute Agent

Figure 1: Multi–agent design architecture

It is important to note that the following discussion pertains to parametric design problems. We do not address the issues related to conceptual design in this paper. We consider a design scenario to be a collection of parameters and decisions. Parameters are composed of attribute and value tuples which describe the physical interpretation of the parameter and value it holds respectively. In the HSCT nozzle example, an attribute would be the exit Mach number and when combined with the value of Mach 3.4 it forms a design parameter. The set of attributes can be partitioned according to their dependencies. Thus, it may not be possible to independently control all of the parameters due to relationships between attributes and design constraints. The parameters and attributes are characterized in two groups: design parameters (attributes) and performance parameters (attributes). Design attributes are the characteristics that define a design configuration. In the HSCT nozzle example, wall thickness, material, length and manufacturing processes can be considered as design attributes. Each design attribute is considered to be independent and dependencies in the design attributes can be modeled by intermediate variables. The collection of design attributes is sufficient represent a complete design. The desired product performance characteristics, such as cost and durability, are represented as performance attributes. These attributes are derived from the design attributes, and hence, are dependent variables. The design attributes are transformed into performance attributes by the collective actions of agents in the MADA design ecology. The collection of decisions form the properties of the final design and represent the high level goals of the designers. In a design environment they represent the choices between design alternatives. Parameters and attributes form the structure of the design scenario, while the decisions shape the outcome.

2.1 Design Ecology

The MADA design ecology, shown in Figure 1, contains four distinct entities, 1) design coordination agents, 2) worker agents, 3) tool agents and 4) tools, in addition to the environment in which the agents reside. As mentioned before, the design is represented in a parametric form. The relationships between the parameters and the analysis tools are defined by parameter maps. The relationships between parameters, such as how the cross sectional area of a HSCT nozzle effects the temperature and pressure profile along the axis of the nozzle, can be inferred as the design iterates through several configurations.

The parameter maps are managed by the design coordination agents and the worker agents. The design coordination and worker agents convert the user's goals into manageable and coordinated tasks. The design coordination agents are responsible for determining the processes needed to calculate parameter values and specific tasks for the worker agents. Thus, they provide the necessary intelligence to ensure complete and valid designs. The worker agents use the parameter maps provided by the design coordination agents to satisfy the dependencies and return the result back to the coordination agent. Specialized worker and coordinator agents interact with multiple tools, thereby providing the means for inter–application collaboration.

The tool agents and tool interfaces provide an abstraction layer, which allows the application programs to consume and produce information in a common data and command/communication infrastructure. The tools are individually managed by the tool agents, which are responsible for coordinating requests for information, instantiating and executing the analysis tools and delivering the results. The tool agents have specific information requirements that must be satisfied and these dependencies are managed by

the design coordination agents. Design and analysis tools take independent design attributes and combine them into composite attributes. Tool agents, who manage this process, can also impose constraints at this point and perform simple transformations. Performance tools processes design attributes and convert them into performance attributes. This is transformation is accomplished by interacting with the design tools and the design coordination agents.

2.2 Implementation

The design architecture is implemented using a multi-layered, multi-agent approach, isolating the complexities of one technology from another. This approach gives the flexibility to change tools and applications without disrupting the entire system. This also gives the environment ability to adapt to the changing technologies without major changes. MADA needs to be able to operate in heterogeneous computing networks and therefore utilizes technologies that facilitate interaction between diverse operating platforms. The MADA environment uses Java as its core language and inherits many key features from it, including the ability to run on any platform that has a Java Virtual Machine (JVM). The tool agents use Remote Method Invocation (RMI) which enables Java applications to invoke methods remotely through lightweight Applications Program Interfaces (API). This allows the agent subsystems to be mobile in non-proprietary ways. Java and RMI by themselves only provide the means in which heterogeneous, mobile agent systems can be built. An agent management system, or Multi-Agent Facility (MAF), on the other hand, provides a common set of resources and services for the mobile agents, such as mobility tracking, data persistence, message passing, naming services and life-cycle support. Individual agents exist in the MAF environment, which provides the required services [2]. The MADA agents communicate information to other agents though a KQML interface [3]. Figure 2 shows a HSCT nozzle being designed using MADA. Additional implementation details of the system can be found in [4].

3 Design Economy

Instead of performing a centralized search on the design space, a distributed methodology is desirable to take advantage of the asynchronous and distributed nature of the underlying design ecology. The search model presented in this paper is based on a collection of individual decision making entities. These entities, or agents, make choices based on limited information and preferences. The choices are formed in a market setting by representing the design and performance attributes as commodities and the stake holders, or decision makers, as consumers.

In addition to the benefits of distributing the computational processes, market based models have also been shown to yield an efficient distribution of stake holder interests through out the system. Thus the combination of design economy and design ecology in MADA provides a means to balance multiple design criteria while maintaining the complex interactions among the design attributes.

We now formulate the design economy problem so that it can be mapped on to a general equilibrium model. By formulating the design problem in the context of general equilibrium theory we can deploy the techniques used in economics to ascertain the global properties of the design system [5]. The global properties are of interest since they represent the final design configuration generated by the design economy. The aforementioned mapping is defined by three basic entities: 1) consumers, 2) producers and 3) commodities. In the following discussion, we first introduce the concept of general equilibrium and then define the market entities in terms of the design problem.

3.1 General Equilibrium

The concept of general equilibrium has been well studied by economists and is used to model market activity [6, 7, 8]. Economists use equilibrium analysis to model the aggregate behavior of market based systems. Questions about market stability, existence of a solution and other global properties are answered by studying the equilibrium points of the system. In general equilibrium models, we can show that under certain assumptions the market behaves in a predictable fashion, which is desirable for the design search process.

In the economic context, the consumer behavior is dictated by their preferences, which in turn determine their desired set of commodities, or the market bundles. In general equilibrium, the consumers choose market bundles in order to maximize their utility subject to the budget constraints. This desire for goods manifests itself in the market as demand. As the market prices shift due to this demand, the agents try to reallocate their market bundles based on their stated preferences. This iterative activity drives the dynamics of the market economy. The market settles at an equilibrium point when all the consumers are satisfied with their market bundles.

A general equilibrium model consists of the following:

- A fixed collection of k goods or commodities, $g^1, \cdots, g^k$, with an associated price vector $\bar{p}$ in the market.

- A collection of m consumer agents

  - having initial endowment of goods $\bar{\omega} = (\omega_1, \cdots, \omega_m)$
  - maximizes stated preferences in the form of a utility function, $u_i = f(\bar{p}, \omega_i \cdot \bar{p})$

- A collection of producer agents

  - with a feasible production set in all feasible production sets $\bar{y} \in Y$, $y_i < 0$ represents inputs, $y_i > 0$ represents outputs
  - maximize profit, $\bar{p} \cdot \bar{y}$

In order to formulate the design problem in terms of the general equilibrium model, we need define consumers, producers and commodities in the design context.
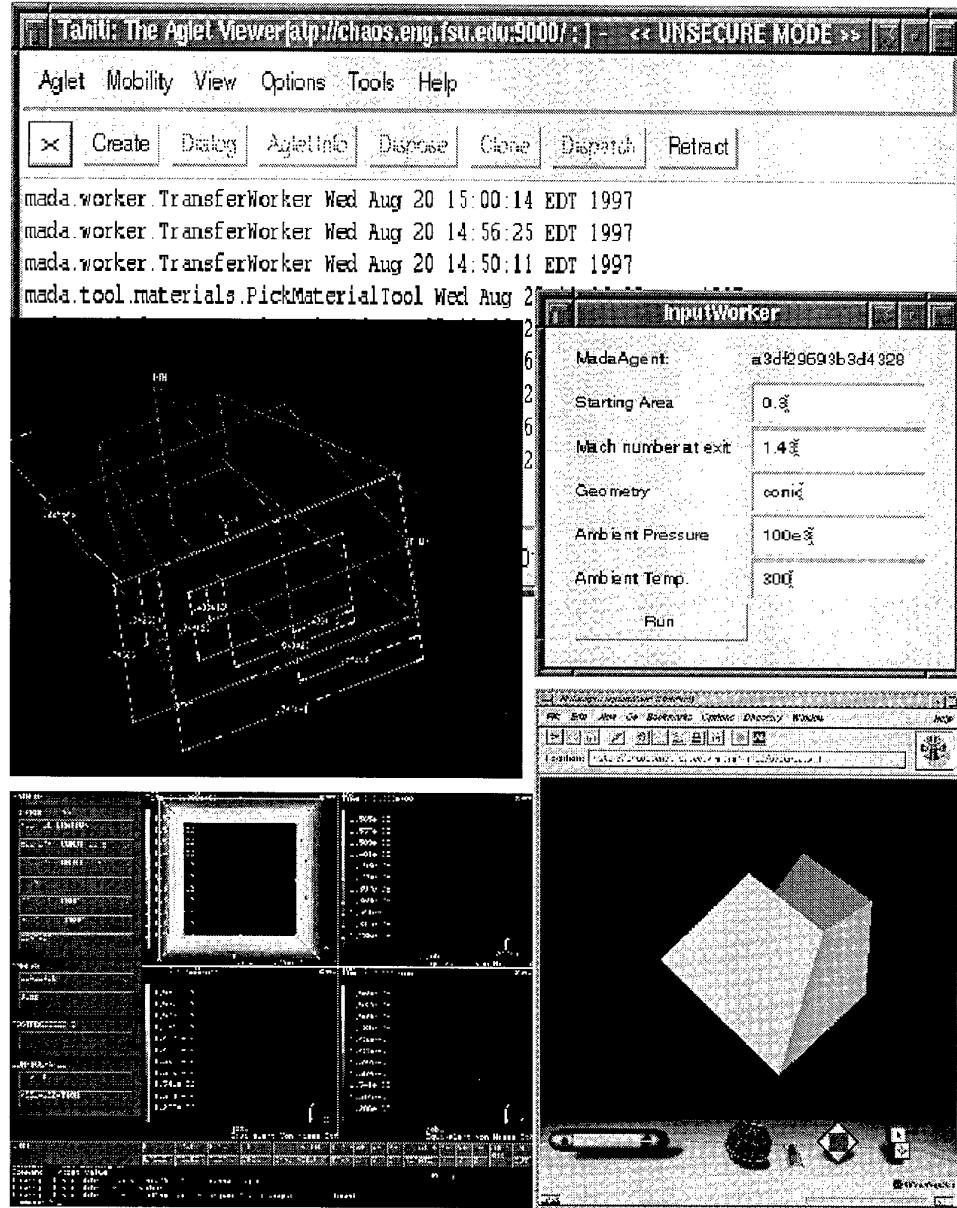
Figure 2: Design of a HSCT nozzle using MADA

3.2 Consumer Agents

Consumer agents are the embodiment of a stake holder in the design process. These agents act in interest of the stake holder they represent. The decision maker's preferences and goals are encoded in the agent using an utility function. Each stake holder's influence on the design is controlled by allocating an initial endowment. This endowment allows us to give different weights to the decision makers in the system.

Definition 1 (Consumer Agent) *Consumer agent i, is a rational economic agent with an initial endowment ω_i that solves the following problem:*

$$\max \quad u_i(\chi)$$
$$s.t. \quad p \cdot x_i \leq \omega_i \qquad (1)$$

where x_i is a set of control commodities, which are explained in the following discussion, and χ is the set of global quantities of the performance commodities, $\chi \equiv f(x_i, g)$, where g is the set of performance commodities.

The consumer agents trade performance measures in order to achieve the highest level of personal utility subject to their resource or endowment constraint. For example, if one stake holder needs a lighter nozzle, it may be willing to allow proportional increase in cost. This activity effectively expresses the consumer's willingness to exchange one performance commodity for another at a marginal rate based on their relative importance. The results in general equilibrium theory ensure that under certain conditions the resulting system will produce an *efficient* or Pareto optimal[1] allocation of performance attributes among the individuals [6, 8]. It is important to note that we are not guaranteed a single equilibrium point or the solution may not be globally optimal according to some aggregate utility metric. However, this problem can be overcome by enumerating through different equilibria in order to ascertain the quality of the design according to a overall utility metric or setting desired utility levels as constraints.

Basing the consumer's utility maximization on the *global* commodity quantity is a departure from the standard general equilibrium model which uses the individual's possession of the commodity to determine the utility. This is done to alleviate the problem of *incremental benefit*, that is, how do you measure the impact of the change in a design attribute on dependent performance attributes and consumer's utility values? In the HSCT nozzle example, if one consumer agent requests a 2% decrease in weight, this decrease may benefit other consumer agents in the economy also. Hence, the utility for an individual consumer needs to be based on the global values of the design and performance attributes. By eliminating the utility proportioning problem the overall system becomes simpler as the consumer agent's utility is based on the global performance measure and not on the fraction of change it is responsible for.

---
[1]It is not possible to increase any one agent's utility without reducing some other agent's utility.

3.3 Performance Commodities

The consumption of commodities drives the market economy and shapes the outcome of the system. Commodities are items that are produced, bought and sold in the market and represent the primary medium through which the consumers interact. In the design economy, the consumers trade performance commodities. The performance commodities are derived from the performance attributes of the design. It is important to note that the consumers do not directly trade in design attributes. Each consumer acquires, or attempts to acquire, performance commodities which will increase its utility value. The price vector, which is based on the demand in the market, governs the cost of trading the performance commodities.

Definition 2 (Performance Commodities) *A performance commodity g^k is a continuously quantifiable real valued performance attribute.*

We consider the commodities in the standard economic sense, *goods*, which generally have positive connotations to the consumer agents. For example, efficiency can be considered a good and having more of this commodity would increase the agent's utility. However, performance attributes do not necessarily conform to this definition. Negative commodities need to be reformulated such that they can be considered as goods. For example, increasing the weight of the HSCT nozzle is generally considered undesirable. Hence, a reformulated commodity could be lightness. Thus, increased consumption of this reformulated commodity would increase the consumer's utility.

3.4 Producer Agents

In order to consume performance commodities they must first be produced. The producers agents consume a set of design attribute as inputs, such as length and material, and convert them into performance attributes, such as weight and cost. The production of performance commodities in MADA is accomplished by performance attribute agents. Formally, this calculation defines the feasible technologies ($y \in Y$) of the producer. The design attributes are managed by the design attribute agents. The performance attribute agents, or producer agents, and the design attribute agents are part of the design economy, as shown in Figure 1.

An interesting situation arises in this formulation when a design attribute (material) creates a positive change in a performance attribute (stiffness) and a negative change in another (weight). It is obvious that if the design attribute where allocated to the two producer agents they would produce conflicting demand patterns. The important issue here is not the allocation of fractional attribute values but possession of control. This conflicting demand for the design attributes is resolved by splitting design attributes into positive and negative control commodities. An intermediate broker (producer) breaks up the design attribute into both positive and negative control commodities. If a producer can increase its profit by lowering a design attribute it acquires more negative control commodities of

the design attribute and vice versa. The producer agents acquire their inputs from the design attribute agents or from their initial endowments.

Definition 3 (Control Commodities) *A control commodity is a guaranteed fractional inclusion (exclusion) of the total value of a design attribute used in the calculation of the performance attributes.*

An agent i can control commodity k in the positive sense by purchasing positive control, $c_i^{k^+}$, or likewise the negative $c_i^{k^-}$. Conservation of control must be maintained, that is $c_i^{k^+} + c_i^{k^-} = x_i^k$ which represents the range of control.

3.5 Design Commodities

Design commodities are derived from the design attributes and can be classified into two types: singular design commodities and composite design commodities. The amount of a design commodity produced to be converted into a design control commodity depends on the range of a design attribute. Composite design commodities represent a class of dependent design attributes, such as weight and volume. Composite commodities provide a means of controlling aggregate values of dependent variables. The conversion of design attribute values to design commodities is a form of normalization.

In the case of a singular design attribute, a producer agent has the sole initial endowment of the design commodity and produces the associated positive and negative control commodities from it. In the case of composite design commodities, only one producer agent controls each commodity. The producer agents representing singular design commodities use this as their production input.

3.6 Market Dynamics

Once the design problem has been decomposed, the consumer preferences encoded and the market economy defined, the interaction dynamics need to be specified. We use an interaction method called *tatonnement*, which uses an incremental price adjustment process through bidding and auction processes to clear market demand. The market clearing process ensures that supply meets the demand by controlling the prices of the commodities. Other market clearing techniques can also be used to produce similar results. A beneficial property of the tatonnement processes is that it can be implemented as a distributed asynchronous protocol which fits well into the MADA distributed environment [9].

The design economy, consisting of the consumers, producers and commodities along with their interaction protocols, evolves through the price negotiation process. This forms the basis of the design search process. The stake holders and their associated consumer agents drive the market with their consumption which cascades down the commodity chain. At every step of the process the production and consumption levels of all commodities are controlled by negotiating their market price through the assistance of the auctioneer and the price bidding processes.

The final market equilibrium represents a balance of the resource usage throughout the system. The equitable distribution of resources results in a robust design as performance commodities are effectively distributed throughout the system. Inequities are represented by a disproportionate amount paid for a commodity by a producer or consumer. Such a point would be represented by market imbalance in a particular commodity.

In general equilibrium the notion of stability has been well studied. The existence of a stable solution, even a unique stable solution, can be guaranteed if the consumers and producers conform to a set of conditions. These conditions are generally based on the convexity of the producer and consumer preferences. In the design context, it is difficult to guarantee these conditions for all the entities. Hence, we empirically test the stability and convergence properties of the systems using our Multi-Agent Diagnostics Convergence Worksheet (MAD–CoW). This worksheet provides a testbed for studying the dynamics of the interaction protocols and the utility values in the market environment. Figure 3 shows an example of three design agents which reach an equilibrium point after 30 iterations.

4 Learning

The market structure of the design environment puts high demands on the analysis software because of the large number of iterations that may be executed before reaching equilibrium. To manage this computational load the tool agents are augmented with a learning mechanism in order to facilitate efficient use of resources. Two mechanisms are currently employed, intelligent tool selection and a output estimation module.

4.1 Intelligent Tool Selection

The parametric nature of the design ecology allows tools with differing capabilities to be substituted into the environment. By allowing multiple tools to be used in the same search process, agents can balance the information fidelity requirements with search time. Analyses performed early in the search processes do not require the same precision as those done later in the search. Hence, faster, lower fidelity tools can be used to focus the search as it progresses. The management of the overall solution quality also important. Using low fidelity inputs makes the use of a high precision analysis tool unnecessary. Managing the entire information quality processes can yield significant computational savings by reducing *fidelity mismatch* and using detailed analysis only when required.

4.2 Neural Network Estimation

Since the market adjustment processes can take many iterations it is desirable to be able to estimate the output of a design tool, thereby reducing the computational overhead.

We present a neural network estimation model for the aerodynamic analysis tool in the HSCT nozzle design, as shown in Figure 4. The aerodynamic analysis tool determines the flow properties inside the nozzle. We presently
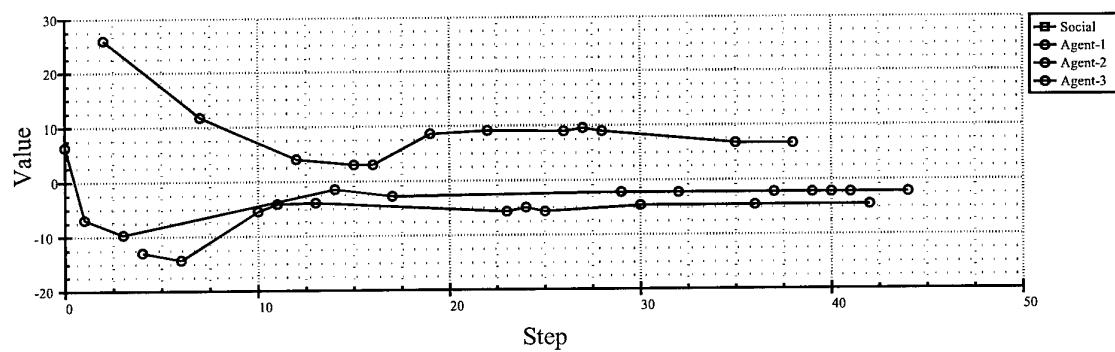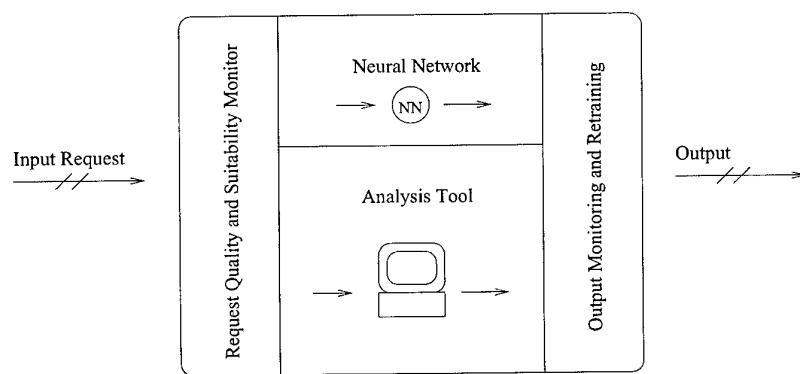
Figure 3: Convergence analysis

Figure 4: Neural network estimation

use a one-dimensional isentropic flow analysis model, that describes the global characteristics of the flow inside the nozzle with reasonable accuracy. Assumption of sonic flow at the throat gives an area-Mach number relation that relates the Mach number at any location in the nozzle to the ratio of the local nozzle to the sonic throat area. An ideal expansion at the nozzle exit is also assumed in the analysis. The ambient conditions, nozzle pressure ratio (NPR: stagnation pressure/ambient pressure) and the temperature ratio (TR: stagnation temperature/ambient temperature) are specified as the initial nozzle parameters. In practice, the turbine outlet conditions are typically known before the design of a nozzle is initiated. The performance of the nozzle is then characterized in terms of the NPR and TR. For a given throat area and exit nozzle angle, the length of the nozzle can be calculated. Although, the aerodynamic analysis carried out here is relatively simple, the values of most of the important flow parameters inside the nozzle, such as the pressure and temperature on the nozzle walls are captured adequately.

This is a pattern association problem and the network best suited for this is the feedforward network with backpropagation. A feedforward type of neural net is a specific connection structure, where neurons of one layer are only allowed to have connections to neurons of other layers. Backpropagation is a learning algorithm used by nets with supervised learning. A graphical representation of this network can be found in Figure 5, with input nodes, hidden layers and output nodes from left to right respectively. The inputs to the network are 1) nozzle pressure ratio 2) Mach number at exit 3) ambient pressure 4) ambient temperature 5) temperature ratio 6) starting area 7) nozzle angle and 8) number of samples. The outputs generated are 1) maximum temperature 2) length and 3) ratio of starting area to the exit area.

The analysis tool is used to generate the training data set for the neural network. The number of hidden layers, nodes in each hidden layer and the learning rate are experimentally determined. Once the network prediction error is below an acceptable level it is used to estimate the design tool outputs. This significantly speeds up the design search process. The network is verified after a series of runs and the analysis tools are used to to update the weight matrix in the net. The decision whether to use the neural net estimation or the analysis tool results can be based on a cost function reflecting the required fidelity and criticality of the results.

Table 1 shows four test results of the neural network for the aerodynamic analysis tool. Best results were obtained when the training was done for 1000 cycles with the structure shown in Figure 5 and the learning rate was set to $0.25(\alpha)$. Note that all inputs to the net were normalized between 0 and 1.

5 Summary

The distributed design environment presented in this paper can be applied to the design of complex products. The distributed nature of the computations and decision making

are well suited for large scale applications. By representing the design search problem in an economic context, we can study the properties of the design configurations generated by this methodology. Although this method does not guarantee an optimal design, it can be used to identify acceptable alternatives.

The future research in this area will focus on testing the architecture on complex assemblies, involving multiple design domains, such as mechanical, electrical and computational systems. The learning tools will also be refined to include the overall design performance prediction capabilities.

6 Acknowledgments

References

[1] S. H. Thomke, "Managing experimentation in the design of new products," *Management Science*, vol. 44, pp. 743–762, June 1998.

[2] R. Levy, K. Erol, and H. Mitchell, "A study of infrastructure requirements and software platforms for autonomous agents," in *Proceedings of ICSE-96*, July 1996.

[3] T. Finin, R. Fritzson, and D. McKay, "A language and protocol to support intelligent agent interoperability," in *Proceedings of the CE & CALS Washington '92 Conference*, June 1992.

[4] A. Deshmukh, A. Krothapalli, T. Middelkoop, and C. Smith, "Multi–agent design architecture for integrated design systems," *AIAA Journal of Aircraft*, 1999. Accepted with revisions.

[5] T. Mullen and M. P. Wellman, "Some issues in the design of market-oriented agents," in *Intelligent Agents II: Agent Theories, Architectures, and Languages*, Springer-Verlag,, 1996.

[6] Y. Balasko, *Foundations of the Theory of General Equilibrium*. Academic Press, Inc., 1988.

[7] J. Quirk and R. Saposnik, *Introduction to General Equilibrium theory and Welfare Economics*. McGraw-Hill, 1968.

[8] T. Rader, *Theory of General Economic Equilibrium*. Academic Press, 1972.

[9] J. Q. Cheng and M. P. Wellman, "The WALRAS algorithm: A convergent distributed implementation of general equilibrium outcomes," *Computational Economics*, vol. 12, pp. 1–23, 1998.

Inputs to the Neural Net						Outputs from the Neural Net			Net Error
npr	me	pa	ta	tr	astar	temp	length	aebast	
0.348	0.607	0.857	0.938	0.332	0.278	0.355	0.337	0.641	0.110
0.961	0.605	0.632	0.685	0.388	0.284	0.248	0.319	0.635	0.080
0.792	0.599	0.774	0.800	0.350	0.230	0.288	0.289	0.622	0.076
0.997	0.594	0.443	0.235	0.005	0.112	0.042	0.247	0.599	0.062
0.573	0.562	0.487	0.534	0.284	0.134	0.145	0.231	0.576	0.050

Table 1: Neural network estimation results
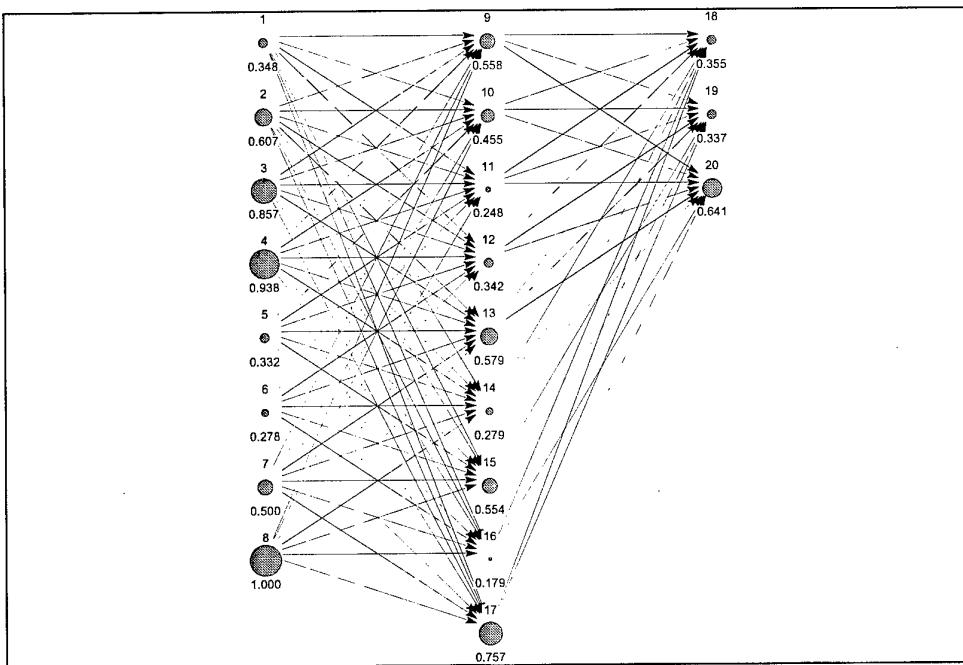
Figure 5: Neural network layout

A Conceptual Design Methodology to Predict the Wave Drag of a Transonic Wing

T. Krißler

Synaps Ingenieur-Gesellschaft mbH
Fahrenheitstr. 1, D-28359 Bremen, Germany
DaimlerChrysler Aerospace Airbus GmbH, EFP
Hünefeldstr. 1–5, D-28183 Bremen, Germany

Abstract

A conceptual design methodology to predict the wave drag of a transonic wing for use within multisdisciplinary aircraft design was developed. To achieve this, a database of cross section designs optimized with respect to total drag was set up varying the design parameters Ma, t/c, c_L and Re. Mathematical formulations for the aerodynamic cross section characteristics total drag, viscous drag and the local shock location were derived from the database as functions of the design parameters. The cross section wave drag was then derived using these formulations. A locally infinite swept wing is assumed and simple sweep theory using the shock sweep angle is used to transform the wave drag. The wave drag of a 3-D wing is predicted summing locally infinite swept wing sections in spanwise direction. The achieved drag prediciton is accurate enough for use within conceptual aircraft design and predicts well the trends in wave drag development as a function of the design parameters Ma, t/c, c_L, Re and the wing planform.

Introduction

Within the scope of multidisciplinary conceptual aircraft design [1] [2], a transonic aerodynamic module to predict transonic effects of a wing is essential. Typically, about 300 parameters and 50 design variables and constraints are used to describe the complete configuration, whereas about 150 parameters and 15 design variables of these are used for aerodynamic purposes [3]. The objective of the presented methodology is to describe transonic aerodynamic effects with a limited number of parameters and predict the correct trends within conceptual aircraft design. Processing time becomes critical for application of the methodology within multidisciplinary design automation and optimization. For this reason, time intensive codes (e.g. 3-D Navier Stokes, 3-D Euler) are not appropriate. Therefor a fast conceptual design methodology to predict the wave drag of a transonic wing as a function of the design parameters Ma, t/c, c_L, Re and the wing planform will be described.

Methodology

Transonic aerodynamic characteristics of a wing are a result of the wing planform, the spanwise distribution of lift, thickness and local flow data. These parameters shall be used as input data for a method to predict aerodynamic effects of a transonic wing.

As a first step, a database of cross section designs was set up using numerical optimization routines. To achieve this, Daimler-Chrysler Aerospace Airbus (DA) inhouse codes were linked to the Synaps optimization tool *PointerPro*^{TM} [4] to set up the database. The aerodynamic codes used were *VICWA* [5] (Full potential code with finite-difference boundary layer calculation) and *XLS6* (Full potential code with integral boundary layer calculation). The database contains about 240 cross section designs optimized with respect to total drag, called optimized performance designs. Typical optimized performance cross section designs of the database are shown in Fig. 1.

All calculations are 2D, without sweep angle. The design parameters to set up the database of optimized performance cross section designs have been varied within the following ranges:

$$0.7 < Ma_{2d} < 0.8$$
$$0.5 < c_{L2d} < 0.9$$
$$0.05 < t/c_{2d} < 0.16$$

For a 3D wing the corresponding Ma range for quarter chord sweep angles of about 30° is $0.8 < Ma_{3d} < 0.95$. The Reynolds number Re was varied from $1 \cdot 10^6$ to $80 \cdot 10^6$.

Using this database of optimized performance cross section designs, analytical approximations for the relationships between aerodynamic cross section characteristics and the design parameters Ma, t/c, c_L and Re were derived from the database using appropriate methods. Formulas were found, ensuring physically plausible trends towards the borders of design parameter ranges. The idea for a methodology to predict the 2D total profile drag as a function of the design parameters Ma, t/c, c_L at constant Re originates from A. Van der Velden.

A refined methodology to predict the 2D cross section total drag and a methodology for the profile viscous drag as a function of the design parameters Ma, t/c, c_L and Re were established.

Methodologies needed for the 2D wave drag:

- Total profile drag

- Profile viscous drag

To predict the wave drag of a transonic 3D wing, locally infinite swept wing sections are assumed which are integrated in spanwise direction. Simple sweep theory using the local shock sweep angle is used to transform the cross section wave drag. To achieve this, methodologies for the following aerodynamic characteristics as functions of the design parameters were developed.

Methodologies needed for the 3D wave drag:

- Profile wave drag

- Local shock sweep angle

The previously mentioned methods for the 2D total profile drag and the profile viscous drag were used to derive the profile wave drag. A

methodology for the local shock sweep angle was developed in previous work [6].

The methodologies are used within multidisciplinary design automation to predict the minimum wave drag, the minimum total drag and trends in drag development of a transonic wing as a function of local values of Ma, c_L, t/c, Re and the wing planform.

The 3D design paramter ranges for the use of the methodologies are as follows:

$$0.7 < Ma < 0.95$$
$$0.1 < c_L < 1.3$$
$$0.03 < t/c < 0.18$$

Analysis

The total drag output from the transonic code of the optimized performance designs in the database was analyzed to determine the relationship between cross section characteristics and design parameters. A drag break down into wave drag due to lift and viscous effects is assumed to be adequately correct for use within conceptual design. Both wave drag due to lift and viscous drag are assumed to be functions of the design parameters Ma, t/c, c_L and Reynolds number Re.

Total profile drag

To describe the total profile drag of the optimized performance designs in the database, an appropriate function was chosen. As a first estimate a third order polynomial (1) was used with mixed terms in the design parameters Ma, c_L and t/c combined with an exponential contribution of Ma, c_L and t/c .

$$c_{Dtot} = \sum_{\substack{i,j,k=0 \\ i+j+k \leq 3}}^{3} A_{ijk}\, x_1^i\, x_2^j\, x_3^k + \cdots$$

$$\cdots + \left(\sum_{i=0}^{3} x_i \right) \cdot exp \left(\sum_{\substack{i,j,k=0 \\ i+j+k \leq 2}}^{2} B_{ijk}\, x_1^i\, x_2^j\, x_3^k \right) \quad (1)$$

where

$$x_1 = f(Ma)$$
$$x_2 = f(c_L)$$
$$x_3 = f(t/c).$$

For better model handling, x_1, x_2 and x_3 are linear functions of the design parameters Ma, c_L and t/c, respectively.

For a specific cross section n in the database, the local quadratic deviation E_{locn} of the total drag model compared to the total drag in the database is described in equation (2). Here $(c_D)_{totdb_n}$ and $(c_D)_{totmod_n}$ are the total drag of the cross section n in the database and of the model following equation (1) respectively.

$$E_{locn} = (|(c_D)_{totdb_n} - (c_D)_{totmod_n}|)^2 \quad (2)$$

The mean global deviation E_{glob} of the mathematical model for the total drag for all N cross sections in the database may then be derived using equation (3).

$$E_{glob} = \frac{1}{N} \sum_{n=1}^{N} E_{locn} \quad (3)$$

To achieve the best fit possible for the model with the database, the coefficients A_{ijk} and B_{ijk} were varied until the minimum of the global deviation E_{glob} was reached. Due to the resulting nonlinear equation system, a numeric optimizer was used to find the coefficients A_{ijk} and B_{ijk} in equation (1).

Primarily a physically correct reproduction of trends in total drag development was intended. The mean deviation of the model compared to the total drag of the cross sections in the database is less than 7.5%. An exact agreement of the total drag determined from the database with the total drag calculated using equation (1) was not required for multidisciplinary design.

The total drag of the optimized cross sections in the database compared to the total drag model for constant Reynolds number at $c_L = 0.5$ is shown in Fig. 2. The total drag coefficient $(c_D)_{tot}$ is plotted as a function of t/c. The Mach number is a curve parameter and is increasing from bottom right to top left. The database total drag is shown as dashed lines and the model total drag as solid lines. Similar plots at $c_L = 0.7$ and $c_L = 0.9$ are shown in Fig. 3 and Fig. 4 respectively.

The finally derived formula of the total drag model principally consists of an absolute term, linear terms in c_L and t/c and functions of $(t/c)^2$. Third order terms in the polynomial contribution were not relevant. An exponential function with linear terms in Ma and c_L and a quadratic term in t/c was used to describe the total cross section drag for a specific Reynolds number.

$$c_{D_{tot}} = P_{tot}(c_L, t/c, (t/c)^2) + \cdots$$
$$\cdots + E_{tot}(Ma, c_L, (t/c)^2) \quad (4)$$

with

P_{tot} polynomial
E_{tot} exponential function

The total drag model for constant Reynolds number at $c_L = 0.5$ is shown in Fig. 5. The total drag coefficient $(c_D)_{tot}$ is plotted as a function of t/c and Mach number Ma. Mach number is increasing from front to back and thickness is increasing from left to right.

The total drag model predicts the correct trends in total drag development as a function of the design parameters Ma, t/c, c_L and Reynolds number Re. The behaviour near the borders of the parameter ranges is physically plausible.

In order to extract the profile wave drag from the profile total drag, the profile viscous drag as a function of the design parameters was needed.

Profile viscous drag

As for the total drag model a similar approach for the viscous drag model was used to find an analytical relationship of the viscous drag dependent on the design parameters t/c, c_L and Re. The optimized performance cross section designs in the database were used for the calculation of viscous drag at Reynolds numbers in the range from $Re = 1 \cdot 10^6$ to $Re = 80 \cdot 10^6$.

A second order polynomial with mixed terms in the design parameters c_L and t/c was used as a starting point for a specific Reynolds number.

$$c_{Dvisc}|_{Re} = \sum_{\substack{j,k=0 \\ j+k\leq 2}}^{2} A_{jk}\, x_2^j\, x_3^k \qquad (5)$$

Again, the coefficients of the mathematical function to describe the viscous drag were found using numerical optimizers. The viscous drag model describing the viscous drag of the cross section designs in the database as a function of the design parameters is shown in equation (6). Note there is no contribution of Mach number to the profile viscous drag.

$$c_{Dvisc} = P_{visc}(c_L,\ t/c,\ (t/c)^2) \qquad (6)$$

with

$$P_{visc} \quad \text{polynomial}$$

The coefficients A_{jk} in equation (5) are functions of the Reynolds number Re. Logarithmic terms or combinations of logarithmic and exponential terms are used, dependent on the coefficient A_{jk}.

$$
\begin{aligned}
A_{00} &= s_0 \; e^{(\ln s_1 Re)} \\
A_{01} &= q_0 + \ln(q_1 Re) \\
A_{10} &= r_0 + \ln(r_1 Re) \\
A_{02} &= p_0 + p_1 Re
\end{aligned} \qquad (7)
$$

The parameters p_i, q_i, r_i and s_i in (7) were calculated as previously described using a numerical optimizer to find a best possible fit for the viscous drag derived from the database. The Reynolds numbers were in the range from $Re = 1 \cdot 10^6$ to $Re = 80 \cdot 10^6$.

The viscous drag of the optimized cross sections in the database compared to the viscous drag model for constant Reynolds number at $c_L = 0.5$ is shown in Fig. 6. The viscous drag coefficient $(c_D)_{visc}$ is plotted as a function of t/c. The Mach number is a curve parameter and there is no variation of viscous drag with Mach number. The database viscous drag is shown as dashed lines and the model viscous drag as solid lines. A similar plot at $c_L = 0.7$ is shown in Fig. 7.

The viscous drag model for constant Reynolds number at $c_L = 0.5$ is shown in Fig. 8. The viscous drag coefficient $(c_D)_{visc}$ is plotted as a function of t/c and Mach number Ma. Mach number

is increasing from front to back and thickness is increasing from left to right.

The viscous drag model predicts the correct trends in viscous drag development as a function of the design parameters c_L, t/c and Re. Additional drag due to possible separation at the upper surface trailing edge at off-design conditions (towards higher t/c at high c_L) is not described with the viscous drag model (Fig. 9). However, these conditions are not relevant for transonic aircraft sizing.

Profile wave drag

Using the profile total drag model and the profile viscous drag model described in the previous sections, a wave drag model can be established using the assumption about drag break down in the section 'Analysis'. Subtracting the viscous drag model at a certain Reynolds number from the total drag model set up for the same Reynolds number, the resulting model describes the wave drag contribution of the optimized cross section designs in the database as a function of Ma, t/c, c_L and Re. The wave drag model comprises the wave drag due to shock waves and pressure drag due to thickening of the boundary layer caused by shock boundary layer interaction.

Combining the wave drag model with the viscous drag model, the total drag of the cross sections can be predicted as a function of the design parameters Ma, t/c, c_L and Re.

The wave drag model for constant Reynolds number at $c_L = 0.5$ is shown in Fig. 10. The wave drag coefficient $(c_D)_{wave}$ is plotted as a function of t/c and Mach number Ma. Mach number is increasing from front to back and thickness is increasing from left to right.

Wing wave drag

Based on the assumption of an isobaric wing design concept, the wave drag can locally be calculated using simple sweep theory based on the local shock sweep angle (Fig. 11). The 3D transonic characteristics of a wing may then be predicted using the 2D models, derived from the database. The wing wave drag can be described as a function of the local values of Ma, c_L, t/c, Re, the local shock sweep angle ϑ_S and the wing planform.

The local shock sweep angle is a function of the local shock location of the upper surface shock and the wing planform. An analytical model of the local shock location as a function of the design parameters was derived from the database simimlar to the drag models described previously. The shock location of the upper surface shock of the optimized cross sections in the database compared to the shock location model at $c_L = 0.7$ is shown in Fig. 12. The shock location $(x/c)_s$ is plotted as a function of t/c. The Mach number is a curve parameter and is increasing from bottom right to top left. The database shock location is shown as dashed lines and the model shock location as solid lines. The shock location model at $c_L = 0.7$ is shown in Fig. 13. The shock location $(x/c)_s$ is plotted as a function of t/c and Mach number Ma. Mach number is increasing from front to back and thickness is increasing from left to right. More detailed information about the shock location model may be found in [6].

Using the viscous drag model, the wave drag model and the methodology described within this paper, the minimum total drag of a 3D wing for a specific design may be predicted and a drag break down into wing viscous drag and wing wave drag is possible.

The wing drag prediction solely is a function of the local design parameters Ma, c_L, t/c, Re and the wing planform. With the drag models being derived from cross section designs optimized with respect to minimum total drag, the methodology predicts the minimum possible drag for a specific wing design. With the assumption of an isobaric wing design concept, a good prediction for the outboard wing and a first good estimate for the inboard wing may be achieved using the methodology. However, the more an isobaric wing design concept is realized in actual wing design, the better the wing drag prediction which can be achieved using the described methodology.

Conclusion

A conceptual design methodology was described to predict the wave drag, viscous drag and total drag of a transonic wing. The methodology is intended for use within multidisciplinary conceptual design. The wave drag and trends in wave drag development of a wing can be predicted as a function of the local design parameters Ma, c_L, t/c, Re and the wing planform. As a result of the analytical description of the drag models used within the methodology, the processing time for a wing drag prediction is only in the order of seconds. Although the methodology is based on 2D cross section designs optimized with respect to minimum drag, the predicted minimum wave drag of a 3D wing compares well with the wing wave drag of current design studies. Future work will consider the implementation of effects of the fuselage and engine installation.

References

[1] Van der Velden, A., Aerodynamic Shape Optimization, AGARD-R-803 AGARD-FDP-VK1 Special Course, April 1994

[2] Van der Velden, A., Tools for Applied Engineering Optimization, AGARD-R-803 AGARD-FDP-VK1 Special Course, April 1994

[3] Sobieczky, H., Seebass, R., Mertens, J., Dulikravich, G., Van der Velden, A., New design concepts for high speed air transport, CISM courses and lectures no. 366, International Center for Mechanical Sciences, Springer, 1997

[4] Synaps Inc., "PointerPro^{TM}4.2", www.synaps-ing.de

[5] Dargel, G., Ein Programmsystem für die Berechnung transsonischer Profil- und konischer Flügelströmungen auf der Basis gekoppelter Potential- und Grenzschichtlösungen, DGLR Bericht 92-07, Köln, 1992

[6] Krißler, T., A Conceptual Design Methodology for the Estimation of the Local Shock Locations on Optimized Transonic Wings, DGLR AG-STAB Symposium, Berlin, 1998
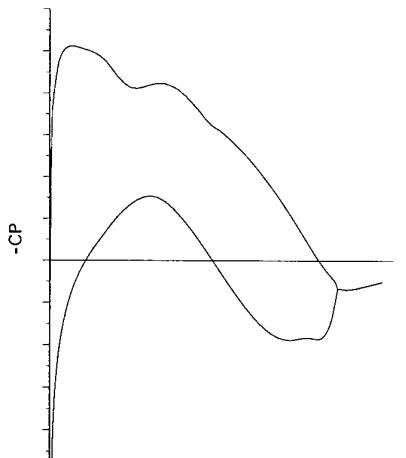
(a) Optimized performance design, $Ma = 0.72$, $c_L = 0.7$, $(t/c) = 0.11$

Fig. 2: Database total drag c_{Dtotdb} versus formulation $c_{Dtotmod}(Ma, c_L, t/c)$ at $c_L = 0.5$

Fig. 3: Database total drag c_{Dtotdb} versus formulation $c_{Dtotmod}(Ma, c_L, t/c)$ at $c_L = 0.7$

(b) Optimized performance design, $Ma = 0.76$, $c_L = 0.5$, $(t/c) = 0.10$

Fig. 1: Typical cross section designs of the database
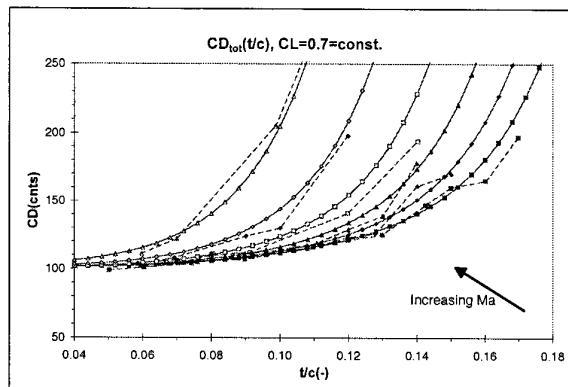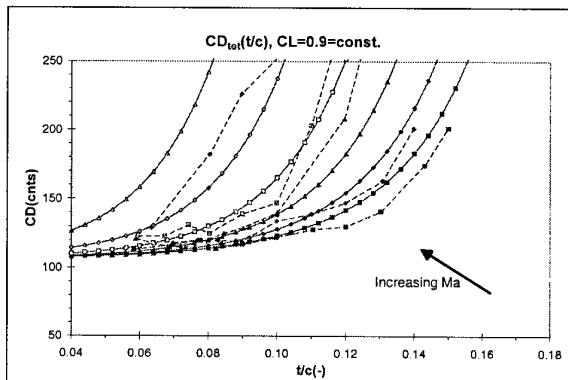
Fig. 4: Database total drag c_{Dtotdb} versus formulation $c_{Dtotmod}(Ma, c_L, t/c)$ at $c_L = 0.9$
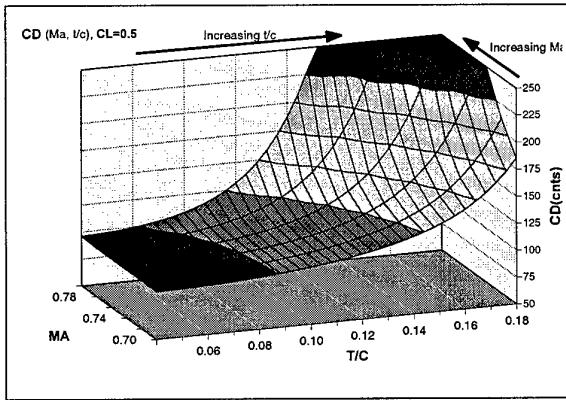
Fig. 5: Total drag $c_{Dtotmod}$ at $c_L = 0.5$
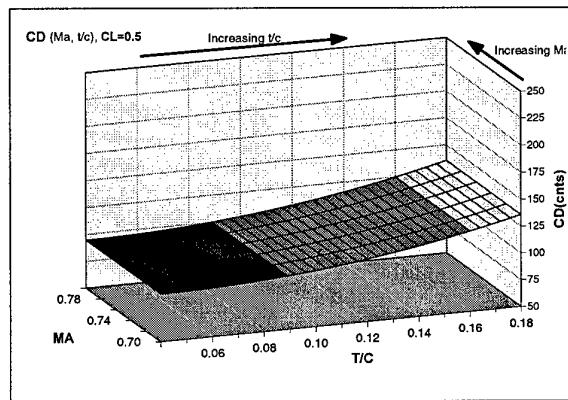
Fig. 8: Viscous drag $c_{Dviscmod}$ at $c_L = 0.5$
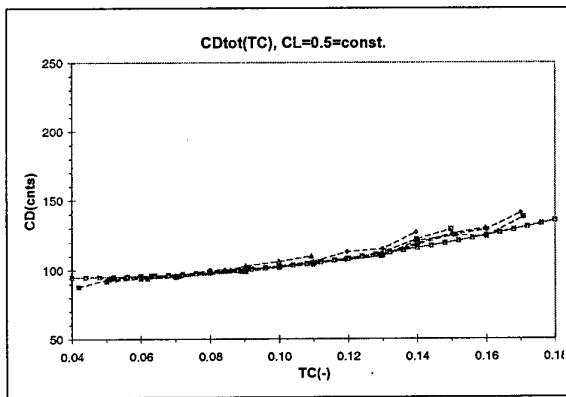
Fig. 6: Database viscous drag $c_{Dviscdb}$ versus formulation $c_{Dviscmod}(c_L, t/c)$ at $c_L = 0.5$
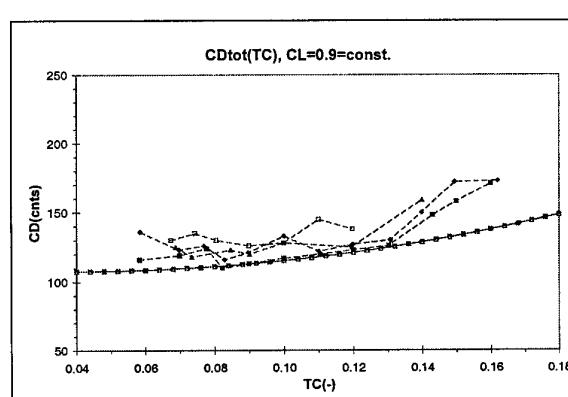
Fig. 9: Database viscous drag $c_{Dviscdb}$ versus formulation $c_{Dviscmod}(c_L, t/c)$ at $c_L = 0.9$
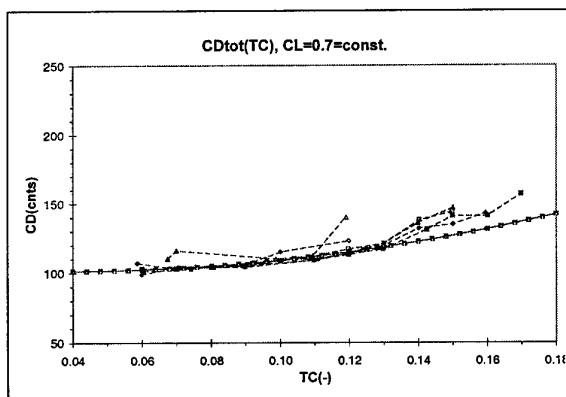
Fig. 7: Database viscous drag $c_{Dviscdb}$ versus formulation $c_{Dviscmod}(c_L, t/c)$ at $c_L = 0.7$
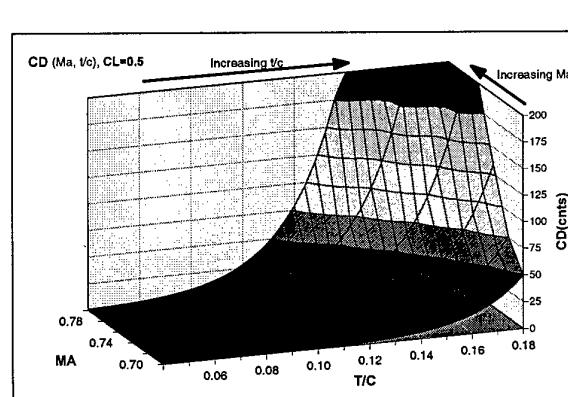
Fig. 10: Wave drag $c_{Dwavemod}$ at $c_L = 0.5$
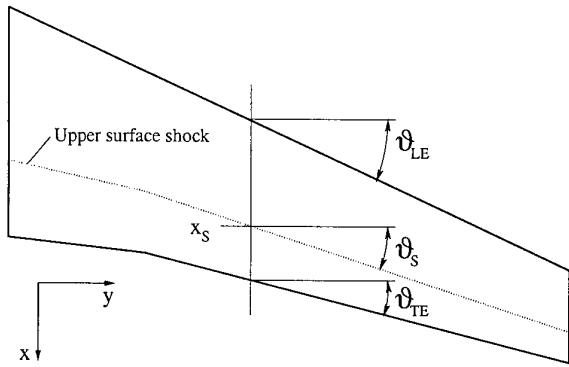
Fig. 11: Local shock sweep angle, isobaric wing design concept
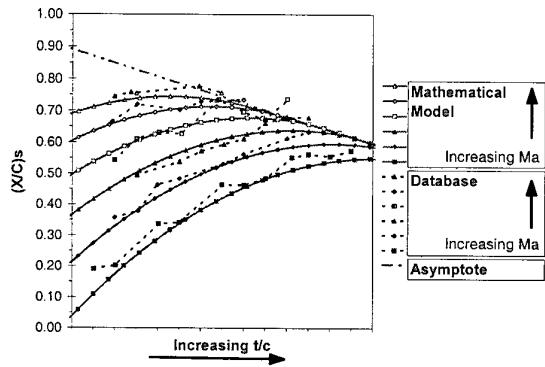
Fig. 12: Database shock location $(x/c)_{S_{db}}$ versus mathematical model $(x/c)_{S_{mod}}(Ma, t/c)$ at $c_L = 0.7$
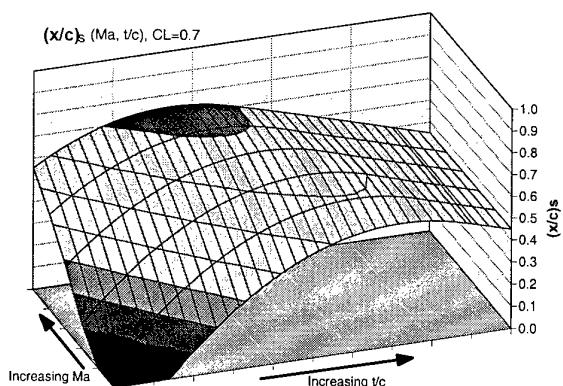
Fig. 13: Shock location model $(x/c)_{S_{mod}}(Ma, t/c)$ at $c_L = 0.7$

Airfoil and Wing Planform Optimization for Micro Air Vehicles

J. G. Sloan, W. Shyy* and R. T. Haftka

*University of Florida
Department of Aerospace Engineering, Mechanics & Engineering Science
P.O. Box 116250
Gainesville, Florida 32611-6250, U.S.A.

ABSTRACT

Low Reynolds number flight for micro air vehicles (μAVs) suffers from laminar separation resulting in reduced lift and increased drag. The objective of the present work is to use the response surface methodology (RSM) to identify correlations between the airfoil and the wing planform to facilitate a two-level optimization procedure in which an optimized airfoil and wing planform are reached simultaneously. Several approaches have been considered in this work. (1) A constant cross-section wing is modeled with maximum camber, y_c, maximum thickness, y_t, and aspect ratio, AR, as design variables at two different Reynolds numbers of 8.0×10^4 and 2.0×10^5. This is done to determine how the optimal airfoil may change for different aspect ratios and Reynolds numbers. (2) A variable cross-section wing defined by root camber and angle-of-attack and tip camber and angle-of-attack is modeled in order to determine how the optimal airfoil may change from the root to the tip of the wing. (3) Due to the size restrictions on μAVs, a fixed-span approach is used to model an aircraft subject to the constraints of steady flight with the aspect ratio and camber as design variables. This third approach balances trade-offs between wing area, aspect ratio, and Reynolds number in determining the overall flight efficiency. Optimal airfoils exhibit characteristics which change little with wing aspect ratio or location on the wing planform. There appears to be a trend of increasing optimal camber with decreasing Reynolds number. While the optimal design seems to favor airfoils with minimum thickness and relatively modest camber of about 4 to 5% of the chord, a higher camber may be a better choice if higher lift coefficient at minimum power is used as a design goal. Measurements of both the global and the local response surface prediction accuracy combined with design space refinement help to assess the reliability of the response surface approximations and optimal design predictions.

1. INTRODUCTION

The low-Reynolds number flight regime of micro air vehicles (μAVs) presents substantial aerodynamic design challenges. Micro air vehicles have length scales under 15 cm and flight speeds of approximately 15 m/s, resulting in Reynolds numbers between 10^4 and 10^5. Airfoil performance at these chord Reynolds numbers suffers from laminar separation and increased sensitivity to changing flow conditions. The increased sensitivity of the flow structure is important since fluctuations in wind velocity are comparable to the flight speed in this regime[1]. Furthermore, since airfoil performance decreases as Reynolds number decreases, attempts to shrink the overall aircraft size while trying to keep a 'workable' chord Reynolds number and sufficient lifting area result in low aspect ratio wing planforms[2].

As the aspect ratio decreases, the percentage of the wing area affected by wing-tip vortices increases, resulting in a largely three-dimensional flow field over most of the wing. An accurate analysis must consider the performance effects of both the airfoil geometry and the wing planform geometry.

The objective of the present study is to optimize airfoil and wing geometries for this flight regime using response surface methodology (RSM)[3]. RSM integrates statistical experimental design fundamentals, regression modeling techniques, and elementary optimization methods. Polynomial approximations are created relating aerodynamic performance measures to the variables which define the wing configuration. The number and the distribution of design points used for fitting response surfaces plays a large role in their predictive accuracy. The various design point selection techniques used in this study have been discussed and compared by Giunta et al.[4] and Unal et al.[5] for aerodynamic approximations in aerospace vehicle design. Design space refinement can improve the response surface prediction accuracy in the region of interest. Narducci et al.[6] and Sobieski et al.[7] used response surfaces fit to successively refined regions around the optimum. Other examples of RSM applied to fluid design problems are given in Madsen et al.[8], Knill et al.[9], and Baker et al.[10].

Since a common obstacle encountered during μAV design is the weight of the onboard energy supply, minimizing the flight power consumption is an appropriate design objective. Attempts are made to identify correlations between the airfoil and the wing planform to facilitate a two-level optimization procedure in which an optimized airfoil is found for an optimized wing planform. Design variables are chosen based on their ability to modify the flow fields under consideration. Governing flow quantities such as mass and momentum fluxes are strongly influenced by wing camber, thickness, aspect ratio, and angle-of-attack. Additionally, flow fields in the Reynolds number range of currently envisioned μAVs are largely dependent on the Reynolds number and freestream disturbance level[11].

Several approaches have been considered in this work. (1) A constant cross-section wing is modeled with maximum camber, y_c, maximum thickness, y_t, and aspect ratio, AR, as design variables at two different Reynolds numbers of 8.0×10^4 and 2.0×10^5. This is done to determine how the optimal airfoil may change for different aspect ratio wings and different Reynolds numbers. Investigations of the sensitivity of optimal camber with changes in the flight Reynolds number may warrant and facilitate the use of a variable camber airfoil. (2) A variable cross-section wing defined by root camber and angle-of-attack and tip camber and angle-of-attack is modeled in order to determine how the optimal airfoil may change from the root to the tip of the wing. (3) Due to the size restrictions on μAVs, a fixed-span approach is

used to model an aircraft subject to the constraints of steady flight with the aspect ratio and camber as design variables. This third approach balances trade-offs between wing area, aspect ratio, and Reynolds number in determining the overall flight efficiency.

Accurate evaluations of low Reynolds number airfoils require aerodynamic models which take into account the performance effects of separation and laminar-turbulent transition. Although precise modeling of the flow structure associated with separation requires a solution of the full Navier-Stokes equations, the effects of thinly separated regions on pressure and viscous shear forces can usually be substantially captured by reduced-equation boundary layer models[12,13]. Such a reduced two-dimensional model combined with a three-dimensional potential flow solver is incorporated in the present study to make an incremental design/optimization procedure feasible.

2. PERFORMANCE CRITERIA

The performance analysis is based on both a three-dimensional potential flow solution provided by $PMARC$[14] and a two-dimensional inviscid/boundary-layer solution (also referred to as viscous/inviscid solution) for the airfoil provided by $XFOIL$[15,12]. Performance is measured by the power index, $C_L^{3/2}/C_D$, which appears explicitly in the equation for the steady flight power requirement, P_r, given by[16,17,18]

$$P_r = \frac{C_D}{C_L^{3/2}} \sqrt{\frac{2W^3}{\rho S}} \tag{1}$$

The lift coefficient, C_L, is the non-dimensional force component perpendicular to the freestream velocity vector. The drag coefficient, C_D, is the non-dimensional force component parallel to the freestream velocity vector. In Eq. (1), W, ρ, and S are, respectively, aircraft weight, air density, and wing reference area.

The drag coefficient, C_D, will be discussed in terms of three drag component coefficients such that

$$C_D = C_{d_f} + C_{d_p} + C_{d_i} \tag{2}$$

where

1) C_{d_f} is known as the frictional drag coefficient, and it results from fluid forces which act tangentially to the airfoil surface due to viscosity and velocity gradients at the solid surface,

2) C_{d_p} is known as the pressure drag coefficient (or alternatively as form drag or afterbody drag), and it results from fluid forces which act normal to the airfoil surface, and

3) C_{d_i} is known as the induced drag coefficient, and it results from a change in the relative wind over the wing from lift-induced wing-tip vortices.

The sum of the friction drag and the pressure drag is commonly known as the 'profile drag'. Since C_{d_f} is a result of viscous shear forces, and the inviscid solution around an arbitrary, 2-D configuration gives a resultant force perpendicular to the freestream, leaving $C_{d_p} = 0$, the profile drag can be termed the viscous drag. The C_{d_p} component of the viscous drag results from modification to the effective airfoil shape caused by boundary layer thickness, separation and the trailing wake.

In the following analyses, the lift coefficient is determined from $PMARC$, and the drag coefficient is determined by adding the profile drag coefficient given by $XFOIL$ and the induced drag coefficient given by $PMARC$. The average profile drag is used for wings with varying cross-section, which offers an approximate estimate with much reduced computing needs.

$XFOIL$ simulates inviscid or coupled inviscid/boundary-layer flow around 2-D airfoils. $XFOIL$'s predictive accuracy was assessed in Shyy et al.[13]. $XFOIL$ uses a two-equation boundary layer integral formulation based on dissipation closure for both laminar and turbulent flows[12]. A two-equation model is necessary in order to uniquely determine the shape parameter in separated flow regions. $XFOIL$ also employs the e^n laminar-turbulent transition prediction model[19,20,21]. The e^n method is based on linear stability analysis using the Orr-Sommerfeld equation to determine the growth of spatially developing waves.

$XFOIL$ determines the lift coefficient from integration of surface pressures, where the surface pressures are obtained from the potential flow solution. The drag coefficient is calculated from the Squire-Young formula[22,23],

$$C_d = \frac{2\theta_\infty}{c}, \tag{3}$$

where θ_∞ is the wake momentum thickness at downstream infinity and c is the airfoil chord. The Squire-Young formula is obtained by applying the momentum theorem to a control volume surrounding the airfoil, and it measures the fluid momentum losses downstream of the airfoil. This measurement provides the 2-d profile drag of the airfoil, namely, $C_d = C_{d_f} + C_{d_p}$.

$PMARC$ is a low-order potential flow panel code for three-dimensional geometries in unsteady flow fields. Laplace's equation for the velocity potentials is resolved by superposition of source and doublet solutions throughout the wing surface and trailing wake. The lift coefficient is determined from integration of surface pressures, and the induced drag coefficient is determined by Trefftz plane analysis[24].

$PMARC$'s accuracy was tested against $XFOIL$ for three different airfoils: the two well-known airfoils, NACA 0012 and CLARK-Y, and a recently proposed low Reynolds number airfoil, S1223[25]. The three airfoils and the results of the assessment are presented by Sloan[26].

3. THE RESPONSE SURFACE METHOD

The approach of RSM is to perform a series of experiments, or numerical analyses, for a prescribed set of design points, and to construct a global approximation (response surface) of the measured quantity (the response) over the design space. In the present context, the response is a measure of wing performance such as $C_L^{3/2}/C_D$, and the design space consists of a set of relevant design variables such as camber, thickness, angle-of-attack, and so on. Quadratic polynomials are used for the response surface approximations for which extremal points are easily found by standard constrained optimization algorithms. The main advantages of RSM over other optimization tools such as gradient-based search algorithms are that it requires minimal interfacing with the analysis tools and avoids the need for expensive derivative calculations. However, RSM is practically limited by the number of design variables which can be considered. A response surface represented by a quadratic polynomial has $(k+1)(k+2)/2$ coefficients, where k is the number

of design variables. So, for example, a quadratic polynomial in 10 variables has 66 coefficients which requires an even higher number of analyses to obtain a reliable fit.

The response surface is fit by standard least squares regression using JMP^{27} statistical analysis software. JMP is an interactive, spreadsheet-based program which provides a variety of statistical analysis functions. A *backward elimination* procedure based on t-statistics is used to discard terms and improve the prediction accuracy[3]. The t-statistic, or t-ratio, is given by

$$t_o = \frac{b_j}{se(b_j)}, \tag{4}$$

where b_j is the regression coefficient and $se(b_j)$ is the standard error of the regression coefficient. The standard error of the regression coefficient is given by

$$se(b_j) = \hat{s}\sqrt{C_{jj}} \tag{5}$$

where $\hat{s}$ is an unbiased estimator of the standard deviation of the observations (also an unbiased estimator of the rms error in prediction based on the response surface) and C_{jj} is the diagonal element of $(X'X)^{-1}$ corresponding to b_j. The standard deviation, $\hat{s}$, is given by

$$\hat{s} = \sqrt{\frac{\sum e_i^2}{n - p}} \tag{6}$$

where the residual, e_i, is the difference between the observation, y_i, and the fitted value, $\hat{y}_i$. X is an $n \times p$ matrix of the levels of the independent variables where n is the number of observations and p is the number of terms in the model. In the present case, X is a 27×10 matrix representing 27 levels of the 10-term model resulting from 27 combinations of the 3 design variables. Looking for a t-statistic > 2 in absolute value is a common rule of thumb since this value corresponds to an approximately 5 percent probability of mistakenly rejecting the null hypothesis that the coefficient is zero. In the backward elimination procedure, the acceptable probability for leaving a term in the model is usually changed until the most accurate reduced model is found. Additionally, it is common to retain linear terms with unacceptable t-statistics if they are included in significant higher-order terms. The global fit and prediction accuracies of the full and reduced response surfaces are assessed through statistical measures such as R^2, R_a^2, and $\hat{s}$.

The R^2 value is determined by

$$R^2 = \frac{SS_R}{SS_{yy}} = 1 - \frac{SS_E}{SS_{yy}} \tag{7}$$

where SS_E is the sum of squares of the residuals ($\sum e_i^2$) or errors, SS_R is the sum of squares due to regression, and SS_{yy} is the total sum of squares about the mean, where

$$SS_{yy} = SS_R + SS_E \tag{8}$$

R^2 measures the proportion of the variation in the response around the mean that can be attributed to terms in the model rather than to random error. R_a^2 is an R^2 value adjusted to account for the degrees of freedom in the model and is given by

$$R_a^2 = 1 - \frac{SS_E/(n - p)}{SS_{yy}/(n - 1)} = 1 - \left(\frac{n - 1}{n - p}\right)(1 - R^2). \tag{9}$$

Since R^2 will always increase as terms are added to the model, the overall assessment of the model may be better judged from R_a^2, since it will often decrease if unnecessary terms are added.

Similar to R_a^2, $\hat{s}$ is corrected for the degrees of freedom in the model. Even though a full response surface with a higher value of R^2 fits the variability in the data better, one or more reduced response surfaces may have higher values of R_a^2 and lower values of $\hat{s}$ making them better predictors. Support for this measure is based on the idea that there is a danger in retaining terms with low t-statistics since the extra degrees of freedom may be fitting noise.

4. OPTIMIZATION OF AIRFOIL SHAPE AND ASPECT RATIO: y_c, y_t, and AR

Shyy et al.[13] have conducted computer analysis which suggests that increased camber and reduced thickness are beneficial to low Reynolds number ($Re = 7.5 \times 10^4$ to 3.0×10^5) airfoil flows. Similar results were obtained experimentally by Jenkins et al.[28] at $Re = 2.0 \times 10^4$ to 1.0×10^5. Experiments conducted by Sunada et al.[29] at a much lower Reynolds number of $Re = 4.0 \times 10^3$ also indicate that airfoils at this Reynolds number should be relatively thin and well-cambered. Their best airfoil as measured by C_L/C_D had 5% camber, whereas their best airfoil as measured by $C_L^{3/2}/C_D$ had 10% camber. However, in these studies, no attempt has been made to optimize the wing and airfoil shapes based on a systematic approach. In this regard, the response surface method (RSM)[3] is used here to determine optimal values of camber and thickness for different aspect ratio wings.

The three design variables initially considered for optimization are the maximum camber, y_c, maximum thickness, y_t, and the wing aspect ratio, AR. The NACA surface distribution is used to create the airfoils based on maximum camber and maximum thickness, where the position of the maximum camber was chosen to be at 40% of the chord. The three design variables are constrained to the following ranges:

$$0.0 \leq y_c \leq 0.10c$$
$$0.05c \leq y_t \leq 0.15c$$
$$1 \leq AR \leq 5$$

The reason for the lower bound on y_t is that convergent *XFOIL* solutions are not obtainable for many airfoils with thicknesses less than 5%, due to numerical ill-conditioning in the potential flow calculation. The analyses are done for both $Re = 2.0 \times 10^5$ and $Re = 8.0 \times 10^4$. A full-quadratic response surface representing this design space consists of 10 terms and is evaluated by analyses of the 27 points of the full three-level factorial design. The response is chosen to be the maximum power index, $C_L^{3/2}/C_D$. The maximum power index for each of the 27 design points is determined by calculating the power index at successively narrower ranges and finer resolutions of angle-of-attack in the vicinity of the maximum. The design

variables are scaled to lie in the range −1 to 1 which improves the numerical conditioning of the problem. Tables 1 and 2 list the coefficients and their associated t-statistics along with values of R^2, R_a^2, and $\hat{s}$ for both the full and reduced response surfaces for $Re = 2.0 \times 10^5$ and $Re = 8.0 \times 10^4$ respectively. Both reduced models in Tables 1 and 2 provide improved values of R_a^2 and $\hat{s}$ over the full models and are chosen for optimization.

The equation describing the response as given by *JMP* is input to *Solver*[30]. *Solver* is an optimization toolbox included with Microsoft Excel which uses the Generalized Reduced Gradient method to find the maximum or minimum of a function with given constraints. Tables 3 and 4 list the maximum $C_L^{3/2}/C_D$ and the corresponding camber for aspect ratios of $AR = 1, 3$, and 5. All optimal airfoils had a thickness of 5%, the lowest allowable value set by the constraints. The predicted response value in Tables 3 and 4 is the response value given from the response surface approximation. The actual response value is the response value obtained by reanalyzing the optimal point given by the response surface approximation. The angle-of-attack listed in Tables 3 and 4 is the angle-of-attack at which the actual response value occurs. The best maximum $C_L^{3/2}/C_D$ values for each aspect ratio from the original data used to construct the response surfaces are also listed. The original data for all of the response surfaces in this paper can be found in Ref. [26].

From the original 27 data points used to fit the response surface at $Re = 2.0 \times 10^5$ the airfoil corresponding to $y_c = 0.05$ and $y_t = 0.05$ gives superior performance over the predicted optima for $AR = 1, 3$, and 5 in Table 3. The same airfoil also gives superior performance over the optima in Table 4 at $Re = 8.0 \times 10^4$. The fact that the response surfaces could not predict an optimal point at least as good as one of the original data reveals their poor prediction accuracy. Figures 1 and 2 show the response surface approximations plotted against actual values taken from Tables 3 and 4 and from the nine original design points in the plane at $y_t = 0.05$ of the full three-level factorial design used to construct the response surfaces. These figures show that the response surfaces are not capturing the actual peak in the data.

The actual errors for the optimal points listed in Table 3 for $Re = 2.0 \times 10^5$ are all smaller than the predicted rms error of 0.619 for that response surface, showing that the prediction accuracy of the response surface at these points is at least as good as expected. However, two of the optimal points listed in Table 4 (the points at $AR = 1$ and $AR = 5$) for $Re = 8.0 \times 10^4$ have actual errors larger than the predicted rms error of 0.655 for that response surface.

The estimated standard error of a predicted response at some location x is given by

$$s_{\hat{y}(x)} = \hat{s} \sqrt{x^{(m)'}(X'X)^{-1}x^{(m)}} \tag{10}$$

where $\hat{s}$ is the rms error, $x^{(m)}$ is a vector which is a function of the location where the (m) notation indicates that $x^{(m)}$ has been expanded to "model space" to reflect the form of the model as X does. For example, in the present case $x^{(m)}$ for the full model is given by

$$x^{(m)'} = [1, y_c, y_t, AR, y_c^2, y_c y_t, y_t^2, AR y_c, AR y_t, AR^2]. \tag{11}$$

The estimated standard errors for the two overly inaccurate points in Table 4 are both 0.327. The actual error is larger than both the predicted rms error and the local estimated standard error at these optimum. It follows that the actual error at these two disappointing optimal points could not have been anticipated based on rms error or local estimated standard error. It appears that the variation in the response over the chosen design space cannot be sufficiently modeled with a quadratic polynomial.

In order to obtain more reliable fits, the design space is reduced by first setting the thickness, y_t, equal to 5% and fitting six separate response surfaces in the single variable camber, y_c, for aspect ratios of $AR = 1, 3$, and 5 for each Reynolds number. The five design points of $y_c = 0.02, 0.03, 0.04, 0.05$, and 0.06 are chosen to fit each response surface. The six response surfaces along with their values of R^2, R_a^2, and $\hat{s}$ are shown in Table 5. In all cases, reduced models did not improve the prediction accuracy. The optimal points predicted by the six response surfaces are listed in Table 6.

The six response surfaces presented in Table 5 all have excellent values of R^2, R_a^2, and $\hat{s}$. All predicted optima in Table 6 are very accurate and all happen to be very close in response value to a design point in the original data. The results show that the optimal camber changes very little with changes in wing aspect ratio over this range. The predicted optimal camber appears to increase by about 0.5% of the chord when the Reynolds number decreases from $Re = 2.0 \times 10^5$ to $Re = 8.0 \times 10^4$. The best maximum $C_L^{3/2}/C_D$ from the raw data also occur at a higher camber on average at $Re = 8.0 \times 10^4$. Overall, it appears from the results in Table 6 that an airfoil with 4% camber and 5% thickness would provide superior performance over this range of flight conditions.

The modest optimal cambers obtained in Table 6 seem to contradict the conclusions of Ref. [13] which suggest that low Reynolds number airfoils should have relatively high camber. In order to determine why modest cambers are favored by the 3-D model, curves of $C_L^{3/2}/C_D$ as a function of angle-of-attack for four different wings at different aspect ratios and different cambers are shown in Figure 3. As can be seen at aspect ratios of both $AR = 1$ and $AR = 5$ the wings with 5% camber exhibit a higher maximum $C_L^{3/2}/C_D$ than the 8% camber wings even though both wings have comparable overall performance. The peaks in the $C_L^{3/2}/C_D$ vs. α curves are due to a sudden drop in the profile drag coefficient, C_d, at the corresponding angle-of-attack as can be seen in Figure 4. The sudden change in C_d looks suspicious and may be largely noise. At $AR = 5$, both the 5% and 8% camber airfoils provide nearly the same overall performance. At $AR = 1$, the $C_L^{3/2}/C_D$ vs. α curves are very flat and the difference in performance between the two airfoils is practically negligible. With such similar performance between the two airfoils, the data of Figure 3 is fit with quadratic polynomials to see if the smoothing effect of the least-squares fit changes the curves enough to result in a different optimum airfoil. The polynomials are plotted in Figure 5 and show that the 5% camber airfoil remains superior after filtering the noise, while the 8% camber airfoil exhibits more steady performance with regard to the change in the angle-of-attack.

Figure 6 shows plots of the lift coefficient, C_L, vs. α for the four wings. The 8% camber airfoil provides superior lift at both aspect ratios. With both the 5% and 8% camber airfoils providing similar power requirements, the 8% camber airfoil may be the better choice if the lift coefficient at minimum power is taken into consideration.

Figure 7 shows pressure distributions at 3 different spanwise locations for wings of $AR = 1$ and $AR = 5$ with a NACA 5405 airfoil and $\alpha = 5°$. The root section and mid-span section pressure distributions for each aspect ratio are nearly the same, showing that the flow is two-dimensional in that region. However, the magnitude of the section lift coefficients along the span as represented by the area between the upper and lower pressure curves is significantly reduced as the aspect ratio decreases. Thus, the spill-over effects at the wing-tips are felt along the entire span at low aspect ratios. Therefore, it can be expected that the 3-D optimal airfoil is different from the 2-D one.

5. SPANWISE DESIGN VARIATION: y_{cr}, y_{ct}, α_r, and α_t

In order to test how the optimal airfoil should vary with spanwise location, a procedure is developed which includes four design variables. The design variables are chosen to be the root camber and root angle-of-attack designated by y_{cr} and α_r, and the tip camber and tip angle-of-attack designated by y_{ct} and α_t. The wing thickness is set at 5%. The response is the power index, $C_L^{3/2}/C_D$, and the analyses are done at $Re = 8.0 \times 10^4$ and $AR = 1$. The ranges of the design variables are chosen to encompass the predicted optimal point for $AR = 1$ in Table 4. Such ranges are as follows:

$$0.05c \leq y_{cr} \leq 0.10c \qquad 0.05c \leq y_{ct} \leq 0.10c$$
$$2.5° \leq \alpha_r \leq 7.5° \qquad 2.5° \leq \alpha_t \leq 7.5°$$

This range was selected before the design space refinement resulting in the optimal points of Table 6. However, this range includes the best point from the raw data at $Re = 8.0 \times 10^4$ and $AR = 1$. The points selected to fit the response surface are the 25 points of a 4-dimensional central-composite design. The equation of the best reduced response surface along with its values of R^2, R_a^2, and $\hat{s}$ and its predicted optimum are shown in Table 7.

The predicted optimal camber and angle-of-attack values decreased from root to tip. However, the actual optimal $C_L^{3/2}/C_D$ is lower than six of the response values used in the response surface construction. The actual error at the optimal point listed in Table 7 could not have been anticipated since it is substantially larger than both the predicted rms error of 0.127 and the local standard error at the optimum of 0.083. Again it appears that a quadratic polynomial cannot sufficiently model the variation in the response for the range of design variables considered.

After reviewing the data used to fit the response surface and identifying design points with relatively high values of the response, the design space is reduced considerably by narrowing the ranges of the design variables to the following:

$$0.05c \leq y_{cr} \leq 0.10c \qquad 0.05c \leq y_{ct} \leq 0.075c$$
$$5° \leq \alpha_r \leq 7.5° \qquad 2.5° \leq \alpha_t \leq 5°$$

Additionally, the number of design points used to construct the response surface is increased to 30. The 30 points are chosen by first generating the 81 points of the full three-level factorial design and using the D-optimality criterion[3] for selecting 30 of these 81 points. The best reduced response surface and its predicted optimum are shown in Table 8.

The optimal point selected in Table 8 corresponds to the best design point from the 30 design points used to fit the

response surface. Reducing the design space resulted in improved prediction accuracy. The rms-error of the response surface in Table 8 is relatively low showing that the quadratic form fits the data rather well over this reduced size design space. In an attempt to further improve the optimal design, the next step retains the size of the design space but shifts it so that the best point in Table 8 is now the center of the design space, resulting in the following ranges for the design variables:

$$0.025c \leq y_{cr} \leq 0.075c \qquad 0.0375c \leq y_{ct} \leq 0.0625c$$
$$3.75° \leq \alpha_r \leq 6.25° \qquad 3.75° \leq \alpha_t \leq 6.25°$$

Five of the design points used to fit the response surface in Table 8 lie in the full three-level factorial design of the current design space and are used in the fit. An additional 25 points are selected from the remaining points in the full three-level factorial design based on the D-optimality criterion. The best reduced response surface and its predicted optimum are shown in Table 9.

The optimal point obtained in Table 9 has a lower actual response value than the best point in the raw data which was selected as the optimum in Table 8. Centering the design space about the optimal point did not improve the prediction accuracy around that point sufficiently enough to identify a better optimum. Adding the flexibility of a variable cross section has not resulted in an improved optimal design for reasons that are unclear. The results identify an optimal wing geometry as having a constant cross section of 5% camber which corresponds to the results in Table 6 for $AR = 1$ and $Re = 8 \times 10^4$.

6. OPTIMIZATION OF FIXED-SPAN WING IN STEADY FLIGHT: y_c and AR

It is apparent that maximum performance will always occur at the highest aspect ratio, which for a given chord Reynolds number means maximizing the span. However, in practice, size restrictions place limits on the span. In this section, the aspect ratio remains a variable, but the span is fixed at 10 inches (25.4 cm). This procedure makes the chord, and therefore the chord Reynolds number, an implicit design variable.

The optimization problem is formulated in the two design variables camber and aspect ratio with the thickness set at 5%. The initial ranges of the design variables are the following:

$$0.0 \leq y_c \leq 0.10c$$
$$0.5 \leq AR \leq 1.5$$

Since the wing area, S, varies with aspect ratio, an appropriate response for minimizing the power requirement is the maximum $C_L^{3/2} \cdot S^{1/2}/C_D$ from Eqn. (1). The aircraft weight, W, is set at 16 oz, and the available thrust power, P_a, is set at 28 watts. The aircraft is modeled in steady flight flying at the minimum power velocity, V_{min}. Steady flight is defined by the following relations:

$$L = W \qquad (12)$$

$$T = D \qquad (13)$$

Equation (12) can be rearranged to obtain the required flight velocity as,

$$V_{min} = \sqrt{\frac{2W}{\rho S C_L}} \qquad (14)$$

For each design point, values for ρ, W, and S are given and C_L (from *PMARC*) is determined independently of the Reynolds number and is therefore only a function of the geometry and the angle-of-attack. Substituting the lift coefficient at minimum power, $C_{L_{minp}}$, into Eqn. (14) gives the minimum power velocity, V_{minp}.

Equation (13) can be rearranged to obtain an expression for the maximum sustainable velocity as,

$$V_{max} = \sqrt[3]{\frac{2P_a}{\rho S C_{D_{minp}}}} \qquad (15)$$

Since the velocity from Equation (14) now determines the Reynolds number, an *XFOIL* solution for the given airfoil at this Reynolds number will complete the calculation for the flight C_D (C_{d_i} is already given from the *PMARC* solution). The design is feasible as long as the minimum power velocity is less than or equal to the maximum sustainable velocity.

In order to determine the maximum $C_L^{3/2} \cdot S^{1/2}/C_D$ for a given wing subject to the constraints of steady flight, an iteration procedure is set up by first guessing a Reynolds number and calculating an initial maximum $C_L^{3/2}/C_D$. The lift coefficient at the initial maximum $C_L^{3/2}/C_D$ will determine the initial V_{minp}. With an initial V_{minp} in hand, a new Reynolds number and a new maximum $C_L^{3/2}/C_D$ can be determined. This procedure converges when the current maximum $C_L^{3/2}/C_D$ occurs at a $C_{L_{minp}}$ and V_{minp} creating the same Reynolds number at which the maximum $C_L^{3/2}/C_D$ is being determined. Typically, the procedure requires between 3 and 7 iterations.

The first response surface is fit using the 9 points of a two-dimensional central composite design shown as Set A design points in Figure 8. According to the flow model calculations, all aircraft in the range of design variables considered are able to fly in steady flight. The full response surface fit to Set A design points is presented as the Set A response surface in Table 10. Reduced models did not improve the prediction accuracy.

Evaluation of the Set A response surface gives an optimal response value of 1.257 m at $y_c = 0.0639$ and $AR = 1.5$. The actual response value for this design is 1.213 m. The discrepancy between the predicted an actual response value along with the observation that aspect ratio was maximized suggests that refinement of the design space may improve the prediction accuracy and the final design. Five successively refined sets of response surface design points are shown in Figure 8. The design points are marked with filled circles and the optimal points predicted by the response surfaces fit to each set of design points are marked with an X. Response surface data for Sets B through E are shown in Table 10. In all cases, reduced response surfaces do not improve the prediction accuracy and are not shown. However, Sets D and E which include only the design variable y_c, found a much better fit with a cubic polynomial rather than a quadratic polynomial. Predicted and actual optimal response values for Sets A through E are shown in Table 11.

Each step of the design space refinement consistently improved the actual optimal design performance. The final optimal design of $AR = 1.5$ and $y_c = 0.0295$ has a chord Reynolds number of $Re = 3.09 \times 10^5$ when flying at its minimum power

velocity of $V_{minp} = 27.2$ m/s. The improvements in $C_L^{3/2}/C_D$ for the higher aspect ratio wings outweighed the negative effects from their smaller area, S. The smaller area wings compensate to meet the steady flight constraints by flying at a slightly higher velocity.

Table 12 shows the rms error and local standard error along with the actual error for the optimal designs for each design point set. It again appears that neither the rms error nor the estimated local standard error provide a reliable way to predict the actual error at the optimum. Also, after reviewing the data used to fit the response surface, it is apparent that the two steps in the design space refinement represented by Sets B and C would not have been necessary if the raw data had been considered when choosing a refined region. The predicted optimum from the Set A response surface is lower than the actual response value in Set A corresponding to $y_c = 0.05$ and $AR = 1.5$. This design point was not predicted as an optimum from a response surface approximation until Set C. A refinement procedure which only follows the predicted optimum, instead of also considering the original data, can result in additional refinement steps.

A single response surface was fit to all of the design points contained in Sets A-E and the best reduced model and its predicted optimum is presented in Table 13. The single response surface fit to all of the design points in Sets A-E had lower values of R^2 and R_a^2 and a higher rms error than any of the response surfaces presented in Table 10. The single response surface fit to all of the design points in Sets A-E spanning the entire initial design space does not provide sufficient predictive accuracy.

7. CONCLUSION

The response surface method has been used to investigate and identify optimal wing geometries providing minimum power consumption for low Reynolds number flight vehicles. In all cases, optimization provided only a modest improvement in the flight power requirement. However, some insight was gained into particular trends concerning low-Reynolds-number, low-aspect-ratio wing design. As anticipated, the wing thickness should be minimized. The results of Table 6 suggest that optimal airfoils change very little with changes in wing aspect ratio. Investigations into how the optimal airfoil changes with spanwise location revealed that the best wing had a constant cross-section with 5% camber oriented at 5° angle-of-attack. The optimal airfoil is not strongly coupled to the wing planform since it does not change much with changes in aspect ratio or with location on the wing. The analyses of Sections 3 and 4 suggest that optimal cambers lie at about 4% or 5%. The fixed-span, steady flight calculations in Section 5 resulted in optimal cambers being significantly lower at about 3%, albeit at a higher Reynolds number. There appears to be a trend of increasing optimal camber with decreasing Reynolds number. Furthermore, a higher camber may be a better choice if higher lift coefficient at minimum power is used as a design goal, instead of simply minimizing the overall power index.

Obtaining accurate response surface approximations requires using an appropriate number of design points for the model being fitted. For some of the response surface approximations created in this work, such as in the first spanwise cross-section variation problem, using too few points may have contributed to the poor prediction accuracy. Also, the original

data as well as the predicted optimum should be considered when conducting a zooming procedure for design space refinement.

8. REFERENCES

1) Liu, H.-T. (1992). Unsteady aerodynamics of a Wortmann wing at low Reynolds numbers. *Journal of Aircraft, 29*, 532-539.

2) Handley, C. (1998, July-August). Tiny planes, big tasks. *Compressed Air*, pp. 14-20.

3) Myers, R. H., & Montgomery, D. C. (1995). *Response surface methodology - process and product optimization using designed experiments.* New York: John Wiley & Sons, Inc.

4) Giunta, A. A., Dudley, J. M., Narducci, R., Grossman, B., Haftka, R. T., Mason, W. H., & Watson, L. T. (1994). Noisy aerodynamic response and smooth approximations in HSCT design. AIAA Paper No. 94-4376.

5) Unal, R., Lepsch, R. A., & McMillin, M. L. (1998). Response surface model building and multidisciplinary optimization using D-optimal designs. AIAA Paper No. 98-4759.

6) Narducci, R., Valorani, M., Dadone, A., Grossman, B., & Haftka, R. T. (1995). Optimization methods for non-smooth or noisy objective functions in fluid design problems. AIAA Paper No. 95-1648.

7) Sobieski, I. P., Manning, V. M., & Kroo, I. M. (1998). Response surface estimation and refinement in collaborative optimization. AIAA Paper No. 98-4753.

8) Madsen, J. I., Shyy, W., Haftka, R. T., & Liu, J. (1997). Response surface techniques for diffuser shape optimization. AIAA Paper No. 97-1801.

9) Knill, D. L., Giunta, A. A., Baker, C. A., Grossman, B., Mason, W. H., Haftka, R. T., & Watson, L. T. (1998). HSCT configuration design using response surface approximations of supersonic euler aerodynamics. AIAA Paper No. 98-0905.

10) Baker, C. A., Grossman, B., Haftka, R. T., Mason, W. H., & Watson, L. T. (1998). HSCT configuration design space exploration using aerodynamic response surface approximations. AIAA Paper No. 98-4803.

11) Mueller, T. J. (Ed.) (1989). *Low Reynolds number aerodynamics.* New York: Springer-Verlag.

12) Drela, M., & Giles, M. B. (1987). Viscous-inviscid analysis of transonic and low Reynolds number airfoils. *AIAA Journal, 25*(10), 1347-1355.

13) Shyy, W., Klevebring, F., Nilsson, M., Sloan, J., Carroll, B., & Fuentes, C. (1999). A Study of Rigid and Flexible Low Reynolds Number Airfoils. *Journal of Aircraft, 36*(3), 523-529.

14) Ashby, D. L., Dudley, M. R., Iguchi, S. K., Browne, L., & Katz, J. (1992). *Potential flow theory and operation guide for the panel code PMARC_12.* Computer Software Management and Information Center (COSMIC), University of Georgia.

15) Drela, M. (1989). XFOIL: An analysis and design system for low Reynolds number airfoils. In T. J. Mueller (1989) *Low Reynolds number aerodynamics.* New York: Springer-Verlag, pp. 1-12.

16) Anderson, J. D., Jr. (1989). *Introduction to flight.* (3rd ed.). New York: McGraw-Hill.

17) Donovan, J. F., & Selig, M. S. (1989). Low Reynolds number airfoil design and wind tunnel testing at Princeton University. In T. J. Mueller (1989) *Low Reynolds number aerodynamics.* New York: Springer-Verlag, pp. 39-57.

18) Foch, R. J., & Ailinger, K. G. (1992). Low Reynolds number, long endurance aircraft design. AIAA Paper No. 92-1263.

19) Smith, A. M. O., & Gamberoni, N. (1956). Transition, pressure gradient, and stability theory. Douglas Aircraft Co., Rept. ES 26388.

20) Ingen, J. L. van (1956). A suggested semi-empirical method for the calculation of the boundary layer transition region. Delft University of Technology, Dept. of Aerospace Engineering, Rept. VTH-74.

21) Cebeci, T., & Bradshaw, P. (1977). *Momentum transfer in boundary layers.* Washington: Hemisphere Publishing Corporation.

22) Squire, H. B., & Young, A. D. (1937). The calculation of the profile drag of aerofoils. *Reports and Memoranda Aeronautical Research Council, London*, No. 1838 (1938 Vol.).

23) Rosenhead, L. (Ed.) (1963). *Laminar boundary layers.* New York: Dover Publications, Inc.

24) Katz, J., & Plotkin, A. (1991). *Low-speed aerodynamics: from wing theory to panel methods.* New York: McGraw-Hill, Inc.

25) Selig, M. S., & Guglielmo, J. J. (1997). High-lift low Reynolds number airfoil design. *Journal of Aircraft, 34*(1), 72-78.

26) Sloan, J. G. (1998). Airfoil and Wing Planform Optimization for Low Reynolds Number Flight Vehicles. Master Thesis, Department of Aerospace Engineering, Mechanics & Engineering Science, University of Florida.

27) SAS Institute Inc. (1995). JMP version 3. Cary, N.C.

28) Jenkins, D. A., Shyy, W., Sloan, J., Klevebring, F., & Nilsson, M. (1998). Airfoil performance at low Reynolds numbers for micro air vehicle applications. RPVs Thirteenth International Conference, Bristol, United Kingdom.

29) Sunada, S., Sakaguchi, A., & Kawachi, K. (1997). Airfoil section characteristics at a low Reynolds number. *Journal of Fluids Engineering, 119*(1), 129-135.

30) Microsoft Corporation. (1985-1996). Microsoft Excel 97.

Table 1. Coefficients and corresponding t-statistics along with overall fit information for both the full and reduced response surfaces for maximum $C_L^{3/2}/C_D$ as a function of y_c, y_t, and AR at Re = 2.0 ×10⁵.

term	coefficient (full)	t-stat (full)	coefficient (red.)	t-stat (red.)
intercept	9.332	28.45	9.211	34.59
y_c	0.8296	5.46	0.8296	5.69
y_t	0.1011	0.67	0.1011	0.69
AR	4.256	28.02	4.256	29.17
y_c*y_c	-1.578	-6.00	-1.578	-6.24
y_t*y_c	-0.6998	-3.76	-0.6998	-3.92
y_t*y_t	-0.1812	-0.69	–	–
$AR*y_c$	0.3905	2.10	0.3905	2.19
$AR*y_t$	0.0433	0.23	–	–
$AR*AR$	-0.5390	-2.05	-0.5390	-2.13
R^2	0.981		0.980	
R_a^2	0.971		0.973	
$\hat{s}$	0.644 (8.25% of mean)		0.619 (7.94% of mean)	

Table 2. Coefficients and corresponding t-statistics along with overall fit information for both the full and reduced response surfaces for maximum $C_L^{3/2}/C_D$ as a function of y_c, y_t, and AR at Re = 8.0 ×10⁴.

term	coefficient (full)	t-stat (full)	coefficient (red.)	t-stat (red.)
intercept	7.778	23.00	7.778	23.33
y_c	0.3733	2.38	0.3733	2.42
y_t	-0.3678	-2.35	-0.3678	-2.38
AR	3.372	21.54	3.372	21.85
y_c*y_c	-1.600	-5.90	-1.600	-5.99
y_t*y_c	-0.9553	-4.98	-0.9553	-5.05
y_t*y_t	-0.3389	-1.25	-0.3389	-1.27
$AR*y_c$	0.1314	0.69	–	–
$AR*y_t$	-0.1916	-1.00	–	–
$AR*AR$	-0.4880	-1.80	-0.4880	-1.83
R^2	0.970		0.967	
R_a^2	0.953		0.955	
$\hat{s}$	0.664 (10.78% of mean)		0.655 (10.63% of mean)	

Table 3. Predicted and actual maximum $C_L^{3/2}/C_D$ with corresponding y_c for a given AR at Re = 2.0 ×10⁵.

AR	y_c	$C_L^{3/2}/C_D$ predicted	$C_L^{3/2}/C_D$ actual	α (deg.)	Best $C_L^{3/2}/C_D$ from raw data
1.0	0.0680	4.52	4.04	1.7	4.12
3.0	0.0742	9.48	9.40	1.3	9.69
5.0	0.0804	13.41	13.63	1.3	14.09

Table 4. Predicted and actual maximum $C_L^{3/2}/C_D$ with corresponding y_c for a given AR at Re = 8.0 $\times 10^4$.

AR	y_c	$C_L^{3/2}/C_D$ predicted	$C_L^{3/2}/C_D$ actual	α (deg.)	Best $C_L^{3/2}/C_D$ from raw data
1.0	0.0708	4.22	3.43	5.7	3.56
3.0	0.0708	8.08	8.05	5.7	8.40
5.0	0.0708	10.97	11.78	5.7	12.20

Table 5. Six refined response surfaces for maximum $C_L^{3/2}/C_D$ as a function of y_c for Re = 2.0 $\times 10^5$ and Re = 8.0 $\times 10^4$ at AR = 1, 3, and 5.

$Re=2\times 10^5$	
AR = 1	$C_L^{3/2}/C_D = 4.159 - 0.0087y_c - 0.2064y_c^2 + 0.1345y_c^3$ $\quad R^2 = 0.999, R_a^2 = 0.998, \hat{s} = 0.006$ (0.15% of mean)
AR = 3	$C_L^{3/2}/C_D = 9.790 - 0.1507y_c - 0.3234y_c^2 + 0.2713y_c^3$ $\quad R^2 = 0.986, R_a^2 = 0.945, \hat{s} = 0.042$ (0.44% of mean)
AR = 5	$C_L^{3/2}/C_D = 14.21 - 0.0862y_c - 0.5541y_c^2 + 0.3984y_c^3$ $\quad R^2 = 0.998, R_a^2 = 0.993, \hat{s} = 0.029$ (0.21% of mean)
$Re=8\times 10^4$	
AR = 1	$C_L^{3/2}/C_D = 3.550 - 0.1029y_c - 0.2177y_c^2 + 0.0807y_c^3$ $\quad R^2 = 1.0, R_a^2 = 1.0, \hat{s} = 0.001$ (0.03% of mean)
AR = 3	$C_L^{3/2}/C_D = 8.454 + 0.0432y_c - 0.4117y_c^2 + 0.1803y_c^3$ $\quad R^2 = 1.0, R_a^2 = 0.999, \hat{s} = 0.010$ (0.12% of mean)
AR = 5	$C_L^{3/2}/C_D = 12.22 + 0.2183y_c - 0.6310y_c^2 + 0.2483y_c^3$ $\quad R^2 = 1.0, R_a^2 = 1.0, \hat{s} = 0.003$ (0.03% of mean)

Table 6. Optimal points selected by the six response surfaces in Table 5.

Re	AR	Optimal y_c	$C_L^{3/2}/C_D$ predicted	$C_L^{3/2}/C_D$ actual	Best $C_L^{3/2}/C_D$ from raw data
2.0×10^5	1	0.0396	4.16	4.15	4.15 @ y_c=0.04
2.0×10^5	3	0.0362	9.80	9.80	9.77 @ y_c=0.03
2.0×10^5	5	0.0386	14.22	14.20	14.19 @ y_c=0.04
8.0×10^4	1	0.0456	3.56	3.56	3.56 @ y_c=0.05
8.0×10^4	3	0.0411	8.46	8.45	8.45 @ y_c=0.04
8.0×10^4	5	0.0439	12.24	12.24	12.22 @ y_c=0.04

Table 7. Best reduced response surface for $C_L^{3/2}/C_D$ and predicted optimum for the first spanwise cross-section variation problem.

Response surface
$C_L^{3/2}/C_D = 3.104 + 0.0839y_{cr} - 0.0199\alpha_r + 0.0340y_{ct} - 0.1048\alpha_t + 0.0779\alpha_r y_{cr}$ $- 0.1245\alpha_r^2 - 0.0362y_{ct}y_{cr} + 0.0922\alpha_t y_{ct} - 0.1192\alpha_t^2$

Statistical measures
$R^2 = 0.777, R_a^2 = 0.642, \hat{s} = 0.127$ (4.34% of mean)

Predicted optimum						
y_{cr}	α_r (deg)	y_{ct}	α_t (deg)	$C_L^{3/2}/C_D$ predicted	$C_L^{3/2}/C_D$ actual	Best $C_L^{3/2}/C_D$ from raw data
0.10	5.58	0.05	2.94	3.28	3.07	3.56

Table 8. Best reduced response surface for $C_L^{3/2}/C_D$ and predicted optimum for the second spanwise cross-section variation problem.

Response surface
$C_L^{3/2}/C_D = 3.207 + 0.0250y_{cr} - 0.1029a_r - 0.0559y_{ct} + 0.0173a_t - 0.0765y_{cr}\,y_{cr}$ $+ 0.1906a_r y_{cr} + 0.0212y_{ct}a_r - 0.0275y_{ct}y_{ct} - 0.0147a_t y_{cr} - 0.0408a_t y_{ct} - 0.0332a_t a_t$

Statistical measures
$R^2 = 0.950, R_a^2 = 0.920, \hat{s} = 0.059$ (1.90% of mean)

Predicted optimum						
y_{cr}	a_r (deg)	y_{ct}	a_t (deg)	$C_L^{3/2}/C_D$ predicted	$C_L^{3/2}/C_D$ actual	Best $C_L^{3/2}/C_D$ from raw data
0.05	5.0	0.05	5.0	3.49	3.56	3.56

Table 9. Best reduced response surface for $C_L^{3/2}/C_D$ and predicted optimum for the third spanwise cross-section variation problem.

Response surface
$C_L^{3/2}/C_D = 3.328 + 0.1654y_{cr} - 0.0688a_r + 0.0648y_{ct} - 0.0758a_t - 0.1104y_{cr}\,y_{cr}$ $+ 0.1431a_r y_{cr} - 0.0882a_r a_r - 0.0531y_{ct}y_{ct} + 0.0604a_t y_{ct} - 0.1380a_t a_t$

Statistical measures
$R^2 = 0.933, R_a^2 = 0.897, \hat{s} = 0.087$ (2.88% of mean)

Predicted optimum						
y_{cr}	a_r (deg)	y_{ct}	a_t (deg)	$C_L^{3/2}/C_D$ predicted	$C_L^{3/2}/C_D$ actual	Best $C_L^{3/2}/C_D$ from raw data
0.075	5.53	0.0565	4.8	3.42	3.35	3.56

Table 10. Five response surfaces for maximum $C_L^{3/2} \cdot S^{1/2}/C_D$ constructed from five successively refined sets (A-E) of design points for the fixed-span aircraft subject to the constraints of steady flight.

Set A	$C_L^{3/2}S^{1/2}/C_D = 1.154 + 0.1930y_c + 0.1115AR - 0.3642y_c^2 + 0.0097ARy_c - 0.0368AR^2$ $R^2 = 0.999, R_a^2 = 0.997, \hat{s} = 0.015$ (1.69% of mean)
Set B	$C_L^{3/2}S^{1/2}/C_D = 1.206 + 0.1960y_c + 0.0374AR - 0.3750y_c^2 + 0.0072ARy_c - 0.0073AR^2$ $R^2 = 0.999, R_a^2 = 0.999, \hat{s} = 0.006$ (0.63% of mean)
Set C	$C_L^{3/2}S^{1/2}/C_D = 1.139 - 0.0895y_c + 0.0433AR - 0.0236y_c^2 - 0.0004ARy_c - 0.0055AR^2$ $R^2 = 1.0, R_a^2 = 0.999, \hat{s} = 0.002$ (0.18% of mean)
Set D	$C_L^{3/2}S^{1/2}/C_D = 1.291 - 0.1739y_c - 0.4249y_c^2 + 0.3782y_c^3$ $R^2 = 0.981, R_a^2 = 0.923, \hat{s} = 0.069$ (6.40% of mean)
Set E	$C_L^{3/2}S^{1/2}/C_D = 1.263 + 0.0936y_c - 0.3127y_c^2 + 0.2002y_c^3$ $R^2 = 0.999, R_a^2 = 0.998, \hat{s} = 0.011$ (0.98% of mean)

Table 11. Predicted and actual maximum $C_L^{3/2} \cdot S^{1/2}/C_D$ with corresponding y_c obtained from the successively refined response surfaces presented in Table 10. AR = 1.5 for all designs.

Design Point Set	y_c	$C_L^{3/2} \cdot S^{1/2}/C_D$ predicted (meter)	$C_L^{3/2} \cdot S^{1/2}/C_D$ actual (meter)
A	0.0639	1.257	1.213
B	0.0635	1.263	1.215
C	0.0500	1.243	1.242
D	0.0416	1.307	1.256
E	0.0295	1.271	1.266

Table 12. Predicted and actual error comparisons for the predicted optimal points of Table 11.

Design Point Set	rms-error	standard error at optimum	actual error at optimum
A	0.015	0.011	0.044
B	0.006	0.004	0.048
C	0.002	0.002	0.001
D	0.069	0.051	0.051
E	0.011	0.007	0.005

Table 13. Best reduced response surface for maximum $C_L^{3/2} \cdot S^{1/2}/C_D$ fit to all of the design points in Sets A-E.

Response surface			
$C_L^{3/2}S^{1/2}/C_D = 1.153 + 0.1586y_c + 0.1504AR - 0.3786y_c^2 - 0.0465ARy_c$			
Statistical measures			
$R^2 = 0.919, R_a^2 = 0.897, \hat{s} = 0.080$ (7.87% of mean)			
Predicted optimum			
y_c	AR	$C_L^{3/2}S^{1/2}/C_D$ predicted	$C_L^{3/2}S^{1/2}/C_D$ actual
0.0574	1.5	1.311	1.226
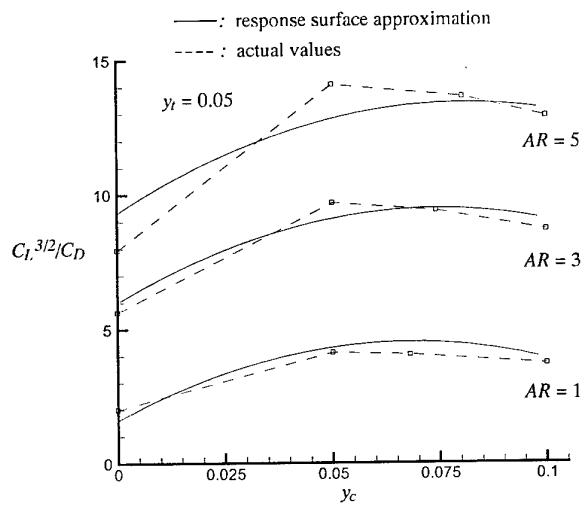
Figure 1. Actual and response surface approximation of $C_L^{3/2}/C_D$ vs. y_c for AR = 1, 3, & 5 at y_t = 0.05 and Re = 2.0 ×10⁵.
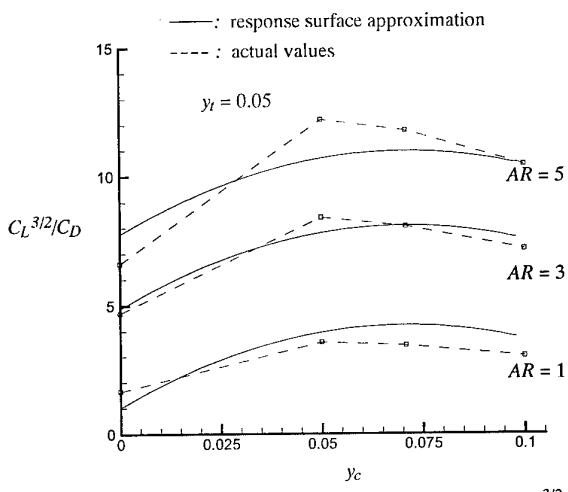
Figure 2. Actual and response surface approximation of $C_L^{3/2}/C_D$ vs. y_c for AR = 1, 3, & 5 at y_t = 0.05 and Re = 8.0 ×10⁴.
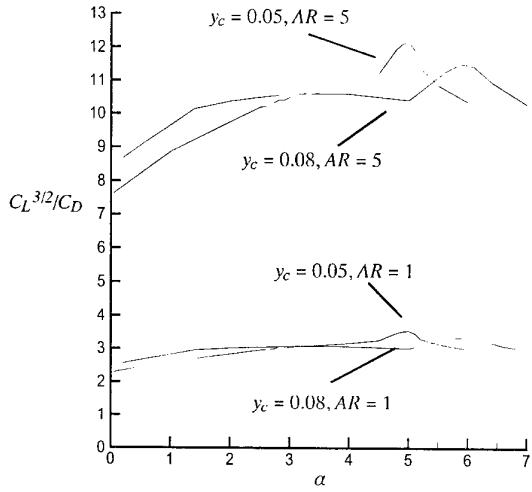
Figure 3. $C_L^{3/2}/C_D$ vs. α for four different wings representing aspect ratios of $AR = 1$ & 5 and cambers of $y_c = 0.05$ & 0.08.
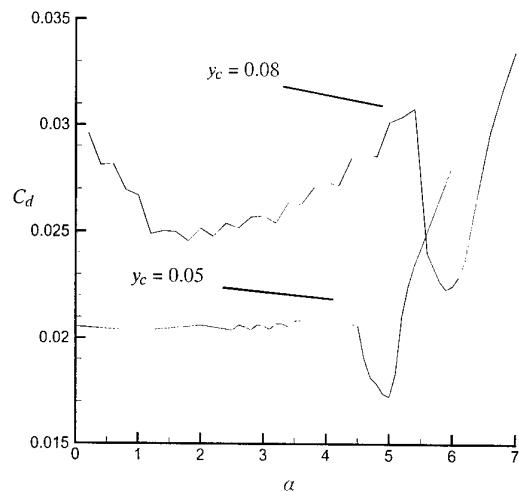
Figure 4. Profile drag coefficient, C_d, vs. α for both NACA 8405 and NACA 5405 airfoils.
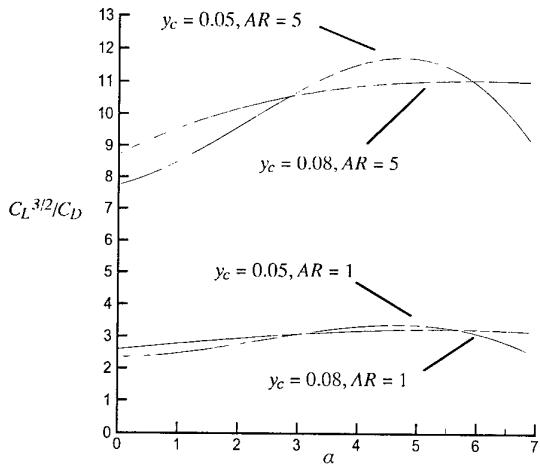
Figure 5. Quadratic polynomial approximations of the $C_L^{3/2}/C_D$ vs. α data in Figure 3 for the four different wings representing aspect ratios of $AR = 1$ & 5 and cambers of $y_c = 0.05$ & 0.08.
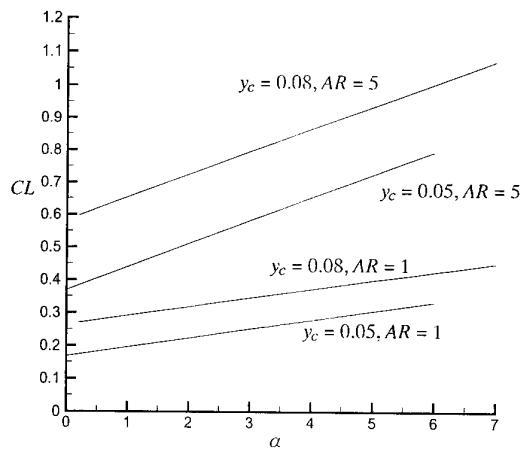
Figure 6. C_L vs. α for the four wings representing aspect ratios of $AR = 1$ & 5 and cambers of $y_c = 0.05$ & 0.08.
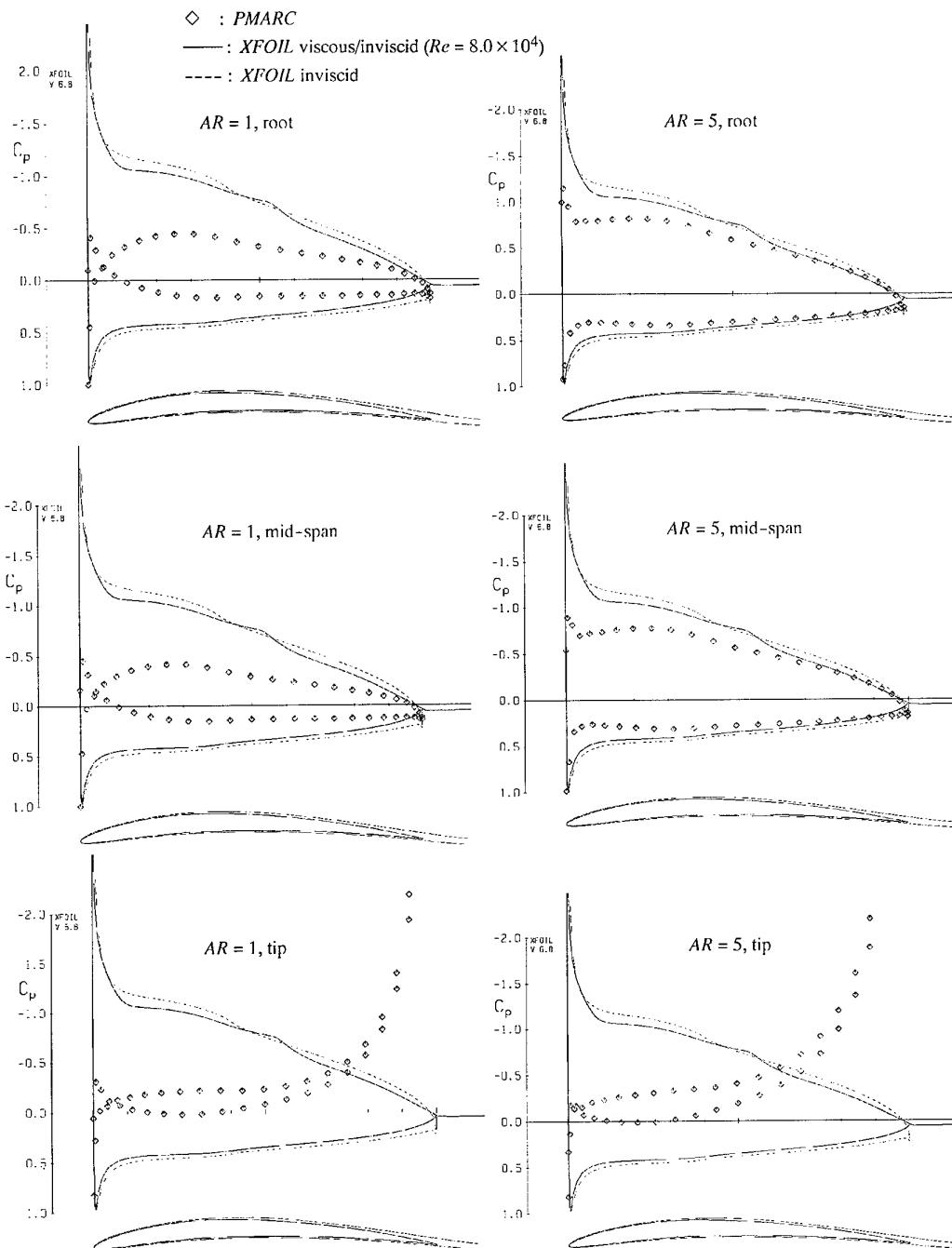
Figure 7. C_p distributions at the root, mid-span, and tip sections for a NACA 5405 airfoil at $\alpha = 5°$ for AR = 1 and AR = 5.
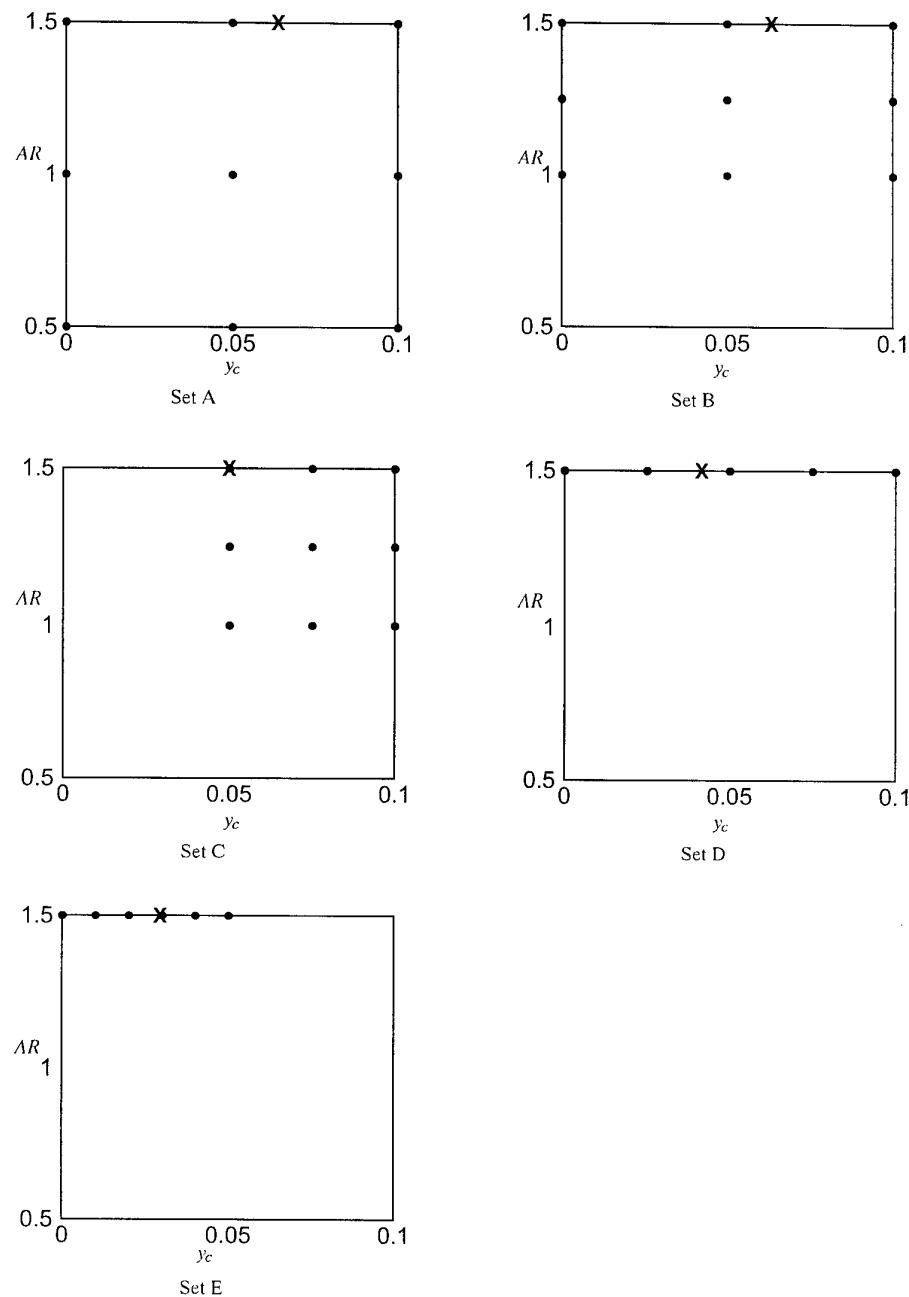
Figure 8. *Five successively refined sets (A-E) of response surface design points. Circles mark the design points, and X marks the optimal point on the response surface selected by Solver.*

DESIGN TOOLS FOR PERFORMANCE ASSESSMENT OF FIGHTER AIRCRAFT INCORPORATING NEW TECHNOLOGIES

Anthony Kutschera[*], Peter M. Render[†]
Department of Aeronautical and Automotive Engineering
and Transport Studies
Loughborough University
Loughborough, Leicestershire LE11 3TU
United Kingdom

Abstract

The performance assessment of modern fighter aircraft has been the subject of considerable research in recent years. A new metric called Nodal Manoeuvre Analysis has been proposed, which allows performance assessment of new technologies to be carried out during the conceptual/preliminary design stages of an aircraft. This paper seeks to demonstrate the uses of the Nodal Manoeuvre Analysis metric by considering three case studies. These studies assess the changes in performance of a baseline aircraft in a vertical turn manoeuvre, when new technology is incorporated. The technologies are 1) an increase in thrust, 2) a reduction in weight, and 3) the incorporation of Thrust Vectoring and Post Stall Manoeuvrability. Through these studies, it is shown that Nodal Manoeuvre Analysis can quantify the advantages/disadvantages of incorporating new technology into the design.

Nomenclature

AoA	Angle of Attack
AFFTC	Air Force Flight Test Center
BVR	Beyond Visual Range
CCT	Combat Cycle Time
C_L	Lift Coefficient
D	Drag
DoF	Degree of Freedom
ITR	Instantaneous Turn Rate
L	Lift
NMA	Nodal Manoeuvre Analysis
n_z	Normal Load Factor
P_s	Specific Excess Power
PSM	Post Stall Manoeuvrability
S	Wing Reference Area
SEP	Specific Excess Power
stsl	Static Thrust at Sea Level
t	Time
T	Thrust
TVC	Thrust Vector Control
V	Velocity
W	Weight
WVR	Within Visual Range
α	Angle of Attack

Introduction

There is a distinct need for the implications of new technologies such as Thrust Vector Control (TVC) and Post Stall Manoeuvrability (PSM) to be known early on in the design stage. Experimental projects such as the X-31a, F-18 HARV (High Alpha Research Vehicle) and the F-16 MATV (Multi Axis Thrust Vectoring) have proven the technology. In fact the X-31a project incorporated simulated combat between the X-31a and an F/A-18. According to Smith[1], this showed that with the TVC/PSM, the X-31a gained an overwhelming combat advantage in a one-on-one scenario. With thrust vector control and post stall manoeuvrability now becoming an operational capability with aircraft such as the F-22 and Su-27/30/35 etc., there is a requirement to be able to assess future concepts so that they can be designed to surpass the performance of likely threats. The connotations of TVC and PSM need to be assessed at the early stages of design, for example when comparing conceptual designs. Because of this, the amount of data known about the aircraft will be limited. Also, TVC and PSM are specific examples of new technologies. In general, any new technologies need to be assessed, and it is possible that existing methods do not allow this.

Over the last decade, there has been much discussion about the types of metric that can be used for the assessment of aircraft performance. Bitten[2] discusses the differences between performance, manoeuvrability and agility metrics. Performance relates to the state variables of the aircraft, for example velocity. Manoeuvrability relates to the time differential of the aircraft state (for this example, acceleration). Agility relates to the time differential of manoeuvrability (for this example, rate of change of acceleration). It is the authors' basic view that control power dominates the agility and controllability of a fighter, whereas simple terms like speed, load factor limit and thrust to weight ratio (T/W) dominate the performance. As aircraft develop to become more agile and manoeuvre closer to physical limits, it is agility (and with it transient response) that becomes more important. Different agility metrics have been proposed to help quantify the capability of aircraft designs, including those suggested by Eidetics International[3] and MBB[4]. Three components of agility are defined in both metrics. These are axial, pitch and torsional agility, which relate to time rate of change of axial load factor, time rate of change of normal load factor, and stability axis roll acceleration, respectively.

Currently there is more interest in agility metrics than in performance metrics. Agility metrics are very useful in describing the ability of the aircraft to move quickly and change state. Comparing two aircraft will easily show that

[*] Research Assistant, GradRAeS, Member AIAA
[†] Senior Lecturer, MRAeS, Member AIAA

one is more *agile* than another. However, there are two problems with agility metrics. One is that these metrics do not give a physical feel of the overall combat situation to the designer, tactician or pilot. Knowing that an aircraft can pull a given load factor faster than the adversary, does not necessarily mean an advantage is conferred. For a simplistic example, a large bomber could be designed with such large control power that its pitch acceleration would be greater than a fighter, and hence its pitch agility would be greater. However, its much lower T/W ratio would mean that it loses energy more quickly than the fighter. This would give away the advantage gained by the bomber in the first seconds of manoeuvring, and eventually lead to a shoot solution for the fighter. According to Bitten[2], the Air Force Flight Test Center (AFFTC) emphasise that it is tactically relevant to obtain a desired final state for the aircraft. Factors like the time to pitch to maximum load factor do not tell the designer about the final state of the aircraft. Also, agility metrics do not allow the designer the ability to assess the performance in relation to air combat. This is demonstrated by considering the above example of the bomber. Its superior rate of pitch acceleration does not confer an advantage in combat, but by considering a pitch agility metric, an advantage could be implied.

The second problem is that agility metrics do not allow the conceptual designer to assess the aircraft. Accurate values of control derivatives cannot be known during conceptual and preliminary design[5]. However, agility metrics are important much later in the design, in order to assess the agility of the aircraft, and to ensure that it has enough control power. This will mean that the aircraft is more controllable and will have superior trackability. Reference 6 states that it has been shown that there is a real combat payoff for a high transient response capability, and hence agility is very important.

Reference 2 states that 'defining a metric that uses the time to achieve a relative state change as a measure of performance incorporates the initial state conditions, the rates affected by manoeuvrability, and the accelerations affected by agility. This is termed functional agility by the AFFTC'. This can basically be interpreted as a requirement to look at closed loop tasks, not simply instantaneous performance, or agility.

As will be discussed in the following section, performance metrics do not fully assess new technologies. The limitations in the performance and agility metrics, and the non existence of manoeuvrability metrics means that the conceptual designer is left with no suitable tools in defining the changes that these technologies will bring. This paper addresses the problem and considers a new metric that has been developed called Nodal Manoeuvre Analysis, which assesses functional agility. The assessment of the metric is done through a set of case studies.

The Need for Nodal Manoeuvre Analysis

Kutschera[7] discusses in detail the lack of suitable tools for the conceptual designer to evaluate advanced technologies such as TVC/PSM. Through a literature survey, the study identified over thirty metrics. The suitability of these metrics was discussed with industry and combat pilots. Based on these discussions, Kutschera chose to analyse six metrics.
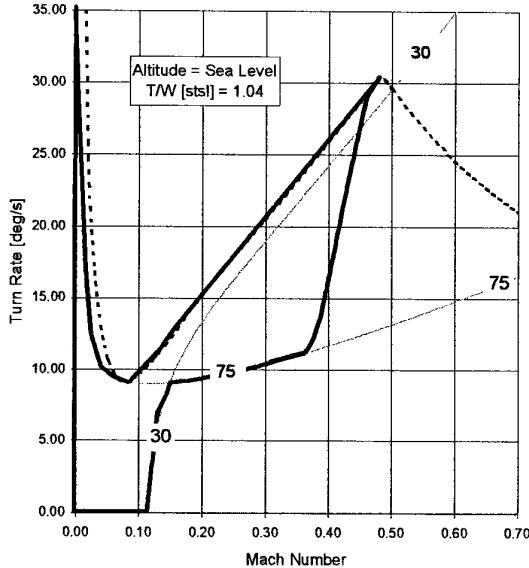
Figure 1 - Post Stall Boundary Shown on a Turn Rate Plot.
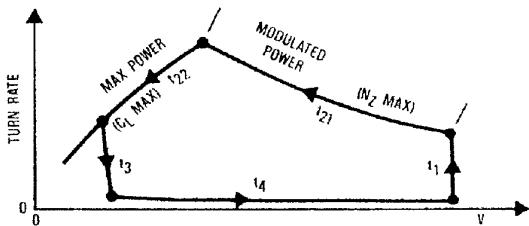
Figure 2 - Concept of CCT.

It was found from the literature review that manoeuvres which are evaluated should consist of closed loop tasks, for example, pitch to a given load factor, not simply pitch to maximum load factor. Since the maximum load factor may vary between aircraft, it is more useful to use a specific load factor, and hence a closed loop task.

The paper shows that metrics such as the turn rate plot can have post stall envelopes added to them, as shown in Figure 1. The figure shows two thin grey lines which are lines of constant AoA (30° and 75°). It also shows a black dashed line which is the Instantaneous Turn Rate (ITR) line. Finally, the thick solid line shows the post stall boundary, constructed from looking at the best possible capability of the aircraft (see Reference 7). The aircraft must be within the thick black line to be able to obtain a post stall AoA. However, these plots only show what is happening in a particular instant during a manoeuvre. In addition, the plots do not assess a closed loop manoeuvre. The same comments also apply to energy manoeuvrability diagrams.

Since existing performance metrics fail to help advanced aircraft assessment, existing functional metrics can be considered. An example of a closed loop metric, discussed in Reference 7, is the Combat Cycle Time (CCT) (this is shown graphically in Figure 2). The CCT is defined as the sum of the times taken to pitch to maximum load factor (t_1), turn

through a heading change of 180° at the ITR (t_{21} + t_{22}), pitch down to 1g (t_3) and accelerate back to the original energy level (t_4). Although this metric includes the time taken to return to the original energy state, it does not consider the position (firing opportunities) of the aircraft.

The definition of the CCT also limits the aircraft manoeuvre to reversing the flight path. Consider the following. The pilot would like to bring the weapons to bear on the enemy by pointing the nose (that is pitching to increased AoA) during the CCT. If the desired AoA is greater than the stall AoA, the turn rate will be reduced, because lift is reduced. This means that reversing the flight path will take longer. Also, because the aircraft will lose energy more quickly while at elevated AoA, the recovery time in the last segment of the CCT will be longer. Although the pilot will have gained a shoot opportunity, the measure of merit will be worse than if the aircraft had followed the original CCT manoeuvre. Hence a full analysis for technology such as TVC/PSM cannot be completed with the CCT metric.
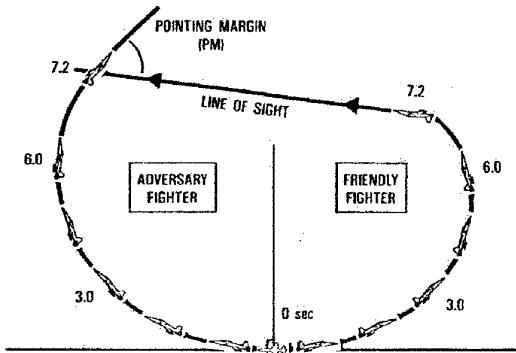
Figure 3 - Definition of Pointing Margin.

Another functional metric, the Pointing Margin, was found to have the most potential. This metric considers two aircraft that have just passed each other and are trying to turn as hard as possible to bear their weapons on the enemy. In Figure 3, the friendly fighter is equipped with TVC/PSM and can point at the enemy aircraft first. The Pointing Margin angle (shown as PM in Figure 3) is used as the measure of merit. However, this metric does not consider variables such as energy, and it depends upon a standard enemy manoeuvre, meaning that absolute performance can not be supplied for an aircraft.

Existing metrics do not really allow new technologies to be assessed at the conceptual design phase. To overcome these problems, a new metric was developed in Reference 7, called Nodal Manoeuvre Analysis (NMA).

Nodal Manoeuvre Analysis

It is of interest to the pilot and hence designer, how quickly the aircraft state can be changed. Questions like, 'How easy is it to manoeuvre the aircraft to a given position with a given direction?', 'How long does it take to get there?', 'How much energy will be expended?' and 'What is the final energy rate?', need to be answered. NMA was developed by considering these questions. Initially, it was thought that the manoeuvres tested should have the objective of getting the aircraft to aim

at a given point. However, there are problems with this approach, such as how far away that point should be and should the point move, to simulate an enemy aircraft. For this reason, the objective was altered to get the aircraft to complete a body axis heading change, so that it is aiming in a given plane, for example the vertical plane. The performance is not only limited to the vertical plane, and other planes should be examined. For a fuller assessment, there are also many more combat realistic manoeuvres that should be considered, for example horizontal turn reversal, and axial acceleration. The assessment of the aircraft is done by measuring parameters like time taken to complete the manoeuvre, turn diameter, and energy bleed rate at the end of the manoeuvre. The results are displayed in the altitude-velocity domain, to allow the designer to see quickly where, for example, the elapsed time of the manoeuvre is a minimum. The ability to assess different manoeuvres, in different planes, allows the designer to assess the performance of the aircraft with relevance to air combat.

To illustrate the concept of NMA, this paper considers only one closed loop manoeuvre. This is a 180° degree, body axis heading change, in the vertical plane. The aircraft starts at a given altitude and velocity at 1g normal loading. Then it pitches up to attain AoA for ITR. The aircraft continues to turn until it gets to a point where pitching to the maximum AoA would mean that the target is acquired. At this point, the aircraft does pitch up, and when the angular difference between the body axis and the target is zero, then the manoeuvre is said to be complete. A typical NMA plot is shown in Figure 4, where the contours show the elapsed time in seconds for the aircraft to complete the heading change.
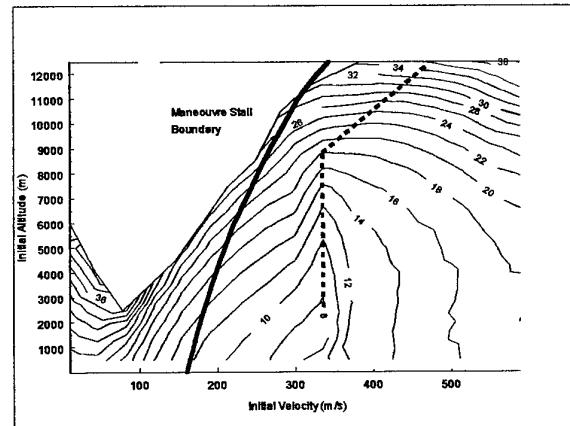
Figure 4 - Time in Seconds to Complete Turn Reversal.

The altitude and velocity axes indicate the initial conditions of the aircraft before the manoeuvre is started. Also shown on the plot are two lines and a boundary. The white area, labelled 'Manoeuvre Stall Boundary' is where an aircraft with initial conditions in this area would stall at some stage during the manoeuvre, and would not be capable of pulling the nose over to point and complete the manoeuvre, without first pitching down to gain speed. The thick black line shows the Corner Velocity in the horizontal plane. Traditionally, this speed is referred to as being where the aircraft is most manoeuvrable since it will have its maximum ITR at this speed. The dashed line shows the best velocity for any given

altitude, to minimise the turn reversal time. Notice the difference between the two lines. This is due to one referring to instantaneous performance, and one referring to a more realistic closed loop manoeuvre.

In principle, any dynamic model of the aircraft of interest can be used for NMA. For the present study, it has been assumed that the amount of data available to the designer is limited to basic geometric data, standard engine data and data derived from the geometry such as weight, lift, drag, etc. It is unlikely that aerodynamic stability derivatives will be known, so it has been deemed acceptable to use a reduced order aircraft model. The model used was reduced to 2 Degrees of Freedom (DoF) with quasi bank freedom. The model was allowed to rotate about the velocity vector and hence turn in the horizontal plane, but the roll response of the model was not modelled. Also, sensitivity analysis showed that pitch response does not have a great effect on final aircraft state variables, and so a very accurate assessment of pitch control derivatives was not required.

The accuracy of the reduced order model was compared with a full 6 DoF non-linear model of the F/A-18a which used unclassified data. Typical accuracy of the reduced order model was such that it was within 5-10% of the full order model, based on a manoeuvre where the objective was to achieve a flight path angle of 90°. For longer manoeuvres, which were not so dependant upon pitch response, the accuracy was improved to less than 5% error.

When using NMA, the designer has to be satisfied that the accuracy of the model being used is acceptable. It should be realised that the outputs will only be as accurate as the inputs provided. If the model used were very inaccurate, then the results of the NMA would also be inaccurate. Any conclusions that were then drawn would be at the discretion of the user executing the analysis.

It should be realised that NMA only provides analysis of the performance of the airframe with initial conditions of speed and altitude. This information is useful for Within Visual Range (WVR) or Beyond Visual Range (BVR) analysis. For WVR analysis, terms such as turn diameter, and turn time are of importance, for BVR, it is turn sustainability (energy usage) which is of importance. Currently, inclusion of a weapons system has not been considered. However, it is suggested that NMA could be adapted to include a weapons system, although this is currently outside the scope of this project. Note that NMA allows the user to use as simple or as complex an aircraft model as required by the analyst. This flexibility, together with the capability to assess performance in WVR and BVR, clearly and concisely using variables that relate directly to combat, gives Nodal Manoeuvre Analysis the potential to be a very powerful tool.

Case Studies

This paper will use the NMA metric for case studies to assess the use of three types of advanced technology. These will be compared to a baseline aircraft, the F/A-18a.

The case studies consider the following three advanced

technologies. 1) The use of advanced engines. The F-404-400 engines used on the F/A-18a have a thrust to engine weight ratio of about 5.0:1 (dry). Using advanced engines with a ratio of about 6.0:1 (dry) would increase the overall thrust by 20%. This example would be similar to exchanging the F-404-400 with the EJ-200, which according to Reference 8 have very similar dimensions. 2) The extensive use of composite/advanced materials in a total redesign of the airframe, but still keeping the same shape and configuration. This could reduce the overall combat weight by as much as 20%, which Reference 9 would suggest to be quite reasonable for future aircraft. Finally, 3) the implementation of a TVC system allowing the aircraft to sustain post stall angles of attack up to 70°. It is assumed that the additional weight of the TVC system is negligible compared to the combat weight, and that there is no effect to the pitching moment of the aircraft due to the added weight at the rear of the aircraft.

To produce the NMA metric, a batch set of simulations of the manoeuvre was run. The simulations ran automatically, using flight control rules discussed in the previous section where the manoeuvre is described, to control the aircraft. Each of the three case studies was run independently. At each point in the altitude-velocity domain, the values were compared to the baseline, and the differences were plotted to show what advantage or disadvantage may come from the addition of a technology. The results are discussed below.

Results

Turning performance and energy performance are both of interest. This is discussed in Reference 10, and is referred to as *angles fighting* and *energy fighting* respectively. The former considers turn time and diameter, and the latter considers energy used in the manoeuvre and energy bleed at the end of the manoeuvre. For this reason, the following plots show turn time, turn diameter, energy consumption and bleed rate.

Baseline F/A-18a.
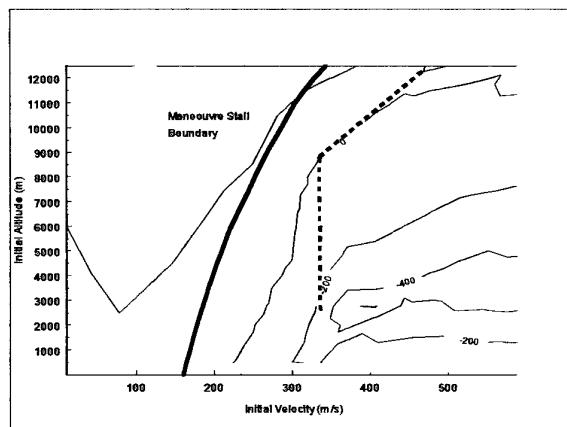
Figure 5 - Specific Excess Power Immediately after Turn Reversal, for the Baseline Aircraft.
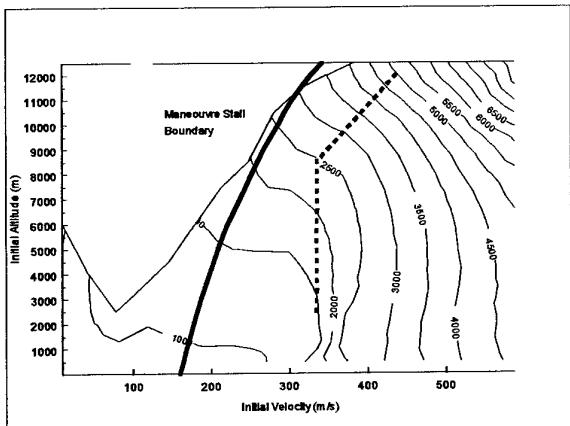
Figure 6 - Vertical Diameter in Metres at the End of the Turn Reversal, for the Baseline Aircraft.
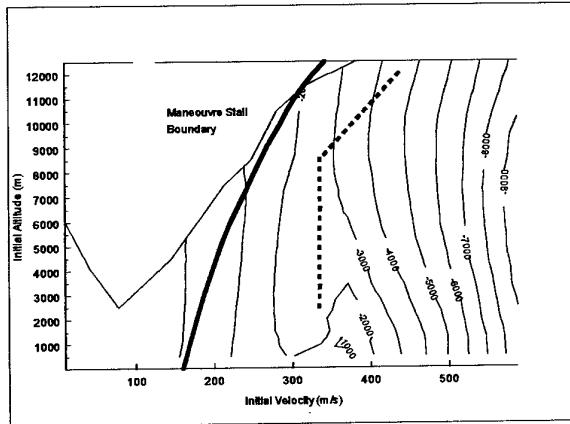
Figure 7 - Energy Gain During Turn Reversal, for the Baseline Aircraft.

Figure 4 shows the time to reverse the turn for the standard F/A-18a. Figures 5 and 6 show the Specific Excess Power (SEP) and the vertical diameter respectively for the standard aircraft. Figure 7 shows the energy gained during the manoeuvre. Values on Figure 7 which are negative, indicate that the aircraft has lost energy during the manoeuvre. These four plots can be used to work out the absolute performance of the three modified aircraft (if so desired), whose performance is shown in later figures. The thick black corner velocity line and the thick black dashed optimum line that exists on Figure 4 are also shown on Figures 5-7.

Case 1: Increase Thrust by 20%.

Figures 8-11 show the effect of changing the engines to increase the overall thrust by 20%. The figures have a thick black line drawn, which is the manoeuvre stall boundary for the standard F/A-18a, taken from Figures 4-7.

Also shown on Figures 8-11, is a thin black line which is similar in shape and position to the thick black line. This limit is the manoeuvre stall boundary for the modified aircraft. It is above the thick line (the standard aircraft), since the advanced technology allows the modified aircraft to turn at
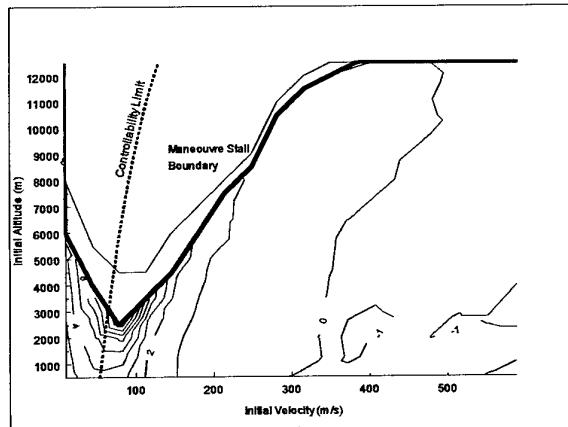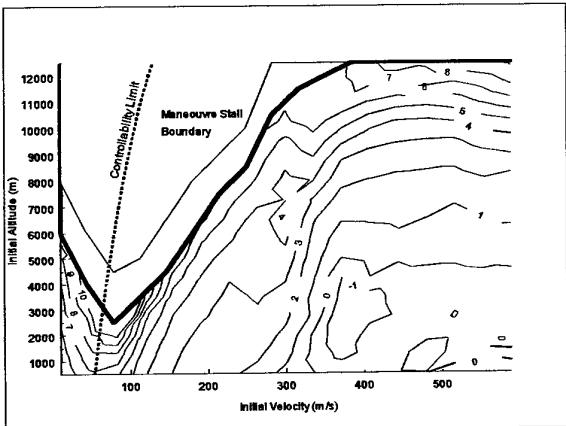

Figure 8 - Difference in Elapsed Time in Seconds to Complete Turn Reversal. Positive Values Show a Shorter Turn Time for the Aircraft with Increased Thrust.

higher altitude without stalling.

Also shown on these figures is a dashed line labelled 'Controllability Limit'. This is the line at which the aircraft is at 1g normal load factor with an AoA of 25°. This angle is deemed the maximum AoA at which the aircraft still has full pitch control, that is, the aircraft is still controllable.

Figure 8 shows contours evaluating the difference in time taken between the standard aircraft and the modified aircraft. Contours with positive values show where the modified aircraft has an advantage in turn time (at any speed to the left of the zero second contour). It can be seen that the maximum amount of time advantage that the modified aircraft has, is about 7 seconds, at just slower than 100m/s velocity and about 2500m altitude. Note though, that this is very close to the controllability limit of the aircraft. It is arguable that no pilot would want to prolong combat in this region and so generally, for the majority of the flight envelope, there is not more than about a second of advantage conferred by increasing the thrust of the engines.

At higher speeds, the modified aircraft appears to have a small disadvantage. However, this result would tell the pilot that at higher speed, the throttle should be reduced in order to reduce the turn time. The turn time would be reduced since the aircraft would slow to the corner velocity quicker, and hence have a higher average turn rate. It should be noted that the simulations were run using full throttle. It was not an objective to optimise the turn with throttle scheduling. However, this example shows that NMA could be used for such a purpose.

Figure 9 shows the SEP difference at the end of the turn reversal. It shows that there is virtually no difference between the two aircraft, except for the 200m/s bubble. At the speed and altitude where the 200m/s bubble exists, the standard aircraft is losing about 200 or more metres of energy height every second. Hence the modified aircraft is maintaining its energy at the end of the turn. This not only means that it is capable of sustaining a continued turn, but also that since less energy was used during the manoeuvre, there is a larger
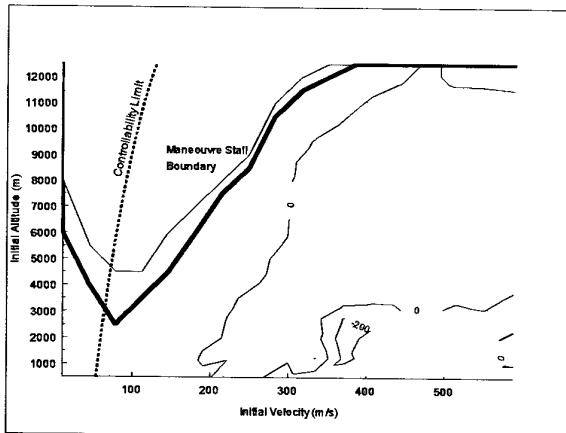
Figure 9 - Difference in Specific Excess Power Immediately after Turn Reversal. Negative Values Show Less Bleed Rate for the Aircraft with Increased Thrust.
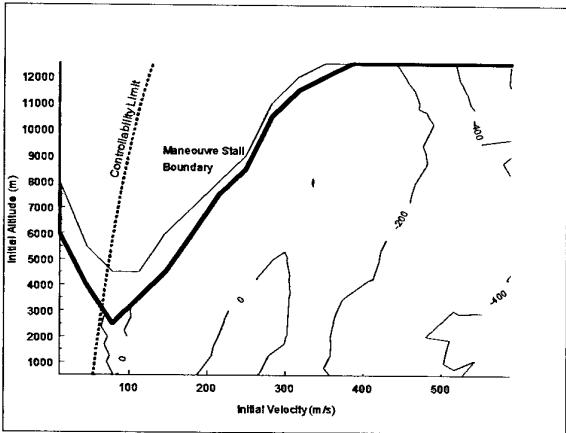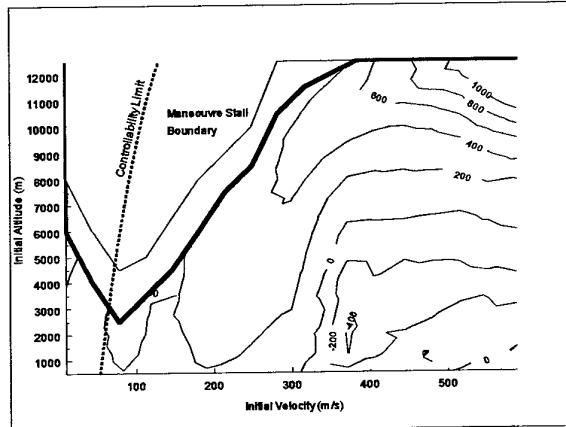

Figure 10 - Difference in Vertical Diameter in Metres at the End of the Turn Reversal. Positive Values Show a Smaller Turn Diameter for the Aircraft with Increased Thrust.

choice of follow on manoeuvres available.

Figure 10 shows the difference in the vertical diameter between the two aircraft. The modified aircraft has a small disadvantage (its turn diameter is typically less than 10% larger when compared to Figure 6 for any speed or altitude). However, for Figure 8 it was stated that thrust could be reduced at higher speed. If this were done, then the turn diameter would reduce, hence equalising any disadvantage shown in Figure 10.

Figure 11 shows the difference in energy gained/lost during the turn reversal. It shows that for higher speeds, the modified aircraft loses slightly less energy height, with the difference between the two aircraft no greater than 800m. Since the modified aircraft has more thrust, it will lose less speed during the turn, leaving it with more energy at the end.

Figures 8-11 show that increasing the thrust by as much as 20% only has a small effect on the performance of the aircraft for the vertical turn manoeuvre. NMA shows that for the modified aircraft there is not much advantage in SEP at the
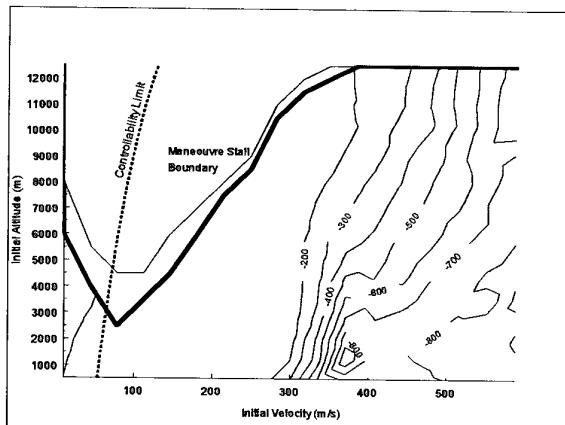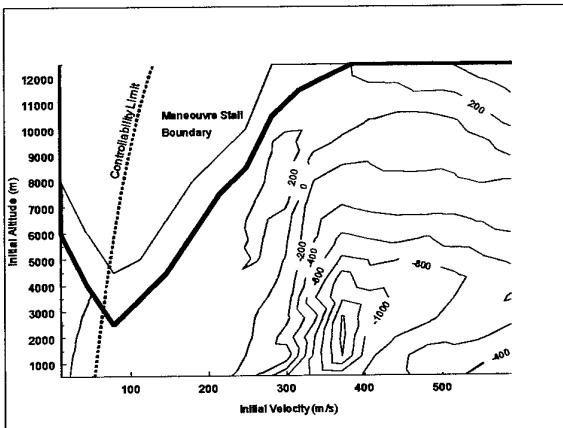

Figure 11 - Difference in Energy Used During Turn Reversal. Negative Values Show Less Energy Used by the Aircraft with Increased Thrust.

end of the manoeuvre, and that there is no real turn diameter disadvantage (less than 10%). The most advantage that comes is from the energy loss during the turn reversal. The modified aircraft has more thrust. This can be used to overcome the drag, and leave the aircraft with more energy at the end of the manoeuvre. Consider equation 1 below.

$$SEP = \frac{V[T\cos(\alpha) - D]}{W} \qquad \text{Equation 1}$$

where, V is velocity, T is thrust, D is drag, and W is weight. This equation is integrated over time to give the energy used during the manoeuvre. At low angles of attack (at which the manoeuvre is performed at high speeds due to the load factor limit), it is dominated by the thrust term, and hence increasing the thrust will reduce the energy used during the manoeuvre.

The high speed, high altitude regime, which is a typical BVR scenario, shows that although there is no turn advantage (in terms of turn time or diameter), there are quite large energy savings made, by increasing the thrust. BVR is dominated by the ability to continue turning without losing energy, and increasing the thrust helps to allow the aircraft to do this.

At low speed near the controllability limit (but above 120m/s), there are no advantages for the increase in thrust. Hence, to increase the WVR performance (which is typically at low speed and low altitude), a much greater thrust increase is required.

Case 2: Decreasing Weight by 20%.

Figures 12-14 show the effect on performance of reducing the combat weight of the aircraft by 20%. The thin black line above the thick black boundary in Figure 12 shows that a reduction in combat weight would mean that the modified aircraft could fly vertical turn reversals at higher altitude while at speeds less than 375m/s. As before, a controllability limit is shown as a dashed line. At any initial speed, the advantage of the modified aircraft increases with increase in altitude. The maximum advantage occurs near the manoeuvre stall boundary and lies between 5 and 10 seconds, for any

initial speed. This is an advantage of around 30% for all speeds, compared to the baseline aircraft. For WVR, an advantage of more than 5 seconds would be enough to obtain a shoot solution, before the enemy can return fire. The figure also shows that at low altitude and high speed, the standard aircraft gains the advantage. This is because the heavier aircraft will slow down quicker and get to its corner velocity sooner. The advantage is however very small, and unlikely to be significant.

Since the modified aircraft will not gain a time advantage from flying low and fast, the difference in SEP is not significant, and hence no plot is shown. The difference in SEP at the end of the manoeuvre is very similar to that for the first case study.

Figure 13 shows the change to the turn diameter. The higher the aircraft flies, the more of an advantage the modified aircraft gets. The maximum is as much as 1km, which is about 15% less than that of the standard aircraft. At low altitude and high speed, there is an advantage for the standard aircraft. This is again because the heavier aircraft will slow

Figure 12 - Difference in Elapsed Time in Seconds to Complete Turn Reversal. Positive Values Show a Shorter Turn Time for the Aircraft with Decreased Weight.
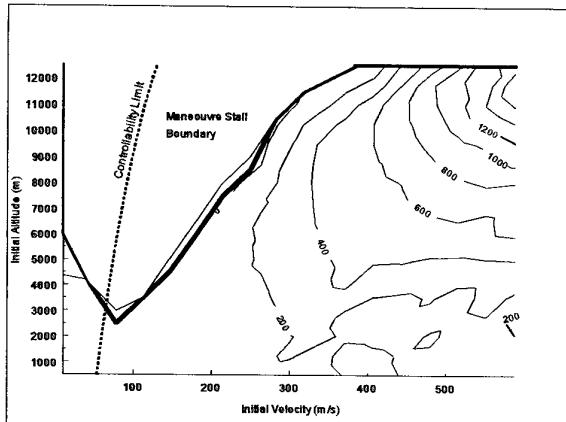

Figure 13 - Difference in Vertical Diameter in Metres at the End of the Turn Reversal. Positive Values Show a Smaller Turn Diameter for the Aircraft with Decreased Weight.

quicker and hence reduce the turn diameter. However, the modified aircraft could match this by reducing thrust as it enters the manoeuvre, although this would not give any time or diameter advantage. To maximise its superiority, the modified aircraft would do much better to fly as high as possible, while still being able to reverse the turn in the vertical plane.

Figure 14 shows the difference in the energy used during the turn reversal. In the areas where there is a time and diameter advantage for the modified aircraft (that is, near the manoeuvre stall boundary), there is also a small energy disadvantage shown by the +200m contours. However, at medium to low altitude and high speed (to the right and below the zero energy contour), the modified aircraft loses significantly less energy than the standard aircraft (up to 1400m less).

Figure 14 - Difference in Energy Used During Turn Reversal. Negative Values Show Less Energy Used by the Aircraft with Decreased Weight.

Case 3: Addition of TVC/PSM.

Figures 15-17 show the effect of implementing a TVC system of negligible extra weight, and allowing the maximum AoA of the aircraft to increase to 70°.

Figure 15 shows the time advantage for the modified aircraft. The contour trends are similar to those shown for Case 2. As with the case study for reduced weight, the biggest advantage to the TVC/PSM aircraft lies close to the manoeuvre stall boundary. The advantage decreases as altitude is decreased. The maximum advantage is again up to 10 seconds, with a minimum of 3 seconds for all speeds, as long as altitude is adjusted. Although it is not shown directly, comparing Figures 12 and 15 shows that the TVC/PSM aircraft has a minimum of a 3 second advantage over the lighter aircraft for most of the flight envelope. At lower speed, the advantage would fall to the lighter aircraft.

Returning to the comparison between the standard aircraft and the TVC/PSM aircraft, it is seen from Figure 15 that the standard aircraft will never have a time advantage. At low altitude and high speed, both aircraft will be load factor limited throughout the manoeuvre. This means that the modified aircraft will not be allowed to go to post stall AoAs,
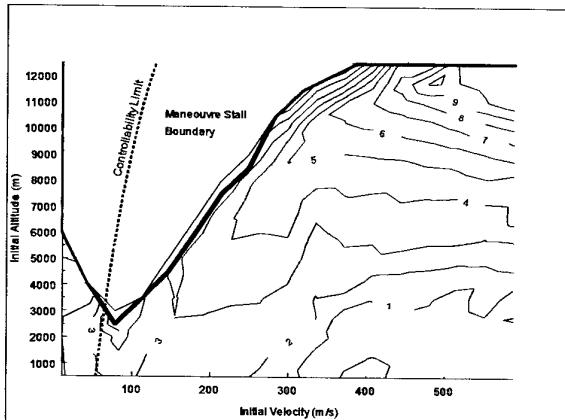
Figure 15 - Difference in Elapsed Time in Seconds to Complete Turn Reversal. Positive Values Show a Shorter Turn Time for the TVC/PSM Aircraft.

and so it will gain no advantage in having this technology. Conversely, the standard aircraft will have no advantage in turn time, and best that it can do is to fly low and very fast, reducing the performance difference to zero.

Figure 16 shows the SEP difference between the two aircraft at the end of the manoeuvre. It shows that the modified aircraft will have as much as a 1600m/s disadvantage. In some cases, this will mean that the modified aircraft will be losing energy at more than twice the rate of the standard aircraft. This issue of losing a lot of energy quickly is characteristic of an aircraft using its PSM ability to the full.

When comparing the energy used during the manoeuvre, the standard and the modified aircraft have very similar results. This is because they are essentially the same aircraft until the very last segment of the manoeuvre where the modified aircraft will go to a post stall AoA. If the pitch acceleration and maximum AoA limit are high enough, it is theoretically possible for the TVC/PSM aircraft to use less energy than the standard aircraft, because it can complete the manoeuvre sooner. For this reason, energy used during the manoeuvre can be very similar when comparing a standard aircraft to a TVC/PSM aircraft. However, the very high AoA of the TVC/PSM aircraft at the end of the manoeuvre means that its energy bleed rate will be much higher, affecting the performance in the next few moments, after the initial manoeuvre is completed. This is why the SEP at the end of the manoeuvre is very important when looking at such aircraft.

Figure 17 shows that the turn diameter is as much as 20% smaller than the standard aircraft (high altitude and high speed), and also that it is as much as 10% smaller than the lighter aircraft (Case 2, not shown). The standard aircraft can only at best match this performance, by flying low and slow.

At very low speed, the modified aircraft would be able to cross to the left of the controllability boundary of the baseline aircraft. This is because the TVC will provide an increased pitching moment (and hence control power) independently of speed. The increase in control power will give the aircraft the
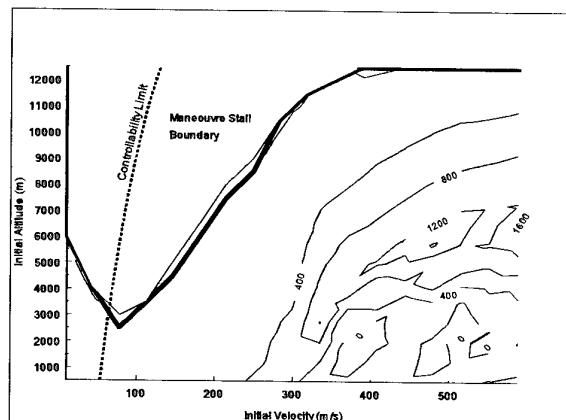
Figure 16 - Difference in Specific Excess Power Immediately After Turn Reversal. Negative Values Show Less Bleed Rate for the TVC/PSM Aircraft.

Figure 17 - Difference in Vertical Diameter in Metres at the End of the Turn Reversal. Positive Values Show a Smaller Turn Diameter for the TVC/PSM Aircraft.

capability to sustain much higher AoAs. Note though, that this very low speed and altitude is unlikely to be used by the pilot, since much greater advantages can be found in other parts of the flight envelope.

For the vertical turn reversal, the addition of TVC and PSM technologies to the aircraft can give very large time and diameter advantages, even in excess of those seen in Case 2 (reduced weight). However, the use of TVC/ PSM will not confer an energy advantage. The SEP at the end of the manoeuvre can be so negative that if a kill is not obtained, then the modified aircraft will be tactically in a very poor slow situation, in only a few seconds. Here, NMA allows the designer to see the trade off between energy and turn performance required for TVC/PSM aircraft.

Discussion of Case Studies

NMA results have been shown for three different case studies. These results show that conclusions could be drawn about the usefulness of the technologies. For the manoeuvre considered, the authors have not drawn any conclusions as to

which technologies are best. It is only intended to demonstrate that the results could be used in helping to determine appropriate levels of new technologies. Note that if NMA is to be used to determine benefits/disadvantages of new technologies, or simply for assessing the performance of aircraft, then a much fuller analysis than that shown here is required. For a fuller assessment, there are many more combat realistic manoeuvres that should be considered, for example horizontal turn reversal, and axial acceleration. When considering technology such as TVC/PSM, it should be realised that this technology provides a capability to execute many new manoeuvres. It is possible that some of these may have tactical relevance, and so these manoeuvres should also be analysed in the full assessment, as long as the limitations of the models used is appreciated.

Once all of the relevant manoeuvres have been considered, and the full analysis has been completed, conclusions can be drawn about where the aircraft is most manoeuvrable. These conclusions can then be used to develop tactics. On the other hand, the designer can determine where the aircraft is under performing, and can use the NMA to execute a parametric study to see what can be modified in the design to give performance closer to that desired.

Conclusions

The NMA metric clearly shows the advantages and disadvantages of different technologies used in the design of an aircraft. The results give values which have meaning to both designer and a pilot.

The results include the performance, the manoeuvrability and the agility of the aircraft, and cover the WVR and the BVR regimes. NMA considers realistic closed loop manoeuvres. This makes NMA a powerful tool for the conceptual or preliminary designer, especially for carrying out parametric studies on the overall combat performance.

NMA simplicity, allows performance assessment of aircraft, quickly and easily. This will aid in the overall aim of a reduction in design cycle time.

Acknowledgements

References

1. R.E. Smith, *'Thrust Vectoring and the X-31 – Lessons to be learned'*, Royal Aeronautical Society Lecture, London, 13 November 1997.
2. Bitten R., *'Qualitative and Quantitative Comparison of Government and Industry Agility Metrics'*, Journal of Aircraft, Volume 27, Number 3, pages 276-282, 1990.
3. Skow A.M., Hamilton W.L., Taylor J.H., *'Transient Agility Enhancements for Tactical Aircraft'*, Technical Report TR89-001, Eidetics International, Torrance California, January 1989.
4. Fox B.A., *'Investigation of Advanced Aircraft Performance Measures of Merit Including New Agility Metrics'*, AFIT/GAE/ENY/91S-3, September 1991.
5. Raymer D.P., *'Aircraft Design: A Conceptual Approach'*, AIAA Education Series, 1992.
6. Hodgkinson J., Skow A., Ettinger R., Lynch U., Laboy O., Chody J., Cord T.J., *'Relationships Between Flying Qualties, Transient Agility, and Operational Effectiveness of Fighter Aircraft'*, Paper Number AIAA-88-4329, 1988.
7. Kutschera A., Render P.M., *'Performance Assessment of Thrust Vector Controlled Post Stall Manoeuvrable Fighter Aircraft Using Minimal Input Data'*, Paper Number AIAA-99-4020, AIAA AFM Conference, August 1999.
8. *'Jane's All the World's Aircraft'*, 1995-1996 Edition, Jane's Publishing Inc.
9. Various, *'Introduction to Aircraft Weight Engineering'*, Society of Allied Weight Engineers, 1996.
10. Shaw R.L., *'Fighter Combat - Tactics and Maneuvering'*, United States Naval Institute, 1985.

Multi-Flight Condition Optimization of Three Dimensional Supersonic Inlets

Gérald Carrier,* Christophe Bourdeau,† Doyle Knight‡
Department of Mechanical and Aerospace Engineering
Center for Computational Design
Rutgers University - The State University of New Jersey
98 Brett Road
Piscataway, NJ 08854-8058, USA

Yan Kergaravat,§ Xavier Montazel¶
Numerical Simulation Department
AEROSPATIALE-MATRA MISSILES
2, rue Béranger B.P. 84
92323 Châtillon Cedex, France

This paper presents an innovative methodology to address the three-dimensional supersonic inlet design problem. An efficient and robust process allows to optimize the aerodynamic performance of inlets for multiple flight conditions. This optimization process links together an optimizer with a fast and accurate simulation tool into an automated optimization loop. The implementation of this new design technique and its applications to two different test cases are presented, namely, the optimization for a single cruise condition, and the optimization for a mission comprised of acceleration, cruise and maneuver phases. The mission-optimized inlet achieves better overall performance than the cruise-optimized inlet.

1 Introduction

The design of high speed inlets for supersonic vehicles is an intricate exercise and a challenging issue. The classical design process mainly relies on engineers' experience and on the limited human capability to cope with a large number of coupled parameters. As a consequence, the design process can be long, laborious and extremely expensive, without any guarantee to lead to the best performing design. In that context, taking into account the progress accomplished in both numerical flowfield simulation and artificial intelligence domains, automated design process strategies appear to be an appropriate answer to the inlet design problem. Actually, the association of efficient optimization algorithms and fast aerodynamic performance analysis tools has proved to be able to give better designs than classical design methods, while reducing the time cost.

Optimizations have already been carried out successfully for several two-dimensional problems. Hussaini et al.[1] and Borivikov et al.[2] have worked on two-dimensional nozzles. Several studies have dealt with two-dimensional supersonic and hypersonic inlets. Zha

et al[3] and Shukla et al[4] performed optimizations of two-dimensional supersonic missile inlets.

Wind tunnel experiments as well as Reynolds Averaged Navier-Stokes (RANS) calculations have shown that the flowfield through supersonic missile inlets is highly three-dimensional,[5] even for inlets with rectangular cross-section under symmetric free stream conditions. Moreover, since the vehicle has to fly an entire mission, the inlets experience very different inflow conditions throughout this mission and its multiple flight conditions. Thus a methodology for inlet optimization which accounts for both the three dimensional feature of the flow field and the different flight conditions met through the mission of the vehicle is clearly needed.

The research presented in this paper describes an efficient and powerful tool to optimize the aerodynamic performance of a full three-dimensional supersonic inlet for a complete, realistic mission. An important issue is the cost of the performance evaluation of such three-dimensional systems, especially when the entire mission is considered, since it leads to several analysis, one for each flight condition. A full RANS simulation of a three-dimensional inlet typically requires several hundred CPU hours on a workstation. While this cpu requirement permits RANS simulations to be used in a manual design process (where only a few designs are

---
*AEROSPATIALE-MATRA MISSILES Engineer
†AEROSPATIALE-MATRA MISSILES Engineer
‡Professor, Dept. of Mechanical and Aerospace Engineering.
§AEROSPATIALE-MATRA MISSILES Engineer
¶AEROSPATIALE-MATRA MISSILES Engineer

considered), it precludes the use of RANS simulations as the basis of an automated design process which requires hundreds of flowfield simulations. Therefore, a hybrid flow solver based upon an innovative combination of an Euler flow-solver and a one-dimensional subsonic diffuser model has been developed. The simulation time with this tool has been reduced to few CPU minutes, allowing the current automated design optimizations.

After describing the problem addressed by the present study, the optimization methodology and the different elements involved are described. Then the results for both a single flight condition and a full mission optimizations are presented and analysed.

2 The Problem of Multi-Flight-Condition Optimization of a Generic Supersonic Inlet

2.1 Overview

The problem is the design of three-dimensional supersonic missile inlet. The function of a supersonic inlet is to capture supersonic flow and efficiently decelerate it in order to provide the engine with a sufficient mass flow rate of high total pressure subsonic flow. This task is performed through three main stages presented in Figure 1.
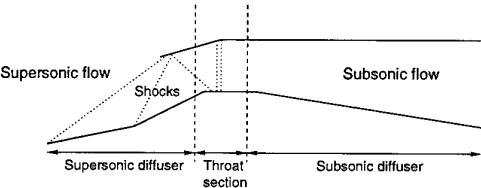
Fig. 1   Supersonic inlet critical operating regime

First, a set of oblique shocks forms in the supersonic part of the inlet and decelerates the supersonic incoming flow. Then a terminal shock system (an approximate normal shock) occurs in the vicinity of the geometrical throat. Finally, the flow is further decelerated in a subsonic diffuser.

To achieve high performance, the inlet design must be optimized for the flight condition according to a set of constraints imposed by manufacturing considerations and engine specifications. But through the entire mission the air-breathing vehicle has to fly, the inlet faces several flight condition which can be very different. Therefore the generic inlet optimization problem can be defined as the maximization of the inlet aerodynamic performance for an entire mission, within a space of feasible designs which corresponds to the given set of constraints imposed on the inlet.

2.2   The Single-Flight-Condition Optimization

Given a particular flight-condition, *i.e.*, a particular inflow condition, two main coefficients are used to assess the aerodynamic performance of the inlet in this condition. The total pressure recovery coefficient η is representative of the efficiency of the flow deceleration performed by the inlet. It is defined as

$$\eta = Pt_{exit}/Pt_0$$

where Pt_{exit} and Pt_0 are respectively the averaged total pressure in the exit plane of the subsonic diffuser and the freestream total pressure.

The mass flow rate coefficient ε represents the relative amount of flow captured by the inlet and is defined as

$$\varepsilon = \frac{\text{mass flow entering inlet}}{\text{maximum mass flow at } \alpha = 0° \text{ and } \beta = 0°}$$

where α and β are the angles of attack and sideslip, respectively.

Therefore, the problem of the inlet optimization for this particular flight condition can be formulated as the search for the global optimum

$$\text{maximize } \eta(\mathcal{G})$$
$$\text{subject to constraints}$$

where $\mathcal{G}$ represents the family of feasible geometries. One of the constraints imposed for the inlet design is to achieve a sufficient mass flow rate coefficient ε.

2.3   The Mission Optimization

Overview

As pointed out previously there is a strong need for the inlet to be optimized not only for one particular flight-condition, but rather for a full mission. The mission, from the point of view of the inlet performance, can be seen as a succession of flight conditions (or flight points).
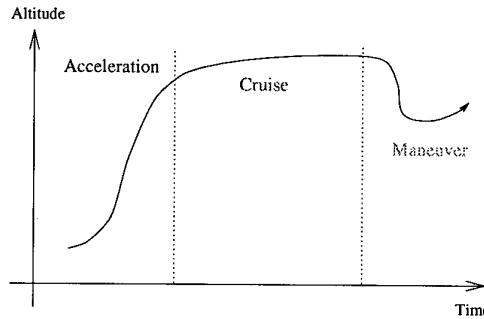
Fig. 2   Profile of a mission

Although this succession is continuous through the mission, this mission can generally be discretised into several stages. Figure 2 represents a typical mission profile. Three different stages are often considered to

define the mission. The first stage is the *acceleration*. It begins at the self-start Mach number of the inlet, which is actually a design parameter (the boost phase is not considered here). During this acceleration stage, the missile has to accelerate and climb to reach its cruise altitude and speed and therefore needs a high thrust. This requirement also implies a high mass flow rate coefficient. At this point, the total pressure recovery is generally high but it is nevertheless important to maximize it. The second stage is the *cruise*. Here, the missile is required to fly the longest distance as possible. Therefore, the fuel consumption is of primary interest and so the total pressure recovery must be maximized. As the missile gets closer to its target, it enters the *maneuver* stage. At this point of the mission, the primary parameter is again the total pressure recovery which must be maximized while the mass flow rate has to be larger than a specified minimum value.

In summary, the mission can be discretised into three different stages which can be considered independently. The total pressure recovery has to be maximized for all the mission stages, while the mass flow rate must be kept larger than a minimum value specified at each stage.

Optimization Strategy

Since the mission yields three different stages, the problem which has to be considered is now multiobjective since the η coefficient is to be maximized for each stage of the mission. But the total pressure recovery cannot be maximized independently for each of the three mission points for a fixed inlet geometry, and the mission optimization is therefore a matter of compromise between the three mission points. The mission problem is handled through the use of a mission target curve for the total pressure recovery. This curve provides a target value for the total pressure recovery for each flight point in the mission. These target values are fixed according to the engine specifications and the mission requirements. However they are slightly overestimated in order to keep the total pressure value achieved by the optimal inlet below it. This target curve for the total pressure recovery will be denoted as $\eta_{target}(Mission\ Point)$. The different constraints applied to the inlet and especially the constraint on the mass-flow rate are also defined independently for each mission-point (See Table 4 in Section §4.2.2).

Given this definition of the mission, the goal of the optimization process is to minimize the gaps between the performance achieved by the candidate inlet on each point of the mission (η_i), and the target curve η_i^t. (See Figure 3). The actual values used to defined the target curve are given in Table 3 of Section §4.2.1.

Therefore the mission problem which will be addressed
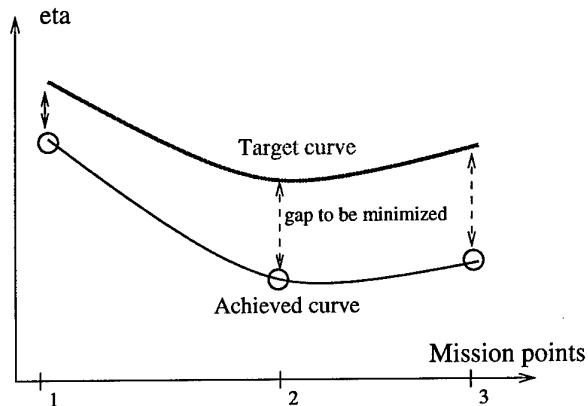
Fig. 3   Example of target and achieved curves

in the following can be expressed as

$$\text{minimize } \phi(\mathcal{G})$$
$$\text{subject to constraints} \qquad (1)$$

where

$$\phi(\mathcal{G}) = \sum_{i\ \in\ \text{mission}} \left[\frac{\eta_i - \eta_i^t}{\eta_i^t}\right]^2$$

where η_i^t is the target value of η at mission point i.

2.4   Geometry Model of the Generic Inlet

Supersonic Part

The geometry investigated is a multi-ramp mixed compression inlet. The cross-section of the inlet is rectangular and the inlet can be considered as "two-dimensional". Nevertheless the three-dimensional features of the flowfield in such inlets have proved to be of considerable importance and are currently included in the simulation. A large amount of internal compression is provided by the cowl which is composed of four different segments, allowing to modify precisely its shapes.
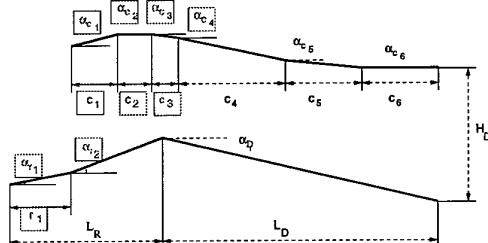
Fig. 4   2D parameters of the inlet

Subsonic Diffuser

A generic diffuser whose shape is fixed during optimizations is added to the supersonic part previously described, respecting some aerodynamic based design rules for its shape. The lower surface of this diffuser is kept flat, forming an angle of $-9.55°$ with the horizontal plane. The upper surface is composed of three equal length planes with increasing angle: $-8.55°$,

−5.05° and −0.55°. These values of angle and length have been chosen to avoid separation and minimize the loss in the subsonic diffuser. The width of the diffuser is assumed to be constant.

This geometry model has been extrapolated from an experimental research performed by S.A. Fisher[6,7] and requires ten parameters to be completely defined. These parameters which describe the two-dimensional shape of the inlet are presented in Figure 4 where the ten design parameters are boxed. This parametrization of the inlet allows to investigate a large spectrum of three-dimensional shapes.

3   Methods Used in Optimal Design Process

3.1   Automated Design Loop

3.1.1   Presentation of the Optimization Loop

The innovative three-dimensional automated optimization process is based on the development of several tools linked within a loop algorithm presented in Figure 5. The optimization software which has been developed and used for the present research can use different optimization algorithms. The optimization has led to the development of a solver fast enough to allow a large number of calls and accurate enough so as to correctly predict the trends between investigated configurations. Outside of the loop, some verifications are made using full Reynolds-averaged Navier-Stokes simulations.
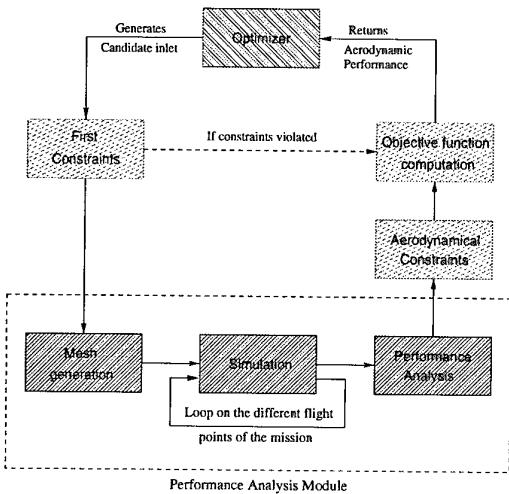
Fig. 5   Automated Optimization Loop

3.1.2   Automated Process Description

The heart of the optimization loop implemented for designing supersonic inlets is called the optimizer. The optimizer generates candidate inlet designs described by ten geometrical parameters (see Section §2.4). These parameters are passed to the analysis

module which returns the aerodynamic performance of the candidate inlet. Based on these simulation results, the objective function and some aerodynamic constraints are calculated. In order to reduce the computational cost of the design process, geometry constraints are also implemented and checked before running the analysis module. If any of those constraints is violated, no evaluation is undertaken and the optimizer is simply given back a penalty for this candidate inlet based upon the amplitude of the constraint violation (see Figure 5). These features, which prevent from the evaluation of non-feasible inlets (from a physical point of view), save a significant amount of time during the optimization process, especially at the very begining.

3.2   Optimization Algorithm

The current optimization loop software is based upon the *Designer's Interface*, developed at Rutgers University. This optimization software includes different optimizers: GADO (a Genetic Algorithm), CFSQP (a gradient based search algorithm) and a random-probe algorithm and allow to choose easily any of this three optimization "engines". The *Designer's Interface* acts as an interface between the optimizer itself and the analysis part.

Previous optimizations[8] have demonstrated that the Genetic Algorithm GADO performs better than CF-SQP for the particular problem of supersonic inlet optimizations. Therefore the present optimizations have been performed using GADO.

Presentation of GADO

GADO (Genetic Algorithm for Design Optimization) is a stochastic optimizer. It first generates a random population of potential candidates. Then mutations and recombinations are applied to individuals of the population in order to make the population evolve towards better solutions. GADO was developed by Khaled Rasheed[9] in the Department of Computer Sciences at Rutgers University. Compared to classical Genetic Algorithms, several improvements have been included that make the search more efficient and reliable for engineering problems.

Each individual is represented by a vector of real numbers, which is particularly well adapted to the parametric description of the inlet. Several innovative crossover and mutation operators have been developed in order to make the search process fast and accurate, *i.e.*, more likely to find the global optimum. Depending on the number of iterations allowed for the search, the stage of the optimization process is taken into account. For example, a guided crossover operator (which mimics a gradient-based method) is applied in the last part of the search, with a view to accelerate the convergence. The shape of the population is also

checked to detect premature clustering and a reseeding of the population can be performed in order the avoid the search process to be stuck near a local optimum of the design space. Finally, the penalty function has been tailored by the use of a penalty coefficient which increases during the process, so as to guide the search towards feasible regions.

This algorithm has already been used successfully for several different engineering test cases.[9-11] The advantage of this optimization tool is its ability to explore large parts of the design space and to reach the global optimum of topologically complex design space.

3.3 Inlet Performance Analysis Methodology

The accuracy and usability of any automated design process is mainly grounded on its performance estimation module. Indeed, the analysis part of the process must be accurate enough to predict the trend between candidate inlets and fast enough for the several hundreds of three-dimensional inlet analyses needed by the optimization to be performed within an acceptable time frame. To answer these requirements a hybrid flow solver, called 2ES3D (an acronym for Euler + Semi-Empirical Simulation 3-D), has been implemented to be used inside the optimization loop and validated.[12]

3.3.1 Simulation Overview

The compression which occurs in the inlet must be achieved with the minimum total pressure loss. Moreover, the engine requires a minimum amount of flow to be captured by the inlet to work in optimal conditions. Figure 1 describes the flow field in the inlet working in critical operating regime, i.e., in the regime which leads to the theoretical maximum efficiency for the compression. First, a supersonic compression is performed through a series of oblique shocks. The flow remains supersonic until the throat region, where a shock system close to a normal shock occurs, downstream of the geometrical throat. After this shock system, the flow is subsonic and is compressed along a diverging duct which acts as a subsonic diffuser. Basically, total pressure losses occur across the various shocks and through the viscous effects in the subsonic diffuser.

The methodology developed for the aerodynamic performance evaluation is based on a physical analysis of the inlet operation (see Figure 1). 2ES3D first uses an Euler simulation to account for the supersonic compression occurring above the inlet ramps. Then corrections are applied for the loss through the terminal shock system and for the viscous losses through the subsonic diffuser. Figure 6 summarizes the different elements of the analysis process performed by 2ES3D.

Fig. 6 2ES3D **automated simulation process**
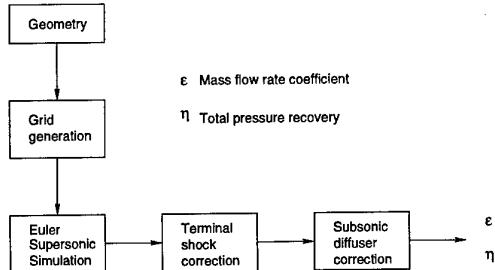
3.3.2 Simulation Models

Euler Calculation

To compute the supersonic compression which occurs above the ramps and the associated losses through the different oblique shocks, an Euler calculation is performed using $\mathcal{GASP}$[13,14] Version 3.2 by AeroSoft, Inc. as the flow solver. In this respect, a grid of the inlet has to be generated. This grid is created with GridPro developed by Program Development Corporation.

The Euler simulation uses a third order accurate upwind scheme (Van Leer scheme) to compute the inviscid fluxes. A Jacobi scheme with inner iterations is used for relaxation. A tangential velocity boundary condition is applied on all the inlet walls and a supersonic outflow condition is used for the inlet exit plane.

$\mathcal{GASP}$ as well as GridPro are run automatically (without any user intervention) in batch mode.

Virtual Terminal Shock Model (VTS)

For the case of supersonic inlets, the main total pressure loss occurs through the terminal shock system previously described. At the critical operating regime, which is the one to be considered for optimization, the terminal shock is located in the vicinity of the aerodynamical throat which is a position known to be close to the geometrical throat or above the boundary layer bleed (if any). Nevertheless, in some cases a subsonic region occurs beneath the cowl which makes the terminal shock unlikely to be stabilized in the region where the flow is subsonic. In that case the terminal shock is applied just downstream of the subsonic area. Finally, the position where the terminal shock is placed is either the geometrical (if no subsonic zone is found) or the downstream position of the subsonic zone if such a subsonic zone exists. This methodology for positioning the terminal shock has proved to give results closer to reality than systematically applying it at the geometrical throat.[8]

This shock is modeled by taking into consideration each individual cell of the mesh at the chosen shock position and by applying the Rankine-Hugoniot formulae for this cell. An averaged value of the total pressure is computed behind the vertical shock. Then

the information about the flow just behind the vertical shock are passed to the one-dimensional subsonic diffuser model.

Subsonic Diffuser Model

The losses which occur in the subsonic diffuser are due to viscous effects. As the boundary layer develops with adverse pressure gradient due to compression, separation is likely to occur in the diffuser[15] , leading to strong reduction of the inlet performance. A one-dimensional model of the subsonic diffuser has been developed based upon a preliminary study done at Stanford University.[16,17] The inflow conditions used to initialize the computation are the averaged flow conditions found immediately behind the terminal shock. The flow field along the diffuser is calculated using a space marching strategy. A "weak-strong" method is applied when separation is detected to take into account the interactions between boundary layers and the non-viscous core flow. The velocity profile of Coles-Van Driest, corrected when boundary layer separate, is used to calculate the stress along the wall. Finally, the geometry of the diffuser is taken into consideration through the definition of its different wall-elements. This model, which is able to predict separation with a reasonable precision,[17] has turned out to be more accurate than empirical formulae for subsonic diffusers.

Bleed Implementation

Supersonic inlets usually incorporate a boundary layer bleed located in the throat region. The bleed role is twofold. Basically, it aims at removing the low energy fluid from the boundary layer which has developed on the supersonic compression ramps in order to prevent separation in the subsonic diffuser. Furthermore, it also helps to stabilize the terminal shock system close to the throat section (see Figure 1). In the present study, the bleed has not been taken into account for optimization, i.e., in 2ES3D, since no boundary layer is computed in the Euler calculation performed by 2ES3D. This strategy is based on the assumption that, given an optimal inlet found with the present method, it is possible, a posteriori, to add to the optimal inlet a bleed which removes a sufficient amount of flow, so as to lead to an excellent final design. This assumption must be validated by performing RANS simulations of the optimal inlet design with bleed.

3.3.3 Validation of 2ES3D

A validation of three-dimensional inlet performance prediction using this method has been conducted,[12] pointing out its domain of validity and showing a 5% accuracy over this domain. The study has demonstrated that 2ES3D enables to correctly predict the trend in performance between inlet configurations. This is the most important feature for its use inside

an optimization loop. Its reliability with regards to the mesh refinement for the Euler simulation has been tested and has shown a good agreement between fine, medium and coarse meshes. The accuracy of the Virtual Terminal Shock model for different positions of the terminal shock was also tested against Euler calculations with back-pressure. The final result is an efficient simulation tool for inlet performance which can accurately predict the trend between inlet configurations and allows important reduction in the computational resources needed for optimizations.

4 Results of Two Optimizations

4.1 Description of the Two Different Optimizations

Two different optimizations have been performed using the methodology and software presented in Section §3. The first optimization is a single flight condition optimization representative of a cruise stage. It served both to validate the automated design software and to provide a reference to assess the improvement obtained using the multi-flight conditions optimization concept. The second optimization is a mission optimization. The mission definition employed during this optimization re-uses the conditions of the first optimization for the cruise stage. The first optimizations intended therefore to provide the best performing inlet for the cruise stage, whereas the second optimization intended to yield a better compromise for flying the entire mission.

4.1.1 Aerodynamic Flight Condition for the Cruise

The first optimization was a single-flight-condition optimization. The inlet has been optimized for a cruise stage which is described in Table 1.

Flight Condition	Cruise
Mach number	3.2
Side-slip angle	0°
Angle of attack	4°
Altitude	12 km
Total pressure	955 kPa
Total temperature	660 K

Table 1 Aerodynamic conditions for cruise optimization

4.1.2 Aerodynamic Flight Conditions Used for the Mission

The second optimization was a multi-flight-condition (mission) optimization. As described previously, the mission was composed of three different stages. The specification of the three different mission stages are described in the Table 2 below. It has to be noted that

the cruise stage of this mission corresponds exactly to the flight-condition used in the first optimization for the single flight condition optimization.

Flight Cond.	Accel.	Cruise	Maneu.
Mach number	2.4	3.2	2.8
Side-slip angle	0°	0°	5°
Angle of attack	1°	4°	0°
Altitude	8 km	12 km	10 km
Total pressure	520 kPa	955 kPa	1306 kPa
Total temperature	508 K	660 K	680 K

Table 2 Aerodynamic conditions for mission optimization

4.1.3 Computer Environment

Both optimizations have been performed on Silicon Graphics R10000 processors. The single-flight-condition optimization took roughly 3.5 days of CPU time to be achieved, whereas the mission optimization took 14 days.

4.2 Settings Used for the Optimization: Objective and Constraint Function Definition

4.2.1 Objective Function

Single-Flight-Condition Optimization (Cruise)

The Genetic Algorithm GADO aims at minimizing the objective function. Since the targeted objective for the single-flight condition optimization is to optimize the total pressure recovery of the inlet, the objective function passed to the optimizer is $-\eta$, the negative value of the total pressure recovery.

Multiple-Flight-Conditions Optimization (Mission)

As it has already been described in Section §2.3, the objective of the mission optimization was to minimize the "gap" between the performance achieved by the inlet through the entire mission and the target performance for this particular mission. The definition of the target curve used for the present optimization is provided in Table 3.

Flight Cond.	Accel.	Cruise	Maneu.
Targeted η	0.8	0.6	0.65

Table 3 Mission optimization targets for η

The expression of the objective function for the mission optimization passed to GADO is Eq (1).

4.2.2 Constraints

The present optimizations are constrained, *i.e.*, the candidate inlet must meet a set of constraint to be considered as "feasible". The constraints intend to eliminate the designs which are not manufacturable,

which do not self-start at the required Mach-number or which shapes are simply not-physical. Figure 7 presents the way these constraints are handled during the optimization process.
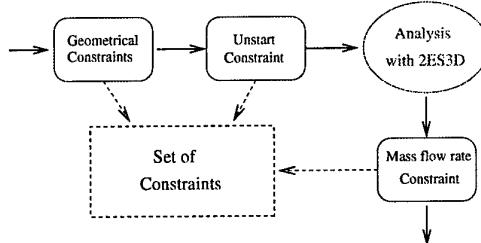
Fig. 7 Constraints verification process

Geometrical Constraints

Prior to the analysis code call, some geometrical constraints are checked, based on the ten geometry parameters passed by the optimizer. These constraints allow to eliminate, early in the process, unfeasible geometries according to manufacturing or physical considerations. This feature saves the time of a performance analysis with 2ES3D.

Unstart of the Inlet

Since the inlet is required to be self-started at a lower Mach number than any of the mission stages, a unstart criterion is applied, prior to the analysis code, to predict if the candidate inlet is started in the required condition. During the two present optimizations, the unstart constraint has been handled using an approximate criterion.

First, the Mach number value at the cowl entrance is computed using Rankine-Hugoniot formulae and taking into account only the two-dimensional geometry of the inlet. Then, the actual contraction ratio, define as (*Entrance Cowl Section Area*)/(*Throat Section Area*), is compared to the maximum contraction ratio which would allow a Pitot type inlet to self-start at the Mach number value calculated previously (Mach number at the cowl entrance). This simplified criterion, which has been used successfuly in previous two-dimensional optimizations[18] has been chosen to avoid an additional costly flow field calculation. During all optimizations, the inlet was required to be self-started at Mach 2.2.

Constraint on the Mass Flow Rate

In the present optimizations the mass flow rate acted as a constraint through two different ways. Since the inlet has to be adapted to a given engine, the mass flow captured by the inlet is required to be large enough to feed this engine. A constraint is consequently applied on the mass flow rate crossing the inlet. The mass flow rate was required to be larger than a specified and stage-dependent value for each stage of the mission, for the candidate inlet to be considered of interest.

To prevent the mass-flow rate constraint to be re-

spected by simply increasing the height of the cowl (scaling effect), a constraint on the mass flow rate coefficient, ε has been added. The mass flow rate coefficient was also required to be larger than a specified and stage-dependent value.

The following table summarizes the constraints related to the mass flow rate which have been considered during the optimizations:

Flight Condition	Accel.	Cruise	Maneu.
Min. MFR	1.6 kg/s	1.4 kg/s	2 kg/s
Min. ε	0.85	0.95	0.8

Table 4   Mass flow rate constraints for the different mission stages

4.2.3   GADO settings

Based on the experience gained during the previous inlet optimizations[8,19] the following settings have been used for the optimizer GADO:

Run	#iter.	Working Pop.	Stored Pop.	Random seed
Cruise	2000	50	2000	45
Mission	2200	50	2000	47

Table 5   GADO settings for the two optimizations

4.3   Analysis of the Results for the Single-Flight-Condition Optimization (Cruise Optimization)

The convergence history of this first optimization is presented in Figure 8. This graph shows that a total pressure recovery of $\eta = 0.45$ is quickly reached by GADO, during the first 100 iterations. The main difficulty encountered by the optimizer during the early stage of the search is actually to find feasible points. Once this first step is accomplished, GADO explores the "feasible" part of the design space by searching around each new best design it finds. This search process yields several flat zones for η in the history curve. Each of these flat zone corresponds roughly to the exploration of new regions in the design space, related to different families of good designs. The notion of family is used to denote groups of designs which have designs parameters close one to another and also close values for the objective function.

Finally the optimal inlet design found by GADO is $\eta_{opt-cruise} = 0.554$. According to the shape of the optimization history curve in Figure 8, the GADO search can be considered as "converged", proving that the 2000 iterations which have been allotted to GADO were sufficient. No reseeding of the working population was performed during this GADO run.

The shape of the optimal inlet for cruise found by GADO is presented in Figure 9.
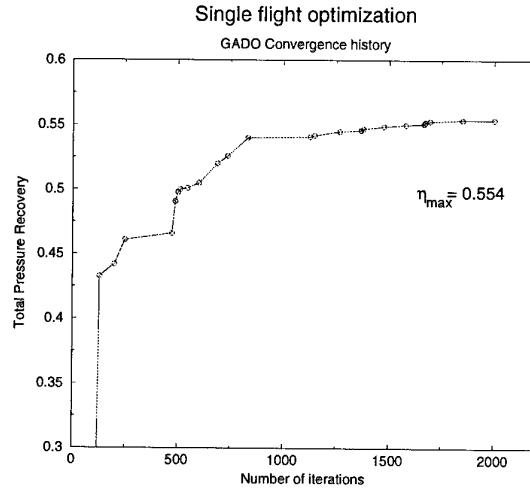
Fig. 8   GADO convergence history for the cruise optimization
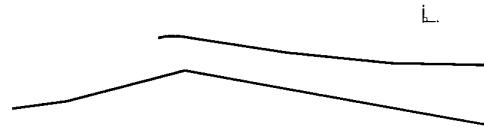
Fig. 9   Optimal design for cruise

Table 6 summarizes the performance of the optimal inlet found during the cruize optimization.

Inlet optimized for	Cruise
η_{2es3d}	0.554
$Massflow\ rate_{2es3d}$	1.911 kg s^{-1}
ε_{2es3d}	1.131

Table 6   Summary of the aerodynamic performance of the optimal inlet for the cruise phase

The performance of the optimal inlet design for cruise has finally been assessed in the two other flight-conditions of the mission, i.e., for the acceleration and maneuver stage. These two computations have been performed using 2ES3D. The results are available in Table 8 (Section § 4.5) .

4.4   Analysis of the Results for the Multi-Flight-Conditions Optimization (Mission Optimization)

The convergence history of the mission optimization is presented in Figure 10. As for the cruise optimization, GADO, after having found the first "feasible" designs, quickly decreases the value of the objective function below 0.03 (See Section §4.2.1). Then the convergence history of the search presents several plateaus, corresponding roughly to the exploration of new-discovered good regions by GADO. Finally, GADO converges to a value of 0.018015 for the objective function. As presented on the Figure 10, the level of 0.0272, which is the value of the mission objective function calculated

for the optimized inlet for cruise is quickly reached and widely overcome by GADO during the mission optimization.

Mission optimization

GADO Convergence history
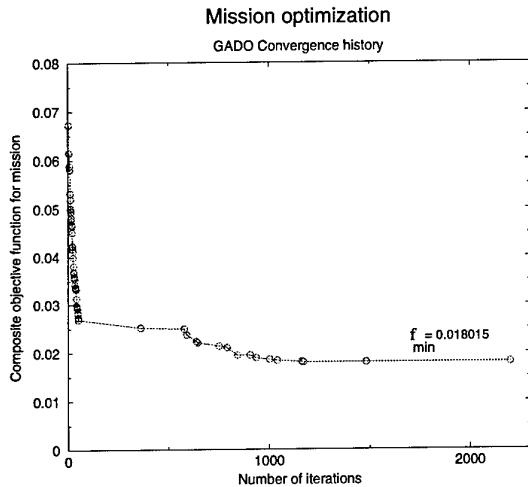
Fig. 10 GADO convergence history for the mission optimization

The shape of the optimal inlet for mission found by GADO is presented in Figure 11.

Fig. 11   Optimal design for mission

Table 7 summarizes the performance of the optimal inlet for the mission, in each of its flight condition.

Opti. Inlet for the mission	Accele.	Cruise	Maneu.
η_{2es3d}	0.714	0.552	0.644
Mass flow $rate_{2es3d}$ (in $kg \cdot s^{-1}$)	1.924	1.884	3.046
ε_{2es3d}	0.874	1.132	0.928

Table 7   Summary of the aerodynamic performance of the optimal inlet for the entire mission

4.5   Comparison Between the Two Optimizations

As it can be seen on Figure 12, or in Table 8, the inlet optimized for cruise performed essentially the same at the cruise condition as the inlet optimized for the mission: $\eta = 0.554$ versus $\eta = 0.552$. Nevertheless, the inlet optimized for the entire mission performed better on the two other flight conditions than the inlet optimized only for the cruise. According to the accuracy of 2ES3D, estimated at 5%, the differences of performance between the two optimal inlet designs are not significant for the cruise stage (where they differ by 0.4%) or acceleration stage (where they differ by 2.6%); however, there is a significant difference in

performance for the maneuver stage (where they differ by 6.1%). This results reveals that the negligible improvement achieved by GADO in the cruise optimization (0.554 to be compared to 0.552) resulted in a degradation of the performance for the maneuver stage of the mission. This demonstrates the benefits of taking into account the entire mission during the optimization.
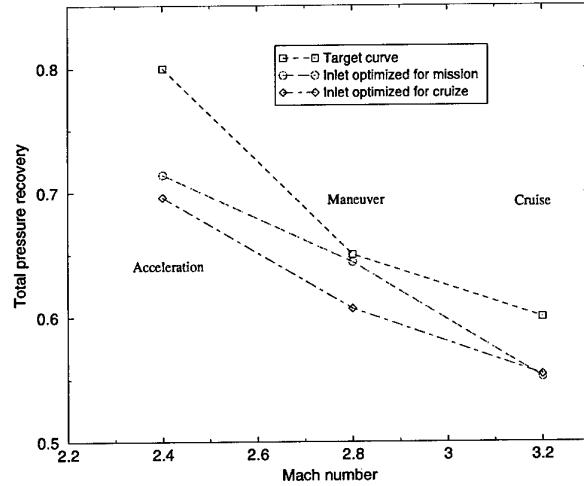
Fig. 12   Comparison between the total pressure recovery achieved by both optima over the three mission stages

Opti. Inlet	Accele.	Cruise	Maneu.
For cruise	0.696	0.554	0.607
For mission	0.714	0.552	0.644
Discrepency	2.6%	0.4%	6.1%

Table 8   Total Pressure recovery of the two optimal inlet designs for the different mission stages, estimated with 2ES3D

Figures 9 and 11 show that the two optimized inlet designs are very close the one to the other. The main difference occurs on the cowl shape for which an enlarged view is shown in Figure 13. This proves the importance of the precision with which the inlet cowl is defined, demonstrating the benefits of a finely parametrized shape of the cowl.

···· Optimal shape for mission

— Optimal shape for cruise
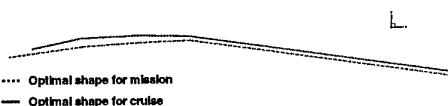
Fig. 13   Comparison of the cowl shape of the two optimized inlets

5   Conclusion and Perspectives

An automated optimal design process, coupling a stochastic optimizer and a three dimensional simulation tool, has been developed.   A multi-flight-conditions optimization of a three-dimensional super-

sonic inlet has been successfully performed, demonstrating the benefits of taking into account the entire mission, rather than a single-flight condition. Compared to the human decision based design cycle currently used in industries, this innovative optimization strategy allows to investigate a larger number of configurations, while looking for maximum aerodynamic performance of the inlet under specific constraints. The use of artificial intelligence techniques guides the search process toward high interest regions of the design space, minimizing the number of computations required to reach a high performance level. The results of the optimizations performed during this study indicate that automated optimal design strategies are very well suited to this kind of critical design problems.

The optimization process presented in this paper has reached the point where industrial application can now be envisaged. The simulation part can address the highly three-dimensional geometries of the most complex industrial problems. The physical modeling used for performance evaluation has proved to be robust and computationally efficient. Current efforts are focused on validation of the inlet designs using RANS simulations.

Acknowledgments

Statement of No Restriction

The authors declare that there is no restriction on the presentation and publication of the present paper.

References

[1] Hussaini, M. and Korte, J., "*Investigation of Low Reynolds-Number Rocket Nozzle Design Using PNS-based Optimization Procedure,*" *NASA T.M. 110295*, November 1996.

[2] Borovikov, A., Gavriliouk, V., Khokhlov, A., Lanshin, A., Sobatchkine, A., and Sokolov, V., "*Optimizing Nozzle Profiling for Orel-2-1 Transport System,*" *32nd AIAA/ASME/SAE/ASEE Joint Propulsion Conference*, July 1996, AIAA-96-2685.

[3] Zha, G., Smith, D., Schwabacher, M., Rasheed, K., Gelsey, A., and Knight, D., "*High Performance Supersonic Missile Inlet Design Using Automated Optimization,*" *6th AIAA/NASA/ISSMO Symposium on Multidisciplinary Analysis and Optimization*, Sept. 4-6 1996, AIAA Paper 96-4142.

[4] Shukla, V., Gelsey, A., Schwabacher, M., Smith, D., and Knight, D., "*Automated Design Optimization for the P2 and P8 Hypersonic Inlets,*" *Journal of Aircraft*, Vol. 34, No. 2, March-April 1997, pp. 228-235.

[5] Montazel, X., Kergaravat, Y., and Blaize, M., "*Navier-Stokes Simulation Methodology for Supersonic Missiles Inlets,*" *13th ISABE*, Sept. 7-12 1997, AIAA-97-3147.

[6] Fisher, S., "*Internal Performance of a Variable Ramp Mixed Compression Intake at Mach 3.05,*" Tech. rep., Department of Defence, Commonwealth of Australia, 1985, Aero Propulsion Report 167.

[7] Fisher, S., "*Three-dimensional Flow Effect in a Two-dimensional Air Intake with Mixed Supersonic Compression,*" *ISABE*, 1985, ISABE 85-7010.

[8] Carrier, G., Bourdeau, C., Knight, D., and Rasheed, K., "*Three Dimensional Optimization of Supersonic Inlets,*" *35th AIAA/ASME/SAE/ASEE Joint Propulsion Conference and Exhibit*, June 20-23 1999, AIAA Paper 99-2108.

[9] Rasheed, K., *GADO : A Genetic Algorithm for Continuous Design Optimization*, Ph.D. thesis, Department of Computer Science, Rutgers University, January 1998.

[10] Blaize, M. and Knight, D., "*Automated Optimization of Two-Dimensional High Speed Missile Inlets,*" *36th AIAA Aerospace Sciences Meeting*, January 1998, AIAA Paper 98-0950.

[11] Blaize, M., Knight, D., Rasheed, K., and Kergaravat, Y., "*Optimal Missile Inlet Design by Means of Automated Numerical Optimization,*" 82nd AGARD Fluid Dynamics Panel Symposium on Missile Aerodynamics, 1998.

[12] Bourdeau, C., Blaize, M., and Knight, D., "*Performance Analysis for an Automated Optimal Design of High Speed Missile Inlets,*" *37th AIAA Aerospace Science Meeting*, January 11-14 1999, AIAA Paper 99-0611.

[13] Aerosoft, Inc., "*$\mathcal{GASP}$*, General Aerodynamic Simulation Program Version 3 User's Manual," Aerosoft, Inc., May 1996.

[14] Aerosoft, Inc., "*$\mathcal{GASP}$* Version 3.2, The General Aerodynamic Simulation Program, User's Manual Addendum," Aerosoft, Inc., Feb. 1998.

[15] Kline, S., Abbott, D., and Fox, R., "*Optimum Design of Straight-Walled Diffusers,*" *Journal of Basic Engineering*, September 1959, pp. 321-331.

[16] Childs, R. and Ferziger, J., "*A Computational Method for Subsonic Compressible Flow in Diffusers,*" *21th AIAA Aerospace Sciences Meeting*, January 10-13 1983, AIAA Paper 83-0505.

[17] Johnston, J., "*Diffuser Design and Performance Analysis by Unified Integral Methods,*" *33rd AIAA/ASME/SAE/ASEE Joint Propulsion Conference and Exhibit*, July 6-9 1997, AIAA Paper 97-2733.

[18] Blaize, M., *Automated Optimization Loop for Two-Dimensional High Speed Inlet ver 5.6*, Aerospatiales Missiles, 1998.

[19] Blaize, M., "*Validation of a Hybrid Methodology To Estimate High Speed Inlet Performance,*" Aerospatiales Missiles, 1998.

DISCUSSION

Session IV, Paper #30

Prof J Hauser (CLE, Germany) asked what advantage there was using Genetic Algorithm rather than Simulated Annealing.

> **Prof Knight** suggested that GAs were more robust in that they did not depend on a valid initial configuration whereas simulated annealing can be sensitive to the initial "temperature", the proper setting of which is experience dependent.

Prof Hauser asked whether the GA could be accelerated by combining it with a deterministic method.

> **Prof Knight** believed that a GA in its later stages of evolution demonstrates some kind of deterministic behaviour, although in general quadratic convergence is not achieved.

Inlet / Body Integration Preliminary Design

for

Supersonic Air-Breathing Missiles Using Automated Multi-Disciplinary Optimization

Yan Kergaravat [*], Eric Vives [#]
Numerical Simulation Department
Aerospatiale Matra Missiles
2 Rue Béranger - B. P. 84
92323 Châtillon CEDEX - France

Doyle Knight [‡]
Department of Mechanical and Aerospace Engineering
Rutgers University - The State University of New Jersey
98 Brett Road - Piscataway
New Jersey 08854-8058 - U.S.A.

Abstract

In order to reduce the design cycle time and cost and to improve the multi-disciplinary interactions at the preliminary design stage of supersonic air-breathing missiles, an automated optimization method has been developed for inlet/body integration in a concurrent engineering environment. Three disciplines of higher relevance have been considered for the *shape* optimization problem: propulsion, aerodynamics and electromagnetics. This paper describes the numerical method, which incorporates a genetic algorithm and three analysis modules into the optimization loop. The parametric model of the generic missile is presented. The optimization problem is defined and solved for a given mission and set of specifications. The problem is addressed in three phases corresponding to an increasing number of concurrent disciplines. This progression enables to emphasize the conflicting goals between the disciplines and to understand how the optimizer yields the best compromises. This preliminary study shows interesting results and strong potential for future development and industrial applications.

* Aerospatiale Matra Missiles Engineer.
# Engineer Intern at Aerospatiale Matra Missiles.
‡ Professor, AIAA Associate Fellow.

1 INTRODUCTION

The main function of the inlet is to provide the engine with airflow at the necessary rate with the highest possible total pressure recovery and the lowest possible flow distortion, external drag and weight [1]. It is relatively easy to meet these objectives for a single Mach number in a uniform flow at a low angle of attack. However, it is a much more challenging task when the fixed geometry inlet must be operated in a forebody flowfield at angles of attack with sideslip and over a range of freestream Mach numbers. Moreover, missile inlets and fairings are generally responsible for a significant part of the overall lift, drag and radar signature of the vehicle. According to A. N. Thomas Jr. [1] "...the need to establish the independent missile variables as early as possible in the inlet design process cannot be overemphasized. Numerous iterations of the inlet design are to be expected because it must be carefully integrated into the engine and vehicle to achieve maximum performance". Fig. 1 gives an overview of the different fields and related constraints involved in this highly multi-disciplinary design problem. This paper presents a new approach to deal with this critical issue in a more efficient way at the preliminary design stage using traditional engineering methods combined with artificial intelligence.

Aerospatiale Matra Missiles and Rutgers University have been working together for several years in the field of shape optimization for supersonic inlet systems [2, 3, 4]. One of the ultimate goals of this collaborative research is the development of an automated methodology for the detailed design of inlets considering the whole mission and all the necessary constraints. The detailed design requires a high level of accuracy for the geometry representation and the performance evaluation. In turn, accurate performance predictions of the exact geometry necessitate sophisticated numerical codes and refined spatial discretizations which are generally expensive in terms of computational time. It is well known that in order to solve such a multidisciplinary problem, computational power still has to increase by several orders of magnitude [5]. Other areas of necessary improvements are optimization formulation [6], advanced approximation methods [7] and multi-level physical modeling and geometry handling [8] [11]. The challenge is schematically represented in Fig. 2 [5]. The horizontal axis gives the number of concurrent disciplines. The vertical axis gives the level of numerical analysis accuracy. And the third axis gives the level of fidelity of the geometrical representation. The ultimate objective is symbolized by the red dot but as said previously, it is not yet accessible. The question is how to get there. The development strategy followed by Aerospatiale Matra Missiles and Rutgers University is threefold. The three development directions are depicted in Fig. 2 by a blue arrow. This paper presents part of the research effort which corresponds to the horizontal blue arrow. The emphasis is on integrating several disciplines into one optimization loop using approximate 2-D/3-D geometrical models and low accuracy physical analysis models.

The global problem we propose to solve in this paper is the following: find the optimum inlet design for a generic ramjet-powered missile and a set of mission specifications. The meaning of *optimum* will be defined in the subsequent sections. Because we intend to focus on the definition of the shape of the missile and inlet, three disciplines have been chosen (shaded ellipses in Fig. 1): aerodynamics, propulsion and electromagnetics. Although these disciplines do not constitute the entire space of design (structures, heat transfer, controls should also be considered) they represent the key conflicting goals. In the following sections, first the missile parametric model is defined. Second, the computational tools are described. Then the results are presented in three phases with an increasing number of concurrent disciplines and mission requirements. The difficulties and benefits of the methodology are discussed.

2 PARAMETRIC MODEL

2.1 Conceptual Model

There is one conceptual configuration for the geometric model of the generic missile. The body is made of a classical ogive/cylinder combination. The missile is equipped with 2 two-dimensional inlets and fairings and 4 fins. A view of the generic missile is given in Fig. 3. The sizes and the locations of the different components are variable parameters. To fully define one configuration, 33 parameters have to be specified. Since the investigated problem is the integration of the inlets to an existing generic missile, it has been chosen to freeze the parameters which are related to the body and fins and to keep variable the parameters which control the external and internal shape and position of the inlets and fairings.

2.2 Fixed Parameters

The fixed parameters, which define the generic missile, are shown in Fig. 4. They are defined in Table 1. The four fins have a root chord and span of 1 caliber. Their planform and position are given in Fig. 4. The ogive is of sharp parabolic type. The ramjet engine of the missile is also assumed to be fixed which has two important consequences. First, the exit location of the inlet subsonic diffuser is fixed. Second, the propulsive performance of the missile can be assessed through the aerodynamic performance of the inlets (total pressure recovery and capture area ratio).

Parameter	Name	Value
1	Missile diameter (caliber)	1 D
2	Base diameter	0.8 D
3	Missile length	14 D
4	Ogive length	2 D
5	Fin longitudinal position	13 D
6	Fin root chord	1 D
7	Fin span	1 D
8	Fin angular position	45 deg.
9	Fin leading edge sweep angle	30 deg.
10	Boattail ending position	14 D
11	Inlet diffuser exit position	11 D

Table 1. Fixed parameters

2.3 Variable Parameters

The 22 variable parameters are shown in Fig. 5. These parameters specify the external and internal shape of the inlets and fairings and their position along and around the missile. The aft parts of the

inlet fairings incorporate boattails. The supersonic diffuser is made of 3 compression ramps and 3 cowl internal ramps. The external part of the cowl is made of a single ramp. The subsonic diffuser is a simple diverging duct with two slopes. The 22 design parameters defined in Fig. 5 are the variables of the automated optimization loop. Each variable parameter belongs to an interval, which is user-defined as shown in Table 2 below.

Variable	Minimum value	Maximum value
V1	90 deg.	160 deg.
V2	5 D	9 D
V3	11 D	13 D
V4	0.7 D	1.5 D
V5	0.5 D	1.3 D
V6	0.6 D	1.45 D
V7	4 D	9 D
V8	0.01 D	1 D
V9	0 deg.	10 deg.
V10	0.01 D	1 D
V11	0 deg.	20 deg.
V12	0.01 D	1 D
V13	0 deg.	30 deg.
V14	0 deg.	15 deg.
V15	0 deg.	13 deg.
V16	0 deg.	10 deg.
V17	0 deg.	10 deg.
V18	0 D	0.5 D
V19	0 D	0.5 D
V20	0 D	0.5 D
V21	0.01 D	3 D
V22	0 deg.	15 deg.

Table 2. Variable parameters

3 OPTIMIZATION LOOP

3.1 Overview

The automated optimization method is essentially a loop combining different tools. An overview of the optimization loop architecture is shown in Fig. 6. The main program is the optimizer GADO. It centralizes the information yielded by the analysis codes and directs the optimization process. The optimizer is a modified version of the genetic algorithm called GADO (acronym for Genetic Algorithm for Design Optimization) which has been developed at Rutgers University [9]. The engineering modules have been developed at Aerospa-

tiale Matra Missiles. The modified genetic algorithm and the analysis codes are presented in the following sections.

3.2 Genetic Algorithm

Genetic Algorithms are search algorithms which mimic the behavior of natural selection to solve given problems [10]. These algorithms first generate a random collection (population) of potential solutions (individuals or candidates). Using mutations and recombinations (crossover operations), they evolve the population towards better solutions, as individuals become adapted to the problem faced. GADO belongs to this same class of optimizers. Compared to classical GAs, GADO has several improvements that have proved to increase the accuracy, speed and reliability of the search process. Further information can be found in [9].

A recent development has been added to GADO at Aerospatiale Matra Missiles, which enables to handle several objectives at the same time. Preliminary runs of the loop had shown that a single objective optimizer was not adequate to treat the multidisciplinary problem. Of course, it is possible to combine different objectives into one function to minimize (or maximize). But it introduces a comparison between measures of merit that cannot necessarily be compared physically (for example, the missile radar cross section and the inlet total pressure recovery). Thus, it was decided to treat each discipline independently. This introduces a difficulty in the ranking process within the optimizer since one design can be better than another one in one discipline and worse in the others. To overcome this issue, the Pareto ranking was used [12] [13] in which an individual is better than another one if all its objective functions are better. The result of this ranking process is the constitution of one family of designs at the end of the optimization in which no individual can be dominated by any other. The main interest of this method lies in the choice of designs which remains at the end of the optimization. The engineer has the possibility to understand afterwards the mechanisms which control the improvements in this or that discipline and to select the final design from a population of good designs.

3.3 Propulsion Code (Internal Aerodynamics)

The analysis code for propulsion performance evaluation is called OCEAS. It computes the total pressure recovery and the capture area ratio of the inlet. The code is based on 2-D analytical methods. The shocks are computed with the Rankine-Hugoniot formula. The expansion fans are modeled with a single Prandtl-Meyer wave chosen to

ensure mass flow conservativity. The influence of the forebody flowfield is given as an input to the code through a table. The viscous losses in the subsonic diffuser are estimated with a one-dimensional semi-empirical code called DIFSUB associated with OCEAS. The typical CPU time needed for one performance evaluation is equal to two seconds with an SGI R10000 processor.

3.4 Aerodynamics Code (External Aerodynamics)

The aerodynamics module called AERO is a 3-D semi-empirical tool. It computes the aerodynamic characteristics of the missile airframe. The lift and drag are estimated through the normal and axial coefficients respectively. The stability of the missile can be evaluated by comparing the position of the center of pressure relative to the position of the center of gravity (static margin). The code combines analytical, semi-empirical methods and database correlations. The computational method is based on the concept of equivalent angle of attack. The vorticity effects are accounted for. The drag of the inlets and fairings is decomposed into pressure and friction drag contributions. Each contribution is evaluated with a specific relevant method. The typical CPU time for one evaluation is one second with an SGI R10000 processor.

3.5 Electromagnetics Code

The electromagnetics code called FIEL2D computes the radar signature of 2-D inlet configurations. The code solves the exact Maxwell equations with a finite element method ignoring the gradients in the third direction. The 2-D geometrical model is extracted from the general missile model and contains the inlet duct. The missile is supposed to be made of perfect electric conducting material. The analysis is limited to monostatic scattering. The measure of merit used to characterize the radar signature is the average for several frequencies of the maximum computed radar cross section over a range of monostatic angles for both the transverse electric (TE) and transverse magnetic (TM) polarizations. The CPU cost for one frequency and one angle is less than one second with an SGI R10000 processor.

3.6 Summary

To summarize, there is a total of 6 measures of merit (Table 3) that can be computed for each missile configuration with the three analysis codes: the total pressure recovery, the capture area ratio, the normal force coefficient, the axial force coefficient, the static margin, and the radar signature. The notations corresponding to Table 3 are given at the end of the paper. Each of these can be treated in

the optimization process either as a constraint (a certain level must be obtained) or as an objective (minimum or maximum search) or it can be deactivated (the discipline is not taken into account). The fitness function (Fig. 6) is a vector of the penalty function and several objective functions (depending on the number of disciplines involved). The penalty function is proportional to geometrical and physical constraint violations. The objective functions which will be the focus of this study are: maximize the inlet total pressure recovery, minimize the missile drag and minimize the inlet radar cross section.

Discipline	Symbol
Propulsion	$\eta_{02} = Pt_2 / Pt_0$
	$\varepsilon = A_0 / A_C$
Aerodynamics	$C_N = N / (\rho_0 V_0^2 S_R / 2)$
	$C_A = D / (\rho_0 V_0^2 S_R / 2)$
	$\Delta s = Xcp - Xcg$
Electromagnetics	$\sigma = \lim_{R \to \infty} 4\pi R^2 \, |E_s|^2 / |E_0|^2$

Table 3. Measures of merit

4 RESULTS

4.1 Mission Specifications

The generic missile flight mission has been modeled with 5 flight conditions presented in Fig. 7. These conditions are representative of a typical ramjet-powered missile mission with an acceleration phase (between t1 and t3), a cruise phase (between t3 and t4) and a maneuver phase (between t4 and t5). These conditions are used for the propulsion and aerodynamic evaluations. The radar signature is estimated for the frequency and bearing domains given in Table 4 below.

Parameter	Range
Frequency	2 - 6 GHz
Bearing	- 45, + 45 deg.

Table 4. Radar signature analysis domain

The general objective of the study is to integrate two square inlets to the generic missile in the best possible way in order to maximize the total pressure recovery and minimize the drag and radar signature. The optimum designs must also satisfy constraints on the inlet capture area ratio, the lift of the missile and its stability. To understand how the design is optimized, the study is performed in three phases (called cases 1, 2 and 3). Case 1 corresponds to the optimization of the inlet from the

propulsion point of view. The aerodynamics and the radar signature of the missile are not taken into account (the disciplines are deactivated). This case should yield the best possible propulsive performance but the multi-disciplinary integration should be poor. The second case corresponds to the integration of the inlet to the missile considering both propulsion and aerodynamics. The radar signature is not taken into account. The result should be a lower performance in propulsion but a lower drag as well. Finally, the third case brings together the three disciplines and should give the best compromise. A summary of the three test cases is given in Table 5 below. The constrained measures of merit must satisfy inequalities that will be specified in the description of each test case.

Case	Discipline(s)	Objective(s)	Constraint(s)
1	Propulsion	maximize η_{02}	ε
2	Propulsion	maximize η_{02}	ε
	Aerodynamics	minimize C_A	Δs, C_N
3	Propulsion	maximize η_{02}	ε
	Aerodynamics	minimize C_A	Δs, C_N
	Electromagnetics	minimize σ	

Table 5. Description of the three test cases

4.2 Case 1

The objective of this test case is to obtain the best possible inlet from the propulsion point of view. The aerodynamics and electromagnetics codes are deactivated.

The two measures of merit associated with propulsion are the inlet total pressure recovery and capture area ratio. The single objective is to maximize the total pressure recovery over the whole mission. The single constraint is that the capture area ratio must be greater than 0.8 for each flight condition.

The shape of the optimized inlet is given in Fig. 8 (dotted lines). The geometry is characterized by its large dimensions. The length and the width are almost maximum to allow for the highest possible amount of compression in the supersonic diffuser and a gentle subsonic diffusion. The optimizer has chosen a design Mach number of 2.6 which gives good performances for cruise and maneuver. The resulting missile is shown in Fig. 9 (top figure). The inlets are located under the missile body to benefit from the inflow pre-compression when at positive angles of attack. The resulting performances are shown in Fig. 10. The top left plot shows the total pressure recovery for each flight condition. The

bottom left plot gives the capture area ratio for each flight condition. It can be noted that the constraint is satisfied. The other measures of merit have been computed afterwards and are shown in the four remaining plots of Fig. 10. It can be seen that the resulting missile is unstable and would not have been selected in a multi-disciplinary optimization. Also the average radar signature is quite high.

4.3 Case 2

The objective of this test case is to understand how the previous design changes when external aerodynamics comes into consideration. The electromagnetic contribution is deactivated.

The two objectives are to maximize the inlet total pressure recovery and to minimize the missile drag over the whole mission. The inlet capture area ratio is constrained as before and the normal force coefficient must be higher than the threshold values given in Table 6. The stability of the missile is constrained through the static margin which must be positive and smaller than 1 D for each flight condition of the mission.

Flight condition	1	2	3	4	5
Minimum C_N	0.	1.	0.8	0.	2.

Table 6. Constraints on normal force coefficient

One optimum inlet has been chosen in the population of the best designs generated by the optimizer. The profile of the inlet is shown in Fig. 8. The design is obviously smaller than the one of case 1 which is logical. Both the length and capture area have been reduced in order to decrease both the pressure and friction drag. Also the design Mach number is smaller (2.5) which helps to reduce the spillage drag contribution during the acceleration phase. The external cowl angle is smaller too. The resulting missile is sketched in Fig. 9. The performances of this second missile are compared to the previous ones in Fig. 10. This second missile is stable (top right plot in Fig. 10) and has a low axial force coefficient (top middle plot). The radar signature has been computed afterwards and is of the same level as the one of case 1.

4.4 Case 3

The last case incorporates the three engineering disciplines. The objective is to understand how the radar signature consideration affects the aerodynamic design.

The three objectives are to maximize the inlet total pressure recovery, to minimize the missile drag

and to minimize the inlet radar signature. The constrained measures of merit are the same as in the previous case and the specified levels are unchanged.

Among the best design family, one individual has been chosen as a reasonable compromise. The inlet geometry is shown in Fig. 8. The capture area of the inlet has been further reduced in order to make the size of the cavity opening smaller in comparison to the considered wave lengths. In order to satisfy the lift constraint, the length of the inlets had to be increased even though it penalized the friction drag contribution. The smaller capture height prevents from having a lot of compression in the supersonic diffuser which explains the loss in propulsive performance.

5 CONCLUSION

An innovative preliminary design method has been developed for the integration of inlets to supersonic air-breathing missiles. This automated method enables to take into account several essential engineering disciplines at the very beginning of the design phase in a fully concurrent way. This study has shown the strong potential of such an approach and the necessity to use a multi-objective optimizer. More work remains to be done in the development concerning the improvement of the analysis codes. In particular, 3-D extensions of the propulsion and radar signature codes would be a significant improvement.

Acknowledgments

Notations

η_{02}	Inlet total pressure recovery
ε	Inlet capture area ratio
C_N	Missile normal force coefficient
C_A	Missile axial force coefficient
Δs	Static margin
σ	Inlet radar cross section
Pt	Total pressure
A	Stream tube cross section
N	Normal force
D	Axial force
V	Velocity
ρ	Air density
S_R	Reference cross section

References

[1] A. N. Thomas Jr., "Tactical Missile Aerodynamics: General Topics", Chapter 7, pp 287-319, *Progress in Astronautics and Aeronautics*, Volume 141, Hemsch/Editor, 1992.

[2] M. Blaize, D. Knight, K. Rasheed, Y. Kergaravat, "Optimal Missile Inlet Design by means of Automated Numerical Optimization", *RTO/AVT Symposium on Missile Aerodynamics*, Sorrento, Italy, May 11-14, 1998.

[3] M. Blaize, D. Knight, "Automated Optimization of Two-Dimensional High Speed Missile Inlets", AIAA Paper 98-0950, *36th AIAA Aerospace Sciences Meeting and Exhibit*, 1998.

[4] M. Blaize, C. Bourdeau, K. Rasheed, D. Knight, "Three-Dimensional Optimization of Supersonic Inlets", submitted to the *35th AIAA/ASME/SAE/ASEE Joint Propulsion Conference*, June 1999.

[5] P. Kutler, "Multidisciplinary Computational Aerosciences", NASA Technical Memorandum 103946, Ames Research Center, June 1992.

[6] E. J. Cramer, J. E. Dennis Jr., P. D. Frank, R. M. Lewis, G. R. Shubin, "Problem Formulation for Multidisciplinary Optimization", Vol. 4, No. 4, pp 754-776, *SIAM Journal Optimization*, November 1994.

[7] J. J. Korte, R. P. Weston, T. A. Zang, "Multidisciplinary Optimization Methods for Preliminary Design", Paper C-40, *AGARD Interpanel (FDP&PEP) Symposium on Future Aerospace Technology in the Service of the Alliance*, April 1997.

[8] J. L. Hunt, C. R. McClinton, "Scramjet Engine/Airframe Integration Methodology", Paper C-35, *AGARD Interpanel (FDP&PEP) Symposium on Future Aerospace Technology in the Service of the Alliance*, April 1997.

[9] K. Rasheed, "GADO: a Genetic Algorithm for Continuous Design Optimization", *Ph. D. Thesis*, Department of Computer Science, Rutgers University, January 1998.

[10] D. Whitley, "A Genetic Algorithm Tutorial", *Technical Report CS-93-103*, Department of Computer Science, Colorado State University, November 1993.

[11] Y. Kergaravat, "Design Optimization of Supersonic Air-Breathing Missiles", 1999 Summer Institute Synthesis Report, Center for Computational Design, Rutgers University, 1999.
http://www.cs.rutgers.edu/CCD

[12] D. E. Goldberg, "Algorithmes Génétiques, Exploration, Optimisation et Apprentissage Automatique", Chapitre 5, Addison-Wesley, 1992.

[13] S. Obayashi, "Pareto Genetic Algorithm for Aerodynamic Design using the Navier-Stokes Equations", Chapter 15, Genetic Algorithm and Evolution Strategies in Engineering and Computer Science, 1998.
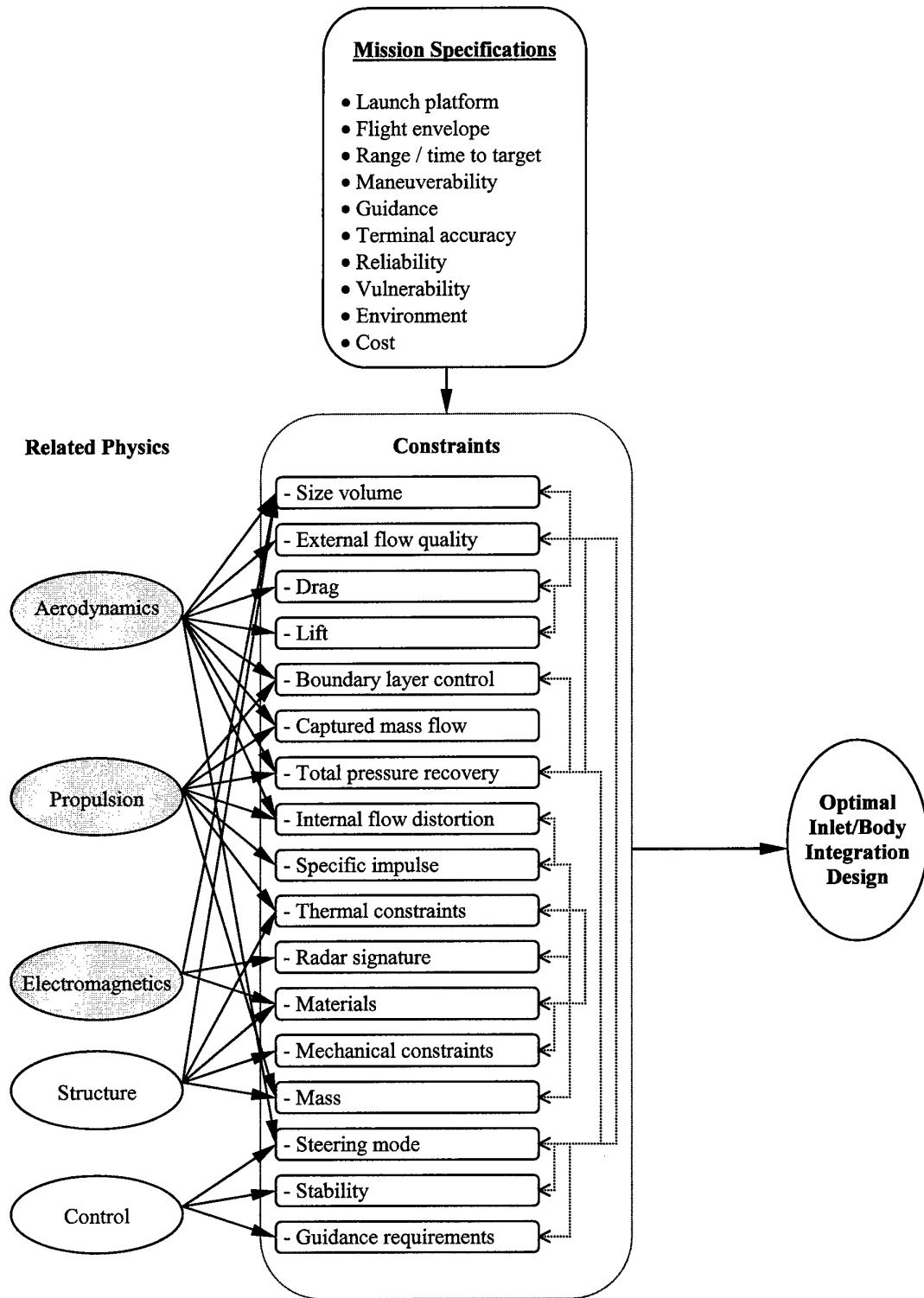
Figure 1. Inlet / missile integration design
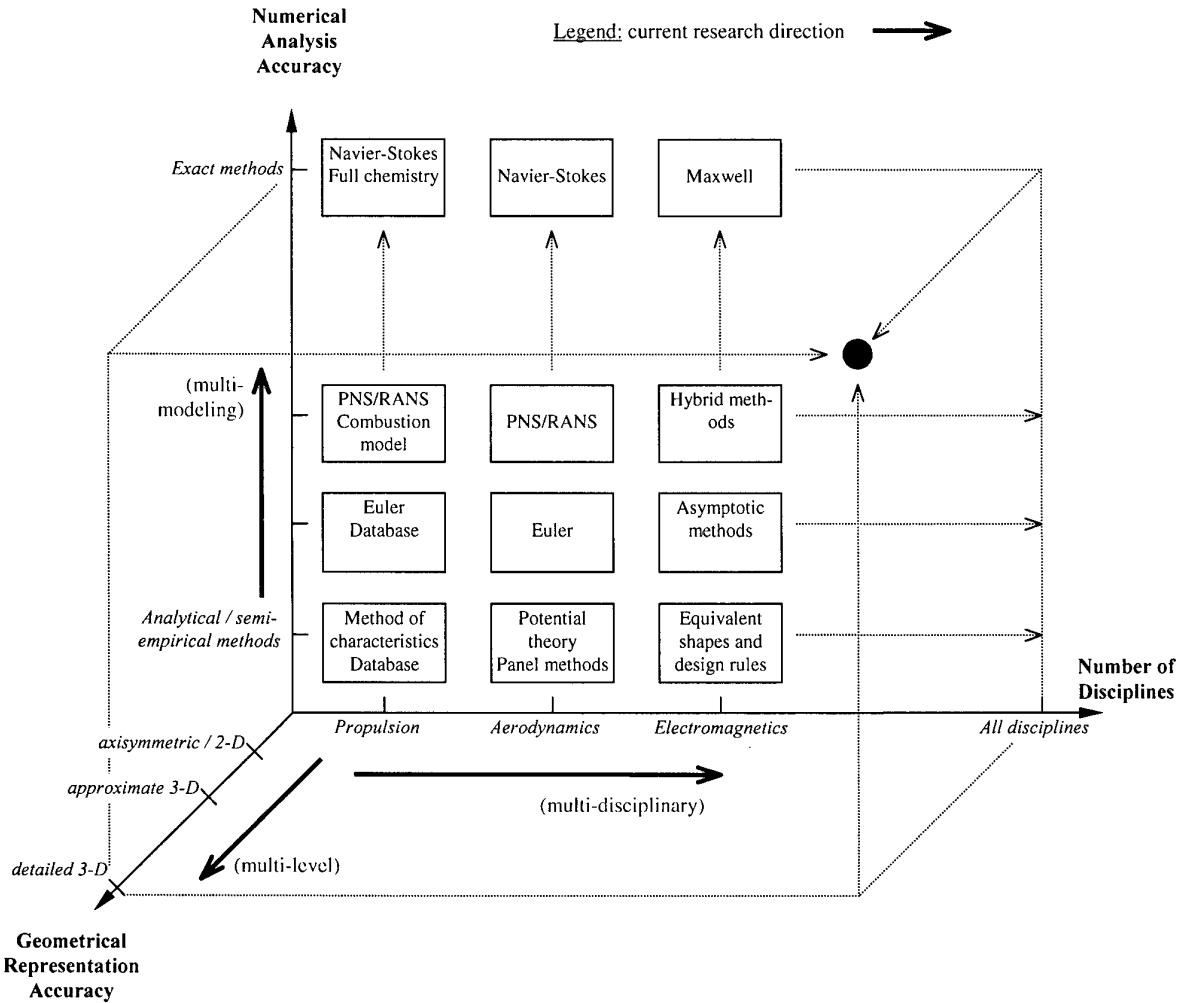
Figure 2. Development directions in the research space for inlet / missile integration optimization
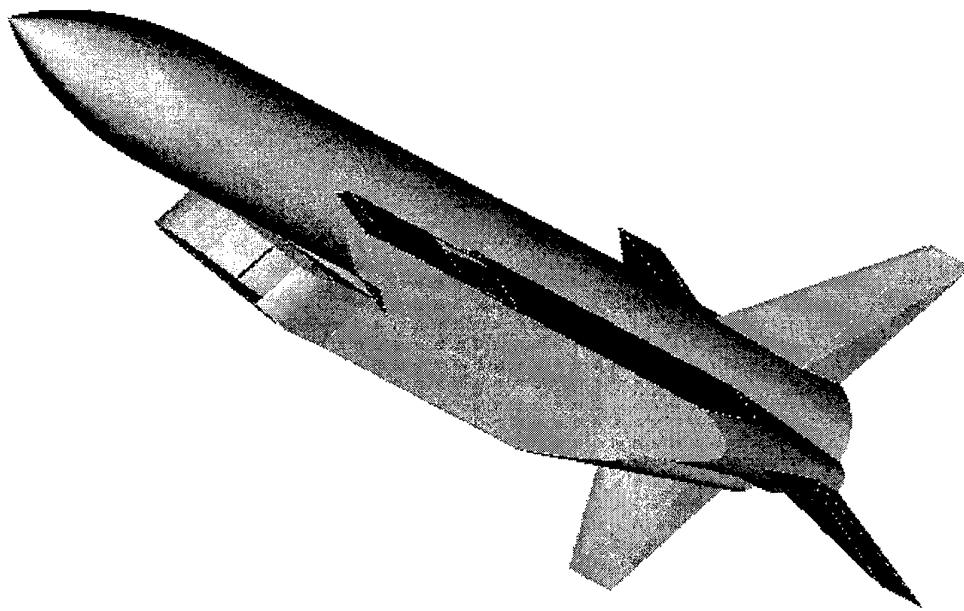
Figure 3. Generic supersonic air-breathing missile
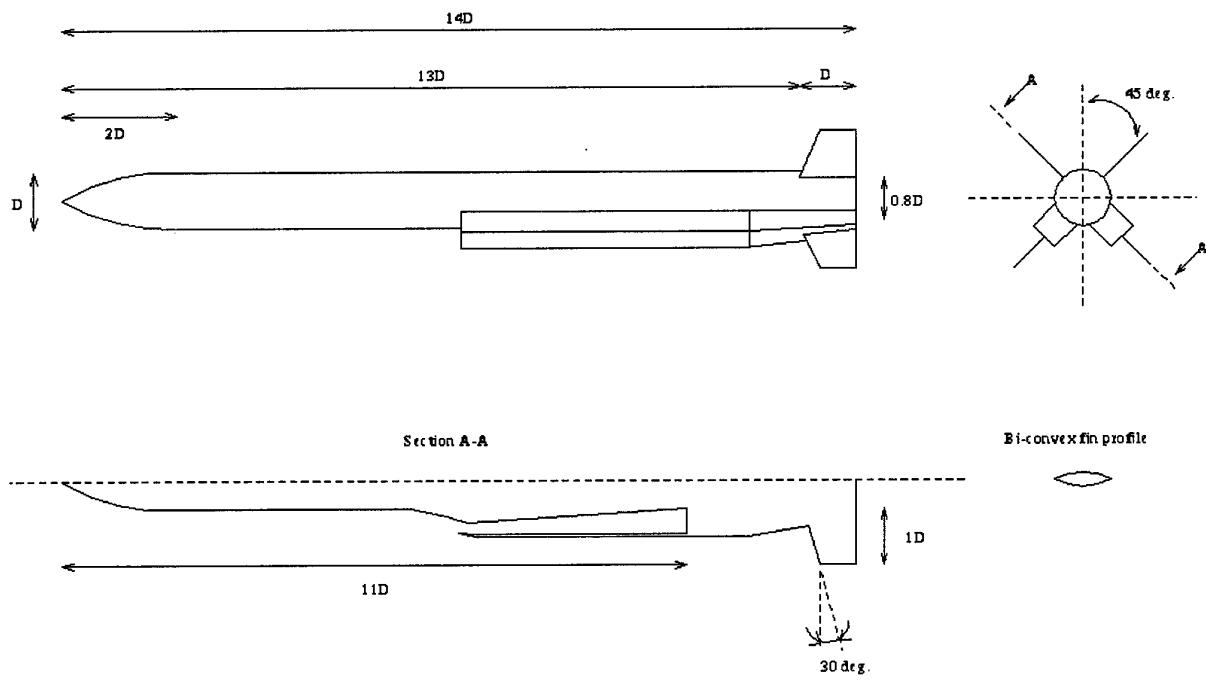
Figure 4. Missile parametric model – Fixed parameters
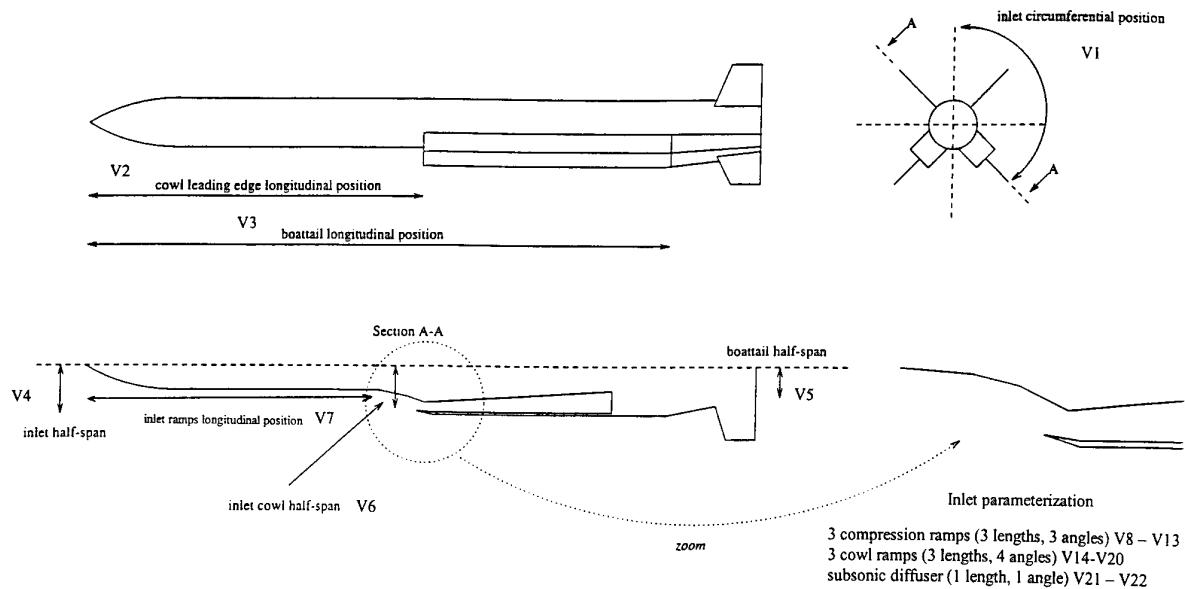
Figure 5. Missile parametric model – Variable parameters
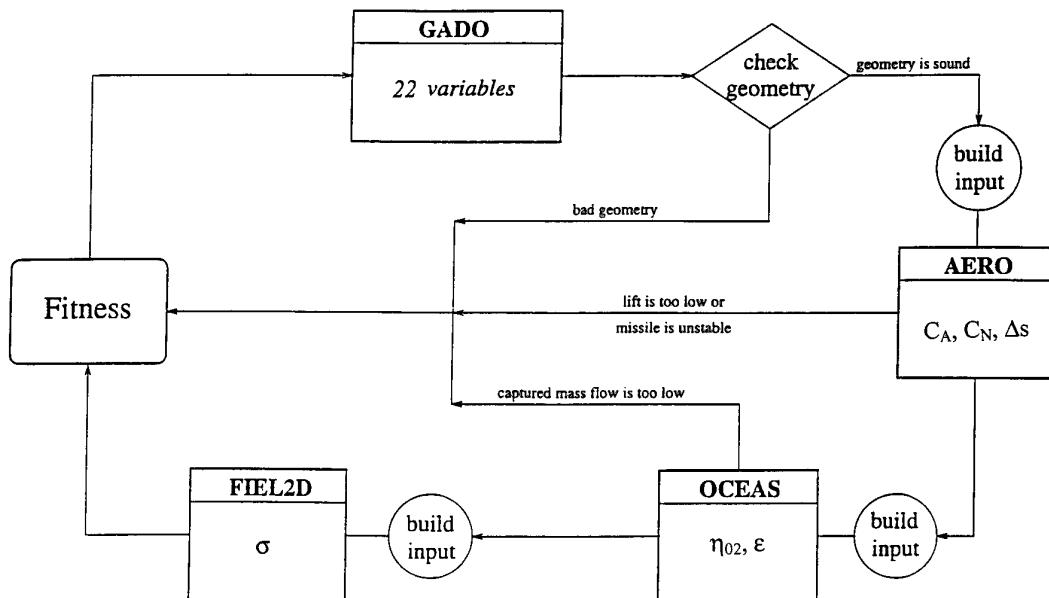
Figure 6. Optimization loop architecture
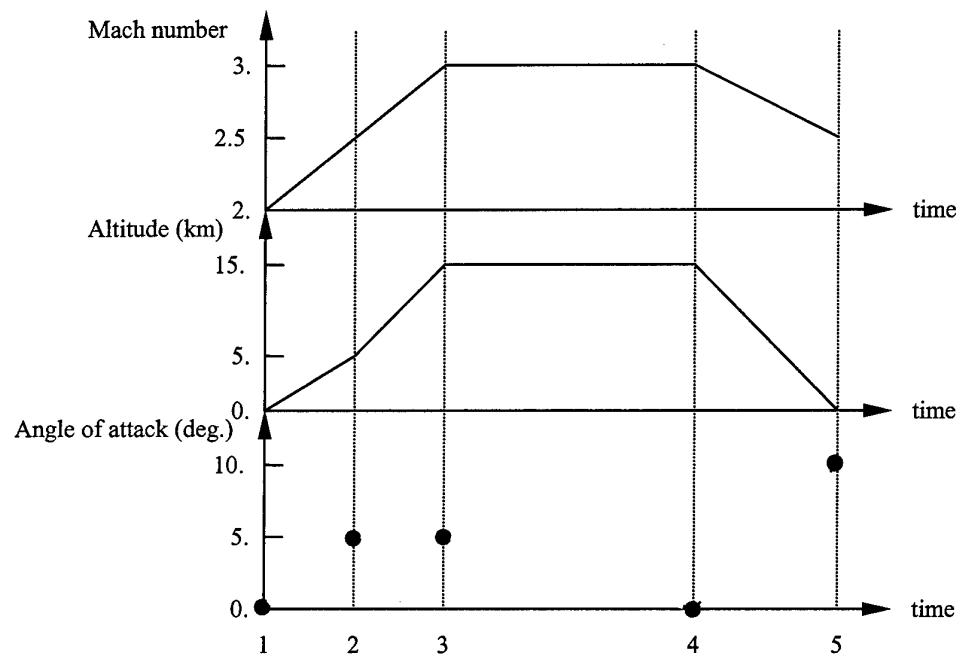
Figure 7. Mission trajectory
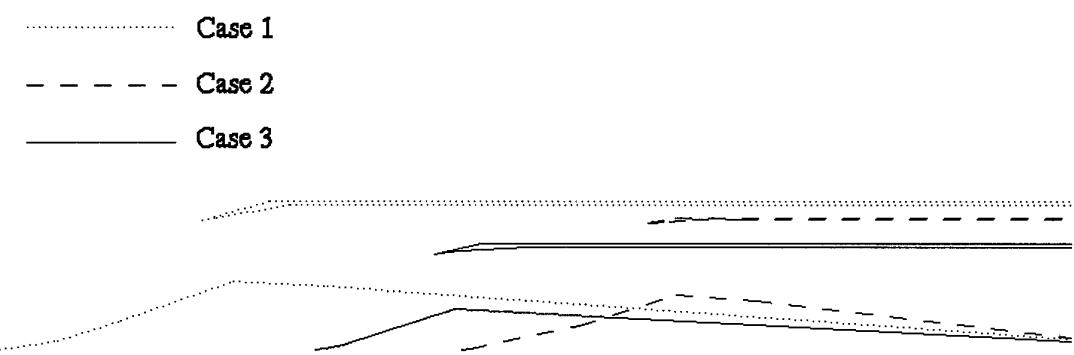
Figure 8. Shape of optimized inlets
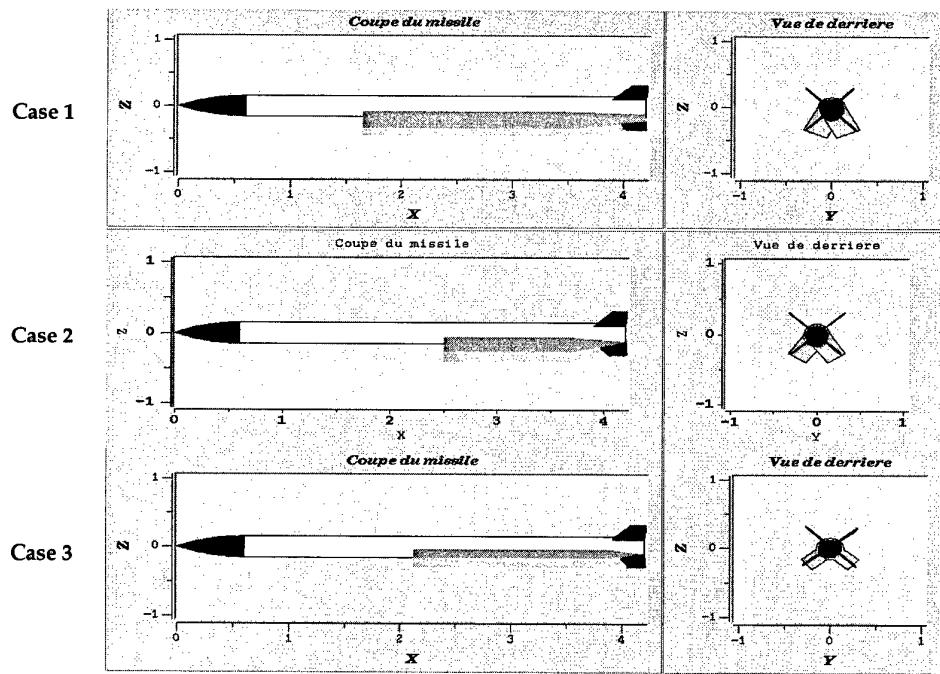
Figure 9. Optimized missile designs
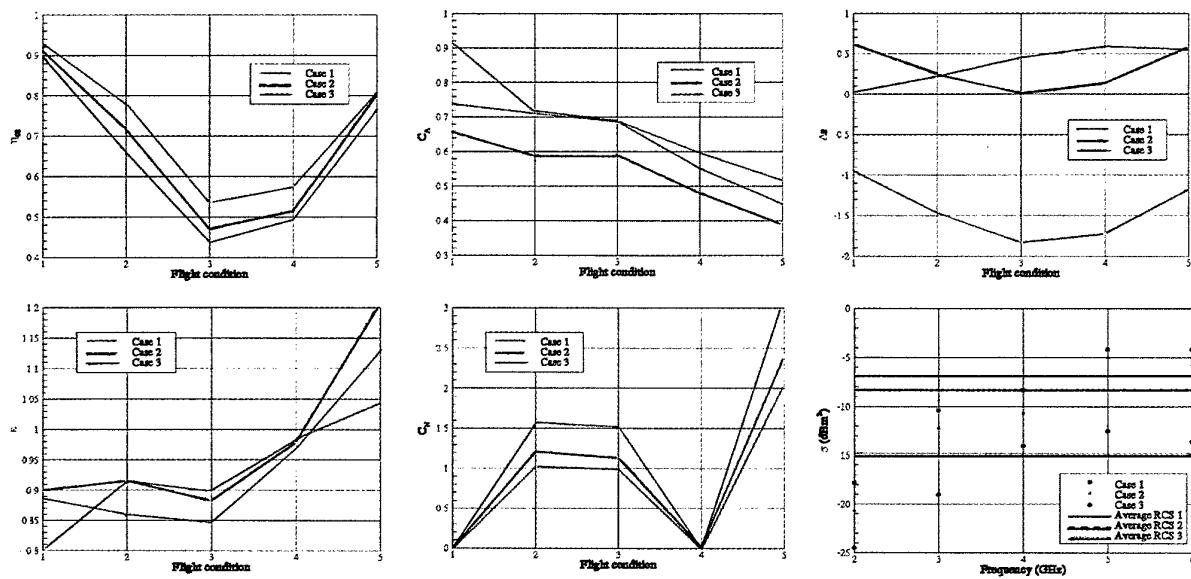
Figure 10. Performances

Development of X-33/X-34 Aerothermodynamic Data Bases: Lessons Learned and Future Enhancements

(October 1999)

C. G. Miller
NASA Langley Research Center
Mail Stop 408A
Hampton, VA 23681-2199
USA

Summary: A synoptic of programmatic and technical lessons learned in the development of aerothermodynamic data bases for the X-33 and X-34 programs is presented in general terms and from the perspective of the NASA Langley Research Center Aerothermodynamics Branch. The format used is that of the "aerothermodynamic chain," the links of which are personnel, facilities, models/test articles, instrumentation, test techniques, and computational fluid dynamics (CFD). Because the aerodynamic data bases upon which the X-33 and X-34 vehicles will fly are almost exclusively from wind tunnel testing, as opposed to CFD, the primary focus of the lessons learned is on ground-based testing. The period corresponding to the development of X-33 and X-34 aerothermodynamic data bases was challenging, since a number of other such programs (e.g., X-38, X-43) competed for resources at a time of downsizing of personnel, facilities, etc., outsourcing, and role changes as NASA Centers served as subcontractors to industry. The impact of this changing environment is embedded in the lessons learned. From a technical perspective, the relatively long times to design and fabricate metallic force and moment models, delays in delivery of models, and a lack of quality assurance to determine the fidelity of model outer mold lines (OML) prior to wind tunnel testing had a major negative impact on the programs. On the positive side, the application of phosphor thermography to obtain global, quantitative heating distributions on rapidly fabricated ceramic models revolutionized the aerothermodynamic optimization of vehicle OMLs, control surfaces, etc. Vehicle designers were provided with aeroheating information prior to, or in conjunction with, aerodynamic information early in the program, thereby allowing trades to be made with both sets of input; in the past only aerodynamic data were available as input. Programmatically, failure to include transonic aerodynamic wind tunnel tests early in the assessment phase led to delays in the optimization phase, as OMLs required modification to provide adequate transonic aerodynamic performance without sacrificing subsonic and hypersonic performance. Funding schedules for industry, based on technical milestones, also presented challenges to aerothermodynamicists seeking optimum flying characteristics across the subsonic to hypersonic speed regimes and minimum aeroheating. This paper is concluded with a brief discussion of enhancements in ground-based testing/CFD capabilities necessary to partially/fully satisfy future requirements.

Introduction: Aerothermodynamics, defined herein as encompassing aerodynamics, aeroheating, and fluid dynamics and physical processes, is the genesis for the design, development, and flight of space transportation vehicles and is in the critical path to success for such vehicles. The aerothermodynamic challenge is to provide the optimum design (i.e., outer mold lines (OML)) to safely satisfy mission requirements including abort scenarios and to reduce design conservatism, risk, and cost; i.e., the optimum flying vehicle with minimum structural (i.e., surface pressure/shear) and heating loads, translating into reduced weight and reduced operation costs. Aerothermodynamics provides crucial information to other key disciplines such as structures, materials, including thermal protection systems (TPS), avionics, guidance, navigation and control, propulsion, etc. The three sources of aerothermodynamic information are: (1) ground-based facilities, (2) computational fluid dynamics (CFD) and/or engineering computer codes, and (3) flight experiments.

In recent years, large volumes of aerothermodynamic information have been generated at the NASA Langley Research Center (LaRC), both experimentally and computationally, in support of high-priority, fast-paced programs such as the RLV/X-33 Phase I and X-34 programs initiated in April 1995, followed a year later by X-33 Phase II, X-34 (second phase), X-38, X-43 (Hyper-X), Missions from Planet Earth (i.e., planetary exploration and Earth sample return missions), and most recently, X-37. These studies, collectively, challenged Langley's aerothermodynamic capabilities/resources. As to be expected, the work environment changed significantly due to the abrupt increase in generation of aerothermodynamic information for external customers. Demands on experimental aerothermodynamicists were especially large since the LaRC Aerothermodynamic Facilities Complex (AFC) (**Micol, 1998**), comprised of five conventional-type, blowdown-to-vacuum hypersonic wind tunnels, represents the Agency's sole source of experimental, ground-based hypersonic aerodynamic and aeroheating data. Downsizing of personnel also occurred in this period, corresponding to experienced aerothermodynamicists and facility technicians who retired, transferred, etc., generally not being replaced, and outsourcing impacted key areas of the aerothermodynamic infrastructure (**Miller, 1998**). Another change to the work environment was due to programs such as X-33 (primarily schedule driven) and X-34 (primarily cost driven) being industry led as opposed to NASA led. Schedules/milestones

established by customers failed to take full advantage of experimental and/or computational aerothermodynamic capabilities or, at the other extreme, were unrealistic in expectations. To satisfy customer milestones, which were often driven more by programmatic considerations (e.g., funding schedules) than technical issues, AFC wind tunnels were operated in a "production-like" manner, running extended/double shifts and weekends.

A review of aerothermodynamic capabilities at the NASA LaRC is provided by **Miller, 1998**. This review includes: (1) the highly iterative aerothermodynamic process for screening initial aerospace vehicle concepts, optimization of aerolines via parametric studies, and benchmark data for final design and establishment of the flight data book (**Fig. 1**); (2) aerothermodynamic methodology which translates to the synergism between ground-based testing and CFD predictions throughout entry into the Earth's atmosphere (**Figs. 2 and 3**); and (3) the resources/infrastructure required to provide accurate/credible aerothermodynamic information in a timely manner. Impacts on Langley's aerothermodynamic capabilities due to programmatic changes, downsizing, outsourcing, etc., are discussed in this review, as are sample applications of these capabilities to the X-33, X-34, X-38, and X-43 programs along with some lessons learned.

The primary purpose of the present paper is to expand upon the lessons learned presented previously by **Miller, 1998** for X-33 and X-34. Programmatic and technical lessons learned from these two programs will be presented in a general manner and will not be identified with a specific program. Many, if not most, of these lessons learned are well known and documented within the aerothermodynamic community. The present synoptic of lessons learned may prove useful for new members of the aerothermodynamic community and to engineers/scientists in other disciplines who are users of aerothermodynamic information, and may serve as a guide/reminder for future programs requiring extensive aerothermodynamic information. These lessons learned are from the perspective of the Aerothermodynamics Branch (AB) of the LaRC, which served as a subcontractor to industry via formal task agreements. (For the convenience of readers, recent publications by the Aerothermodynamics Branch on X-33 and X-34 are given in the "**References**.")

Lessons Learned:
Preface: The aerodynamic data bases upon which the X-33 and the X-34 will fly (i.e., the aerodynamic flight data books) are essentially exclusively from wind tunnel testing. Relatively comprehensive aerodynamic data bases across the subsonic through hypersonic speed regimes were generated for both programs via testing in a number of wind tunnels at the LaRC (e.g., Low Turbulence Pressure Tunnel (LTPT), 14- by 22-Foot Subsonic Tunnel, 16-Foot Transonic Tunnel, Unitary Plan Wind Tunnel (UPWT) Legs 1 and 2, and the hypersonic wind tunnels of the AFC), the NASA Marshall Space Flight Center (MSFC) 14- by 14-Inch

Trisonic Wind Tunnel, and several industry subsonic-to-supersonic wind tunnels. The role of CFD in the generation of X-33 and X-34 aerodynamic data bases was complementary in nature. There are two primary reasons for the dominance of wind tunnel testing over CFD for these programs. Once models and associated hardware are available, wind tunnels provide huge quantities of aerodynamic performance information over wide ranges of attitude (alpha, beta), control surface deflections, individually and in combination, and flow conditions in a relatively short period of time and with a high degree of credibility based on decades of previous experience. The second reason is available wind tunnels cover the flight regimes for the X-33 and X-34 nicely, in that the maximum flight Mach number for X-33 is expected to be around 10 and to be around 7 for the X-34. As observed from **Figs. 2 and 3**, the contribution of CFD increases significantly above Mach 10, or so, where reacting flowfields influence aerodynamic characteristics. In the generation of aeroheating data bases, CFD was an equal and synergistic partner with wind tunnel testing. Because of the major role played by wind tunnels in establishing aerothermodynamic data bases for X-33 and X-34, a significant portion of the subsequent lessons learned are associated with ground-based testing.

Lessons learned presented in this section are loosely organized based on the "aerothermodynamic chain" of **Miller, 1998** (**Fig. 4**). The links of this chain are personnel, facilities, models/test articles, instrumentation, testing techniques, and CFD. These links are universal to all aerothermodynamic activities and, again, are viewed herein from an Aerothermodynamics Branch perspective. No attempt has been made to prioritize the following lessons learned, nor to separate programmatic lessons learned from technical ones. Where deemed appropriate, recommendations are provided which are subjective and may not be universally applicable.

Personnel: To ensure a successful program from the viewpoint of flyability and survivability, it is imperative that certain groups work closely together as a true team:

(1) Experienced, senior aerothermodynamicists who have worked similar programs (e.g., Shuttle Orbiter) should be blended with junior aerothermodynamicists who have not yet learned what is impossible and are eager to learn and to try new approaches, etc. The advantages provided by such a blending have been demonstrated in numerous programs, yet this approach is not always utilized.

(2) Aerothermodynamicists and systems analysis engineers responsible for the initial vehicle concept, for applying engineering codes and interpolation procedures to populate the aerodynamic and aeroheating data bases, and for generating flight trajectories should work closely together from the beginning to the end of the program. Experienced aerothermodynamicists often will identify

deficiencies in initial concepts, thereby allowing system analysis engineers to iterate on the concept prior to its entering the aerothermodynamic process (**Fig. 1**), specifically screening and optimization. Such an exchange can save considerable time and resources. Systems analysis engineers should be involved in the development of wind tunnel test matrices and decisions relative to the output of data reduction procedures. Personnel working guidance, navigation and control (GN&C) issues should also be brought into the aerothermodynamic process early, as they are the ultimate customer for aerodynamic measurements and predictions. Likewise, designers of the thermal protection system (TPS), who are customers for aeroheating measurements and predictions, should be included.

(3) It is imperative that experimental and computational aerothermodynamicists work together from the beginning to the end of the program. The ultimate creditability of aerodynamic and aeroheating information is achieved when independently performed wind tunnel measurements and CFD predictions for wind tunnel cases are compared and found to be in excellent agreement over a range of attitude and flow conditions. Wind tunnel measurements and CFD predictions are highly complementary and together provide accurate aerothermodynamic information throughout the flight trajectory; i.e., across the subsonic to hypersonic regimes. There is a tendency of computationalists to bypass comparing CFD predictions to wind tunnel measurements and to apply CFD only to flight conditions. This bypass should be avoided for reasons discussed previously. In one of the subject programs, an aerothermodynamicist capable of performing both high level experimental work and high level computational (via CFD) work proved to be extremely valuable. Knowledge of the strengths and weaknesses of both disciplines allowed the strengths to be systematically combined and optimized. This demonstration of the advantages provided by an individual having combined experimental and computational skills/capabilities has led to the ongoing development of additional aerothermodynamicists with both skills.

(4) It is important to have experimental and computational aerothermodynamicists working aerodynamic issues and those working aeroheating issues establish strong lines of communication. Often, "anomalies" observed in aerodynamic force and moment measurements can be explained by the detailed surface information achieved in experimental aeroheating studies. Detailed studies of shock-shock interactions, flow separation-reattachment phenomena, boundary layer transitions, etc., via aeroheating measurements are beneficial to aerodynamicists in explaining force and moment trends. Naturally, inputs from computationalists who generate detailed surface and flowfield information are extremely valuable in this process. Working aerodynamic and aeroheating issues together, OMLs may be varied to both enhance the aerodynamic performance and to minimize aeroheating levels.

(5) The same team of experimental aerodynamicists should test across the subsonic-to-hypersonic speed regimes, as opposed to different teams testing at subsonic, transonic, supersonic, and hypersonic conditions. The continuity and flexibility provided by a single team testing across the speed regimes is believed to outweigh the collective outputs of specialists in each regime that must be coordinated and assembled into one story.

Facilities: Typically, initial aerodynamic screening or assessment is performed in relatively low-cost, low-performance subsonic tunnels and using rapidly fabricated, inexpensive stereolithography (SLA) resin models in the unheated flow of the LaRC 22-Inch Mach 15/20 Helium Tunnel. Configuration OMLs are modified/varied in an iterative manner to provide acceptable hypersonic aerodynamic performance, generally at relatively high angles of attack, and subsonic approach and landing characteristics. Vehicle designers may be approaching closure on OMLs via this approach before testing at transonic conditions reveal significant aerodynamic performance problems. It is imperative for most all aerospace vehicle concepts that transonic aerodynamic information be obtained early in the program, such that subsonic, transonic, and hypersonic information is used concurrently in the optimization of OMLs to achieve desired flying characteristics across the entire speed regime, from high altitude hypersonic conditions to approach and landing.

In most cases, the credibility of the experimental aerodynamic data base is enhanced considerably with the simulation of flight values of Reynolds number based on appropriate full-scale vehicle dimensions. Generally, existing hypersonic wind tunnels within NASA and the United States Air Force simulate flight values of Reynolds number, for a given Mach number, and provide a sufficient Reynolds number range to produce fully laminar and equilibrium turbulent boundary layer/shear layer flow about the test article (**Miller, 1998**). However, the simulation of flight Reynolds numbers at subsonic, transonic, and low supersonic conditions is a formidable task and can be accomplished in relatively few facilities. One is the NASA National Transonic Facility (NTF) through the use of cryogenic nitrogen for the test medium. Stringent model design and fabrication requirements and facility operation costs make tests in the NTF relatively expensive and require a long lead time. The vehicle designer is confronted with a trade of reduced risk for increased time and money. As a minimum, limited tests at transonic flight values of Reynolds number on the baseline configuration are recommended to determine if the major portion of the subsonic-to-supersonic aerodynamic data base obtained at lower than flight values of Reynolds number is credible.

An alternative approach is to apply CFD to wind tunnel conditions corresponding to relatively low values of Reynolds number; and, if prediction compares well with measured aerodynamic forces and moments, apply CFD to flight values of Reynolds number to determine the aerodynamic performance. Thus, subsonic-to-low supersonic wind tunnel testing at flight values of Reynolds number or the use of CFD to extend wind tunnel conditions to flight should be used to decrease the risk level associated with the development of the aerodynamic flight data book.

In high-priority, fast-paced programs involving testing in numerous facilities to achieve a wide range of flow conditions, there is a tendency to accept facility performance without questioning nor understanding facility and associated instrumentation limitations. For example, in the case of hypersonic wind tunnels, radial and axial flow uniformity, partial flow blockage phenomena, flow particulate levels, vibrational excitation and possible departure from equilibrium, flow liquefaction, free-stream disturbance level due to particulates but primarily due to acoustic disturbances radiated from the nozzle wall boundary layer, etc., are all factors that must be understood to enhance the data credibility. It is imperative that experimental aerodynamicists, within Government and industry, understand facility and instrumentation limitations and the corresponding influences on data accuracy.

On several occasions, significant delays occurred in the reduction of data acquired in wind tunnel tests to the required form. In some cases, data transfer mechanisms/procedures between wind tunnels and customers were not compatible. Potential incompatibilities related to data transmission and receiving need to be addressed upfront and early in the planning process. Careful planning and coordination are required by experimental aerothermodynamicists to minimize/eliminate delays in data reduction.

Conflicts that occur because of competition among concurrent programs for resources such as facility occupancy, model design/fabrication, etc., are generally resolved through negotiations and compromise. In most cases, major milestones are built around freezing of OMLs, which in turn depends on testing in specific facilities at specific times. When two or more major programs request the same resources for the same time, it is important that clearly defined priorities be established by the appropriate level at the host laboratory and be provided to all involved workers to minimize confusion and dysfunctionality.

Models: The major contributor to the failure to meet wind tunnel schedules and the corresponding milestones for delivery of aerodynamic data was delays in design and fabrication of metallic force and moment models (**Fig. 5**). In Phase I of the X-33 program involving the aerodynamic assessment and optimization of three industry concepts in parallel with the X-34, all models tested in these fast-paced programs were fabricated in-

house at the LaRC and were delivered on time and within cost. This success was achieved by assigning a high priority to the X-33 and X-34 programs and the Fabrication Division operating numerical cutting machines 24-hours per day and 7 days per week. Modifications to model components to enhance aerodynamic performance were generally performed in a day or two, and often overnight. Metallic model fabrication began to be outsourced about the time that Phase II of the X-33 program was initiated. The impact of model delivery delays and the testing of models without verification of the accuracy of OMLs due to insufficient time was substantial. The time associated with fabrication of metallic models represents the major contributor to the total time to perform an experimental aerodynamic test in a wind tunnel (**Fig. 6**).

In an attempt to more rapidly obtain hypersonic aerodynamic data, ceramic force and moment models were made and tested. Ceramic models can be made in about an order of magnitude less time than stainless steel models. Although not a total success, due primarily to the lack of surface fidelity in critical aerodynamic surfaces, lack of precise determination of transfer distances, and challenges associated with precision alignment of the strain-gauge balances, preliminary findings were nevertheless encouraging. High temperature resin SLA models of the X-34 were also tested in heated hypersonic wind tunnels, again with partial success. Stainless steel continues to be the material of choice for precision force and moment models benchmark tested in the heated hypersonic wind tunnels of the AFC. Attempts to refine/enhance fabrication of ceramic and high-temperature resin force and moment models will continue in an effort to reduce the time to generate hypersonic aerodynamic information for assessment/optimization phases of the aerothermodynamic process; i.e., reduce design cycle time.

On the positive side, significant advances were made in the fabrication of precision ceramic models for aeroheating studies. One example is scaling of metallic TPS panels to simulate the bowing that will occur in the hypersonic portion of the X-33 flight trajectory (**Horvath et al., 1999**). These high fidelity models were made and tested to determine the influence of surface roughness due to panel bowing on boundary layer transition.

Instrumentation: Protecting strain-gauge balances from adverse thermal gradients during a run in the heated flow of a hypersonic wind tunnel, or accurately compensating for such gradients proved to be quite challenging. Although the balances were water cooled, heat conduction through the stainless steel walls of the model and/or along the sting/blade support and into the balance compromised accuracy. In both the LaRC 20-Inch Mach 6 Air and 31-Inch Mach 10 Air Tunnels, the force and moment models were pitched-paused and exposed to the flow from one to three minutes. Heat conduction along the sting or through the blade mount was reduced by water cooling. Balances were not actively compensated

for temperature gradients and were passively compensated only for two temperatures, namely room temperature and a temperature higher than this valve. The relatively small models offered little heat sink capacity. Minimizing the contact surface of the balance with the model provided the best protection against unacceptable temperature gradients and proved successful in most cases. Credible aerodynamic data was obtained, but only after many repeat runs, comparison of runs for which the angle of attack was increased with run time to those where alpha was decreased, soak runs where alpha was held constant for the entire run, and so forth. Needed is a fully temperature compensated strain-gauge balance and/or improved methods for balance cooling or protection of the balance from heat conduction.

On at least one occasion, differences between experimental measurements and computational predictions were attributed primarily to uncertainties in the model attitude (i.e., alpha and beta). Uncertainties in the model attitude, which is generally measured with conventional inclinometers for a no-flow case, contributed to corresponding uncertainties in aerodynamic and aeroheating trends and levels and resulted in several repeat runs having to be made. Needed is a user friendly, nonintrusive, precision method to measure model alpha and particularly beta in real time during a tunnel run (i.e., flow-on condition).

On the positive side, the Langley developed phosphor thermography technique (**Fig. 7**) was heavily utilized for the X-33, X-34, and a number of other programs and performed in an outstanding manner. This technique for measuring global, quantitative aeroheating distributions on models truly revolutionized the aerothermodynamic process and is indeed "better, faster, cheaper" than previously used techniques. (Details and capabilities of this technique are discussed by **Merski, 1999**.) One new capability with this technique is to extrapolate heating distributions measured on a model in a hypersonic wind tunnel to flight values of vehicle surface temperature (**Fig. 8**), and to do so immediately following a tunnel run. The accuracy of this extrapolation of ground-based data to flight has been substantiated with comparisons to CFD predictions for both wind tunnel conditions and flight conditions for the X-34 (**Merski, 1999**).

Testing Techniques and Procedures: All force and moment models, including those for benchmark studies, should be designed and fabricated for configuration buildup (i.e., each component attached to the basic body or fuselage may be removed and replaced with a section contoured to the basic body) as opposed to being fabricated in one piece. Models with configuration buildup capability are, naturally, required in the assessment and optimization phases of the aerothermodynamic process and should also be employed in the benchmark phase. "Theoretically OMLs are frozen prior to entering the benchmark phase in the current environment of reduced design time; but, the reality is that the OMLs generally continue to change well into benchmarking. Configuration buildup

capability allows OML changes to be more rapidly and less expensively incorporated into the model, and also contributes to addressing concerns when/if measured aerodynamic data does not follow intuition. Such a situation occurred during benchmarking of hypersonic aerodynamic performance for the X-33, whereby the forces and moments associated with body only were quickly measured and each set of components (i.e., fins, flaps, tails) added one at a time to deduce the contribution to aerodynamic characteristics (**Murphy et al., 1999**; see **Fig. 9**). Testing the same model (and strain-gauge balance(s)) in multiple hypersonic wind tunnels providing a range of normal-shock density ratio from 4 to 12 (i.e., range of ratio of specific heats within the shocklayer of the model from 1.15 to 1.67) (**Fig. 10**) provides aerodynamicists with additional insight as to the cause and effect of both geometric and flow variables.

Other than discrete surface pressure measurements made on models in support of flush air data system (FADS) development and a 0.03 scale X-33 pressure model tested in the LaRC 16-Foot Transonic Tunnel by engineers working structures problems, very few pressure measurements were performed in wind tunnels for the X-33 and X-34 programs. One reason for the dearth of pressure measurements is conventional pressure models using electronically scanned pressure (ESP) systems require a relatively long time to fabricate and are correspondingly expensive; also, lengthy setups and checkouts/shakedowns are generally required for such models. Situations did occur in the X-33 and X-34 programs when aerothermodynamicists would have benefited significantly from measured pressure distributions, particularly in comparisons of CFD predicted aerodynamic coefficients with measured values and in resolving anomalous trends or levels in these coefficients. If successfully developed and applied, nonintrusive, optical-video based, global surface pressure measurement techniques for heated and unheated wind tunnels should be utilized in future studies similar to X-33 and X-34. These techniques will be faster, better, and cheaper than conventional ESP systems and provide detailed information in critical areas on the model; e.g., in regions of shock-shock interaction, flow separation-reattachment (including the entire leeward surface), etc.

Hypersonic boundary layer transition from laminar to turbulent during descent from suborbit or orbit typically results in an increase in heating to the windward surface of the vehicle by a factor of 3 to 5. Thus, a reasonably accurate determination of flight conditions where boundary layer transition occurs is essential for most aerospace vehicles to ensure that aeroheating levels and loads remain within TPS design limits. Ideally, such information would be incorporated into the design of the TPS, including material selection, split line definition, and material thickness. Although progress has been made in developing computational techniques for predicting hypersonic boundary layer transition onset, aerothermodynamicists still rely primarily on semi-empirical methods used for the Shuttle Orbiter and other vehicles. However, these methods today enjoy the

capabilities provided by advances in computers and by the phosphor thermography technique. Accurate determination of boundary layer transition on hypersonic wind tunnel models with and without discrete trip elements over a wide range of attitude and flow conditions (primarily Reynolds number) is possible with the thermography technique. This information can be obtained quickly and inexpensively. For the X-33 program, Langley attempted to develop a boundary layer transition criteria applicable to flight. Approximately 275 runs were performed in the Langley 20-Inch Mach 6 Tunnel over a wide range of Reynolds number with ceramic aeroheating models having different discrete trip arrangements. Inviscid flowfield solutions coupled with boundary layer solutions (**Hamilton et al., 1998**) provided local conditions of interest about the model, specifically boundary layer thickness, edge Mach number, and Reynolds number based on momentum thickness at the location of the surface disturbance(s). The wind tunnel results in terms of these local flow properties were observed to correlate nicely (**Berry et al., 1999**; see **Fig. 11(a)**) and allowed a region in terms of altitude, velocity, and angle-of-attack to be predicted for which the boundary layer would be laminar at altitudes above this region, and turbulent below it (**Thompson et al., 1998**; see **Fig. 11(b)**). This boundary layer transition criteria for the X-33 has proven to be extremely valuable in tailoring trajectories so to not exceed limits on the metallic TPS yet satisfy mission requirements. The accuracy of this approach will be determined by the first flights of the X-33. If proven accurate, as expected, this approach is recommended for all aerospace vehicles expected to experience boundary layer transition near the region of peak heating during descent, and should be performed as early in the program as appropriate. (A major concern with this approach is the measurement of transition onset in a conventional-type hypersonic wind tunnel for which the freestream flow is acoustically contaminated. Freestream disturbances are expected to promote early transition on the model, hence the findings as applied to flight should be conservative. It is primarily because of these acoustic disturbances in the freestream of the wind tunnel, which result from the turbulent boundary layer on the nozzle wall, that flight measurements of transition onset are needed to substantiate this approach.)

Because of the long lead time in the design and fabrication of a force and moment model or pressure model with jets at various locations to simulate reaction control system (RCS) interactions by blowing of various gases, this important phase of the aerothermodynamic study should be initiated just prior to or immediately following the freezing of OMLs. The RCS jets should be calibrated in a vacuum chamber, model setup and shakedown is generally laborious, and there is little room for error with the flow-through five-component strain-gauge balance. Another challenge associated with RCS testing is that the effect of the RCS interaction to be measured is often on the same order of, or smaller than, the balance accuracy (as the balance must be sized for full scale model loads), or the thermal drift. The test

matrix is quite large due to the number of variables involved, hence tunnel occupancy time is substantial, and data reduction and incorporation into the flight aerodynamic data book may not be straightforward. The RCS data will enrich the aerodynamic data base via comparisons of forces and moments without blowing to those obtained with the benchmark force and moment model. An effort should be made to include diagnostics that provide insight as to the characteristics of the flow, including state of the boundary layer, approaching the jet and downstream of the jet (e.g., surface streamline patterns via oil flow, surface temperature via infrared emission, focused schlieren, etc.). Complementary CFD predictions for RCS plume, vehicle flowfield, and possibly vehicle surface interactions should be performed. The upcoming comparisons of X-33 flight results with an active RCS to CFD predictions and to wind tunnel data, including the methods used to extrapolate ground-based data to flight, should be of tremendous benefit to the aerothermodynamic community.

In the haste of performing high-priority, fast-paced aerothermodynamic studies, the general tendency is to omit complementary diagnostics to the force and moment tests and thus lose a valuable tool for explaining trends in the data that may be unexpected. Complementary diagnostics such as oil flow (**Fig. 12**), schlieren, infrared emissions, etc., should be employed whenever feasible. As noted previously, it is very beneficial for experimentalists and computationalists performing aerodynamic studies and for colleagues performing aeroheating studies to interact with one another to obtain a thorough understanding of flow characteristics (e.g., boundary layer/shear layer transition, shock-shock and shock-boundary layer interactions, flow separation and reattachment, sonic line location, etc.) about the complete vehicle.

Computational Fluid Dynamics (CFD): CFD contributed significantly to the development of aeroheating data bases for X-33 and X-34, addressed specific, localized phenomena such as shear layer impingement on the X-33 engine modules, and played a complementary role in the development of aerodynamic data bases which required full tip-to-tail solutions. Through these applications to complex configurations over wide ranges of flow conditions and attitudes, CFD capabilities increased considerably as codes were modified to enhance accuracy, increase speed, and provide new capabilities such as RCS interactions, full wake solutions, etc. Extensive comparisons were performed between the two primary Navier-Stokes solvers for hypersonic flows used within NASA, namely the Langley developed LAURA code and the commercially available GASP code from Aerosoft, Inc., in which strengths and weaknesses were identified. (See, for example, **Fig. 13**.) Efficiency and effectiveness of surface and volume grid generation were enhanced, although generation of these grids remained the major portion of the total time to generate a solution (**Fig. 14**). Advantage was taken of massive parallelization techniques to significantly reduce the running time

required for LAURA. Most importantly, confidence in using CFD to provide aerodynamic and aeroheating data for aerospace vehicles was increased appreciably by comparisons of CFD predictions to wind tunnel measurements and code to code. These comparisons provided a better understanding of what physical and numerical models to use (**Hollis et al., 1999; see Fig. 15**) in future applications.

From X-33 and X-34 experiences in aerothermodynamics, it is strongly recommended that computational and experimental aerothermodynamicists work together in the development of both aerodynamic and aeroheating data bases. The strengths of CFD and ground-based testing are complementary and, used together, provide a better product. Due to expected advances in CFD in the future, particularly in reduced times required to run full Navier-Stokes solvers tip-to-tail, and to dedicated computers for a given program, the time will come when CFD plays a dominant role in the development of aerothermodynamic data bases. However, for the next decade, it is believed that vehicle designers will rely primarily on wind tunnels for subsonic-to-low-hypersonic (i.e., Mach 0.1 to 10) aerothermodynamic information and on CFD predictions for hypersonic-hypervelocity flows (i.e., Mach numbers in excess of 10, or so).

Future Enhancements: Plans to advance aerothermodynamic capabilities at the NASA Langley Research Center in the future will not become reality without adequate resources in terms of personnel (i.e., expertise/competency), equipment and sources of relatively long-term (3 to 5 years) funding. Within the present resources of the Aerothermodynamics Branch, several enhancements have been, or are in the process of being, initiated. For the sake of brevity, example enhancements will only be mentioned briefly; additional information on enhancements is provided by **Miller, 1998**.

The emphasis on future enhancements is to provide aerothermodynamic information faster (**Fig. 16**) for all phases of the aerothermodynamic process; i.e., development of initial concepts, assessment, optimization, and benchmarking. Factors in computational and experimental aerothermodynamics that now require relatively long periods of time to perform are being worked on an effort to reduce time. Computationally, an ambitious effort is underway to develop an unstructured hypersonic viscous solver having all the capabilities of the benchmark Langley LAURA code but with a reduction in the total time to generate grids and obtain a full viscous, tip-to-tail solution by an order of magnitude or more. Until such time this unstructured solver is operational, the optimization of the LAURA code for massive parallel processing on nonvector machines will continue. Significant advances have been made in reducing the time required to generate structured surface/volume grids and work is in progress to further achieve an order of magnitude reduction in time. An unstructured version

of the Langley LATCH (boundary layer solver) code (**Hamilton et al., 1998**) has been developed and coupled with the FELISA code, an unstructured inviscid solver. This combination of FELISA and UNLATCH (UNstructured LATCH) will greatly accelerate the development of comprehensive aeroheating data bases for the windward surfaces of vehicles. This combination is also an important ingredient to a process recently developed to rapidly predict peak heating and heating loads for a given trajectory and "automatically" select optimum TPS materials, determine split lines between different TPS materials, and size the TPS.

Additional computational plans include the continued development and validation of advanced turbulence models for hypersonic flows; enhancement of jet plume-flowfield-surface interaction (i.e., reaction control system) capabilities; possible revival of equilibrium radiation codes to address aerothermodynamic issues associated with very high velocity return to Earth missions; continued advancements in DSMC by coupling to continuum Navier-Stokes solvers to predict RCS phenomena in the rarefied flow regime and extension of DSMC capabilities lower into the atmosphere; the exploiting of boundary-layer theory and triple-deck theory to compute the effects of global and local changes to surface catalysis on computed heating rates; and development of laminar wall function approximation to help reduce grid requirements and accelerate convergence of CFD solutions for hypersonic, viscous flow.

A strong emphasis has been placed on obtaining high performance, precision machining of stainless steel force and moment and pressure models, whereby models would be fabricated in days instead of several months. Rapid, precision machining capability exists, is rapidly evolving, and should be routinely available to customers for model fabrication in the relatively near future. Until such time, techniques to construct complex, high fidelity metal-matrix/composite matrix force and moment models amenable for heated flows will continue, along with high temperature resins for SLA. Techniques for ceramic force and moment models will continue to be refined to decrease time of construction and increase fidelity. Models having remotely controlled surfaces will be explored. This technique is commonly used in Langley subsonic to supersonic tunnels, but has not been used in the AFC primarily because of small model size and cost (trade between increased model cost and cost to operate facility). Model support systems will be designed and built for multiple-body separation studies in preparation for Shuttle Orbiter enhancement studies such as liquid flyback boosters and two-stage-to-orbit-concepts. Development and application of a non-intrusive, three-color surface fluorescence technique for simultaneous global measurements of model surface pressure and temperature in heated hypersonic wind tunnels (including the CF_4 tunnel) continues. This technique will extend the temperature range of the presently used phosphor thermography system and provide a smoother model surface via a different coating technique. The subject technique will represent a critical step towards the

ultimate goal of simultaneous force and moment, pressure, and temperature (heat transfer) measurements. This three-color technique will eventually replace the highly successful two-color phosphor thermography technique presently used for essentially all aeroheating studies in the Langley AFC. Until that time, the two-color technique will continue to be improved. Two or three systems will be applied simultaneously to provide multiple views of the model, thereby providing more information faster and reducing the number of tunnel runs required (i.e., cost). Fluorescence techniques will be used during force and moment testing to identify the state of the boundary layer (i.e., laminar, transitional, or turbulent) and locations of flow separation and reattachment often important in the interpretation of force and moment data (e.g., for deflected control surfaces and for wings/fins). Theories/procedures for the extrapolation of phosphor thermography aeroheating measurements to vehicle flight surface temperatures will continue to be developed, calibrated against the rich flight data base for the Shuttle Orbiter and upcoming flight data for X-33 (**Fig. 17**) and X-34, and applied to future aerospace vehicle concepts.

Strides are being taken to more accurately infer heating to thin model surfaces such as fins, tails, wings, and surfaces with small radii of curvature such as leading edges by advances in fluorescence techniques including time response, routine use of 2D/3D conduction codes and/or use of model materials having extremely low thermal conductivity to minimize conduction.

Optical techniques are under development for monitoring model attitude during the run when under pressure and thermal loads. Although the pitch-pause method for force and moment measurements is a tried and proven standard in the Langley AFC, continuous pitch capability may be implemented to substantially increase productivity and reduce thermal effects on the balance. Continuous pitch will require a sufficient increase in strain-gauge balance and data acquisition response, as well as real-time model attitude measurements.

References:

Berry, S. A., Horvath, T. J., DiFulvio, M., Glass, C. E., and Merski, N. R., "X-34 Experimental Aeroheating at Mach 6 and 10," *Journal of Spacecraft and Rockets*, Vol. 36, No. 2, March-April 1999, pp. 171-178.

Berry, S. A., Horvath, T. J., Hollis, B. R., Thompson, R. A., and Hamilton II, H. H., "X-33 Hypersonic Boundary Layer Transition," AIAA Paper 99-3560, June 1999.

Brauckmann, G. J., "X-34 Vehicle Aerodynamic characteristics," *Journal of Spacecraft and Rockets*, Vol. 36, No. 2, March-April 1999, pp. 229-240.

Hamilton II, H. H., Weilmuenster, K. J., Berry, S. A., and Horvath, T. J., "Computational/Experimental Aeroheating Predictions for X-33 Phase II Vehicle," AIAA Paper 98-0869, January 1998.

Hollis, B. R., Horvath, T. J., Berry, S. A., Hamilton II, H. H., and Alter, S. D., "X-33 Computational Aeroheating Predictions and Comparisons with Experimental Data," AIAA Paper 99-3559, June 1999.

Hollis, B. R., Thompson, R. A., Murphy, K. J., Nowak, R. J., Riley, C. J., Wood, W. A., Alter, S. J., and Prabhu, R. K., "X-33 Aerodynamic and Aeroheating Computations for Wind Tunnel and Flight Conditions," AIAA Paper 99-4163, August 1999.

Horvath, T. J., Berry S. A., Hollis, B. R., Liechty, D. S., Hamilton II, H. H., and Merski, N. R., "X-33 Experimental Aeroheating at Mach 6 Using Phosphor Thermography," AIAA Paper 98-3558, June 1999.

Kleb, W. L., Wood, W. A., Gnoffo, P. A., and Alter, S. J., "Computational Aeroheating Predictions for X-34," *Journal of Spacecraft and Rockets*, Vol. 36, No. 2, March-April 1999, pp. 179-188.

Merski, N. R., "Global Aeroheating Wind-Tunnel Measurements Using Improved Two-Color Phosphor Thermography Method," *Journal of Spacecraft and Rockets*, Vol. 36, No. 2, March-April 1999, pp. 160-170.

Micol, J. R., "Langley Aerothermodynamic Facilities Complex: Enhancements and Testing Capabilities," AIAA Paper 98-0147, January 1998.

Miller, C. G., "Aerothermodynamic Flight Simulation Capabilities for Aerospace Vehicles," AIAA Paper 98-2600, June 1998.

Murphy, K. J., Nowak, R. J., Thompson, R. A., Hollis, B. R., and Prabhu, R. K., "X-33 Hypersonic Aerodynamic Characteristics," AIAA Paper 99-4162, August 1999.

Prabhu, R. K., "A Computational Study of an X-33 Configuration at Hypersonic Speeds," NASA/CR-1999-209366, July 1999.

Riley, C. J., Kleb, W. L., and Alter, S. J., "Aeroheating Predictions for X-34 Using an Inviscid Boundary-Layer Method," *Journal of Spacecraft and Rockets*, Vol. 36, No. 2, March-April 1999, pp. 206-215.

Thompson, R. A., Hamilton II, H. H., Berry, S. A., and Horvath, T. J., "Hypersonic Boundary Layer Transition for X-33 Phase II Vehicles," AIAA Paper 98-0867, January 1998.

Wurster, K. E., Riley, C. J., and Zoby, E. V., "Engineering Aerothermal Analysis for X-34 Thermal Protection System Design," *Journal of Spacecraft and Rockets*, Vol. 36, No. 2, March-April 1999, pp. 216-228.
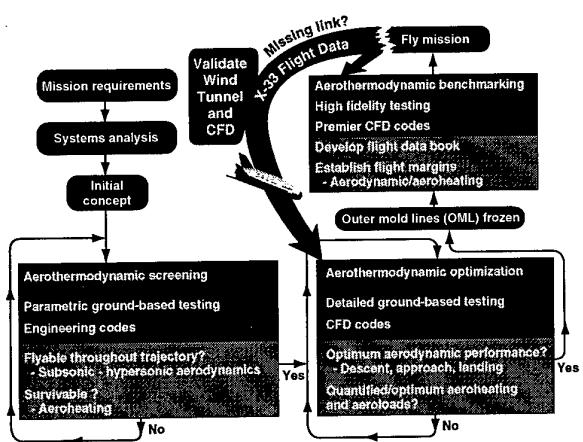
Fig. 1 Aerothermodynamic process.
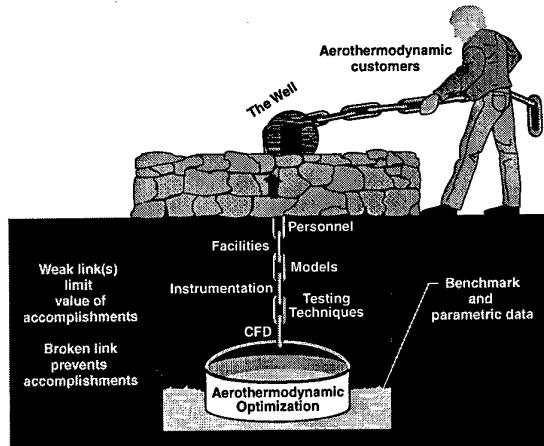
Fig. 4 "Aerothermodynamic chain" representing infrastructure.
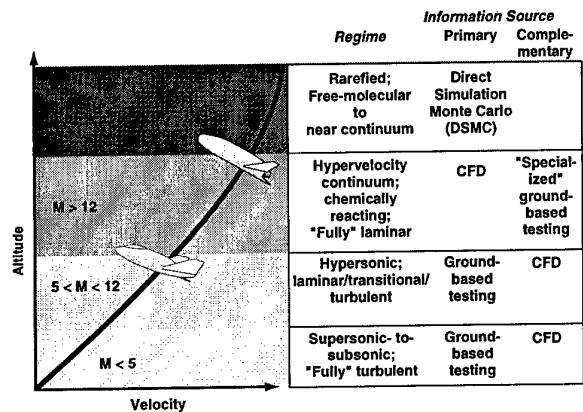
Fig 2. Aerothermodynamic methodology.
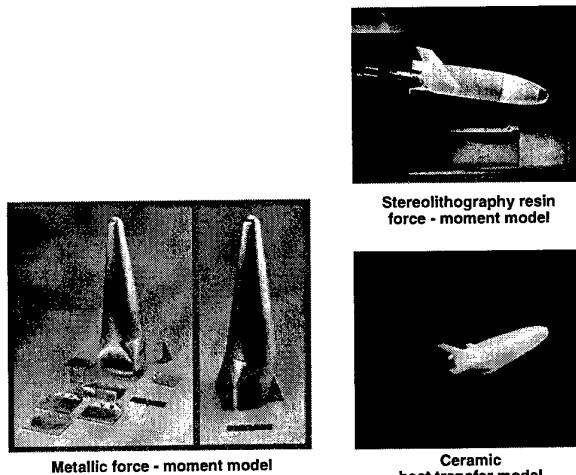
Fig. 5 Representative models for testing in LaRC AFC.
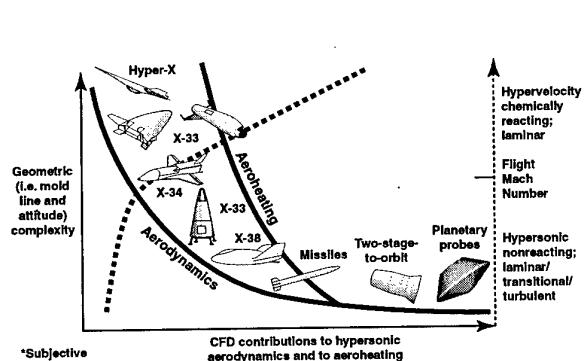
Fig. 3 Relative contribution of CFD.
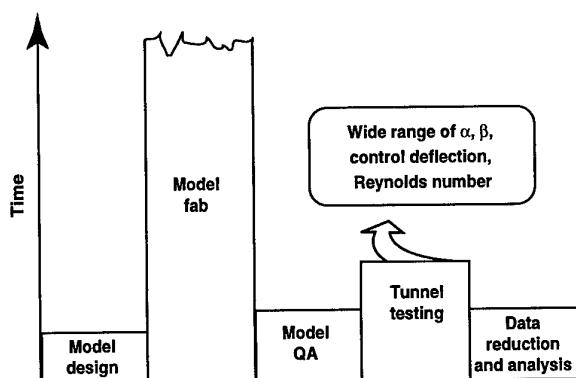
Fig. 6 Relative times associated with typical force and moment study in LaRC AFC.
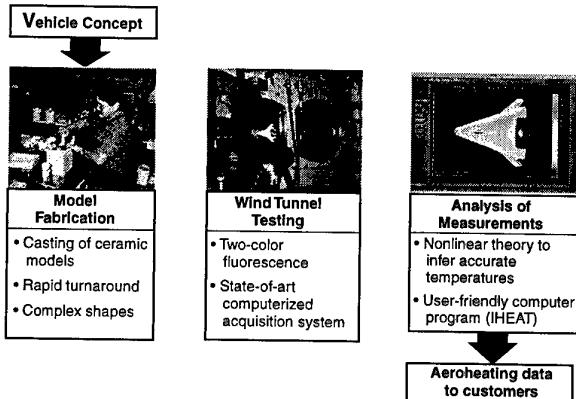
Fig. 7 Phosphor thermography quantitative aeroheating process.
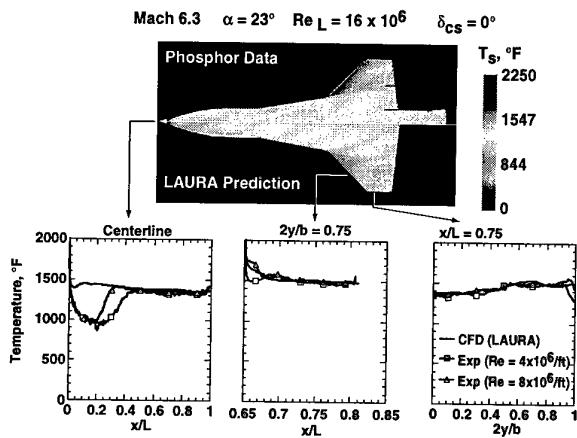
Fig. 8 Extrapolation of X-34 wind tunnel aeroheating measurements to flight; turbulent boundary layer. From Merski et al., 1999.
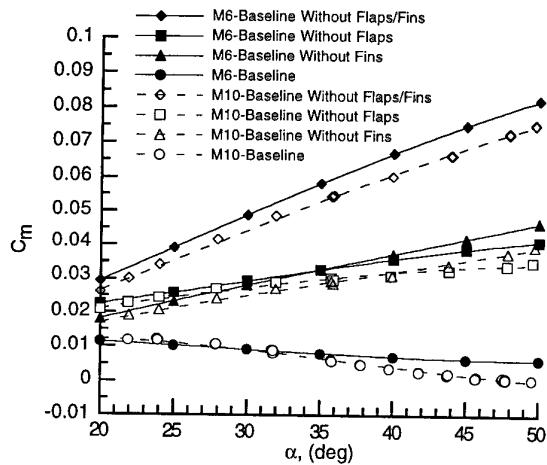
Fig. 9 Measured pitching moment coefficient for X-33 configuration build-up; Mach 6 and 10. From Murphy et al., 1999.
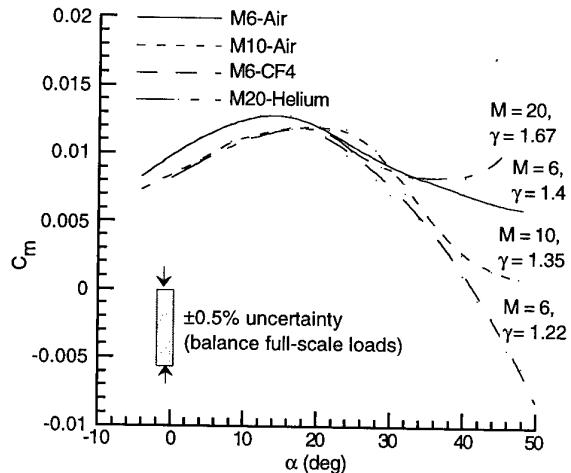
Fig. 10 Effect of Mach Number and shock density ratio on measured pitching moment coefficient for X-33. From Murphy et al., 1999.
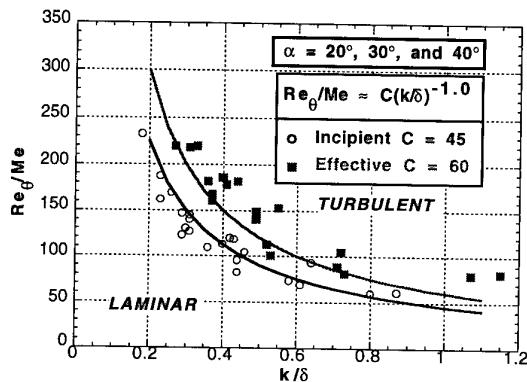
(a) Roughness transition correlation. From Berry et al., 1999.

Fig. 11 X-33 boundary layer transition correlation.
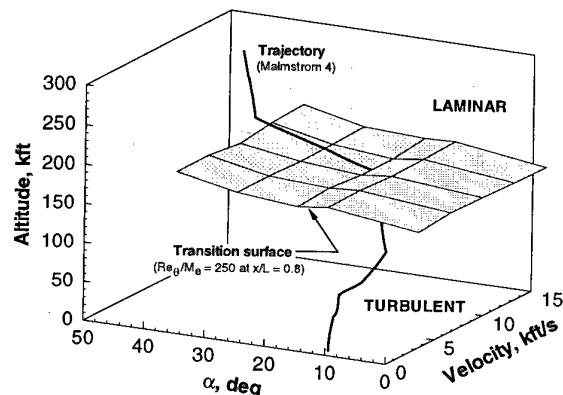
(b) Altitude – angle of attack – velocity. From Thompson et al., 1998.

Fig. 11 Concluded.
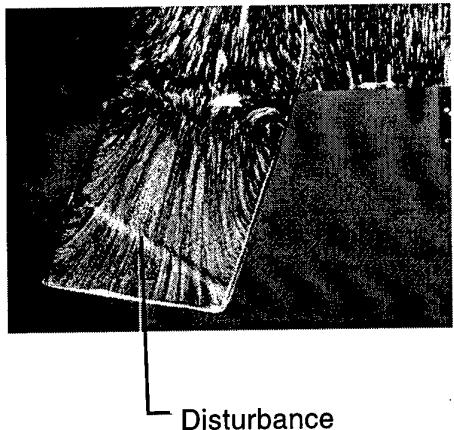
Fig. 12. X-33 body flap surface streamlines.
$M_\infty = 6$, $\alpha = 40°$, $\delta_{BF} = 20°$, $Re_\infty = 2 \times 10^6/ft$.
From Horvath et al., 1999.

(a) Flux formulation.

Fig. 15 Effect of flux formulation and TVD limiter on
centerline X-33 heating distribution; $\alpha = 40°$
From Hollis et al., 1999.

Fig. 13 Phosphor/CFD X-34 centerline comparison.
From Merski et al., 1999.
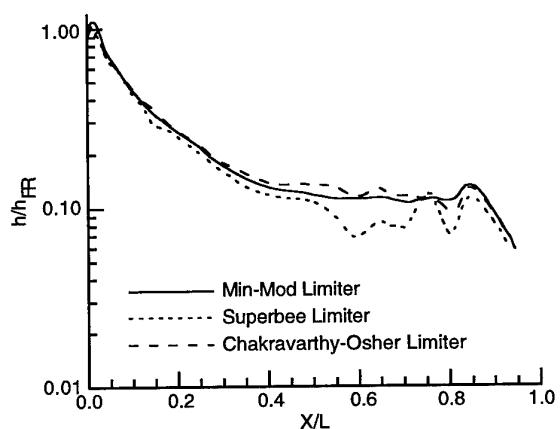
(b) TVD limiter.

Fig. 15 Concluded.

Fig. 14 Relative times associated with typical CFD
application.

• **Experimental hypersonic aerodynamics**

Present

Future

(Factor of 4)

Time

▨ Model   ▦ Model   ▧ Model   ▨ Tunnel   ▨ Data reduction/
design   fab   QA   testing   analysis

• **Experimental aeroheating**

Present

Future

(Factor of 1.5)

Time

• **Computational aerodynamics/aeroheating**

Present

Future

(Factor of 3)

Time

▨ Surface   ▦ Volume grid   ▦ Running first   ▨ Additional
grid   with wake   case   cases

Fig. 16 Aerothermodynamic future goals.
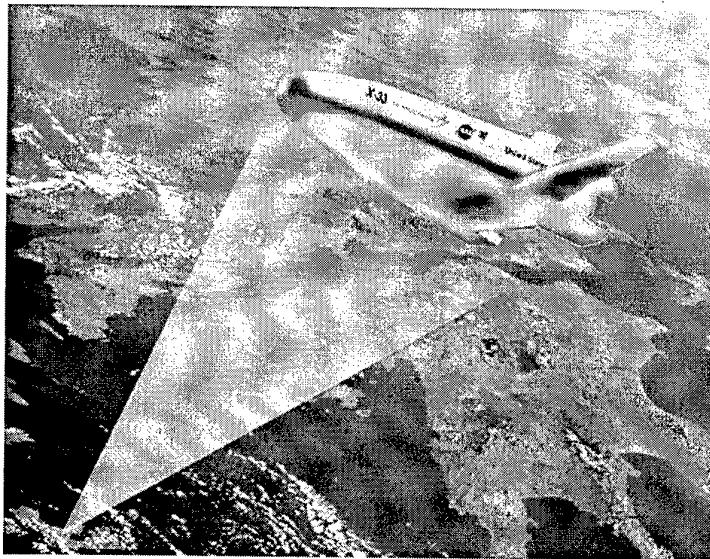
Fig. 17 X-33 flight data extraction and comparison to ground-based data and CFD predictions.

Rapid Aerodynamic Data Generation using an Iterative Approximation Method.

C. A. Toomer
British Aerospace Sowerby Research Centre,
CFD Group, Mathematical Modelling Department,
FPC 267, PO Box 5, Filton, Bristol,
United Kingdom BS34 7QW

Nomenclature

a	Coefficient used in function fitting expression
c	Chord length
CFD	Computational Fluid Dynamics
C_D	Coefficient of drag
C_L	Coefficient of lift
C_M	Pitching moment (y-direction)
Cp	Coefficient of pressure
M	Mach number
MDO	Multi-disciplinary Design Optimisation
PosMaxT	Position of Maximum thickness design variable
t	Parametric variable
x	Axial co-ordinate
y	Normal co-ordinate
z	Vertical co-ordinate
α	Angle of attack (degrees)
β	Design variable (shape or operating condition)

Subscripts

∞	Freestream conditions

Introduction

Aerodynamic design and optimisation is a costly and complicated process in which numerically generated information about the design space plays a vital role. Hence the information needs to be of good quality, i.e. describing the correct physics, and to be easily accessible from databases using standardised formats. To make this process affordable and efficient, the codes must be fast, robust and accurate. Aerodynamic design problems tend to involve a large number of design parameters and constraints on the design. Large data sets are generated and so it is wise to automate the data generating and processing whenever possible.

Data generation is only part of the process. Efficient algorithms to access and interpret the data are required, as is an efficient means of negotiating through the design space. Optimisation is the usual method by which the data are analysed, and regions within the design space identified as possible design solutions or improvements to existing designs.

One of the aims of the work presented here is to use approximation methods to resolve functions of interest, through the use of simpler or easier to compute functions. These computed functions depend on the variables chosen in the parameterisation of the vehicle shape and the conditions at which it flies. The functions of interest are those describing the vehicle's performance, e.g. coefficients of lift, drag and pitching moment. The modelling enables the designer to learn about the relations between the design parameters and their effects on the vehicle performance. It is important to understand: the trade-offs between the accuracy of the model and the complexity of the function, and the amount of data & time required to achieve a useful description of the design space.

Another aim is to create frameworks of methods that allow the designer to easily and quickly enhance and modify the problem as knowledge is built up. For example, having run an optimisation case the designer may wish to amend the existing constraints or to add into the problem constraints on new quantities.

The Sowerby Research Centre of British Aerospace has a number of computational tools available for use in the conceptual design phase of a vehicle. Some are developed in-house, others obtained from outside, some tools are mature, others in development. For many of these programs physical accuracy is the prime concern, e.g. Navier-Stokes/Euler finite volume codes. Others are developed where it is felt that some accuracy can be sacrificed for substantial reductions in the time to identify viable solutions to the problem considered.

In this second category of codes are a forward design perturbation code (developed in-house) based on sensitivity analysis, and response surface methods. When combined in a multi-level optimisation strategy, reductions of between 70% to 95% have been obtained in the computational time required to find one or more solutions, compared with using a Computational Fluid Dynamics (CFD) code to produce the required aerodynamic data. The design variables used are both operating condition parameters (angle of attack and freestream Mach number) and geometric parameters (B-splines, bezier curves or "super-variables" for each aerofoil section: camber, thickness, position of maximum thickness and twist angle etc).

This paper is structured into three main sections. In the first section the routes chosen to obtain an improved design are discussed. In the second section are described the complementary methods used to parameterise the vehicle shape, generate the data describing its performance and to interpret this data for design problems. The third and final section details the conditions imposed in a design improvement study and

some of the results obtained. A generic wing-body is used as the testcase. Both single-point and multi-point results are shown. Multi-point analyses are extremely valuable in assessing the off-design performance of the vehicle. Modifying a design through single point optimisation may produce a configuration that is very sensitive to changes in design parameters.

The work presented here is the first stage of a two-part design improvement study. Only the results from the first stage are reported in this paper. The second stage, in which the viscous flow around the vehicle is studied, involves the predictions from the first stage, in particular the region of design space to be investigated. For configurations with regions of separated flow, the inviscid and viscous optimisation results may not indicate the same region of design space.

Routes to Design Improvement

There is no route that consistently provides the best solution for all types of aerodynamic design optimisation problems. Both sequential approximate programming and direct insertion approaches are commonly used. In order to make these standard approaches more cost-effective; approximation techniques are included in the sequences used here. The codes linked together include a surface and field grid generator, a CFD code, a sensitivity code, curve fitting techniques and an optimiser.

Four approaches have been compared. Approaches 1 & 2 are sequential approximate programming approaches where the maximum benefits of approximations are used to speed up the time to find an improved design. Approaches 3 & 4 use a direct insertion approach, where the use of approximate data is limited and hence the accuracy of the data used by the optimiser is better than in approaches 1 & 2.

Approach 1.
The design space is chosen by setting, for each design variable, the range over which it can vary. A representative sample of points is chosen to model this design space, and at each point the CFD code is run to produce forces and moments data. The results are function fitted using polynomials, so that a mathematical representation exists for each force & moment coefficient as a function of the perturbed design variables. By partially differentiating these expressions, the first and second order gradients can be obtained. The expressions for the forces & moments and their sensitivities provide the optimiser with sufficient information at any point in the design space to perform its search for the minimum of the objective function.

Approach 2.
Approach 2 follows that of 1 except that the perturbation code is used to generate some of the data in place of the CFD code. This reduces the time required to find potential design configurations that satisfy the constraints in the optimisation problem. The CFD code is always used to evaluate information at the initial design point. All data required at points reasonably close to the initial design point are generated using the perturbation code. The tiered CFD/perturbation/function-fitting approach has been successfully used to improve aerofoil shape design for cruise conditions. The reduction in time of approach 2 compared with approach 1 can be up to 90% ([1]).

Approach 3.
Approach 3 is a direct insertion approach where the optimiser directs the path taken through the design space to find the minimum of the objective function. At each design point selected, data are evaluated by the CFD code to give the values of the objective and constraints and their sensitivities for each design parameter. The gradients are created by forward differencing. No response surface fits are used. The advantage with the method is that all data are as accurate as the CFD code can produce and so the optimiser follows a search path based on accurate information. There are disadvantages too. Care must be taken with the production of the gradients, in that reasonable step sizes must be used. Inaccurate gradients are produced using too large a stepsize, and also by using very small step-sizes since the gradient calculation is influenced by rounding errors and any cycling in the CFD solution. Substantial time is required by approach 3 to generate the required data as each design parameter must be perturbed to evaluate the gradient and that involves multiple runs of the CFD code at each design point considered. Finally information may be required at a design point for which the surface and/or volume grid poses problems for the flow code. In the case of the latter problem arising, an alternative design point, close to the specified point, must be used for which the analysis codes are successful, or the optimisation must be taken from a different initial point.

Approach 4.
Substantial savings in time can be made on approach 3 if the gradient calculation is performed by the perturbation code. Approach 4 uses the perturbation code not just for the gradient calculation but also when the new point chosen by the optimiser is reasonably near to the previous point. In that case the perturbation code is instructed to march to this point. In tests conducted by van Etten [2] using a line search with small steps, this approach can reduce the time required to find the minimum by 60-90% over approach 3.

Convergence of the design search
For all approaches except approach 3, the solution obtained by the optimiser is based on approximation data. Therefore the CFD code must be run at the design point proposed by the optimiser so as to provide the accurate values for the forces and moments. If the solution does not satisfy the problem within required design and accuracy limits, the approach is repeated.

In approaches 1 & 2, whenever a new design space is chosen or an existing one modified or sub-divided, sufficient data are evaluated to the limits of each new design space for the function fits. A new polynomial fit is found for each quantity modelled. New smaller design spaces are often constructed around solutions suggested by the optimiser, with this point at the centre of the new design space. The changes to the design space must make the functions described more accurate and relevant without excluding possible solutions. The optimisation is started using the new formulae and the sequence is continued until the agreed accuracy is met.

Parameterisation and Design Tools

Surface parameterisation and grid generation
Many different parameterisations can be adopted to perform shape variation on vehicle configurations. In this case the parameterisation is that developed for the European Consortium MDO wing-body test case [3]. This generic civil aircraft has a wingspan of 80m, a take-off weight of 550 tonnes and seats 650 passengers. The

planform of the aircraft is kept constant during these design studies and only the sectional shape of the wing is allowed to vary. The wing is constructed from five aerofoil sections: at the root, crank, tip and intermediate (in-board and out-board) positions (see Figure 1).

The formulation ensures specific set values in each section for trailing edge angles, and the curvature of the nose, crest and trough. Other rules are applied to preserve the planform area, aspect ratio, sweep and dihedral. Hence there is limited opportunity for greatly altering the shape.

Each aerofoil is constructed in (x, z) space from four Bezier curves of fifth-order using the general formulation:

$$x(t) = x_0 - 5t(x_0 - x_1) + 10t^2(x_0 - 2x_1 + x_2)$$
$$-10t^3(x_0 - 3x_1 + 3x_2 - x_3) + 5t^4(x_0 - 4x_1 + 6x_2 - 4x_3 + x_4)$$
$$-t^5(x_0 - 5x_1 + 10x_2 - 10x_3 + 5x_4 - x_5)$$

A similar formulation for the z co-ordinate is used. t is a parametric variable and the (x_n, z_n) are Bezier curve vertices for n=0,...5.

Two curves are on the upper surface of the aerofoil, two on the lower surface. For each surface, one curve extends from the leading edge to the crest (on the upper surface) or trough (on the lower surface). The other curve from the crest or trough to the trailing edge. In Figure 2 the four curves for the crank section of the wing in its default configuration, with the associated Bezier curve control points are shown.

The user or the optimiser influences the shape of the aerofoil through assigning values to "super-variables": camber, twist, maximum thickness and position of maximum thickness for each aerofoil section. These values are used to evaluate the Bezier vertices. The aerofoil lengths are non-dimensionalised by the chord length, c. The position of maximum thickness variable, PosMaxT, controls the chordwise position of the trough and crest (Figure 3). These are located at the same z-coordinate value. Camber is restricted such that it affects only the rear portion of the aerofoil. An increase in camber causes the trailing edge to move downwards (Figure 4), and the trailing edge tangents to be rotated. The formula used is:

$$z(tail) = z(tail\_orig) - camber(1 - PosMaxT)^2$$

Once the aerofoils are created they are positioned on the wing planform. Each aerofoil is rotated to the specified twist angle, and then the aerofoil is scaled to obtain the correct chord on the three-dimensional planform. Finally the aerofoils are placed on the 3D planform by applying dihedral, deriving the wing twist axis at quarter chord and positioning the aerofoil chordline to intersect with this reference axis.

After the wing is constructed, a surface mesh is produced and the multi-block field mesh extended from this. As structured meshes are used throughout this study, it is necessary to maintain the same number of blocks, and cells within each block, as in the original mesh.

Figure 1: Schematic of the model geometry
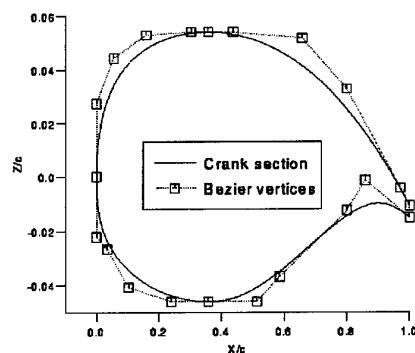
Figure 2. A parameterised wing section using Bezier curves. The position of the Bezier vertices is also plotted.

Figure 3 Effect on the aerofoil shape of varying the Position of maximum thickness parameter, PosMaxT
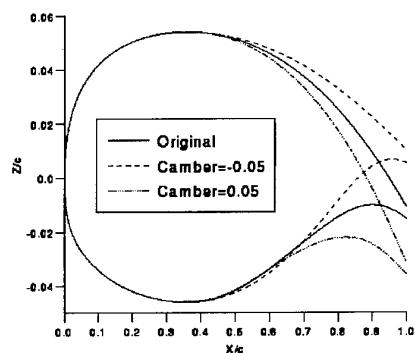
Figure 4 Effect on the rear aerofoil shape of varying the camber parameter from its original value of zero.
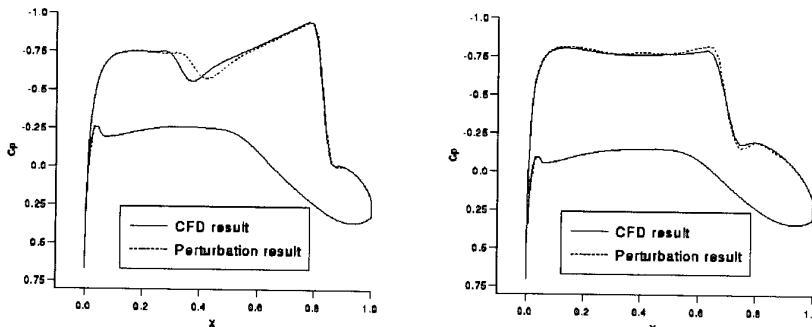
Figure 8. Comparison between the CFD and the perturbation surface Cp distributions at 41% and 74% chord respectively for the shape variation in the MDO wing. The results are sectional cuts of the Cp distributions in Figure 5. The x values have been scaled by the chord length.

The perturbation code produces flowfield predictions as well as forces and moments. The pressure coefficient distribution on the wing-body and on the symmetry plane at the final point of (0.35, 0.43, 0.44, 0.44, 0.42). is shown in Figure 5, as is the corresponding CFD solution on the final geometry. The same range and number of contours are used in both diagrams.

The range of values for Cp, [-1.044,1.122] is predicted extremely well by the perturbation code. The only differences between the CFD and perturbation predictions occur on the upper wing surface in the vicinity of the shock, where the latter code has a tendency to smear a shock.

This effect can be shown better by taking sectional cuts through the wing. Comparison between the CFD and perturbation predictions for the surface Cp distributions at 41% and 74% chord are given in Figure 8. The upper surface distribution is not accurate in the mid-section of the wing where there is a small shock. The perturbation code prediction for this shock is in error by 1-2 cells in the 41% chord diagram. The position of the shock and the number of grid cells used to capture it are the predominant source of error in the perturbation results. However as shown by Figure 7, the error is not large enough to significantly affect the forces and moments data. It will be shown in the next section that the errors in the shock region do not deter from the code's usefulness in design improvement problems.

The methods used in the perturbation code may be applicable to other sets of nonlinear equations that describe well-behaved, continuous functions, e.g. forces and moment coefficients. Work is currently underway to evaluate the approach using nonlinear equations in structural modelling problems.

Function-fitting

There is a wealth of possible functions that can be used to model the available data. Aerodynamic forces and moments data tends to be smooth and continuous with few turning points per variable, even though there are discontinuities (shocks) present in the transonic flow around the vehicle. The function fits utilised in these cases involve those with and those without cross terms. For expressions with cross terms, the data are targeted toward more specific regions that are known to be of interest.

In these examples the shape design parameters are themselves functions of other variables (i.e. the Bezier vertices). Hence the parameters are not necessarily independent of each other. Function fitting using the

summation of separate expressions for each design variable may miss any inter-dependence. The use of cross-terms in the function fitting, and using data in which more than one parameter has been varied, can be used to establish the inter-dependence of the parameters.

The expression used without cross terms involves a three-level star design: a central point, points near the centre, and points toward the design boundary. A fourth order polynomial is used for each parameter perturbed, and these polynomials are summed to give the coefficient expression. The advantage with this type of expression is that as the number of design parameters is increased, the number of data points required to model the extended function increases linearly. The accuracy does not degrade with an increase in design parameters as long as care is taken not to make the parameter ranges too large.

The disadvantages with this type of modelling is the small number of points used to describe the response due to each parameter and the lack of information on parameter interactions due to no cross-terms.

The drag coefficient can be represented as:

$$C_D = a_0 + \sum_{j=1}^{NTOT} \sum_{n=1}^{4} a_{nj} \beta_j^n$$

where NTOT is the number of design variables, β_j are the design variables, a_0, a_{nj} are the polynomial coefficients whose values are found from function fitting the data. Similar expressions are used for the other functions (e.g. lift coefficient, pitching moment, surface Mach number) with different values for the coefficients. The response surfaces for the lift and drag coefficients (in one of the typical design spaces considered in this study), showing the variation with crank and tip camber (all other design variables kept to those of the reference position) are shown in Figure 9.

Expressions with cross-terms can be computationally more complex in requiring far larger amounts of data to fit, but they are not more complex in terms of the design parameters being modelled. The data are initially selected from the simpler no cross-term data, with additional points generated within regions of the domain known to be of interest where more than one parameter varies from the values at the initial/central point. The advantage is that parameter interactions are considered in the modelling. The disadvantages with this type of function are the time to generate the required data, and
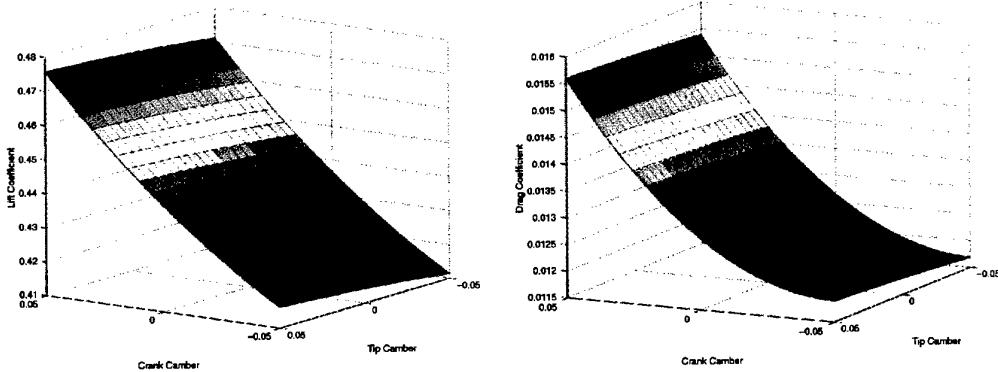
Figure 9 Function fitted data for the lift and drag coefficients on the wing using a quadratic expression with cross-terms. The crank and tip cambers are allowed to vary. All other parameter values are set to those at the reference point in design space.

deciding which points are good representatives of the design space. This problem increases as the number of design parameters increase. The cross term function used in this study uses a summation of linear and quadratic terms.

$$C_D = a_0 + \sum_{j=1}^{NTOT} a_j \beta_j + \sum_{j=1}^{NTOT} a_{jj} \beta_j^2 + \sum_{1 \leq j \leq k \leq NTOT} a_{jk} \beta_j \beta_k$$

With NTOT design variables the quadratic expression requires

$$\frac{1}{2}(NTOT + 1)(NTOT + 2)$$

data points. Hence for the 20 shape variables and the angle of attack, 253 data points are required.

The values from the functions generally compare well with the corresponding values obtained from the CFD code for small design spaces. However it is important to work within the design space defined by the function fitted data. As the amount of data describing a domain increases, the domain can be sub-divided and function fits of the data within each sub-domain can be used. The drawback with this approach is that at the boundary between sub-domains, the gradients of objective and constraint functions may be different in each region. The large domain space also needs to be shrunk to a number of smaller, isolated, sub-domains, each modelling the design space around a potentially favourable design solution.

Function fits substantially simplify the application to optimisation studies where the objective and constraint functions consist of these explicit mathematical expressions from which the partial derivatives are readily available. The optimisation strategy permits the design space size to be amended and/or additional constraints to be quickly added to the problem, through utilisation of the data stored when using the CFD and perturbation codes. These situations occur when either the designer wishes to test the solutions to the optimisation problem and evaluate which designs are most suitable, or when the designer wishes to pose a slightly different optimisation problem to the same design space. A further advantages with using function fits is that estimates of the quantities needed by the optimiser are available for any point in the design space, and the search does not stop due to problems obtaining surface or volume geometries at specified design points.

The disadvantages to be overcome with function fitting: the accuracy depends on the function model and on the choice of experimental design. Large inaccuracies can arise if the range over which a design parameter is being modelled is large and/or if a parameter is highly sensitive.

The Optimisation Routine
The optimisation algorithm used is a sequential quadratic programming algorithm from the NAG Fortran library [6]. The search direction is the solution of a quadratic programming problem. Since a gradient-based optimiser is effective in searching for a local minimum, in all the experiments described here, runs are performed at different initial design points. This increases the chance that the optimiser will consider design points in different regions. The larger the number of design variables, the more test cases need to be performed.

Design Improvement Studies

Test case considered
In the following optimisation problems, the MDO aircraft is assumed to be flying at cruise conditions of M_∞ 0.85.

The CFD and sensitivity codes are run for steady state inviscid flow only. The design parameters permitted to vary are the angle of attack and for each aerofoil section: the camber and the twist. In some cases the position of maximum thickness varies too. The chosen starting point has α=0.5 degrees, zero camber and the twist and position of maximum thickness vectors are:

(2.364, 1.286, 0.155, -0.684, -1.638),
(0.287, 0.350, 0.358, 0.358, 0.341)

respectively. The thickness for each aerofoil section is kept to the original values of:
(0.14, 0.12, 0.10, 0.094, 0.088)

The design space is set to [-0.01, 0.05] for each cambered section, [-7, 5] degrees for the twist angles, [0.25, 0.45] for the positions of maximum thickness and [-1.5, 2.5] degrees for the angle of attack. The set of design points used in the function fits contain points relatively close to the original points and points at the boundary.

The drag coefficient on the wing at the original design point is 0.012630. The lift coefficient & pitching moment (on the wing) are 0.44397 and -0.14365 respectively.

The aim of the optimisation is always to improve the design when compared with the wing performance at the initial chosen design point.

The objective in the single-point optimisations is to minimise the drag over the wing whilst retaining the lift, and not permitting the pitching moment to reduce. It is also important to ensure that constraints are added to the fuselage to maintain the lift and prevent the drag from increasing and the pitching moment from decreasing. Other requirements are to maintain the planform area, to prevent the drag over the whole configuration from increasing and to weaken the shocks on the wing surface.

Many optimisers increase the rear wing loading when attempting to weaken the wing shock, so this tendency must be avoided through the use of further constraints on the surface Mach number and the surface pressure. This increases the number of constraints by up to another 10 for the wing surfaces and up to another 20 for the fuselage surfaces from the multi-block mesh.

In the multi-point problems three points in design space with different angles of attack are used. The objective function is a weighted combination of the drag coefficients at these points. The same types of constraints as in the single point optimisation are then applied at the three points.

Time savings
The run-time saved by using the perturbation code where possible during the data gathering and optimisation procedures is between 75% - 86% in using approach 2 compared with approach 1, and 82%-87% for approach 4 compared with approach 3.

The CFD runs use a previous converged flow field as starting data (when appropriate) and are run until changes between iterations in the density and velocity are less than 10^{-3}. The inaccuracies from the perturbation code do not cause the optimisation to take greatly different vectors through the design space during the line search process, or to invoke more iterations before convergence. As expected approach 3, where all the data are from the CFD code and no function-fits or perturbation data are used, is the most expensive approach.

In approach 2 the cost of solving the problem, including running the CFD code on the predicted design point is equivalent to 7 CFD runs for cases where the function fitting is adequate. If the design space needs to be shrunk and the optimisation re-run, and then the prediction point checked by CFD, the further cost is 3 CFD runs.

Single point design improvements
The following results are from approaches 1 & 2. The optimised solutions are in agreement with those found using approaches 3 & 4.

Inequality constraints on the lift and the pitching moment allow the lift to increase by a few percent above the original value whilst the pitching moment is prevented from decreasing.

The results from four cases are shown in Table 1. The first case (10 design variables) has the twist, angle of attack and camber varying, excepting the root camber, which is fixed at zero. Case 2 permits the root camber to vary as well. Cases 3 & 4 also have the position of maximum thickness varying. Case 3, the 15 variable case, does not allow the root camber to vary, whereas case 4 does (i.e. 16 design variables).

Comparing the values from the function fits with the corresponding CFD values on the optimised geometries shows an error of up to 1.9% for the drag and 0.3% for the lift and pitching moment.

For example, for the 16 design variable case, the percentage reduction in the coefficient of drag on the optimised wing compared with that on the original wing is 7.7% with C_D=0.011657. (The values compared are from the CFD code on the original and optimised geometries.) Considering both the wing and fuselage sections, total lift is maintained, the drag coefficient reduces by 5.5% and the pitching moment increases by 2%.

The change to the design variables is to introduce camber (negative) into the wing sections (except for the root section, which is fixed at zero) causing the tail to rise slightly. The position of maximum thickness moves forward to 0.25 at all but the crank section, where it moves back to 0.426. The twist vector is now (1.09, 2.44, -0.17, -0.56, -1.40) whereas the angle of attack is relatively unaffected by the optimisation and changes to 0.47 degrees. The variation in shape is shown in Figure 10 at the crank and the tip.

The Cp distribution on the upper wing for the optimised solution from the 15 variable case is shown in Figure 11. Also shown are sectional cuts at 10%, 40% and 75% of the wingspan. Compared with the original the optimised distributions show no increase in wing loading to the rear of the aerofoil, but there is in-board loading. There is a small change in the position of the shock near the trailing edge and a slight reduction in its strength. On the 10% and 40% diagrams, there is a small shock in the middle of the upper surface. In the optimised case this shock has moved in the trailing edge direction with a definite reduction in strength. This movement is due to the shift in the position of maximum thickness.

The preferred Cp distribution is a continuing decrease along the upper surface, indicating that supersonic flow is decelerated along the surface. The non-monotonic Cp distributions at the 10% and 40% wingspan positions show that there is room for further improvement in the design. Locating solutions in design space with a smooth, monotonic distribution requires adding extra constraints (after, say, 10% chord) on the pressure gradient. This information is also stored by the perturbation code.

In the cases where the position of maximum thickness is kept fixed at the original value in each section, there the maximum Mach numbers on the upper and lower surfaces reduce slightly. If the position of maximum thickness is allowed to vary in the optimisation, the drag reduction is higher, but the maximum Mach number increases. On the lower surface, this rises from M1.07 on the original geometry to M1.5 on the optimised geometry. On the upper surface there is a slight reduction from M1.39 on the original to M1.37 on the optimised wing. By setting constraints on the surface Mach number, the shock strengths can be prevented from increasing. The surface Mach numbers evaluated when the forces and moments coefficients were calculated are function fitted and added to the problem as inequality constraints.

If the constraints are set on the wing surfaces such that their value cannot be larger than the original maximum surface Mach numbers, the drag coefficient becomes 0.012407, a reduction from the original value of 2%. The wing shape lies between that of the original and the

	Design variables	% reduction in C_D	% increase in C_L	% increase in C_M
10	4 camber, 5 twist, α	2.1	0.0	0.7
11	5 camber, 5 twist, α	5.1	0.0	0.7
15	4 camber, 5 twist, α, 5 PosMaxT	3.1	1.0	0.0
16	5 camber, 5 twist, α, 5 PosMaxT	7.7	0.4	0.7

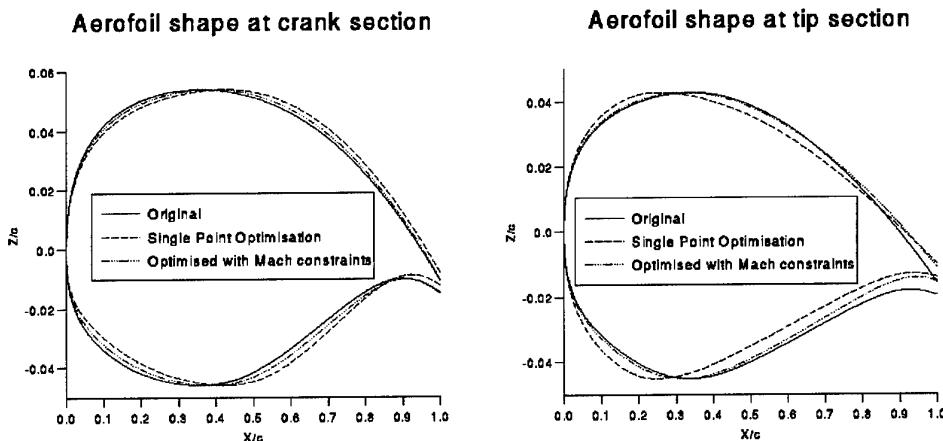Table 1 Percentage reduction in drag for the optimisation cases compared with the values on the original wing. The number of design variables perturbed varies from 10 to 16.

Aerofoil shape at crank section   Aerofoil shape at tip section

Figure 10 Wing sections at the crank and the tip. Comparison is made between the original, the optimised result without surface constraints and the result from optimising with surface constraints on the wing.

Section at 10% wingspan   Section at 40% wingspan

Section at 75% wingspan
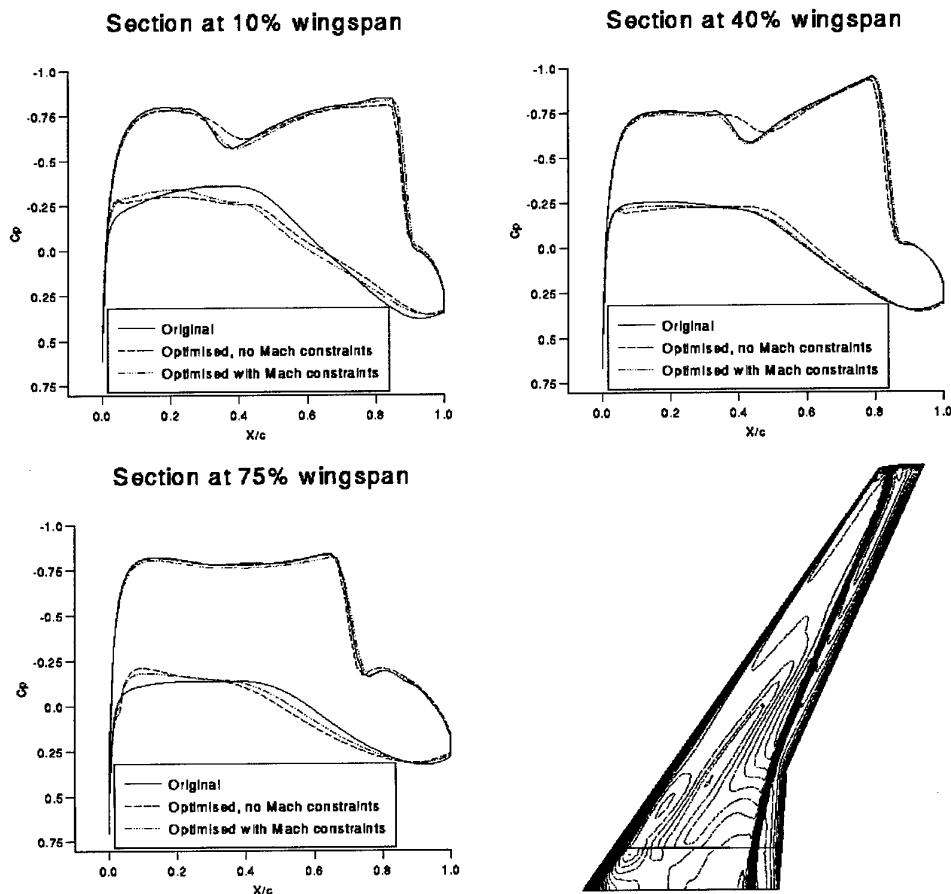
Figure 11. Cp distributions at 10%, 40% and 75% of the wingspan. On each graph are displayed the Cp distribution on the original and optimized wings including the Cp distribution from the case where constraints are applied to the surface Mach number. Also shown is the Cp distribution on the upper surface of the optimized wing.

Aerofoil shape at Crank section

Section at 75% wingspan
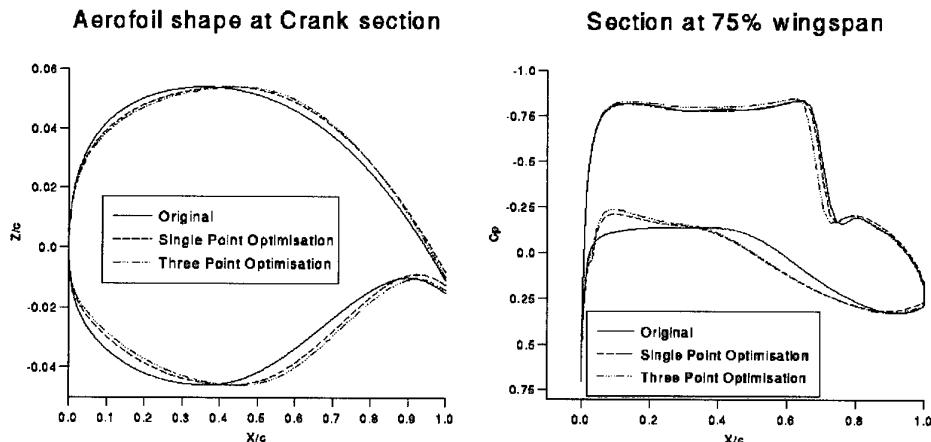
Figure 12. Results from the 3-point optimization run. On the left hand diagram comparison is made between the aerofoil sections at the crank for the original, single point and three point cases. On the right hand diagram comparisons are shown of the Cp distributions at 75% of the wingspan for the three cases.

optimised (without Mach constraints) shape (see Figure 10). The angle of attack drops to 0.37 degrees.

Design improvements through multi-point optimisation

In this investigation of off-design conditions, three points are chosen for their wing lift coefficient values of 0.44397, 0.4 and 0.37. On the original wing-body configuration, these correspond to angles of attack at 0.5, 0.21 and 0.0 degrees. Hence the problem has 18 design variables: fifteen shape (i.e. camber, twist and position of maximum thickness) and 3 angles of attack. Constraints are set on the lift coefficients to maintain the same lift as on the original wing and the pitching moments to ensure that they do not become more negative. The objective function is a weighted sum of the drag coefficient values at each of the three angles of attack.

The first case shown is where equal weighting has been adopted, the second case is where 90% weighting is on the point with lowest C_L and 5% each on the points with larger C_L. The third case has 90% weighting on the point with highest C_L and 5% each on the other points.

In this type of case, approach 2 can save between 75%-86% of the time required by approach 1, and approach 4 is 84%-89% cheaper than approach 3.

Table 2 lists the change in the angle of attack from the original values for the case with equal weighting. The change to the shape of the wing is in keeping with the single point result: the introduction of camber, small changes in twist and a shift in the positions of maximum thickness in each wing section (see Figure 12).

C_L	Angle of attack (degrees)	
	Original	Optimised
0.44397	0.5	0.690
0.4	0.21	0.408
0.37	0.0	0.204

Table 2: Change in angle of attack in the three-point optimisation case with equal weighting.

The combined drag reductions for the equal and unequal weighted cases are shown in Table 3. The equal-weighted case is less successful in reducing the combined drag than cases where the weighting is unequal.

The Cp distribution on the optimised wing at 75% wingspan is shown in Figure 12. The results of the three point optimisation enhance the trends seen with the single point optimisation with the shock position being moved forward slightly.

	Combined C_D	
	Original	Optimised
Weighting		
Case 1 (0.33,0.33,0.33)	0.010219	0.009423
Case2 (0.05,0.05,0.9)	0.008658	0.007074
Case3 (0.9,0.05,0.05)	0.012108	0.010525

Table 3: Change in the combined C_D due to different weightings. Values on the original & optimised aerofoils.

Conclusions

Approximation methods can be valuable tools in design improvement studies. Careful use can reduce the time to find suitable solutions to design problems by up to 90% compared with using the very accurate CFD codes for production of all required data. If due care is taken, methods of varying accuracy, e.g. perturbation methods, CFD and function fitting algorithms can be complementary in proving the optimiser with good quality, useful data.

The development of a perturbation code can be a valuable aid in design studies, particularly in the evaluation of gradients, rapid production of data and as an exploration tool over a small region of design space.

Function fitting data rapidly reduces the cost of optimisation cases as long as the response surfaces are good representative views of the design space. To reach this stage, the function fits may need to be improved in a number of optimisation runs. This enables regions of

interest to be identified, new data evaluated and function fits of each local area improved.

The frameworks used to find design improvement configurations need to be easily modified as knowledge is built up about the design space considered. The response surface functions should be easily amenable to include more design parameters. Constraint functions may need to be amended or new constraints added in an attempt to enhance or remove certain features in the results.

To produce design improvements that are of practical use, multi-point studies are important. This prevents designs being considered in which small changes in flight conditions produce large changes in the vehicle's performance.

Although the results presented here are for Euler flows, the aim of the research is to use the design improvement approach(es) as the first of two stages. The second stage uses the Euler predictions of which design points are of interest but includes viscous flow predictions. In this way considerable time can be saved compared to evaluating all data for the optimisation studies from Navier-Stokes CFD codes.

Acknowledgements

References

[1]- Aerodynamic Optimisation using Analytic Descriptions of the Design Space.
C. A. Toomer, M. E. Topliss & D. P. Hills.
AIAA-96-4141 and 6th AIAA/NASA/USAF Multi-disciplinary Analysis & Optimization Symposium, Bellevue, WA., Sept. 1996

[2]- Research of Projected Implicit Reconstruction in Optimisation. A. J. A. van Etten. Report No. WFW 96.063, Eindhoven University of Technology, May 1996.

[3]- MDO process and Specification for the Primary Sensitivities Study. Industrial & Materials Technology Programme. S. Allwright. British Aerospace PLC.
April 1996

[4]- MULTI-BLOCK Navier-Stokes solver RANSMB user guide. J. J. Benton. British Aerospace internal report ADE-ETA-R-FM-0121. 1993

[5]- Rapid Design Space Approximations for a Two-Dimensional Transonic Aerofoil.
M. E. Topliss, C. A. Toomer & D. P. Hills. AIAA-96-0095 and AIAA Journal of Aircraft, Vol. 33, No. 6 Nov.-Dec. 1996, pp 1101-1108.

[6]- E04UCF. NAG Fortran library Mark 16. NAG Ltd., 1993.

Design and Aerodynamic Optimization of a New Reconnaissance Very Light Aircraft through Wind-Tunnel Tests

V. Giordano D. P. Coiro   F. Nicolosi   L. Di Leo

Dipartimento di Progettazione Aeronautica
University of Naples "Federico II"
Via Claudio 21 - 80125 Napoli - Italy
Fax : +39 081 624609   e-mail : fabrnico@unina.it

ABSTRACT

Design of a new Very Light Aircraft (V.L.A.) called G97 *Spotter* has been carried out at DPA (Department of Aeronautical Engineering) and an extensive wind tunnel test campaign has been performed on both aircraft and airfoil models. Wind tunnel tests have guided in the design phase allowing configuration optimization. Effects of nacelle and air intake shape, fuselage stretching, wing incidence and flap/aileron effectiveness have been analyzed through wind tunnel tests.

The airfoil has also been designed and modified with the help of wind tunnel test results obtained for a model.

Optimization of the airfoil leading edge shape has been done and has brought to a sensible drag reduction at high speed conditions. Optimization of the air intake shape on the aircraft model has been performed leading to a configuration characterized by lower drag. Influence of an air intake fairing has been analyzed and tested through wind tunnel tests. Wing stall path has been studied.

Importance of wind tunnel tests as a device to analyze and design light aircraft configuration has been highlighted.

INTRODUCTION

Primary applications of G97 *Spotter* V..L.A. are observation/reconnaissance, offering helicopter-like view from cockpit and good low-speed handling and loiter capabilities. The fuselage shape has been designed in order to achieve these goals with a large transparent nose section with two wide transparent doors. The airplane is characterized by an high cantilever wing and is powered by rear pushing propeller engine.

The aircraft schematic views are shown in fig. 1.

Due to the unusual configuration an extensive wind tunnel test campaign has been performed on a 1:5.7 scale model (figg. 2, 3) to obtain aircraft aerodynamic characteristics.

Wind tunnel tests will be presented in this paper as a fundamental tool to carry on a good design, even for very light and ultra-light aircraft.

The performances of light aircraft in commerce are really close between them and only through an accurate design of aircraft components and through an accurate configuration study a new aircraft can be really competitive. When unusual configurations (like that one studied in the present paper) are designed, wind tunnel tests becomes essential to understand the aerodynamic behavior, to estimate the importance of each of aircraft components (i.e. for the drag breakdown) and to help in the design of particular part like engine nacelle, air intake and aircraft tail which can be easily modified on the model and tested in the design phase.
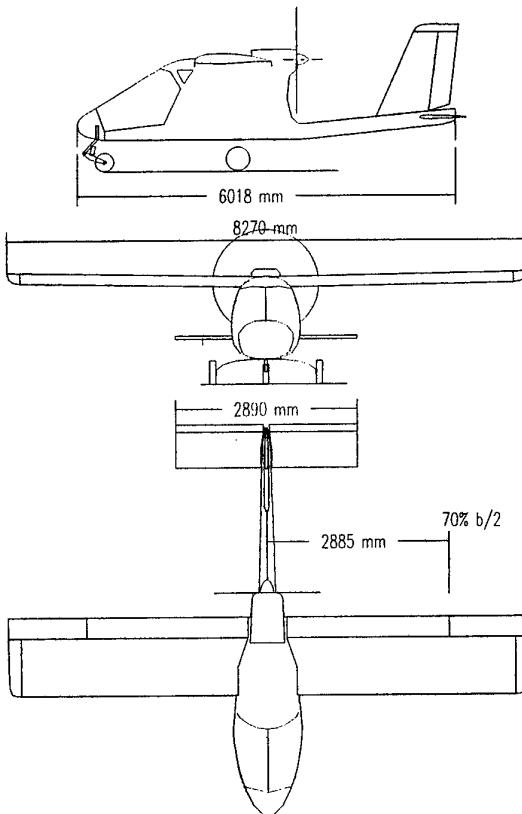
Fig. 1: G97 aircraft schematic views
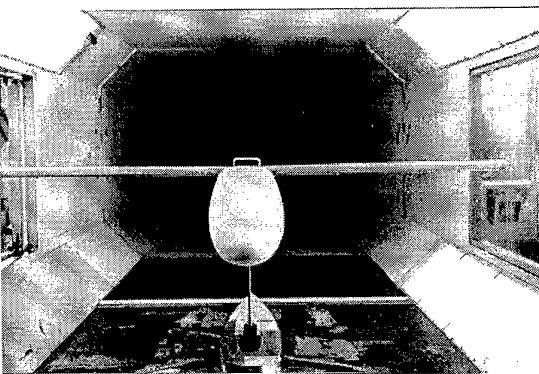
Fig. 2 : G97 model in DPA WT test section
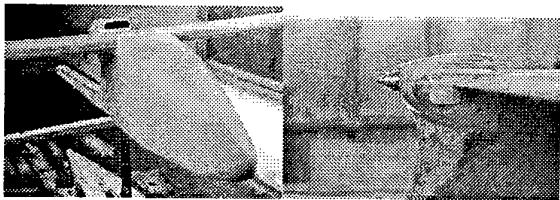
Fig. 3 : G97 model - Lateral view
Particular of Engine Nacelle

For G97 aircraft the airfoil design has been a fundamental step for the whole configuration. The high lift airfoil, called VG1-13 (13% thickness) and specifically designed for this aircraft, has been extensively tested in DPA wind tunnel.

Numerical investigations have also been performed on this airfoil and some of numerical codes developed in the past at DPA have been used to estimate airfoil aerodynamic characteristics and to guide the designer in modifying the model tested in the tunnel. Through wind tunnel tests performed on the airfoil model has been possible to verify if the l.e. modification were in accord with numerical prediction. Primary goals of leading edge modification was the reduction of drag through the improvement of lower surface flow.

In the past other light aircraft like P92 and P96 have been extensively tested [1] at DPA in the wind tunnel and optimized configurations have been the result of the test campaign. In example the leading edge fairing of P96 low-wing aircraft has been designed through wind tunnel tests that have shown reduced separation at wing root.

Wind tunnel tests, paying carefully attention to Reynolds number effects, can lead to an estimation of aircraft performances which can be compared to data coming from numerical evaluations (panel code [ref. 2] , semi-empirical methods[ref. 3]) or comparison with similar aircraft with the same engine.

Flight tests can give indications on some possible improvements in the aircraft aerodynamics which can be verified through wind tunnel tests before implementing the final modification on the aircraft.

TEST SETUP

Wind tunnel tests on the aircraft model and on the 2D airfoil model (see fig. 4) have been performed in the DPA wind tunnel which is a closed circuit low speed tunnel with a test section of 2 m. wide and 1.4 m. height.

The maximum Reynolds number is about 3 million per meter and the turbulence level is about .1% at the test section center.

Tests on the airfoil have been performed by pressure measurements on a 2D model with 0.75 m. chord spanning the test section and a wake rake has been used to estimate airfoil drag. Tests on the aircraft model have been performed using a strain gage based three-component balance to measure lift, moment and drag.

AIRFOIL TESTS

An aluminum model with 0.75 m chord spanning vertically the test section (see fig. 4) has been tested. The airfoil shape is shown in fig. 5.

The airfoil characterized by forward and rearward camber, is 13.4 % thick and has been designed to have good high lift capabilities.

The original airfoil showed very high drag characteristics at high speed conditions and it was then modified at the leading edge (fig. 6) to improve flow conditions on the lower surface.

The original airfoil showed at negative angles of attack (cruise conditions) an high negative pressure peak which leads to flow separation on forward part of lower surface.

Airfoil optimization has been performed through numerical codes developed at DPA and a new leading edge shape has been designed. The airfoil model has been modified and tested again.

Lift curves relative to the original and to the modified airfoil (called VG1-13H) are shown in fig. 7. The airfoil maximum lift coefficient at Re=1.8 mil. is about 1.60 and the airfoil can be then considered like a high lift airfoil. The leading edge modification does not lead to any considerable lift decrease.

Due to strong blockage effect at high angles of attack (the airfoil chord over test section width ratio is 0.4) the airfoil stall has been measured on a new model with 0.45 m chord.

In fig. 8 the experimental lift curve at Re=1.1 mil. of the smaller model compared to that one relative to the 0.75 m chord model at the same Reynolds number is shown. The airfoil maximum lift coefficient has been measured to be 1.62 and different post-stall behavior respect to the bigger model can be observed. At Re=1.8 mil. (flight conditions at stall) the airfoil maximum lift coefficient is expected to be between 1.65 and 1.70.

Airfoil drag polar at Re=1.8 mil. of original and modified airfoil are shown in fig. 9. The original airfoil was characterized by a high negative pressure peak on the lower surface at low and negative angles of attack.

In fig. 10 pressure distributions on original and modified airfoils at low angle of attack are shown. The graph put in evidence the different flow conditions on airfoil lower surface which leads to lower drag. The original airfoil at alpha=-4 deg. is characterized by a separated flow region on lower surface, while the modified airfoil shows a high negative pressure peak with completely attached flow. The airfoil was then characterized by small separated area on lower surface with consequent drag increase at high speed cruise conditions. In fact the original airfoil has very high drag at lift coefficients lower than 0.30÷0.40. The modified airfoil shows improved behavior at low lift coefficient, being characterized by acceptable drag also at high speed cruise conditions (Cl around 0.20).

Drag coefficient at high speed conditions have then been reduced and brought to acceptable values.

In fig. 11 airfoil moment coefficient (respect to 0.25 c) at Re=1.8 mil. are shown. The airfoil is characterized by quite high moment coefficient (around -.10) which is a penalty regarding tail trim drag and torsional loads at high speed. The airfoil on the aircraft will be mounted with the rear part deflected 5 deg. upward to reduce moment coefficient.

The airfoil is currently under a refinement phase through both numerical and experimental investigations.

Numerical versus experimental data comparison has been presented in [4].
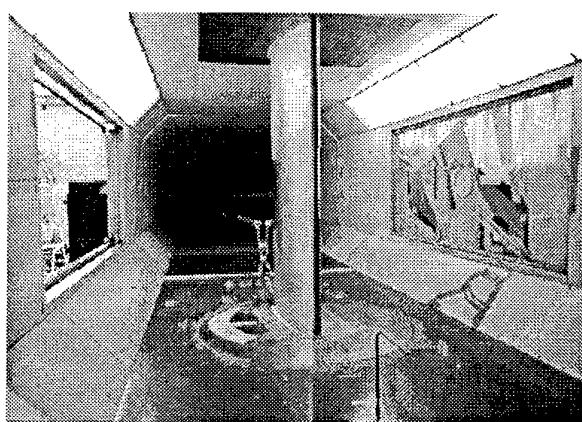
Fig. 4 : Airfoil model in DPA wind tunnel test section
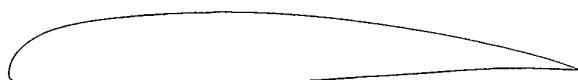
Fig. 5 : VG1-13 Airfoil
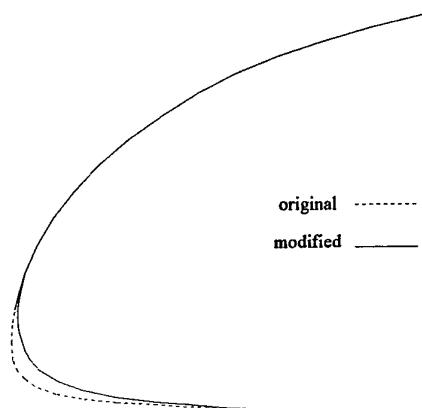
Fig. 6 : VG1-13 Airfoil – leading edge
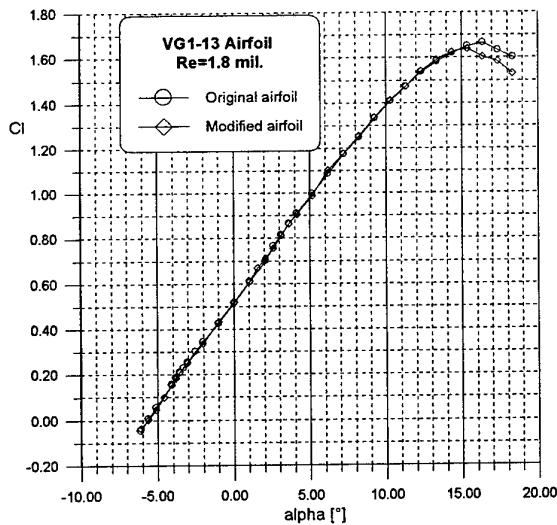
Fig. 7 : VG1-13 original and modified airfoil – lift curve
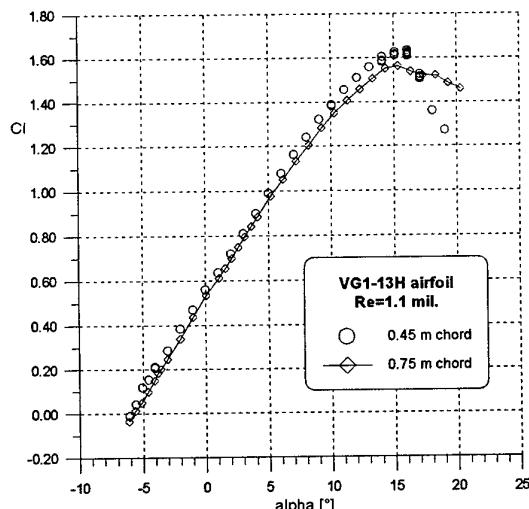
Fig. 8 : VG1-13H airfoil – lift curve of 2 models
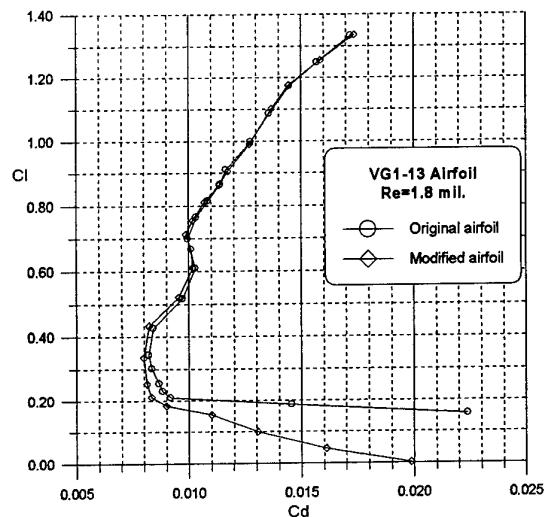
Fig. 9 : VG1-13 Airfoil – drag polar
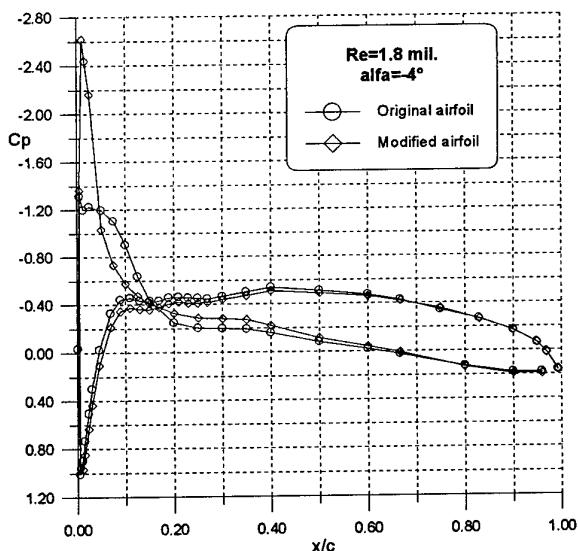
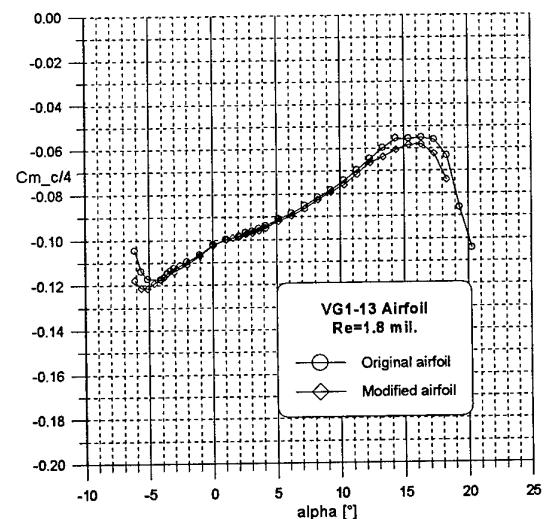Fig. 10 : VG1-13 Airfoil - press. coeff. distribution

Fig. 11 : VG1-13 Airfoil – moment coeff. curves

AIRCRAFT MODEL TESTS

Configuration aerodynamic analysis and optimization has been performed through wind tunnel tests on the aircraft model.

Wind tunnel tests have been performed on a 1:5 scale wood model of G97 wing-body. The model has been built reproducing the exact configuration, including the real engine nacelle and air intake shape. Pictures showing the wing-body model mounted in DPA wind tunnel test section are shown in fig. 2 and 3. In fig. 3 the lateral view shows the fuselage shape and the engine nacelle reproduction in scale.

Different flap/aileron configurations

The wing on the model has been built in such a way to allow various settings of flap/aileron deflections. The goal was to test also the configuration obtained deflecting the flap and aileron 5° upward obtaining a reduced moment coefficient suitable for high-speed cruise. The model airfoil geometry with trailing edge movable part deflected 5° upward and set at 0° is shown in fig. 12. The wing with flap and aileron top view is shown in fig. 13. Other tested configurations obtained deflecting flap/aileron are shown in table 1.

chord =220 mm   movable part = 47.5 mm
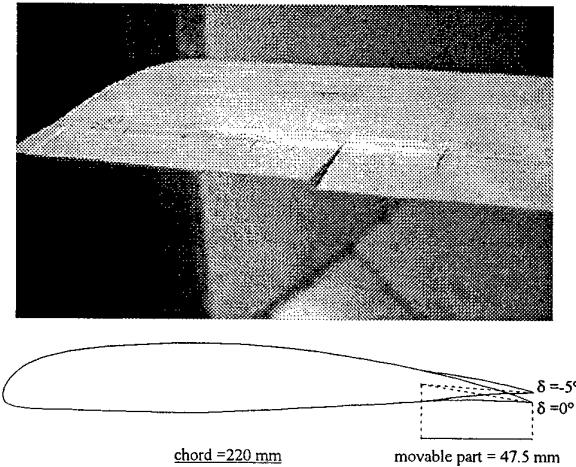
Fig. 12 : wing model flap/aileron
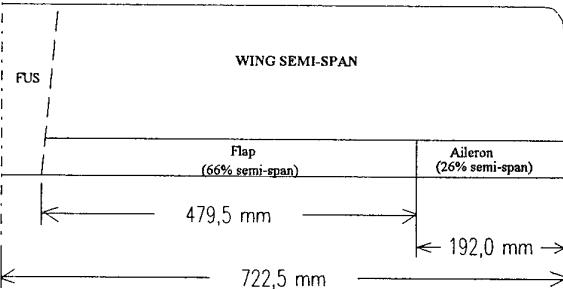
Fig. 13 : Wing semi-span model top view

CONF.	Flap	Aileron
A (High speed)	δ=-5°	δ=-5°
B (Low speed)	δ=0°	δ=-5°
C	δ=0°	δ=0°

Table 1 : Wing flap/aileron configurations

The test Reynolds number referred to the wing chord (c=0.22 m) is about 0.6 mil. The difference of Reynolds number between wind-tunnel tests and flight has to be taken carefully in account comparing aerodynamic coefficients obtained for both airfoil models and flight. Wind tunnel tests for flap/aileron configuration A,B,C have been performed. Configuration A (with flap and aileron deflected -5° upward) is thought to be the final aircraft configuration for high speed. At lower speed, with flap set at 0°, conf. B is the other operative configuration. The upward deflection has been foreseen to reduce the moment coefficient which is too high for VG1-13H airfoil. Configuration C is not an operative condition for the real aircraft, but it is useful to check aileron effectiveness.

In fig. 14 the lift coefficient curves versus alpha for the 3 different configurations is shown. The maximum lift coefficient for configuration A is reduced form 1.45 (conf. C) to 1.35. Wing-body lift coefficients are in good agreement with scaled (to 3D effects) two-dimensional values measured on the airfoil model. The flap and aileron effectiveness have been evaluated.

The flap effectiveness $\tau=(d\alpha/d\delta)$ is :$\tau=(1.75°/5°)=0.35$

The aileron effectiveness is : $\tau=(0.95°/5°)=0.19$

The moment coefficient curves for the 3 different configurations, evaluated respect to the estimated real aircraft C.G. position (Xc.g. = 23.3% chord and Z c.g. = 29.3% chord under wing level) are shown in fig. 15.The moment coefficient at alpha=0° with flap and aileron deflected 5° upward (conf. A) is reduced from -0.12 (relative to conf. C) to -0.08. This value seems reasonable to limit wing torsional load and tail equilibrium load at high speed. The moment coefficient versus CL curve shows a static stability for CL greater than 0.6, typical of high-wing configurations. The slope in the linear range indicates a position of the wing-body aerodynamic center of about 19% of the chord.

In fig. 16 the drag polars for conf. A,B,C are shown. Conf. A is characterized by a drag coefficient of 0.028 while conf. C has a considerable increase of drag at low lift coefficient with a value around 0.035. The advantage of adopting conf. A at high speed instead of conf. B is also underlined by this favorable effect. The drag increase of conf. C at low lift coefficients is mainly due to the airfoil which is working at negative angles of attack and is characterized by areas of separated flow on lower surface (like in fig. 11). The polar curve for conf. A is parabolic for CL between 0.20 and 1.00 and is characterized by a CDo=0.025 and an Oswald efficiency factor of 0.72.
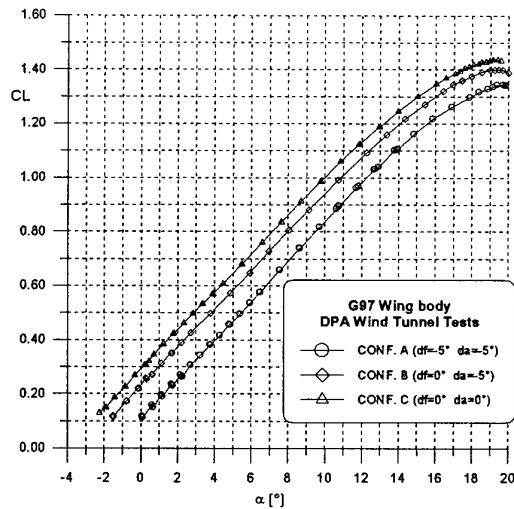
Fig. 14 : Wing-body Lift curves for different flap/aileron configurations
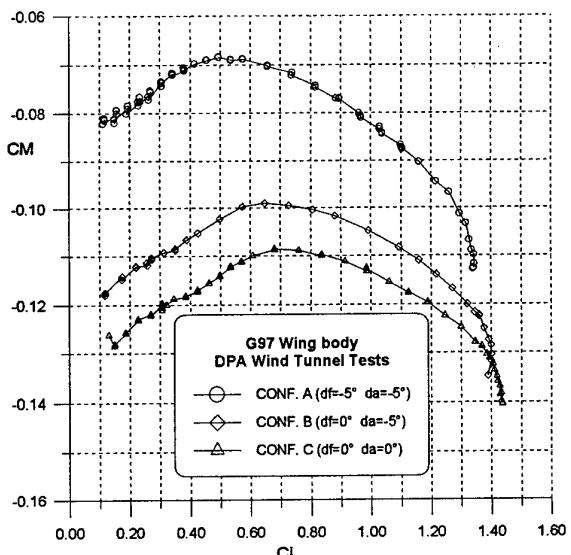
Fig. 15 : Wing-body moment curves for different flap/aileron configurations
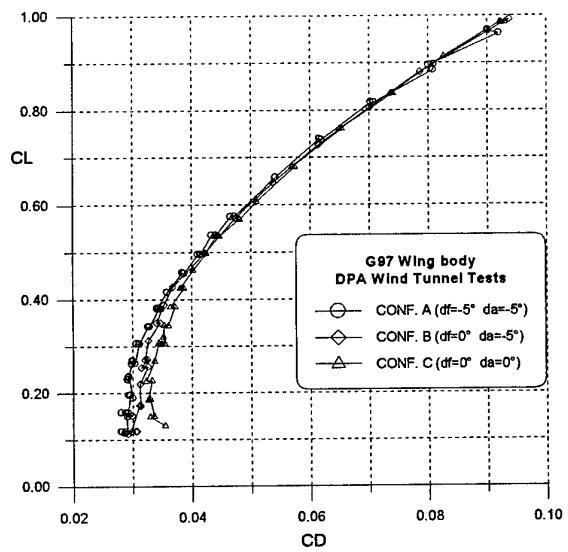
Fig. 16 : Wing-body drag polars for different flap/aileron configurations

Effect of engine nacelle and air intake

Effect of engine nacelle and air intake has been investigated.

Two different nacelles with different air intake frontal area have been tested. Tests have been performed also with a fin instead of the nacelle and the air intake to estimate their contribution to the total drag.

Pictures of lateral views of nacelle N1, N2 and fin are shown in fig. 17.

In fig. 18 is clearly noticeable the difference in air intake frontal area between nacelle N1 and N2. The intake of nacelle N1 was modified to reduce frontal area and flow separation on the top and shape N2 was chosen.

With nacelle N2 (smaller than the first one) a 25% drag reduction has been obtained as shown in the wing-body drag polar relative to wing configuration A (fig.19).

In the same figure the drag polar relative to the configuration with fin is shown. It can be seen that configuration N2 leads to drag values not so higher than those relative to the configuration with fin. The influence of air intake frontal area is not so critical for configuration N2, however the most

critical aspect which contributes to the high drag increase for configuration N2 appears to be the flow separation on air intake upper surface. In fig. 20 flow visualization with tufts on configuration N1 and N2 at alpha=1° are shown. It is clearly visible that conf. N1 presents separated flow (which leads to the higher drag in fig. 19) while conf. N2 is characterized by attached flow conditions.

Preliminary flight tests on the aircraft prototype have shown that the second nacelle with smaller air intake does not lead to any danger of insufficient engine cooling.

NACELLE N1

NACELLE N2

FIN
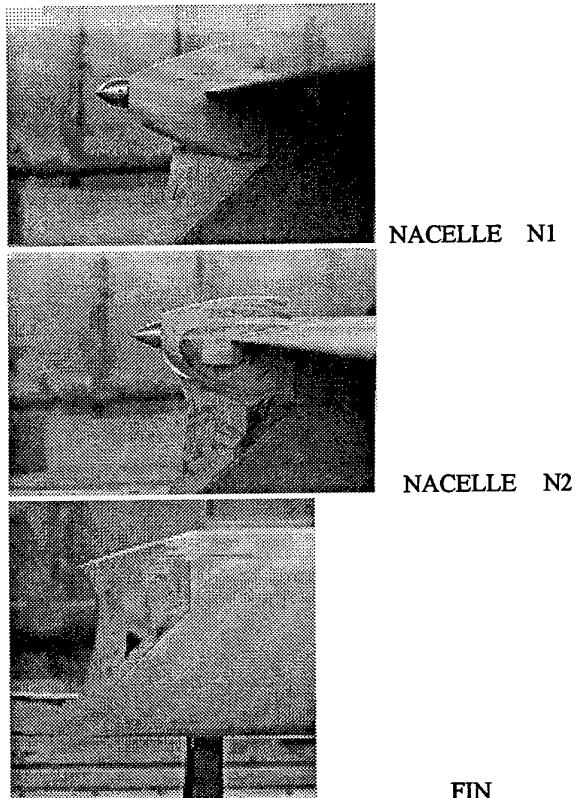
Fig. 17 : Nacelle N1, N2 and fin
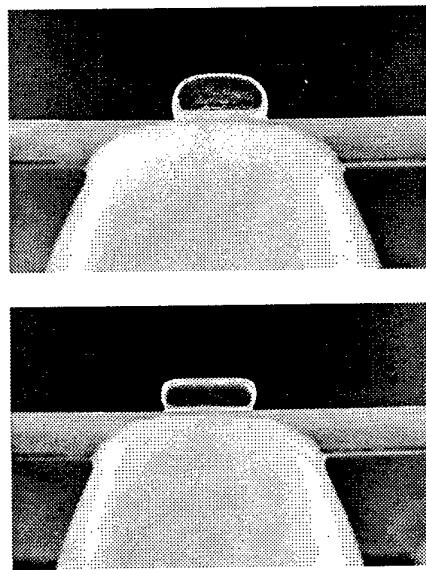
Fig. 18 : Nacelle N1, N2 – frontal view
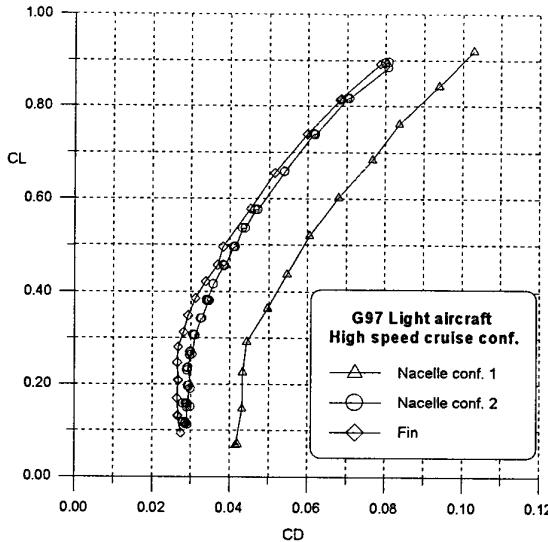
Fig. 19 : Drag Polar, Nacelle N1,N2 and fin
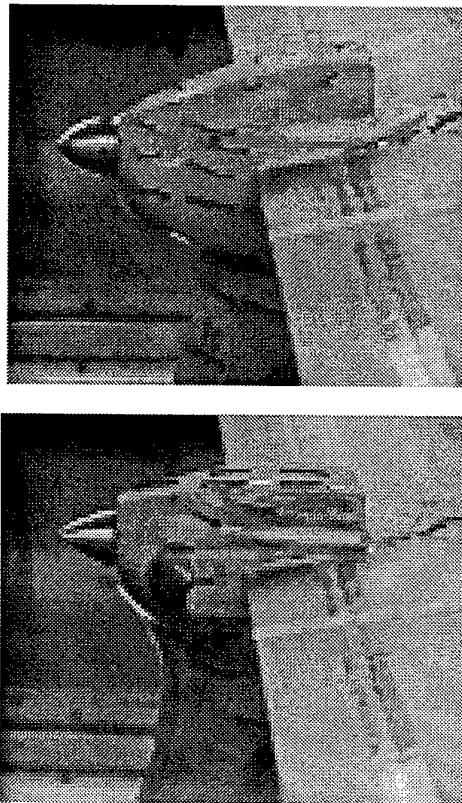
Fig. 20 : Flow visualization on nacelle N1 and N2
alpha=1 deg.

Wing-fuselage junction fairing

The experimental results presented in figg. 14, 15, 16, 19 were obtained with a fairing at both wing fuselage junction and air intake. Wing-fuselage interference effects have been pointed out through panel method calculations [4]. These effects together with more complicated and unpredictable 3D viscous interference effects lead to a drag increase which can be reduced through the use of a proper fairing.

More than one fairing shape has been tested and a final very small fairing has been found which leads to a considerable drag reduction.

In fig. 21 the picture shows the fairing at the junction. In fig. 22 drag polars relative to the wing-body configuration A (and nacelle N2) with fairing (also shown in fig. 16 and 19) and without fairing are shown.

It is possible to notice that the fairing is particularly effective at low angles of attack. In fact the fuselage without fairing induces high negative angles of attack at wing root but with the fairing this effect is diminished. This is a desirable effect in view of the fact that the VG1-13H airfoil is characterized by separations and high drag values in this range of angles of attack (fig. 9).
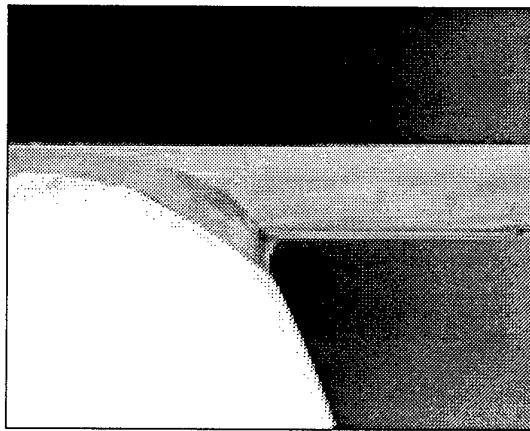
Fig. 21 : Wing-fuselage junction fairing
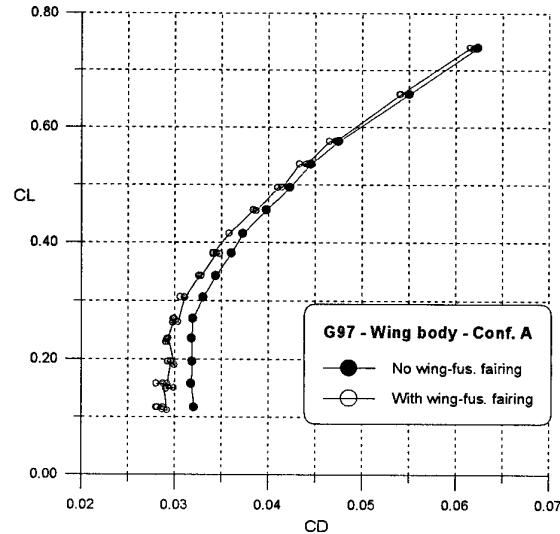
Fig. 22 : Effect on drag of wing-fuselage junction fairing

Air intake fairing

Effect of a small air intake fairing has been tested. From flow visualization with tufts it appeared that separated flow conditions were present on air intake sides.

To improve and streamline the air intake an air intake fairing has been thought and applied to the model. The air intake is represented in fig. 23 and 24.

Drag polar of configuration A with nacelle N2 and with air intake fairing and without air intake fairing are shown in fig. 25. The use of the air intake fairing leads to a further drag coefficient reduction of almost 10% .
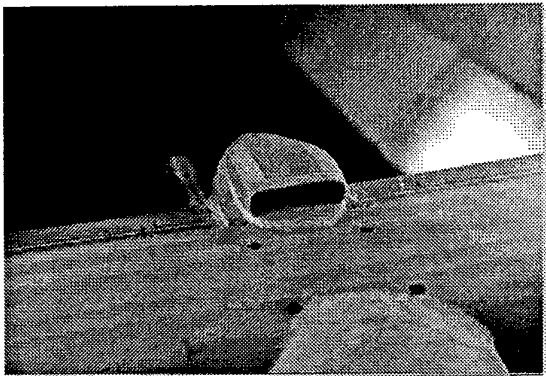
Fig. 23 : Air intake fairing
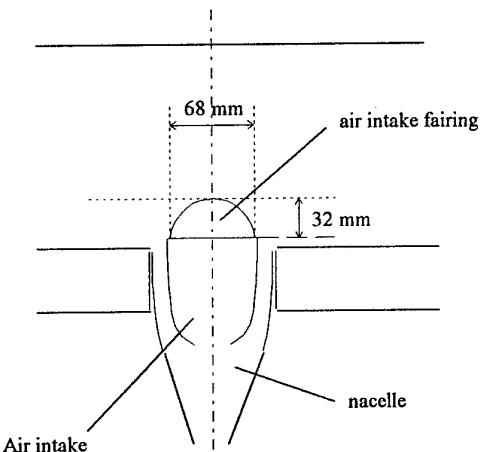
Fig. 24 : Air intake fairing
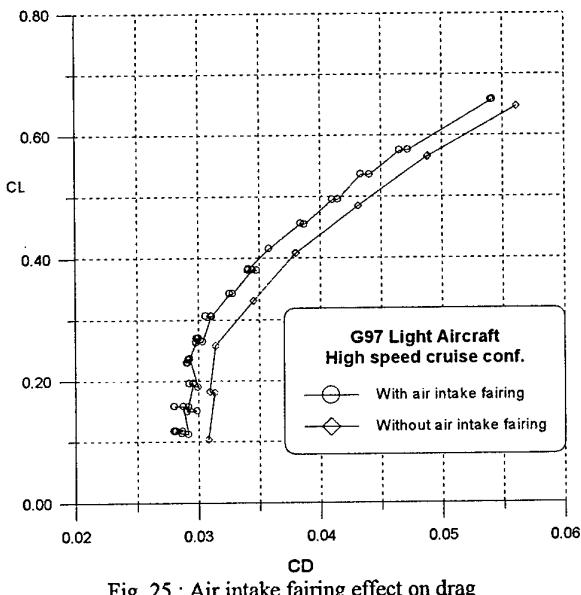
Fig. 25 : Air intake fairing effect on drag

Fuselage length increase

To shift the C.G. position toward the aircraft nose (it is well known that the rear pushing propeller configuration is critical because the engine weight leads to balance problems) it has been necessary to increase the fuselage length. Effect of fuselage length increase has been tested.

In fig. 26 the lateral view of both original and stretched fuselages is presented.

The fuselage length has been increased of 5 cm on the model (corresponding to about 25 cm for the full scale aircraft).

The effect of length increase (and also of wetted area) on fuselage drag is shown in fig. 27. In this figure the drag coefficient versus angle of attack of the original and stretched fuselage with nacelle is shown. The length increase leads to an average drag coefficient increase of 1÷2 counts (about 10% of fuselage drag). It can be seen that the fuselage drag decreases with incidence due to the air intake which becomes less exposed.

The effect of length increase on wing-body moment coefficient (evaluated respect to the aircraft CG position, Xcg=23.3%c - Zcg on middle of fuselage height) is shown in fig. 28. It can be noticed that in the linear range (CL between 0 and 0.5) the stretched fuselage is characterized by an increased instability respect to the original one. The aerodynamic center of the wing-body configuration is at 19% of the chord with the original fuselage and at 18% for the stretched fuselage. The moment coefficient (also due to the different wing-fuselage interference effects) is reduced of about 0.01 and this is favorable for equilibrium loads.
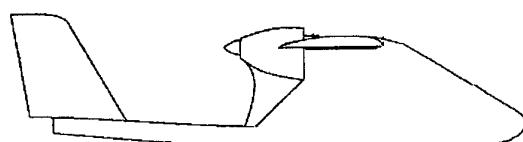
Fig. 26 Original and stretched(on the top) fuselage
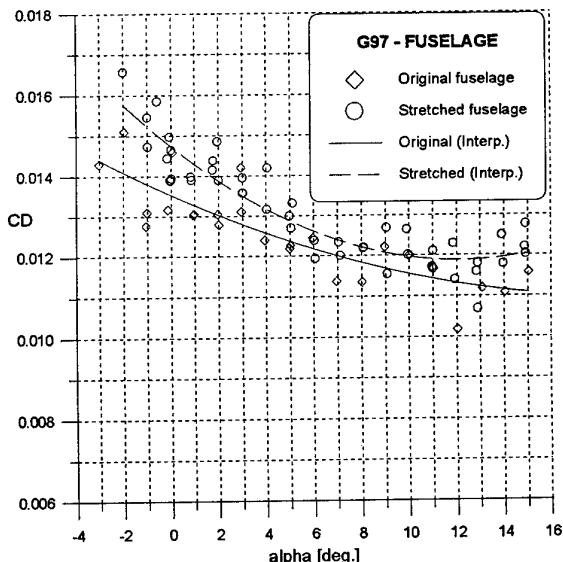
Fig. 27 Fuselage Drag coefficient
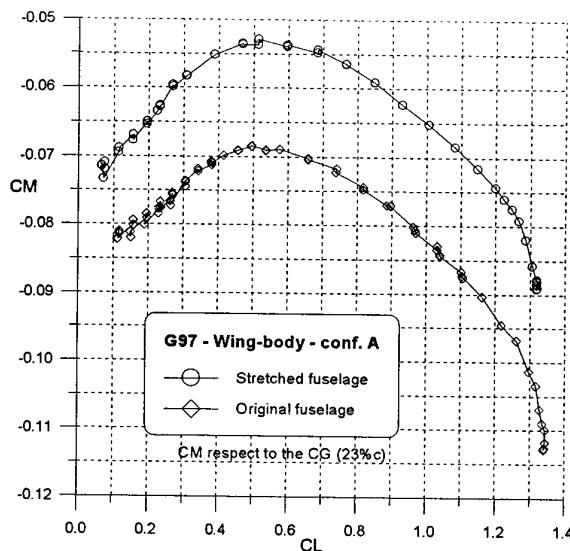
Fig. 28 : Wing-body moment coefficient

Wing stall path

Investigation on the wing stall path has been performed by visualization with tufts.

Visualizations indicate a stall path similar to a tapered wing due to the effect of the air intake in the middle of the wing.

In fig. 29 flow visualization on wing upper surface at alpha=17 deg. is shown. The separated flow region is evidenced in fig. 30. It is clear that the air intake and the nacelle in the center of the wing influences the wing stall and reduces separations at wing root. The aileron region is unaffected by flow separation.
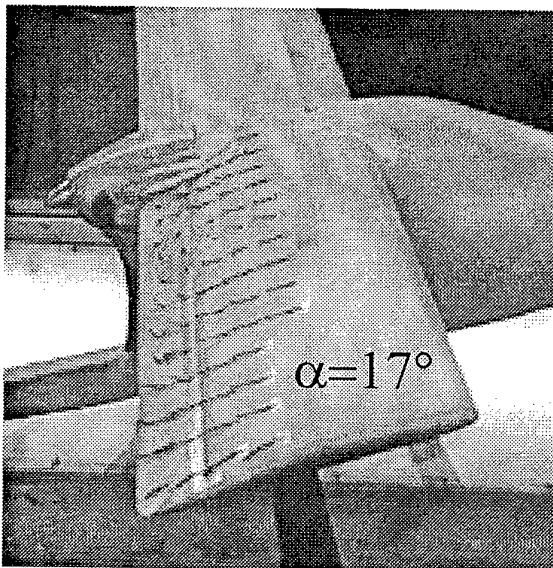
Fig. 29 : Flow visualization, α=17 deg.
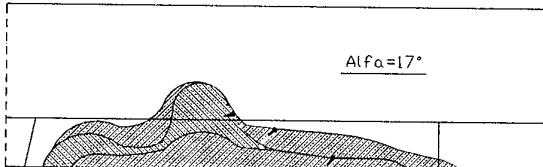
Fig. 30 : Separated region

Conclusions

Wind tunnel tests have been performed in the low speed wind tunnel belonging to D.P.A. on airfoil and aircraft models of G97 *Spotter* light aircraft.

The airfoil leading edge shape has been optimized leading to a reduced drag coefficient at high speed cruise conditions.

The aircraft model has been tested in several flap/aileron configurations giving indications on flap/aileron effectiveness and a necessary moment coefficient reduction has been obtained deflecting the flap 5 deg. upward.

An accurate analysis has been performed on nacelle and air intake shape. Two different nacelles with different air intake frontal area have been tested. It has been obtained a relevant drag coefficient reduction through a well streamlined nacelle shape. Effect of an air intake fairing has been tested. The fairing leads approximately to a 10% drag reduction on wing-body configuration.

Effect of fuselage length increase has been tested. The "stretched" fuselage leads to a very small drag increase and modifies the moment coefficient and the aerodynamic center of wing-body configuration.

The wing stall path has been analyzed through flow visualization with tufts on wing upper surface.

The air intake at wing center leads to a reduced load and reduced separation at wing root.

Further investigations through wind tunnel tests have been planned in the next future.

Flight tests will give further indications of accuracy of wind tunnel aerodynamic analysis and optimization of this light aircraft.

References

[1] Coiro D.P., Marulo F., Nicolosi F., Ricci F.: "Numerical, Wind Tunnel and Flight Tests for P92J and P96 Light Aircraft" XXI I.C.A.S. Congress, Melbourne, AUSTRALIA, Sept. 1998.

[2] F. Nicolosi, D.P. Coiro : "Fuselage Design and wing integration for Sailplanes and Light Aircraft", XIV AIDAA Congress , Naples October 1997

[3] Wolowicz, H. C. and Yancey, B. R., " Longitudinal Aerodynamic Characteristics of Light, Twin-Engine, Propeller-Driven Airplanes ," NASA TN D-6800, 1972

[4] Giordano V., Coiro D.P., Nicolosi F., : "Reconnaissance Very Light Aircraft Design. Wind-Tunnel and Numerical Investigation". EHAE 99 Conference, Prague, Sept. 1999. To be published on Journal for theoretical and applied mechanics – Czech Republic.

Rapid Generation of Conceptual and Preliminary Design Aerodynamic Data by a Computer Aided Process

Luciano Fornasier, Thomas Gottmann

DaimlerChrysler Aerospace AG – Military Aircraft

P O Box 801160

D 81663 Ottobrun, Germany

ABSTRACT

A multidisciplinary integration framework (MIDAS- an acronym for Multidisciplinary Integration for Design and Analysis Software) is developed for a quick and accurate assessment of aircraft performance. The system allows for the continuos integration of the conceptual and preliminary design stages. The MIDAS system is starting from the definition of the configuration layout to provide basic aerodynamic data- for performance analysis, sizing, structural layout and early handling qualities. The first aerodynamic dataset is provided by an Excel-based module in a highly automated way. This data base can be updated by computational and experimental fluid dynamics findings. Another MIDAS module integrate the preparation of CFD meshes. The paper deals with the integration of aerodynamic methods within the aircraft design.

INTRODUCTION

Within the frame of a series of initiatives aimed at improving effectiveness of its aircraft design and analysis capabilities, the Military Division of DaimlerChrysler Aerospace AG (Dasa) is developing MIDAS, a multidisciplinary integration framework for aircraft design process. MIDAS targets specifically configuration studies in a conceptual and preliminary design environment, where peculiar requirements such as flexibility and robustness of the system components, reliability of results, user friendliness, and fast response times have to be properly addressed. The overall objective here is to reduce response times of analysis and iterative design cycles of one order of magnitude while increasing design quality and decreasing design uncertainties. The basic approach selected consists of cross-linking methodologies and numerical simulation tools already existing in the specific disciplines across a common interface, streamlining the data flow between the different building blocks by standardization of exchange data structures and creation of common data bases. In this paper the generation and integration of the aerodynamic data within the MIDAS system is presented.

INTEGRATION OF AERODYNAMICS IN THE DESIGN PROCESS

In the conceptual design phase, mission performance, trajectory optimizations, sizing, and stability and control require generation of a proper longitudinal aerodynamic

data set. The aerodynamic data typically are presented as function or in tabular form, **Figure. 1**.
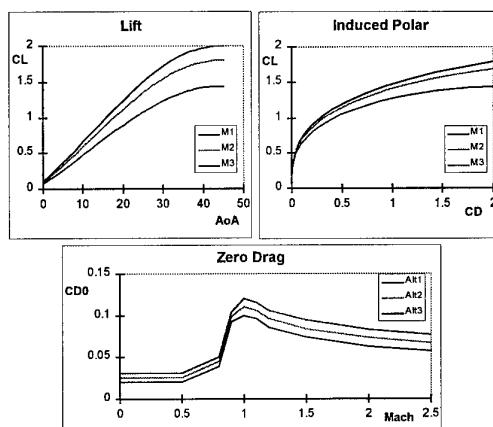
Figure 1 – Example of a [Trimmed] Aerodynamic Data Set as used for Point Performance Calculations

In general, the predicted aerodynamic data are derived from different sources. At the very beginning of the conceptual design loop, prediction of aerodynamic characteristics relies on handbook methods, existing databases, approximate methods, and correlation methodologies, often blended with sensible 'guess-estimated' values. Due to obvious limitations of this methodology, especially when applied to innovative – i.e. not evolutionary - designs, application of numerical methods of Computational Fluid Dynamics (CFD) can be beneficially used to improve the estimated aerodynamics as the design evolves into the preliminary design phase. To this purpose, numerical flow solvers of different degree of flow modelling fidelity are nowadays available, ranging from panel methods for prediction of linear flow characteristics to Euler flow solvers for assessment of non-linear aerodynamics – e.g. transonic flow and high-angle of attack characteristics, and Navier-Stokes solvers for viscous flow conditions. CFD and wind tunnel experiments are used to validate the aerodynamic design and to assess the risks for the following phase of the project.

An important feature of MIDAS is the inclusion of high fidelity numerical simulation methods in the early design process.

When applying CFD methodology, rapid and efficient ways to set-up the numerical models, run the flow simulations, analyze the results and extract the desired information must be devised for containing the required time and human

efforts within values affordable and acceptable to conceptual and preliminary design project timeframes and budgets. Extrapolation of the progress in computing power of the last years let expect application of high fidelity CFD methods become the primary aerodynamic tool in the near future, but currently their use has to be limited to the analysis of critical flow conditions. Thus, since today CFD calculations do not cover the entire flight envelope of interest, predictions of different accuracy level have to be matched and balanced carefully. The generation of a consistent aerodynamic data set from the 'raw' aerodynamic data is a process which certainly requires sound engineering experience and may still involve time-consuming manual work, representing a severe bottle-neck within the entire design process chain.

In the following, the basic approach taken to overcome the present limitations and allow MIDAS 'open the way' to CFD methodology in conceptual and preliminary design analysis is presented and discussed.

BUILD UP OF THE AERODYNAMIC DATA SET

In a first development step, the MIDAS building blocks necessary to realize the coupling between configuration layout, aerodynamics, propulsion and masses – left side of Figure 2 - have been developed, ref. [1].
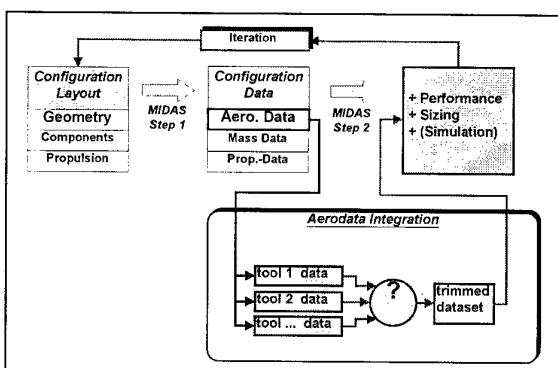
Figure 2: A/C Conceptual Design Iteration Principle and MIDAS Steps 1 & 2

In the second development step of MIDAS, an interactive build-up procedure for integrating the aerodynamic data and yielding the trimmed data-set required as input for operating the performance, sizing and flight simulation modules has been implemented. The position and the function of the aerodynamic integration module within the iterative design process is indicated by a question mark in the circle of the lower box in Figure 2.

The design and implementation of this aerodynamic integration module have been mainly driven from the specific functional requirements deriving from applications at Dasa conceptual design environment. Some of the main 'drivers' are presented here.

Unlike design of conventional transport aircraft systems, design of advanced military configurations may rely on a variety of different or novel arrangements of aerodynamic means for aerodynamic control and maneuvers. This in turn implies a high flexibility in the tool used for building up

the aerodynamic set, which should be able to accommodate a broad variety of application rules.

Another requirement stems from the necessity to progressively refine and adjust the data set, as new information and more accurate data are becoming available during the design process. One common method to generate the initial aerodynamic data set is to provide the derivatives and the zero values for lift, drag and pitch moment coefficients integration of the functions by assuming some appropriate blending interpolation between the given data yields generally smooth functions, which can be used as first guess for performance and sizing calculations, Figure 3. These 'initial' curves are later adjusted as more accurate results – such as CFD calculations and wind tunnel experiments data – become available later, Figure 3.
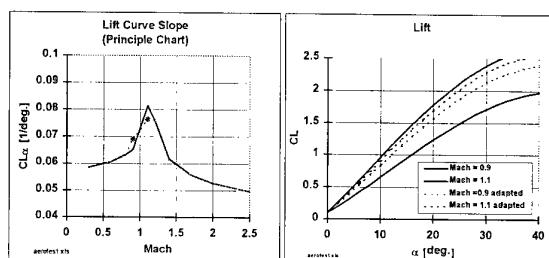
Figure 3: Example of Data set Adaptation Using Derivative Representation of Aerodynamic Data

The left hand side of the figure shows a preliminary crude derivative function and the right hand side contains the integrated coefficient. As an example, two adaptations are sketched as dots (left diagram) and the corresponding adapted curves as dashed curves (right diagram). In the same way fast variations and scaling of the data set can be performed.

With respect to trim, two different procedures are available. Initially, some 'educated-guess' of trim effects are added to the clean aerodynamic data. These trim losses are dependent on the stability characteristics of the configuration and on the zero pitching moment. Hence they can be neglected to the first order for configurations which are aerodynamically marginally stable and at design conditions. Later, initial assumptions must be refined by performing a trim calculation, by balancing all pitching moment contributions with respect to the actual center of gravity position. The effort in this case is clearly unlike higher but the trim losses can be determined with higher accuracy. In addition, better knowledge on the configuration become available, like required control power, control surface deflection settings and static stability margin.

An important feature for the integration module is the compatibility of the data set build-up procedure with the one incorporated in the Aero Data Module (ADM), a Dasa proprietary software tool used at the pre-design level, Ref. [2]. ADM contains and interpolates a complete 6 degree-of-freedom aerodynamic data set, which includes all control elements of an aircraft, and is used in flight mechanics and flight simulation. Output options of ADM in combination with the AERO-Module are clean and/or trimmed dataset or only parts of the dataset, gradient matrices and others **(Figure 4)**.
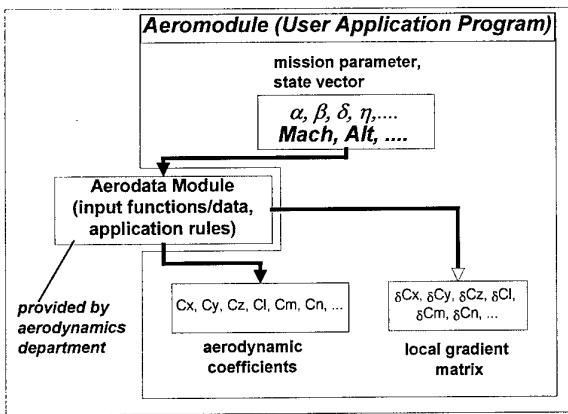
Figure 4: ADM and AeroModule (6 –DOF /11/)

The required compatibility with ADM allows to obtain a tight integration of the conceptual with the preliminary design phase, since the data sets established in conceptual design to be taken over in a later pre-design phase in terms of data and/or application rules.

QuADBUS Basic Layout Features

According to the set requirements, a software tool called QuADBUS -Quick Aero Data Build Up System- has been developed. The overall integration of QuADBUS within the aerodynamic data set generation procedure for the conceptual design is sketched in **Figure 5**.
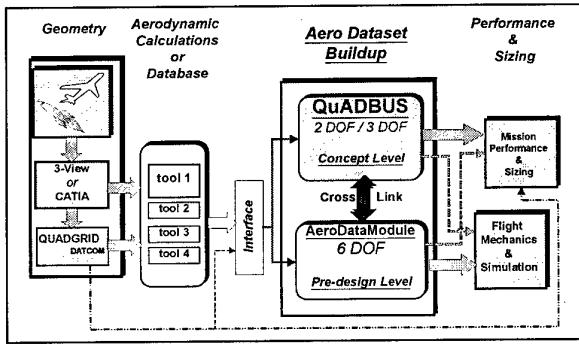
Figure 5: Flowchart of Aerodynamic Dataset Generation

This scheme shows that the data: flow can either incorporate the QuADBUS or the ADM (Aero Data Module) software tools (QuADBUS is used at the *conceptual design level*, whereas ADM serves for the *pre-design level*).

Unlike ADM – which consists of a series of FORTRAN library that must be linked together with the specific application program - QuADBUS is implemented as an EXCEL-based standalone application. Using the de-facto standard EXCEL spreadsheet environment, the user can perform the data manipulations using the EXCEL interactive cell operations, while visually controlling the effect of the data alterations – in real time – using the EXCEL-built-in graphic capabilities. Plug-ins to specific

macro functions written in VisualBasic allow the execution of calculation tasks (e.g. interpolation, gradient computation, solution of linear systems, appliaction rules). Although the computational speed of the Excel implementation is several orders of magnitude more slowly compared to an equivalent implementation in FORTRAN, no appreciable drawback has been perceived so far. For an application using a calculation matrix of following dimensions:

Variable Type	No of Variables
Mach number	15
Angle of Attack	20
1st Control Surface (Preset)	15
2nd Control Surface (Trim Element)	10
Altitude	10

and requiring the usage of about ten Visual Basic routines in the background, a PENTIUM II-233 processor takes about 10 seconds for the entire calculation process with trimming and update of all graphs. The associated size of the Excel file is 4.5 Mbyte.

QuADBUS Internal Dataflow and Module Arrangement

The required flexibility in building up the data set using a broad variety of application rules is obtained combining the spreadsheet feature of the EXCEL software itself with the VisualBasic capability to realize calculation program modules.. **Figure 6** illustrates schematically the migration of the data within QuADBUS from the definition of the input data for the clean configuration (left side) to the output of the trimmed data for the complete configuration.
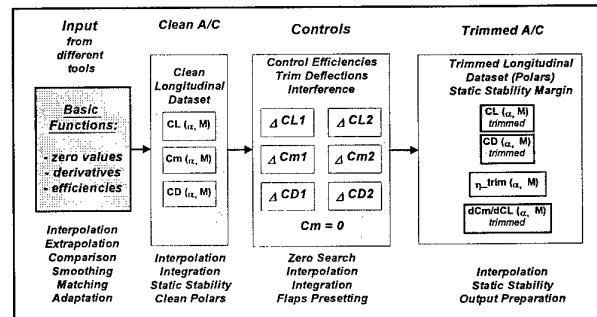
Figure 6: QuADBUS Principle Dataflow

The parts relevant to the controls (input data and associated application rules) are always present but become inactive for those components that have not been explicitly defined. The application rules used for the coefficients build-up are defined as VisualBasic functions in separate files.

The user interface used to communicate with the internal data flow structure is represented by an EXCEL template, **Figure 7**: The workfile contains several worksheets (for geometry, mission, input functions, clean configuration aerodynamics, ...) and VisualBasic sheets with the routines

as necessary e.g. for the application rules and for the trim calculation.

Separate input sheets include groups the input data which are read in by an EXCEL macro or which may be copied from an ASCII file. The same kind of presentation – tables, graphs - are realized for the output of the calculated datasets.
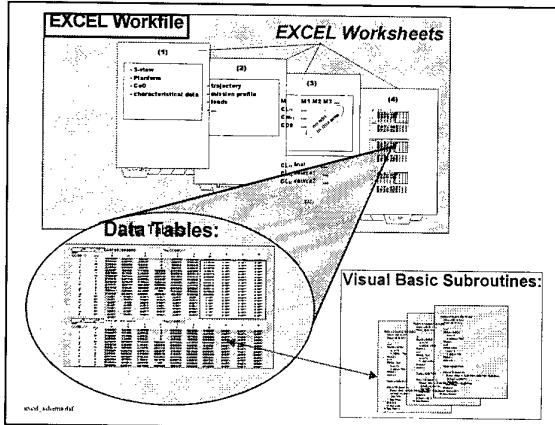

Figure 7: QuADBUS User Interface (EXCEL Workfile)

For the build-up of a new configuration aero dataset, first a copy of the QuADBUS *master file* must be opened and filled with the data of the actual configuration under concern. At the beginning, the cells relevant to the input are empty. The worksheets are marked for the various inputs and in addition are prepared for the dataset build-up process. The user can either type or copy the data into the tables, from an existing data set or from plain ASCII files as available, and can watch the dataset growing. As navigational aids, cells eligible to receive user's input are highlighted with different colors, depending whether the input is necessary or optional. All remaining cells, where intermediate and final results are stored, are write-protected in order to prevent accidental modification or deletion.

The calculations can be performed either step-wise, sheet-wise or for the entire workfile. Data generally may be changed by editing of the single cells and/or by drag-and-drop mouse operation in the graphs.

Application Rules Handling

Internally in QuADBUS, each aerodynamic coefficient is represented by a sum of additive terms, whereas the application rules specify how these terms are combined together in dependency of the independent variables, e.g. Mach number, altitude, angle-of-attack, control settings. For example, the lift and drag curves for the clean configuration are defined using the zero-values, linear slopes, non-linear terms, minimum and maximum values, interference and flow separation dependent terms, resulting in the final lift curve shape and drag polars, as shown in **Figure 8**.

This decomposition mechanism allows to separate the effect of each particular influence parameter on the global curves, a useful feature in conceptual design, where estimated values for these parameters can be assumed to be dependent from the geometrical characteristics of the configuration by

means of semi-empirical formulas (like e.g. body influence on wing planform efficiency, wing leading edge suction, vortex lift) .
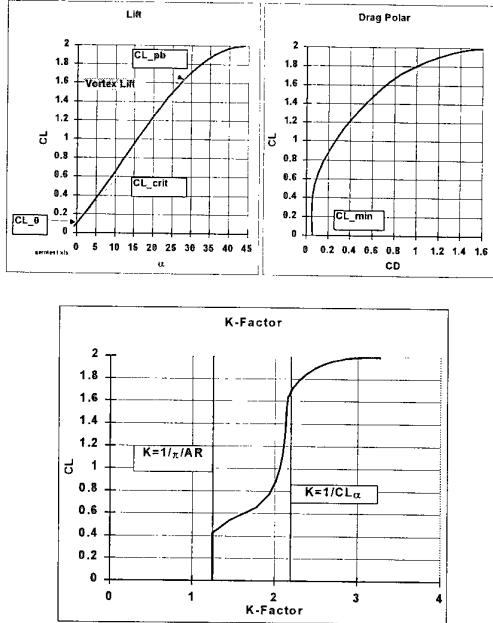
Figure 8: Elements of Lift and Drag Build-up of the clean A/C

To this purpose, a limited geometry description and analysis capability is optionally available in QuADBUS, which allows to extract automatically the geometrical parameters relevant for the aero data build-up process (e.g. wing planform, surface area, mean aerodynamic chord, control volumes, cross-section area distributions.) from a schematic three view layout of the configuration, **Figure 9**.
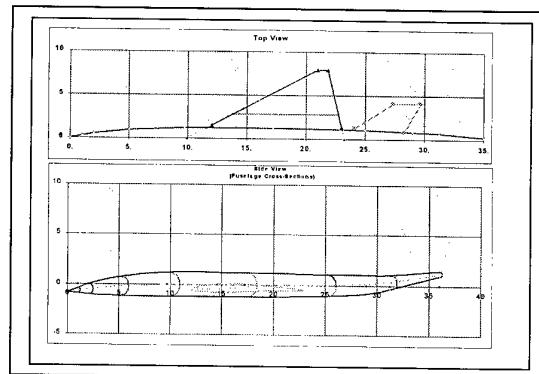

Figure 9: Planform and Cross-Section Input Options

In this way, the total lift curve may be obtained by adding non-linear contributions from leading edge and tip vortices computed according to DATCOM /12/, Schemenski /13/, Polhamus /14/ relations. The non-linear lift contribution of low aspect ratio wings, e.g. can be described as $CL_v = Fv$ $(1-R)$ Kv $\sin^2\alpha$ $\cos\alpha$ where Kv is a function of the LE and TE sweep angles and Mach number, and Fv is a vortex breakdown factor vs. aspect ratio and angle of attack, **Figure10**.
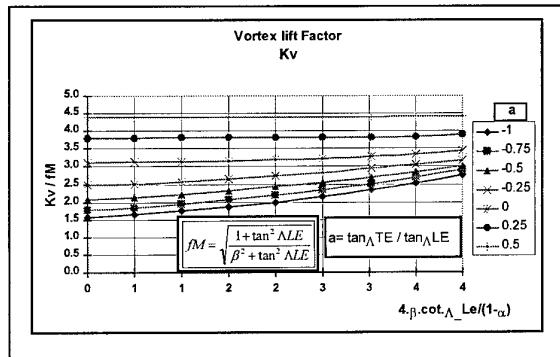
Figure 10: QuADBUS: Vortex Lift Factor Dependency

The leading edge suction parameter R of course is depending on the profile of the wing, the angle-of-attack and the aspect ratio. In QuADBUS parameters and factors like the above described ones can either be imported from outside or interpolated from the tables located in the background sheets of QuADBUS, using the geometry parameters as calculated from the geometry sheet.

In a similar way, the induced drag of the A/C is computed by a special procedure that allows a broad variety of manipulations, which take in account the real flow behaviour and still may be adapted to the data which are available to the user:

The strategy for the induced drag build-up within QuADBUS is sketched in **Figure 11**, where four options can be chosen by the user: As basic solution, the induced drag for the clean aircraft is automatically computed according to DATCOM/Schemensky methods /12, 13/ as a function of the Mach number and lift coefficient using the available geometrical information.
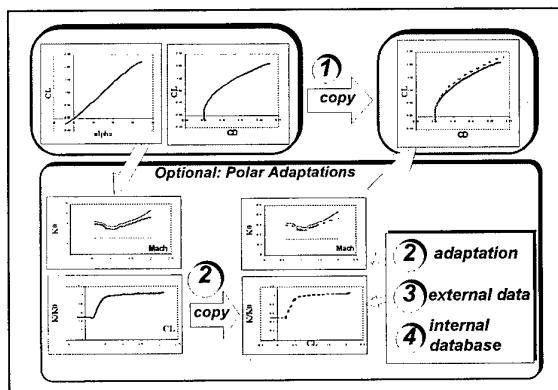
Figure 11: Options in Composition of Drag-Polars

1. *Implemented Procedure and/or*
2. *by Comparison of Similar A/C and Manipulation of K-Factor*
3. *Input of K-Factor Tables (external data)*
4. *Using internal database*

The first option consists of using directly this estimated polar in all further calculations ①.

For the other options, the basic polar is presented in the following parabolic fitting form:

$$CDi = K0\,(Ma)\cdot K/K0\,(CL, Ma)\cdot (CL-CLmin)^2$$

where the K0 and K factors depends on the Mach number and on both Mach and lift coefficient respectively. This kind of representation is – in fact – quite usual in conceptual design and allows an experienced user to make sensible educated-guess for the K-factor values when no better estimates are available. Hence the second option allows the user to operate directly on the K-factors tables, while verifying the effect of the adaptation on the induced polar curves(Figure 11). The third option allows to import K-factor tables or CDi tables from outside- e.g. produced by CFD calculations ③ and to start the polar calculation at this point.

The fourth option is using a QuADBUS internal database ④, where statistical values of typical K-factors are stored for different aircraft categories. **Figure 12** shows the upper and lower bounds of the stored K-factors for fighter type aircraft. The user is then required to define the actual curve he intends to use within the shown bandwith.
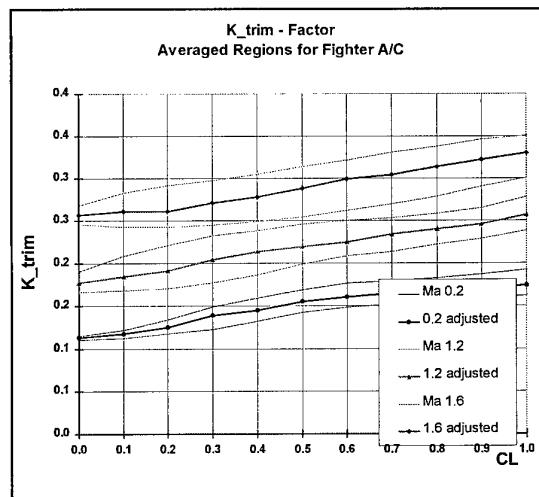

Figure 12: Example for using the K-Factor Database in QuADBUS (here: Combat Aircraft)

EXAMPLES OF APPLICATION

In the following two application examples are given for demonstrating the capability of the QuADBUS module.

QuADBUS Application Example 1: Clean Polar Buildup

An existing pre-design data set has been used as benchmark in an evaluation exercise aiming at assessing QuADBUS capability in the generation of the aerodynamic data set for an advanced fighter-type configuration. For simulating the operability conditions typical of a conceptual design phase, no other 'external' information but zero values and linear gradients have been used in QuADBUS. The reference

data set –generated by the ADM module – is based on CFD and wind tunnel data.

Figure 13 shows the comparison of lift and drag polars for a subsonic and a supersonic Mach number. As can be seen, QuADBUS predictions of non linear effects on both lift and induced drag compare well with the reference data.

The effort required to operate QuADBUS for generating the data is orders of magnitude lower compared to ADM operation.
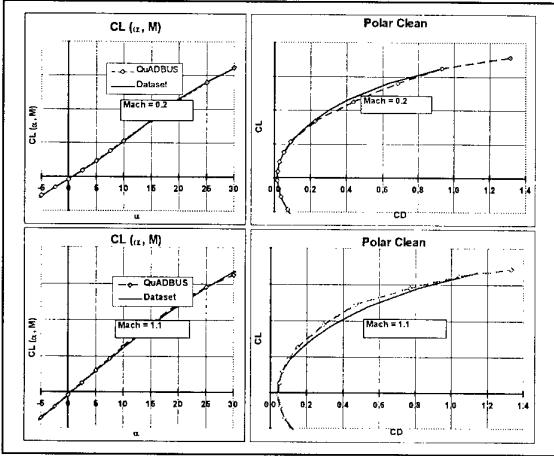

Figure 13: Comparison of Original Dataset (Generic Combat Aircraft, Experimental & CFD Data) and QuADBUS Integration Procedure Results

QuADBUS Application Example 2:Trim Calculation for Two Different Center of Gravity Positions

In this application, the trim capability of QuADBUS is used to investigate the aerodynamic variations due a rearward shift of the configuration center of gravity.
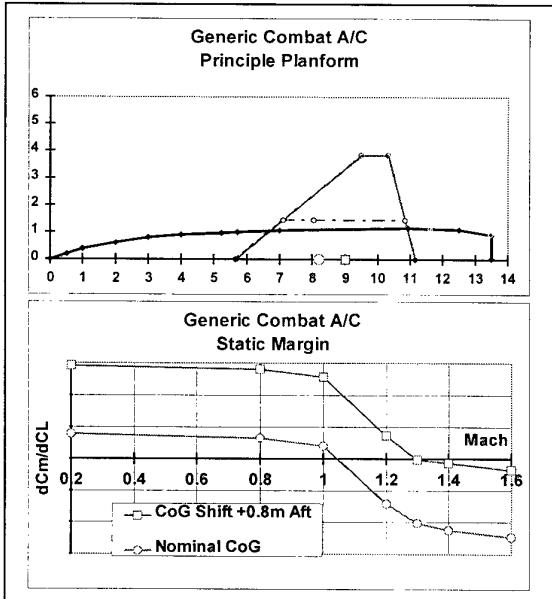
Figure 14a Generic Combat Aircraft Planform and: Static Margin Stability

.**Figure 14** .shows the planform of the configuration and the two center-of-gravity positions used in this example. The lower part of Fig.14a contains the resulting static stability margin vs. Mach for the two CoG positions, as calculated by QuADBUS.

A selection of typical output graphs from QuADBUS, the aerodynamic performance L/D_trim, and the corresponding elevator trim angle δ_trim is presented in Fig. 22b (nominal CoG position) and Fig.14c (rearward shifted CoG position). The wing trailing edge flap schedule for this example was (M=0.3: η_TE = 10°; M=0.9: η_TE = 5°,; M>1: η_TE = 0°).

From Figure 14c it can be seen that for M=0.2 the curve for the trim angle of the elevator reaches saturation at an angle of attack 20. The variations illustrated in Figure 14 are performed in less than half a minute, including all graphs, (not shown here; related to that example, about 150 graphs in the background were active for control purposes). The user interaction is limited to update the x-position of the center of gravity in one cell.
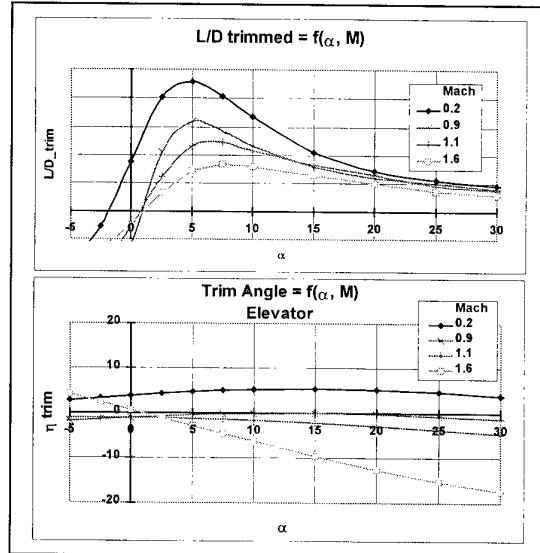

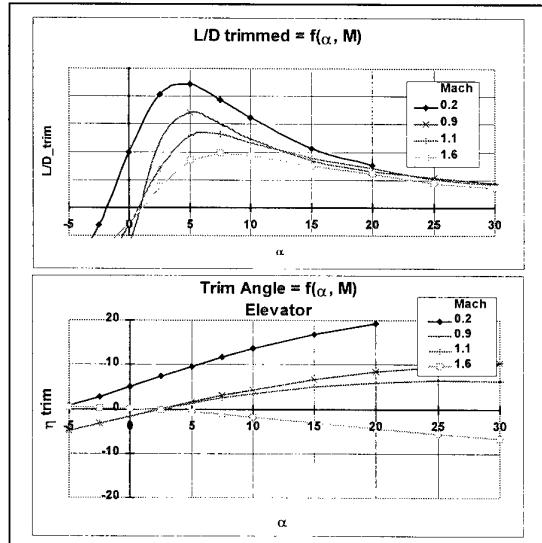*Figure 14b: Trim Results for nominal X_CoG*

Figure 14c Trim Results for rearward X _CoG (+ Δ0.8m)

RAPID SURFACE MESH GENERATION

Presently the HISSS panel method – **Ref. 6** and AIRPLANE+ -an in-house development of the AIRPLANE Euler unstructured flow solver of **Ref. 7-8-10** - are integrated in MIDAS. The mesh generator FLITE – **Ref 9** – is used to generate the unstructured volume grid used by the Euler solver. Both the panel method and the unstructured mesh generator require as geometry input the definition of a structured surface grid. The generation of a valid surface mesh about a complex aircraft configuration is a demanding task, which requires considerable amount of skill and effort, **Figure 15**.
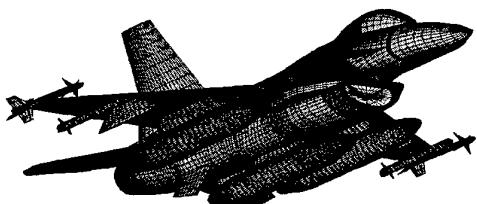
Figure 15 – Surface panelling for a F16-type Fighter
Aircraft -

At the very beginning of a conceptual study a complete lofting model does not exist, therefore a simplified geometry definition is integrated in MIDAS. To this purpose, the geometry generator PGRID has been developed, that allows to obtain a valid surface model in a highly automatic way from a limited amount of geometrical data. The surface model generated by PGRID can be directly used as input to the panel method and/or to the unstructured mesh generation.

Later in the design stages, it is desirable to start the grid generation process from a high-quality CAD model, that is the repository of geometrical layout of the configuration during the design phase. Since CAD models are normally defined for constructive purposes, they are normally not readily suitable for mesh generation. Filtering and un-cluttering of superfluous elements, restoration of surface integrity by closure of gaps and removal of overlap, modification of badly meshable regions are required before the meshing process can start. When done manually, this preparation activity may take several labour weeks. In the ESPRIT Project JULIUS a CAD Repair tool is being specifically developed to reduce substantially the effort of extracting a 'ready-to-mesh' surface model from a 'dirty' CAD model.

The two tools are briefly presented in the next setions.

The Geometry Generator PGRID

The lofting strategy adopted in PGRID – Parametric Geometry by Reduced Input Data - focusses on typical aeronautical applications, without any claim to generality, and combines different elements from existing approaches, **Ref.s 3-4**. The basic idea is to reduce the amount of information required to define an airplane geometry by decomposing the whole configuration into a set of isolated parts, like fuselage, wings, tails,. and letting the geometry generator itself performing all the operations necessary to yield a geometrical model satisfying the surface mesh generation requirements (i.e. surface continuity, closed-volume domains).

The whole configuration is broken down into its constructive parts, i.e. fuselage, engine inlet and outlet or nacelle, wings, control surfaces, external pods. Each of these components are defined and modeled in isolation, and subdividing it into a set of geometrically less complex surface elements (patches). The three-dimensional surface of each patch is then described by bi-dimensional parametric polynomial functions. The actual shaping of these parametric surface is controlled by the user via specification of a set of variables. Three different types of surface specification are available:

Body-like component patches are described by defining the evolution of a conic curve between two opposite boundary curves by means of blending functions. 4th-order parametric polynomial functions after –**Ref.4** - are used for both the conic and the blending curves;

Wing-like component patches are defined by assuming a linear variation between two wing sections arbitrarily positioned in space. A database of over 200 different wing sections is directly accessible from the program; if necessary, the profile thickness can be scaled to the user specified value;

B-Splines surface patches can be used indifferently to describe body- or wing-like components; they are defined starting from a rectangular array of grid points and using a least-square deviation procedure to determine the set of control points which 'best-fit' the given points; once computed, the B-spline parameters - i.e. control points and parametrical vectorbase, /4/ are stored in IGES format into a local database for later use; a similar technique is followed for determining and storing b-splines curves used for interpolating airfoils section originally available in tabular form;

Starting from the individual specification of the configurations components the grid generator performs automatically a series of operations, which, requiring only a few additional user's directives allow to yield a 'valid' a surface mesh:

Definition of the initial mesh: according to the user's specifications, each patch is discretised into a rectangular **mxn** array of points - i.e. a certain number **n** of sections each carrying **m** points; the location of the inner points is found from the given point distribution along the boundaries by applying a Laplace solver in the parametric space:

Generation of connectivity relationships: a topology information table is automatically built to keep trace of the connectivity relationships of each patch to its neighbors; all

patches connected together are stored into a special data structure called *thread*; depending along which boundary curve the patches are connected a distinction is made between m- and n-threads; in order to satisfy the contiguity meshing requirements the number and the location of the points along the edges shared by two patches must be identical; as a general rule, the number of points for each patch is raised to the largest dimension found in the local threads;

Calculation and regridding of part intersections: curves between two intersecting parts are discretised by calculating the piercing points between the curves of one part - defined as *master* - and the surface of the other part - defined the *slave* - ; hence, 'master' parts retain their original topology, while slaves parts must be re-gridded in order to fit the intersection curves; again the points on the slave patches are redistributed by using the Laplace smoother in the parametric space. In general, master patches retain their original number of points, unless the case when one or more slaves are intersected by topologically independent masters - e.g. short-coupled wing-foreplane.

Final regridding and validity check: After having intersected all compenetrating parts, fulfillment of the contiguity condition is checked again and, when necessary, gridding of patches with insufficient number of points is updated. Then a check is performed breaking up contiguous boundary curves into identical *segments*: a necessary condition for a 'valid' mesh is that each segment must bound exactly two patches or - for symmetrical configurations, one patch and lie on the symmetry plane.

Application to a Business Jet Aircraft

The generation of a surface mesh for a typical business-jet configuration is presented. The general layout of the configuration has been derived from the GULFSTREAM IV three-views drawing from /4/.

Figure 16a shows the build up of the airplane configuration. The fuselage and the engine nacelle have been described using the body-like input form, while wing, winglets, wing/winglets fairing, horizontal and vertical tail, and engine pylon make use of the wing-like description scheme. The fuselage has been further subdivided into smaller parts, for achieving a better control of the cross section distribution The solid lines represents the patch boundary curves. For sake of simplicity the wing and the engine pylon has been extended up to the symmetry plane.
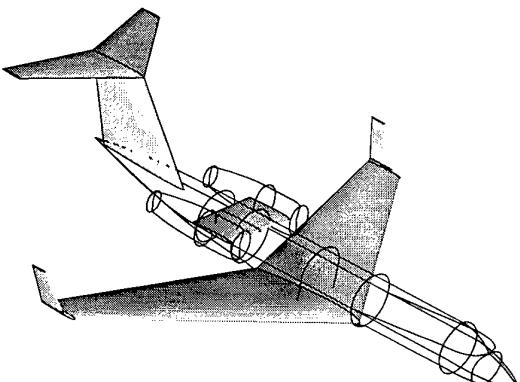

Figure 16 - Business Jet Configuration
(a) Schematic representation of user defined input

The Figure 16b represents the grid of the central part of the fuselage after the calculation of the intersections with the wing and the engine pylon. The patch boundaries are rendered by thicker solid lines. The two blank areas represent the footprints of the innermost sections of the wing and of the pylon. Aiming at obtaining a smooth transition from the wing to the fuselage grid lines, a special user's directive has been used to wrap the body grid around the wing leading edge - the so-called C-type topology option. An H-topology type intersection has been produced at the pylon intersection (default topology).
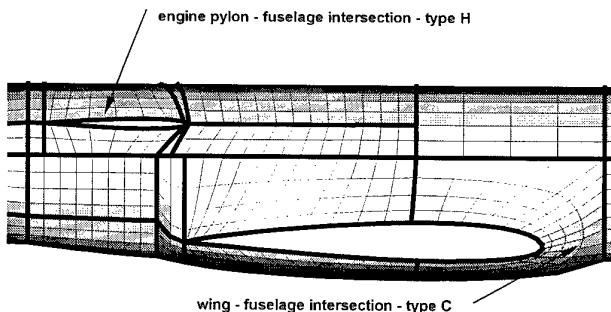

Figure 16 (b) Intersection regions on fuselage

Due to local topological constraints, the number of chordwise points of the pylon have been automatically decreased from its original value.

The appearance of the final surface grid for the complete configuration is rendered in figure 16c. The topology information are used to obtain a 'closed- volume', contiguous grid.
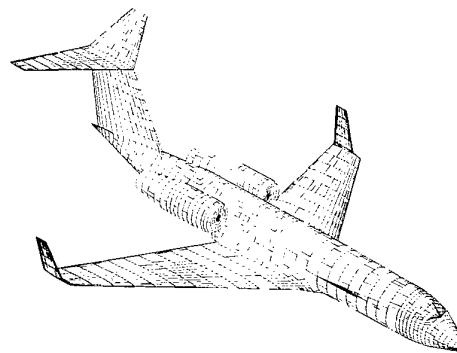

Figure 16 (c) Final surface grid

B.C. specification and wake generation: To complete the modeling for the panel method calculation, the boundary conditions and the geometry of the wake surfaces shed from the lifting parts of the configuration must be specified. Both these items have been addressed in PGRID, in such a way to comply with the modeling requirements of the panel code HISSS. Without PGRID, the generation of a correct wake geometry is almost an art and requires a good deal of practice. The approach followed here has been to transfer the expertise directly to the mesh generator, leaving to the user the task to check the validity of the automatically generated wakes, and providing him/her the possibility to

define or modify the wake modeling manually. Figure 16d, next page - presents the wakes generated in full automatic mode by PGRID for the GULFSTREAM configuration.
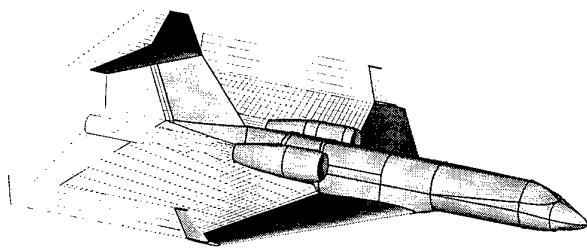
Figure 16 - Modelling of a Business-Jet Aircraft
(d) automatic wake arrangement

The GULFSTREAM modelling presented here has been computed in a couple of minutes on an intel 486 lap-top with only 8Mb RAM. The basic configuration input data have been defined by hand in two hours work back in 1995 as first application of PGRID to a complete wing-fuselage - tails and nacelle. The engine pylon has been introduced later for demonstrating the multiple intersection capability.

The JULIUS CADR Tool

In compliance with the technical requirements specified by end-user partners of the ESPRIT Project EP the Institute for Production Systems and Design, IPK, Berlin, is developing the interactive application software CADR – CAD Repair. The CADR tool integrates a commercial CAD translator which imports a CAD model from an IGES description and transforms the imported data into a NURBS-based data structure. Based on an analysis of these data, the topological information tree of the model is performed, that in turn, is used for detecting topological and geometrical errors of the models. Interactive commands or predefined operation sequence are used to obtain a 'waterproof' surface models that satisfies the requirements of the downstream application modules. At the end of the 'repairing' actions, all the geometrical and topological information are stored into a BREP+ data structure. The geometrical part of BREP+ structure is based on trimmed NURBS-patches. In cooperation with the partners CSCS and SMR, IPK is presently implementing the capability to detect 'badly'-meshable elements, as tiny faces, high aspect ratio elements. Merging of patches by reparametrisation and carpeting techniques are then used to improve the local mesh quality.

CADR Application: Business Jet Airplane

For sake of comparison, the aircraft configuration defined by PGRID is presented. The Business Jet geometry is imported in CADR using an IGES description of the surface patches of the isolated components, **Figure 16a**. Executing the default sequence of operation, CADR performs automatically following operations: splitting of folded surfaces, finding of common edges, calculation of

intersecting curves, trimming of surfaces by edge curves, detection of gaps. At the end of the sequence, visualisation of patch attributes is used to help the user to remove the trimmed parts of the wing, tails and engine pylon parts falling inside the fuselage and the engine nacelle. Visualisation of the attribute 'gaps' allows to selectively pick the pairs of free edges eligible to be closed by automatic construction of proper surfaces that are added to
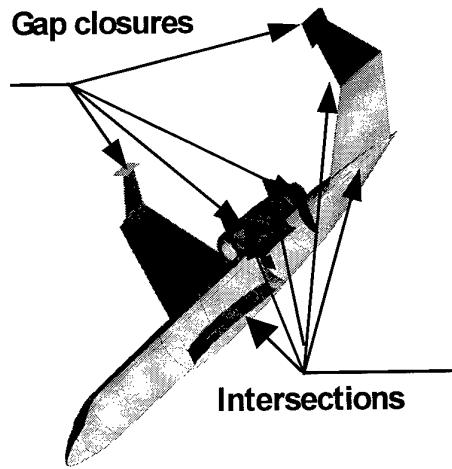
the data structure, **Figure 17.**

Figure 17 – CADR repairing operations

Running the verification sequence it can been verified that the model is now geometrically and topologically valid. The model can be now be stored into the BREP+ data structure. A FLITE-compatible file is written for the unstructured mesh generator. A detail of the surface triangulation obtained by FLITE is shown in **Figure 18**. By comparison with figure 16b it can be seen that the use of trimmed patches by the CADR module allows to avoid the segmentation of the original patches in the intersection regions, improving the quality of the local mesh. The CAD repair for this model takes less than half an hour for a user
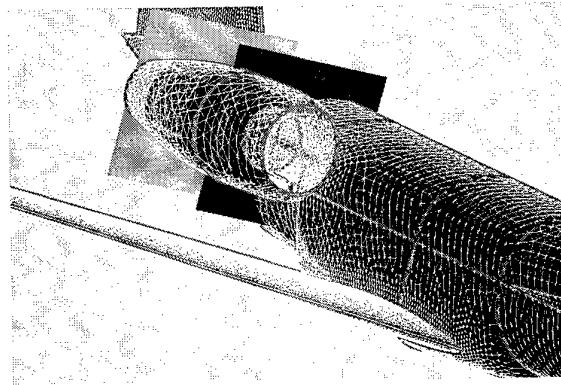
with little specific experience.

Figure 18 – Detail of the unstructured surface mesh

CFD RESULTS

In this section some selected CFD results are presented. The whole process, from the definition of the geometrical models to the CFD computation has been carried out using the tools discussed in this paper.
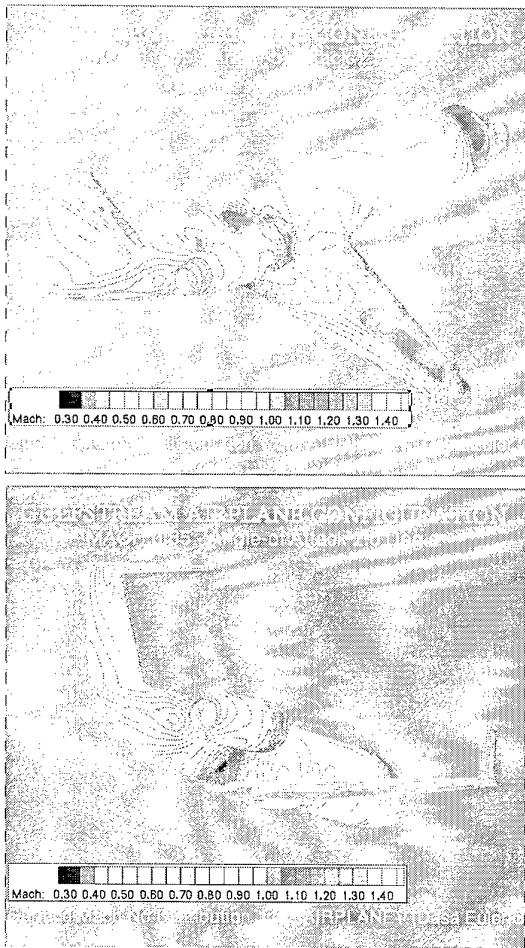

Figure 18 – Visualisation of AIRPLANE+ calculation

CONCLUSIONS

Integration of CFD methodology in the generation of the aerodynamic data set gives the opportunity to reduce design risks already in the earliest design studies. The system presented here allows to remove two bottle-necks in the application of CFD tools and to obtain accurate aerodynamic data already in the initial conceptual design phase.

A typical bottleneck within the conceptual design process is the integration of the aerodynamic results from the various tools and data sources into a consistent aerodynamic dataset. A software platform (QuADBUS) was developed to allow rapid build-up of the trimmed aerodynamic data set using interactive data manipulation. The system is suitable for execution of design variations/trade-offs calculations and of sensitivity analysis. The tool is based on commonly available spreadsheet software, allowing the user to work in an open, but well structured environment –

comparable to the former engineering work using pencil, rubber and pocket calculator – but having the full digital support of modern information technology.

A new set of tools covering both the geometry definition and the mesh generation task has been developed for reducing the effort when generating computational meshes around complex airplane configurations. The applications presented here demonstrate the present capability and the potential of the proposed approach. Requiring a minimum of training and few more data than a three view layout to start with, the new system allows to generate within reasonable response times structured surface meshes about geometrically complex airplane configuration, thus allowing to promote the use of powerful CFD analysis tools in the conceptual and preliminary aircraft design.

REFERENCES

1. Fornasier, L., 'Multidisciplinary Integration of Numerical Simulation Methods in Conceptual Design of Advanced Aircraft and Space Vehicles', AIAA 96-4131, 1996
2. Raymer, D.P., 'Aircraft Design: A Conceptual Approach', AIAA Educational Series, 1992
3. Sobieckzky, H., private communication, 1994
4. JANE'S, 'All the World's Aircraft', 1987-88 Ed., pp. 433.
5. Mortenson, M.E., 'Geometrical Modeling', John Wiley and Sons, 1991
6. Fornasier, L., 'HISSS - A Higher-Order Panel Method for Subsonic and Supersonic Attached Flow about Arbitrary Configurations', in *Panel Methods in Fluid Mechanics*, Notes on Numerical Fluid Mechanics, Vol. 21, Vieweg Verlag, 1987
7. Jameson;A. Baker T.J., and Weatherill, N.P., 'Calculation of Inviscid Transonic Flow over a Complete Aircraft', AIAA Paper 86-0103, 1986
8. Jameson,A, and Baker, T.J., 'Improvements to the Aircraft Euler Method', AIAA Paper 87-0452, 1987
9. Weatherill, N.P., and Hassan, O., 'Efficient Three-Dimensional Delauney Triangulation with Automatic Point Creation and Imposed Boundary Constraints', International Journal of Numerical methods in Engineering, Vol. 37, 1996, pp. 2005-2039
10. Rieger, H,. et al., 'Development of an Aerospace Design System into a Parallel User Simulation Environment', Proceedings of the HPCN Europe 1996 Conf. , Springer Verlag, 1996, pp. 340-351
11. Cucinelli, Giancarlo "Projekt IFA: Vorstellung des Aero Data Moduls" Daimler-Benz Aerospace, Militärflugzeuge, asa-MT631-3100-TN-S-485, 31.7.98
12. USAF Stability and Control DATCOM Air Force Flight Dynamics Laboratory, October 1960 (Revised August 1968)
13. Schemensky, R.T. "Development of an Empirically Based Computer Program to Predict the Aerodynamic Characteristics of Aircraft" Convair Aerospace Division of General Dynamics Corporation, AFFDL-TR-73-144, Vol.1, Nov. 1973
14. Polhamus, E.C."Charts for Predicting the Subsonic Vortex-Lift Characteristics of Arrow, Delta, and Diamond Wings" NASA TN D-6243, April 1971

ACKNOWLEDGMENTS

REPORT DOCUMENTATION PAGE

1. Recipient's Reference	2. Originator's References	3. Further Reference	4. Security Classification of Document
	RTO-MP-35 AC/323(AVT)TP/15	ISBN 92-837-1040-1	UNCLASSIFIED/ UNLIMITED

6. Title

Aerodynamic Design and Optimisation of Flight Vehicles in a Concurrent Multi-Disciplinary Environment

7. Presented at/sponsored by

the Symposium of the RTO Applied Vehicle Technology Panel (AVT) held in Ottawa, Canada, 18-21 October 1999.

8. Author(s)/Editor(s)	9. Date
Multiple	June 2000

10. Author's/Editor's Address	11. Pages
Multiple	382

12. Distribution Statement   There are no restrictions on the distribution of this document. Information about the availability of this and other RTO unclassified publications is given on the back cover.

13. Keywords/Descriptors

Aerodynamics	High lift devices	MDO (Multidisciplinary Design Optimization)
Design	Fluid dynamics	
NATO	Wings	Procurement
International cooperation	Airfoils	Tools
Optimization	Computer aided design	Rapid design system
Aerospace engineering	Missiles	Aerospace craft
Aerodynamic configurations	Data bases	Military Operations
Military aircraft	Data processing	Requirements

14. Abstract

The Symposium dealt with Design Issues and more specifically Aerodynamic Design and Optimization of Flight Vehicles in a Concurrent Multi-Disciplinary Environment. Thirty two papers and a Keynote address were presented with the objective to survey the current and future scene given the trend towards a more concurrent and multi-disciplinary approach to aerospace vehicle engineering.

There were six sessions covering the following topics:

• Lessons Learnt/Requirements for the Future Regard to the Role of Aerodynamicists in a Concurrent Multi-Disciplinary Design Process

• The Role of Aerodynamics in Concept Phase of a Project Design

• MDO and the Aerodynamics Design Process

• Methodologies/Tools for Aerodynamic Optimisation

• Application of Methodologies/Tools for Aerodynamic Optimisation

• Techniques for Rapid Database Generation

NORTH ATLANTIC TREATY ORGANIZATION

R T

RESEARCH AND TECHNOLOGY ORGANIZATION

BP 25 • 7 RUE ANCELLE

F-92201 NEUILLY-SUR-SEINE CEDEX • FRANCE

Télécopie 0(1)55.61.22.99 • E-mail mailbox@rta.nato.int

DIFFUSION DES PUBLICATIONS

RTO NON CLASSIFIEES

L'Organisation pour la recherche et la technologie de l'OTAN (RTO), détient un stock limité de certaines de ses publications récentes, ainsi que de celles de l'ancien AGARD (Groupe consultatif pour la recherche et les réalisations aérospatiales de l'OTAN). Celles-ci pourront éventuellement être obtenues sous forme de copie papier. Pour de plus amples renseignements concernant l'achat de ces ouvrages, adressez-vous par lettre ou par télécopie à l'adresse indiquée ci-dessus. Veuillez ne pas téléphoner.

Des exemplaires supplémentaires peuvent parfois être obtenus auprès des centres nationaux de distribution indiqués ci-dessous. Si vous souhaitez recevoir toutes les publications de la RTO, ou simplement celles qui concernent certains Panels, vous pouvez demander d'être inclus sur la liste d'envoi de l'un de ces centres.

Les publications de la RTO et de l'AGARD sont en vente auprès des agences de vente indiquées ci-dessous, sous forme de photocopie ou de microfiche. Certains originaux peuvent également être obtenus auprès de CASI.

CENTRES DE DIFFUSION NATIONAUX

ALLEMAGNE
Streitkräfteamt / Abteilung III
Fachinformationszentrum der
  Bundeswehr, (FIZBw)
Friedrich-Ebert-Allee 34
D-53113 Bonn

BELGIQUE
Coordinateur RTO - VSL/RTO
Etat-Major de la Force Aérienne
Quartier Reine Elisabeth
Rue d'Evére, B-1140 Bruxelles

CANADA
Directeur - Recherche et développement -
  Communications et gestion de
  l'information - DRDCGI 3
Ministére de la Défense nationale
Ottawa, Ontario K1A 0K2

DANEMARK
Danish Defence Research Establishment
Ryvangs Allé 1, P.O. Box 2715
DK-2100 Copenhagen Ø

ESPAGNE
INTA (RTO/AGARD Publications)
Carretera de Torrejón a Ajalvir, Pk.4
28850 Torrejón de Ardoz - Madrid

ETATS-UNIS
NASA Center for AeroSpace
  Information (CASI)
Parkway Center
7121 Standard Drive
Hanover, MD 21076-1320

FRANCE
O.N.E.R.A. (ISP)
29, Avenue de la Division Leclerc
BP 72, 92322 Châtillon Cedex

GRECE (Correspondant)
Hellenic Ministry of National
  Defence
Defence Industry Research &
  Technology General Directorate
Technological R&D Directorate
D.Soutsou 40, GR-11521, Athens

HONGRIE
Department for Scientific
  Analysis
Institute of Military Technology
Ministry of Defence
H-1525 Budapest P O Box 26

ISLANDE
Director of Aviation
c/o Flugrad
Reykjavik

ITALIE
Centro documentazione
  tecnico-scientifica della Difesa
Via Marsala 104
00185 Roma

LUXEMBOURG
Voir Belgique

NORVEGE
Norwegian Defence Research
  Establishment
Attn: Biblioteket
P.O. Box 25, NO-2007 Kjeller

PAYS-BAS
NDRCC
DGM/DWOO
P.O. Box 20701
2500 ES Den Haag

POLOGNE
Chief of International Cooperation
  Division
Research & Development Department
218 Niepodleglosci Av.
00-911 Warsaw

PORTUGAL
Estado Maior da Força Aérea
SDFA - Centro de Documentação
Alfragide
P-2720 Amadora

REPUBLIQUE TCHEQUE
VTÚL a PVO Praha /
  Air Force Research Institute Prague
Národní informační středisko
  obranného výzkumu (NISČR)
Mladoboleslavská ul., 197 06 Praha 9

ROYAUME-UNI
Defence Research Information Centre
Kentigern House
65 Brown Street
Glasgow G2 8EX

TURQUIE
Millî Savunma Başkanliği (MSB)
ARGE Dairesi Başkanliği (MSB)
06650 Bakanliklar - Ankara

AGENCES DE VENTE

**NASA Center for AeroSpace
  Information (CASI)**
Parkway Center
7121 Standard Drive
Hanover, MD 21076-1320
Etats-Unis

**The British Library Document
  Supply Centre**
Boston Spa, Wetherby
West Yorkshire LS23 7BQ
Royaume-Uni

**Canada Institute for Scientific and
  Technical Information (CISTI)**
National Research Council
Document Delivery
Montreal Road, Building M-55
Ottawa K1A 0S2, Canada

Les demandes de documents RTO ou AGARD doivent comporter la dénomination "RTO" ou "AGARD" selon le cas, suivie du numéro de série (par exemple AGARD-AG-315). Des informations analogues, telles que le titre et la date de publication sont souhaitables. Des références bibliographiques complétes ainsi que des résumés des publications RTO et AGARD figurent dans les journaux suivants:

Scientific and Technical Aerospace Reports (STAR)
STAR peut être consulté en ligne au localisateur de
ressources uniformes (URL) suivant:
    http://www.sti.nasa.gov/Pubs/star/Star.html
STAR est édité par CASI dans le cadre du programme
NASA d'information scientifique et technique (STI)
STI Program Office, MS 157A
NASA Langley Research Center
Hampton, Virginia 23681-0001
Etats-Unis

Government Reports Announcements & Index (GRA&I)
publié par le National Technical Information Service
Springfield
Virginia 2216
Etats-Unis
(accessible également en mode interactif dans la base de
données bibliographiques en ligne du NTIS, et sur CD-ROM)

Imprimé par le Groupe Communication Canada Inc.
(membre de la Corporation St-Joseph)
45, boul. Sacré-Cœur, Hull (Québec), Canada K1A 0S7

NORTH ATLANTIC TREATY ORGANIZATION

RT

RESEARCH AND TECHNOLOGY ORGANIZATION
BP 25 • 7 RUE ANCELLE
F-92201 NEUILLY-SUR-SEINE CEDEX • FRANCE
Telefax 0(1)55.61.22.99 • E-mail mailbox@rta.nato.int

DISTRIBUTION OF UNCLASSIFIED
RTO PUBLICATIONS

·NATO's Research and Technology Organization (RTO) holds limited quantities of some of its recent publications and those of the former AGARD (Advisory Group for Aerospace Research & Development of NATO), and these may be available for purchase in hard copy form. For more information, write or send a telefax to the address given above. **Please do not telephone**.

Further copies are sometimes available from the National Distribution Centres listed below. If you wish to receive all RTO publications, or just those relating to one or more specific RTO Panels, they may be willing to include you (or your organisation) in their distribution.

RTO and AGARD publications may be purchased from the Sales Agencies listed below, in photocopy or microfiche form. Original copies of some publications may be available from CASI.

NATIONAL DISTRIBUTION CENTRES

BELGIUM
Coordinateur RTO - VSL/RTO
Etat-Major de la Force Aérienne
Quartier Reine Elisabeth
Rue d'Evére, B-1140 Bruxelles

CANADA
Director Research & Development
Communications & Information
Management - DRDCIM 3
Dept of National Defence
Ottawa, Ontario K1A 0K2

CZECH REPUBLIC
VTÚL a PVO Praha /
Air Force Research Institute Prague
Národní informační středisko
obranného výzkumu (NISČR)
Mladoboleslavská ul., 197 06 Praha 9

DENMARK
Danish Defence Research
Establishment
Ryvangs Allé 1, P.O. Box 2715
DK-2100 Copenhagen Ø

FRANCE
O.N.E.R.A. (ISP)
29 Avenue de la Division Leclerc
BP 72, 92322 Châtillon Cedex

GERMANY
Streitkräfteamt / Abteilung III
Fachinformationszentrum der
Bundeswehr, (FIZBw)
Friedrich-Ebert-Allee 34
D-53113 Bonn

GREECE (Point of Contact)
Hellenic Ministry of National
Defence
Defence Industry Research &
Technology General Directorate
Technological R&D Directorate
D.Soutsou 40, GR-11521, Athens

HUNGARY
Department for Scientific
Analysis
Institute of Military Technology
Ministry of Defence
H-1525 Budapest P O Box 26

ICELAND
Director of Aviation
c/o Flugrad
Reykjavik

ITALY
Centro documentazione
tecnico-scientifica della Difesa
Via Marsala 104
00185 Roma

LUXEMBOURG
See Belgium

NETHERLANDS
NDRCC
DGM/DWOO
P.O. Box 20701
2500 ES Den Haag

NORWAY
Norwegian Defence Research
Establishment
Attn: Biblioteket
P.O. Box 25, NO-2007 Kjeller

POLAND
Chief of International Cooperation
Division
Research & Development
Department
218 Niepodleglosci Av.
00-911 Warsaw

PORTUGAL
Estado Maior da Força Aérea
SDFA - Centro de Documentação
Alfragide
P-2720 Amadora

SPAIN
INTA (RTO/AGARD Publications)
Carretera de Torrejón a Ajalvir, Pk.4
28850 Torrejón de Ardoz - Madrid

TURKEY
Millî Savunma Başkanliği (MSB)
ARGE Dairesi Başkanliği (MSB)
06650 Bakanliklar - Ankara

UNITED KINGDOM
Defence Research Information
Centre
Kentigern House
65 Brown Street
Glasgow G2 8EX

UNITED STATES
NASA Center for AeroSpace
Information (CASI)
Parkway Center
7121 Standard Drive
Hanover, MD 21076-1320

SALES AGENCIES

NASA Center for AeroSpace
Information (CASI)
Parkway Center
7121 Standard Drive
Hanover, MD 21076-1320
United States

The British Library Document
Supply Centre
Boston Spa, Wetherby
West Yorkshire LS23 7BQ
United Kingdom

Canada Institute for Scientific and
Technical Information (CISTI)
National Research Council
Document Delivery
Montreal Road, Building M-55
Ottawa K1A 0S2, Canada

Requests for RTO or AGARD documents should include the word 'RTO' or 'AGARD', as appropriate, followed by the serial number (for example AGARD-AG-315). Collateral information such as title and publication date is desirable. Full bibliographical references and abstracts of RTO and AGARD publications are given in the following journals:

Scientific and Technical Aerospace Reports (STAR)
STAR is available on-line at the following uniform
resource locator:
  http://www.sti.nasa.gov/Pubs/star/Star.html
STAR is published by CASI for the NASA Scientific
and Technical Information (STI) Program
STI Program Office, MS 157A
NASA Langley Research Center
Hampton, Virginia 23681-0001
United States

Government Reports Announcements & Index (GRA&I)
published by the National Technical Information Service
Springfield
Virginia 22161
United States
(also available online in the NTIS Bibliographic
Database or on CD-ROM)

Printed by Canada Communication Group Inc.
(A St. Joseph Corporation Company)
45 Sacré-Cœur Blvd., Hull (Québec), Canada K1A 0S7

ISBN 92-837-1040-1